Bioactivities and structural diversity of natural products derived from fungi

Inaugural dissertation

for the attainment of the title of doctor
in the Faculty of Mathematics and Natural Sciences
at the Heinrich Heine University Düsseldorf

presented by

Viktor Emanuel Simons

from Mönchengladbach

Düsseldorf, January 2023

from the Institute of Pharmaceutical Biology and Biotechnology
at the Heinrich Heine University Düsseldorf

Published by permission of the
Faculty of Mathematics and Natural Sciences at
Heinrich Heine University Düsseldorf

Supervisor: Prof. Dr. Rainer Kalscheuer

Co-supervisor: Prof. Dr. Dr. hc. Peter Proksch

Date of the oral examination: 31.03.2023

Table of Contents

Abbreviations

ABC	ATP-binding cassette
AHC	N-acyl-homoserine lactones
AIC	autoinducing peptide
AMR	antimicrobial resistance
antiSMASH	antibiotics and secondary metabolite analysis shell
ATCC	American Type Culture Collection
ATP	adenosine triphosphate
C3 convertase	complement component 3 convertase
CAT	chloramphenicol acetyltransferase
DNA	deoxyribonucleic acid
EF-G	elongation factor G
e.g.	exempli gratia
EPS	extracellular polymeric substances
ESKAPE	Group of highly drug-resistant and clinically important human pathogens
et al.	*et aliae*
ExoS	exoenzyme S
GARDP	Global Antibiotic Research and Development Partnership
GTPases	guanosine triphosphate hydrolase enzymes
HAC	histone acetylases
HDAC	histone deacetylases
HGT	horizontal gene transfer
HPLC	high performance liquid chromatography
LPS	lipopolysaccharides
MBE	mobile genetic element
MDR-PA	multidrug resistant *Pseudomonas aeruginosa*
MexXY	multidrug efflux system XY
MexZ	multidrug efflux protein Z
MIC	minimal inhibitory concentration
MIC_{90}	minimal concentration at which 90% of isolates are inhibited

µM	mikromolar
MRSA	methicillin-resistant *Staphylococcus aureus*
NaBr	sodium bromide
NaI	sodium iodide
OMP	outer membrane protein
OprD	outer membrane protein D
OSMAC	one strain many compounds
OXA-48	oxacinillase 48
PBP	penicillin-binding protein
pH	pondus hydrogenii
QS	quorum sensing
RNA	ribonucleic acid
ROS	reactive oxygen species
rRNA	ribosomal ribonucleic acid
SAB	*Staphylococcus aureus* bacteremia
SCIN	*staphylococcal* complement inhibitor
sp.	species
Tet(M)	tetracycline resistance protein M
Tet(O)	tetracycline resistance protein O
UV	ultraviolet
VCD	vibrational circular dichroism
WHO	World Health Organization

Acknowledgement

First of all, I would like to deeply thank my supervisor Prof. Dr. Rainer Kalscheuer for the great guidance and support during my years as a PhD-student. The countless meetings and talks helped me to grow and find my way in this interesting field of research and have an indispensable value to me.

Also, I would like to thank Prof. Dr. Dr. h.c. Peter Proksch for being my co-supervisor and with his former work to build up the opportunity so that I could find my way into the research field of natural products and compound isolation.

I also want to thank my colleagues and former colleagues Marian Frank, Lasse van Geelen, Nam Tran-Cong, Dieter Meier, Yvonne Gröner, Mohammed Rizwan Babu Sait, Steffen Schindler, Tino Seidemann, Lin Wang, Anna-Lene Kiffe-Delf, Emmanuel Tola Adeniyi, Kristin Schwechel, Di He, Violetta Krisilia, Meng Yun Zhang, Haiqian Yu, Dina Elkashef and Arta Kuci. And, I want to thank Heike Goldbach-Gecke not only for the cytotoxicity testings of isolated fungal compounds, but for the general support. In this regard I also want to thank Simone Miljanovic and Katja Friedrich. There was not one day where I could not count on your help. All of these great people helped me to learn, develop and improve new skills and in general to grow as a person. Thank you for always sharing kind and helpful words and thoughts and for filling the institute with life. Thanks to you, I will always wear a wide smile when thinking about my time at the university.

Further, I want to express my deepest gratitude to my research partners Prof Dr. Tibor Kurtán and Attila Mándi for the exceptional knowledge and support in the measurements of the circulardichroism data.

Also, I want to thank Prof. Dr. Christoph Janiak and Dennis Woschko for the measurements of the X-ray crystallographic data.

Furthermore, I want to thank my research partners and colleagues Marian Frank, Lasse van Geelen, Nam-Tran Cong, Flamminia Mazzone, Sebastian Scharf, Philipp Spohr, Peter Eze and Lin Wang for the great and professional cooperation throughout the whole process of the development of our manuscripts.

I want to express a very special thank you to my family and especially my mother, which comes from the bottom of my heart. Your steady support throughout my whole life, on so many different levels, paved the way so I was able to develop and grow to the person I am today. I am very grateful to have such a wonderful family.

Finally, I want to thank my girlfriend Melanie. During the last years your immense support was of immeasurable value to me. You helped me to find and maintain the balance in life, which was necessary to walk this road. The countless talks, both serious and cheery, granted me inner strength and improved my attitude. Thank you for always being there for me.

1. Introduction

1.1. Antibiotics

In 1899, Emmerich and Löw firstly described the clinical use of bacterial extracts to treat infections [1]. By that time, they could only speculate on the nature of the compounds they were using. Later in 1910, Paul Ehrlich was the first person to introduce a synthetic antibiotic for clinical use to the world, Salvarsan, a triphenylic compound with arsenic atoms bound covalently to it, and which was used for treatment against syphilis [2]. A huge downside was its rather strong toxicity. A random occasion in 1928 led to the discovery of penicillin by Alexander Fleming [3], surely one of the most famous and iconic moments in the history of drug discovery.

One of the first systematic studies in the history of antibiotic drug discovery from microorganisms was conducted by Selman Waksman and H. Boyd Woodruff in 1940 [4], where the focus was on the isolation of microorganisms from soil samples and the subsequent isolation of antibacterial compounds produced by these microorganisms. These scientists were the discoverers of the peptidic antibiotic class of actinomycins [5]. With their studies, they initiated the entry into the so-called "Golden Age" of antibiotic discovery from 1950 to 1970, where dozens of new antibiotical classes from different sources were introduced to the world [6]. Unfortunately, in the time past these years, the discovery of new antibiotics strongly decreased, while antibiotic resistance steadily increased. Today we are facing the challenge of finding new solutions to the emerging microbial resistance crisis to prevent the death of millions of people that otherwise could occur in the future [7].

1.1.1. Fungal antibiotics

The history of fungal antibiotics that are still in use today started around the "golden age" of antibiotic drug discovery. Some of these compound classes were so successful that new semisynthetic derivatives with improved activity and safety were investigated. Here, a short overview of the most important fungal antibiotics classes is given.

As described above, the penicillins introduced the world to a completely new class of medication: antibiotics. Penicillin G (see **Figure 1**) is one of the early discovered members of this class of β-lactam antibiotics and still has a therapeutic meaning. An inexpensive isolation process for its application for systemic use in humans was first described in 1945 by Berger *et*

al. [8]. In 1948 a derivative, penicillin V, being more acid-stable and therefore improving oral intake, was introduced to the world [9]. Decades later amoxicillin was synthesized, which on the one hand improved the bioavailability even more and on the other hand had a broader spectrum of action by also including some gram-negative bacteria that were not tackled by the penicillins described before [10]. The mode of action, the inhibition of the transpeptidase that is damaging the cell wall of bacteria indirectly resulting in a bactericidal effect, was already described in 1957 [11].

The cephalosporins are structurally close relatives of the penicillins, also bearing the beta-lactam group as the central element, necessary for its antibiotic activity (see Figure 1). In 1953 the first compound of this class, cephalosporin N, was isolated from a *Cephalosporium sp.*[12]. Even though the naturally occurring cephalosporins only inherit a weak antibacterial activity, it was recognised that they could not be inactivated by certain enzymes, namely penicillinases or beta-lactamases, which at that time already led to the first antibiotic resistances against the penicillins [13]. Semisynthetically derived compounds from the class of cephalosporins, like cefuroxime, led to a strong increase in its antibiotic activity, by also killing bacteria resistant to penicillins [14].

Griseofulvin was isolated in 1939 from *Penicillium griseofulvum* (see **Figure 1**) [15]. Its special ability to influence the morphology of the germ tubes of certain fungi also gave it the name "curling factor" [16]. This spiro compound with a grisan base structure is selectively active against dermatophytes by inhibiting the function of microtubules [17, 18], allowing its clinical use for treatment ofskin infections caused by these pathogens.

The first antibiotic isolated from the genus *Fusarium* was enniatin (see **Figure 1**), which was discovered in 1947 by Gaumann *et al.* and showed good antibacterial activity against *Mycobacterium paratuberculosis* [19]. More of these cyclic depsipeptides were isolated in the following years, namely enniatin A and B and beauvericin [20, 21]. However, their high level of genotoxicity made them unapplicable for use as antibiotics [22].

In 1951, the antibacterial class of the pleuromutilins (see **Figure 1**) was discovered from the basidiomycetes *Pleurotus mutilus (*now *Omphalina mutila)* and *Pleurotus passeckerianus* [23]. The lead compound pleuromutilin showed bacteriostatic activity against *Staphylococcus aureus* via inhibition of the peptidyl transferase of the ribosomal 50S subunit [24, 25]. Nevertheless, concerns of hepatotoxicity, gastrointestinal side effects, low bioavailability and stability, and the complicated side chain chemistry regarding semisynthesis, stopped this interesting class of diterpenes from its entry into the world of antibiotics for clinical use for around 50 years [26].

Now, with the semisynthesis of lefamulin, there is another systemic antibiotic for use in infected humans [27, 28].

In 1962, fusidic acid (see **Figure 1**) was isolated from the genus *Fusidium* and is a fungal antibiotic mainly active against Gram-positive bacteria [29]. The bacteriostatic effect can be explained through the inhibition of prokaryotic elongation factor EF-G and thus the inhibition of protein biosynthesis [30]. This steroid antibiotic is mainly in use in the treatment of skin infections, but systemic application is possible [31].

This summary of the history of antibiotics derived from fungal sources shows only a part of the underlying potential that is still to be unfolded. While in the last decades the focus was mainly put on the semisynthetic modification of known compounds, it is about time that yet another new class of naturally derived antibiotics will be discovered.

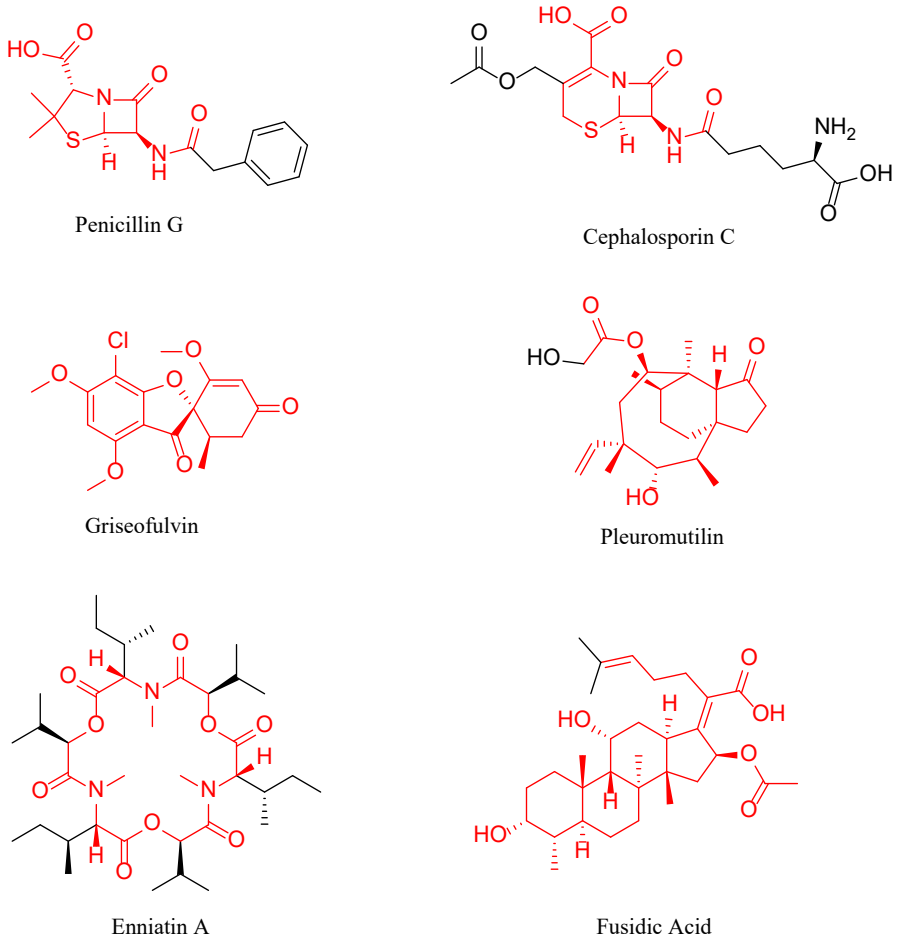

Figure 1. Chemical structures of antibiotic lead compounds derived from fungi. The core structures that are being shared in most derivatives of a group are marked in red.

1.1.2. Resistance mechanisms

Ever since antibiotics were introduced to the world of medications, antimicrobial resistance sooner or later emerged [32], limiting the effectiveness and applicability of many antibiotics that had been in use for several decades. Antimicrobial resistance to antibiotics can be achieved through different mechanisms, which are shortly described in this chapter.

Some bacteria exhibit an intrinsic resistance against several drugs, meaning the resistance already exists preexposure and is not induced mainly through the use of antibiotics. Mycobacteria, for example, have a high lipid content in their cell wall so that hydrophilic compounds cannot pass. In contrast, relatively lipophilic compound, such as rifampicin, can permeate through it and passively diffuse into the cell [33]. Furthermore, gram-negative bacteria are often less susceptible to most antibiotics if compared with their gram-positive counterparts. This is because of their sophisticated cell wall structure, consisting of an outer membrane in addition to the cytoplasmic membrane. The outer membrane is an additional selective permeability barrier, which can be passed by hydrophilic molecules only through porins [34]. Adaptation of these porins, for instance, is described for *Pseudomonas sp.*, leading to more limited uptake of certain drugs and subsequently to higher resistance rates [35].

Another resistance mechanism is the protection or modification of a drug target. Target protection is being achieved, for example, by the tetracycline-resistance determinants Tet(M) and Tet(O). These proteins, belonging to the superfamily of the GTPases, prevent the antibiotic tetracycline from binding to the 16S rRNA by conformational changes in the 30S ribosomal subunit, and, therefore, from inhibiting the protein translation [36, 37].
A modification of the drug target is something that can be observed, for example, in rifampin resistance of certain bacteria. Single nucleotide polymorphism in the *rpoB* gene leads to an amino acid exchange in the rifampin target site and loss of affinity of rifampicin to the beta-subunit of the RNA polymerase [38].

The inactivation of the drug is a resistance mechanism that can be achieved through cleavage or minor modification of the antibiotic. A prominent example of a cleavage-based resistance mechanism is the production of β-lactamases to dismantle penicillins and other beta-lactam antibiotics. The general mechanism of action of bacterial β-lactamases is to hydrolyze the amide group of the β-lactam antibiotic. This can be accomplished by both gram-positive and gram-negative bacteria. Nowadays, a variety of different classes of beta-lactamases with differing specificity to the wide range of β-lactam antibiotics is known, such as OXA-48 from *Acinetobacter baumannii* responsible for carbapenem resistance, to threaten the impact of

antibiotics that are saving human lives for many decades [39].

An example of the modification of a drug is found in the acetylation of chloramphenicol, leading to a strongly decreased binding affinity to its target [40]. Different types of chloramphenicol acetyltransferases (CAT) are described, yielding 3-mono- and 1,3-diacetylchloramphenicol [41]. An example is EC 2.3.1.28 originating from *Escherichia coli* and leading to high-level resistances [42].

Bacteria possess efflux pumps that among other substrates can also expel antibiotics. These pumps can be encoded intrinsically, can acquire selectivity towards certain antibiotics due to mutations driven by selective pressure or can be recruited by horizontal gene transfer. We know different types of bacterial efflux pumps, some of them being relatively unspecific multidrug transporters, such as the ATP-binding cassette (ABC) transporters, some of them being highly specific for certain antibiotics, such as Tet-pumps conferring resistance towards tetracycline in *E. coli*. Efflux pumps reduce the effective concentration of antibiotics inside the cell, circumventing them from reaching lethal concentrations [43, 44].

An overview of the most important antimicrobial resistance mechanisms is provided in the following **Figure 2**.

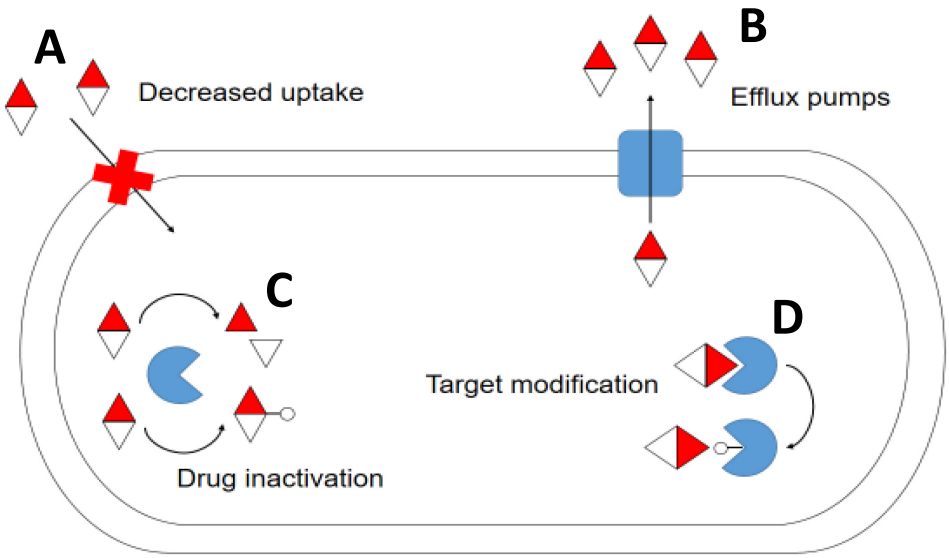

Figure 2. Summary of the most important antimicrobial resistance mechanisms. A: Decreased uptake can be achieved through transport proteins (e.g. porins) that control the uptake of hydrophilic compounds. In the case of gram-negative bacteria, the special membrane structure is highly controlling the uptake of drugs. **B**: Specialized or multidrug efflux pumps can efficiently reduce the concentration of antibiotics inside the bacterial cell. **C**: Drug inactivation via enzymes can either dismantle an antibiotic or add a molecular group to it, both reducing its activity. **D**: Target modification alters the molecular target of the antibiotic, reducing or completely abolishing its affinity to it.

1.1.3. Biofilms

The bacterial biofilm is an accumulation of bacterial cells embedded in extracellular polymeric substances (EPS) forming the biofilm matrix consisting of polysaccharides, proteins, and extracellular nucleic acids. Bacteria can grow as a biofilm on biotic (e.g. soft tissues) or abiotic (e.g. medical devices) surfaces [45]. A biofilm can be formed by only one bacterial species, but most of the time it consists of different species living together in a community [46]. Also, a biofilm can consist of only a monolayer or of multilayers, where the cells are attached to the surface as well as to other organisms [47].

The formation of a bacterial biofilm is mainly divided into five steps (see **Figure 3**). Step one is the reversible attachment phase. In this phase, the bacteria can attach to a certain surface, but this binding is not very specific and therefore completely reversible. In step two, the irreversible attachment phase, additional more specific cell-cell- and cell-surface interactions are established, amongst others *via* adhesins, which lead to a stronger attachment. In step three, the EPS are synthesized and secreted, which is induced by the recognition of quorum sensing (QS) molecules. These QS molecules are an essential part of infection and biofilm formation and are different among gram-positive and gram-negative bacteria. The main QS molecule in gram-positive bacteria is called autoinducing peptide (AIP) and is recognised by a sensor-kinase, which phosphorylates a transcription factor that regulates the expression of genes involved in infection and biofilm formation (two-component system). In gram-negative bacteria, N-acyl homoserine lactones (AHL) are the main QS molecules and bind directly to a transcription factor controlling the expression of virulence- and biofilm-related genes. After the release and recognition of QS molecules, biofilm maturation is the fourth step in biofilm formation. Step five is the dispersal or detachment phase, in which cells are dispersed from the biofilm and transformed back to the planktonic state [48, 49].

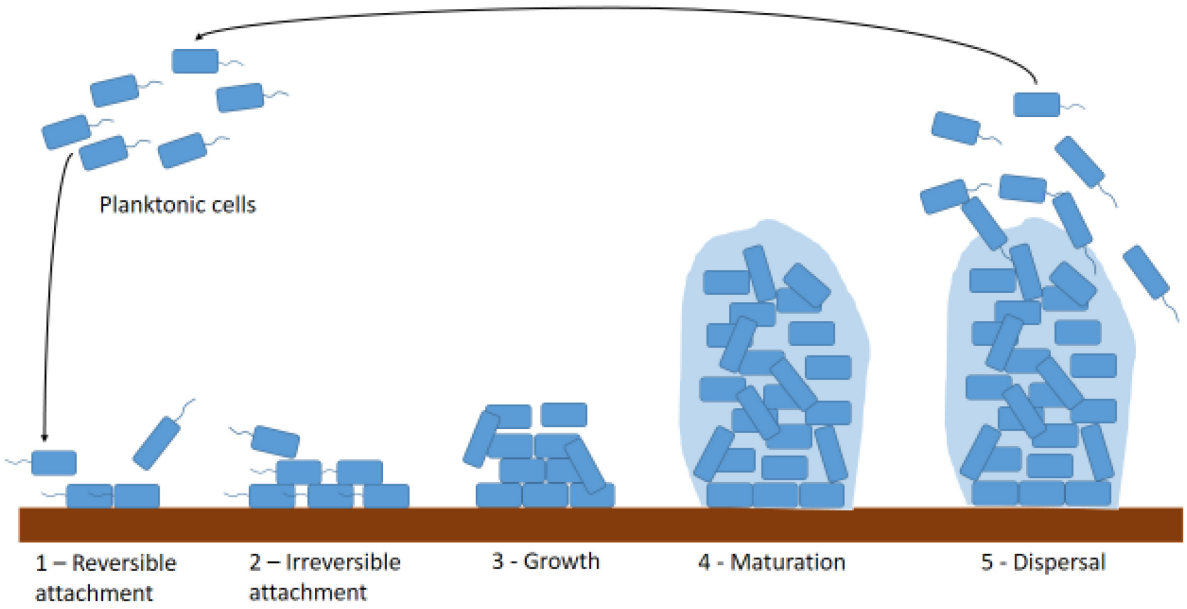

Figure 3. The five main phases of biofilm formation. **1** – Reversible attachment to a surface. **2** – Irreversible attachment via specific binding mechanisms. **3** – Growth via secretion of extracellular polymeric substances (EPS) and quorum sensing molecules. **4** – QS molecules induce the maturation of the biofilm. **5** – Cells can leave the biofilm and transform back into the planktonic state. Figure adapted from [48].

The production of a biofilm gives a lot of advantages to microorganisms. While nutrients can diffuse through the biofilm and spread homogenously, the biofilm matrix forms a physical barrier and protects the bacteria against harsh environmental conditions, like extreme temperatures, pH values and UV light, but also against antibiotics rising the tolerance against antibiotic treatment up to 1000-fold [50, 51]. For *E. coli* and *Myxococcus xanthus,* it has been described that a lack of nutrients can convert them from the biofilm state back to the planktonic state, suggesting that biofilms are preferably built under good nutritive circumstances [52].

Bacterial persisters are a slow-growing or even growth-arrested sub-population of cells. Because many antibiotics are most effective on fast-growing bacteria, persisters are hard to treat. This subpopulation is being found in high concentrations in bacterial biofilms and is one of the reasons for the long-term treatment of infections caused by *Mycobacterium tuberculosis* [53].

The flexibility of microorganisms to form biofilms depending on the environmental situation is also advantageous in terms of host-immune defence mechanisms during infections in humans [54]. A variety of diseases is described where the production of biofilms plays a crucial role in

its pathophysiological development. Some examples are auditory, cardiovascular, respiratory, or urinary diseases, to name but a few [55]. However, the formation of biofilms is not always connected to human diseases, such as biofilms inside the healthy mouth that are commonly found and consist of different bacterial species living together. A problematic situation occurs when biofilm formation leads to persistent infections that cannot be cured within short periods [56]. An example is an infection with *Mycobacterium tuberculosis*, forming cavities in the lung tissue, where the mycobacteria are surrounded by EPS within a biofilm-like structure that some antibiotics are not able to permeate through to reach single cells, increasing the bacteria's intrinsic drug tolerance. Also, the higher amount of persistent cells within the biofilm turns the treatment into a lengthy and tedious purpose [57]. Another example is the infection with the gram-negative bacterium *Pseudomonas aeruginosa* that can occur in patients with a weak immune system and is especially endangering patients suffering from cystic fibrosis. The big armamentarium of antimicrobial resistances, which commonly is found in *P. aeruginosa*, together with the ability to form biofilms that can even grow on implant materials such as joints or catheters, makes it hard to treat after an productive infection has been established [58]. A big threat of high clinical relevance is the gram-positive bacterium *Staphylococcus aureus*, which often also carries a variety of resistances against common antibiotics and can grow biofilms on medical devices [59].

Finding compounds that can inhibit or disrupt biofilms gained additional interest in recent years because of the threatful character in medicine and industry causing a health burden [60].
The difference between the inhibition of biofilm formation and its disruption is as follows: Compounds that inhibit the biofilm formation are active before the biofilm is built, disturbing the complex interbacterial signalling, so that the biofilm is not formed properly. In contrst, biofilm disrupting compounds can break up already existing, mature biofilm structures [61]. A mechanistic example of the inhibition of biofilm formation is the inhibition of QS, called quorum quenching [62]. A rather recent example of natural compounds able to inhibit biofilm formation are the cytochalasans. Yuyama *et al*. isolated 13 cytochalasan derivatives from different fungal organisms that were able to inhibit biofilm formation of *S. aureus* efficiently, while providing a good cytotoxic profile. Yet the mode of action still needs to be investigated [63]. An example of a compound showing biofilm disrupting activity is the antibacterial agent triclosan. Even though this compound is in use since a long time as an antibacterial agent in a wide range of consumer goods, it is connected to a variety of side effects ranging from an increase in thyroid hormone levels, and higher abortion rates to increased risk of asthma, allergies and food sensitization [64, 65]. Furthermore, there is a variety of macromolecular

compounds showing biofilm disrupting activities. Amongst these are peptides, enzymes, synthetic polymers, polycationic materials, and peptidomimetics [66]. When it comes to natural products, the field of known antibiofilm compounds is rather scarce and therefore requires a stronger focus of researchers worldwide [67].

1.1.4. Resistance Crisis

The appearance of antimicrobial resistance (AMR) in the history of antibiotics has always been tightly connected to the application of antibiotic drugs. Ever since antibiotics were used, at some point sooner or later antimicrobial resistance occurred [32].
Following the "golden age" of antibiotic drug discovery, the time between 1962 and 2000 sometimes is referred to as an innovation gap because no new antibiotic classes have been introduced to the world [68]. Nevertheless, the extensive development of (semi-)synthetic antibiotics till the early 1990s made the scientific world not pay enough attention to possibly one of our most threatening problems of the future [69]. Recently, based on predictive statistical models, it was calculated that in 2019 already 1.27 million deaths worldwide were directly attributable to bacterial AMR alone, and the yearly death toll will possibly increase to approx. more than 10 million deaths within the next 30 years [70, 71].

The reasons for this widespread occurrence of AMR that is affecting every part of the world are assembled by a multicausal nature. First of all, problems occur during the prescription process of antibiotics. Wrongly chosen antibiotics with insufficient effectiveness, an unspecific treatment against unknown pathogens, or the premature termination of drug intake are some problems arising from the management of antibiotics in the clinical environment. This leads to a high selective pressure, and mutations are more likely to spread increasing the risk of AMR. Another issue is the overuse of antibiotics in livestock and food industries. Antibiotics are widely used to prevent infections in animals and to promote growth for maximum productivity. H this immense overuse perfectly paves the way for AMR [72].
Another problem is that incentives for the pharmaceutical industry are rather low. Research in the field of antibiotics was becoming less fruitful and ineffective since not only the discovery of new antibacterial natural products proved more and more difficult, but also the high expectations placed in the high-throughput screening of synthetic compound libraries were fulfilled only to a very limited extent. Furthermore, mode of action studies are very elaborate and a high number of failures had a discouraging effect. Additionally, the clinical testing of

drug candidates is cost-intensive usually devouring several hundred million dollars. If the drug is successfully introduced to the pharmaceutical market, a new antibiotic, especially if it belongs to a completely new class, is likely to be used as a drug of last resort and even if used will naturally be applied only during a short period. Altogether, this is limiting its economical value for the producer drastically. These are reasons why many antibiotics developed or isolated by researchers in universities never leave the state of basic research and go into the cost-intensive clinical phase [73].

AMR is severely threatening our future health system. If there is no substantial change in finding new and effective antibiotics, calculations estimate more than 10 million deaths annually by the year 2050 worldwide caused only by AMR. This is more than the predicted number of deaths caused by cancer for the same year [74].
In May 2019, there were 407 projects worldwide, focussing on the development of antibacterial agents in preclinical development. Some of them took new routes, like strategies modifying the microbiome, constructing phages and probiotics, or approaching antivirulence therapy. Nevertheless, this number is still too low and will not alone overcome the resistance crisis [75].

While some companies also recognise this problem, organisations were founded to tackle AMR. One such organisation is the Global Antibiotic Research and Development Partnership (GARDP), which aims to develop four new treatments against drug-resistant infections by 2023 [76]. Also, 20 leading biopharmaceutical companies created the AMR action fund. One billion dollar of funding shall support small companies developing new antibiotics to bring two to four new antibiotics to patent by the year 2030 [77].

For future times, the current efforts should be strongly increased and improved to defeat the silent pandemic of AMR.

1.2. High Priority Pathogens

In 2017, the World Health Organisation (WHO) published a list of 12 bacteria for which new antibiotics are urgently needed. This high-priority pathogens list itself is divided into three subsections, ranking these 12 bacteria into the levels of medium, high, and critical risk. The risk level is determined based on criteria like mortality rate, nosocomial infections, or broad resistance and therefore gives a clear sign on which pathogens research should be focused on the most. The authors highlighted that *M. tuberculosis* is not included because its treatment is already targeted in different other programs but bears the same importance [78].

Table 1. High-priority pathogens list as determined by the WHO in 2017. Pathogens with frequently acquired resistances are divided into the three risk and priority levels "Critical", "High" and "Medium". Table adapted from [78].

Risk level/Priority	**Pathogen**	**Resistance**
Critical	*Acinetobacter baumannii*	Carbapenem
	Pseudomonas aeruginosa	Carbapenem
	Enterobacteriaceae	Carbapenem, ESBL-producing
High	*Enterococcus faecium*	Vancomycin
	Staphylococcus aureus	Methicillin, Vancomycin
	Helicobacter pylori	Clarithromycin
	Campylobacter spp.	Fluoroquinolone
	Salmonellae	Fluoroquinolone
	Neisseria gonorrhoeae	Cephalosporin, Fluoroquinolone
Medium	*Streptococcus pneumonia*	Penicillin (non-susceptible)
	Haemophilus influenzae	Ampicillin
	Shigella spp.	Fluoroquinolone

This information is based on surveillance worldwide. Every few years, the WHO publishes surveillance data from countries around the world, showing new developments in the field of AMR [79].

Another classification of microorganisms with multidrug resistances and an endangering armamentarium of virulence factors are the ESKAPE pathogens. These were grouped by "The Infectious Diseases Society of America" to highlight them as important hospital-acquired pathogens, being able to "escape" the effect of antibiotics [80, 81]. The acronym ESKAPE includes the bacteria ***E****nterococcus faecium,* ***S****taphylococcus aureus,* ***K****lebsiella pneumonia,* ***A****cinetobacter baumannii,* ***P****seudomonas aeruginosa* and ***E****nterobacter spp.* It is of high importance to discover new antibiotics being able to tackle these microorganisms efficiently to increase our scope of potential treatments [82]

In the following subchapters, two of the most important pathogens, *Staphylococcus aureus* and *Pseudomonas aeruginosa*, will be described, and the special importance of developing new antimicrobials that can efficiently eradicate these bacteria will be highlighted.

1.2.1. *Staphylococcus aureus*

The gram-positive bacterium *Staphylococcus aureus* was named after its cluster-like colonisation and its gold-like pigmentation compared to other *Staphylococcus* species. Additionally, it reacts positively to testing for coagulase, mannitol fermentation, and deoxyribonuclease [83].
The first person isolating this bacterium was the Scottish surgeon Alexander Ogston in 1880, who recognised it being content of pus in one of his patients. Remarkably, he already understood it is one of the reasons for the high mortality rate after operations by that time. He also found out that heat sterilisation and the use of disinfectants remove the infectiousness of the pus [84].

S. aureus can cause a wide range of different infections, including the skin or respiratory system. This is of huge concern regarding hospitalized patients when they suffer from staphylococcal pneumonia. Also, immune deficient patients are especially endangered or patients with viral infections, which can be superinfected by *S. aureus*. In these situations, the infections can cause endocarditis, osteomyelitis, or toxic shock syndrome, to name but a few [85]. One of the most problematic situations occurs when an infection leads to sepsis, so-called

S. aureus bacteremia (SAB), where the bacterium spreads over the blood circulation throughout the whole body leading to mortality rates of around 20 % [86].

The high versatility of *S. aureus* gives it a threatening character. Often, *S. aureus* strains comprise mobile genetic elements (MBEs) that can bear virulence factors. The exchange of plasmids for example can thus transfer virulence factors via horizontal gene transfer (HGT) from one bacterium to another [87]. These virulence factors are also called toxins because they support the pathogenicity of *S. aureus* drastically. One example is the α-toxin, which helps the cocci to efficiently penetrate the skin through different molecular mechanisms. The next step could then be a systemic infection. Also, the bacteria can encapsulate in an abscess, which limits the effectiveness of attacks by the host immune system. While being transported by the circulation of the bloodstream, *S. aureus* can produce leukocidins, which destroy phagocytes indirectly by inducing cell lysis via a cell membrane receptor. Also, the bacterium is capable of inhibiting the innate immune system via the complement system by the production of staphylococcal complement inhibitor (SCIN), which inhibits C3 convertases, altogether weakening the immune response [88].

Furthermore, the high genetic adaptability of *S. aureus* is also notable in its acquisition of antibiotic resistances. Already in 1942, the first clinical isolate with penicillin resistance was described [89]. In 1959 methicillin was developed, being the first beta-lactam antibiotic that was not dismantled by penicillinases [90]. But it took only two years to again discover the first *S. aureus* isolate with methicillin resistance [91], which the bacterium achieves through the expression of high levels of penicillin-binding protein 2a (PBP2a) [92]. This subtype is not inhibited by methicillin but can take over the main transpeptidation function of the host PBP.

S. aureus is a common nosocomial pathogen because of its ability to produce biofilms on catheters and other medical devices and thus can be easily transmitted. The formation of biofilms overcomplicates the therapy because some antibiotics are not able to penetrate them, while others are less effective on the higher number of persistent bacteria embedded in the EPS [93].

The standard treatment for a methicillin-resistant *S. aureus* (MRSA) infection with bacteremia is the glycopeptide antibiotic vancomycin. A lot of experience has been made with this compound because it is already in use for decades. To optimize treatment success, it is important to exactly adjust the serum concentration. In some cases, its slow bactericidal effect unfortunately can decrease the chances of successful treatment.
Other possible treatments are the use of the glycopeptide teicoplanin or the lipoglycopeptide

telavancin, with the latter having higher nephrotoxicity compared to vancomycin. The lipopeptide daptomycin has a fast bactericidal effect, but is less effective in pneumonia and has a toxic effect on muscles. The mechanism of the muscle toxicity of daptomycin, which in severe cases can cause rhabdomyolysis, has not completely been elucidated. A study in 2020, however, has revealed *in vitro* results proposing membrane damage via the necroptotic pathway [94]. Also, the use of the fifth-generation cephalosporine ceftaroline and the bacteriostatic-acting oxazolidinones is possible. Finally, the combination of vancomycin or daptomycin with a beta-lactam antibiotic can be used [95].

Clinical isolates with combined resistance against methicillin and vancomycin have been described, but the cases are fortunately still rather scarce. Responsible use of existing antibiotics is a key factor to continue limiting these numbers in the future and not generating virtually untreatable pathogens [96].

1.2.2. *Pseudomonas aeruginosa*

In 1882, the French pharmacist Carle Gessard managed to isolate *Pseudomonas aeruginosa* from green and blue coloured bandages of wounded soldiers. At that time it was known under the name *Bacillus pyocyaneus* [97]. The pigment, which is blue under basic conditions and could change to green at neutral pH, was named pyocyanin and investigated in more detail by Edwin Jordan at the end of the 19th century [98].

P. aeruginosa is a gram-negative rod-shaped bacterium that is an oxidase-positive glucose non-fermenter [99]. It is found in nearly every surrounding because of its high adaptability. It thus can be found in soil, water, or in plants as an endophyte [100]. Also, it was found to be associated with nematodes, insects, and amoebae [101].

For humans, *P. aeruginosa* is an opportunistic pathogen that is mainly infecting immunosuppressed and weak patients. Examples are patients with severe burns, HIV infections, or tumour diseases. It is a dangerous threat for patients with cystic fibrosis and people in intensive care units. It is estimated that *P. aeruginosa* is responsible for around 10% of nosocomial infections in European hospitals [102].

Once infected, *P. aeruginosa* is a hard-to-treat pathogen. It has developed a variety of molecular mechanisms to efficiently protect itself from the immune system, both defensively and aggressively. The central key point in this regard are the diverse virulence factors.

P. aeruginosa, like most gram-negative bacteria, has lipopolysaccharides (LPS) incorporated into its outer membrane. While these lipid molecules can be used by the host immune system to detect and eliminate the bacterial cell, the bacterium itself can use them to bind to host cells, cause damage to tissues, develop the bacterial biofilm and create resistance to certain antibiotics [103].

Outer membrane proteins (OMPs) are used for adhesion, antimicrobial resistance, and exchange of nutrients. An example is the OMP OprD, which normally is used by carbapenem antibiotics like imipenem to passage through the bacterial cell membrane. Mutations in this protein can lead to resistance to this antibiotics class [104].

The formation of biofilms is of huge concern in *P. aeruginosa*. It leads to a bunch of effects that severely limit the successful treatment. The bacterial cells become much more evasive while being attacked by antibiotics less efficiently, the community has a higher amount of persistent cells in comparison to the planktonic state, and phagocytes can be repelled easier. Biofilms of *P. aeruginosa* pave the way to long-term resistance and chronic infections in the lung, wounds, and paranasal sinuses, to name but a few [105].

Another virulence factor is the type III secretion system. This secretion system is used to inject effector proteins into host cells, such as exoenzyme S (ExoS), which is even able to induce apoptosis in phagocytes and thus reduce the bacterial clearance of the infected organism [106].

The mentioned pyocyanin also acts as a bacterial virulence factor, by inhibiting prostacyclin release, cell respiration, ciliary functions, and host enzymes [107]. It is described that the pathogenicity of pyocyanin is also connected to the production of reactive oxygen species (ROS), but further studies need to be undertaken to confirm these suggestions [108].

Its success as a nosocomial pathogen is surely also driven by its ability to form biofilms in sinks, plumbings, and other areas with ponding water in hospital surroundings [109]. In addition to these non-specific antibiotic resistances also a variety of specific resistance mechanisms are described. A mutation in the gene encoding the porin OprD for instance drives a resistance against the carbapenem antibiotic imipenem [110]. This is of huge concern because the carbapenem-resistant *P. aeruginosa* is one of the three critical level bacteria on the WHO high priority pathogens list [78]. Another example of a specific AMR is the overexpression of the MexXY multidrug transporter operon by a mutation in the *mexZ* gene. This mutation increases the activity of an efflux pump responsible for transporting aminoglycosides, fluoroquinolones and β-lactam-antibiotics out of the bacterial cell, reducing the susceptibility against these antibiotics drastically [111].

Effective treatment options for *P. aeruginosa* infections comprise β-lactam-antibiotics, like penicillins, cephalosporins or carbapenems, and aztreonam in case of a penicillin allergy, fluoroquinolones and aminoglycosides. β-Lactam-antibiotics can be combined with a β-lactamase-inhibitor, such as clavulanic acid. While fluoroquinolones can be administered orally, they exhibit a higher rate of resistance development. For multi-drug-resistant *P. aeruginosa* (MDR-PA) infections, treatment with the polymyxins colistin or polymyxin B is possible. In general, the decision for a certain treatment should be based on the local resistance situation and, if tolerable, the treatment period should be long enough to reduce the chance of AMR. Also, a combination therapy with different antibiotics might be carried out to reduce the risk of acquiring resistances [112].

As an interesting alternative treatment approach, phage therapy has gained more attention during the last years. While there is still more scientific investigation necessary to improve these therapies to a level allowing usedful clinical application, promising results have already been published, for example focusing on biofilm deformation to lower intrinsic resistances and improve the effectiveness of available antibiotics [113].

1.3. Isolation of microorganisms from environmental samples

The isolation of microorganisms from environmental samples and the subsequent isolation of bioactive compounds derived from these organisms was already initiated in the middle of the 20th century when Waksman and Woodruff as pioneers isolated actinomycin A and B from the soil-derived bacterium *Streptomyces antibioticus* [4]. This was the starting point for a new era of microbial research and drug discovery. Some scientists discussed that the isolation of antibiotics from soil-derived microorganisms is a promising strategy due to the limitation of resources and space in the soil. Thus, the production of antimicrobial compounds can lead to a selective advantage. Others argued that in nature these antimicrobial compounds are normally present in sublethal concentrations and are rather being used as signal molecules. Inhibition of other microorganisms in unnaturally high concentrations is therefore a random occasion [114-116].

Compared to synthetically derived antibiotics, isolation of antimicrobial compounds from environmental microorganisms can most of the time be accomplished faster and easier. This might be due to the fact that these compounds have been steadily developed and improved

under conditions of constant microbial competition during evolution over thousands of years [117].

Of huge concern is the limitation of the cultivability of environmental microorganisms. It is estimated that around 99 % of the microorganisms living in soil are not able to grow under standard laboratory conditions [118]. This led to approaches of developing new cultivation techniques in recent years, to grow microorganisms in artificial surroundings, that have been tagged to be uncultivable before [119]. In 2015, for example, a special chip-based process led to the discovery of the new peptide antibiotic teixobactin. The researchers were able to use a special plastic chip with semipermeable membranes to grow the gram-negative bacterium *Eleftheria terrae* in its natural soil habitat while isolating the antibiotic compound at the same time [120].

In the last decades, the focus more and more shifted to lesser investigated environmental niches to reduce the frequent rediscovery of already known natural products. Endophytic microorganisms for example are microorganisms associated with a plant host in a mutually supportive relationship. This special natural habitat has an influence on the metabolic pathways of these microorganisms, which led to the discovery of a variety of new bioactive natural products from endophytes [121]. Other prominent ecological niches that have contributed to increase our treasure chest of natural products and antibiotics are marine surroundings [122], microorganisms associated with insects [123], and microorganisms derived from animal faeces [124].

This short overview is supposed to provide a glimpse of the diversity and sheer scale that is connected to environmental microorganisms. New developments and progress in this field of research will continue to deliver new natural products with antimicrobial activities for many years.

1.3.1. Soil

The soil as a source for antimicrobial metabolites produced by microorganisms was firstly discovered by Waksman and Woodruff in 1940 with the isolation of actinomycin A and B [4]. The idea that led to their intense investigations was that pathogenic microorganisms for hundreds of years must have been in contact with soil microorganisms, being constantly transmitted by humans and animals. Nevertheless, the proportion of pathogenic microorganisms in soil remains very low, suggesting mechanisms that inhibit the growth of these organisms.

In the years after the pioneering work of Waksman and Woodruff, Albert Schatz continued with the isolation of streptomycin, the first antitubercular antibiotic, from soil-borne *Streptomyces griseus [125]*. Later, chlortetracyclin was firstly described as a metabolite from *Streptomyces aureofaciens* [126], and chloramphenicol was isolated by Ehrlich from another *Streptomyces sp.* from a soil sample [127].

The content and diversity of microorganisms in soil are subject to huge differences and depend on a lot of different factors. In 1 g of soil, an estimated number of several billion bacteria comprising around 200 million actinomycetes can be found [128]. There are 100-9,000 different prokaryotic organisms per cm^3 and 200-235 different fungi per gram of soil [129]. However, there is an immense variety of the richness of different organisms that depends on the quality of the soil. The amount and diversity of prokaryotes in arable soil for example are markedly lower compared to natural forest soil [130]. The preference for certain species of fungi also differs strongly with respect to pH values and the general content of soils [131]. Generally, more microorganisms can be found at soil depths of 0-25 cm, because of a higher content of organic materials that serve as nutrients [132]. Also, a variety of microorganisms reside in the rhizosphere, showing different diversifications of microorganisms depending on the particular plant species [133].

To expand the range of cultivable microorganisms from soil samples, a lot of new methods have been developed in recent years. A rather crude but effective approach is the intense adaptation of the parameters used for laboratory culturing of soil microorganisms. For example, new species from the divisions acidobacteria and verrucomicroba were isolated by adding humic acid and quorum-signalling compounds to the growth medium, prolonging the growth phase to more than 30 days, building up an anoxic or hypoxic atmosphere or protecting the bacteria from endogenous peroxides [134].

A more sophisticated approach was the construction of a diffusion bioreactor that should mimic the naturally occurring environmental conditions in forest soil. This bioreactor contains an outer and an inner chamber that is separated by a perforated layer. The outer layer is filled with forest soil, while the inner layer is filled with the soil sample distributed in the growth medium. During the growth process, natural components from the forest soil can diffuse through fine pores into the inner chamber and promote the growth of microorganisms that are dependent on certain ingredients that synthetical media cannot provide [119].

Another modern approach tackling the problem of unculturable soil microorganisms was accomplished by Hover *et al.* in 2018. They discovered the new antibacterial class of the malacidins without the need of culturing any bacteria in a process known as “genome mining”.

Microbial DNA was directly isolated from soil samples, and the genetic information was used to rationally search for calcium-dependent antibiotic-like tags [135].

These works impressively show the complexity and diversity of microbial life in the soil. Further, they give an insight into the intertwined dependences that the different contents, living and not living, have in this gigantic natural community.

1.3.2. Plants

Endophytes are microorganisms, mostly bacteria, and fungi, which live inside plant tissues mainly in a symbiotic relationship. Normally these microorganisms are harmless to the plant host, and endophytic organisms have been described for nearly every known plant [136]. Interestingly, it strongly depends on the part of the plant that is being processed, which endophytes and what pattern of microorganisms can be isolated from it [137].

Endophytes can be very useful for their plant host. It is described that they can improve the uptake of minerals into the plant [138], support nitrogen fixation [139], play a crucial role in the host defence mechanisms [140], increase cellulose and lamina density in the plant tissues and thus reducing herbivory of insects [141], and protect from oxidative stress by the production of enzymes like the superoxide dismutase [142].

In recent years research work suggested an even closer relationship between the endophytic organism with its host. Some publications even described that horizontal gene transfer (HGT) can happen between the plant and its endophytes. An example is the subtilisin gene that is relatively typical for plants, which was found in an endophytic *Colletotrichum sp.* [143]. Also, the transfer of genes from endophytic fungi to their host plants was reported. An example is the transfer of the hemerythrin gene to mosses, where it plays a role in oil body biogenesis and dehydration resistance [144]. There is still a need for extensive research on this exciting topic, but there is a high possibility that the contact of the endophyte with its host plant can lead to the acquisition of genes necessary for the production of bioactive secondary metabolites [145]. This theory is supported by the description of plant hosts and their corresponding endophytes, that both are capable of producing the same bioactive metabolite. An early and famous example is the biosynthesis of the cytotoxic taxol, which was found to be a secondary metabolite produced both by *Taxus brevifolia* and its fungal endophyte *Taxomyces andreanea* [146]. Other examples are the biosynthesis of hypericin by *Hypericum perforatum* and its endophyte

Chaetomium sp. and camptothecin by *Fusarium solani* and its host plant *Apodytes dimidiate* [147, 148].

In the last years, a colourful spectrum of new and bioactive compounds exclusively found in endophytic organisms has been described, ranging from peptidic structures to a huge variety of small molecules with different bioactivities [149]. Endophytes have proven to be a precious and prolific complementation to other natural sources of microorganisms and attempts in finding new antimicrobials. Each plant's unique fingerprint of endophytic organisms and the possible genetic interactions between the microorganisms and their host turn the research of endophytes into a fruitful and promising field with high potential.

1.3.3. Other ecological niches

Microorganisms can be found in various places to form ecological niches, which shows their huge potential to adapt. In the following, three additional ecological niches shall be highlighted that could possibly play an important role in the discovery of new bioactive natural products.

The frequent rediscovery of compounds from terrestrial microorganisms shifted the interest towards lesser explored ecological niches. Marine microorganisms are of special interest in this respect because research in this area is still very scarce [150]. This is quite surprising because marine organisms, in general, comprise the biggest part of the overall known biodiversity of the world because of the immense size of the oceans [151]. The conditions in marine environments often are more extreme and very different from terrestrial surroundings. The hydrostatic pressure, salt content and a big range of temperatures up to extreme points influence the living microorganisms here, forcing them to develop a range of diverse adaptations also leading to the production of unique secondary metabolites [152].
In the past, a wide range of interesting compounds with different bioactivities was isolated from marine microorganisms. Some examples are salinosporamide A from *Salinospora sp.*, which showed strong cytotoxic activities on cancer cells [153]; dolastatin 10 from a marine cyanobacterium, a precursor of one of the strongest cytotoxic compounds on earth; the semisynthetic monomethylauristatin E [154]; the antiviral antimycin A [155]; and salinopostin A, which is an antimalaria compound with a strong activity in the nanomolar range [156].

Another interesting ecological niche for microorganisms that gained more and more interest especially in recent decades are insects. Most of the time these microorganisms live in a symbiotic relationship with the insect, similar to that of the endophytes [157]. Interestingly, the

microorganisms can live inside different parts of the insect, like the gut, but also in specialized cells called “bacteriocytes” and thus play an important role in the uptake and processing of nutrients for the insect [158-160].

Some new bioactive compounds have been isolated from microorganisms obtained from insects. A symbiotic *Serratia marcescens* from the microbiota of the *Anopheles* mosquito was found to produce the lipodepsipeptides stephensiolides A-K that possess activities against *Bacillus subtilis* and *Plasmodium falciparum* [161]. Furthermore, from a *Streptomyces sp.* found in the fungus-growing ant *Cyphomyrmex sp.*, a macrocyclic polyketide named cyphomycin has been isolated that showed a range of different antifungal activities, including antifungal activity against the multiresistant yeast *Candida auris* [162].

Microorganisms also play an important role in the gut of animals as symbionts, where they improve and increase the nutrient uptake for the host while also profiting from the nutrients and strengthening the host’s immune defence against pathogenic microorganisms [124]. The composition of the nutrient uptake is central here because it also influences the diversity and composition of the gut microbiome of the animal [124, 163, 164]. The faeces of herbivore animals for example is made up of a unique diversity of microorganisms because of the plant-based diet that is also rich in the uptake of endophytic organisms that live inside the plant tissue and have extensive probiotic effects [165].

Research on bioactive compounds from microorganisms derived from animal faeces is rather scarce. The isolation of new azaphilone pigments and the compound pyrenophorin from the goose dung-derived fungus *Coniella fragariae*, which possesses strong cytotoxic activity, has been described [166]. Further, the isolation of new anti-inflammatory metabolites from a *Streptomyces sp.* isolated from zebra dung can be found in the literature [167]. Nevertheless, this ecological niche is still underexplored and potentially rich in unique metabolites with interesting bioactivities.

1.4. Activation of silent gene clusters and the OSMAC concept

Biosynthetic gene clusters (BGCs) are genes that are physically located close to each other and together are responsible for the synthesis of certain metabolic products [168]. There are different types of BGCs, each developing different structural classes of metabolites, like polyketides, non-ribosomal peptides or terpenes, to name a few [169]. Interestingly, not all BGCs are expressed constitutively, meaning some are only active under certain conditions. Some of them need triggers from the environment or are being expressed stronger under special genetic influences. These BGCs are silent and if activated can lead to cryptic metabolites that are not present under standard conditions [170]. The possibilities for the isolation of undiscovered and bioactive secondary metabolites from microorganisms, therefore, are substantially increasing by approaches trying to address these activation processes. This is further supported by the increasing number of whole genome sequencing data during the last years that underline that most of the BGCs microorganisms likely possess the genetic capacity to produce many metabolites we still have not discovered yet [171]. The potential for the isolation of new and bioactive secondary metabolites through the activation of silent BGCs thus is high and promising.

There are different strategies to access these cryptic and potentially interesting compounds. A biotechnological method is the heterologous expression of a certain inactive BGC. The BGC of interest is being transferred from the parental and naturally occurring host strain to a known lab strain, where it can be expressed to exploit the metabolites. The biggest challenge here is the size of the BGCs, which often can exceed 100 kilobases [172].

Another methodology is the so-called refactoring of BGCs. This means the substitution of transcriptional regulatory elements to turn the silent BGCs into permanently active ones. Of special interest here is the promotor engineering because promotors drive the transcription of a BGC [173].

Addionally, epigenetic modifications are able to change the metabolic profile of an organism. This is typically not specific and leads to changes in different genetic positions. An example is the knockout of genes that encode histone deacetylases. In eukaryotic cells, histone proteins form a condensed structure with DNA, which is called nucleosome. The interaction of the histone proteins with the DNA and consequently the structural appearance of the nucleosome influences the activity of certain genes. This is tightly connected to the acetylation status of the histone proteins, which is being controlled by histone acetylases (HATs) and deacetylases (HDACs). Hyperacetylation of histones, which can be achieved by downregulation and

knockout of HDACs, leads to transcriptional activation of silent chromosomal regions, and this migth result in the biosynthesis of secondary metabolites that are not produced otherwise [174-176].

A strategy not directly focussing on biotechnological methods, but on the activation of silent gene clusters is the OSMAC concept (see figure 4). OSMAC was conceived in 2002 by Bode *et al.* and is the acronym for **O**ne **S**train **Ma**ny **C**ompounds, meaning that different cultural conditions of the same strain can lead to different secondary metabolite profiles. This effect can occur on different levels, concerning transcription, translation, or activation and inhibition of different enzymes [177]. The big advantage of OSMAC is the ease of use. Prominent and easy-to-apply examples for the OSMAC concept are changes in physical parameters, like the temperature during cultivation or changing the oxygen concentration, co-cultivations with other microorganisms to mimic situations that occur in nature, or the supplementation of different nutrients or other small compounds to the cultivation medium [178].

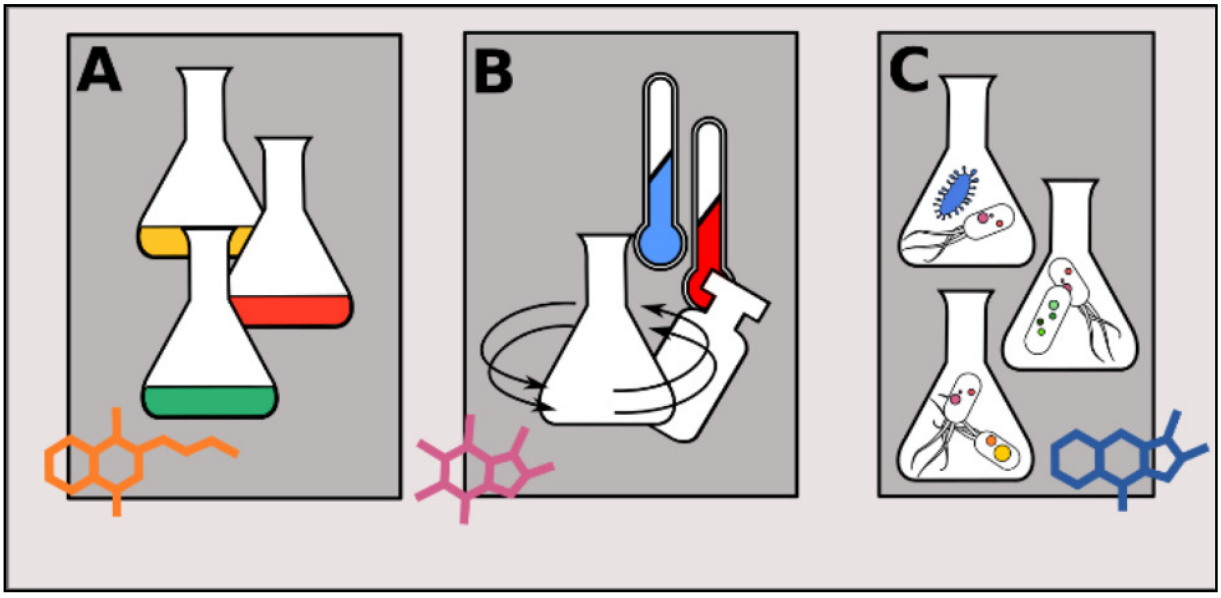

Figure 4. Examples of OSMAC approaches in the cultivation of a microorganism. A: alteration of the nutrient medium, B: adaptation of the physical parameters, C: co-cultivation with different microorganism (prokaryotic-prokaryotic, prokaryotic-eukaryotic or eukaryotic-eukaryotic). Figure adapted from [178].

The heterologous expression of BGCs was already quite fruitful and yielded a variety of different metabolites. Taromycin A is an antibiotic from the bacterium *Saccharomonospora sp.* that was isolated by transferring its BGCs to *Streptomyces coelicolor* [179]. Also, the BGC from a marine *Streptomyces sp.* coding for the antibiotics class of the berninamycins was expressed in *Streptomyces albus* and led to two new members of this family of thiopeptides,

named berninamycin J and K [180].

Cryptic metabolites that were isolated through the OSMAC concept are also quite manifold. An interesting example is the supplementation of fruit and vegetable juice to the cultivation medium of *Fusarium tricinctum*, which gave new fusarielin derivatives, a class of compounds with members being active against human ovarian cancer cells [181]. The addition of different salts to the cultivation medium of the endophytic fungus *Bulgaria inquinans* isolated from mistletoe led to the biosynthesis of new butyrolactones [182]. Furthermore, the co-cultivation of *Bacillus subtilis* with the endophytic fungus *Trichocladium sp.* from the Vietnamese medicinal plant *Houttuynia cordata* gave the new spiro compound 5-epi-pestafolide A and increased the production of the antibiotic colleketol by tenfold [183].

1.5. Bioassay-guided compound isolation

While the isolation of new natural products is steadily increasing our knowledge about the chemical space covered by nature, often compounds with no detected activities are not followed any further after discovery because of a lack of practical use. In fact, the major aim of natural product isolation is the discovery of bioactive molecules that could lead to potential therapeutic applications. A rational design for the isolation process of bioactive compounds from natural sources that track certain activities starting from the crude extract to the pure compound is purposeful and time-saving. This is what bioassay-guided compound isolation is focussing on. Any kind of bioactivity can be traced throughout the whole isolation process and only the samples with promising bioactivities are further processed. It can also be used to explore lesser investigated bioactivities to isolate known compounds that inherit these activities but were never tested for them. Especially in high-throughput screening processes, it helps reduce the number of samples to the most important ones and thus saves a lot of unnecessary work and time [184].

A good example of the helpfulness of bioassay-guided isolation of natural products is a study from 2009, where 126 different *Actinomycetes* from the Aegean region of Turkey have been isolated and screened for bioactivity against MRSA and *E. coli*. The bioactivity guidance helped the authors reduce this total amount of bacteria to the most interesting isolate and precisely let them isolate the two antimicrobial compounds 4'-deacetyl griseusin A and griseusin A, both showing MICs lower than 1 µg/mL against MRSA and *E. coli*, respectively [185]. Another study from 2018 aimed to isolate compounds with biofilm-inhibiting properties against different *Candida sp.*. The bioactivity-guided isolation of *Salvia officinalis* extracts yielded the two biofilm-inhibiting compounds carnosol and 12-methoxy-trans-carnosic acid [186]. A cell-based activity-guided screening in 2013 led to the isolation of the bacterial steroids bendigole D-F with anti-inflammatory properties [187].

These examples underline the versatility and benefit of bioassay-guided isolation processes. The tracking of interesting activities throughout a complete isolation process, in addition to searching for new and structurally interesting compounds, helps to improve the outcome for natural product isolation-based studies.

2 Aim

The increasing resistance rates of microorganisms against known antibiotics and a lack of discovery of new, clinically applicable antimicrobial compounds endanger our health system. We are in urgent need of finding new antibiotics to secure the use of effective antibiotic therapies against life-threatening pathogens in the future. Additionally, compounds being able to inhibit and disrupt the formation of microbial biofilms, which can lead to high tolerance and resistance against antimicrobial compounds are of special interest. Microorganisms from environmental samples in this regard have proven to be rich sources of bioactive compounds. In this work, the isolation of natural products from microbial fungi isolated from different environmental niches with a focus on bioactivity and molecular novelty was the main target. Endophytic microorganisms are interesting sources of bioactive compounds. The close and intense contact with their host has been shown to play an important role in their production of secondary metabolites.

In chapter 4, the endophytic fungus *Paraboeremia selaginella* was isolated from *Philodendron monster*a. Because information about secondary metabolites from this fungus is hardly found in the literature the main metabolites should be isolated and tested for interesting bioactivities. Special focus was put on bioactivity testing against the apicomplexan pathogen *Toxoplasma gondii.*

The endophytic fungus *Trichocladium sp.* has already been shown to be influenced by different OSMAC approaches in earlier studies. Especially high protein and amino acid concentrations seem to change the metabolic profile in different ways. In the study presented in chapter 5, we highlight the influence of a new OSMAC approach with high concentrations of the amino acid L-phenylalanine on the production of secondary metabolites. The isolated compounds are tested for different bioactivities and new compounds should be elucidated to their absolute configuration.

The genus *Fusarium* even if well known, is still interesting because of its high versatility when it comes to the activation of silent BGCs. In chapter 6, we introduce an OSMAC approach, where we co-cultivate the soil-borne fungus *Fusarium oxysporum* together with different bacteria. The isolation and structure elucidation of compounds derived from the most promising co-cultivation with *Paenibacillus ehimensis* and their bioactivities should be described. Special focus is put on bioactivities regarding biofilm disruption. Finally, a proposal of the biosynthesis

of interesting compounds on the basis of a whole genome sequencing approach should be carried out.

3 Summary

Looking back on the last decades, we face a period with a lack of new antibiotics. Together with the increasing emergence of multi- and extensively drug-resistant pathogens, the discovery of new antimicrobial compounds becomes a key factor in not losing the race against AMR. Since we have an increasing rate of rediscovery in the research field of natural product isolation, it becomes important to go new routes. The focus on lesser investigated ecological niches, new cultivation strategies and activation of silent gene clusters is promising and provides us with nearly unlimited possibilities.

Toxoplasma gondii is an apicomplexan parasite that can infect different warm-blooded animals and humans. Toxoplasmosis is a related infection that can cause severe damage in immunocompromised patients and lead to fetal abortion in pregnant women. Since therapeutic options are limited, the discovery of new anti-toxoplasma compounds with a low side effect profile is of special interest. In the study "*In vitro* biological activity of natural products from the endophytic fungus *Paraboeremia selaginellae* against *Toxoplasma gondii"* presented in chapter 4, the isolation of the endophytic fungus *Paraboeremia selaginellae* and the subsequent isolation of eight compounds from a culture on solid rice medium was accomplished. The structures were elucidated and *5S,6S*-phomalactone VCD data were measured for the first time. All eight compounds were tested for antibacterial, cytotoxic, and anti-toxoplasma activity. Results showed that six of the eight compounds had moderate to good anti-toxoplasma activity while having a preferably good cytotoxic profile against the tested human cell lines.

In chapter 5, the endophytic fungus *Trichocladium sp* was cultivated in an OSMAC-based approach on solid rice medium supplemented with high concentrations of the aromatic amino acid L-phenylalanine. From the crude extract, ten compounds were isolated and their structures were elucidated. In previous studies, supplementation with a high protein medium or the aromatic amino acid L-tyrosine already yielded new compounds. In this study, five new compounds were successfully isolated and described. Interestingly three of the five new compounds are structural precursors of the cyclic dilactone colletodiol and derivatives. Although colletodiol or closely related derivatives were isolated in the previous studies, we describe their linear derivatives for the first time and propose L-phenylalanine to be an inhibitor of the cyclisation of colletodiol and related cyclic dilactones, leading to additional alternative metabolites.

Soil samples were one of the early sources for the isolation of microorganisms. Since the rediscovery of known microorganisms from soil samples happens frequently under standard lab conditions, researchers started to focus on lesser-investigated natural sources. *Fusarium oxysporum* is a well-investigated microbial fungus often associated with plant diseases as a pathogen. Even though a plethora of interesting compounds from the genus *Fusarium* was already isolated in the last decades, recent studies still reveal that there is a huge hidden treasure chest of unknown natural products that can be assessed by activation of silent BGCs. In chapter 6, we present our study of an *F. oxysporum* that was isolated from a soil sample. Employing the OSMAC concept, co-cultivation with five different bacteria was carried out on a solid rice medium to activate silent BGCs and reveal cryptic secondary metabolites. The co-cultivation with the soil-borne bacterium *Paenibacillus ehimensis* showed a strong shift in its macroscopic appearance on rice medium. While the axenic culture of *F. oxysporum* and the four other co-cultivations only showed an orange to red colour inside the rice medium, the co-cultivation with *P. ehimensis* led to the appearance of dark purple coloured spots. The HPLC-chromatogram showed a strong increase in the production of 9-*O*-methylfusarubin, which in high concentrations could be connected to the appearance of the purple colour. From this crude extract, ten compounds were isolated and resulted in three yet undescribed structures. Two of the three new compounds, named fusapurpurin A and B had the 9-*O*-methylfusarubin core structure that was extended by a phenyl pyruvic acid moiety, leading to a new structural subclass of fusarubin derivatives. A nanopore whole genome sequencing approach revealed a biosynthetic gene cluster (BGC) that could be responsible for the synthesis of the 9-*O*-methylfusarubin core structure. Genes encoding for an amino acid transporter and a L-amino acid oxidase inside this BGC supported the hypothesis that fusapurpurin A and B are formed over a reaction of 9-*O*-methylfusarubin and a structural derivative of L-phenylalanine. Interestingly, these compounds disrupt pre-formed biofilms of *Staphylococcus aureus, Pseudomonas aeruginosa* and, in the case of fusapurpurin B, *Mycobacterium tuberculosis*. This study underlines that new natural products can still be isolated from well-investigated microorganisms. The power of the OSMAC concept is immense and can help to increase and revive the potential of already-known species.

4. In Vitro Biological Activity of Natural Products from the Endophytic Fungus Paraboeremia selaginellae against Toxoplasma gondii

Manuscript published in: MDPI Antibiotics

Impact factor: 5.222 (2021)

DOI: 10.3390/antibiotics11091176

Contribution to the paper:

- Isolation and identification of the fungus
- Fermentation of the fungus and preparation of the crude extract
- Isolation and structure elucidation of the fungal compounds
- Large contribution to the writing of the manuscript

antibiotics

MDPI

Article

In Vitro Biological Activity of Natural Products from the Endophytic Fungus *Paraboeremia selaginellae* against *Toxoplasma gondii*

Flaminia Mazzone [1,†], Viktor E. Simons [2,†], Lasse van Geelen [2], Marian Frank [2], Attila Mándi [3], Tibor Kurtán [3], Klaus Pfeffer [1,*] and Rainer Kalscheuer [2,*]

[1] Institute of Medical Microbiology and Hospital Hygiene, Heinrich Heine University, 40225 Duesseldorf, Germany
[2] Institute of Pharmaceutical Biology and Biotechnology, Heinrich Heine University, 40225 Duesseldorf, Germany
[3] Department of Organic Chemistry, University of Debrecen, 4002 Debrecen, Hungary
* Correspondence: klaus.pfeffer@hhu.de (K.P.); rainer.kalscheuer@hhu.de (R.K.); Tel.: +49-211-8112459 (K.P.); +49-211-8114180 (R.K.)
† These authors contributed equally to this work.

Abstract: *Toxoplasma gondii* is an apicomplexan pathogen able to infect a wide range of warm-blooded animals, including humans, leading to toxoplasmosis. Current treatments for toxoplasmosis are associated with severe side-effects and a lack efficacy to eradicate chronic infection. Thus, there is an urgent need for developing novel, highly efficient agents against toxoplasmosis with low toxicity. For decades, natural products have been a useful source of novel bioactive compounds for the treatment of infectious pathogens. In the present study, we isolated eight natural products from the crude extract of the endophytic fungus *Paraboeremia selaginellae* obtained from the leaves of the plant *Philodendron monstera*. The natural products were tested for inhibiting *Toxoplasma gondii* proliferation, and their cytotoxicity was evaluated in different human cell lines. Six natural products showed antitoxoplasma activity with low or no cytotoxicity in human cell lines. Together, these findings indicate that biphenyl ethers, bioxanthracenes, and 5*S*,6*S*-phomalactone from *P. selaginellae* are potential candidates for novel anti-toxoplasma drugs.

Keywords: *Toxoplasma gondii*; *Paraboeremia selaginellae*; endophytic fungi; natural products; bioactivity; biphenyl ether; bioxanthracene; phomalactone

Citation: Mazzone, F.; Simons, V.E.; van Geelen, L.; Frank, M.; Mándi, A.; Kurtán, T.; Pfeffer, K.; Kalscheuer, R. In Vitro Biological Activity of Natural Products from the Endophytic Fungus *Paraboeremia selaginellae* against *Toxoplasma gondii*. *Antibiotics* **2022**, *11*, 1176. https://doi.org/10.3390/antibiotics11091176

Academic Editors: Valério Monteiro-Neto and Elizabeth S. Fernandes

Received: 12 August 2022
Accepted: 29 August 2022
Published: 31 August 2022

1. Introduction

Toxoplasma gondii is an obligate intracellular protozoan parasite member of the phylum Apicomplexa, which includes known human pathogens such as *Plasmodium* sp., *Eimeria* sp., *Neospora*, *Babesia*, *Theileria*, and *Cryptosporidium* spp., with which it shares significant biological similarities [1]. Beyond these organisms, the study of *T. gondii* has experimental advantages since its basic biology and the methodology for the genetic manipulation and quantification of its different stages are well established. Thus, *T. gondii* is considered a major model for the study of apicomplexan biology and for anti-apicomplexan drug target validation [2]. *T. gondii* infections are among the most common human zoonoses, leading to toxoplasmosis disease [3]. *T. gondii* is considered one of the world's most successful parasites due its ability to infect a wide range of warm-blooded vertebrate intermediate hosts [4]. *T. gondii* is estimated to chronically infect one-third of the world's human population and is acquired mainly through two ways: by ingesting oocysts shed from feline hosts (the definitive hosts) in contaminated food or water and by the consumption of raw or undercooked meat containing viable tissue cysts [5]. Waterborne and food-borne outbreaks of toxoplasmosis have been reported from countries with diverse cultural, social,

and ethnic backgrounds [6]. In immunocompetent individuals, infection with *T. gondii* is usually asymptomatic or has a subclinical course with mild symptoms. In contrast, immunocompromised (i.e., acquired immune deficiency syndrome (AIDS), organ transplant or cancer) patients can develop the disease, leading to life-threatening cerebral and ocular toxoplasmosis due to a reactivation of the latent infection. Additionally, primary infection in pregnant women may result in fetal death, spontaneous abortion, and birth defects [7–9]. Although many gaps have been filled in the epidemiological, diagnostic, and biological fields to understand of the interaction of the parasite with the host, little progress has been made in drug discovery for the treatment of toxoplasmosis.

Current treatments of acute toxoplasmosis are largely limited to anti-folate therapy. Pyrimethamine and sulfadiazine, the current gold-standards for the treatment of toxoplasmosis, can suppress the parasite growth in the active stage of the infection by targeting the tachyzoite stage, but they have no effect in the bradyzoites stage. Additionally, they have been found to have high rates of toxic side effects, leading to discontinuation of therapy. Thus, there is an urgent need to identify novel potent candidates that would be well-tolerated to eradicate latency as well as to treat the acute infection [10,11]. Natural products profoundly impact the history of drug discovery, especially in the research of novel anti-cancer, anti-bacterial, and anti-parasitic treatments. Nature continues to provide diverse and unique chemical sources of bioactive lead compounds that inspire novel drug discoveries [12]. The antiparasitic bioactivity of natural products from various sources, especially plant-derived secondary metabolites, has been deeply investigated in in vitro and in vivo studies [13]. Many fungal metabolites have also been reported to exhibit antimicrobial properties against parasitic pathogens. However, most of these studies focused on bioactivity against *Plasmodium falciparum*, whereas there is a scarcity of investigations to explore the potential of fungi as a source of novel anti-toxoplasma agents [14].

In this study, we extracted and purified eight natural products from the crude extract of *Paraboeremia selaginellae*, an endophytic fungus isolated from the ornamental plant *Philodendron monstera*. Isolated compounds were structurally characterized and evaluated for their anti-toxoplasma activities. Biphenyl ethers, bioxanthracenes, and phomalactone showed substantial activity against *T. gondii* proliferation. Therefore, we suggest these compounds as promising candidates for novel anti-parasitic therapies.

2. Results

2.1. Isolation of Compounds from Paraboeremia selaginella

We isolated an endophytic fungus from fresh surface-sterilized leaves of the ornamental plant *Philodendron monstera*. The isolated strain was identified as *Paraboeremia selaginella* by the internal transcribed spacer (ITS) sequence with 99.56% identity in comparison with the ITS database of the National Center for Biotechnology Information. From the crude extract of a culture of *Paraboeremia selaginella* grown on solid rice medium, eight compounds were isolated by chromatographic methods and structurally elucidated by complementary spectroscopic analyses (Figure 1). All eight compounds have previously been reported from other sources but are reported here for the first time as natural products occurring in the genus *Paraboeremia*.

Different stereoisomers of phomalactone (**F**) were isolated and reported previously from various sources [15–18], and some papers did not specify the absolute configuration [19,20], while others assigned the (5*R*,6*R*) absolute configuration to the large positive specific rotation [21], which was opposite to previous studies [15–18,22]. In order to determine the absolute configuration of phomalactone independently and unambiguously, we performed TDDFT-ECD, TDDFT-OR, and DFT-VCD studies, which consistently confirmed the (+)-*cis*-(5*S*,6*S*) absolute configuration (see Supplementary Materials) [23,24]. Comparisons of the experimental and computed VCD spectra of *cis*-(5*S*,6*S*) are shown in Figure 2, which produced good agreement. Other computational results are shown in the Supplementary Materials.

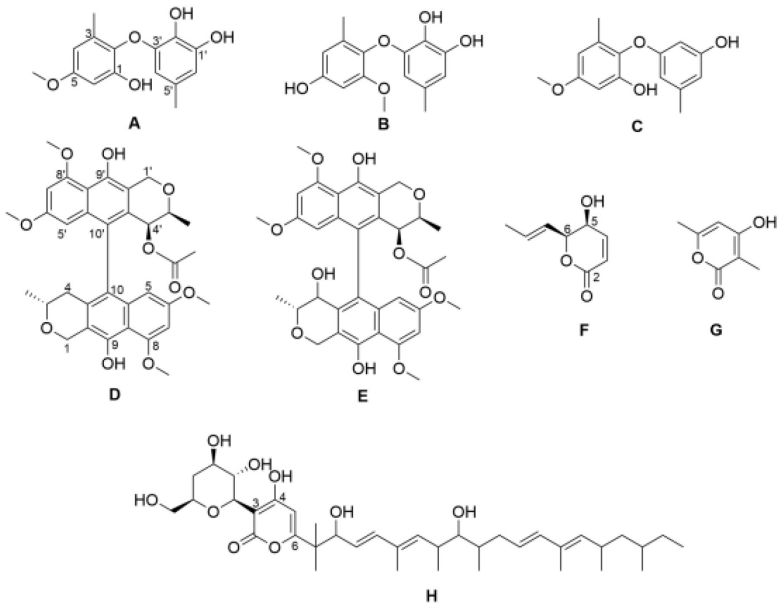

Figure 1. Chemical structures of the isolated compounds. NK-A 17e233 (**A**); 1,2-benzenediol, 3-(4-hydroxy-2-methoxy-6-methylphenoxy)-5-methyl-(ACI) (**B**); cyperin (**C**); ES-242-1 (**D**); ES-242-3 (**E**); 5*S*,6*S*-phomalactone (**F**); methyltriaceticlactone (**G**); S 39163/F-1 (**H**).

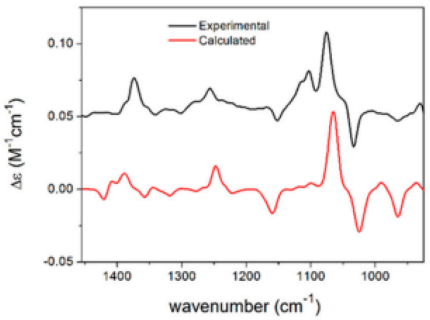

Figure 2. Comparison of the experimental VCD spectrum of **F** measured in $CDCl_3$ and the calculated VCD spectrum of *cis*-(5*S*,6*S*)-**F** computed at the B3LYP/TZVP PCM/$CHCl_3$ level for the eight lowest-energy conformers gained from the DFT optimization performed at the same level.

2.2. *Anti-T. gondii* Activity

The eight natural products isolated from *P. selaginellae* were tested for anti-*T. gondii* activity. Interestingly, **A**–**F** showed activity against *T. gondii* growth, with IC_{50} values of 5.75, 22.16, 27.22, 7.38, 17.99, and 5.13 μM, respectively (Table 1 and Figure 3). Therefore, we further explored the in vitro cytotoxicity of the natural compounds in different human cell lines.

Table 1. In vitro activity (IC_{50} values) of the natural compounds (**A**–**H**) from *P. selaginellae* against the *T. gondii* strain ME49. All experiments were conducted in triplicate.

Compound	IC_{50} (µM)
NK-A 17e233 (**A**)	5.75
1,2-benzenediol, 3-(4-hydroxy-2-methoxy-6-methylphenoxy)-5-methyl-(ACI) (**B**)	22.16
cyperin (**C**)	27.22
ES-242-1 (**D**)	7.38
ES-242-3 (**E**)	17.99
5*S*,6*S*-phomalactone (**F**)	5.13
methyltriaceticlactone (**G**)	Not active
S 39163/F-1 (**H**)	Not active
pyrimethamine	0.06

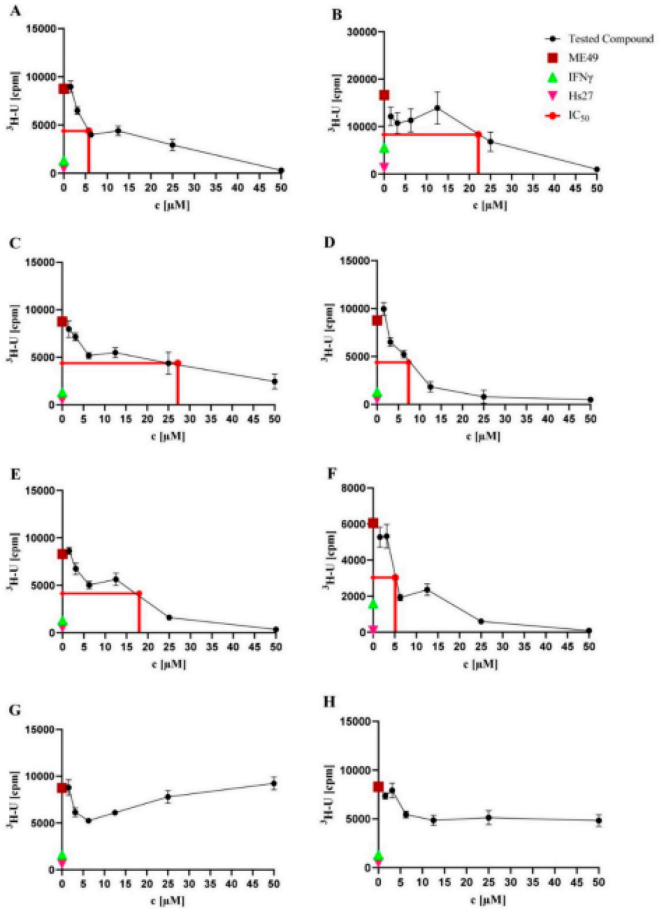

Figure 3. Toxoplasma proliferation assays. Toxoplasma proliferation assays were performed to investigate the activity of the natural products against *T. gondii* strain ME49. Hs27 cells were cultured in a monolayer in 96-well plates and infected with *T. gondii* (3×10^4). Cultures were treated with the

natural products at the concentration range of 0.56–50.00 µM for 48 h at 37 °C. Afterwards, the cultures were labelled with ^{3}H-U (5 mCi, diluted 1:30) for 28–30 h at 37 °C. Based on the incorporation of ^{3}H-U into the parasite nucleic acid, the parasite growth was quantified. As controls, uninfected Hs27 cells without treatment (pink triangles) and IFNγ pre-stimulated infected Hs27 cells (green triangles) were used, while untreated *T. gondii*-infected Hs27 cells (red squares) served as a negative control. Values shown in (**A**–**H**) represent the means of three independent experiments each done in duplicate ($n = 6$) ± SEM. The mean of the IC_{50} values (red line) of each compound is shown. Activity of NK-A 17e233 (**A**); 1,2-benzenediol, 3-(4-hydroxy-2-methoxy-6-methylphenoxy)-5-methyl-(ACI) (**B**); cyperin (**C**); ES-242-1 (**D**); ES-242-3 (**E**); 5*S*,6*S*-phomalactone (**F**); methyltriacetiolactone (**G**); S 39163/F-1 (**H**).

2.3. Cytotoxicity Assays

First, we evaluated the cytotoxicity of compounds **A** to **F** in an MTT assay against Hs27 human fibroblasts (same cell type used for the *T. gondii* proliferation assay). The results of the MTT assay are shown in Figure 4 and Table 2. **A**–**E** showed no cytotoxicity at 100 µM against Hs27 cells. Only **F** showed moderate cytotoxicity with a cytotoxic concentration $CC_{50} = 81 \pm 2.16$ µM.

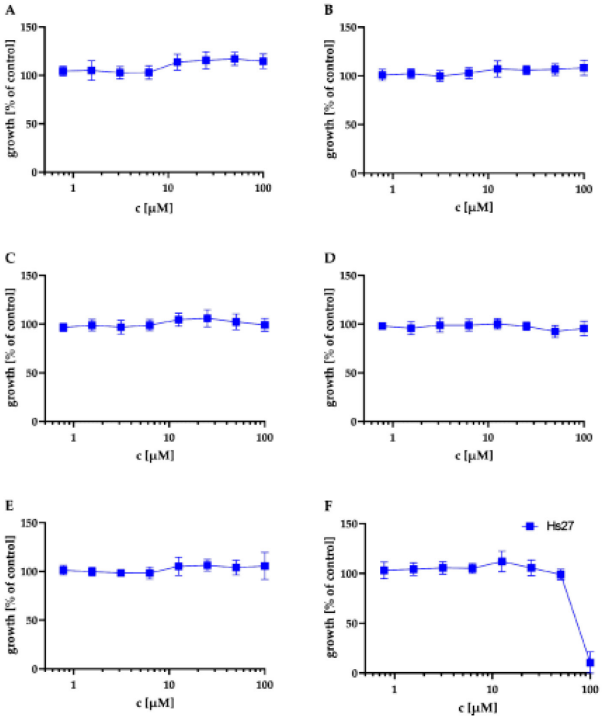

Figure 4. Effect of the natural products on the metabolic activity of Hs27 cells via MTT assay. Hs27 cells were plated in 96-well plates and grown to confluence prior to incubation at 37 °C for 24 h with the natural products in the concentration range of 0.56–100.00 µM. The cultures were incubated with 10 µL of the 12 mM MTT stock solution for approximately 4 h. Afterwards, 100 µL of SDS dissolved in HCl was added to each well and incubated again for 4 h at 37 °C. Finally, the absorbance was measured at 570 nm by spectrophotometry. Values shown in (**A**–**F**) represent the means of three independent experiments each done in duplicate ($n = 6$) ± SEM. Cytotoxicity in Hs27 cells of NK-A 17e233 (**A**); 1,2-benzenediol, 3-(4-hydroxy-2-methoxy-6-methylphenoxy)-5-methyl-(ACI) (**B**); cyperin (**C**); ES-242-1 (**D**); ES-242-3 (**E**); 5*S*,6*S*-phomalactone (**F**).

Table 2. In vitro cytotoxicity (CC_{50} values) of the natural compounds (**A**–**F**) from *P. selaginellae* against human fibroblasts Hs27. Concentration >100 µM indicates no activity in the experimental setup. All experiments were conducted in triplicate.

Compound	CC_{50} (µM)
A	>100
B	>100
C	>100
D	>100
E	>100
F	81
Pyrimethamine	44

These compounds also were tested against the THP-1, Huh-7, and Hek 293 cell lines in a Resazurin assay. The mean IC_{50} values of the Resazurin assay are shown in Table 3. While compounds **A**–**C** showed no cytotoxic effect in concentrations < 100 µM against any of the tested cell lines, **D** had only a weak cytotoxic activity against the Hek 293 cell line with an IC_{50} of 93.8 µM. **E** showed moderate cytotoxic activity against all of the three tested cell lines and thus was the most cytotoxic of the tested compounds. **F** showed no or weak cytotoxic effects against the Huh-7 and Hek-293 cell lines. The cytotoxic effect against the THP-1 cell line was higher, with an IC_{50} of 24.3 µM. The graphs for the Resazurin assay are shown in Figure 5.

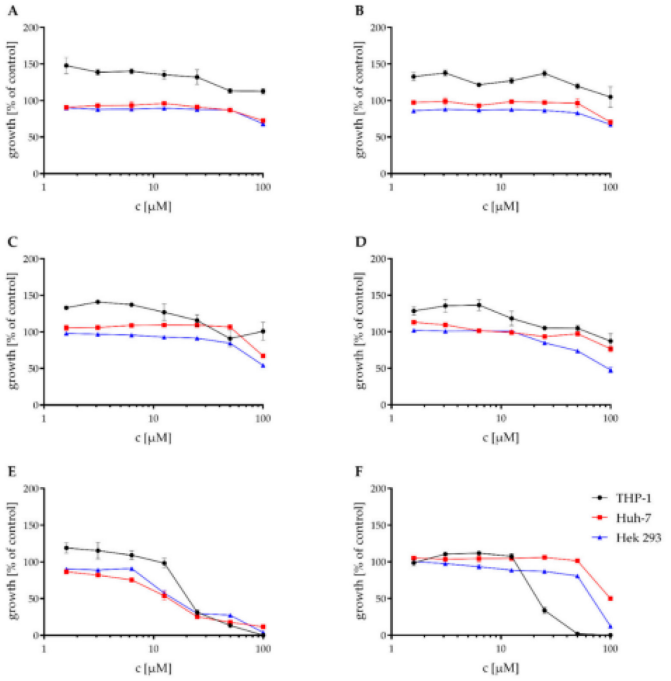

Figure 5. Effect of the natural products on the viability of THP-1, Huh-7, and HEK-293 cells. Cytotoxic effect of NK-A17e233 (**A**); 1,2-benzenediol,3-(4-hydroxy-2-methoxy-6-methylphenoxy)-5-methyl- (ACI) (**B**); cyperin (**C**); ES-242-1 (**D**); ES-242-3 (**E**); 5*S*,6*S*-phomalactone (**F**) against the human cell lines THP-1, Huh-7, and HEK-293 as determined by resazurin assay. 100% growth control DMSO, 0% growth control cycloheximide. Values represent the means of triplicates ± SEM.

Table 3. Mean IC_{50} values of compounds **A**–**F** against human cell lines THP-1, Huh-7, and Hek293. All concentrations are shown in µM. Concentration >100 µM indicates no activity in the experimental setup. All experiments were conducted in triplicate. The IC_{50} values were calculated using GraphPad Prism 7.

Compound	Mean IC_{50} [µM]		
	THP1	Huh-7	HEK-293
A	>100	>100	>100
B	>100	>100	>100
C	>100	>100	>100
D	>100	>100	93.8
E	21.9	13	16.95
F	24.3	100	66.9

2.4. Determination of Anti-Bacterial Activity

In our ongoing research for antibacterial and particularly antitubercular compounds, **A** to **H** were also tested in a minimal inhibitory concentration assay against *S. aureus* ATCC 700699, *P. aeruginosa* ATCC 87110, and *M. tuberculosis* H37Rv. Compounds **A** to **H** had no inhibitory effect on *S. aureus* ATCC 700699 and *P. aeruginosa* ATCC 87110, except for compound **F**, which showed a weak inhibitory effect on *P. aeruginosa* ATCC 87110 with an MIC_{90} of 100 µM. Compounds **A**, **B**, **C**, **F**, **G**, and **H** had no inhibitory effect on the growth of *M. tuberculosis*, and compounds **D** and **E** showed a weak inhibitory effect with an MIC_{90} of 50 and 100 µM, respectively. The results are shown in Table 4, highlighting that compounds **A** to **F** had a specific anti-toxoplasma effect and were devoid of broad, unspecific antimicrobial activity.

Table 4. MIC_{90} against *S. aureus* ATCC 700699, *P. aeruginosa* ATCC 87110, and *M. tuberculosis* H37Rv. All concentrations are shown in µM. Concentration >100 µM indicates no activity in the experimental setup. All experiments were conducted in triplicate.

Compound	MIC_{90} [µM]		
	S. aureus ATCC 700699	*P. aeruginosa* ATCC 87110	*M. tuberculosis* H37Rv
A	>100	>100	>100
B	>100	>100	>100
C	>100	>100	>100
D	>100	>100	50
E	>100	>100	100
F	>100	100	>100
G	>100	>100	>100
H	>100	>100	>100

3. Discussion

Natural products have played an important role in the history of drug discovery for infectious disease. In the quest for new anti-*T. gondii* drugs, natural products have been proven to exhibit high potential for the discovery and development of new lead compounds with strong anti-*T. gondii* activity [25,26]. In this study, we isolated eight natural products from the crude extract of the endophytic fungus *P. selaginellae*. A previous report on the inhibitory activity of one of these compounds (phomalactone, **F**) against the apicomplexan parasite *Plasmodium falciparum* with an IC_{50} of 84.32 µM [27] prompted us to test the natural products for anti-*T. gondii* activity. Interestingly, six compounds showed activity against *T. gondii* proliferation with no or low cytotoxicity in different human cell lines and no or low antibacterial activity against a gram-positive, a gram-negative, and a mycobacterial representative, revealing reasonable anti-*T. gondii* specificity and promising therapeutic windows. These results establish diphenyl ethers, bioxanthracenes, and lactones from *P. selaginellae* as potential candidates for further preclinical development of novel anti-toxoplasma therapeutics.

Some of the isolated compounds share similar structural elements, which give insights into a structure–activity relationship of the natural products against the tested *T. gondii* strain ME49. Compounds **A**, **B**, and **C** are biphenyl ether derivatives that differ either in the position of the methoxy group or in the number of substituted hydroxyl groups. The most potent of these compounds is **A** (IC_{50} = 5.75 µM), followed by **B** (IC_{50} = 19.35 µM) and **C** (IC_{50} = 27.22 µM). While **A** only differs from **B** by a switch in the position of the methoxylated hydroxyl group from position 2 to 4, it differs from **C** only by an additional hydroxyl group in position 2′, which it shares with **B**. Because of the higher potency of **A** in the toxoplasma proliferation assay compared to **B** and **C**, the position of the methoxy group in 4 and the amount and position of hydroxyl groups in 2′ and 3′ both are likely to have an influence on the antitoxoplasma activity of these derivatives. This suggestion, nevertheless, needs further experimental evidence. Furthermore, diphenyl ethers **A**, **B**, and **C** are structurally related to triclosan, a well-known broad spectrum antifungal and antibacterial agent targeting lipid synthesis [28]. It has been shown that triclosan also inhibits the growth of apicomplexans by inhibition of the enoyl reductase ENR (FabI) enzyme, the second reductive step in the type II fatty acid biosynthesis pathway. Nevertheless, due the poor solubility of triclosan, there is considerable interest in finding novel potent triclosan analogs with improved properties such as solubility, activity, and toxicity [29,30]. The mechanism of action of **A**, **B**, and **C** may be similar to that of triclosan, but further studies are necessary to explore and confirm their mode of action and cellular target. Furthermore, in vitro and in vivo pharmacokinetic characterization is needed to reveal whether any of the compounds reported here has superior properties compared to triclosan.

Compounds **D** and **E** represent bioxanthracenes belonging to the ES-242 class and share the same structure, differing only in position 4′ by the hydroxyl group that is present only in **E**. The IC_{50} values in the toxoplasma proliferation assay were 7.38 µM and 17.99 µM for **D** and **E**, respectively, suggesting a reduction in the antitoxoplasma activity if position 4′ is substituted by a hydroxyl group. The bioxanthracenes **D** and **E** were previously isolated from *Verticillium* spp. and are well-known to act as *N*-methyl-*D*-aspartate receptor antagonists [31]. Both compounds were also found to be active against the apicomplexan parasite *P. falciparum* with IC_{50} values of 8.44 and 13.22 µM, respectively [32]. Interestingly, the activities of **D** and **E** against *T. gondii* in this study were comparable to their reported activity in *P. falciparum* with IC_{50} values of 7.38 µM and 17.99 µM (see Table 1). Nevertheless, the mechanism of action of **D** and **E** on apicomplexans is still unknown and is probably independent from their activity as NMDA receptor antagonists [32].

Compounds **F** and **G** are small δ-lactonic molecules; 5*S*,6*S*-phomalactone (**F**) differs from methyltriaceticlactone (**G**) in the length of the sidechain in position 6, the hydroxyl group in position 5, and in the absence of the methyl group that is present in methyltriaceticlactone in position 2. Interestingly, antitoxoplasmal activity was observed for **F**, but not for **G**, suggesting that one or more of these structural differences and not only the presence of the δ-lactonic base structure plays a crucial role in the bioactivity against *T. gondii*. Phomalactone (**F**) is a frequent fungal metabolite and was first isolated from the plant-pathogenic fungus *Nigrospora* sp. [16]. It has a wide range of activities such as antifungal, immunomodulating, insecticide, nematocidal, and phytotoxic activity [15,19,33–35]. In addition, it has been found to be active against the apicomplexan parasite *P. falciparum*, with an IC_{50} of 84.32 µM [27]. In the present study, we tested **F** for inhibition of *T. gondii* proliferation and, interestingly, it showed a more potent activity with an IC_{50} of 5.13 µM (see Table 1). No target or mode of action has been suggested for phomalactone in *P. falciparum*, and the target of this compound in *T. gondii* also remains elusive and has to be determined in the future. Importantly, the newly identified natural products with inhibitory activity against *T. gondii* showed very little in vitro toxicity and should be evaluated in in vivo infection model systems in the future. In general, this study highlights the potential of endophytic fungi as a promising source for novel antitoxoplasma compounds.

4. Materials and Methods

4.1. General Experimental Procedures

Optical rotations were measured on a Jasco P-2000 polarimeter (Jasco, Pfungstadt, Germany). UV-spectra were obtained by the use of a Dionex P580 system in combination with a diode array detector (UVD340S) and an Eurosphere 10 C18 column (125 mm × 4 mm). ECD spectra were measured on a JASCO J-810 spectropolarimeter. VCD spectra were recorded on a BioTools Chiral-IR-2X at a resolution of 4 cm^{-1} under ambient temperature for 18 × 3000 scans. Samples were dissolved in $CDCl_3$, and the solution was placed in a 100 µm BaF_2 cell. 1D and 2D NMR spectra were recorded on a Bruker Avance III (^1H, 600 MHz; ^{13}C 150 MHz) spectrometer. Mass spectra were measured on a Finnigan LCQ Deca (Thermo Quest, Egelsbach, Germany) mass spectrometer and for HRESIMS, on a UHR-QTOF maXis 4G (Bruker Daltonics, Bremen, Germany) mass spectrometer. Semipreperative HPLC was performed on a Lachrom-Merck Hitachi system (pump L7100, UV-detector L7400, Eurospher 100 C18 column 300 mm × 8 mm, Knauer, Everswinkel, Germany). VLC and non-vacuum-column chromatography were accomplished using Macherey Nagel silica gel 60M (0.04–0.063 mm). Precoated TLC silica gel 60 F254 plates (Merck, Darmstadt, Germany) were used for tracking separation using detection under UV light at 254 and 365 nm wavelengths or spraying anisaldehyde–sulfuric acid reagent. Sephadex LH20 (GE Healthcare Bio.Sciences AB, Uppsala, Sweden) was used as a stationary phase for column chromatography. The measurement of optical rotations was accomplished by using spectral grade solvents.

4.2. Fungal Material

The fungus was obtained from the leaves of the plant *Philodendron monstera* as an endophyte. A single leaf was surface sterilized by soaking it with 70% ethanol for 30 s and letting it dry under sterile conditions. With a heat-sterilized scalpel, the leaf was cut into pieces and put onto a YPD agar plate, which was enriched with 100 mg/L chloramphenicol to suppress bacterial growth. After seven days of incubation at room temperature, distinct fungal growth was observed on the plate. A 1 cm^2 piece of the fungus was cut out of the agar medium using a heat-sterilized scalpel under sterile conditions and was transferred onto a new sterile YPD agar plate to isolate a pure organism. The isolated strain was identified as *Paraboeremia selaginella* by the internal transcribed spacer (ITS) sequence with 99.56% identity in comparison with the ITS database of the National Center for Biotechnology Information (GenBank Accession ON231784).

4.3. Fermentation and Extraction

The fungus was fermented on solid rice medium. Ten Erlenmeyer flasks were used; 100 g of rice and 100 mL of demineralized water were added to each flask and autoclaved at 121 °C for 15 min. Under sterile conditions, 1 cm^2 of fungal material was cut out of an agar plate using a sterile scalpel and transferred onto the autoclaved rice medium. The fungus was grown for 4 weeks under static conditions at room temperature. Each flask was soaked with 250 mL of ethylacetate for at least 12 h. The rice medium was then cut into small pieces and shaken for 8 h at 150 rpm. The liquid crude extract was filtrated into round flasks and evaporated using a rotary evaporator to yield 14.66 g of dry crude extract.

4.4. Isolation

The crude extract (14.66 g) obtained from the fermentation was separated using vacuum liquid chromatography with silica gel as a stationary phase. A step gradient from 100% hexane to 100% ethylacetate followed by a step gradient from 100% dichloromethane to 100% methanol gave 18 fractions (V1–V18). Two fractions (V4 and V6) were chosen based on initial bioactivity observed against *Candida albicans*. However, this bioactivity was lost during the purification process. Fraction V4 (200.7 mg) was further separated using a Sephadex LH20 column with MeOH as eluent to give five subfractions (V4-S1–S5). Fraction V4S3 (47.3 mg) was subjected to semipreparative HPLC using a MeOH-H_2O step gradient

from 50% to 80% MeOH followed by a washing step with 100% MeOH to yield **A** (20.7 mg), **B** (2.8 mg), and **C** (7.7 mg). Fraction V6 (1010 mg) was purified using a Sephadex LH20 column with CH_2Cl_2 and MeOH (50/50) as eluent to yield six subfractions (V6-S1–S6). Subfraction S2 (72.0 mg) was purified using a silica column with 40% hexane and 60% ethylacetate to elute **D** (25.0 mg) and **E** (8.6 mg) as pure compounds. Subfraction V6-S4 (516 mg) was further purified by using a Sephadex LH20 column with MeOH as eluent to yield five subfractions (V6S4-S1–S5). Subfraction V6S4S2 (496 mg) was subjected to a silica column with a mixture of CH_2Cl_2 and MeOH (95/5) as eluent to give four subfractions (V6S4S2-K1–K4). Silica subfraction V6S4S2K2 (47 mg) was then purified by semipreparative HPLC using a MeOH-H_2O step gradient from 10% to 30% MeOH followed by a washing step with 100% MeOH to yield **F** (22.2 mg) and **G** (4.5 mg). Fraction V12 (744.1 mg) was separated using a Sephadex LH20 column with 50% MeOH and 50% CH_2Cl_2 to yield six subfractions (V12-S1–S6). Subfraction S2 (180.3 mg) was then further separated using a silica column with 10% MeOH and 90% CH_2Cl_2 as eluent to give seven subfractions (V12S2-K1–K7). Silica subfraction K7 (56.1 mg) was subjected to semipreparative HPLC using a step gradient from 70% to 100% MeOH to yield **H** (5.0 mg).

NK-A 17e233 (A): Brown oil; UV (MeOH) λ_{max} 220.0, 234.3, 279.7 nm; ^{1}H NMR (DMSO-d6) see Supplementary Materials Figure S1; HRESIMS *m/z* 277.1075 $[M + H]^+$ (calcd. for $C_{15}H_{17}O_5$ 277.1071 *m/z*).

3-(4-Hydroxy-2-methoxy-6-methylphenoxy)-5-methylbenzene-1,2-diol (B): Brown oil; UV (MeOH) λ_{max} 211.7, 286.3 nm; ^{1}H NMR ($CDCl_3$), see Supplementary Materials Figure S6; HRESIMS *m/z* 277.1065 $[M + H]^+$ (calcd. for $C_{15}H_{17}O_5$ 277.1071 *m/z*).

Cyperin (C): Brown oil; UV (MeOH) λ_{max} 212.1, 279.8 nm; ^{1}H NMR ($CDCl_3$), see Supplementary Materials Figure S10; HRESIMS *m/z* 261.1126 $[M + H]^+$ (calcd. for $C_{15}H_{17}O_4$ 261.1121 *m/z*).

ES-242-1 (D): Brown amorphous powder; $[\alpha]^{24}_D$ *+18* (c 1.0, MeOH); UV (MeOH) λ_{max} 239.0, 309.8, 345.8 nm; ^{1}H NMR ($CDCl_3$) and ^{13}C NMR ($CDCl_3$), see Supplementary Materials Figures S14 and S15; HRESIMS *m/z* 622.2644 $[M + NH_4]^+$ (calcd. for $C_{34}H_{40}NO_{10}$ 622.2647 *m/z*).

ES-242-3 (E): Brown amorphous powder; $[\alpha]^{24}_D$ *+66* (c 1.0, $CHCl_3$); UV (MeOH) λ_{max} 239.2, 298.6, 309.4 nm; ^{1}H NMR ($CDCl_3$) and ^{13}C NMR ($CDCl_3$), see Supplementary Materials Figures S19 and S20; HRESIMS *m/z* 638.2588 $[M + NH_4]^+$ (calcd. for $C_{34}H_{40}NO_{11}$ 638.2596 *m/z*).

Phomalactone (F): light yellowish oil; $[\alpha]^{24}_D$ *+172* (c 1.0, EtOH); UV (MeOH) λ_{max} 216.0 nm; For the details of VCD, ECD, and OR calculations, see Supplementary Materials; ^{1}H NMR ($CDCl_3$) and ^{13}C NMR ($CDCl_3$), see Supplementary Materials Figures S24 and S25; HRESIMS *m/z* 155.0702 $[M + H]^+$ (calcd. for $C_8H_{11}O_3$ 155.0703 *m/z*) and *m/z* 137.0597 $[M - OH^-]^+$ (calcd. for $C_8H_9O_2$ 137.0597 *m/z*).

Methyltriaceticlactone (G): White amorphous powder; UV (MeOH) λ_{max} 290.5 nm; ^{1}H NMR (DMSO-d6) and ^{13}C NMR (DMSO-d6), see Supplementary Materials Figures S29 and S30; HRESIMS *m/z* 141.0549 $[M + H]^+$ (calcd. for $C_7H_9O_3$ 141.0546 *m/z*).

S 39163/F-1 (H): Brown amorphous gum; $[\alpha]^{24}_D$ *−11* (c 1.0, MeOH); UV (MeOH) λ_{max} 218.2, 238.8, 291.9 nm; ^{1}H NMR ($CDCl_3$), see Supplementary Materials Figure S34; HRESIMS *m/z* 661.4312 $[M + H]^+$ (calcd. for $C_{38}H_{61}O_9$ 661.4310 *m/z*).

4.5. Preparation of Compounds for T. gondii Proliferation Assay

The purified natural products **A**–**F** and pyrimethamine [36] were dissolved in DMSO as 10 mM stocks and stored at −20 °C. The compounds were diluted in Iscove's Modified Dulbecco's medium (Gibco–Thermo Fisher Scientific, Braunschweig, Germany) immediately prior to use.

4.6. Parasites and Cell Culture for T. gondii Proliferation Assay

T. gondii ME49 tachyzoites (ATCC/LGC Standards GmbH, Wesel, Germany) were cultured in human foreskin fibroblast Hs27 cells (ATCC/LGC Standards GmbH, Wesel, Germany)

as host cells as described previously [37]. The cells were maintained in Iscove's modified Dulbecco's medium (Gibco–Thermo Fisher Scientific, Braunschweig, Germany) supplemented with 10% heat-inactivated fetal bovine serum (Invitrogen, Karlsruhe, Germany) and 50 mM 2-mercaptoethanol (Gibco–Thermo Fisher Scientific, Braunschweig, Germany) and were grown in a humidified incubator at 37 °C with 5% CO_2 in air atmosphere. For toxoplasma propagation, 25 cm^2 cell culture flasks, containing a confluent monolayer of Hs27 cells, were infected with 5×10^6 *T. gondii* tachyzoites after medium change. After three days, the supernatant of the cell culture containing parasites was harvested and transferred to a 15 mL centrifuge tube and centrifuged at 700 rpm for five minutes and resuspended in cell culture medium. The number of parasites was counted using a hemocytometer.

4.7. T. gondii Proliferation Assay

Microtiter plates (96-well) with a final volume of 200 µL per well were used for the assay. Hs27 fibroblast monolayers were infected with 3×10^4 freshly harvested tachyzoites per well (MOI = 1) and incubated for 48 h at 37 °C, after which various concentrations of the tested compounds (0.04, 0.09, 0.19, 0.39, 0.78, 1.5, 3.12, 6.25, 12.5, 25, 50 µM) in culture medium were added to the cells. Pyrimethamine (0.007, 0.01, 0.03, 0.06, 0.125, 0.25, 0.5, 1 µM) was added under identical conditions as a positive drug control [37]. Hs27 cells were pre-stimulated for 24 h with IFNγ (300 U/mL) and infected with *T. gondii* cells without further treatment as the growth inhibition control. After 48 h, proliferating toxoplasma parasites were radioactively labelled with tritiated uracil (5 mCi, Hartmann Analytic, Braunschweig, Germany) and diluted 1:30 (10 µL per 200 µL total culture volume per well) in order to determine parasite proliferation [38]. After 28–30 h, the microtiter plates were frozen at −20 °C. To evaluate the assay, the microtiter plates were thawed at room temperature. Cells were transferred to glass-fiber filters (Printed Filtermat A 102 mm × 258 mm, PerkinElmer, Waltham, MA, USA) using a cell harvester (Basic96 Harvester, Zinsser Analytic, Skatron Instruments, Northridge, CA, USA). The filters were dried for 20 min at 130 °C in a drying cabinet and were then soaked in 10 mL of scintillation fluid (Betaplate Scint, PerkinElmer, Waltham, MA, USA) and shrink-wrapped in plastic covers (Sample Bag for Betaplate, PerkinElmer, Waltham, MA, USA). The filters were then clamped in cassettes and evaluated using a beta-counter device (Betaplate Liquid Scintillation Counter 1205, LKB-WALLAK, Melbourne, Australia) to measure the Cherenkov radiation, which refers to the amount of incorporation of tritiated uracil into the RNA of *T. gondii*. IC_{50} values, the concentration of inhibitors necessary to inhibit the growth of tachyzoites by 50%, were determined for each experiment with the use of Prism GraphPad version 9.2.0 software.

4.8. Cell Viability Assay against Hs27 Cells

The 3-[4,5-dimethylthiazole-2-yl]-2,5-diphenyltetrazolium bromide (MTT) test was used to assess cell viability of the isolated active compounds against Hs27 cells. The MTT assay is a colorimetric reaction based on the enzymatic reduction of MTT to MTT-formazan, which is catalyzed by mitochondrial succinate dehydrogenase [39].

In brief, Hs27 cells were seeded 96-well plates in a monolayer in Iscove's modified Dulbecco's medium (Gibco–Thermo Fisher Scientific, Braunschweig, Germany) and incubated at 37 °C with different concentrations of the tested natural products (1.56, 3,12, 6.25, 12,5, 25, 50, 100 µM) in the culture media. Staurosporine (0.007, 0.01, 0.03, 0.06, 1.25, 0.25, 0.5, 1 µM), a well-known cytotoxicity-inducing kinase inhibitor [40], untreated Hs27 cells, and DMSO were used as controls. After 24 h, the medium of the culture was removed and replaced with 100 µL of DMEM without red phenol (Gibco–Thermo Fisher Scientific, Braunschweig, Germany) plus 10% heat-inactivated fetal bovine serum (Invitrogen, Karlsruhe, Germany), and 50 mM 2-mercaptoethanol (Gibco–Thermo Fisher Scientific, Braunschweig, Germany). Afterwards, the 12 mM MTT solution was added to each well according to the manufacturer's instruction (Vybrant MTT Cell Proliferation Assay Kit, Thermo Fisher Scientific, Braunschweig, Germany). The OD value of each well was assayed at the wavelength of 570 nm on a microplate reader (TECAN Sunrise, Männedorf, Switzerland). The 50%

cytotoxic concentration (CC_{50} values) of the tested natural products on Hs27 cells was calculated and all data were analyzed using Prism GraphPad version 9.2.0 software.

4.9. Determination of the Minimal Inhibitory Concentration against Different Pathogenic Bacteria

Testing for antibacterial activity was done as described previously [37]. Briefly, a single colony of Methicillin-resistant *Staphylococcus aureus* (MRSA strain Mu50, ATCC 700699) or *Pseudomonas aeruginosa* (strain PAO1, ATCC 87110) were grown in Mueller-Hinton broth (MHB) at 37 °C shaking at 120 rpm to reach an optical density of approx. 0.4. The cell suspension was adjusted to 10^6 CFU/mL, of which 50 µL was seeded into a prepared 96-well polystyrene round-bottom plate containing test compounds diluted in MHB in a 1:1 serial dilution ranging from 100 µM to 0.78 µM. The plates were incubated at 37 °C statically for 24 h, and readout was performed using the BacTiter Glo assay (Promega) following the manufacturer's instructions. Briefly, BacTiter Glo reagent was added to a white flat-bottom 96-well plate, and an equal volume of bacteria suspension was added to each well and mixed carefully. After 5 min, the luminescence was measured using a TECAN plate reader. The growth was calculated in regard to the vehicle (DMSO) and sterile control. Moxifloxacin and cefuroxime were used as a positive and negative control, respectively. All compounds were tested in triplicate.

For the testing against *M. tuberculosis* H37Rv, the Minimal Inhibitory Concentration (MIC) was determined in 96-well microtiter plates containing a total volume of 100 µL employing a resazurin reduction assay [41]. Briefly, a 96-well plate was prepared containing 7H9 medium supplemented with 10% ADS (0.81% NaCl, 5% BSA, 2% dextrose), 0.5% glycerol, and 0.05% tyloxapol. Compounds were two-fold serially diluted with the highest tested concentration of 100 µM. A *M. tuberculosis* culture was pre-grown to an $OD_{600\,nm}$ of approx. 0.4–0.6 by shaking at 37 °C in PETG square bottles (ThermoFisher Scientific, Braunschweig, Germany) containing 10 mL supplemented 7H9 medium. The cell density was adjusted to an $OD_{600\,nm}$ of 0.08 (10^6 CFU/mL, and 5×10^4 CFU were added to each well). Rifampicin and DMSO were used as a positive and solvent control, respectively. The 96-well plates were incubated for 5 days at 37 °C and 5% CO_2 in humidified atmosphere. Afterwards, 10 µL of a 100 mg/mL resazurin solution was added to each well and resuspended carefully. After another 24 h at room temperature, the cells were fixed by adding 100 µL of a 10% formalin solution to each well. The readout was performed using a TECAN plate reader at 535 nm excitation and 590 nm emission. The growth was calculated in relation to the solvent control being 100% growth. The experiment was performed in triplicate.

4.10. Cytotoxicity Assay against Different Human Cell Lines

The cytotoxicity study was carried out using the THP-1 (human monocytic leukemia cell line), Huh-7 (Human liver carcinoma cell line), and HEK293 (human embryonic kidney cell line) cell lines as described before [37]. The THP-1 cells were cultured using RPMI 1640 medium containing 2 mM L-glutamine and supplemented with 10% fetal calf serum (FCS) and 1% sodium pyruvate. Huh-7 cells were cultured using a 1:1 mixture of RPMI 1640 medium containing 2 mM L-glutamine and 10% FCS medium and DMEM containing 10% FCS and 1% sodium pyruvate. The HEK-293 cells were cultured with DMEM including 2 mM L-glutamine and supplemented with 1% NE amino acids, 1% 1.0 mM sodium pyruvate and 10% FCS. All three cell lines were then incubated at 37 °C in an atmosphere of 5% CO_2 under humid conditions for 2 weeks while renewing the medium twice weekly. Subsequently, the cells were suspended and adjusted to a density of 2×10^5 cells/mL. In a 96-well flat-bottom microtiter plate, the cells were adjusted to a total volume of 100 µL containing 2-fold serial dilutions of the tested compounds **A**–**F** ranging from 100 to 1.56 µM. Cycloheximide (4, 2, 1, 0.5, 0.25, 0.13, 0.06, 0.03 µg/mL) was used as a positive control. After an incubation time of 48 h at 37 °C in an atmosphere of 5% CO_2 under humid conditions, 10 µL resazurin solution (100 µg/mL) was added to each well and incubated for another 4 h. The fluorescence was then quantified using a Tecan Infinite 200pro microplate reader

(excitation 540 nm, emission 590 nm). The residual growth was calculated relative to non-inoculated conditions (0% growth) and controls treated with DMSO (100% growth).

Supplementary Materials: The following supporting information can be downloaded at: https://www.mdpi.com/article/10.3390/antibiotics11091176/s1, Figures S1–S58: Spectroscopic data used for the structure elucidation of compounds A–H; Figure S59: Comparison of the experimental ECD spectrum of F measured in MeCN and the calculated ECD spectra of (5S,6S)-F computed at various levels of theory for the 10 lowest-energy ωB97X/TZVP PCM/MeCN conformers; Figure S60: Geometries of the low-energy ωB97X/TZVP PCM/MeCN conformers of (5S,6S)-F; Figure S61: Geometries of the low-energy B3LYP/TZVP PCM/CHCl3 conformers of (5S,6S)-F; Table S1: Boltzmann populations and specific optical rotations of the low-energy conformers of (5S,6S)-F computed at various levels for the low-energy ωB97X conformers. References [42–45] are cited in Supplementary Materials.

Author Contributions: Conceptualization, R.K. and K.P.; methodology, F.M., V.E.S., T.K., R.K. and K.P.; investigation, F.M., V.E.S., L.v.G. and A.M.; data curation, F.M., V.E.S., M.F., T.K., R.K. and K.P.; writing—original draft preparation, F.M. and V.E.S.; writing—review and editing, funding acquisition, T.K., R.K. and K.P. All authors have read and agreed to the published version of the manuscript.

Funding: This work was supported by the Deutsche Forschungsgemeinschaft (DFG, German Research Foundation)–project number 270650915/GRK 2158 (to RK and KP). T.K. and A.M. were supported by the National Research, Development and Innovation Office (K138672 and FK134653).

Institutional Review Board Statement: Not applicable.

Informed Consent Statement: Not applicable.

Data Availability Statement: All data presented in this study are contained within the article and the supplementary materials. The internal transcribed spacer (ITS) sequence for *Paraboeremia selaginellae* has been deposited in the National Center for Biotechnology Information (NCBI) GenBank under accession number ON231784.

Acknowledgments: We thank the CeMSA@HHU (Center for Molecular and Structural Analytics@Heinrich Heine University) for recording the mass-spectrometric and the NMR-spectroscopic data. We thank Heike Goldbach-Gecke for testing and measuring the cytotoxic effect of the isolated compounds against the tested human cell lines. The Governmental Information-Technology Development Agency (KIFÜ) is acknowledged for CPU time. We thank Karin Buchholz for expert technical assistance and Daniel Degrandi as well as Ursula Sorg for scientific advice and discussions.

Conflicts of Interest: The authors declare no conflict of interest. The funders had no role in the design of the study; in the collection, analyses, or interpretation of data; in the writing of the manuscript, or in the decision to publish the results.

References

1. Frolich, S.; Entzeroth, R.; Wallach, M. Comparison of protective immune responses to apicomplexan parasites. *J. Parasitol. Res.* **2012**, *2012*, 852591. [CrossRef] [PubMed]
2. Kim, K.; Weiss, L.M. Toxoplasma gondii: The model apicomplexan. *Int. J. Parasitol.* **2004**, *34*, 423–432. [CrossRef] [PubMed]
3. Toxoplasmosis of Animals and Man. By J.P. Dubey and C. P. Beattie. 220 pages. ISBN 0 8493 4618 5. CRC Press, Boca Raton, 1988. £108.00. *Parasitology* **2009**, *100*, 500–501. [CrossRef]
4. Dubey, J.P. *Toxoplasmosis of Animals and Humans*; CRC Press: Boca Raton, FL, USA, 2016.
5. Saadatnia, G.; Golkar, M. A review on human toxoplasmosis. *Scand. J. Infect. Dis.* **2012**, *44*, 805–814. [CrossRef] [PubMed]
6. Dubey, J.P. Outbreaks of clinical toxoplasmosis in humans: Five decades of personal experience, perspectives and lessons learned. *Parasites Vectors* **2021**, *14*, 263. [CrossRef] [PubMed]
7. Furtado, J.M.; Smith, J.R.; Belfort, R., Jr.; Gattey, D.; Winthrop, K.L. Toxoplasmosis: A global threat. *J. Glob. Infect. Dis.* **2011**, *3*, 281–284. [CrossRef]
8. de Jong, P.T. Ocular toxoplasmosis; common and rare symptoms and signs. *Int. Ophthalmol.* **1989**, *13*, 391–397. [CrossRef]
9. Elbez-Rubinstein, A.; Ajzenberg, D.; Dardé, M.L.; Cohen, R.; Dumètre, A.; Yera, H.; Gondon, E.; Janaud, J.C.; Thulliez, P. Congenital toxoplasmosis and reinfection during pregnancy: Case report, strain characterization, experimental model of reinfection, and review. *J. Infect. Dis.* **2009**, *199*, 280–285. [CrossRef]
10. Dunay, I.R.; Gajurel, K.; Dhakal, R.; Liesenfeld, O.; Montoya, J.G. Treatment of Toxoplasmosis: Historical Perspective, Animal Models, and Current Clinical Practice. *Clin. Microbiol. Rev.* **2018**, *31*, e00057-17. [CrossRef]

11. Gopalakrishnan, A.M.; López-Estraño, C. Comparative analysis of stage specific gene regulation of apicomplexan parasites: Plasmodium falciparum and Toxoplasma gondii. *Infect. Disord. Drug Targets* **2010**, *10*, 303–311. [CrossRef]
12. Newman, D.J.; Cragg, G.M. Natural Products as Sources of New Drugs over the Nearly Four Decades from 01/1981 to 09/2019. *J. Nat. Prod.* **2020**, *83*, 770–803. [CrossRef] [PubMed]
13. Cheraghipour, K.; Masoori, L.; Ezzatpour, B.; Roozbehani, M.; Sheikhian, A.; Malekara, V.; Niazi, M.; Mardanshah, O.; Moradpour, K.; Mahmoudvand, H. The Experimental Role of Medicinal Plants in Treatment of Toxoplasma gondii Infection: A Systematic Review. *Acta Parasitol.* **2021**, *66*, 303–328. [CrossRef] [PubMed]
14. Lenzi, J.; Costa, T.M.; Alberton, M.D.; Goulart, J.A.G.; Tavares, L.B.B. Medicinal fungi: A source of antiparasitic secondary metabolites. *Appl. Microbiol. Biotechnol.* **2018**, *102*, 5791–5810. [CrossRef] [PubMed]
15. Fukushima, T.; Tanaka, M.; Gohbara, M.; Fujimori, T. Phytotoxicity of three lactones from Nigrospora sacchari. *Phytochemistry* **1998**, *48*, 625–630. [CrossRef]
16. Evans, R.H.; Ellestad, G.A.; Kunstmann, M.P. Two new metabolites from an unidentified nigrospora species. *Tetrahedron Lett.* **1969**, *10*, 1791–1794. [CrossRef]
17. Gusmao, A.S.; Abreu, L.S.; Tavares, J.F.; de Freitas, H.F.; Silva da Rocha Pita, S.; Dos Santos, E.G.; Caldas, I.S.; Vieira, A.A.; Silva, E.O. Computer-Guided Trypanocidal Activity of Natural Lactones Produced by Endophytic Fungus of Euphorbia umbellata. *Chem. Biodivers* **2021**, *18*, e2100493. [CrossRef]
18. Hussain, H.; Kock, I.; Al-Harrasi, A.; Al-Rawahi, A.; Abbas, G.; Green, I.R.; Shah, A.; Badshah, A.; Saleem, M.; Draeger, S.; et al. Antimicrobial chemical constituents from endophytic fungus Phoma sp. *Asian Pac. J. Trop. Med.* **2014**, *7*, 699–702. [CrossRef]
19. Khambay, B.P.S.; Bourne, J.M.; Cameron, S.; Kerry, B.R.; Zaki, M.J. A nematicidal metabolite from Verticillium chlamydosporium. *Pest Manag. Sci. Former. Pestic. Sci.* **2000**, *56*, 1098–1099. [CrossRef]
20. Meepagala, K.M.; Johnson, R.D.; Techen, N.; Wedge, D.E.; Duke, S.O. Phomalactone from a Phytopathogenic Fungus Infecting ZINNIA elegans (ASTERACEAE) Leaves. *J. Chem. Ecol.* **2015**, *41*, 602–612. [CrossRef]
21. Trisuwan, K.; Rukachaisirikul, V.; Sukpondma, Y.; Preedanon, S.; Phongpaichit, S.; Sakayaroj, J. Pyrone derivatives from the marine-derived fungus *Nigrospora* sp. PSU-F18. *Phytochemistry* **2009**, *70*, 554–557. [CrossRef]
22. Wu, S.H.; Chen, Y.W.; Shao, S.C.; Wang, L.D.; Yu, Y.; Li, Z.Y.; Yang, L.Y.; Li, S.L.; Huang, R. Two new solanapyrone analogues from the endophytic fungus *Nigrospora* sp. YB-141 of Azadirachta indica. *Chem. Biodivers* **2009**, *6*, 79–85. [CrossRef] [PubMed]
23. Mandi, A.; Kurtan, T. Applications of OR/ECD/VCD to the structure elucidation of natural products. *Nat. Prod. Rep.* **2019**, *36*, 889–918. [CrossRef] [PubMed]
24. Szabo, Z.; Paczal, A.; Kovacs, T.; Mandi, A.; Kotschy, A.; Kurtan, T. Synthesis and Vibrational Circular Dichroism Analysis of N-Heterocyclic Carbene Precursors Containing Remote Chirality Centers. *Int. J. Mol. Sci* **2022**, *23*, 3471. [CrossRef]
25. Atanasov, A.G.; Zotchev, S.B.; Dirsch, V.M.; Orhan, I.E.; Banach, M.; Rollinger, J.M.; Barreca, D.; Weckwerth, W.; Bauer, R.; Bayer, E.A.; et al. Natural products in drug discovery: Advances and opportunities. *Nat. Rev. Drug Discov.* **2021**, *20*, 200–216. [CrossRef] [PubMed]
26. Guo, H.-Y.; Jin, C.; Zhang, H.-M.; Jin, C.-M.; Shen, Q.-K.; Quan, Z.-S. Synthesis and Biological Evaluation of (+)-Usnic Acid Derivatives as Potential Anti-Toxoplasma gondii Agents. *J. Agric. Food Chem.* **2019**, *67*, 9630–9642. [CrossRef] [PubMed]
27. Jiménez-Romero, C.; Ortega-Barría, E.; Arnold, A.E.; Cubilla-Rios, L. Activity against *Plasmodium falciparum* of Lactones Isolated from the Endophytic Fungus *Xylaria* sp. *Pharm. Biol.* **2008**, *46*, 700–703. [CrossRef]
28. McMurry, L.M.; Oethinger, M.; Levy, S.B. Triclosan targets lipid synthesis. *Nature* **1998**, *394*, 531–532. [CrossRef]
29. McLeod, R.; Muench, S.P.; Rafferty, J.B.; Kyle, D.E.; Mui, E.J.; Kirisits, M.J.; Mack, D.G.; Roberts, C.W.; Samuel, B.U.; Lyons, R.E.; et al. Triclosan inhibits the growth of Plasmodium falciparum and Toxoplasma gondii by inhibition of apicomplexan Fab I. *Int. J. Parasitol.* **2001**, *31*, 109–113. [CrossRef]
30. Tipparaju, S.K.; Muench, S.P.; Mui, E.J.; Ruzheinikov, S.N.; Lu, J.Z.; Hutson, S.L.; Kirisits, M.J.; Prigge, S.T.; Roberts, C.W.; Henriquez, F.L.; et al. Identification and development of novel inhibitors of Toxoplasma gondii enoyl reductase. *J. Med. Chem.* **2010**, *53*, 6287–6300. [CrossRef]
31. Toki, S.; Ando, K.; Kawamoto, I.; Sano, H.; Yoshida, M.; Matsuda, Y. ES-242-2, -3, -4, -5, -6, -7, and -8, novel bioxanthracenes produced by *Verticillium* sp., which act on the N-methyl-D-aspartate receptor. *J. Antibiot.* **1992**, *45*, 1047–1054. [CrossRef]
32. Jaturapat, A.; Isaka, M.; Hywel-Jones, N.L.; Lertwerawat, Y.; Kamchonwongpaisan, S.; Kirtikara, K.; Tanticharoen, M.; Thebtaranonth, Y. Bioxanthracenes from the insect pathogenic fungus. Cordyceps pseudomilitaris BCC 1620. I. Taxonomy, fermentation, isolation and antimalarial activity. *J. Antibiot.* **2001**, *54*, 29–35. [CrossRef] [PubMed]
33. Komai, S.-I.; Hosoe, T.; Nozawa, K.; Okada, K.; de Campos Takaki, G.M.; Fukushima, K.; Miyaji, M.; Horie, Y.; Kawai, K.-I. Antifungal activity of pyranone and furanone derivatives, isolated from *Aspergillus* sp. IFM51759, against *Aspergillus fumigatus*. *MYCOTOXINS-TOKYO-* **2003**, *53*, 11–18. [CrossRef]
34. Krasnoff, S.B.; Gupta, S. Identification of the antibiotic phomalactone from the entomopathogenic fungusHirsutella thompsonii var. synnematosa. *J. Chem. Ecol.* **1994**, *20*, 293–302. [CrossRef] [PubMed]
35. Krivobok, S.; Thomasson, F.; Seigle-Murandi, F.; Steiman, R.; Bottex-Gauthier, C. 6-Allyl-5, 6-dihydro-5-hydroxypyran-2-one, a lactone produced by a new Drechslera species: Specified 1H and 13C NMR assignments, mutagenic and immunomodulating testings. *Die Pharm.* **1994**, *49*, 605–607.

36. Kumarihamy, M.; Ferreira, D.; Croom, E.M., Jr.; Sahu, R.; Tekwani, B.L.; Duke, S.O.; Khan, S.; Techen, N.; Nanayakkara, N.P.D. Antiplasmodial and Cytotoxic Cytochalasins from an Endophytic Fungus, *Nemania* sp. UM10M, Isolated from a Diseased *Torreya taxifolia* Leaf. *Molecules* **2019**, *24*, 777. [CrossRef]
37. Meier, D.; Hernandez, M.V.; van Geelen, L.; Muharini, R.; Proksch, P.; Bandow, J.E.; Kalscheuer, R. The plant-derived chalcone Xanthoangelol targets the membrane of Gram-positive bacteria. *Bioorg Med. Chem.* **2019**, *27*, 115151. [CrossRef]
38. Pfefferkorn, E.R.; Pfefferkorn, L.C. Specific Labeling of Intracellular Toxoplasma gondii with Uracil. *J. Protozool.* **1977**, *24*, 449–453. [CrossRef]
39. Mosmann, T. Rapid colorimetric assay for cellular growth and survival: Application to proliferation and cytotoxicity assays. *J. Immunol. Methods* **1983**, *65*, 55–63. [CrossRef]
40. Tamaoki, T.; Nomoto, H.; Takahashi, I.; Kato, Y.; Morimoto, M.; Tomita, F. Staurosporine, a potent inhibitor of phospholipid/Ca++dependent protein kinase. *Biochem. Biophys. Res. Commun.* **1986**, *135*, 397–402. [CrossRef]
41. Rehberg, N.; Akone, H.S.; Ioerger, T.R.; Erlenkamp, G.; Daletos, G.; Gohlke, H.; Proksch, P.; Kalscheuer, R. Chlorflavonin Targets Acetohydroxyacid Synthase Catalytic Subunit IlvB1 for Synergistic Killing of *Mycobacterium tuberculosis*. *ACS Infect. Dis.* **2018**, *4*, 123–134. [CrossRef]
42. MacroModel; Schrödinger LLC. 2015. Available online: http://www.schrodinger.com/MacroModel (accessed on 31 July 2022).
43. Frisch, M.J.; Trucks, G.W.; Schlegel, H.B.; Scuseria, G.E.; Robb, M.A.; Cheeseman, J.R.; Scalmani, V.; Barone, G.; Mennucci, B.; Petersson, G.A.; et al. *Gaussian 09 (Revision E.01)*; Gaussian, Inc.: Wallingford, CT, USA, 2013.
44. Stephens, P.J.; Harada, N. ECD cotton effect approximated by the Gaussian curve and other methods. *Chirality* **2009**, *22*, 229–233. [CrossRef] [PubMed]
45. Varetto, U. *Molekel 5.4*; Swiss National Supercomputing Centre: Manno, Switzerland, 2009.

Supplementarty Material.

In Vitro Biological Activity of Natural Products from the Endophytic Fungus *Paraboeremia selaginellae* against *Toxoplasma gondii*

Flaminia Mazzone [1,#], Viktor E. Simons [2,#], Lasse van Geelen [2], Marian Frank [2], Attila Mándi [3], Tibor Kurtán [3], Klaus Pfeffer [1,*] and Rainer Kalscheuer [2,*]

[1] Institute of Medical Microbiology and Hospital Hygiene; Heinrich Heine University, Duesseldorf, Germany; Flaminia.Mazzone@med.uni-duesseldorf.de (F.M.); klaus.pfeffer@hhu.de (K.P.)

[2] Institute of Pharmaceutical Biology and Biotechnology, Heinrich Heine University, Duesseldorf, Germany; viktor.simons@hhu.de (V.E.S.); marian.frank@hhu.de (M.F.); lasse.geelen@hhu.de (L.v.G.); rainer.kalscheuer@hhu.de (R.K.)

[3] Department of Organic Chemistry, University of Debrecen, P.O. Box 400, 4002 Debrecen, Hungary; mandi.attila@science.unideb.hu (A.M.); kurtan.tibor@science.unideb.hu (T.K.)

# F.M. and V.E.S. contributed equally

*Correspondence: rainer.kalscheuer@hhu.de; Tel.: +49 211 8114180 (RK),; klaus.pfeffer@hhu.de; Tel.: +49 211 8112459 (KP)

Table of Contents

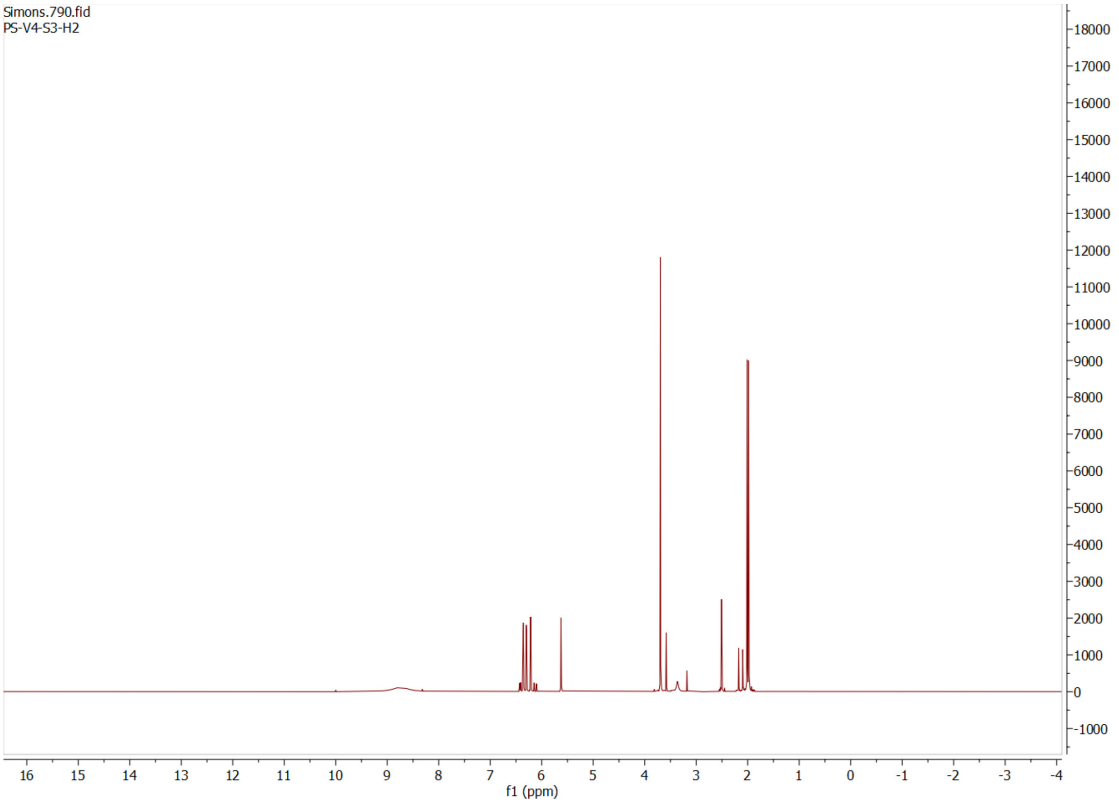

S1. ^{1}H-NMR spectrum (DMSO-d6 – 600 MHz) of Compound A

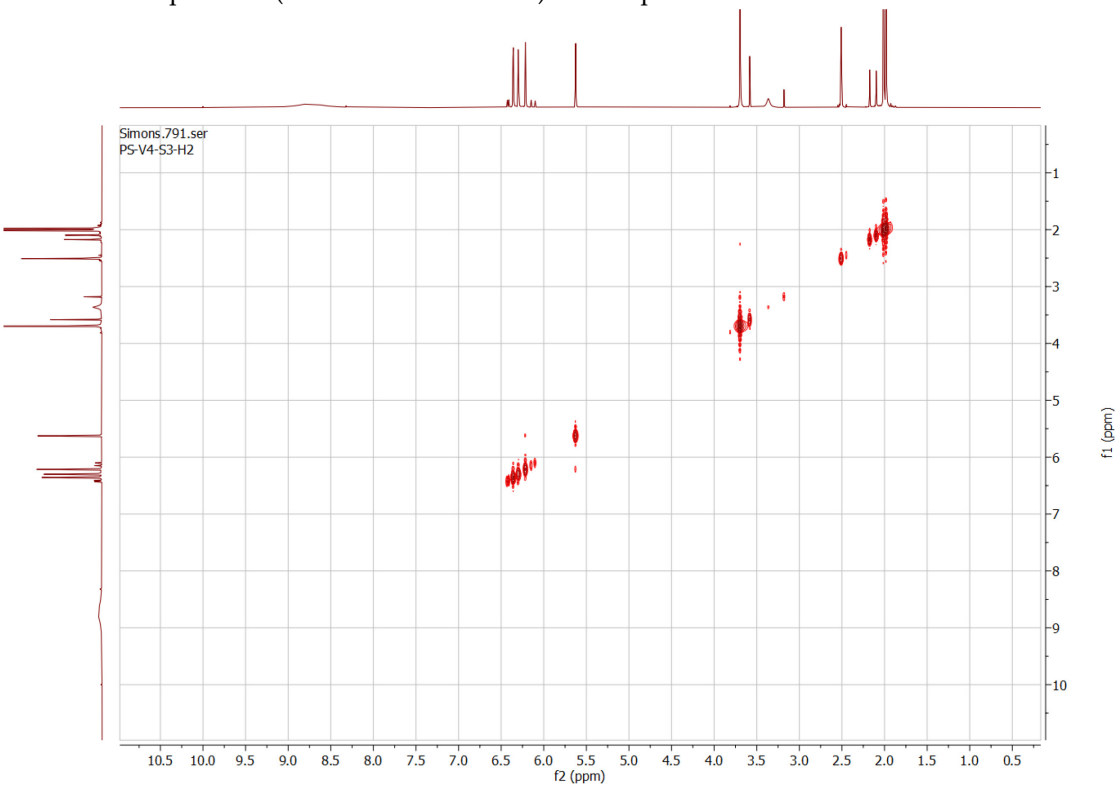

S2. COSY NMR spectrum (DMSO-d6 – 600 MHz) of compound A

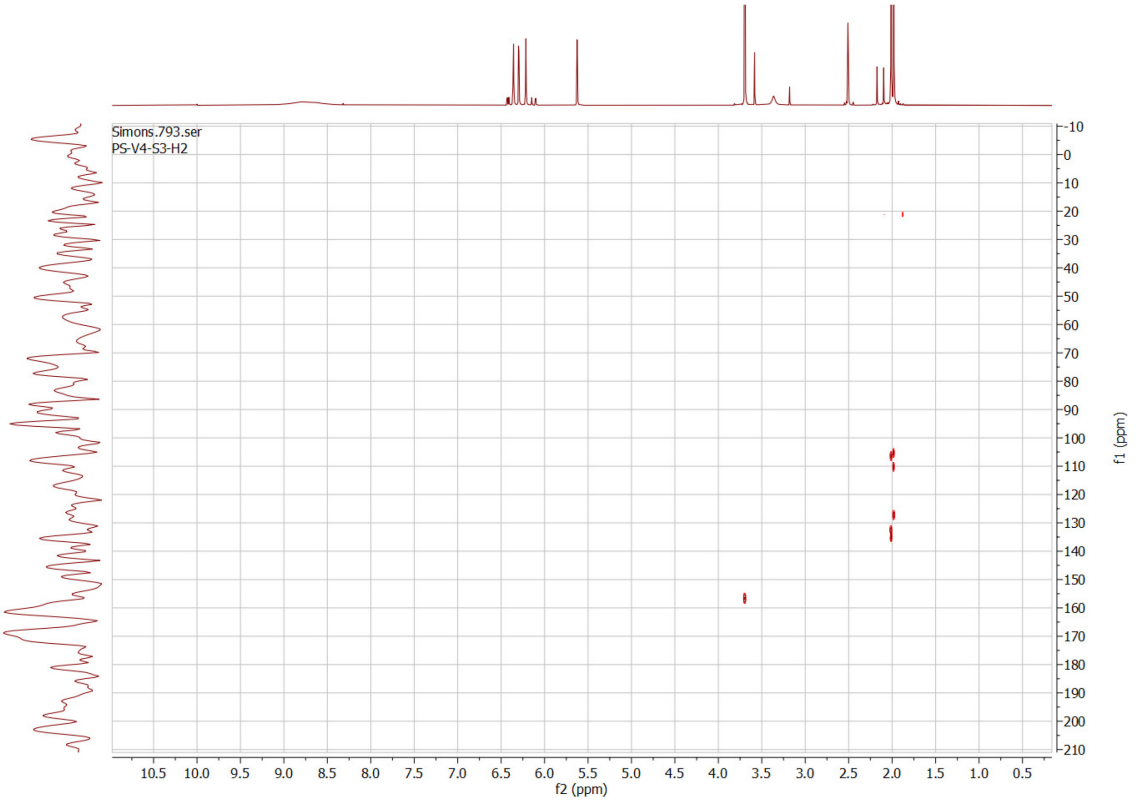

S3. HMBC NMR spectrum (DMSO-d6 – 600 MHz) of compound A

S4. HSQC NMR spectrum (DMSO-d6 – 600 MHz) of compound A

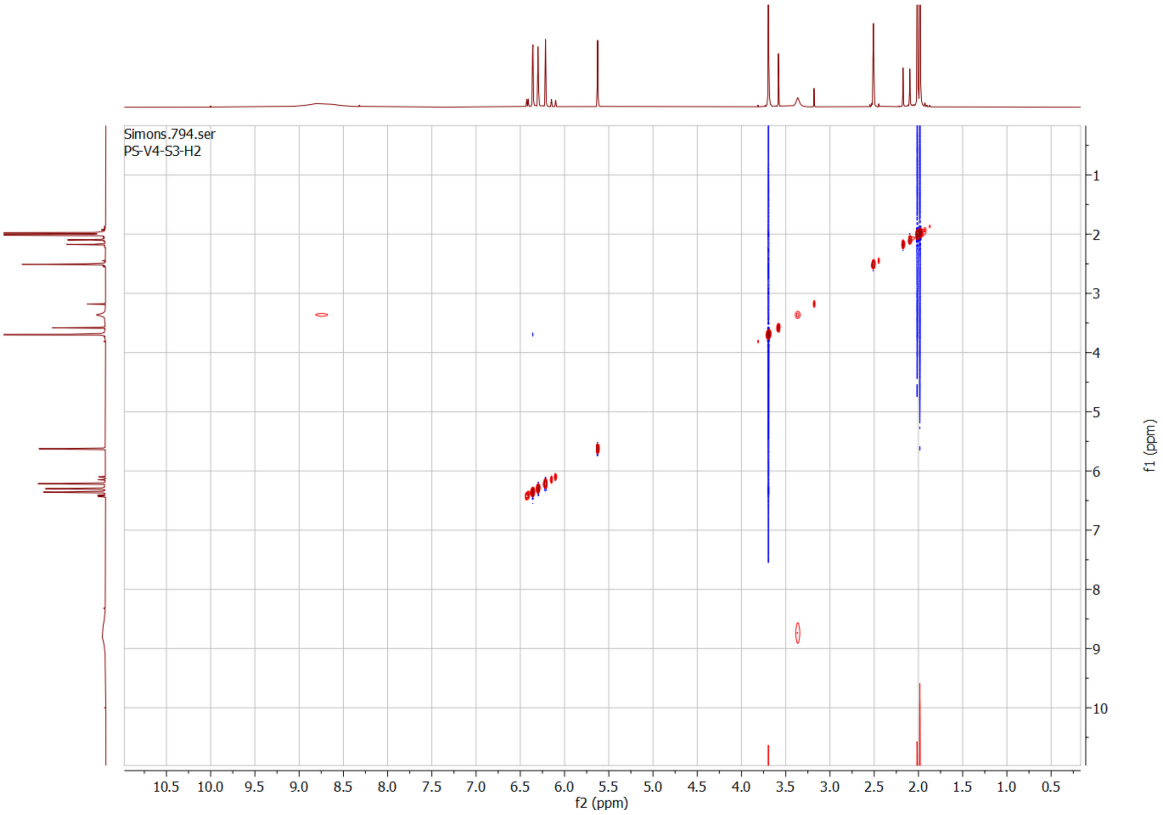

S5. NOESY NMR spectrum (DMSO-d6 – 600 MHz) of compound A

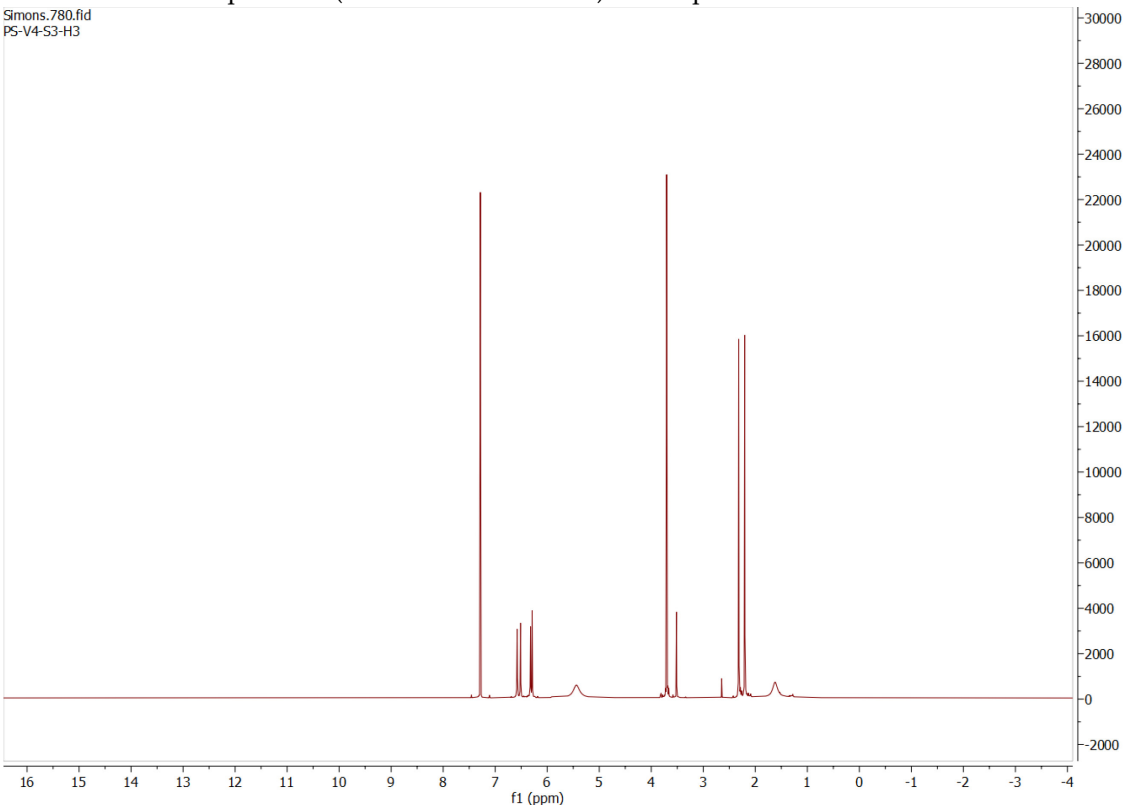

S6. 1H NMR spectrum (CDCl3 - 600 MHz) of compound B

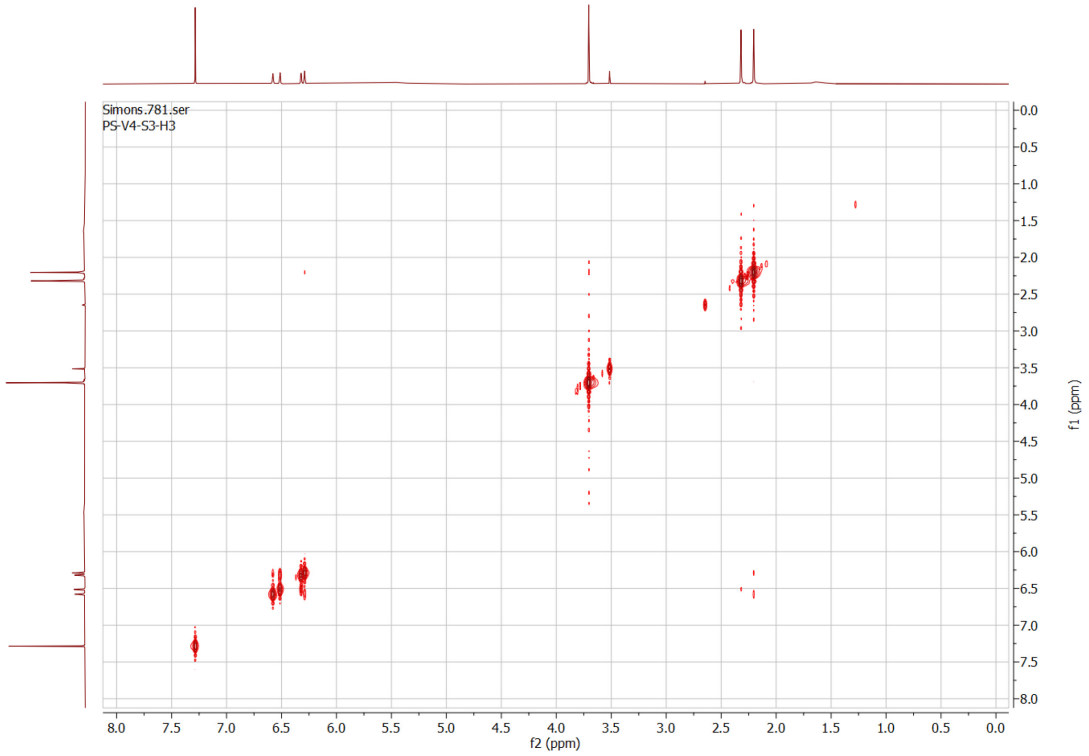

S7. COSY NMR spectrum ($CDCl_3$ - 600 MHz) of compound B

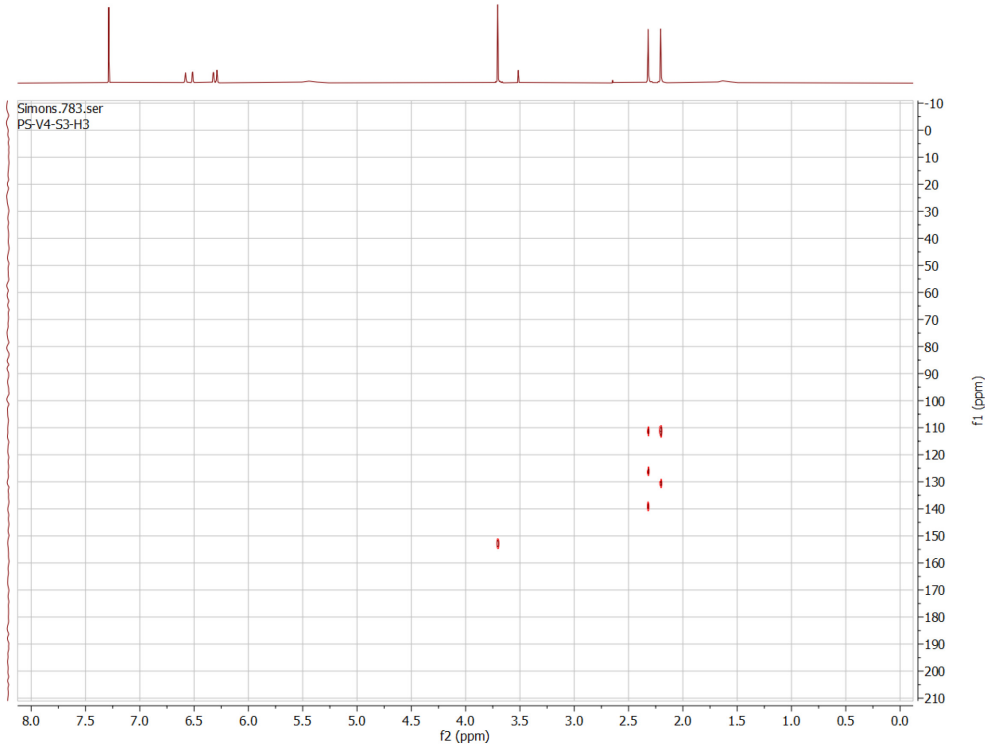

S8. HMBC NMR spectrum ($CDCl_3$ - 600 MHz) of compound B

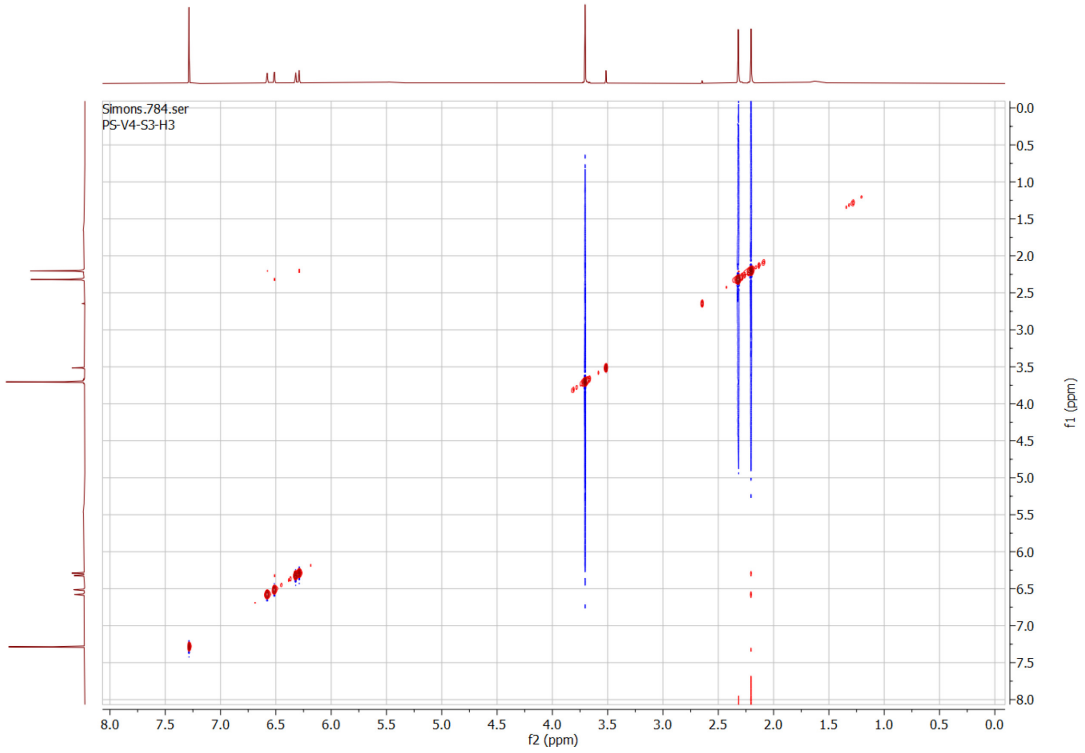

S9. NOESY NMR spectrum ($CDCl_3$ - 600 MHz) of compound B

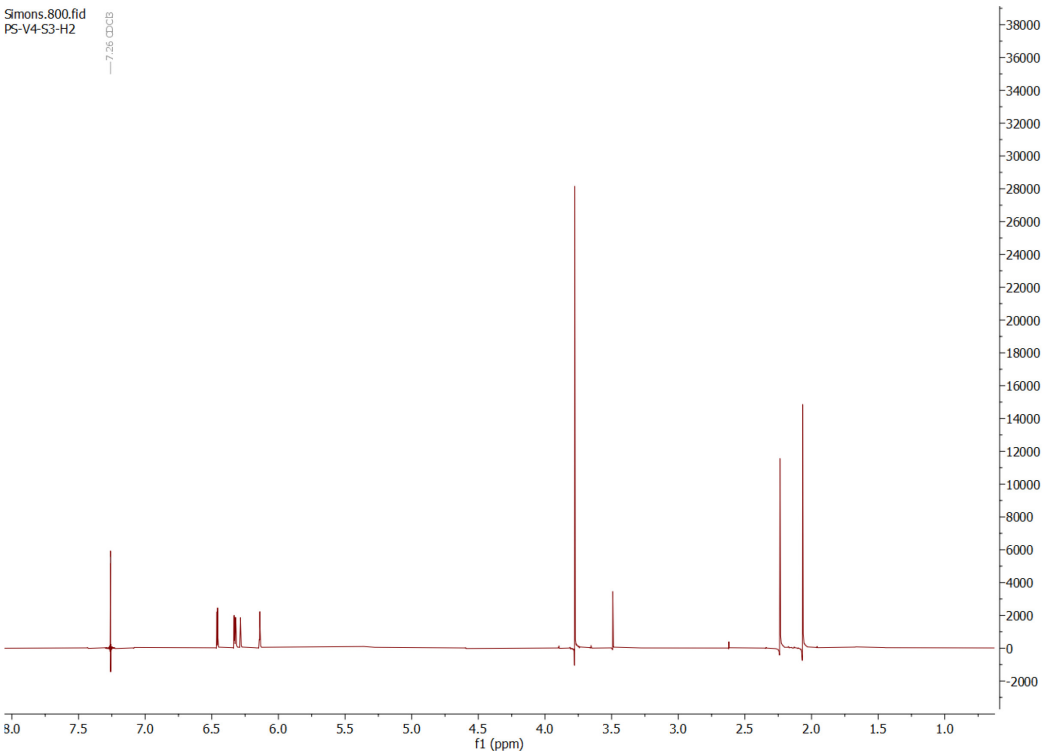

S10. ^1H NMR spectrum ($CDCl_3$ - 600 MHz) of compound C

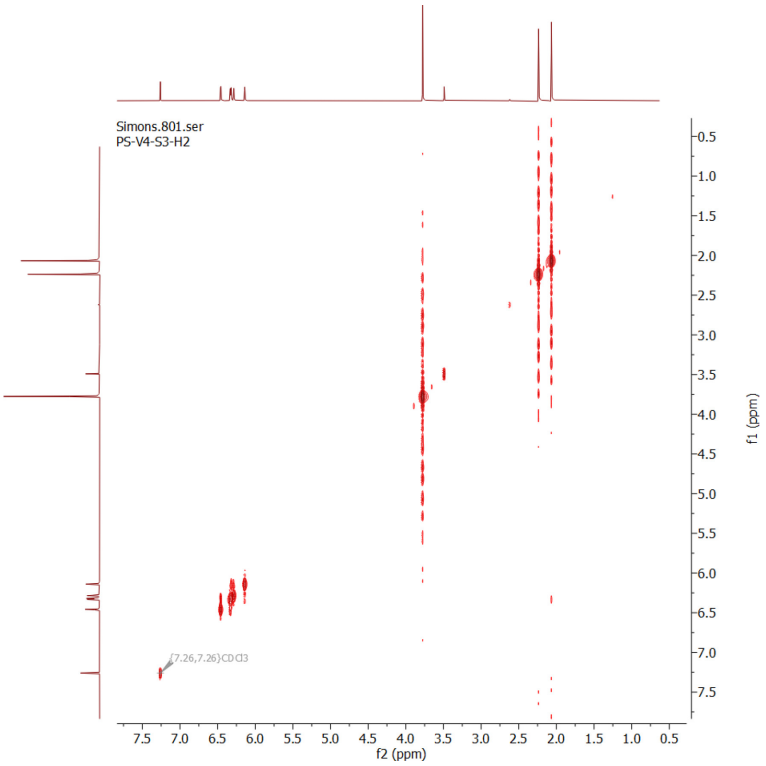

S11. COSY NMR spectrum ($CDCl_3$ - 600 MHz) of compound C

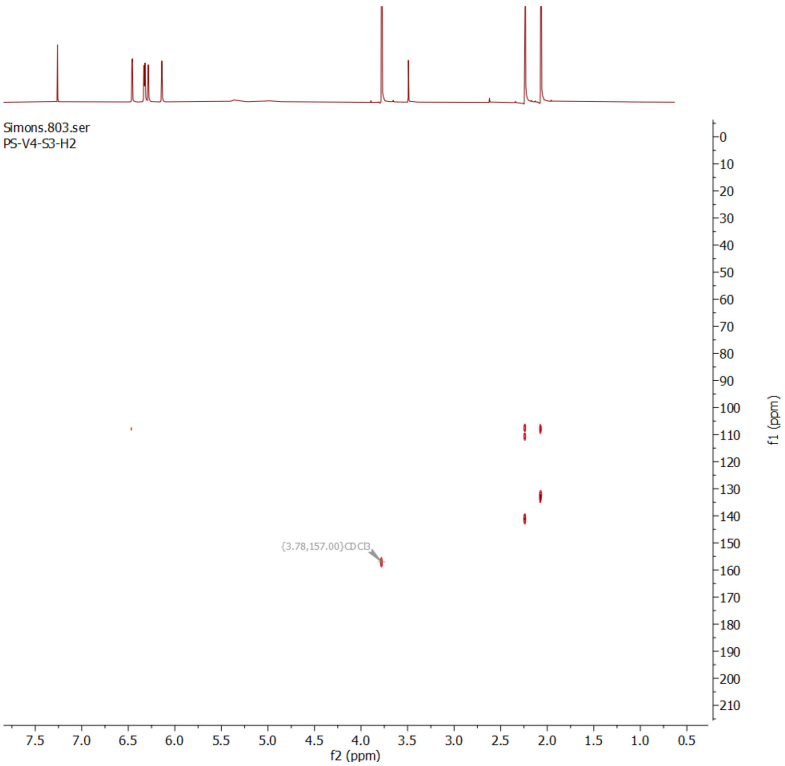

S12. HMBC NMR spectrum ($CDCl_3$ - 600 MHz) of compound C

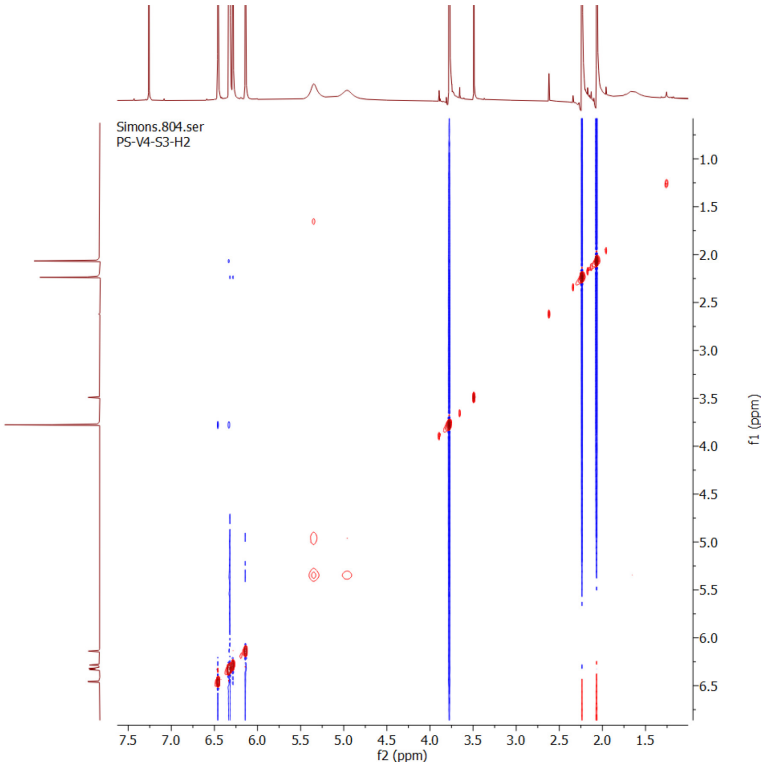

S13. NOESY NMR spectrum ($CDCl_3$ - 600 MHz) of compound C

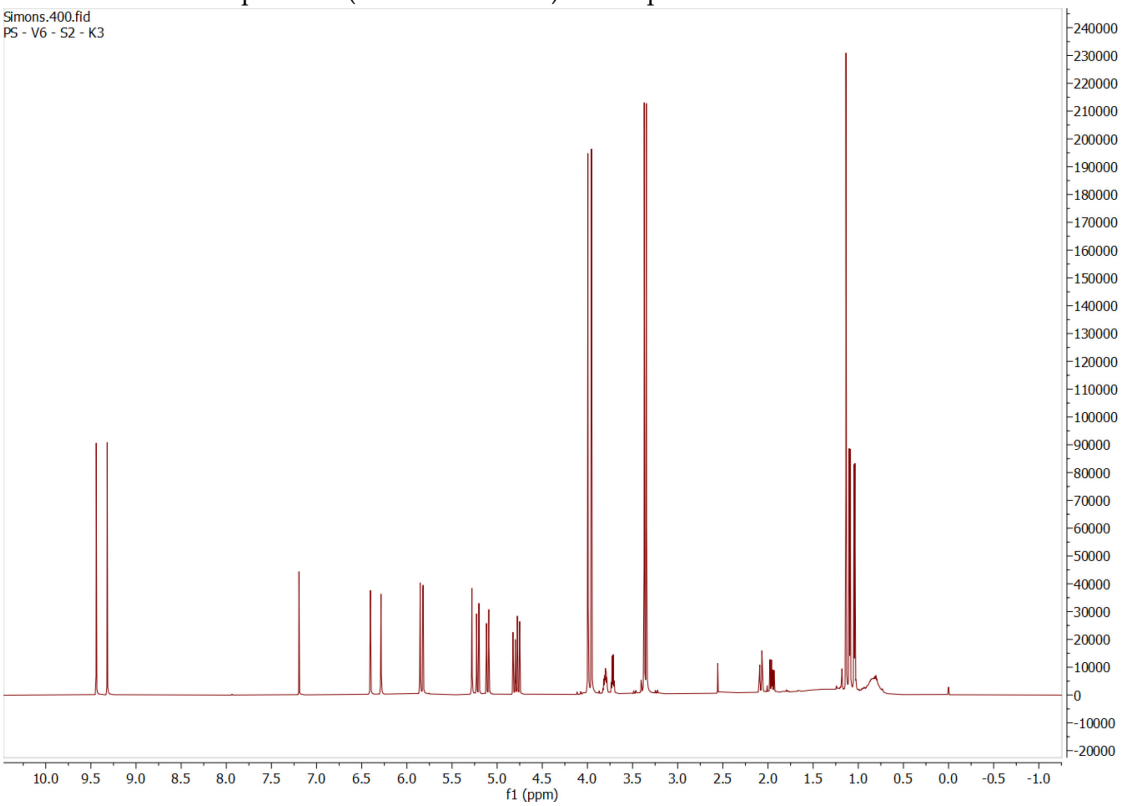

S14. ^1H NMR spectrum ($CDCl_3$ - 600 MHz) of compound D

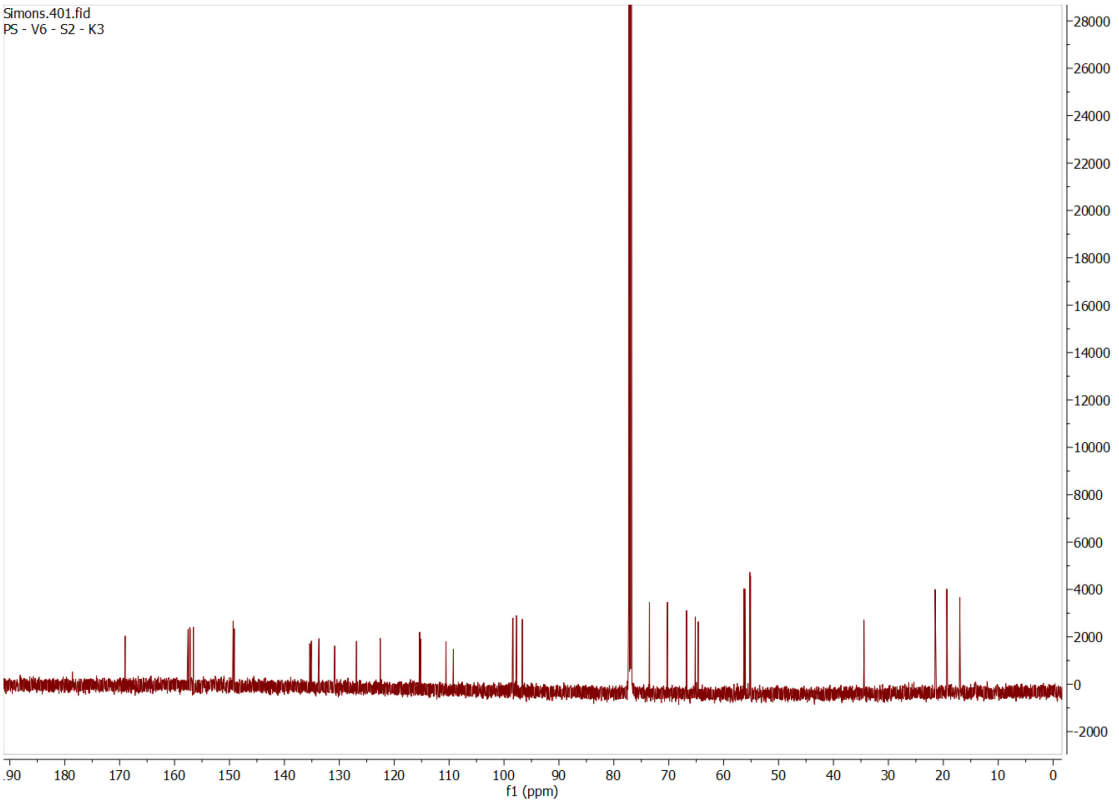

S15. ^{13}C NMR spectrum ($CDCl_3$ - 150 MHz) of compound D

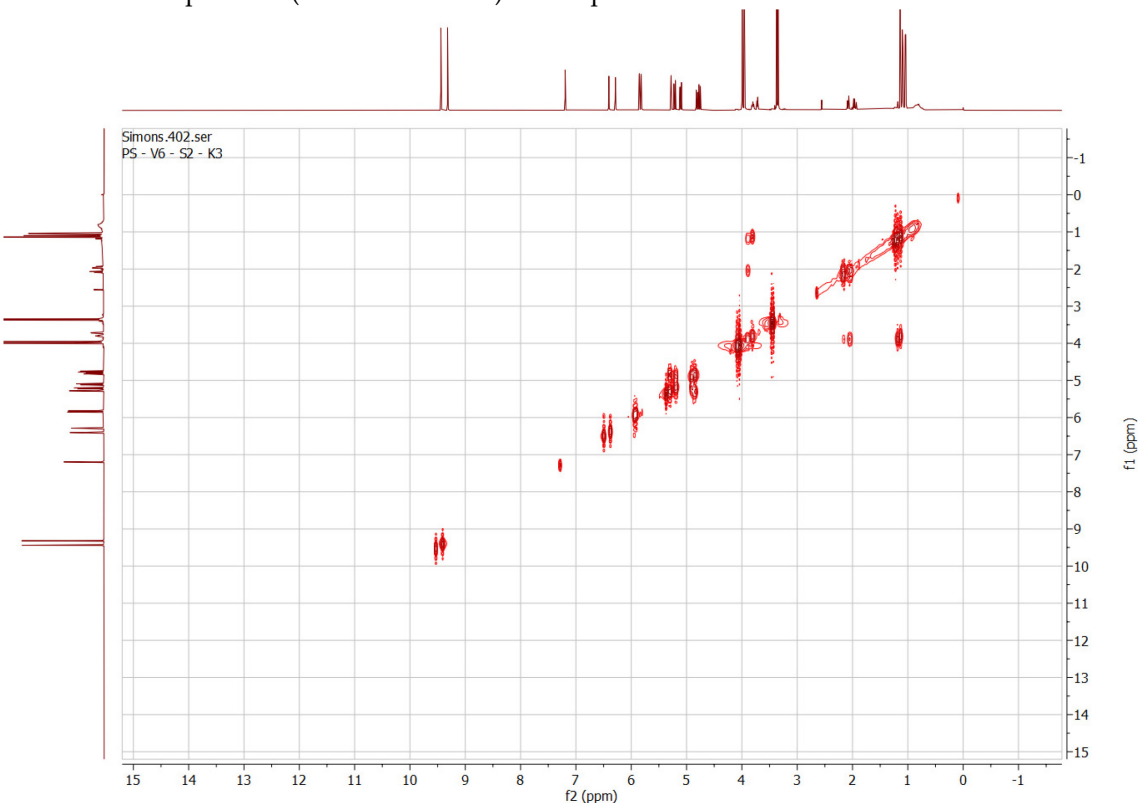

S16. COSY NMR spectrum ($CDCl_3$ - 600 MHz) of compound D

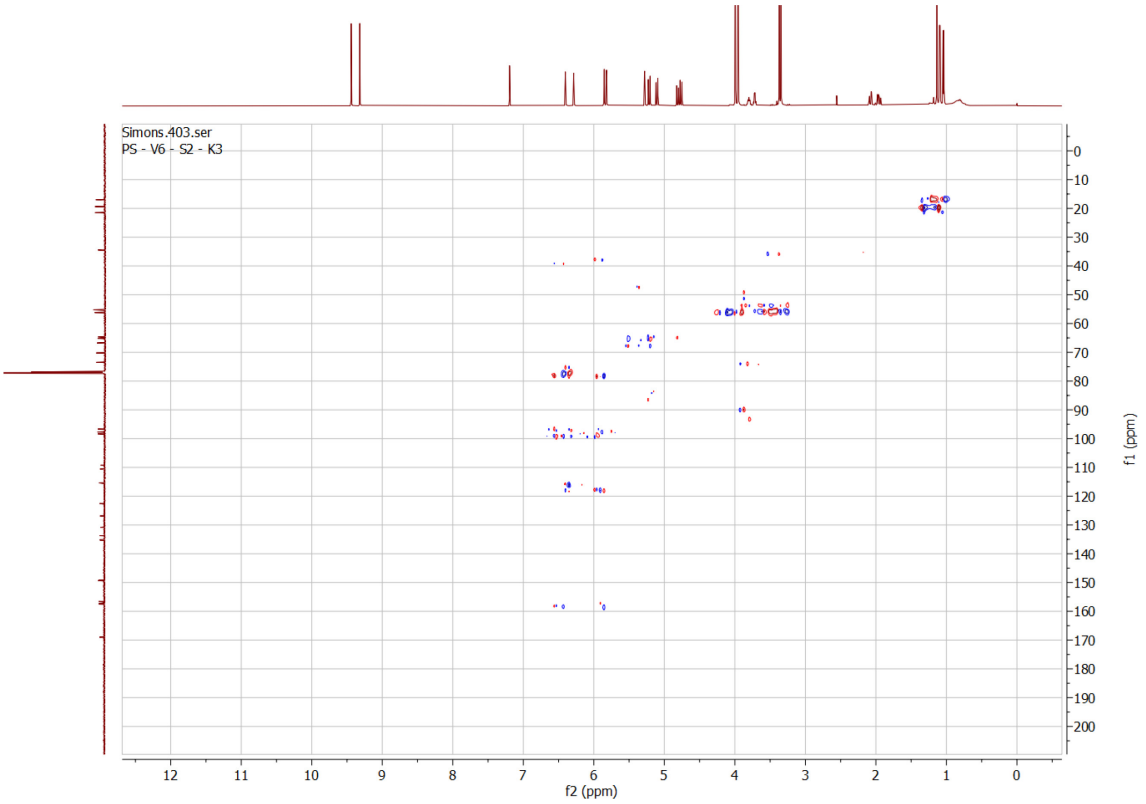

S17. HSQC NMR spectrum ($CDCl_3$ - 600 MHz) of compound D

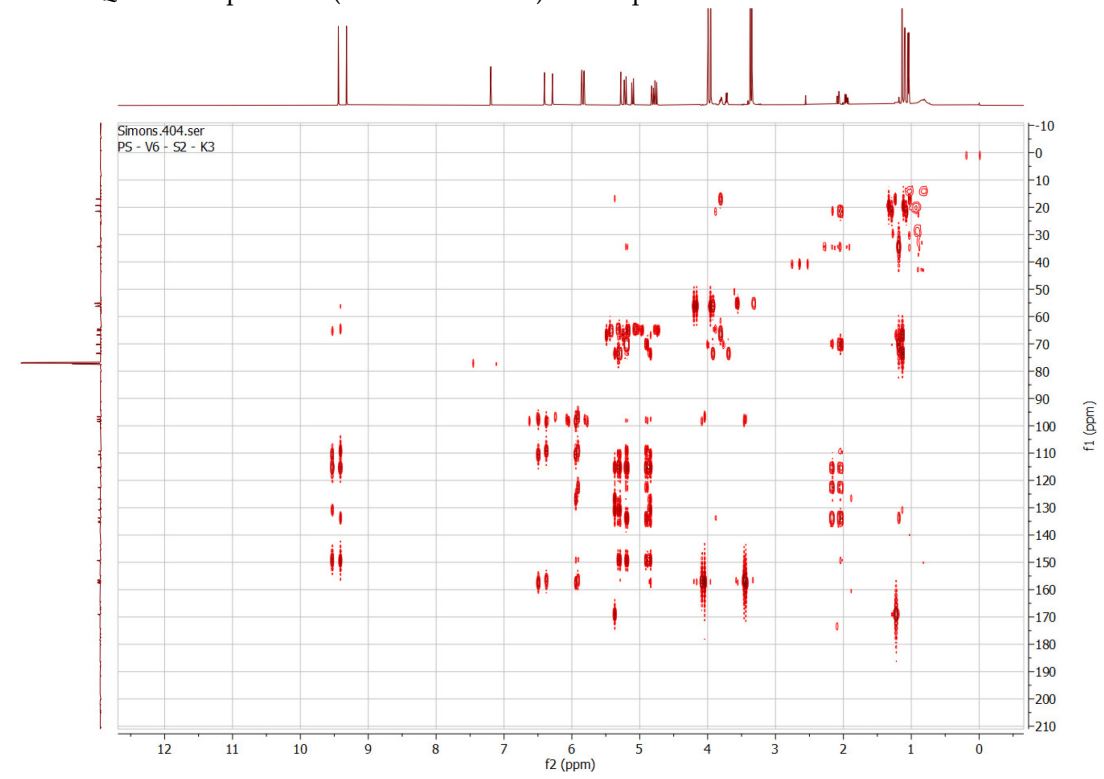

S18. HMBC NMR spectrum ($CDCl_3$ - 600 MHz) of compound D

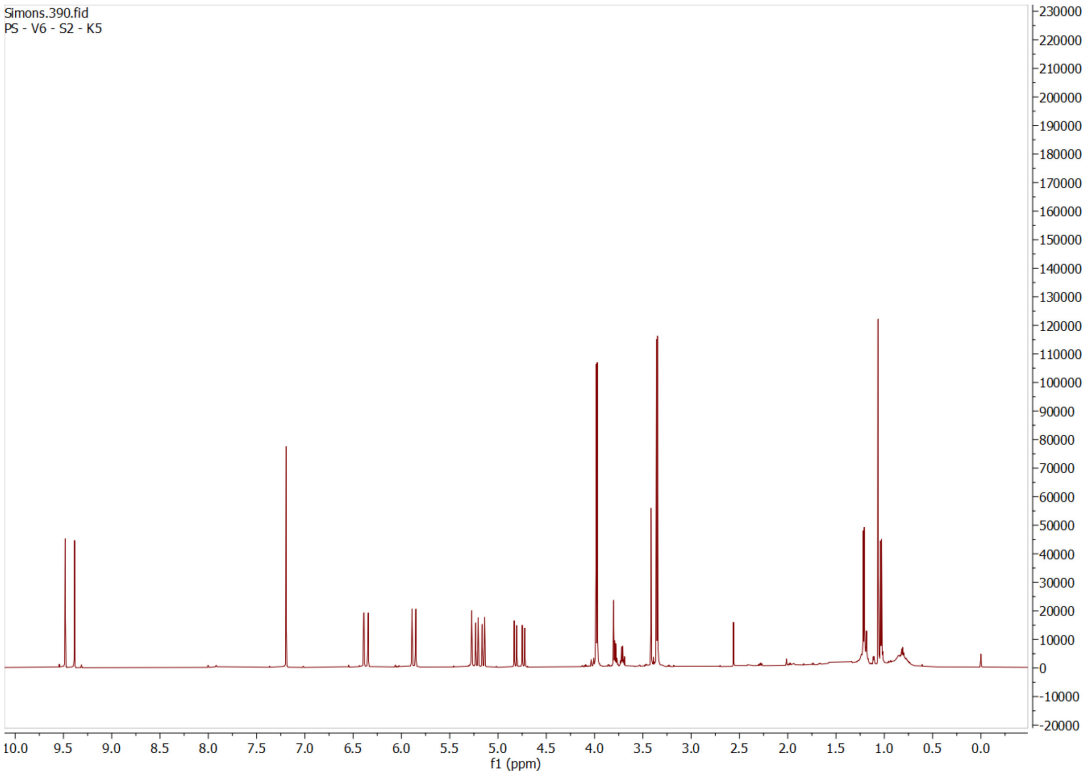

S19. ^{1}H NMR spectrum ($CDCl_3$ - 600 MHz) of compound E

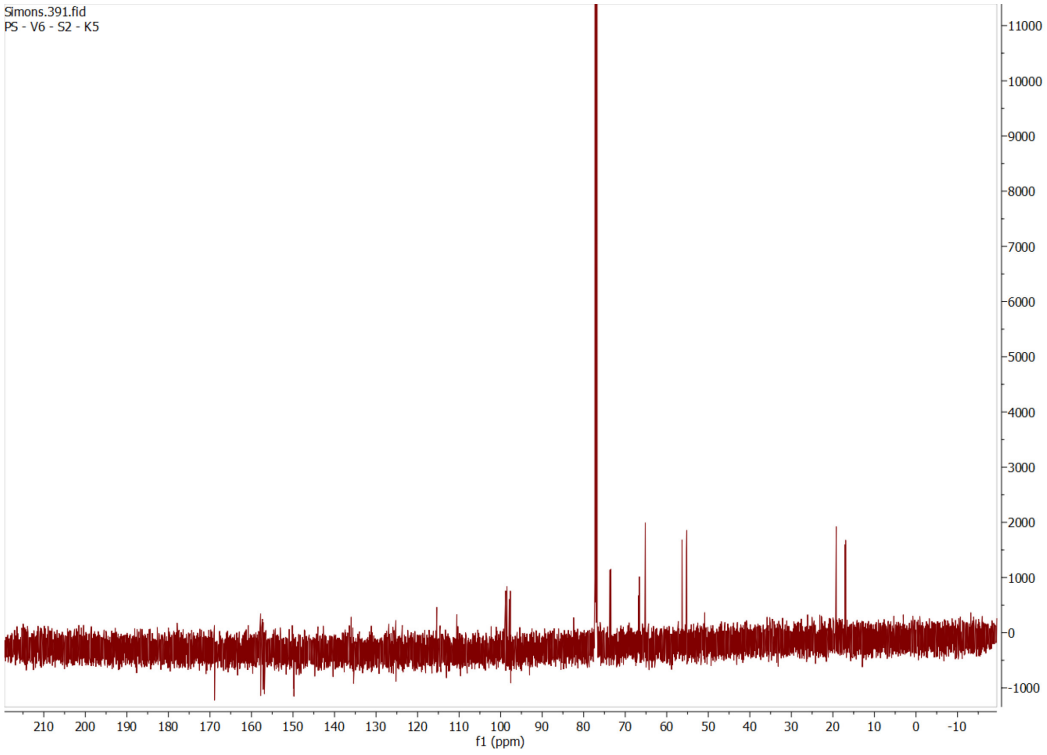

S20. ^{13}C NMR spectrum ($CDCl_3$ - 150 MHz) of compound E

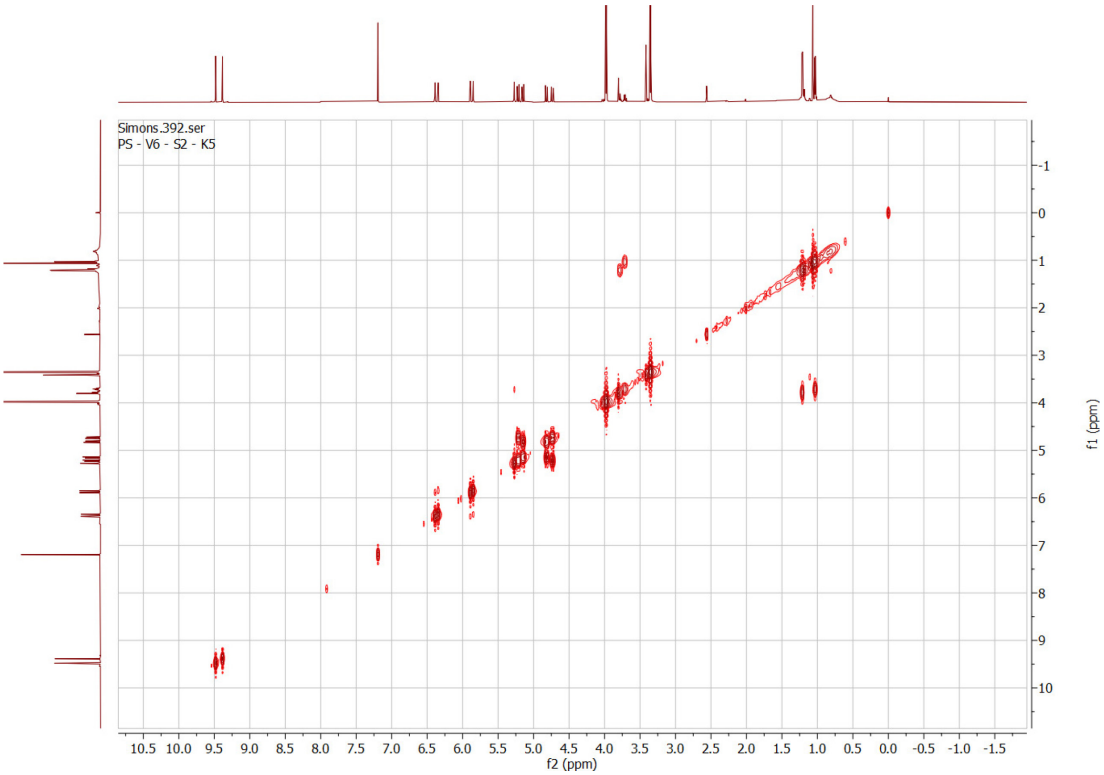

S21. COSY NMR spectrum ($CDCl_3$ - 600 MHz) of compound E

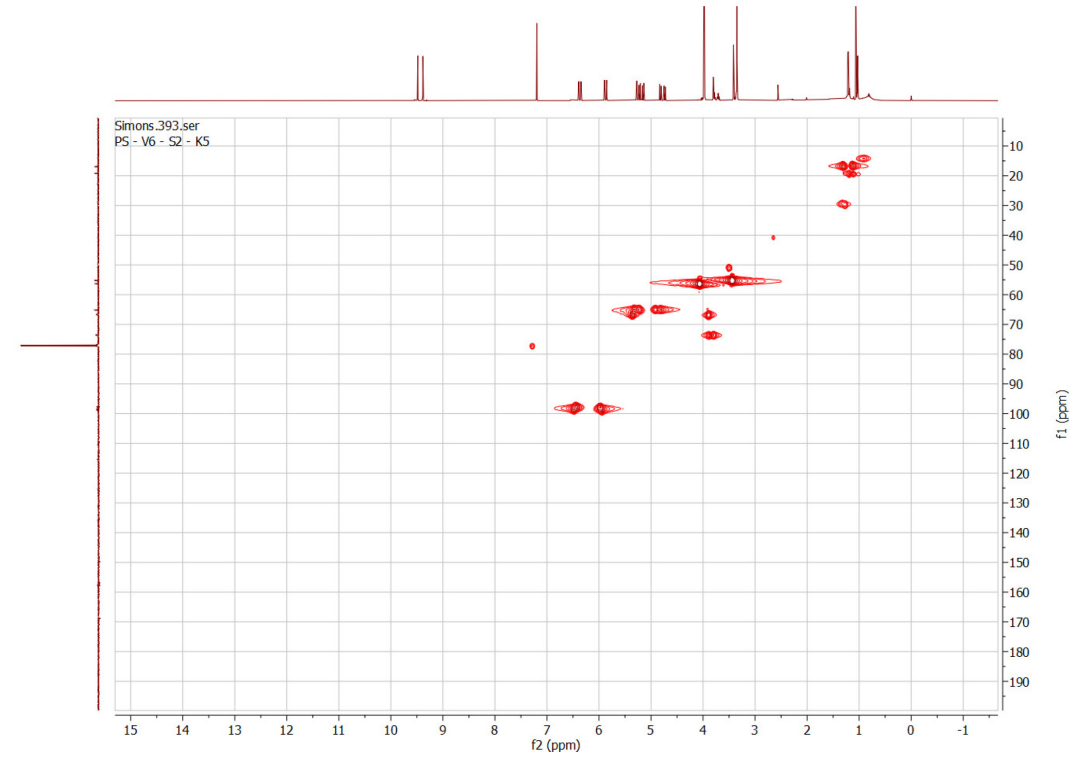

S22. HSQC NMR spectrum ($CDCl_3$ - 600 MHz) of compound E

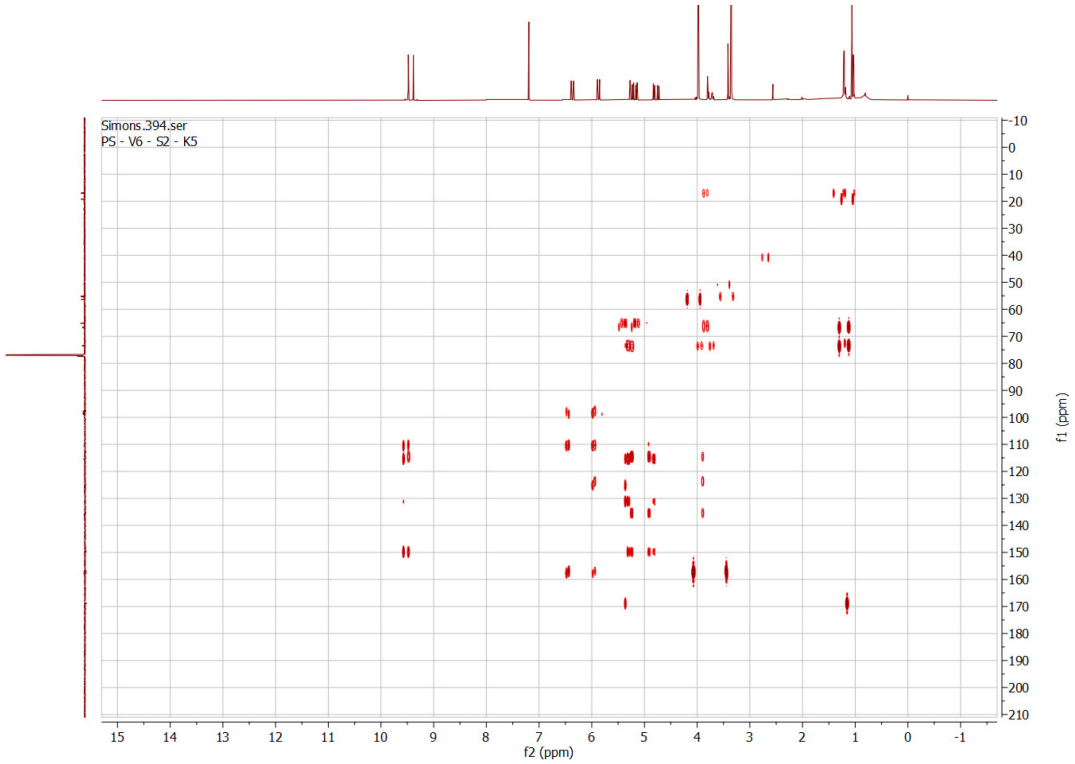

S23. HMBC NMR spectrum ($CDCl_3$ - 600 MHz) of compound E

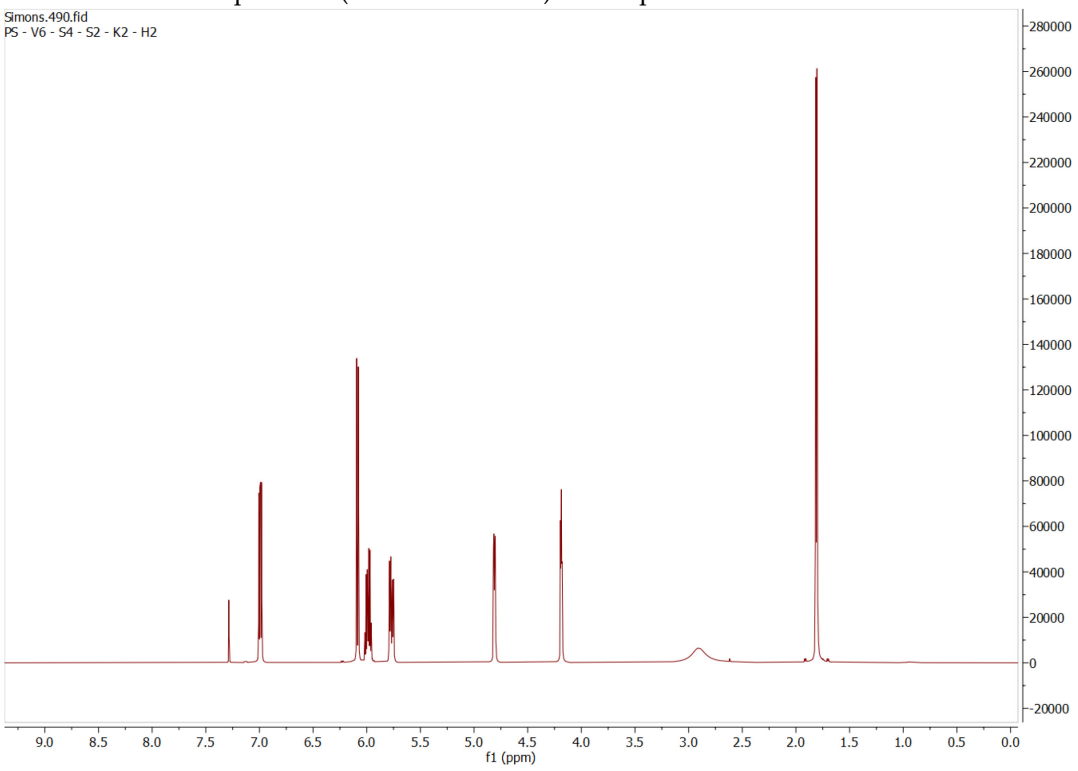

S24. ^1H NMR spectrum ($CDCl_3$ - 600 MHz) of compound F

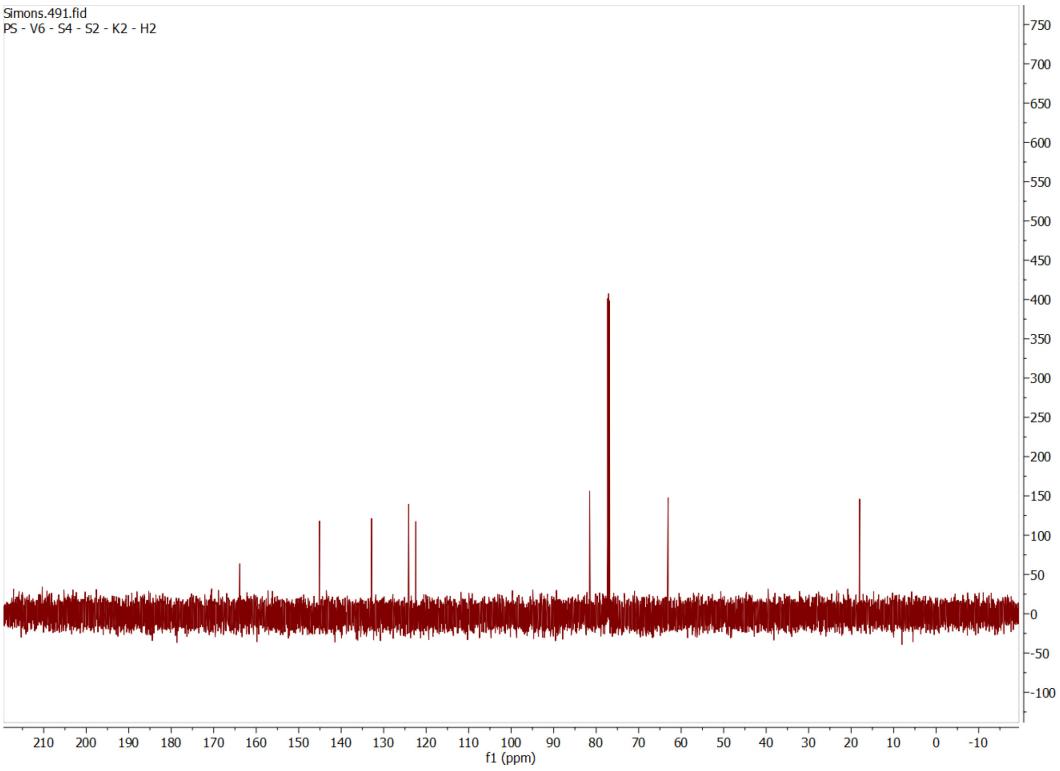

S25. ^{13}C NMR spectrum ($CDCl_3$ - 150 MHz) of compound F

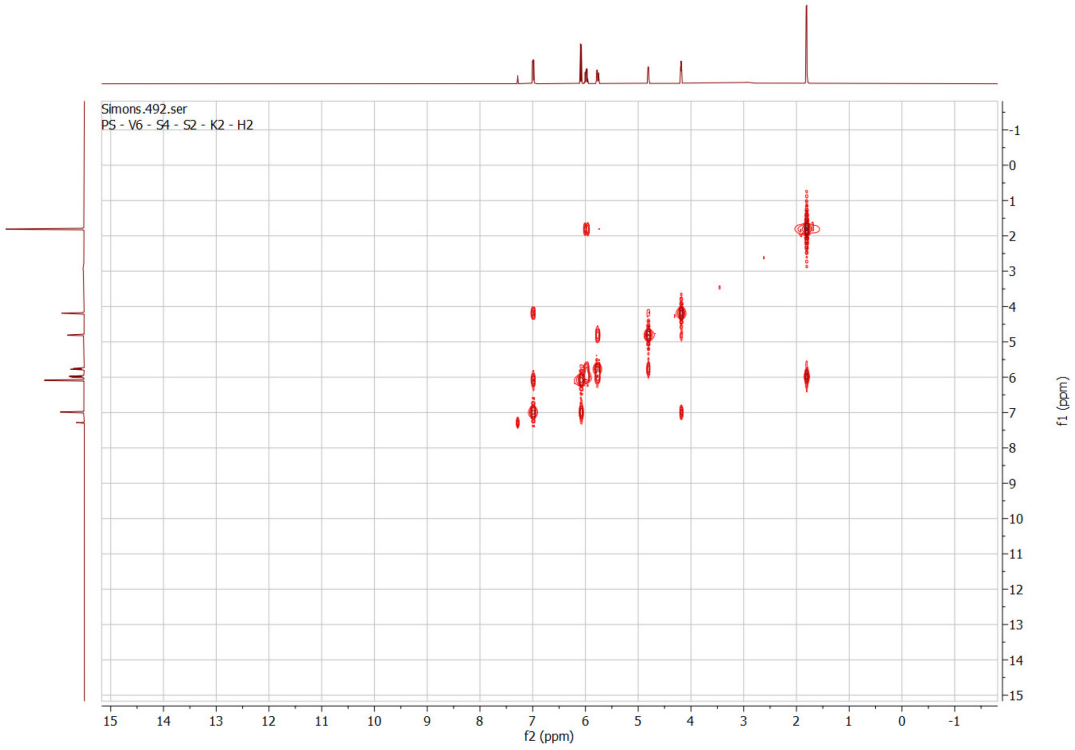

S26. COSY NMR spectrum ($CDCl_3$ - 600 MHz) of compound F

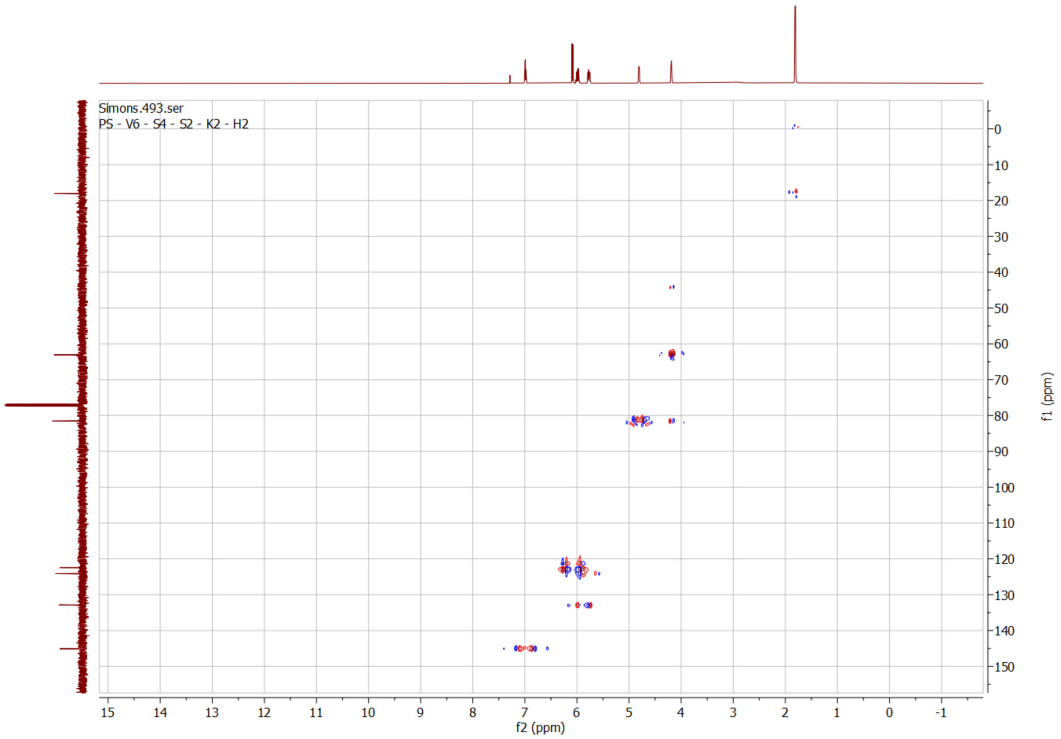

S27. HSQC NMR spectrum ($CDCl_3$ - 600 MHz) of compound F

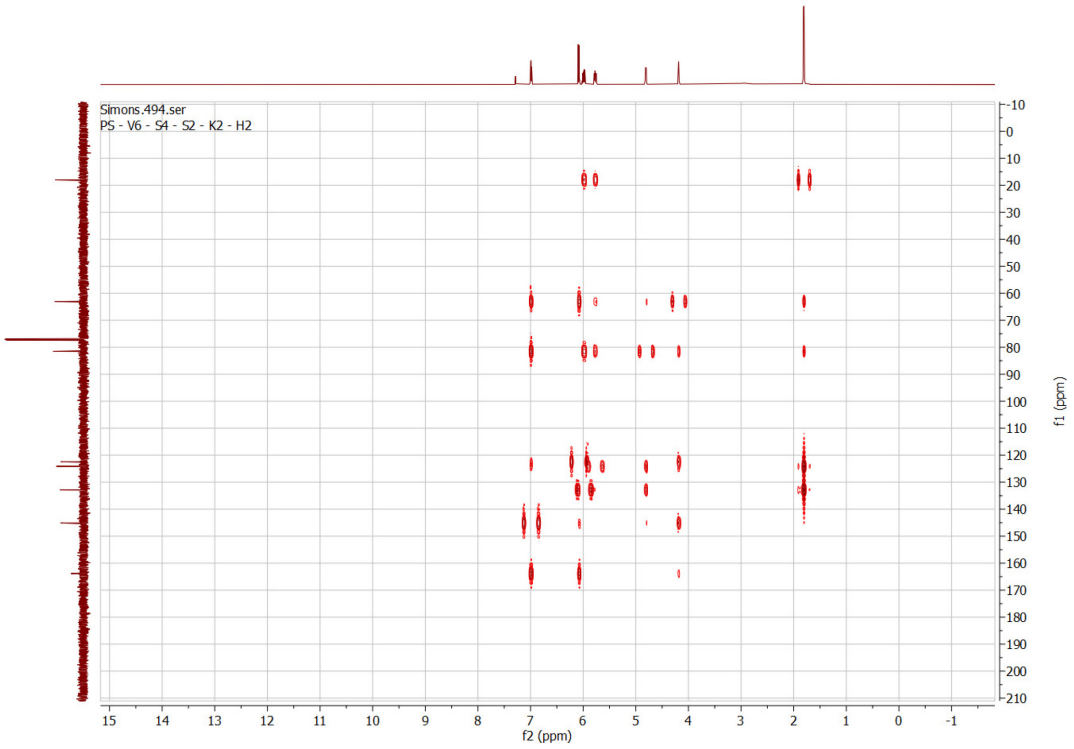

S28. HMBC NMR spectrum ($CDCl_3$ - 600 MHz) of compound F

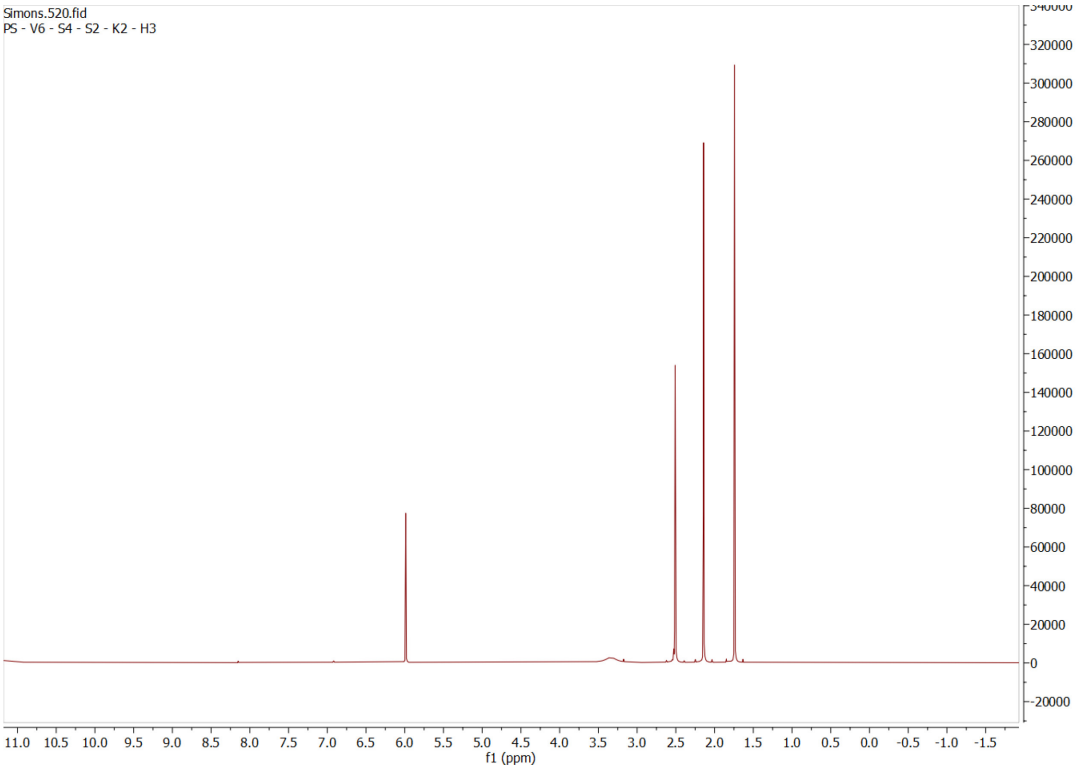

S29. ^{1}H NMR spectrum (DMSO-d6 – 600 MHz) of compound G

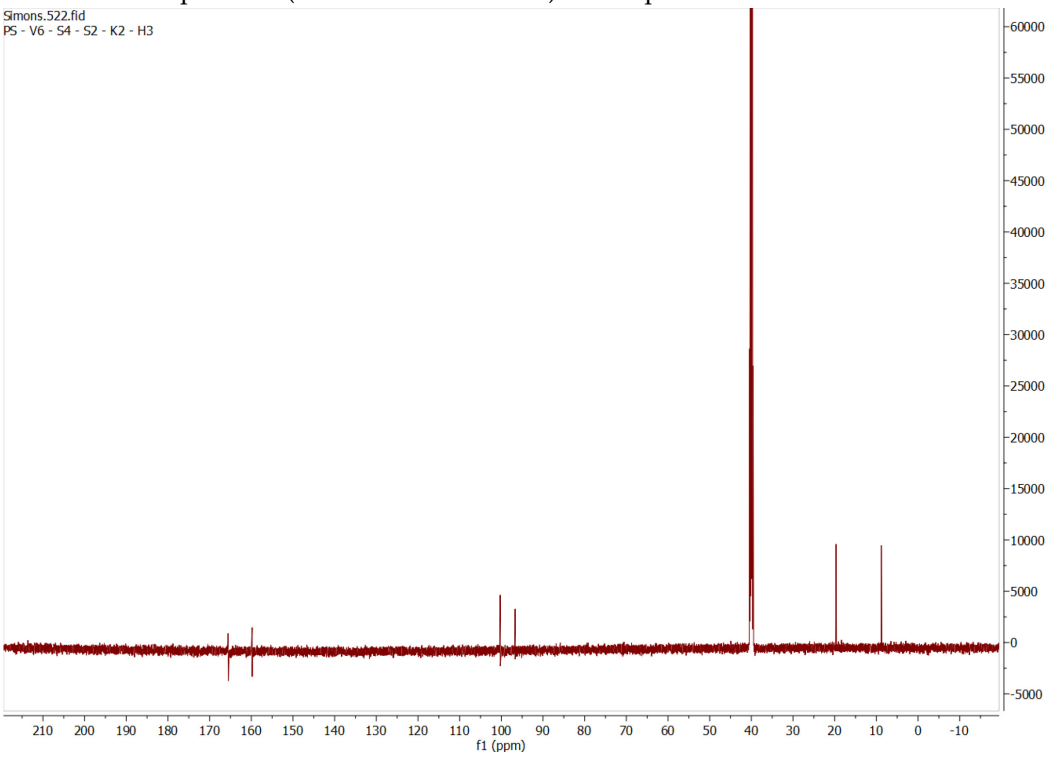

S30. ^{13}C NMR spectrum (DMSO-d6 – 150 MHz) of compound G

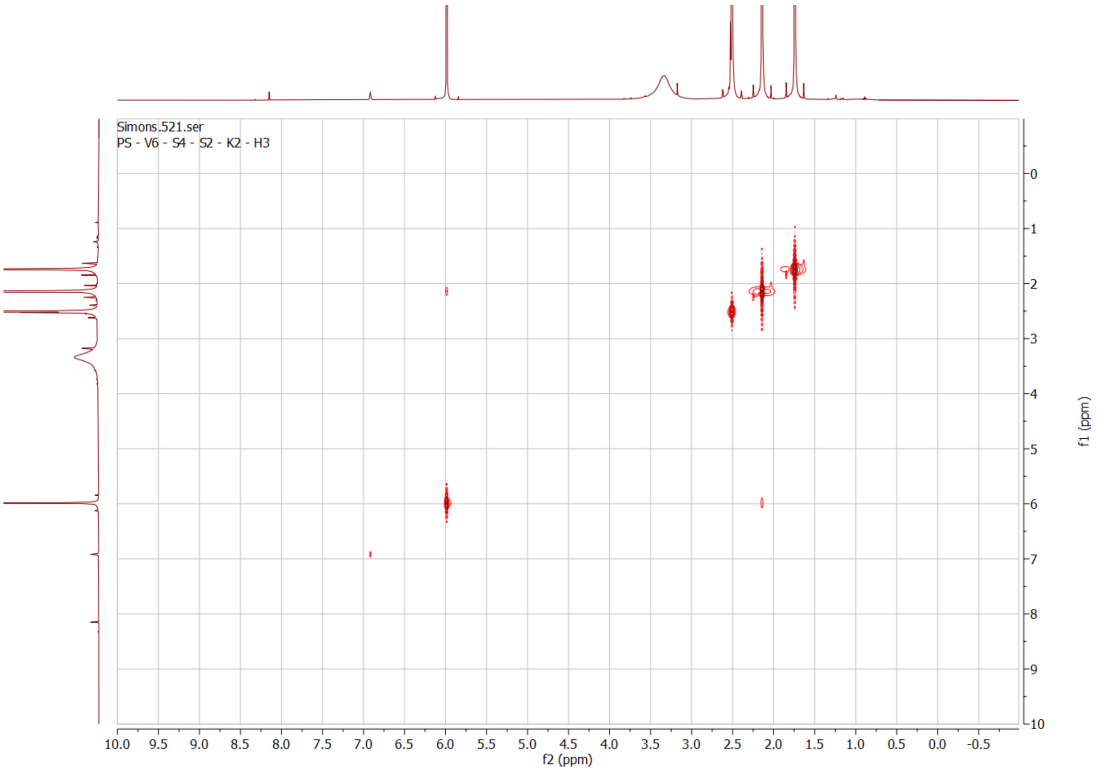

S31. COSY NMR spectrum (DMSO-d6 – 600 MHz) of compound G

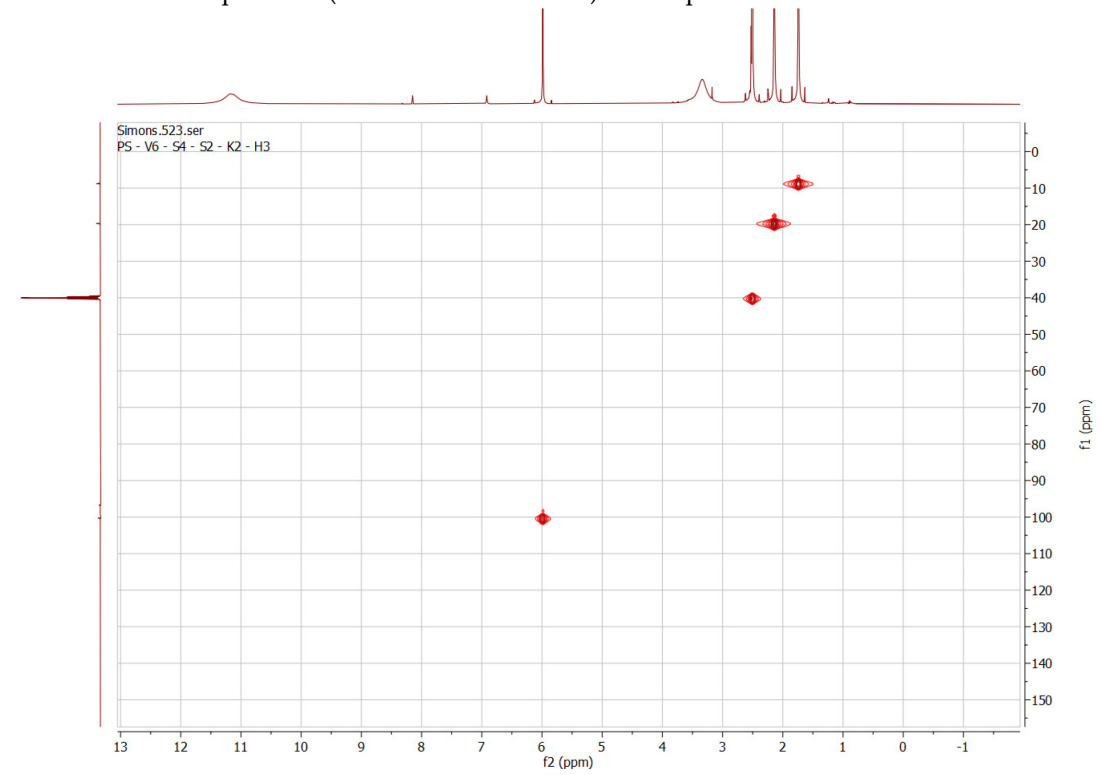

S32. HSQC NMR spectrum (DMSO-d6 – 600 MHz) of compound G

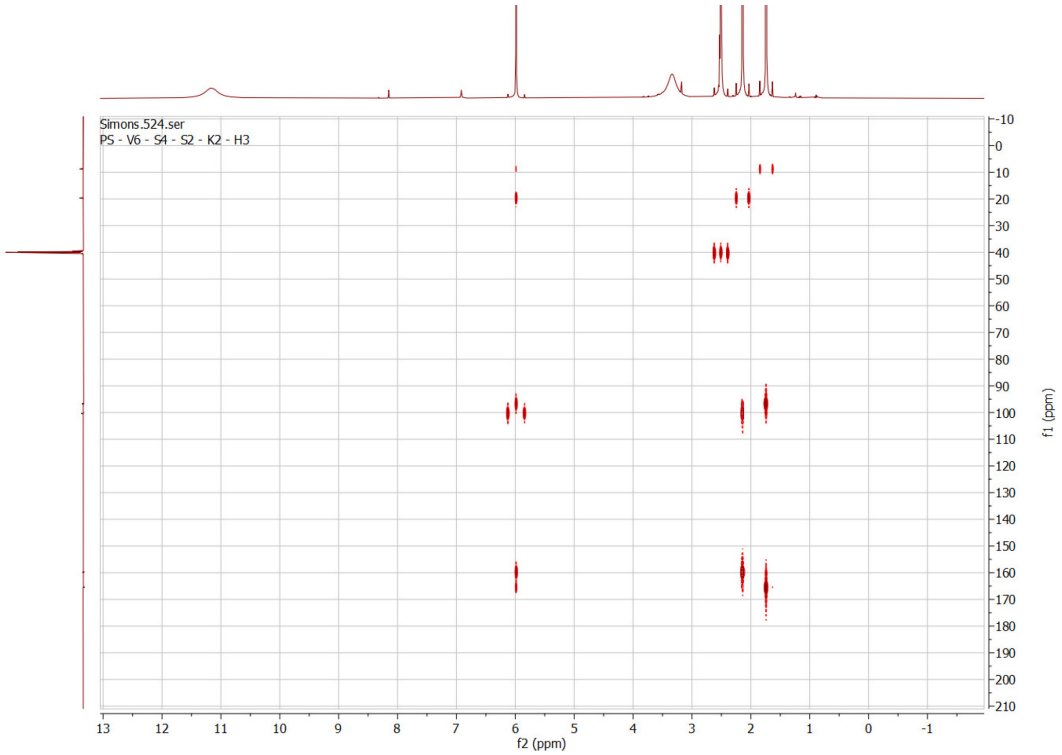

S33. HMBC NMR spectrum (DMSO-d6 – 600 MHz) of compound G

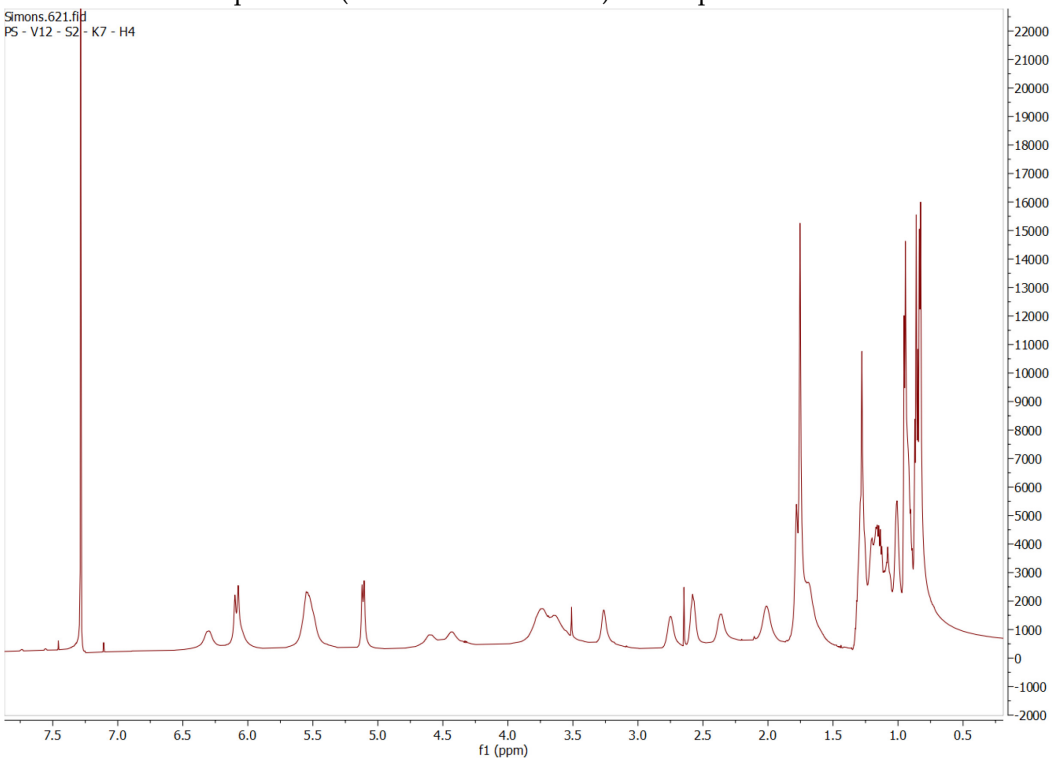

S34. ^{1}H NMR spectrum ($CDCl_3$ - 600 MHz) of compound H

Acquisition Parameter

Source Type	ESI	Ion Polarity	Positive	Set Nebulizer	0.3 Bar
Focus	Not active	Set Capillary	4000 V	Set Dry Heater	180 °C
Scan Begin	50 m/z	Set End Plate Offset	-500 V	Set Dry Gas	4.0 l/min
Scan End	1500 m/z	Set Collision Cell RF	600.0 Vpp	Set Divert Valve	Source

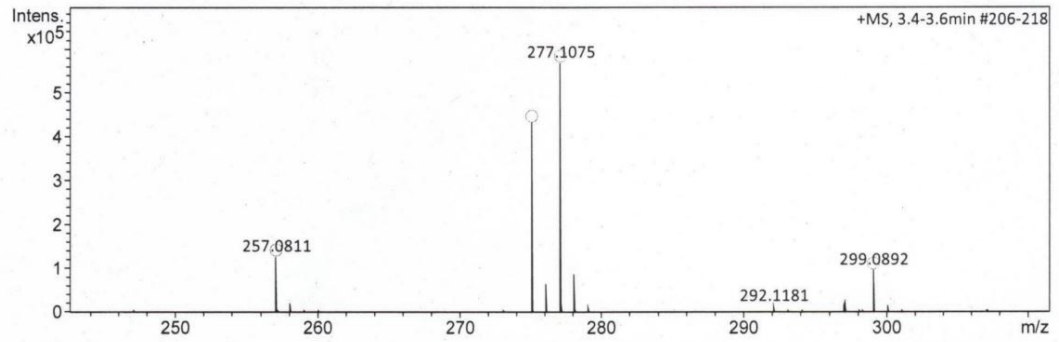

Meas. m/z	#	Ion Formula	m/z	err [ppm]	mSigma	# mSigma	Score	rdb	e⁻ Conf	N-Rule
257.0811	1	C15H13O4	257.0808	-1.1	7.2	1	100.00	9.5	even	ok
275.0919	1	C15H15O5	275.0914	-1.8	581.8	1	100.00	8.5	even	ok
277.1075	1	C15H17O5	277.1071	-1.6	8.4	1	100.00	7.5	even	ok
299.0892	1	C15H16NaO5	299.0890	-0.8	0.6	1	100.00	7.5	even	ok

S35. HRESIMS (MeOH) of compound A

Acquisition Parameter

Source Type	ESI	Ion Polarity	Positive	Set Nebulizer	0.3 Bar
Focus	Not active	Set Capillary	4000 V	Set Dry Heater	180 °C
Scan Begin	50 m/z	Set End Plate Offset	-500 V	Set Dry Gas	4.0 l/min
Scan End	1500 m/z	Set Collision Cell RF	600.0 Vpp	Set Divert Valve	Source

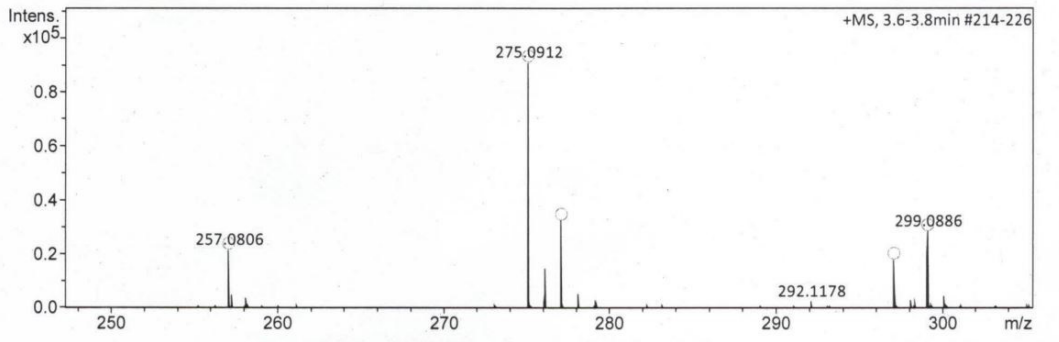

Meas. m/z	#	Ion Formula	m/z	err [ppm]	mSigma	# mSigma	Score	rdb	e⁻ Conf	N-Rule
257.0806	1	C15H13O4	257.0808	1.1	5.7	1	100.00	9.5	even	ok
275.0912	1	C15H15O5	275.0914	0.7	192.5	1	100.00	8.5	even	ok
277.1065	1	C15H17O5	277.1071	2.1	4.8	1	98.95	7.5	even	ok
	2	C14H14N4NaO	277.1060	-1.8	6.5	2	100.00	9.5	even	ok
297.0730	1	C13H9N6O3	297.0731	0.3	11.1	1	100.00	12.5	even	ok
	2	C15H14NaO5	297.0733	1.2	602.8	2	0.00	8.5	even	ok
299.0886	1	C13H11N6O3	299.0887	0.4	3.4	1	100.00	11.5	even	ok
	2	C15H16NaO5	299.0890	1.3	4.2	2	87.30	7.5	even	ok

S36. HRESIMS (MeOH) of compound B

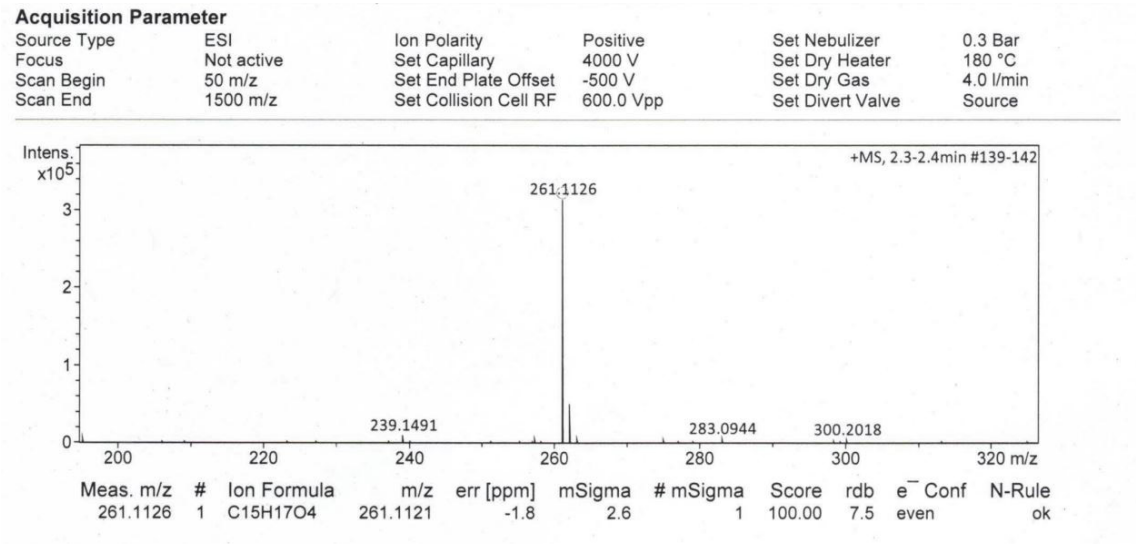

S37. HRESIMS (MeOH) of compound C

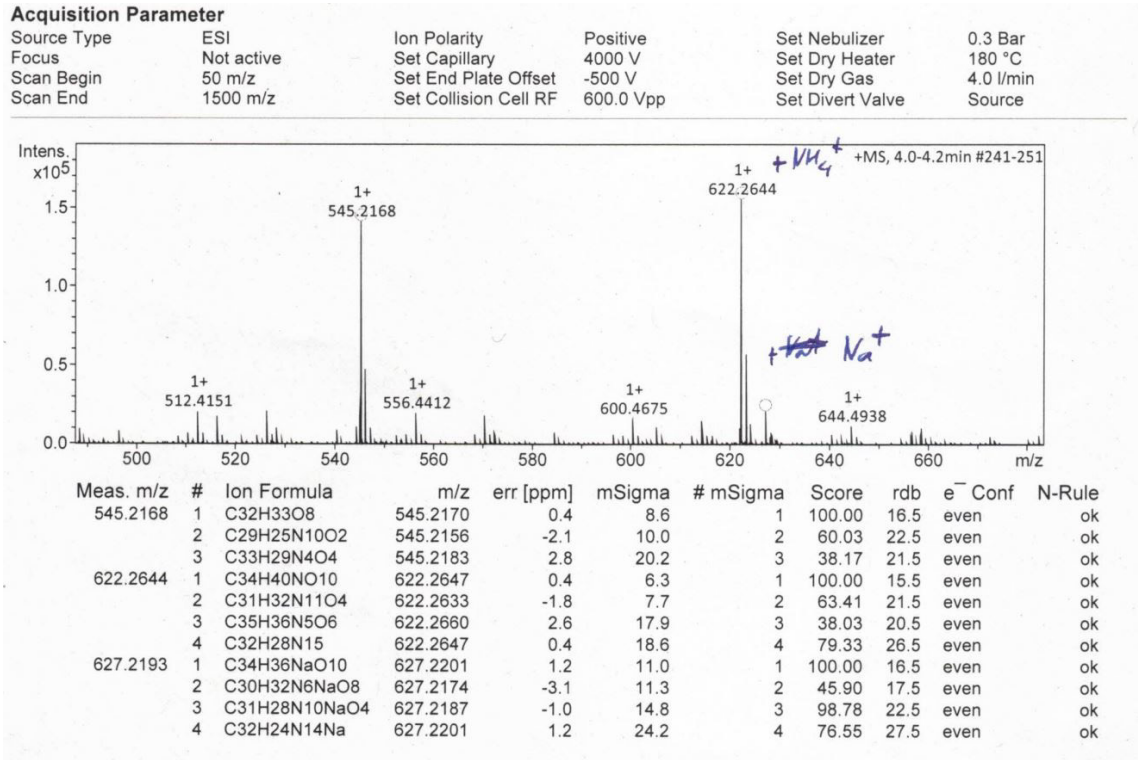

S38. HRESIMS (MeOH) of compound D

Acquisition Parameter

Source Type	ESI	Ion Polarity	Positive	Set Nebulizer	0.3 Bar
Focus	Not active	Set Capillary	4000 V	Set Dry Heater	180 °C
Scan Begin	50 m/z	Set End Plate Offset	-500 V	Set Dry Gas	4.0 l/min
Scan End	1500 m/z	Set Collision Cell RF	600.0 Vpp	Set Divert Valve	Source

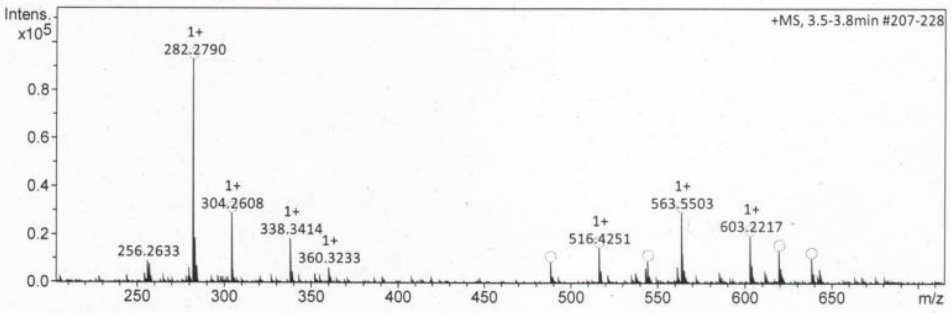

Meas. m/z	#	Ion Formula	m/z	err [ppm]	mSigma	# mSigma	Score	rdb	e¯ Conf	N-Rule
282.2790	1	C18H36NO	282.2791	0.4	30.2	1	100.00	1.5	even	ok
304.2608	1	C18H35NNaO	304.2611	0.9	13.8	1	100.00	1.5	even	ok
	2	C15H34N3O3	304.2595	-4.5	20.4	2	48.40	0.5	even	ok
488.3939	1	C23H50N7O4	488.3919	-4.1	27.1	1	34.39	2.5	even	ok
	2	C24H46N11	488.3932	-1.4	27.8	2	79.11	7.5	even	ok
	3	C27H54NO6	488.3946	1.4	29.9	3	100.00	1.5	even	ok
	4	C26H51N5NaO2	488.3935	-0.8	30.4	4	85.24	3.5	even	ok
	5	C28H50N5O2	488.3959	4.1	39.6	5	24.93	6.5	even	ok
516.4251	1	C29H58NO6	516.4259	1.5	9.1	1	100.00	1.5	even	ok
	2	C28H55N5NaO2	516.4248	-0.6	11.1	2	90.44	3.5	even	ok
	3	C26H50N11	516.4245	-1.1	13.2	3	76.15	7.5	even	ok
	4	C25H54N7O4	516.4232	-3.7	24.7	4	26.14	2.5	even	ok
544.4564	1	C31H62NO6	544.4572	1.4	11.0	1	83.99	1.5	even	ok
	2	C27H58N7O4	544.4545	-3.5	13.4	2	39.01	2.5	even	ok
	3	C30H59N5NaO2	544.4561	-0.5	14.2	3	100.00	3.5	even	ok
	4	C28H54N11	544.4558	-1.1	14.5	4	65.37	7.5	even	ok
563.5503	1	C36H71N2O2	563.5510	1.3	54.5	1	100.00	2.5	even	ok
	2	C34H72N2NaO2	563.5486	-3.0	61.2	2	44.45	-0.5	even	ok
	3	C32H67N8	563.5483	-3.5	63.6	3	33.38	3.5	even	ok
603.2217	1	C34H35O10	603.2225	1.3	4.9	1	83.81	17.5	even	ok
	2	C33H32N4NaO6	603.2214	-0.5	7.7	2	100.00	19.5	even	ok
	3	C31H27N10O4	603.2211	-1.0	10.0	3	83.93	23.5	even	ok
	4	C34H28N8NaO2	603.2227	1.7	11.6	4	64.05	24.5	even	ok
	5	C32H23N14	603.2225	1.2	12.8	5	73.02	28.5	even	ok
	6	C30H24N14Na	603.2201	-2.7	13.7	6	41.54	25.5	even	ok
	7	C32H36NaO10	603.2201	-2.7	16.0	7	39.93	14.5	even	ok
	8	C30H31N6O8	603.2198	-3.2	17.6	8	31.61	18.5	even	ok
619.6126	1	C40H79N2O2	619.6136	1.6	28.2	1	100.00	2.5	even	ok
	2	C38H80N2NaO2	619.6112	-2.3	35.7	2	64.89	-0.5	even	ok
	3	C36H75N8	619.6109	-2.7	38.1	3	50.45	3.5	even	ok
638.2588	1	C32H41NNaO11	638.2572	-2.5	5.5	1	56.61	12.5	even	ok
	2	C30H36N7O9	638.2569	-3.0	7.4	2	44.83	16.5	even	ok
	3	C34H40NO11	638.2596	1.2	13.7	3	81.16	15.5	even	ok
	4	C33H37N5NaO7	638.2585	-0.4	15.4	4	100.00	17.5	even	ok
	5	C31H32N11O5	638.2582	-0.9	15.8	5	87.00	21.5	even	ok
	6	C30H29N15NaO	638.2572	-2.6	18.7	6	43.63	23.5	even	ok
	7	C32H28N15O	638.2596	1.2	26.8	7	61.67	26.5	even	ok
	8	C34H33N9NaO3	638.2599	1.6	26.8	8	52.80	22.5	even	ok
	9	C47H32N3	638.2591	0.4	87.5	9	10.66	33.5	even	ok

S39. HRESIMS (MeOH) of compound E

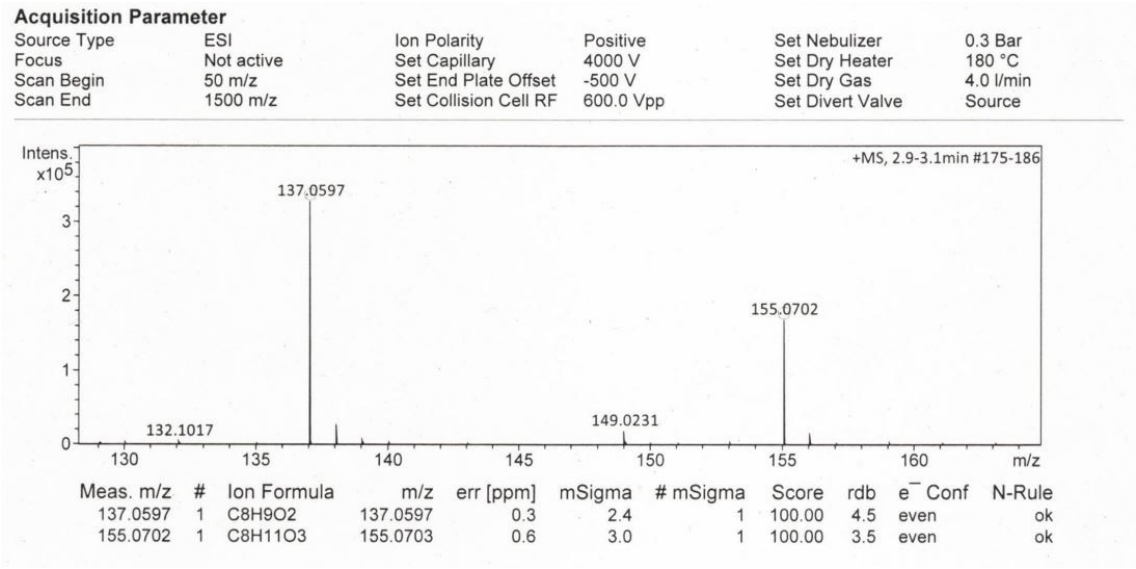

S40. HRESIMS (MeOH) of compound F

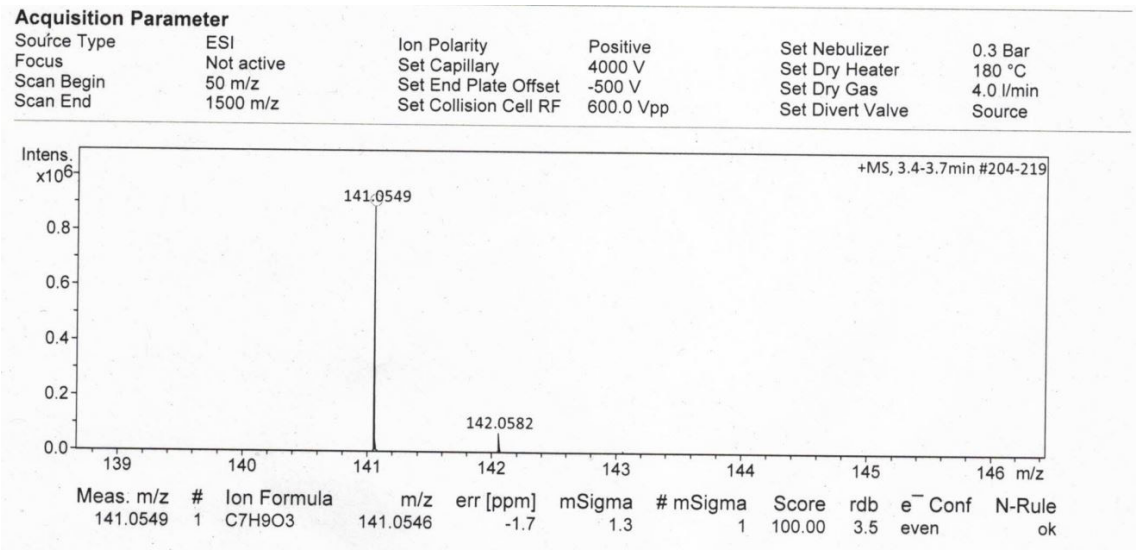

S41. HRESIMS (MeOH) of compound G

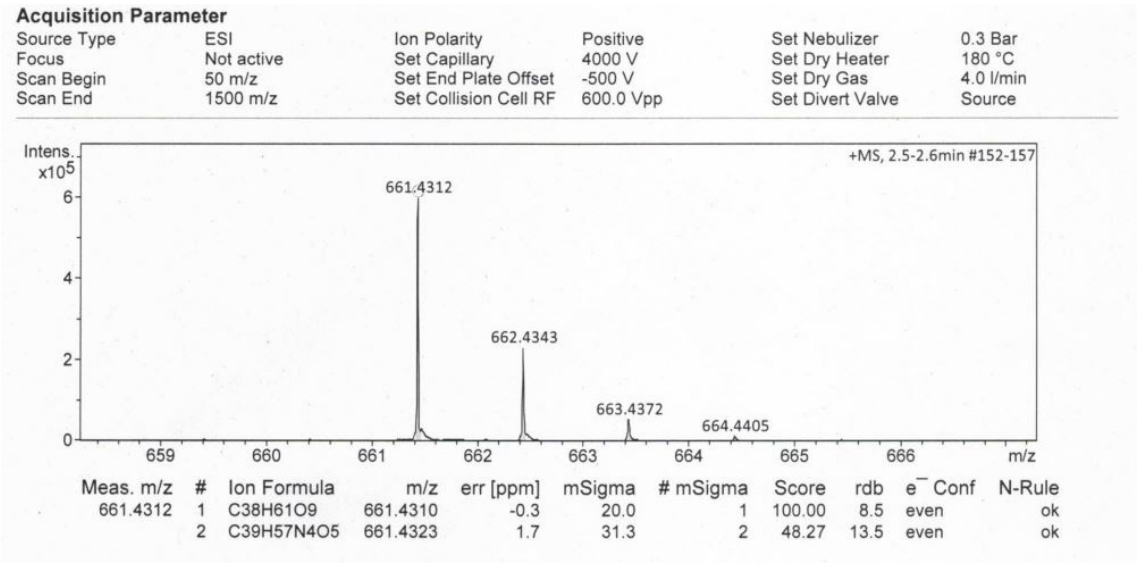

S42. HRESIMS (MeOH) of compound H

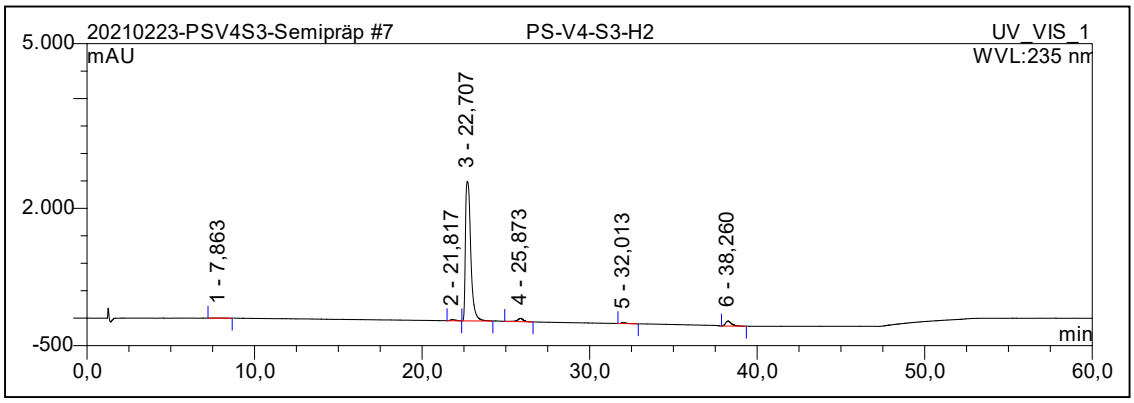

S43. HPLC chromatogram (MeOH) of compound A

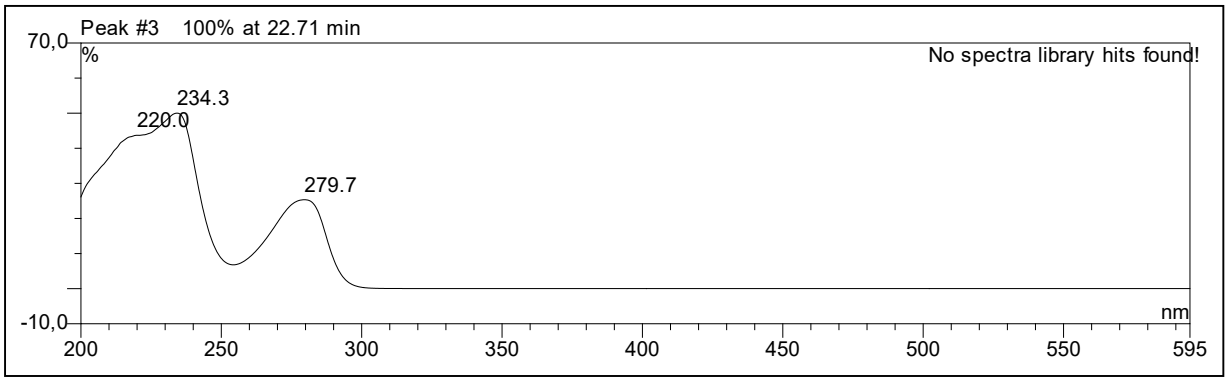

S44. UV-Vis spectrum (MeOH) of compound A

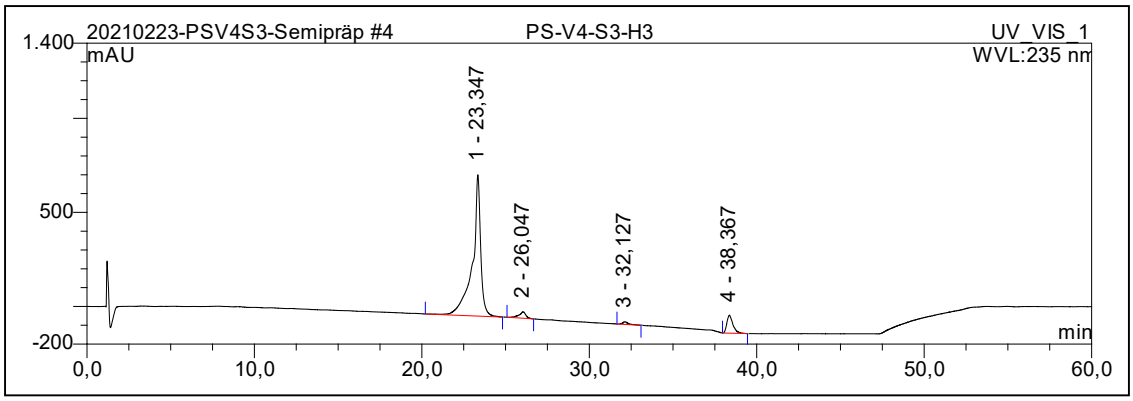

S45. HPLC chromatogram (MeOH) of compound B

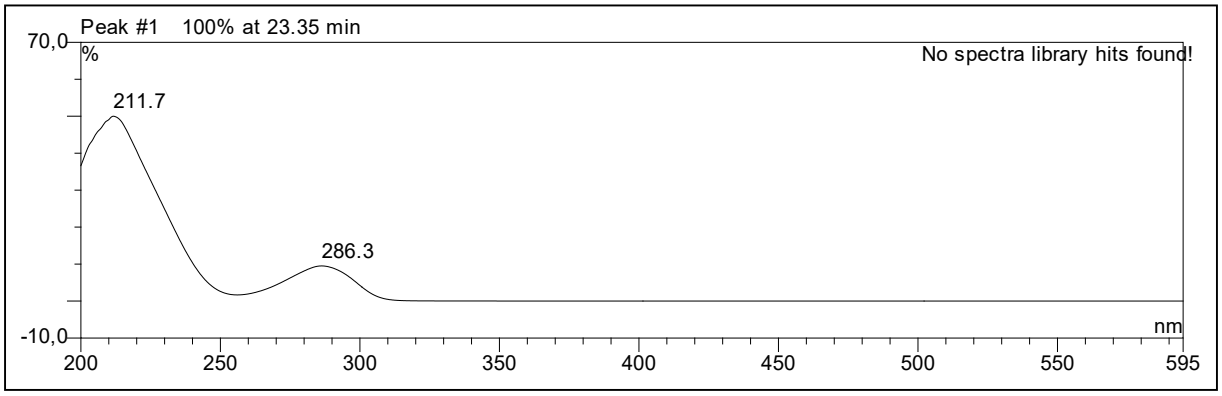

S46. UV-Vis spectrum (MeoH) of compound B

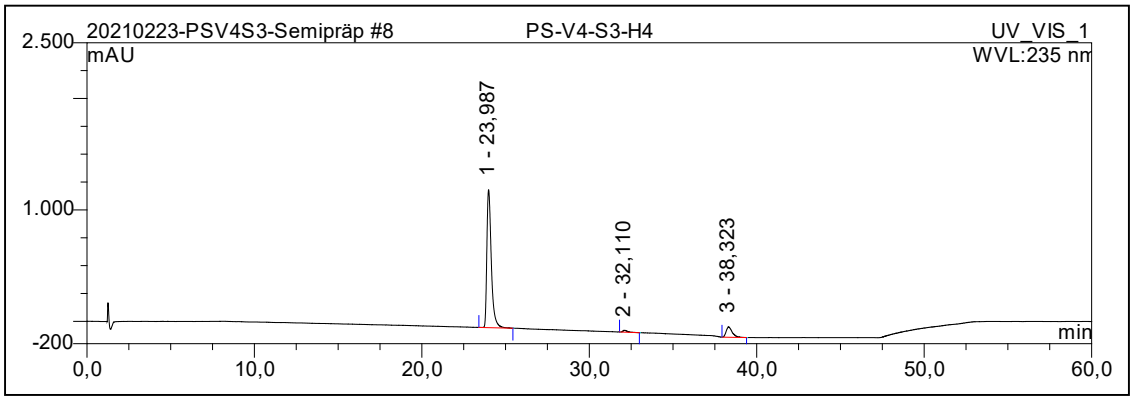

S47. HPLC chromatogram (MeOH) of compound C

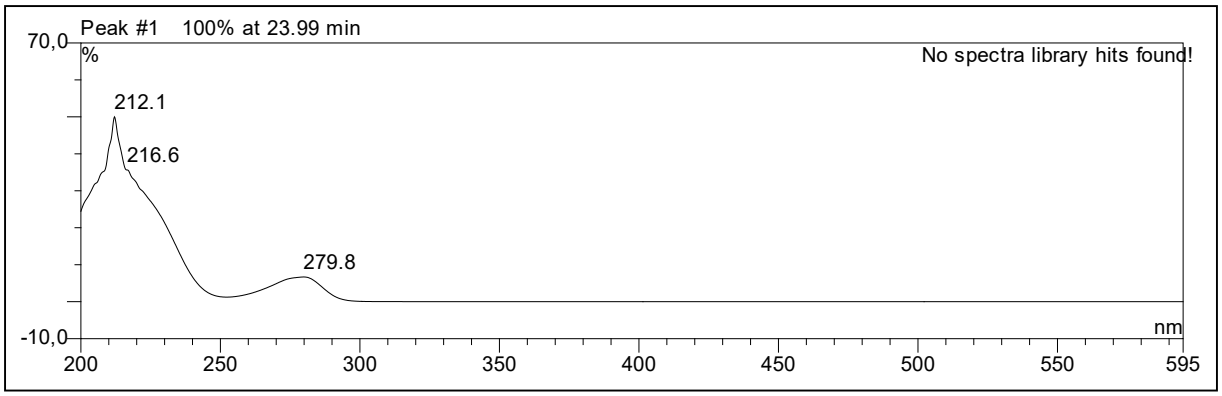

S48. UV-Vis spectrum (MeOH) of compound C

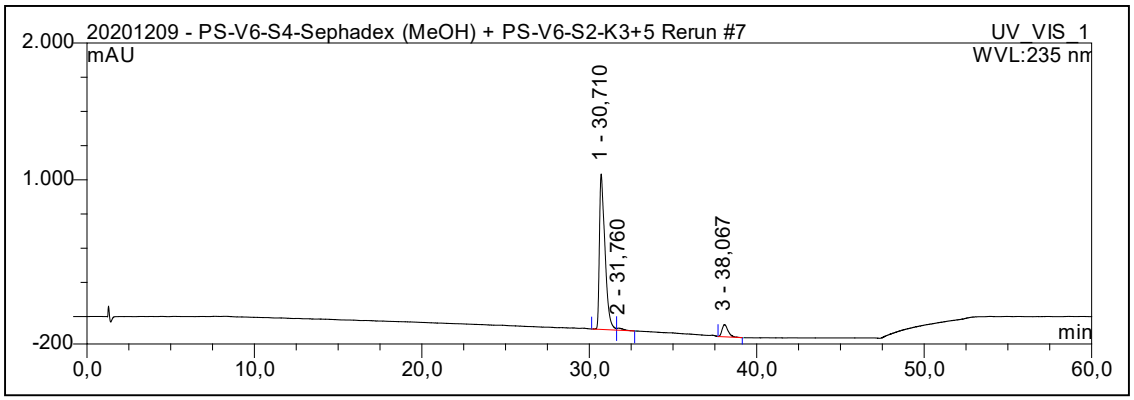

S49. HPLC chromatogram (MeOH) of compound D

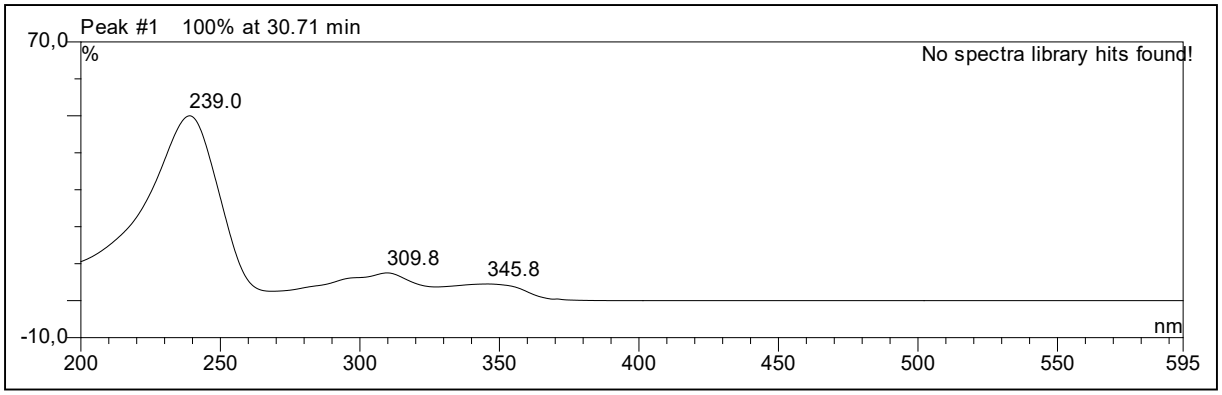

S50. UV-Vis spectrum (MeOH) of compound D

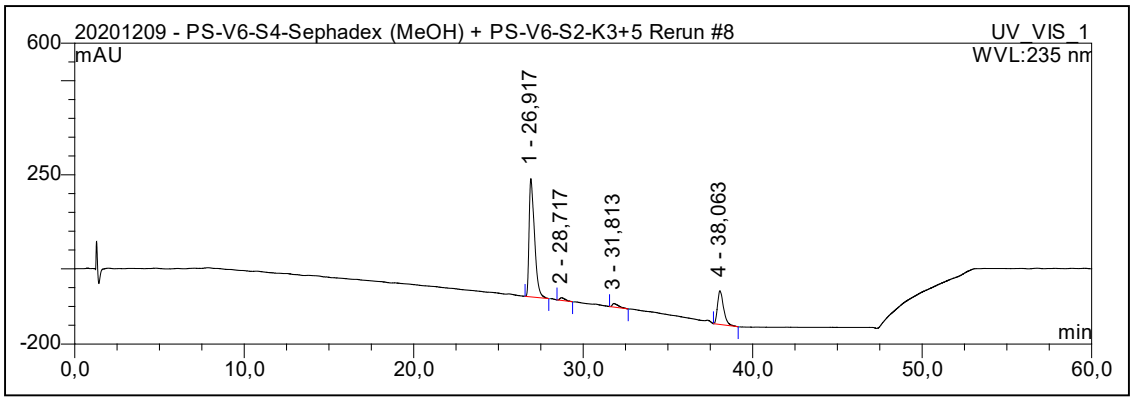

S51. HPLC chromatogram (MeOH) of compound E

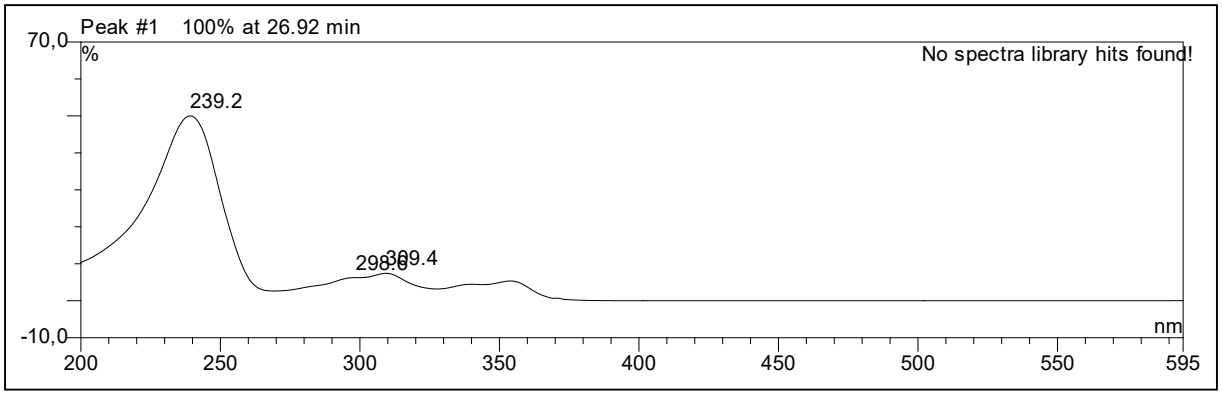

S52. UV-Vis spectrum (MeOH) of compound E

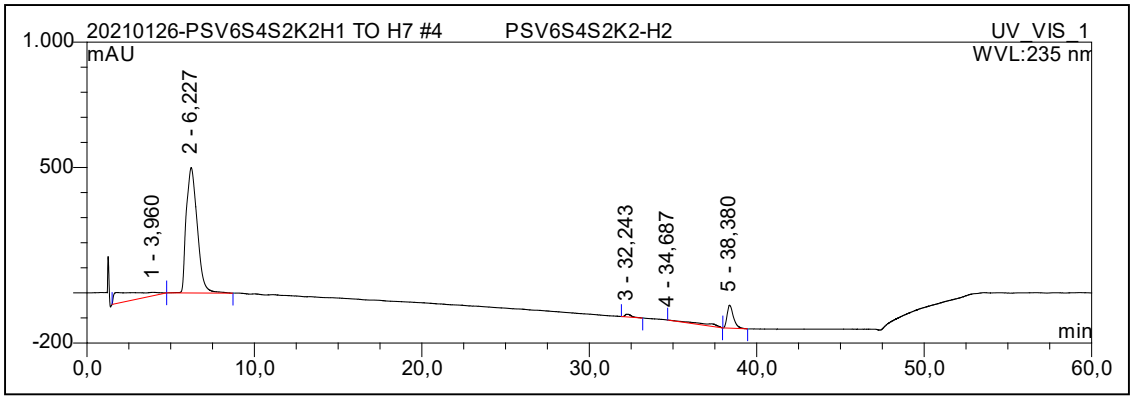

S53. HPLC chromatogram (MeOH) of compound F

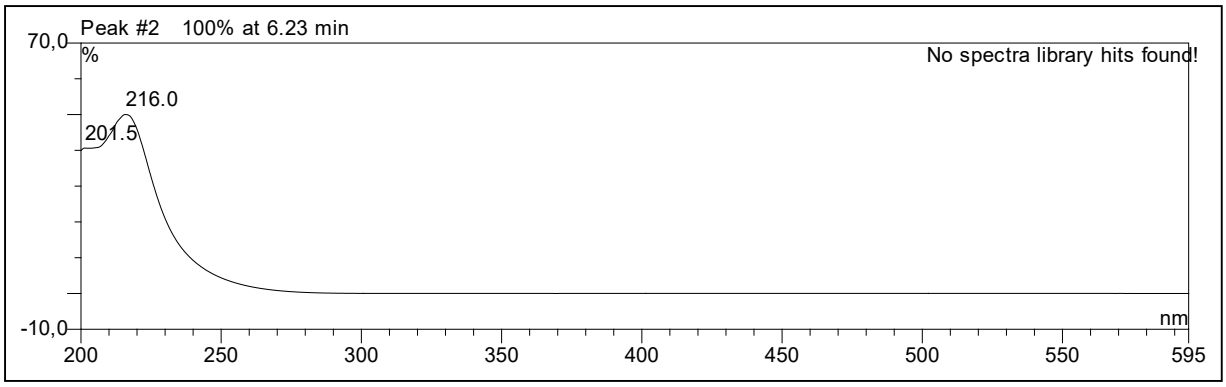

S54. UV-Vis spectrum (MeOH) of compound F

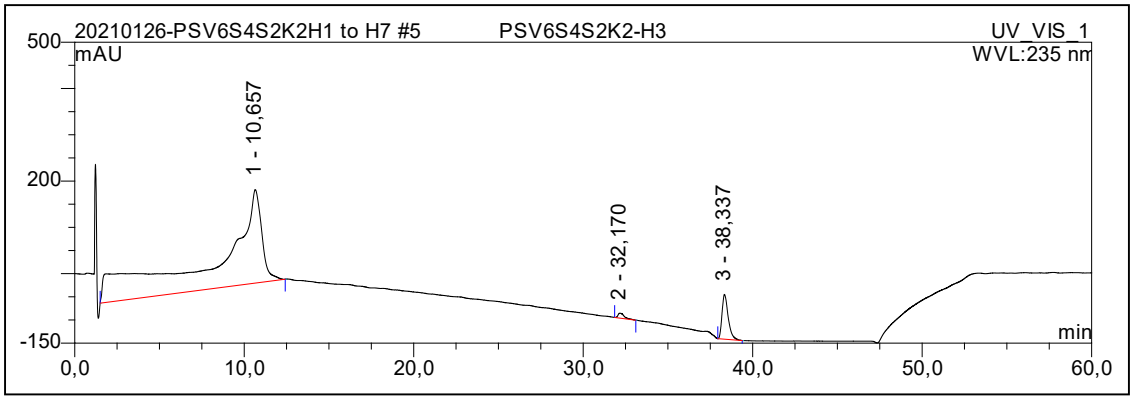

S55. HPLC chromatogram (MeOH) of compound G

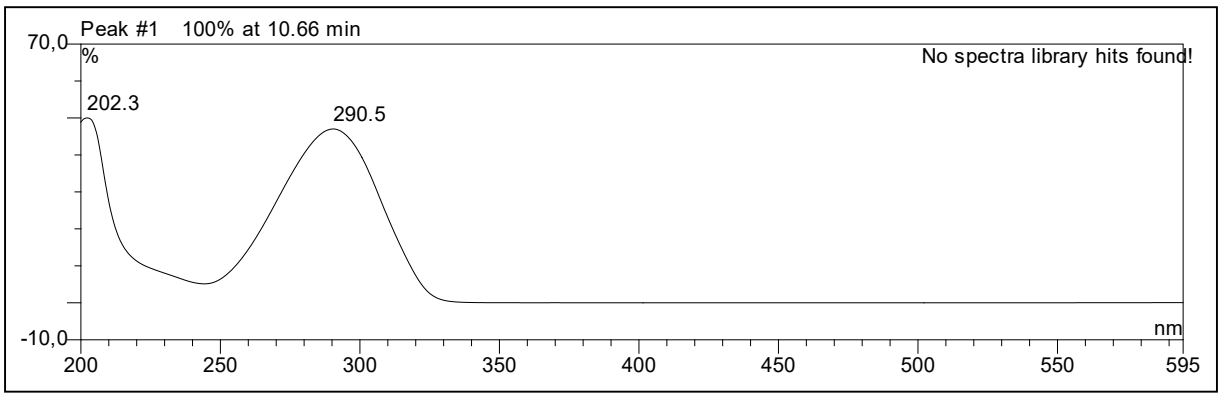

S56. UV-Vis spectrum (MeOH) of compound G

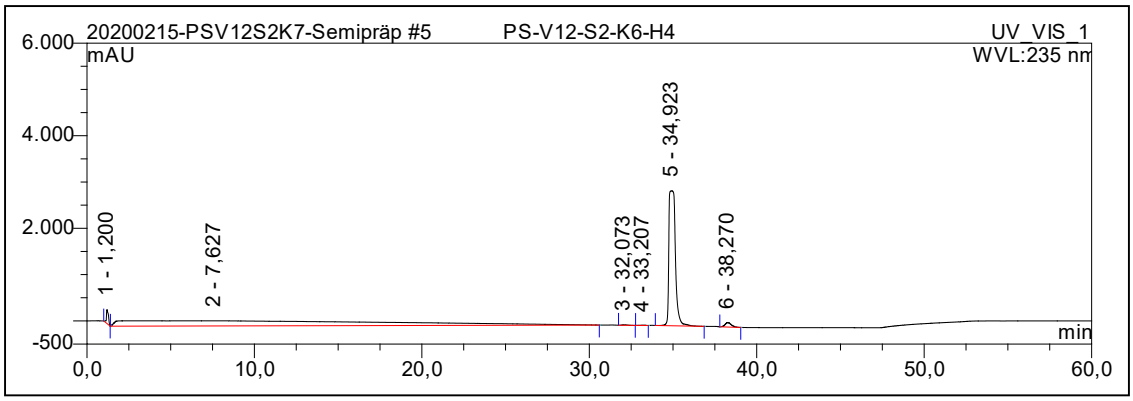

S57- HPLC-chromatogram (MeOH) of compound H

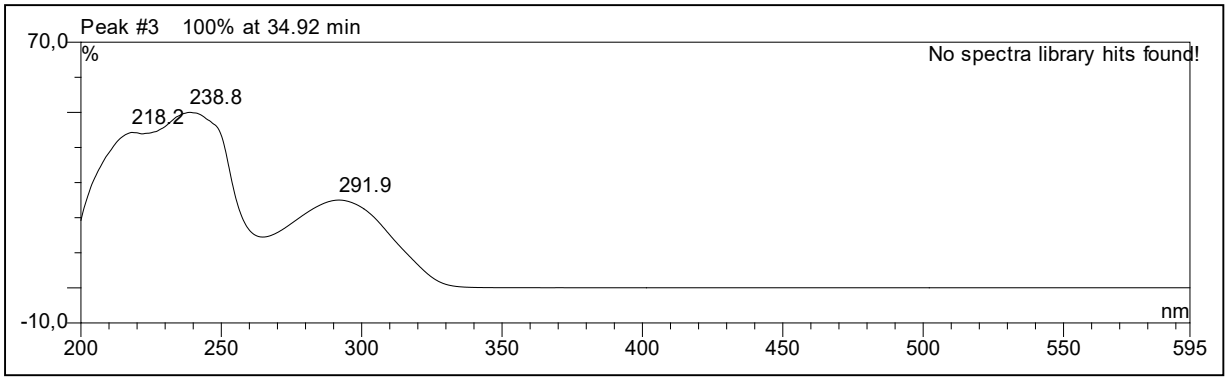

S58. UV-Vis spectrum (MeOH) of compound H

Stereochemical studies of F

The ROESY spectrum of **F** showed correlation between the 5-H and 6-H protons of the adjacent stereogenic centers indicating their *cis* relative configuration. Therefore the conformational analysis and chiroptical calculations were performed on the arbitrarily selected *cis*-(5*S*,6*S*) stereoisomer. The Merck molecular force field (MMFF) conformational search produced 16 conformers in a 21 kJ/mol energy window which were re-optimized at the ωB97X/TZVP PCM/MeCN and the B3LYP/TZVP PCM/$CHCl_3$ levels, separately, yielding 10 and 8 low-energy conformers over 1% Boltzmann population, respectively (Figures S60 and S61). In the low-energy computed conformers, the 5,6-dihydro-α-pyrone moiety adopted a conformation, which oriented the C-5 hydroxyl group to axial and the C-6 prop-1-en-1-yl substituent to equatorial position. ECD spectra computed at four levels for the ωB97X conformers gave acceptable agreement with the experimental ECD spectrum (Figure S59) with CAM-B3LYP/TZVP giving the best agreement. Optical rotation calculations performed for the same conformers at four levels and PCM solvent model for EtOH reproduced the large experimental positive value {$[\alpha]^{24}_D$ *+172}* in the range of +81 – +99 (Table S1). VCD spectra computed at the B3LYP/TZVP PCM/$CHCl_3$ level for the same level optimized conformers gave good agreement with the experimental VCD spectrum (Figure X3). That is, all three applied chiroptical methods suggested (5*S*,6*S*) absolute configuration for **F** allowing elucidation of the absolute configuration as (5*S*,6*S*).

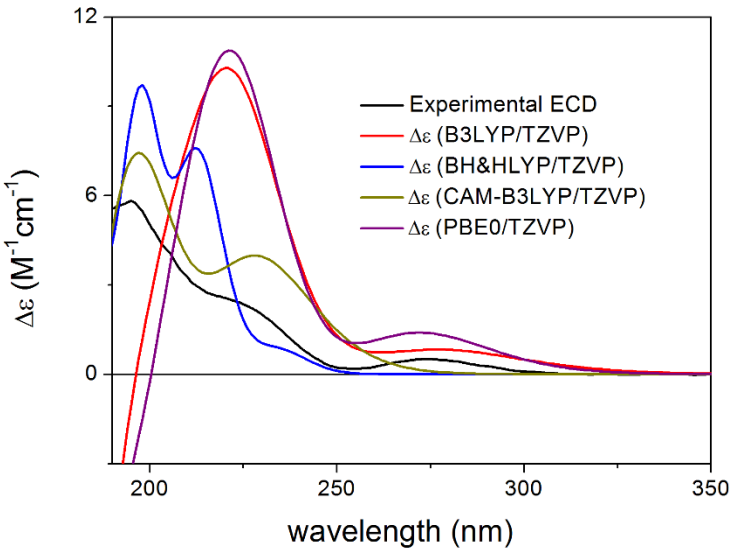

S59. Comparison of the experimental ECD spectrum of F measured in MeCN and the calculated ECD spectra of (5S,6S)-F computed at various levels of theory for the 10 lowest-energy ωB97X/TZVP PCM/MeCN conformers. Black: experimental, red: B3LYP/TZVP PCM/MeCN with half-height width 4200 cm^{-1}, blue: BH&HLYP/TZVP PCM/MeCN with half-height width 2100 cm^{-1}, olive: CAM-B3LYP/TZVP PCM/MeCN with half-height width 4200 cm^{-1}, purple: PBE0/TZVP PCM/MeCN with half-height width 4200 cm^{-1}.

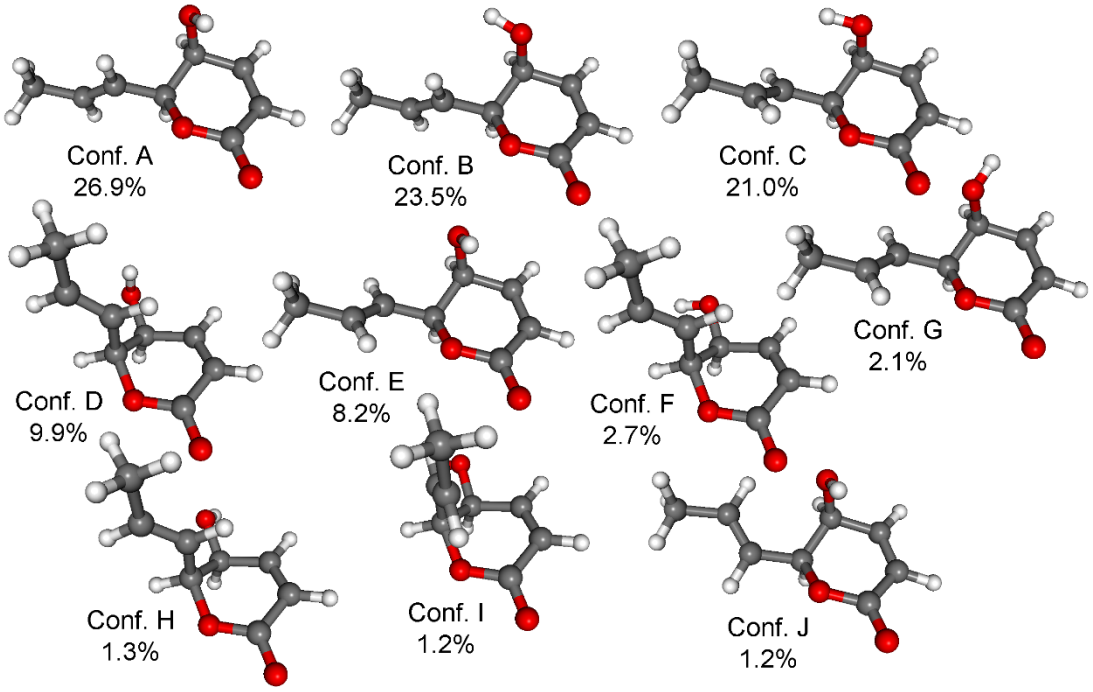

S60. Geometries of the low-energy ωB97X/TZVP PCM/MeCN conformers of (5S,6S)-F.

S61. Boltzmann populations and specific optical rotations of the low-energy conformers of (5S,6S)-F computed at various levels for the low-energy ωB97X conformers.

Conformer	Boltzmann population	B3LYP/TZVP PCM/EtOH	BH&HLYP/TZVP PCM/EtOH	CAM-B3LYP/TZVP PCM/EtOH	PBE0/TZVP PCM/EtOH
Conf. A	26.93%	134.70	98.20	104.21	130.74
Conf. B	23.55%	29.58	5.44	9.46	29.68
Conf. C	20.95%	214.32	199.47	197.39	211.76
Conf. D	9.90%	-104.45	-80.52	-97.75	-93.21
Conf. E	8.24%	211.30	192.34	193.43	209.37
Conf. F	2.73%	-128.11	-87.40	-111.23	-111.39
Conf. G	2.09%	228.43	189.15	199.16	223.73
Conf. H	1.32%	-56.67	-26.86	-45.34	-45.81
Conf. I	1.24%	-155.48	-96.97	-122.07	-146.94
Conf. J	1.19%	263.77	211.06	223.80	260.09
Average	N/A	98.79	81.43	81.10	98.73

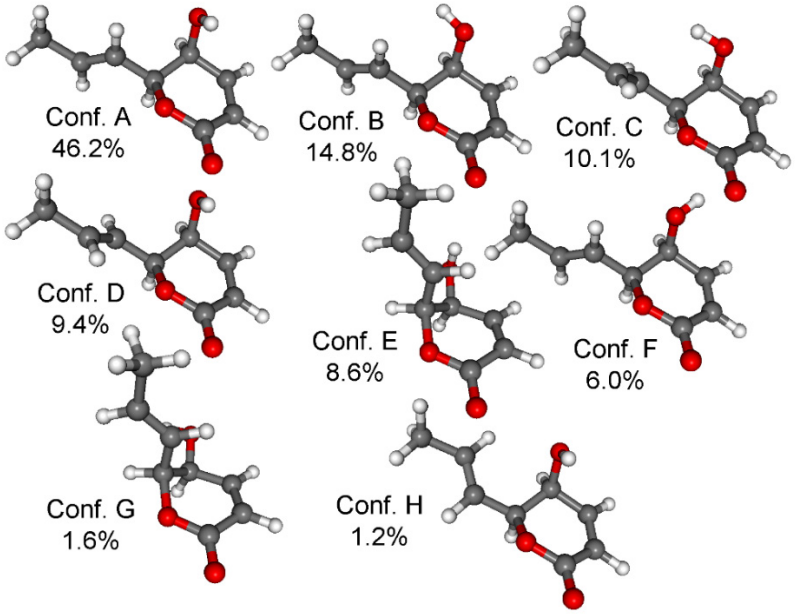

S62. Geometries of the low-energy B3LYP/TZVP PCM/CHCl3 conformers of (5S,6S)-F.

Computational details

Mixed torsional/low-frequency mode conformational searches were carried out by means of the Macromodel 10.8.011 software by using the MMFF with an implicit solvent model for $CHCl_3$ [1]. Geometry re-optimizations were carried out at the ωB97X/TZVP level with the PCM solvent model for MeCN and the B3LYP/TZVP level with PCM solvent model for $CHCl_3$. TDDFT-ECD and OR calculations were run with various functionals (B3LYP, BH&HLYP, CAMB3LYP, and PBE0) and the TZVP basis set as implemented in the Gaussian 09 package with the PCM/MeCN and the PCM/EtOH solvent models, respectively [2]. ECD spectra were generated as sums of Gaussians with 2100-4200 cm^{-1} width at half-height, using dipole-velocity-computed rotational strength values [3]. VCD spectra were generated with 8 cm^{-1} half-height width and scaled by a factor of 0.99. Boltzmann distributions were estimated from the ωB97X and the B3LYP energies. The Molekel software package was used for visualization of the results [4].

References

[1] MacroModel; Schrödinger LLC, 2015, http://www.schrodinger.com/MacroModel.

[2] Frisch, M. J.; Trucks, G. W.; Schlegel, H. B.; Scuseria, G. E.; Robb, M. A.; Cheeseman, J. R.; Scalmani, V.; Barone, G.; Mennucci, B.; Petersson, G. A.; Nakatsuji, H.; Caricato, M.; Li, X.; Hratchian, H. P.; Izmaylov, A. F.; Bloino, J.; Zheng, G.; Sonnenberg, J. L.; Hada, M.; Ehara, M.; Toyota, K.; Fukuda, R.; Hasegawa, J.; Ishida, M.; Nakajima, T.; Honda, Y.; Kitao, O.; Nakai, H.; Vreven, T.; Montgomery, J. A., Jr.; Peralta, J. E.; Ogliaro, F.; Bearpark, M.; Heyd, J. J.; Brothers, E.; Kudin, K. N.; Staroverov, V. N.; Kobayashi, R.; Normand, J.; Raghavachari, K.; Rendell, A.; Burant, J. C.; Iyengar, S. S.; Tomasi, J.; Cossi, M.; Rega, N.; Millam, J. M.;

Klene, M.; Knox, J. E.; Cross, J. B.; Bakken, V.; Adamo, C.; Jaramillo, J.; Gomperts, R.; Stratmann, R. E.; Yazyev, O.; Austin, A. J.; Cammi, R.; Pomelli, C.; Ochterski, J. W.; Martin, R. L.; Morokuma, K.; Zakrzewski, V. G.; Voth, G. A.; Salvador, P.; Dannenberg, J. J.; Dapprich, S.; Daniels, A. D.; Farkas, Ö.; Foresman, J. B.; Ortiz, J. V.; Cioslowski, J.; Fox, D. J. Gaussian 09 (Revision E.01); Gaussian, Inc.: Wallingford, CT, 2013.

[3] Stephens, P. J.; Harada, N. Chirality 2009, 22, 229–233.

[4] Varetto, U. MOLEKEL 5.4; Swiss National Supercomputing Centre: Manno, Switzerland, 2009.

5. Colletodiol derivatives of the endophytic fungus Trichocladium sp.

Manuscript draft (unpublished)

Overall contribution to the paper:

- Fermentation and extraction of the fungal culture
- Isolation of the fungal metabolites
- Spectral analysis of the isolated compounds
- Measurement of the optical rotations of chiral compounds
- Structure elucidation
- Writing of the first version of complete manuscript draft

Colletodiol derivatives of the endophytic fungus *Trichocladium sp*.

Viktor E. Simons[a], Marian Frank[a], Lasse van Geelen[a], Nam Tran-Cong[a], Dorothea Albrecht[a], Annika Coort[a], Christina Gebhard[a], and Rainer Kalscheuer*[,a]

[a]Institute of Pharmaceutical Biology and Biotechnology, Heinrich Heine University, Universitätsstrasse 1, 40225 Düsseldorf, Germany

*Corresponding author: rainer.kalscheuer@hhu.de (R. Kalscheuer)

Abstract: The OSMAC (one strain many compounds) concept is a cultivation-based approach to increase the diversity of secondary metabolites in microorganisms. In this study, we applied the OSMAC-approach to the endophytic fungus *Trichocladium sp.* by supplementation of the cultivation medium with 2.5 % phenylalanine. This experiment yielded five new compounds, trichocladiol (**1**), trichocladic acid (**2**), colletodiolic acid (**3**), colletolactone (**4**) and colletolic acid (**5**), together with five previously described ones (**6-10**). The structures were elucidated via comprehensive spectroscopic measurements, and the absolute configurations of compounds **1** and **3-5** was elucidated using CD calculations. For formation of compounds **3-5**, a pathway based on colletodiol biosynthesis is proposed. Compound **6** exhibited strong antibacterial activity against methicillin-resistant *Staphylococcus aureus* with a minimal inhibitory concentration (MIC) of 0.78 µM as well as a strong cytotoxic effect against the human monocytic cell line THP1 with an IC_{50} of 0.7 µM. Compound **8** showed moderate antibacterial activity against *Mycobacterium tuberculosis* with a MIC of 25 µM and a weak cytotoxic effect against THP1 cells with an IC_{50} of 42 µM.

Keywords: Trichocladium sp.; OSMAC; dihydronaphthalenone; macrocarpon; colletodiol precursors; biosynthesis; antibacterial activity; cytotoxicity

1. Introduction

Since the early 20th century, microorganisms derived from natural samples became a promising source for novel bioactive compounds. The isolation and characterization of penicillin in 1929 by Alexander Fleming marked the beginning of a new era of natural product-based drug discovery [1]. In 1940, Waksman and Woodruff firstly described soil microorganisms able to inhibit the growth of pathogenic bacteria and isolated the peptide antibiotic actinomycin [2]. This was the beginning of a prolific area of discovery of bioactive natural compounds from soil-derived microorganisms. The isolation of taxol from the endophytic fungus *Taxomyces andreanae* in 1993 then shed light onto endophytic microorganisms and showed a glimpse of their potential as a promising source of bioactive secondary metabolites [3]. Endophytic microorganisms live in a symbiotic relationship with their plant host and are able to release antibiotics and other compounds as a defense mechanism [4]. Previously studied plant species mostly contain at least one microbe, and growth in unique environmental surroundings often lead to the discovery of novel endophytes. Thus, the given opportunities for the isolation of promising microorganisms from plants are manifold [4, 5]. Under laboratory cultivation conditions, many biosynthetic gene clusters (BGCs) of microbes are not expressed in axenic cultures. This led to different approaches trying to activate these silent genes in order to isolate new cryptic metabolites [6]. A cultivation-based concept termed OSMAC (**O**ne **S**train **Ma**ny **C**ompounds) was described by Bode et al. in 2002 where even small changes in the cultivation conditions such as modification of the cultural medium, temperature or the introduction of co-cultivation attempts are able to activate silent gene clusters and thus can result in the discovery of new natural products [7]. Previous work has indicated that the endophytic fungus *Trichocladium sp.* is amenable to triggering of secondary metabolism by the OSMAC approach [8]. Building upon this observation, we now extended the OSMAC concept to an axenic culture of *Trichocladium sp.* by enrichment of solid rice medium with the amino acid L-phenylalanine. This fermentation yielded ten natural compounds including five new compounds (**1**-**5**) and five already described ones (**6**-**10**). The two macrolides colletoketol and colletodiol were isolated previously from cultures of *Trichocladium sp.*[8]. Compounds **3**-**5** now seem to represent intermediates or alternative metabolites of the fungal biosynthesis pathway for these macrolides. The molecular structures of the compounds **1**-**10** were elucidated using high-resolution electrospray ionization mass spectrometry (HRESIMS) combined with 1D- and 2D-NMR measurements. All isolated compounds were tested for their antimicrobial activity against the human pathogens *Staphylococcus aureus* ATCC 700699, *Pseudomonas aeruginosa* ATCC 87110, *Candida albicans* ATCC 24433 and *Mycobacterium tuberculosis* ATCC 27294, and for their cytotoxic activity against the THP1 human cell line.

2. Results and discussion

During our ongoing investigation of the endophytic fungus *Trichocladium sp.* HCRSW, which was isolated from roots of the Vietnamese plant *Houttuynia cordata*, we have already reported on the isolation of natural compounds resulting from an OSMAC-approach employing L-tryptophane feeding as well as from a fungal-bacterial co-cultivation experiment [8]. We now present the results of an additional OSMAC experiment employing 2.5% (w/v) phenylalanine supplementation to solid rice medium. HPLC-DAD chromatographic comparison of ethylacetate (EtOAc) extracts of the phenylalanine cultures to the control cultures revealed the presence of formerly undetected secondary metabolites in the semi-polar range. Chromatographic workup of the extract resulted in the isolation of the five known compounds chaetochromin A (**6**) [9], phenazine-1-carboxylic acid (**7**) [10], phenazine-1-carboxamide (**8**) [11], dechlorodihydromaldoxin (**9**) [12] and fuscoatramide (**10**) [13], as well as of five new compounds including a new dihydronapthalenone compound **(1)**, a new macrocarpon [14] derivative **(2)** and three new open chain derivatives **(3-5)** of the macrocyclic dilactones colletol [15] and colletodiol [16]. Colletodiol itself is a direct precursor of the antibiotic grahamimycin A1 [17], which is equal to colletoketon. Interestingly, compounds **3-5** are structurally closely related monoesters to colletodiol and dilactonic derivatives. The planar structures of all isolated compounds were unequivocally elucidated based on NMR and MS spectral data, and their bioactivity against several pathogenic microorganisms and the human THP1 cell line was investigated. We present the structure elucidation of new compounds **1-5** together with a proposal of a pathway to build compounds **3-5**.

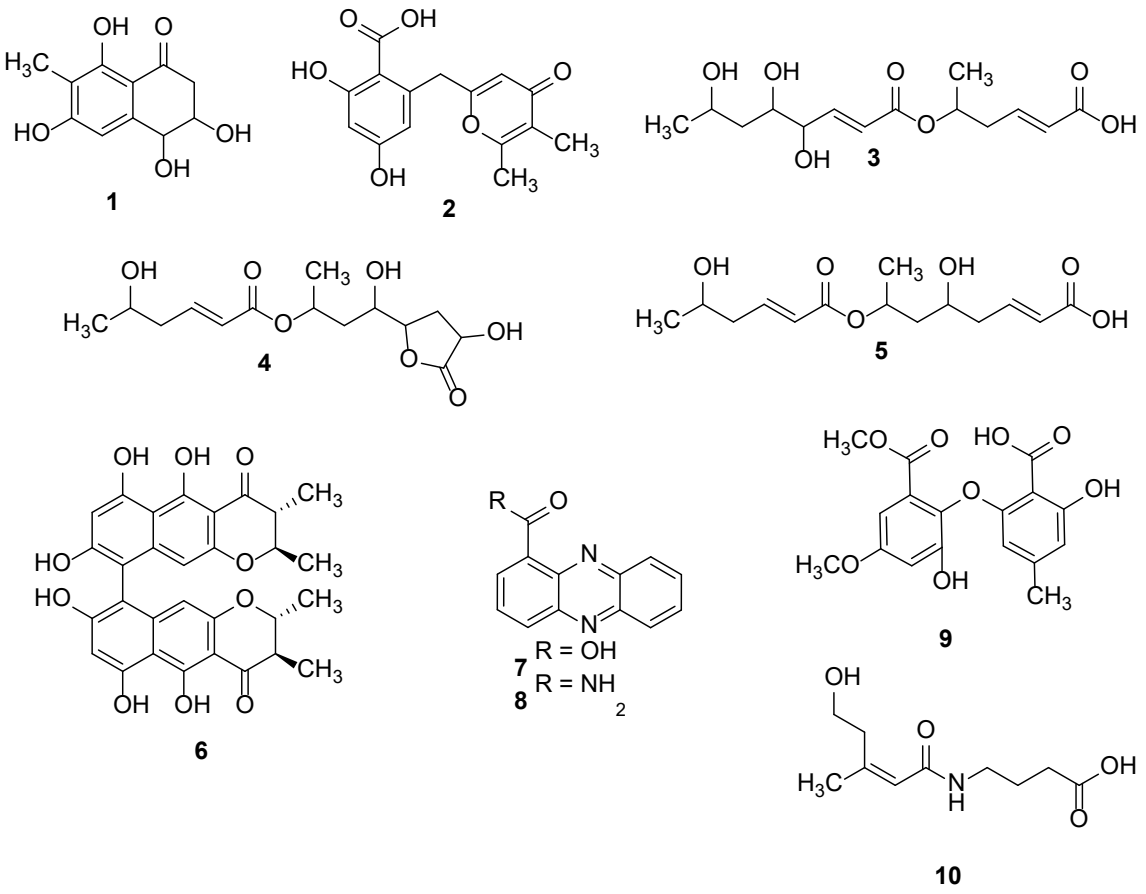

Fig. 1. Structures of isolated compounds from *Trichocladium sp.* resulting from OSMAC approach with 2.5% n(w/v) L-phenylalanine.

2.1 Structure elucidation

Structure elucidation of compound **1:**

Compound **1** was isolated as a yellowish solid and showed UV absorption maxima at 219 and 291 nm. Its molecular formula was assigned as $C_{11}H_{12}O_5$ based on its HRESIMS pseudomolecular ion peak at 225.0756 m/z (calcd. for $C_{11}H_{13}O_5$) with six degrees of unsaturation. When analyzing the ^{1}H- and ^{13}C-spectra (Table 1), the presence of a strongly deshielded, chelated δ 13.03 ppm (OH-8) and non-chelated phenol δ 10.56 ppm (6-OH), one aromatic singlet δ 6.61 ppm (H-5) and one aromatic methyl singlet δ 1.93 ppm (CH_3-9) suggested the presence of a pentasubstituted phenyl ketone unit. This was confirmed by detailed analysis of the HMBC correlation from H-5 to quaternary C-7 (δ 108.5 ppm), C-8a (δ 108.5 ppm) and C-4a (δ 144.6 ppm) and from chelated OH-8 to adjacent quaternary C-8 (δ 162.0 ppm), C-7 and C-8a. The relative configuration can be accessed through the NOESY measurement. Because H-3 (δ 4.29 ppm, acetone-d6) and H-4 (δ 4.77 ppm, acetone-d6) give a clear cross signal, both atoms have the same axial orientation, showing that atoms H-3 and H4 are syn-positioned. The absolute configuration was then calculated on the basis of CD measurements.

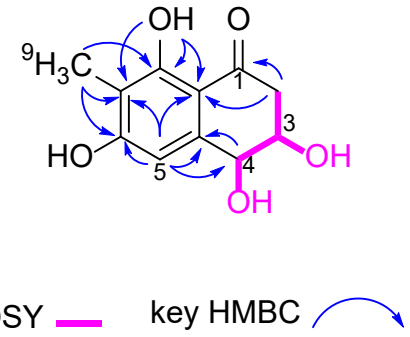

Figure 2: Key NMR correlations for **1**

Table 1: NMR data for **1** (measured in DMSO-d_6 , MeOH-d_4 and acetone-d_6 at 150 Hz and 600 MHz, respectively)

position	δ_C* DMSO-d_6	δ_H, m (*J* in Hz) DMSO-d_6	δ_H, m (*J* in Hz) MeOH-d_4	δ_C Acetone-d_6	δ_H, m (*J* in Hz) Acetone-d_6
1	201.2, C			201.7, C	
2	43.1, CH_2	2.80, dd (17.2, 3.4) 2.66, dd (17.2, 5.8)	2.88, dd (17.2, 3.9) 2.77, dd (17.2, 7.4)	43.7, CH_2	2.83, d (3.6)
3	69.0, CH	4.11, m	4.20, ddd (7.4, 3.9, 2.9)	70.3, CH	4.29, br s
3-OH		4.94, d (4.1)			4.12, d (4.6)
4	68.9, CH	4.61, dd (6.7, 2.0)	4.70, d (2.9)	70.8, CH	4.77, br s
4-OH		5.38, d (6.7)			4.41, d (6.7)
4a	144.6, C			144.8, C	
5	105.8, CH	6.61, br s	6.58, s	107.4, CH	6.72, s
6	162.9, C			163.6, C	
6-OH		10.56, br s			9.38, br s
7	108.5, C			111.0, C	
8	162.0, C			163.6, C	
8-OH		13.03, s			13.09, s
8a	108.5, C			111.5, C	
9	6.9, CH_3	1.93, s	2.02, s	7.5, CH_3	2.03, s

*Signals were extracted from HSQC and HMBC spectra.

Structure elucidation of compound **2**:

Compound **2** was isolated as a white powder and showed UV absorption maxima at 256 and 300 nm. The molecular formula was assigned as $C_{15}H_{14}O_6$ based on its HRESIMS pseudomolecular ion peak at 291.0866 m/z (calcd. for $C_{15}H_{15}O_6$) with nine degrees of unsaturation. Analysis of the ^{1}H-NMR spectrum (Table 2) showed strongly deshielded aromatic OH-groups with δ 10.14 ppm (3-OH) and 13.22 ppm (1-OH), three aromatic protons H-4 (δ 6.20 ppm), H-6 (δ 6.20 ppm) and H-10 (δ 5.67 ppm), a methylenic group H-8 (δ 4.11 ppm) and two methyl groups H-14 (δ 2.24 ppm) and H-15 (δ 1.77 ppm). Analysis of the HMBC correlations of the three aromatic protons revealed H-4 and H-6 being meta-positioned in a tetrasubstituted phenyl group, while H-10 is positioned in a different aromatic ring system. HMBC correlations from H-8 to C-10 (δ 110.9 ppm), C-2 (δ 106.4 ppm) and C-6 (δ 110.9 ppm) highlighted H-8 being a methylene group connecting two aromatic ring systems. HMBC correlations from H-4 to C-1 (δ 172.4 ppm), C-2 and C-3 (δ 164.2 ppm), H-5 to C-2 and C-5

(δ 161.6 ppm) and H-8 to C-2, C-6 and C-7 (δ 139.0 ppm) revealed the structure of a dihydroxybenzoic acid moiety, while HMBC correlations from H-8 to C-9 (δ 167.7 ppm) and C-10, from H-10 to C-11 (δ 178.3 ppm) and C-12 (δ 119.6 ppm), from H-14 to C-12 and C-13 (δ 161.3 ppm) and adjacent H-15 to C-11, C-12, C-13 and C-14 (δ 17.4 ppm) elucidated the structure of a dimethyl-pyranone.

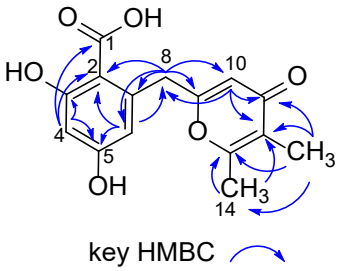

Figure 3: Key NMR correlations for **2**

Table 2: NMR data for **2** (measured in DMSO-d_6 at 150 Hz and 600 MHz, respectively)

position	δ_C*	δ_H, m (J in Hz)
1	172.4, C	
2	106.4, C	
3	164.2, C	
4	101.6, CH	6.20, br s 2H
5	161.6, C	
6	110.9, CH	6.20, br s 2H
7	139.0, C	
8	38.2, CH_2	4.11, s
9	167.7, C	
10	110.9, CH	5.67, s
11	178.3, C	
12	119.6, C	
13	161.3, C	
14	17.4, CH_3	2.24, d (0.9)
15	9.3, CH_3	1.77, d (0.9)
1-OH		13.22, br s
3-OH		10.14, s

*Signals were extracted from HSQC and HMBC spectra.

Structure elucidation of compound **3**:

Compound **3** was isolated as a yellowish oil and showed only one UV absorption maximum at 218 nm near the solvent cut-off. The molecular formula was assigned as $C_{14}H_{22}O_7$ based on its HRESIMS pseudomolecular ion peak at 303.1439 m/z (calcd. for $C_{15}H_{23}O_7$) with four degrees of unsaturation. Detailed analysis of ^{1}H-NMR, ^{13}C-NMR, COSY and HSQC spectra revealed two distinct spin systems starting from an *E*-double bond (H-2/H-3 and H-8/H-9) connected to an oxygenated alkyl chain ending in a terminal methyl moiety each. The *E*-double bonds both exhibit asymmetrically deshielded protons (H-2/H-8: 5.8-6.0 ppm and H-3/H-9: 6.7-7.0 ppm) suggesting an adjacent carbonyl

moiety. Furthermore, investigation of the HMBC spectrum revealed these two carbonyl moieties to be esters or carboxylated by observing the correlation of H-3 (δ_H 6.74 ppm) to C-1 (δ_C 166.9 ppm) and H-9 (δ_H 6.97ppm) to C-7 (δ_C 165.2 ppm). With this information, COSY, HSQC and HMBC revealed two scaffold subunits. Carbons C-1 to C-6 formed a hex-2-enoic acid substructure with an oxygenated position CH-5 (δ_H 4.99 ppm, δ_C 68.9 ppm) and C-7 to C-14 formed an oct-2-enoic acid substructure with oxygenated positions CH-10 (δ_H 4.12 ppm, δ_C 72.8 ppm), CH-11(δ_H 3.61 ppm, δ_C 71.5 ppm) and CH-13(δ_H 3.78 ppm, δ_C 64.5 ppm). Connection of these subunits was determined to be through an ester bond between position CH-5 and carboxyl C-7 based on HMBC correlation from H-5 to C-7 and the stronger relative deshielding of H-5 (δ_H 4.99 ppm) when compared to other oxygenated methin protons (δ_H < 4.12 ppm) in the molecule. The remaining oxygenated methins where determined to be hydroxyl moieties based on the calculated molecular formula, as there were no missing degrees of unsaturation. Thus, the planar structure of **3** was elucidated as shown. The compound may be interpreted as a linear non-lactonized precursor to colletodiol [18], which has been isolated from this fungal strain before [8].

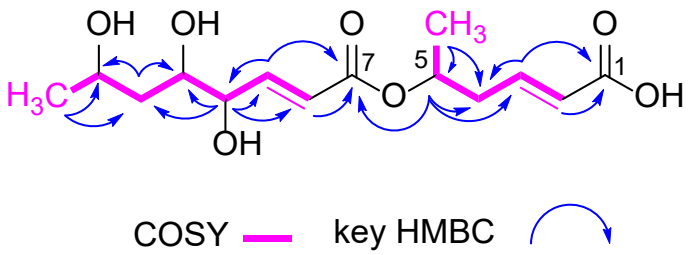

Figure 4: Key NMR correlations for **3**

Table 3: NMR data for **3** (measured in DMSO-d_6 at 150 Hz and 600 MHz, respectively)

position	δ_C	δ_H, m (J in Hz)
1	166.9, C	
2	124.6, CH	5.83, dt (15.6, 1.5)
3	143.7, CH	6.74, dt (15.6, 7.3)
4	37.6, CH_2	2.48, m 2H
5	68.9, CH	4.99, m
6	19.6, CH_3	1.21, d (6.3) 3H
7	165.2, C	
8	120.0, CH	5.96, dd (15.7, 1.9)
9	150.1, CH	6.97, dd (15.7, 4.1)
10	72.8, CH	4.12, m
11	71.5, CH	3.61, dt (9.4, 4.0)
12	41.0, CH_2	1.42, ddd (13.6, 6.3, 3.7) 1.35, ddd (13.6, 9.4, 6.7)
13	64.5, CH	3.78, m
14	23.4, CH_3	1.04, d (6.2) 3H

Structure elucidation of compounds **4** and **5**:

Compound **4** was isolated as a colorless oil and showed only one UV absorption maximum at 218 nm near the solvent cutoff. Its molecular formula was determined as $C_{14}H_{22}O_7$ with four degrees of unsaturation. This was based on the HRESIMS signals of the pseudomolecular ion at 303.1442 m/z and ammonium adduct at 320.1708 m/z, which calculated for $C_{14}H_{23}O_7$ and $C_{14}H_{26}NO_7$, respectively. Analysis of the ^{1}H- and ^{13}C-NMR spectra revealed a high degree of similarity to **3**. The common substructure was revealed to be a similar oxygenated hex-2-enoic acid subunit with *E* configuration (*J* 15.6 Hz) between CH-10 (δ_H 5.85 ppm, δ_C 122.7 ppm) and CH-11 (δ_H 6.89 ppm, δ_C 146.6 ppm). The major difference compared to **3** was the relative shielding (- 1.24 ppm) of the oxygenated methin CH-13 (δ_H 3.74 ppm, δ_C 65.0 ppm) and the presence of hydroxyl 13-OH (δ_H 4.67 ppm), which was detectable via COSY correlation to H-13. This confirmed the connection to the remaining molecule to be established through an ester bond via carbonyl C-9 (δ_C 165.0 ppm) rather than through a hydroxyl function as in **3**. Detailed analysis of the COSY spectrum revealed that the remaining signals all belonged to a single second spin system starting from a terminal methyl CH_3-8 (δ_H 1.22 ppm), which is connected to a series of oxygenated methin protons CH-7 (δ_H 5.04 ppm), CH-5(δ_H 3.51 ppm), CH-2(δ_H 4.45 ppm) and methylene units CH_2-3 (δ_H 2.38/1.87 ppm), CH_2-6 (δ_H 1.78/1.59 ppm), ending in a tertiary alcohol 2-OH (δ_H 5.19 ppm). Analysis of the HMBC spectrum revealed the connection to the *(E)*-5-hydroxyhex-2-enoic acid subunit through ester bond with oxygenated methin CH-7 via correlation from H-7 to C-9, as well as the deshielded chemical shift of H-7 compared to the remaining oxygenated methin units (δ_H 5.04 ppm). Furthermore, HMBC correlations from H-2 and H-3 revealed an adjacent carbonyl C-1 (δ_C 177.0 ppm) with unusually strong deshielding, suggesting incorporation into a five membered ring system. This ring system was established as a lactone bond between carboxylate C-1 and oxygenated methin C-4 (δ_C 78.3 ppm) which is in agreement with the unusually strong deshielding of both carbons. The position of the hydroxyl moiety 5-OH (δ_H 5.19 ppm) was unequivocally determined via COSY correlation to H-5. Thus, all signals and degrees of unsaturation were assigned and the planar structure of **4** was elucidated as shown. The proposed structure reflects the same biosynthetic building blocks for colletodiol as **3** with a reversed order of the hex-2-enoic acid and oct-2-enoic acid. Additionally, a water molecule was added to the *E* double bond of the oct-2-enoic acid, thus removing the stereochemical obstacle and allowing for intramolecular lactonization to take place.

Compound **5** was isolated as a colorless oil and exhibited one UV absorption maximum at 219 nm near the solvent cutoff. The molecular formula was determined to be $C_{14}H_{22}O_6$ based on the HRESIMS pseudomolecular ion signal at 287.1492 m/z and ammonium adduct ion signal at 304.1759 m/z, which were calculated for $C_{14}H_{23}O_6$ and $C_{14}H_{26}NO_6$, respectively. This molecular formula suggested **5** to be a desoxy derivative of **3** or **4**. Comparison of ^{1}H-, ^{13}C-NMR, COSY, HSQC and HMBC spectra of **5** with those of **3** and **4** revealed that **5** contains a terminal (*E*)-5-hydroxyhex-2-enoic acid subunit identical to the one expressed in **4** with proton chemical shifts differing less than

0.1 ppm and carbon chemical shifts less than 0.4 ppm. Analysis of COSY for the remaining signals revealed a singular additional spin system consisting of an *E* double bond (*J* 15.7 Hz) between H-2 (δ_H 5.66 ppm) and H-3 (δ_H 6.66 ppm), followed up by alternating methylene CH_2-4 (δ_H 2.37/2.26 ppm), CH_2-6 (δ_H 1.78/1.54 ppm) and oxygenated methin protons CH-5 (δ_H 3.37 ppm), CH-7 (δ_H 4.76 ppm) and ending in a terminal methyl unit CH_3-8 (δ_H 1.17 ppm). Analysis of HMBC correlations from H-3 revealed carboxylic C-1 (δ_C 167.2 ppm), and the connection to the (*E*)-5-hydroxyhex-2-enoic acid subunit via ester bond was established based on the HMBC correlation of H-7 to C-9 (δ_C 165.1 ppm), as well as the strongly deshielded chemical shift of H-7. Furthermore, the position of hydroxyl unit 5-OH (δ_H 4.71 ppm) was ascertained based on its COSY correlation to H-5, thus unequivocally confirming the second part of the structure to be a (*E*)-7, 5-dihyroxy-oct-2-enoic acid. Thus, the planar structure of **5** was elucidated as shown.

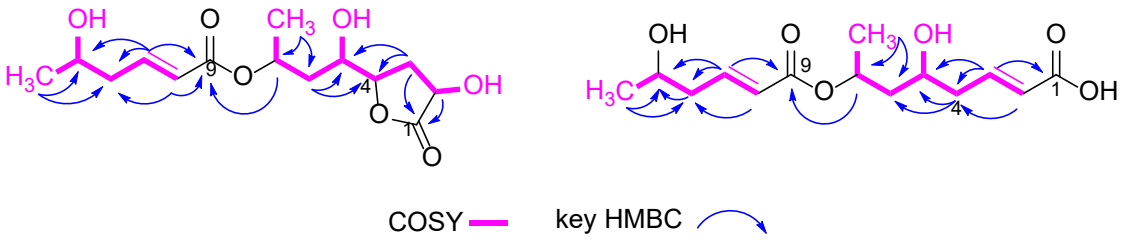

Figure 5: Key NMR correlations for compounds **4** (left) and **5** (right).

Table 4: NMR data for compounds **4** and **5** (measured in DMSO-d_6 at 150 Hz and 600 MHz, respectively)

position	compound **[4]**		compound **[5]**	
	δ_C	δ_H, m (*J* in Hz)	δ_C	δ_H, m (*J* in Hz)
1*	177.0, C		167.2, C	
2	67.4, CH	4.45, dd (11.2, 8.1)	122.5, C	5.66, dd (15.7, 0.9)
2-OH		5.89, m		
3	32.8, CH_2	2.38, ddd (12.0, 8.6, 5.4) 1.87, dt (12.0, 10.9)	149.3, CH	6.66, dd (15.7, 9.1)
4	78.3, CH	4.21, dt (10.3, 5.1)	41.2, CH_2	2.37, ddd (15.7, 8.1, 3.7) 2.26, m 3H
5	67.8, CH	3.51, q (4.5)	63.7, CH	3.37, dt (6.3, 3.6)
5-OH		5.19, d (5.7)		4.71, br s
6	38.3, CH_2	1.78, ddd (13.5, 9.3, 5.5) 1.59, ddd (13.5, 8.1, 4.1)	36.2, CH_2	1.78, ddd (13.8, 9.7, 3.8) 1.54, ddd (13.9, 10.3, 3.5)
7	67.9, CH	5.04, dp (8.0, 6.3)	68.0, CH	4.79, dqd (9.7, 6.1, 3.4)
8	19.3, CH_3	1.22, d (6.2) 3H	20.1, CH_3	1.17, d (6.2)
9*	165.0, C		165.1, C	
10	122.7, CH	5.85, dt (15.6, 1.5)	122.1, CH	5.84, dt (15.6, 1.5)
11*	146.6, CH	6.89, dt (15.6, 7.3)	146.8, CH	6.89, dt (15.6, 7.3)
12	41.4, CH_2	2.25, m 2H	41.2, CH_2	2.26, m 3H
13	65.0, CH	3.74, h (6.1)	64.6, CH	3.75, m
13-OH		4.67, br s		not detected
14	23.4, CH_3	1.05, d (6.2) 3H	23.0, CH_3	1.06, d (6.2)

*Signals were extracted from HSQC and HMBC spectra.

2.2 Determination of antibacterial activity

Compounds **1-10** were tested in a minimal inhibitory concentration assay against methicillin resistant *Staphylococcus aureus* ATCC 700699 (MRSA), *Pseudomonas aeruginosa* ATCC 87110, *Candida albicans* ATCC 24433 and *Mycobacterium tuberculosis* ATCC 27294. None of the new compounds (**1-5**) showed inhibition against the pathogenic microorganisms in concentrations up to 100 µM. The cytotoxic mycotoxin chaetochromin A [19] (**6**) on the other hand showed strong inhibition against MRSA with a MIC_{90} of 0.78 µM, which fits antibacterial activity against *S. aureus* reported in the literature [20]. Interestingly, compound **8** showed a moderate inhibition of *M. tuberculosis* with a MIC_{90} of 25 µM, whereas its carboxylic acid derivative (**7**) showed no inhibition even at 100 µM. The results are shown in Table 5.

Table 5: MIC_{90} against *S. aureus* ATCC 700699, *P. aeruginosa* ATCC 87110, *C. albicans* ATCC 24433 and *M. tuberculosis* H37Rv. All concentrations are shown in µM. Concentration >100 µM indicate no activity in the experimental setup. Values represent means of experiments conducted in triplicates.

	MIC_{90} [µM]			
Compound	***S. aureus* ATCC 700699**	***P. aeruginosa* ATCC 87110**	***C. albicans* ATCC 24433**	***M. tuberculosis* ATCC 27294**
1	>100	>100	>100	>100
2	>100	>100	>100	>100
3	>100	>100	>100	>100
4	>100	>100	>100	>100
5	>100	>100	>100	>100
6	0.78	>100	>100	>100
7	>100	>100	>100	>100
8	>100	>100	>100	25
9	>100	>100	>100	>100
10	>100	>100	>100	>100

2.3 Determination of cytotoxic activity

Compounds **1-10** were also tested for cytotoxic potential against the human monocytic cell line THP-1 using a resazurin assay. The mean IC_{50} values are shown in table 6. Compound **6** (chaetochromin A) had a strong cytotoxic effect with 0.7 µM that is similar to values described in the literature [19], while compound **8** (phenazin-1-carboxamide) had a weak cytotoxic effect with 42 µM on the THP-1 cell line. All remaining compounds including the five new compounds **1-5** showed no cytotoxic effect up to a concentration of 100 µM.

Table 6: IC_{50} values of the isolated compounds **1-10** against human cell line THP1. All concentrations are shown in µM. Concentrations >100 µM indicate no activity in the experimental setup. Values represent means of experiments conducted in triplicates. IC_{50} values were calculated using GraphPad Prism 7.

Compound	**Mean IC_{50} [µM]**
1	>100
2	>100
3	>100
4	>100
5	>100
6	0.7
7	>100
8	42
9	>100
10	>100

2.4 Proposed biosynthesis of linear colletodiol-derivatives

Structures of compounds **3-5** suggest that they represent direct precursors or alternative metabolites of the macrocyclic dilactones colletodiol and of close biosynthetic derivatives like colletol and colletoketol. It seems that this variation is related to one of the later biosynthetic steps, in which the closed ring form of the metabolites is being formed [21, 22]. The last steps of the biosynthetic pathway of colletodiol and derivatives as proposed by O'Neill *et al*. [22] are presented in Figure 6.

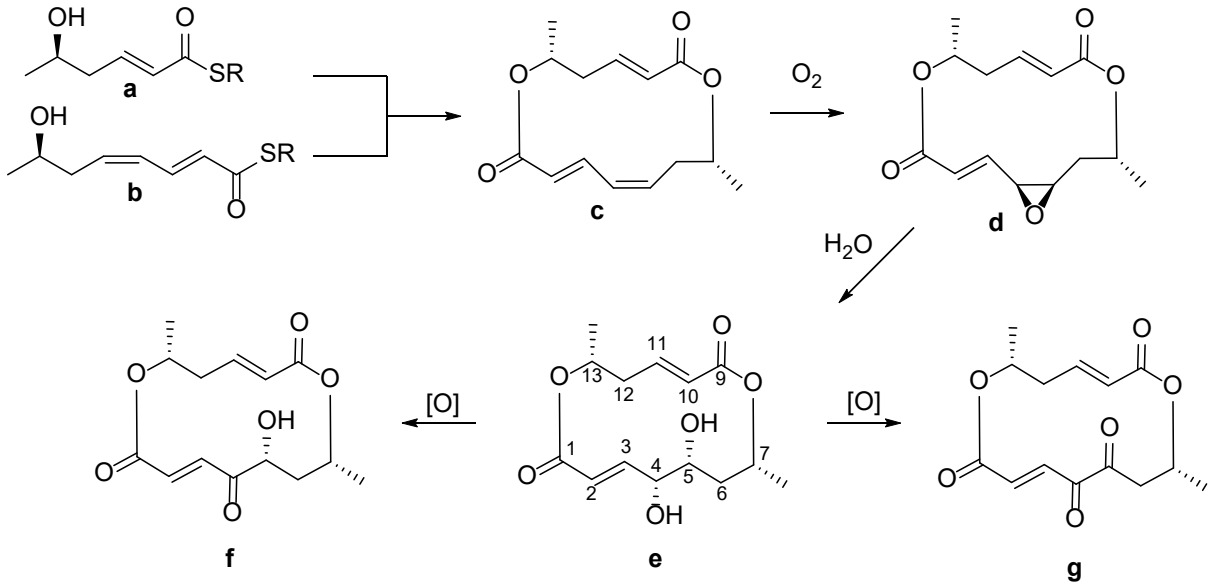

Figure 6: Biosynthesis of colletodiol (**e**), colletoketol (**f**) and colletoketon (**g** = grahamimycin A1) from **a** and **b** as described by O'Neill *et al*. [22]. After cyclisation of **c**, an oxidative step introduces an epoxide group to form intermediate **d**. Hydrolysis of the epoxide leads to colletodiol, which can be oxidized to yield colletoketol and colletoketon.

On the basis of the given information about the biosynthetic pathway of colletodiol and derivatives in *Cytospora sp*. from the literature [21, 22], we propose a possible biosynthetic pathway in Figure 7 that leads to the production of compounds **3-5**. However, it remains unclear whether the colletodiol biosynthetic pathways of *Cytospora sp.* and *Trichocladium sp.* are identical.

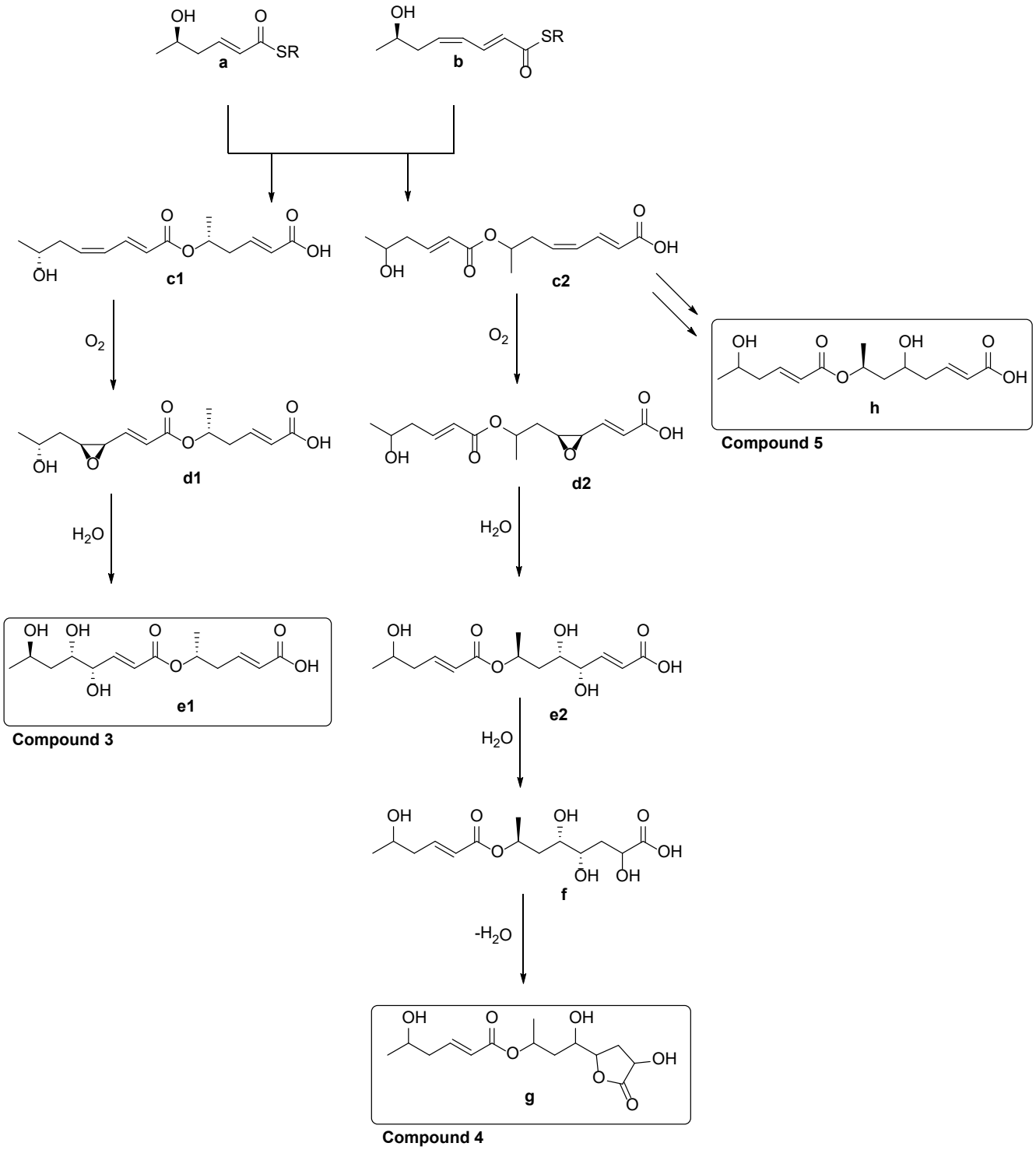

Figure 7: Proposed biosynthesis to form compounds **3-5**. An alternative route starting from **a** and **b** results in the two different linear monoesters **c1** and **c2**. The following biosynthetic steps are likely similar to those of colletodiol biosynthesis, yielding **e1 (compound 3)** and **e2** over **d1** and **d2**. **g (compound 4)** and **h (compound 5)** might be formed from **e2** over **f** and **c2**, respectively, through undescribed metabolic steps.

3. Experimental section

3.1 General experimental procedures

Optical rotations were measured on a Jasco P-2000 polarimeter. UV-spectra were obtained using a Dionex P580 system in combination with a diode array detector (UVD340S) and an Eurosphere 10 C18 column (125 x 4 mm) with a flow rate of 1 ml/min. 1D and 2D NMR spectra were recorded on a Bruker Avance III (^{1}H, 600 MHz; ^{13}C 150 MHz) spectrometer. Mass spectra were obtained on a Finnigan LCQ Deca (Thermo Quest) mass spectrometer and for HRESIMS on a UHR-QTOF maXis 4G (Bruker Daltonics) mass spectrometer. Semipreperative HPLC was performed on a Lachrom-Merck Hitachi system (pump L7100, UV-detector L7400, Eurospher 100 C18 column, 300 x 8 mm, Knauer Germany) and a Knauer system (pump Azura P6.1L, autosampler Smartline 3950, UV-detector Smartline 2600, autocollector FOXY R1, column thermostat CT 2.1), respectively, with a flow rate of 5 ml/min. Precoated TLC silica gel 60 F254 plates (Merck) were used for tracking separation using detection under UV-light at 254 and 365 nm wavelengths or spraying with anisaldehyde-sulfuric acid reagent. VLC and non-vacuum-column chromatography was accomplished using Macherey Nagel silica gel 60M (0.04-0.063 mm). Sephadex LH20 and RP18 was used as stationary phase for column chromatography. For the measurement of optical rotations, spectral grade solvents were used.

3.2 Fungal material

The isolation and identification of the endophytic fungus was described by Tran-Cong *et al.* [8]. Briefly, the fungus was isolated from the roots of the plant *Houttuynia cordata* (voucher specimen GOET038305, Göttingen University Herbarium) as an endophyte and was identified as *Trichocladium sp.* by sequencing of the ITS-sequence and data base comparison via the NCBI Blast tool (accession number MK241585). The voucher strain is deposited in the Institute of Pharmaceutical Biology and Biotechnology, Heinrich Heine University, Düsseldorf, Germany, under the code HCRSW.

3.3 Fermentation and extraction

Fermentation of the fungus was carried out in ten 1-L Erlenmeyer flasks using solid rice medium enriched with L-phenylalanine. For this, for each flask 2.5 g of phenylalanine were dissolved in 100 ml water and then added to 100 g of rice followed by autoclaving. Agar plates section of 1 x 1 cm^2 fungal material was inserted into each Erlenmeyer flask using a flame sterilised scalpel. The fungus was then grown for 21 days at 22 °C under static conditions. Each flask was extracted with 600 ml of EtOAc. The rice medium was cut into small pieces and shaken for 8 hours followed by evaporation of the EtOAc.

3.4 Isolation

The crude extract (5.5 g) obtained from the fungal rice culture enriched with L-phenylalanine was seperated using a silica gel vacuum liquid chromatography (VLC). A step gradient of *n*-hexane/EtOAc and CH_2Cl_2/MeOH was used that yielded 16 fractions (V1-V16). Fractions V6 (510 mg) and V7 (53 mg) were combined and further purified using a LH20 sephadex column with MeOH as eluent giving nine subfractions (V6S1-V6S9). Subfraction V6S4 (31 mg) was conducted to semi-preparative HPLC using a MeOH-H_2O step gradient from 58-78 % MeOH to give **1** (0.8 mg), **8** (5.4 mg) and **9** (1 mg). Fractions V9 (792 mg), V10 (301 mg) and V11 (186 mg) were combined and then further separated by reverse-phase vacuum liquid chromatography using a step gradient of H_2O and MeOH, ranging from 0-100 % MeOH, to give 7 subfractions (V9-11RP1-V9-11RP7). Subfractions V9-11RP1 (218 mg) and V9-11RP2 (146 mg) were purified similarly to V6S4 via semi-preparative HPLC using MeOH-H_2O gradients of 5-50 % MeOH and 30-56 % MeOH respectively to yield **2** (3.4 mg), **3** (43.7 mg), **4** (5.4 mg), **5** (5.6 mg) and **10** (1.3 mg). Subfractions V4 (750 mg) and V5 (545 mg) were combined and conducted to silica column liquid chromatography using EtOAc as eluent followed by a step gradient of CH_2Cl_2/MeOH to give five subfractions (V4-5K1-V4-5K5). Subfraction V4-5K2 (207 mg) was purified by semi-preparative HPLC with a H_2O-MeOH step gradient from 50-80 % MeOH giving **7** (3.4 mg). Subfraction V4-5K1 (221 mg) was transferred to a LH20 sephadex column using MeOH as eluent to yield **6** (106.9 mg).

Spectral data:

Trichocladiol ((3R*,4S*)-3,4,6,8-tetrahydroxy-7-methyl-3,4-dihydronaphthalen-1(2H)-one **- compound 1):** white powder; $[\alpha]_D^{26}$ -8.4 (c 0.225, MeOH); UV (MeOH) λ_{max} 291 nm; ^1H and ^{13}C NMR data, Table 1; HRESIMS m/z 225.0756 $[M + H]^+$ (calcd for $C_{11}H_{13}O_5$, 225.0757).

Trichocladic acid (2-((5,6-dimethyl-4-oxo-4H-pyran-2-yl)methyl)-4,6-dihydroxybenzoic acid **– compound 2):** white powder, UV (MeOH) λ_{max} 256 and 300 nm; ^1H and ^{13}C NMR data, Table 2; HRESIMS m/z 291.0866 $[M + H]^+$ and 313.0683 $[M + Na]^+$ (calcd for $C_{15}H_{15}O_6$, 291.0863 and $C_{15}H_{14}NaO_6$, 313.0680).

Colletodiolic acid ((E)-5-(((E)-4,5,7-trihydroxyoct-2-enoyl)oxy)hex-2-enoic acid **– compound 3):** colorless oil, $[\alpha]_D^{23}$ + 15.3 (c 1.0, MeOH), UV (MeOH) λ_{max} 218 nm; ^1H and ^{13}C NMR data, Table 3; HRESIMS m/z 303.1439 $[M + H]^+$, 320.1703 $[M + NH_4]^+$ and 325.1257$[M + Na]^+$ (calcd for $C_{14}H_{23}O_7$, 303.1438; $C_{14}H_{26}NO_7$, 320.1704 and $C_{14}H_{22}NaO_7$, 325.1258).

Colletolactone (4-hydroxy-4-(4-hydroxy-5-oxotetrahydrofuran-2-yl)butan-2-yl (E)-5-hydroxyhex-2-enoate – **compound 4):** colorless oil, $[\alpha]_D^{22}$ - 18.4 (c 1.0, MeOH), UV (MeOH) λ_{max} 218 nm; ^1H and ^{13}C NMR data, Table 4; HRESIMS m/z 303.1442 $[M + H]^+$ and 320.1708 $[M + NH_4]^+$ (calcd for $C_{14}H_{23}O_7$, 303.1438 and $C_{14}H_{26}NO_7$, 320.1704).

Colletolic acid ((E)-5-hydroxy-7-(((E)-5-hydroxyhex-2-enoyl)oxy)oct-2-enoic acid – **compound 5):** colorless oil, $[\alpha]_D^{22}$ – 43.2 (c 1.0, MeOH), UV (MeOH) λ_{max} 219 nm; ^1H and ^{13}C NMR data, Table 4; HRESIMS m/z 287.1492 $[M + H]^+$ and 304.1759 $[M + NH_4]^+$ (calcd for $C_{14}H_{23}O_6$, 287.1489 and $C_{14}H_{26}NO_6$, 304.1755).

3.5 Media and strains

Nosocomial bacteria Methicillin-resistant *Staphylococcus aureus* (MRSA) ATCC 700699 and *Pseudomonas aeruginosa* ATCC 87110 were grown in Mueller-Hinton-broth (MHB). The pathogenic yeast *Candida albicans* ATCC 24433 was grown in standard YPD medium (1% yeast extract, 2% peptone, and 2% glucose). The pathogenic bacterium *Mycobacterium tuberculosis* (Mtb) ATCC 27294 was grown in 7H9 supplemented with ADS (0.85% NaCl, 5% BSA, 2% dextrose), 0.5% glycerol, and 0.05% tyloxapol. Nosocomial bacteria and *C. albicans* were grown shaking at 120 rpm and 37 °C, Mtb was grown at 37 °C shaking at 80 rpm.

3.6 Determination of the minimal inhibitory concentration

Microbroth dilution assays were performed to determine the minimal inhibitory concentration (MIC_{90}) of compounds. Briefly, a serial 1:1 dilution of compounds was prepared in a 96-well round-bottom polystyrene plate in 50 µL growth medium ranging from 200 µM to 1.56 µM. The $OD_{600\ nm}$ of pre-grown bacterial cultures was determined, and a cell suspension in growth medium was adjusted to 10^6 CFU/mL. Afterwards, 50 µL of the cell suspension were added to each well thereby changing the compound concentration range to 100 µM to 0.78 µM. For MRSA ATCC 700699, *P. aeruginosa* ATCC 87110 and *C. albicans* ATCC 24433, the BacTiter Glo assay (Promega) was used to quantify growth after 24 h of incubation following the manufacturer's manual. Briefly, equal volumes of bacterial cell suspension and BacTiter Glo reagent were mixed in a white flat-bottom 96-well plate. After 5 minutes, luminescence was measured with a TECAN plate reader. Moxifloxacin was used as positive control for MRSA and *P. aeruginosa*, hygromycin was used as positive control for *C. albicans,* while DMSO was used as solvent control for all of the three organisms. For quantifying growth of Mtb ATCC 27294, the resazurin assay was used following a protocol as described previously [23]. Briefly, 10 µL of a 100 µg/mL resazurin solution were added to each well of the 96-well plate after five days of incubation at 37 °C, 5% CO_2, and in humified atmosphere. The plates were incubated for another 18 hours at room temperature before stopping the reaction by addition of 100 µL 10% formalin solution to each well. The fluorescence was measured at 535 nm excision and 590 nm emission using a TECAN plate reader. Rifampicin and DMSO were used as positive and vehicle control, respectively. All experiments have been conducted in triplicates.

3.7 Determination of the cytotoxic activity against THP1 cells

The cytotoxicity assay was performed using THP-1 cells (human monocytic leukemia cell line) in a procedure described before [24]. The cells were cultivated in RPMI 1640 medium containing 2 mM L-glutamine and supplemented with 10% fetal calf serum (FCS) and 1% sodium pyruvate at 37 °C in an atmosphere of 5% CO_2. Cells were adjusted to a density of 2 x 10^5 cells/ml, and 50 µl of this suspension was transferred per well to 96-well flat bottom microtiter plates containing 2-fold serial dilutions of the tested compounds resulting in final concentrations ranging from 100 to 0.78 µM in a total volume of 100 µl. Cycloheximide at concentrations of 4 to 0.03 µg/ml was used as positive control. The cells were then incubated for 48 h at 37 °C in a humidified atmosphere with 5% CO_2. Subsequently, 10 µl of a resazurin solution (100 µg/ml) was added to each well, followed by another incubation step for 4 h. The fluorescence was quantified using a Tecan Infinite 200pro microplate reader (excitation 540 nm, emission 590 nm). The residual growth was calculated relative to non-inoculated (0 % growth) and controls treated with DMSO (100 % growth), respectively.

Acknowledgments

We thank the CeMSA@HHU (Center for Molecular and Structural Analytics@Heinrich Heine University) for recording the mass-spectrometric and the NMR-spectroscopic data. We thank Heike Goldbach-Gecke for testing the cytotoxic activity against the human monocytic cell-line THP1.

References

1. Fleming, A., *On the Antibacterial Action of Cultures of a Penicillium, with Special Reference to their Use in the Isolation of B. influenza.* Br J Exp Pathol., 1929. **10**: p. 226-236.
2. Waksman, S.A. and H.B. Woodruff, *The soil as a source of microorganisms antagonistic to disease-producing bacteria.* Journal of Bacteriology, 1940. **Volume 40**: p. 581-600.
3. Stierle, A., G. Strobel, and D. Stierle, *Taxol and taxane production by Taxomyces andreanae, an endophytic fungus of Pacific yew.* Science, 1993. **260**(5105): p. 214-6.
4. Strobel, G.A., *Endophytes as sources of bioactive products.* Microbes and Infection, 2003. **5**(6): p. 535-544.
5. Ryan, R.P., et al., *Bacterial endophytes: recent developments and applications.* FEMS Microbiol Lett, 2008. **278**(1): p. 1-9.
6. Rutledge, P.J. and G.L. Challis, *Discovery of microbial natural products by activation of silent biosynthetic gene clusters.* Nat Rev Microbiol, 2015. **13**(8): p. 509-23.
7. Bode, H.B., et al., *Big effects from small changes: possible ways to explore nature's chemical diversity.* ChemBioChem, 2002. **3**: p. 619-627.
8. Tran-Cong, N.M., et al., *Induction of cryptic metabolites of the endophytic fungus Trichocladium sp. through OSMAC and co-cultivation.* RSC Adv, 2019. **9**(47): p. 27279-27288.
9. Koyama, K., S. Natori, and Y. Iitaka, *Absolute Configurations of chaetochromin A and related bis(naphtho-Gamma-pyrone) mold metabolites.* Chem. Pharm. Bull., 1987. **35**: p. 4049-4055.
10. Mehnaz, S., et al., *Lahorenoic acids A-C, ortho-dialkyl-substituted aromatic acids from the biocontrol strain Pseudomonas aurantiaca PB-St2.* J Nat Prod, 2013. **76**(2): p. 135-41.
11. Kumar, R.S., et al., *Characterization of antifungal metabolite produced by a new strain Pseudomonas aeruginosa PUPa3 that exhibits broad-spectrum antifungal activity and biofertilizing traits.* J Appl Microbiol, 2005. **98**(1): p. 145-54.

12. Yu, M. and B.B. Snider, *Syntheses of chloroisosulochrin and isosulochrin and biomimetic elaboration to maldoxin, maldoxone, dihydromaldoxin, and dechlorodihydromaldoxin.* Org Lett, 2011. **13**(16): p. 4224-7.
13. Joshi, B.K., J.B. Gloer, and D.T. Wicklow, *Bioactive natural products from a sclerotium-colonizing isolate of Humicola fuscoatra.* J Nat Prod, 2002. **65**(11): p. 1734-7.
14. Ola, A.R., et al., *Inducing secondary metabolite production by the endophytic fungus Fusarium tricinctum through coculture with Bacillus subtilis.* J Nat Prod, 2013. **76**(11): p. 2094-9.
15. MacMillan, J., *Fungal Products Part V. The Absolute Stereochemistry of Colletodiol and the Structures of Related Metabolites of Colletotrichum capsici.* J.C.S., 1973. **3**((170)): p. 1487-1493.
16. Grove, J.F., *Metabolic Products of Colletotrichum capsici. Isolation and Characterisation of Acetylcolletotrichin and Colletodiol.* J. Chem. Soc., 1966. **5**(791): p. 230-234.
17. Ohta, K. and O. Mitsunobu, *Formal total synthesis of grahamimycin A1.* Tetrahedron Letters, 1991. **32**((4)): p. 517-520.
18. MacMillan, J. and R.J. Pryce, *The structure of colletodiol, a macrocyclic dilactone from Colletotrichum capsici.* Tetrahedron Letters, 1968. **9**(53): p. 5497-5500.
19. Koyama, K., et al., *Cytotoxicity and antitumor activities of fungal bis(naphtho-gamma-pyrone) derivatives.* J Pharmacobiodyn, 1988. **11**(9): p. 630-5.
20. Xu, G.B., et al., *Isochaetomium A2, a new bis(naphthodihydropyran-4-one) with antimicrobial and immunological activities from fungus Chaetomium microcephalum.* Arch Pharm Res, 2014. **37**(5): p. 575-9.
21. Simpson, J., *Studies of Polyketide Chain assembly Processes. Origins of the Hydrogen and Oxygen Atoms in Colletodiol.* J. Chem. Soc., Chem. Commun., 1985: p. 1822-1824.
22. O'Neill, J.A., *Biosynthesis of Colletodiol and Related Polyketide Macrodiolides in Cytospora sp. ATCC 20502: Synthesis and Metabolism of Advanced Intermediates.* J. Chem. Soc., Chem. Commun., 1993.
23. Rehberg, N., et al., *3-O-Methyl-Alkylgallates Inhibit Fatty Acid Desaturation in Mycobacterium tuberculosis.* Antimicrob Agents Chemother, 2019. **63**(9).
24. Meier, D., et al., *The plant-derived chalcone Xanthoangelol targets the membrane of Gram-positive bacteria.* Bioorg Med Chem, 2019. **27**(23): p. 115151.

Supplementary Material.

Colletodiol derivatives of the endophytic fungus *Trichocladium sp*.

Viktor E. Simons[a], Marian Frank[a], Lasse van Geelen[a], Nam Tran-Cong[a], Dorothea Albrecht[a], Annika Coort[a], Christina Gebhard[a], and Rainer Kalscheuer*[,a]

[a]Institute of Pharmaceutical Biology and Biotechnology, Heinrich Heine University, Universitätsstrasse 1, 40225 Düsseldorf, Germany

[b]Department of Organic Chemistry, University of Debrecen, P.O. Box 400, 4002 Debrecen, Hungary

*Corresponding author: rainer.kalscheuer@hhu.de (R. Kalscheuer)

Table of contents

S1. NMR Table of Compound 1 (DMSO-d_6, ^{1}H: 600MHz, ^{13}C: 150 MHz)

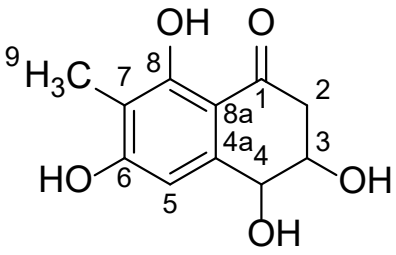

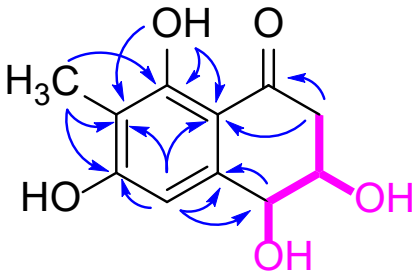

3,4,6,8-tetrahydroxy-7-methyl-3,4-dihydronaphthalen-1(2*H*)-one

Chemical Formula: $C_{11}H_{12}O_5$

Molecular Weight: 224,21

COSY ▬ key HMBC ↷

position	δ_C*	δ_H, m (*J* in Hz)	δ_H, m (*J* in Hz) MeOH-d_4	δ_C Acetone-d_6	δ_H, m (*J* in Hz) Acetone-d_6
1	201.2, C			201.7, C	
2	43.1, CH_2	2.80, dd (17.2, 3.4) 2.66, dd (17.2, 5.8)	2.88, dd (17.2, 3.9) 2.77, dd (17.2, 7.4)	43.7, CH_2	2.83, d (3.6)
3	69.0, CH	4.11, m	4.20, ddd (7.4, 3.9, 2.9)	70.3, CH	4.29, br s
4	68.9, CH	4.61, dd (6.7, 2.0)	4.70, d (2.9)	70.8, CH	4.77, br s
4a	144.6, C			144.8, C	
5	105.8, CH	6.61, br s	6.58, s	107.4, CH	6.72, s
6	162.9, C			163.6, C	
7	108.5, C			111.0, C	
8	162.0, C			163.6, C	
8a	108.5, C			111.5, C	
9	6.9, CH_3	1.93, s	2.02, s	7.5, CH_3	2.03, s
3-OH		4.94, d (4.1)			4.12, d (4.6)
4-OH		5.38, d (6.7)			4.41, d (6.7)
6-OH		10.56, br s			9.38, br s
8-OH		13.03, s			13.09, s

*signals were extracted from HSQC and HMBC spectra.

S2. [1]H-NMR Spectrum of Compound 1 (DMSO-d_6, 600 MHz)

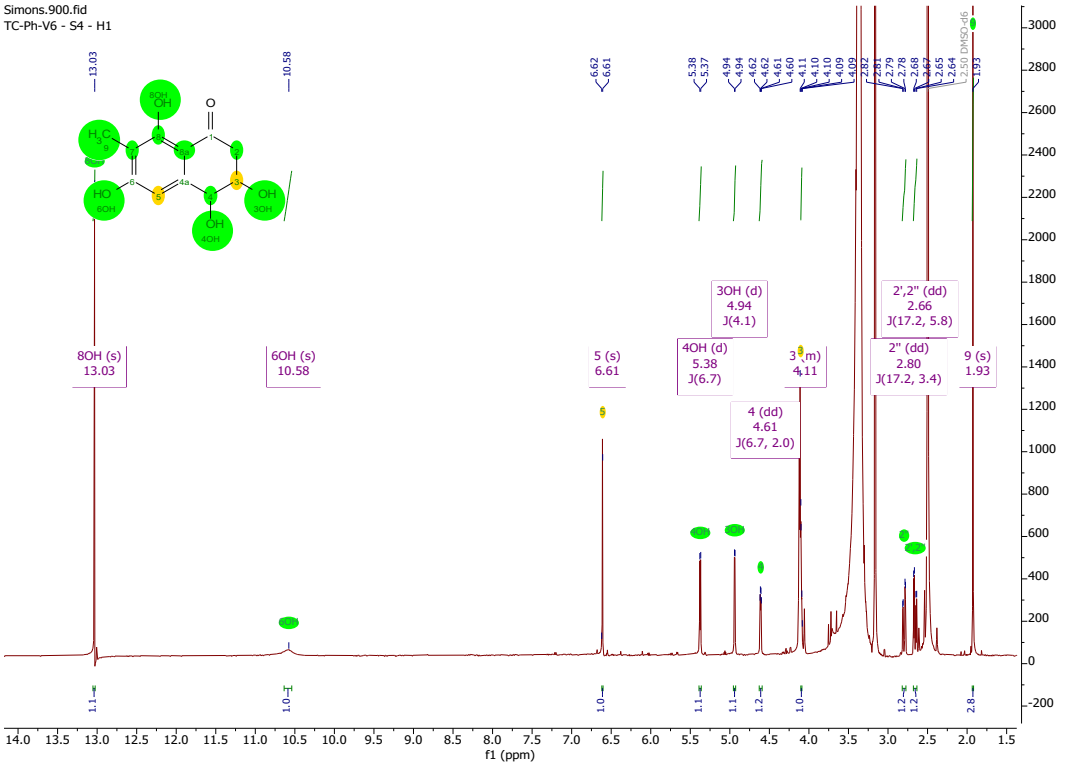

S3. [13]C-NMR Spectrum of Compound 1 (DMSO-d_6, 150 MHz)

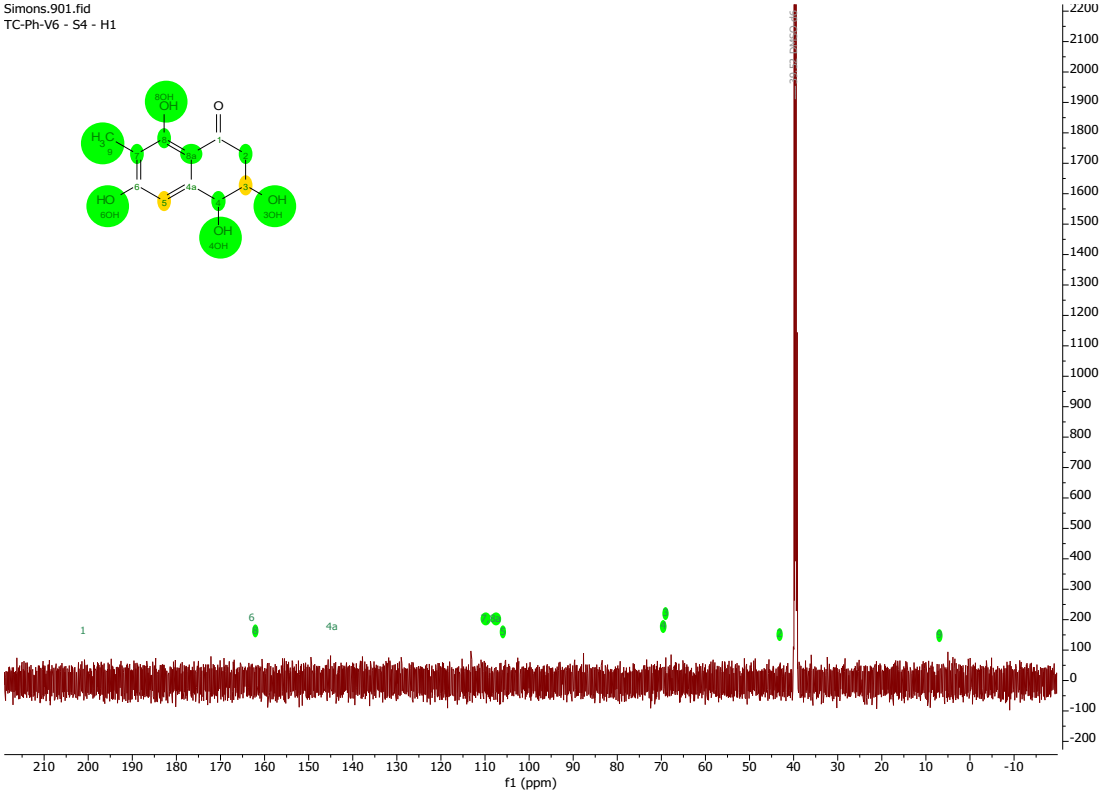

S4.^{1}H-^{13}C-HSQC Spectrum of Compound 1 (DMSO-d_6, ^{1}H: 600MHz, ^{13}C: 150 MHz)

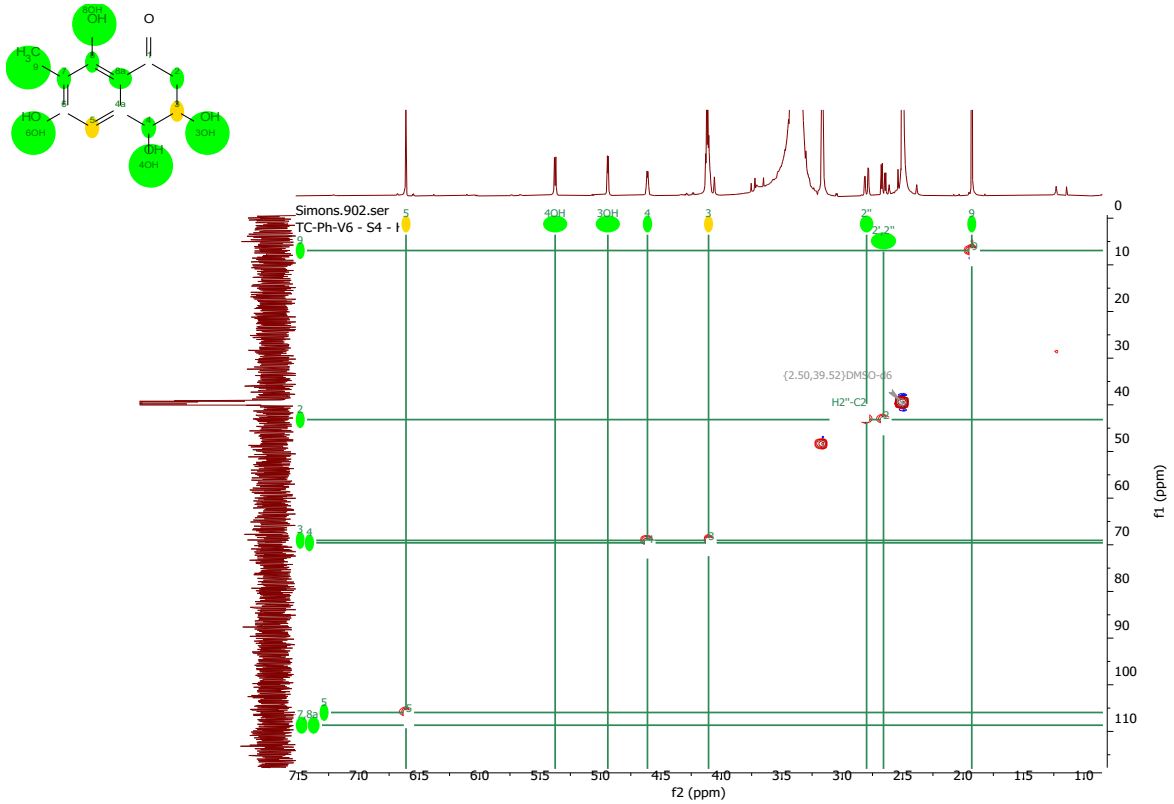

S5.^{1}H-^{13}C-HMBC Spectrum of Compound 1 (DMSO-d_6, ^{1}H: 600MHz, ^{13}C: 150 MHz)

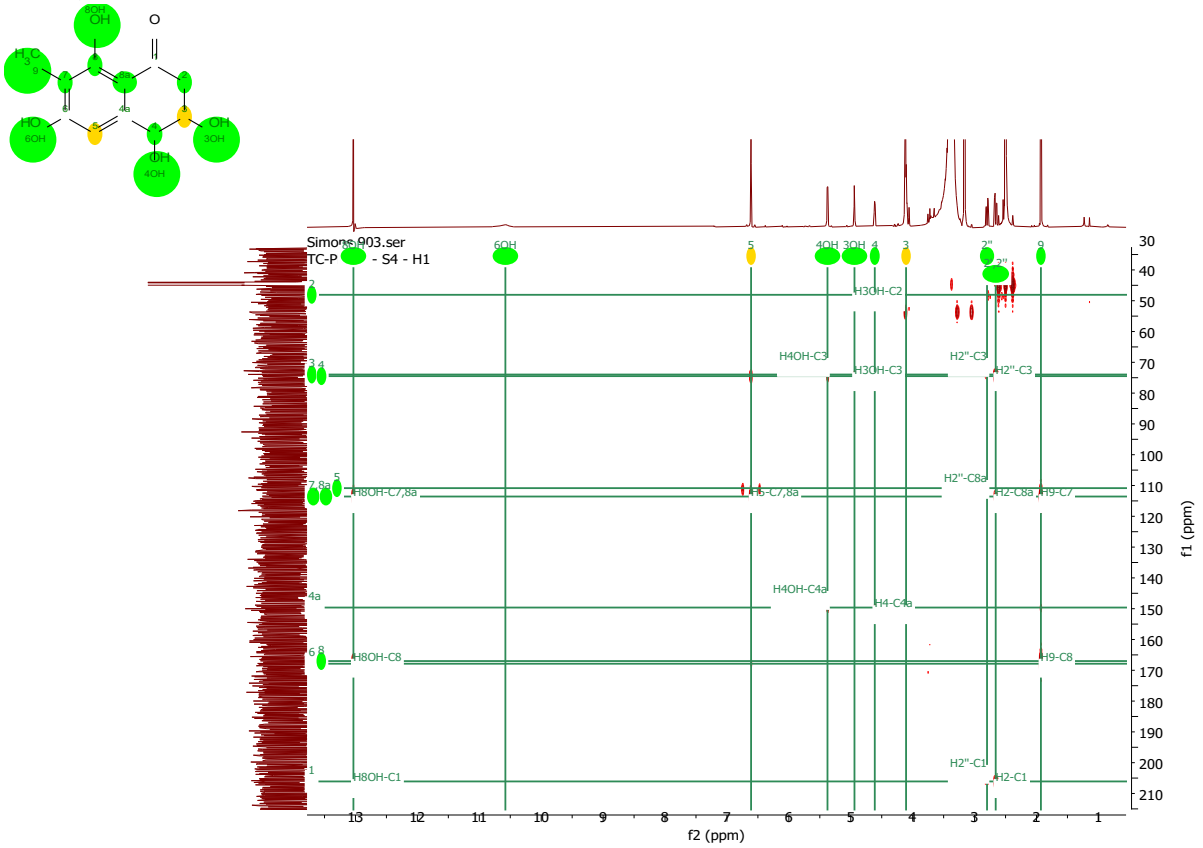

S6.^{1}H-^{1}H-COSY Spectrum of Compound 1 (DMSO-d_6, 600MHz)

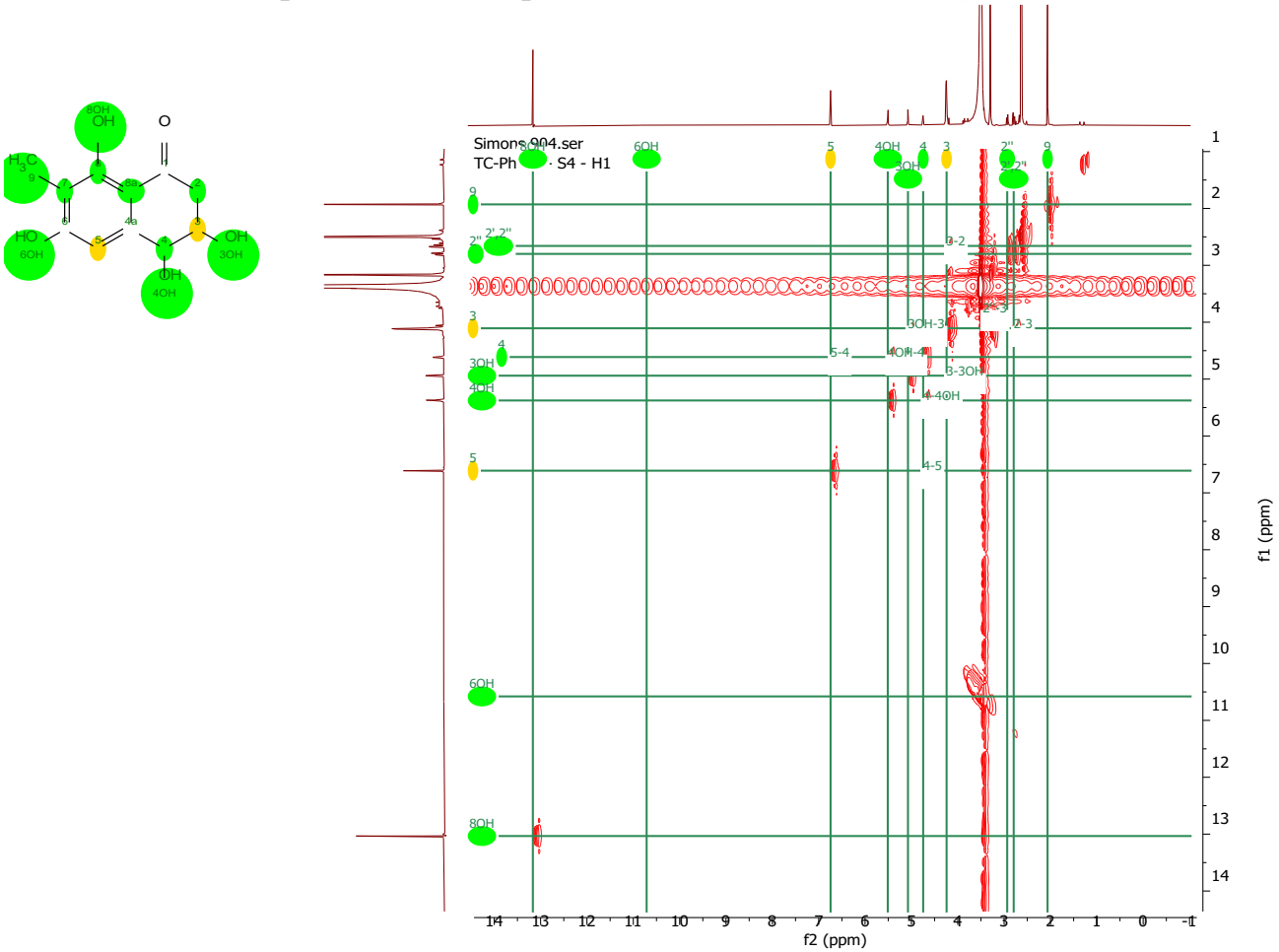

S7.HPLC-DAD UV-Vis Spectrum of Compound 1 (Methanol)

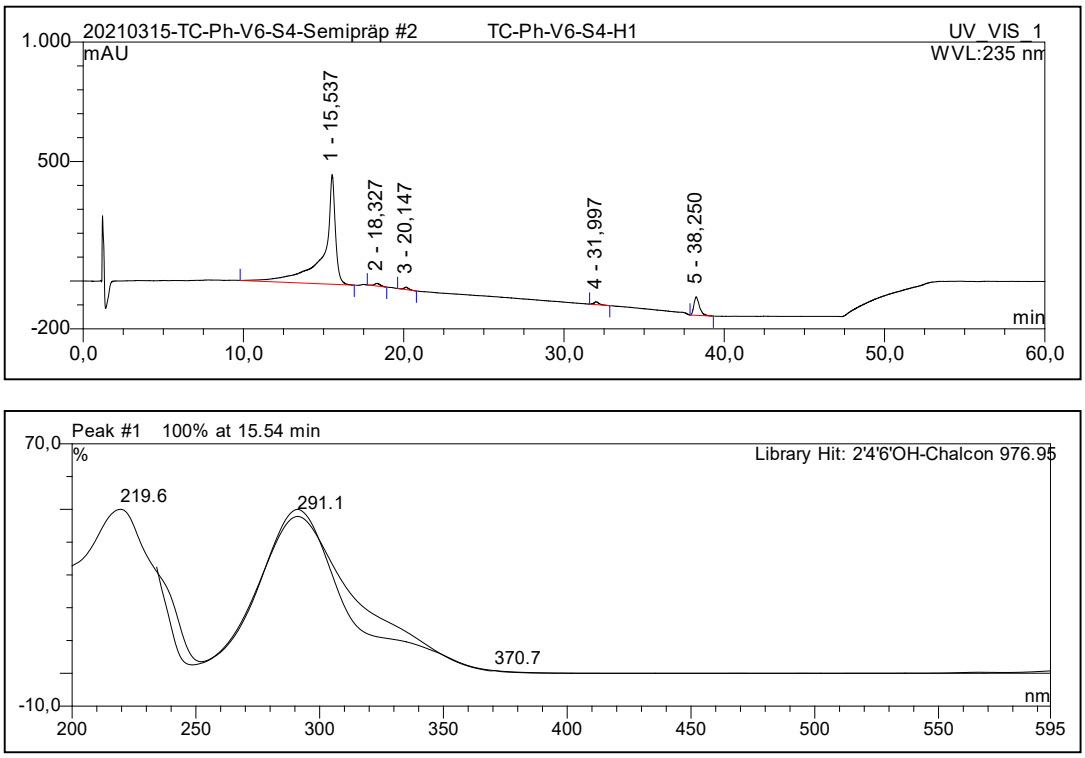

S8.ESI(+)MS Spectrum of Compound 1

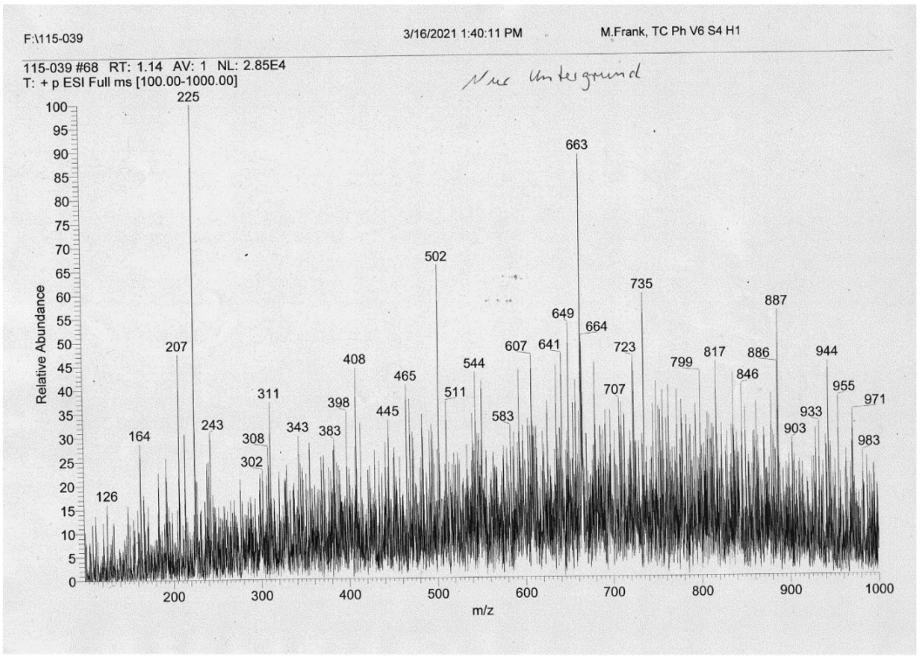

S9.High Resolution ESI(+)MS Spectrum of Compound 1

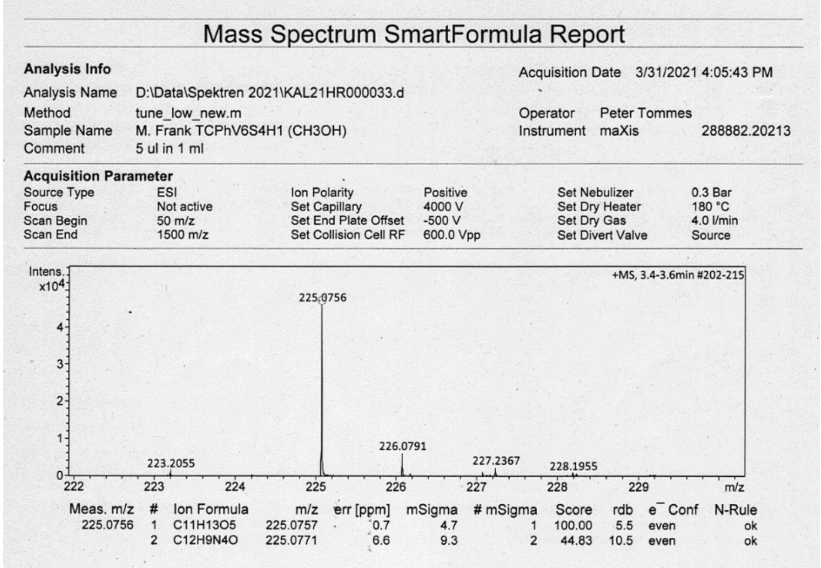

S10.NMR Table of Compound 2 (DMSO-d_6, ^{1}H: 600MHz, ^{13}C: 150 MHz)

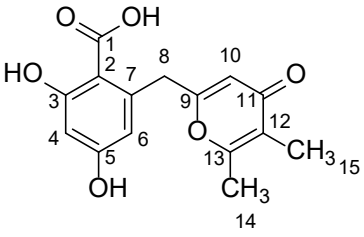

Chemical Formula: $C_{15}H_{14}O_6$
Molecular Weight: 290,27

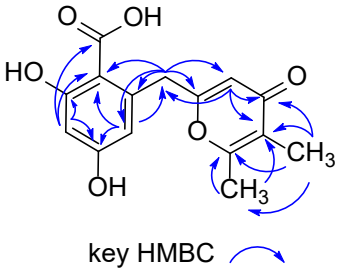

key HMBC

position	δ_C*	δ_H, m (J in Hz)
1	172.4, C	
2	106.4, C	
3	164.2, C	
4	101.6, CH	6.20, br s 2H
5	161.6, C	
6	110.9, CH	6.20, br s 2H
7	139.0, C	
8	38.2, CH_2	4.11, s
9	167.7, C	
10	110.9, CH	5.67, s
11	178.3, C	
12	119.6, C	
13	161.3, C	
14	17.4, CH_3	2.24, d (0.9)
15	9.3, CH_3	1.77, d (0.9)
1-OH		13.22, br s
3-OH		10.14, s

*signals were extracted from HSQC and HMBC spectra.

S11.[1]H-NMR Spectrum of Compound 2 (DMSO-d_6, 600 MHz)

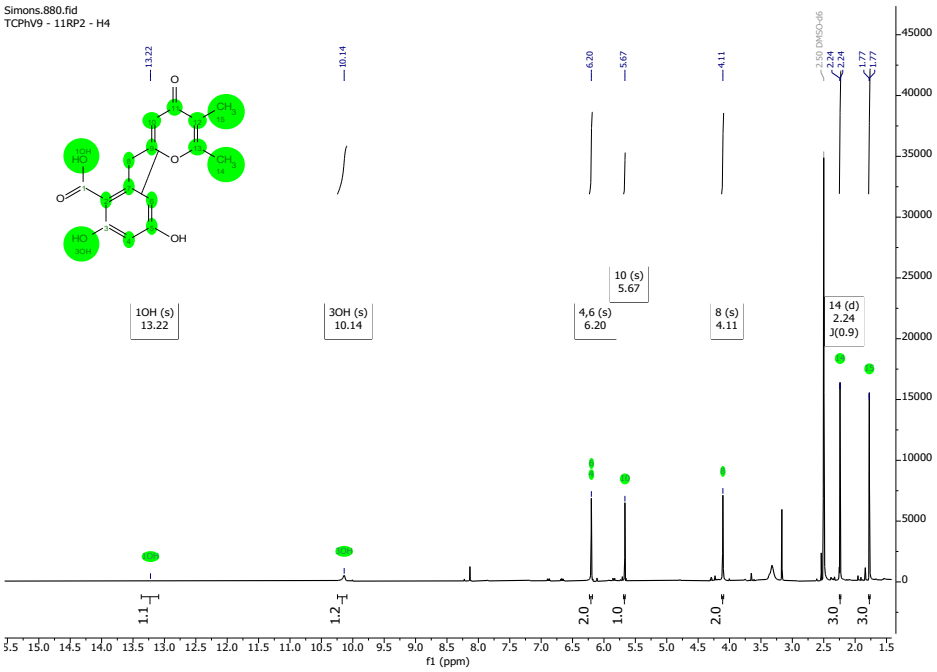

S12.[13]C-NMR Spectrum of Compound 2 (DMSO-d_6, 150 MHz)

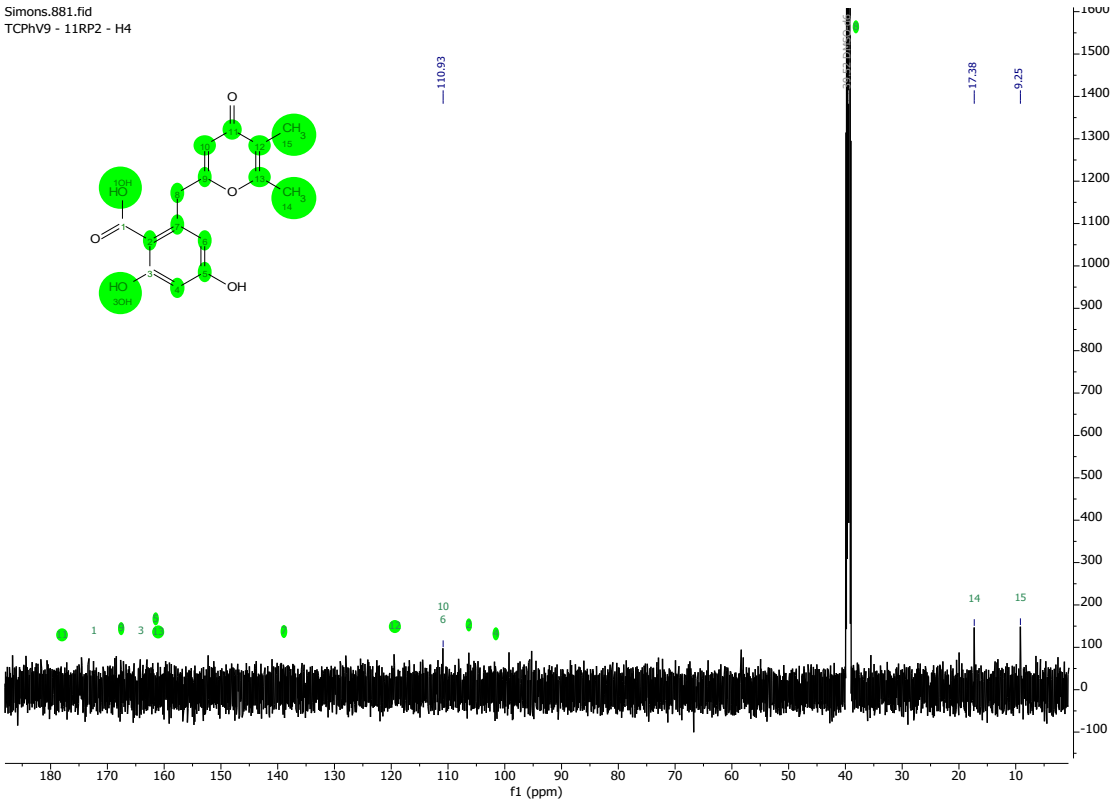

S13.^{1}H-^{13}C-HSQC Spectrum of Compound 2 (DMSO-d_6, ^{1}H: 600MHz, ^{13}C: 150 MHz)

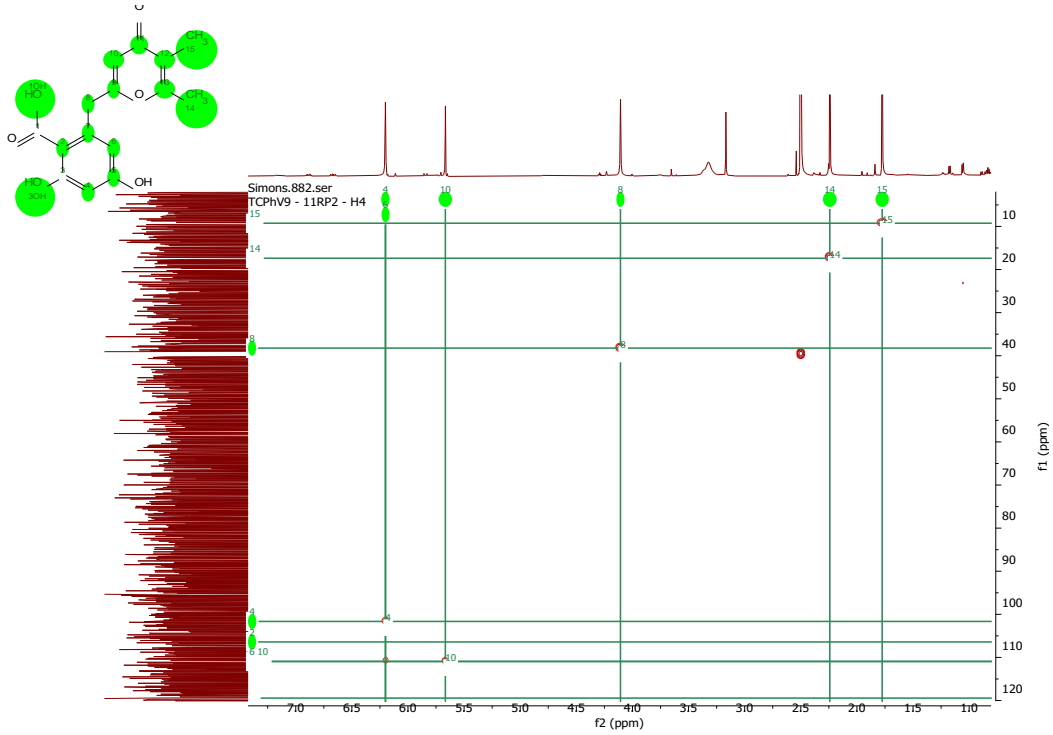

S14.^{1}H-^{13}C-HMBC Spectrum of Compound 2 (DMSO-d_6, ^{1}H: 600MHz, ^{13}C: 150 MHz)

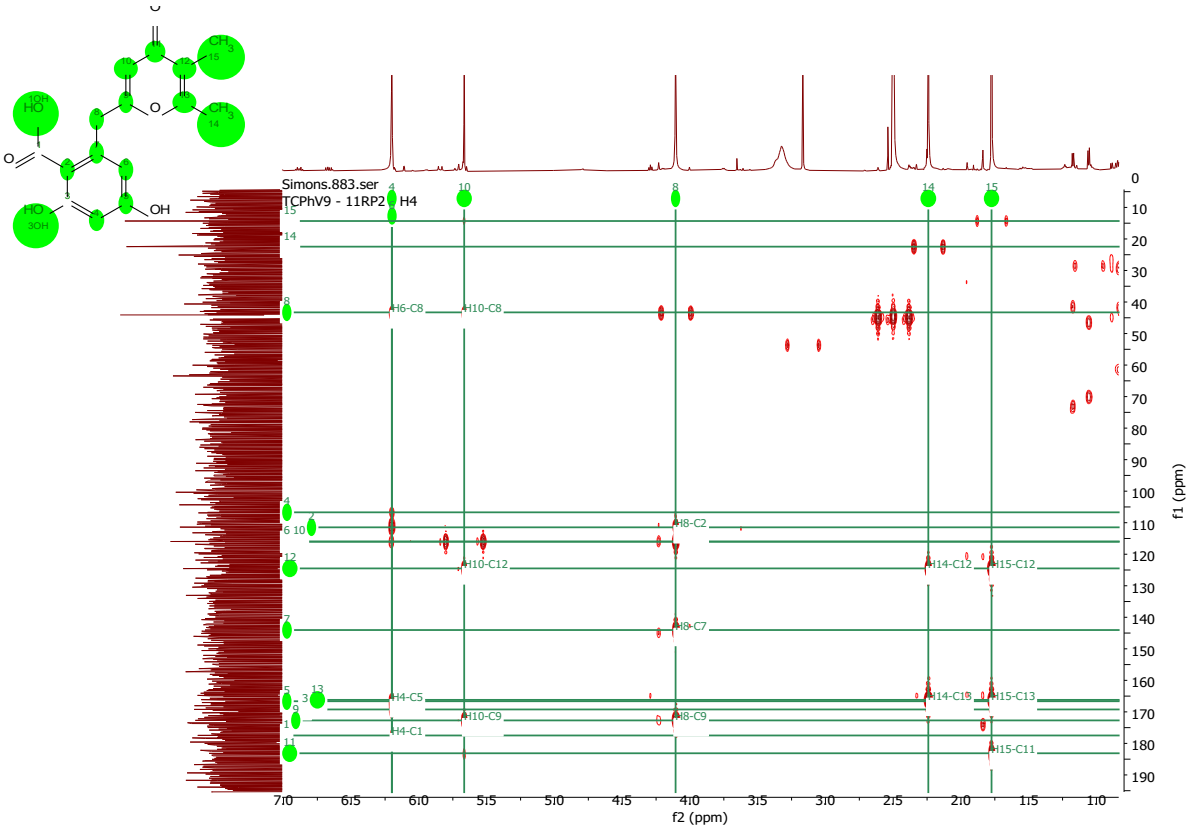

S15.HPLC-DAD UV-Vis Spectrum of Compound 2 (Methanol)

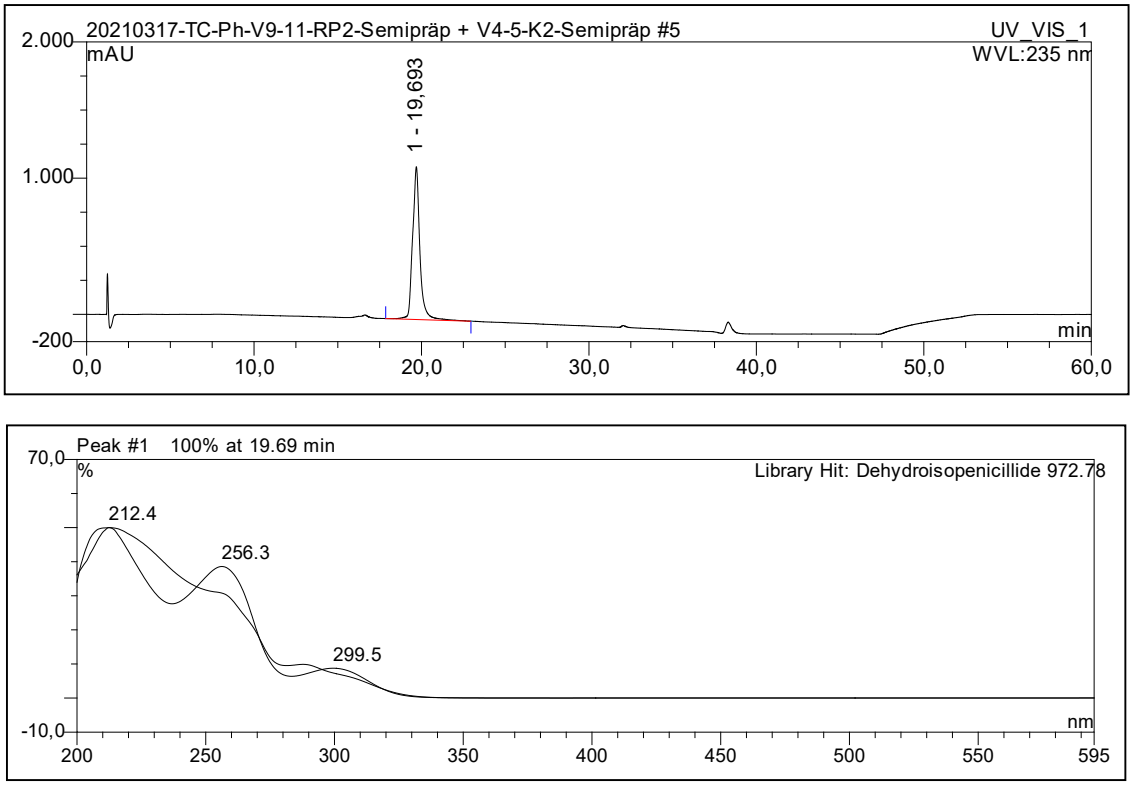

S16.ESI(+)MS Spectrum of Compound 2

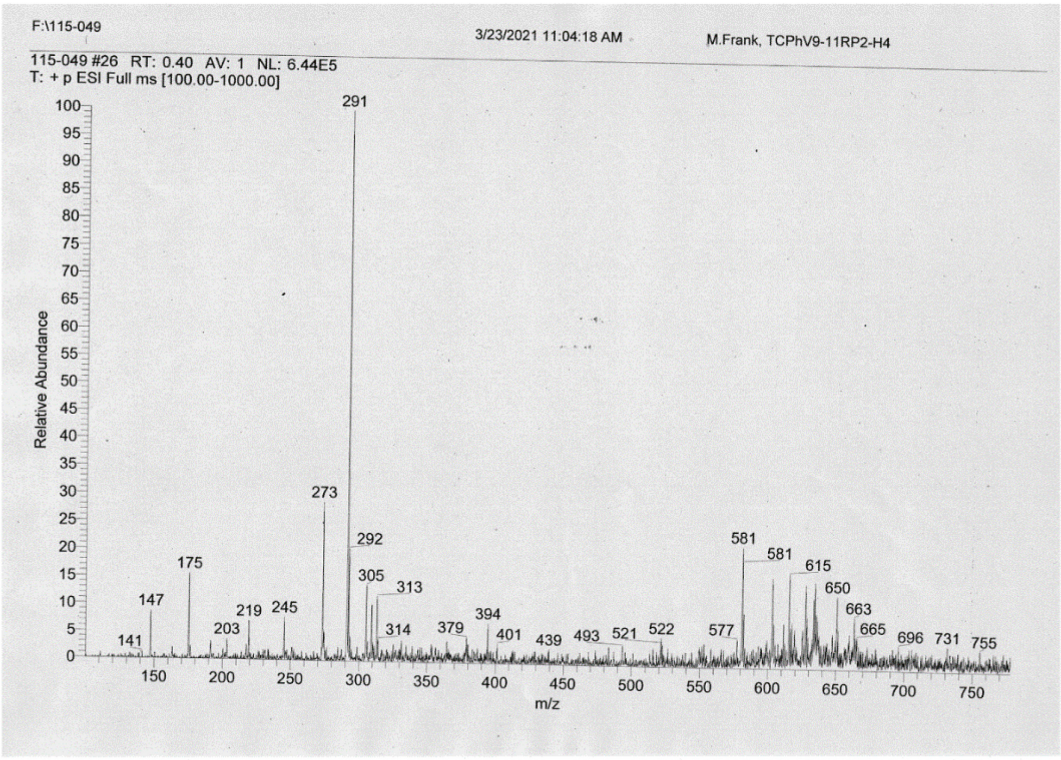

S17.High Resolution ESI(+)MS Spectrum of Compound 2

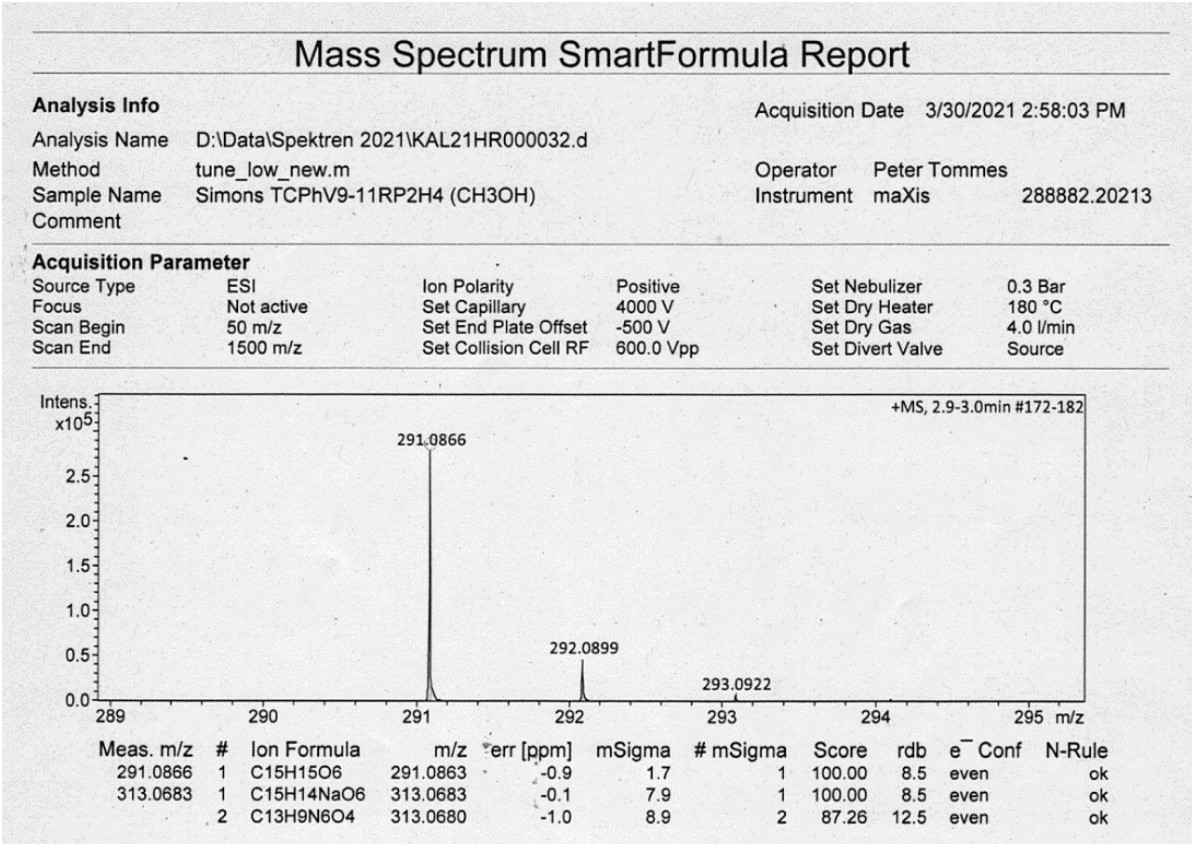

Mass Spectrum SmartFormula Report

Analysis Info

Analysis Name	D:\Data\Spektren 2021\KAL21HR000032.d	Acquisition Date	3/30/2021 2:58:03 PM
Method	tune_low_new.m	Operator	Peter Tommes
Sample Name	Simons TCPhV9-11RP2H4 (CH3OH)	Instrument	maXis 288882.20213
Comment			

Acquisition Parameter

Source Type	ESI	Ion Polarity	Positive	Set Nebulizer	0.3 Bar
Focus	Not active	Set Capillary	4000 V	Set Dry Heater	180 °C
Scan Begin	50 m/z	Set End Plate Offset	-500 V	Set Dry Gas	4.0 l/min
Scan End	1500 m/z	Set Collision Cell RF	600.0 Vpp	Set Divert Valve	Source

Meas. m/z	#	Ion Formula	m/z	err [ppm]	mSigma	# mSigma	Score	rdb	e⁻ Conf	N-Rule
291.0866	1	C15H15O6	291.0863	-0.9	1.7	1	100.00	8.5	even	ok
313.0683	1	C15H14NaO6	313.0683	-0.1	7.9	1	100.00	8.5	even	ok
	2	C13H9N6O4	313.0680	-1.0	8.9	2	87.26	12.5	even	ok

S18.NMR Table of Compound 3 (DMSO-d_6, ^{1}H: 600MHz, ^{13}C: 150 MHz)

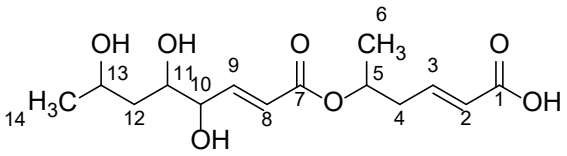

(*E*)-5-(((*E*)-4,5,7-trihydroxyoct-2-enoyl)oxy)hex-2-enoic acid
Chemical Formula: $C_{14}H_{22}O_7$
Molecular Weight: 302,32

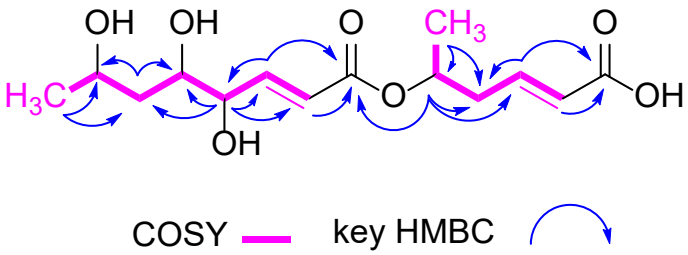

COSY — key HMBC ⌒

position	δ_C	δ_H, m (J in Hz)
1	166.9, C	
2	124.6, CH	5.83, dt (15.6, 1.5)
3	143.7, CH	6.74, dt (15.6, 7.3)
4	37.6, CH_2	2.48, m 2H
5	68.9, CH	4.99, m
6	19.6, CH_3	1.21, d (6.3) 3H
7	165.2, C	
8	120.0, CH	5.96, dd (15.7, 1.9)
9	150.1, CH	6.97, dd (15.7, 4.1)
10	72.8, CH	4.12, m
11	71.5, CH	3.61, dt (9.4, 4.0)
12	41.0, CH_2	1.42, ddd (13.6, 6.3, 3.7) 1.35, ddd (13.6, 9.4, 6.7)
13	64.5, CH	3.78, m
14	23.4, CH_3	1.04, d (6.2) 3H

S19.[1]H-NMR Spectrum of Compound 3 (DMSO-d_6, 600 MHz)

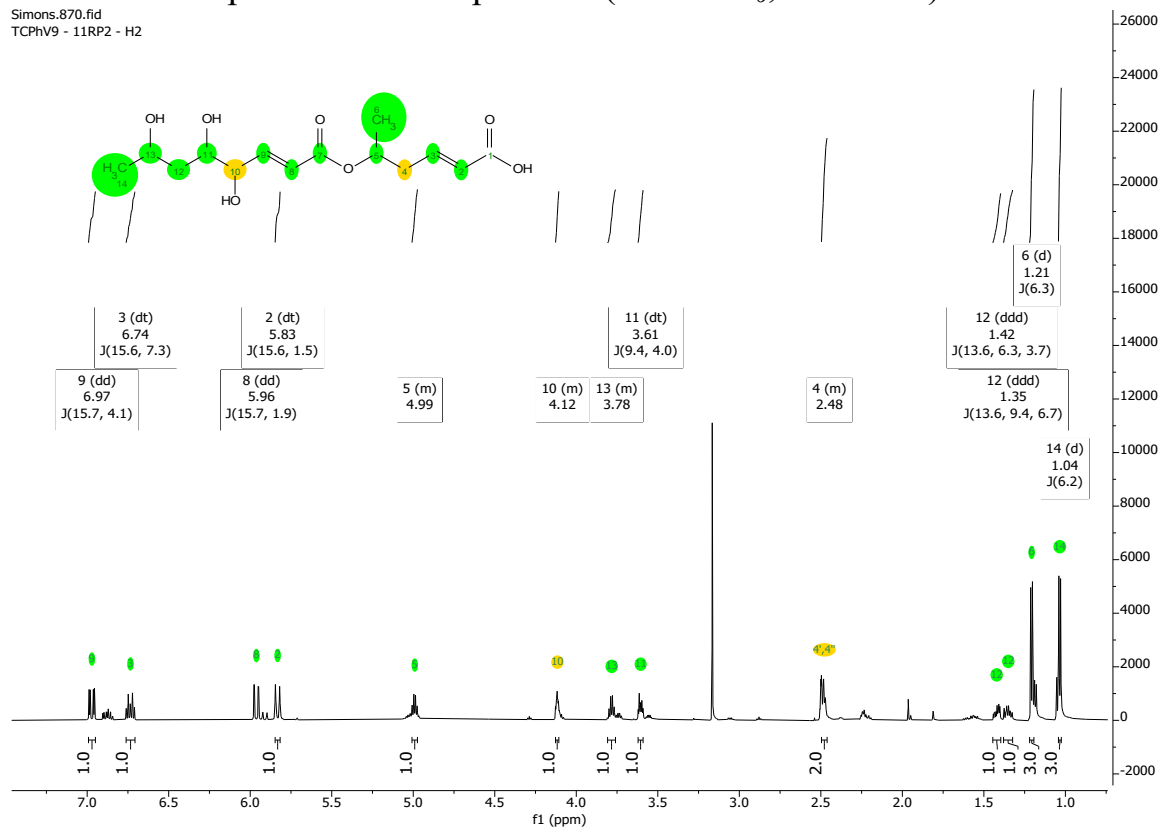

S20.[13]C-NMR Spectrum of Compound 3 (DMSO-d_6, 150 MHz)

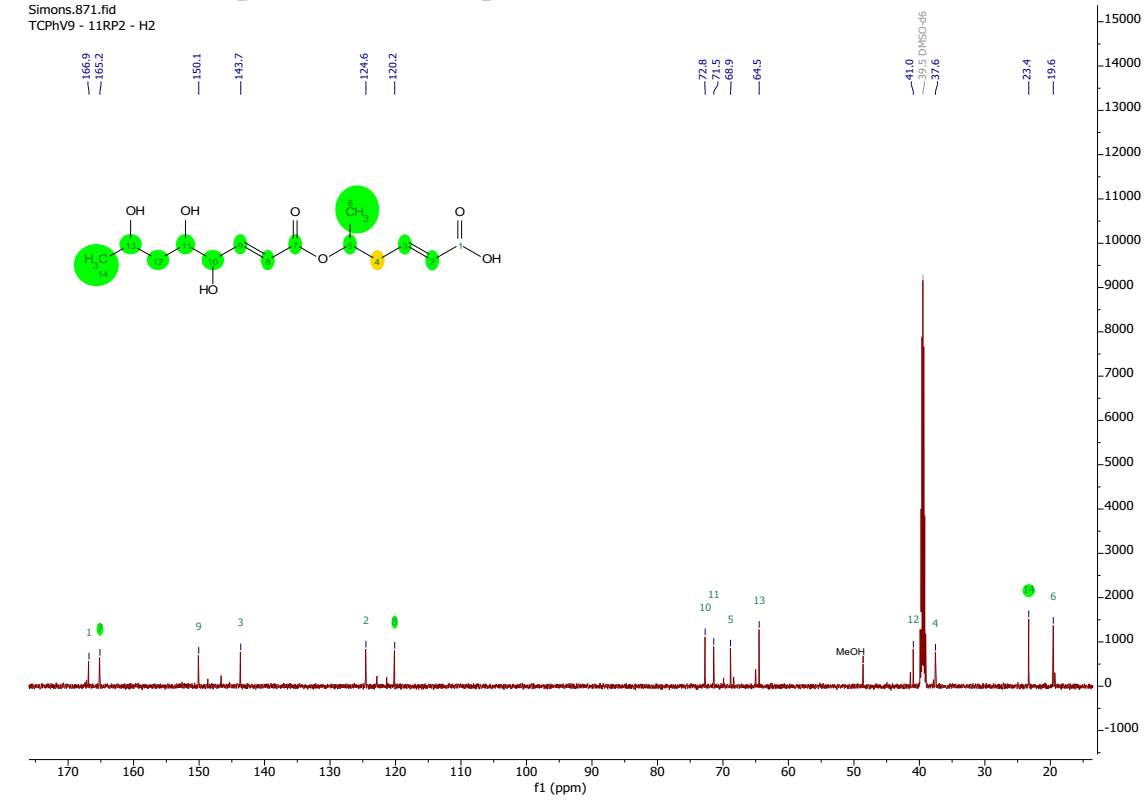

S21.^{1}H-^{13}C-HSQC Spectrum of Compound 3 (DMSO-d_6, ^{1}H: 600MHz, ^{13}C: 150 MHz)

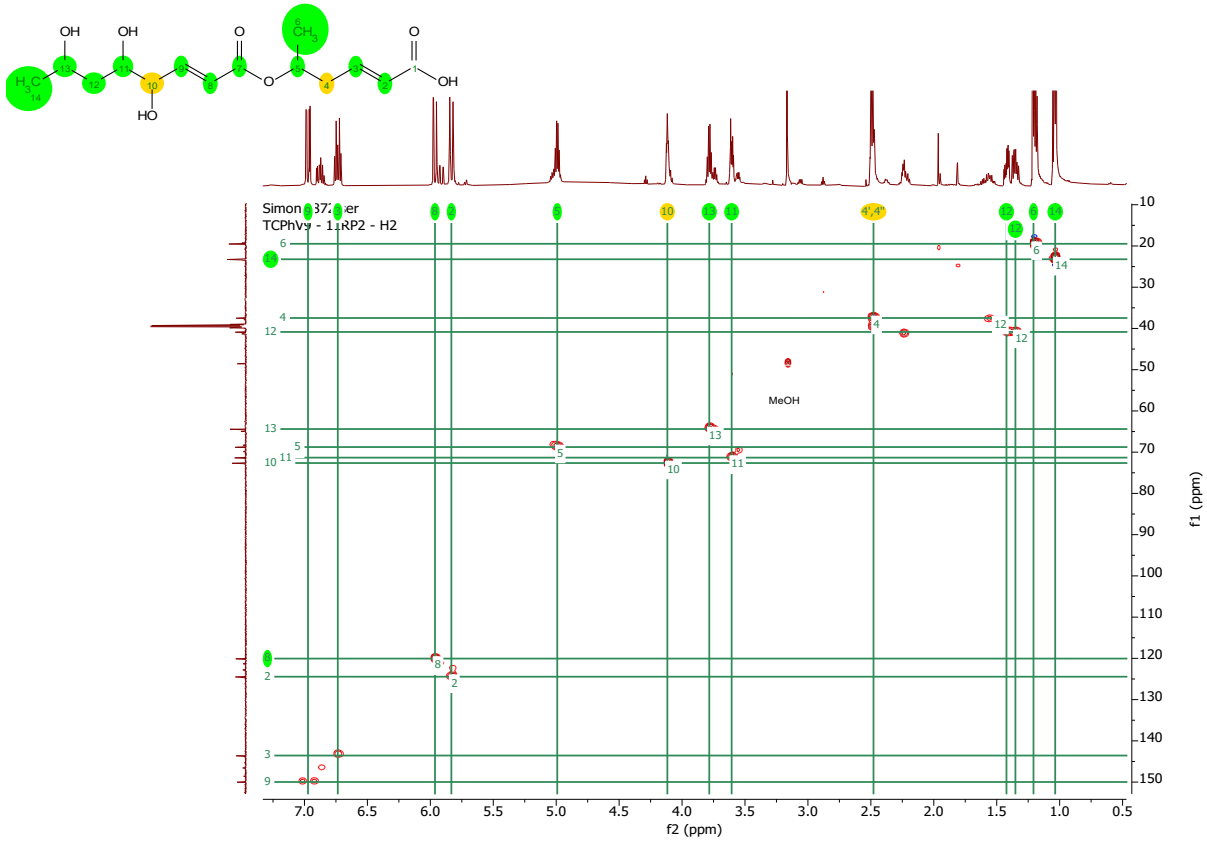

S22.^{1}H-^{13}C-HMBC Spectrum of Compound 3 (DMSO-d_6, ^{1}H: 600MHz, ^{13}C: 150 MHz)

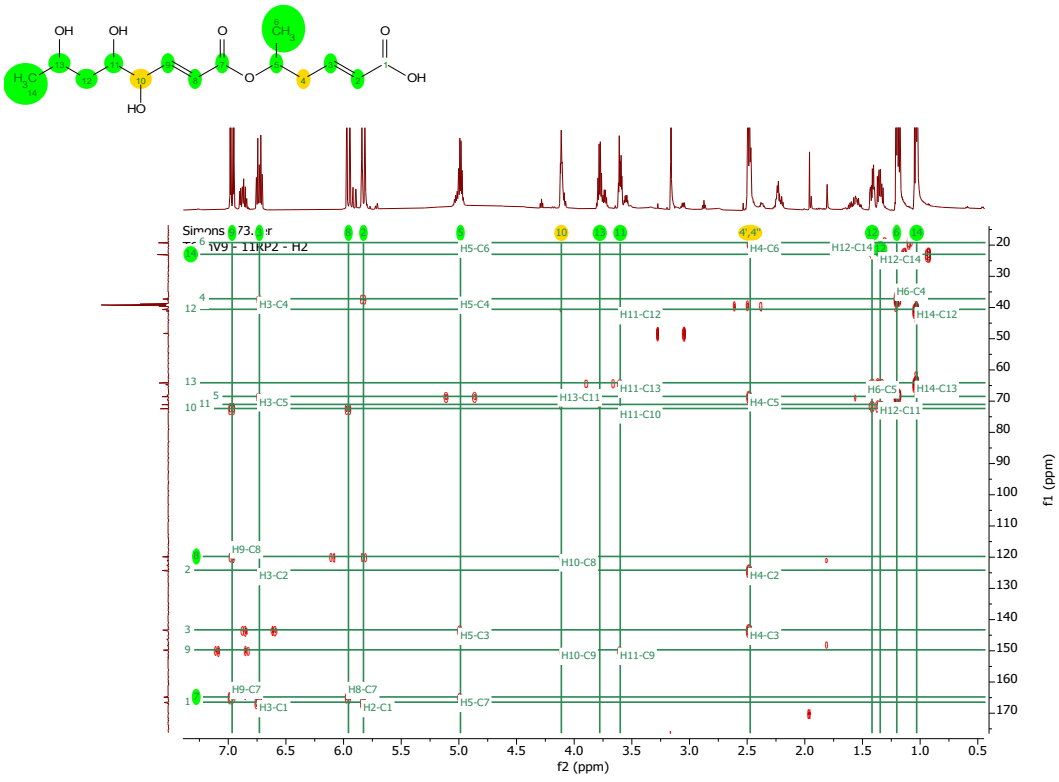

S23.^{1}H-^{1}H-COSY Spectrum of Compound 3 (DMSO-d_6, 600MHz)

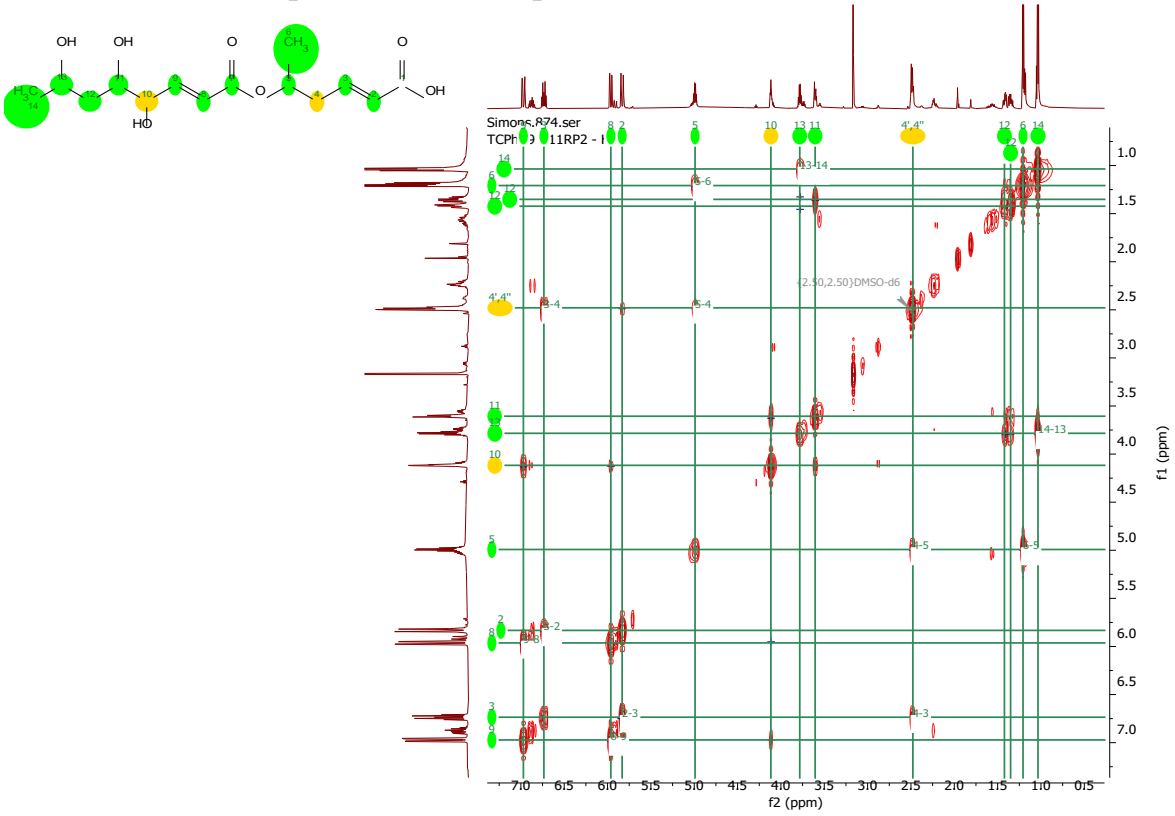

S24.UV-Vis Spectrum of Compound 3 (Methanol)

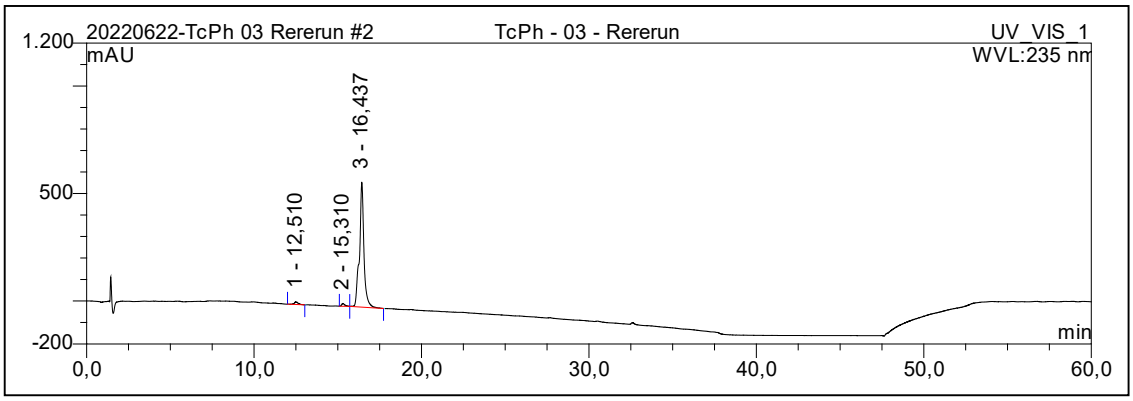

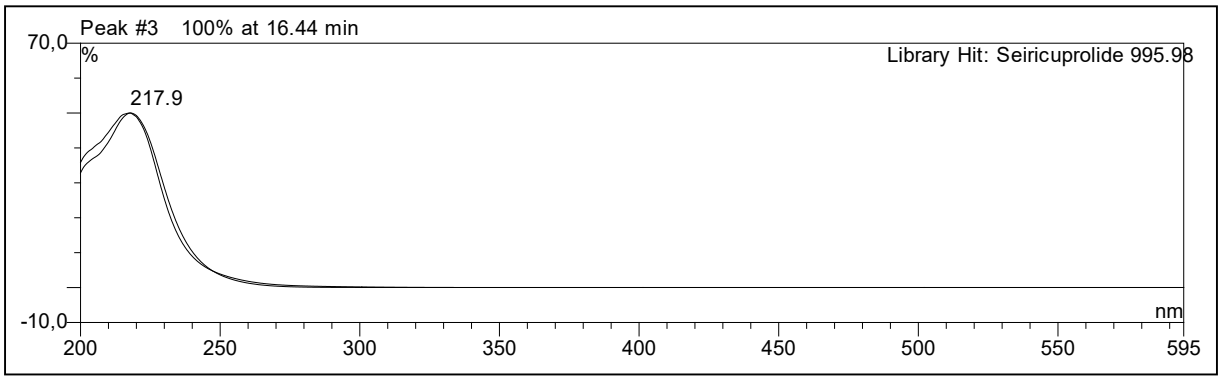

S25.ESI(+)MS Spectrum of Compound 3

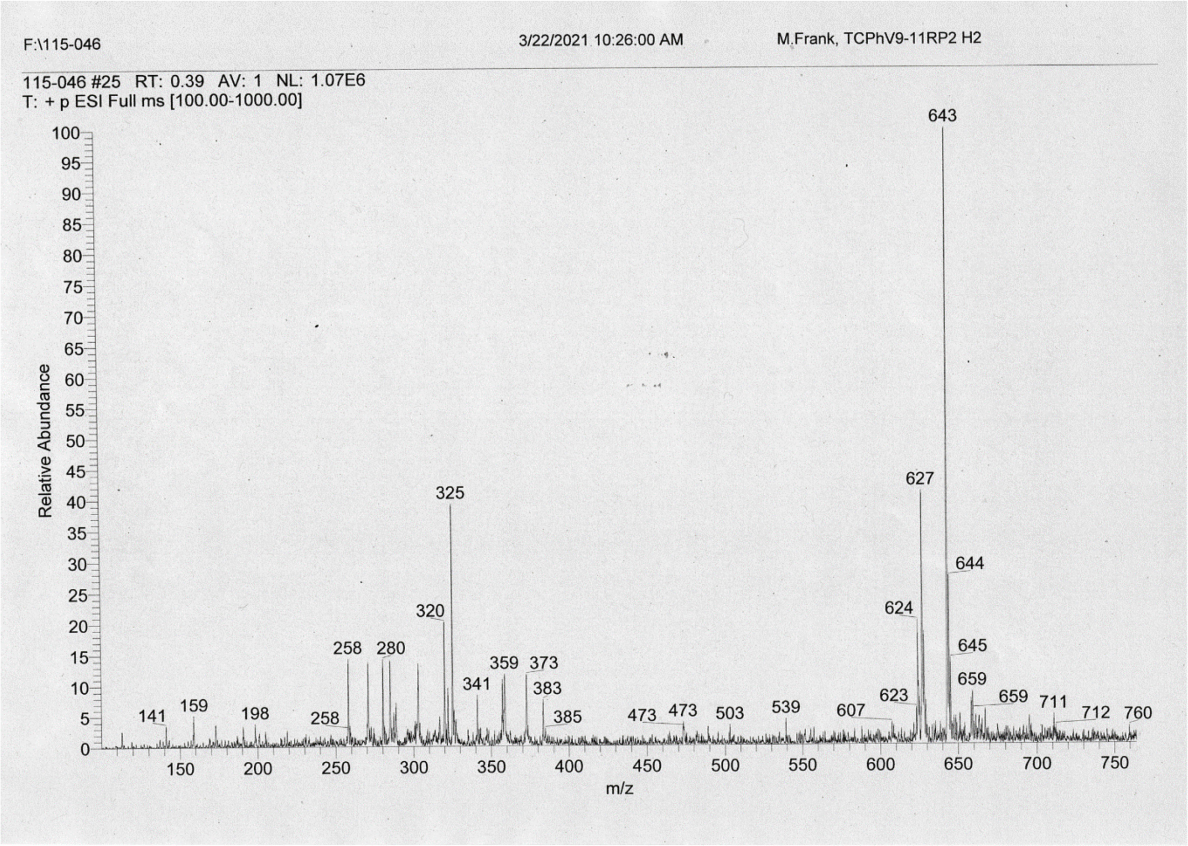

S26.High Resolution ESI(+)MS Spectrum of Compound 3

Acquisition Parameter

Source Type	ESI	Ion Polarity	Positive	Set Nebulizer	0.3 Bar
Focus	Not active	Set Capillary	4000 V	Set Dry Heater	180 °C
Scan Begin	50 m/z	Set End Plate Offset	-500 V	Set Dry Gas	4.0 l/min
Scan End	1500 m/z	Set Collision Cell RF	600.0 Vpp	Set Divert Valve	Source

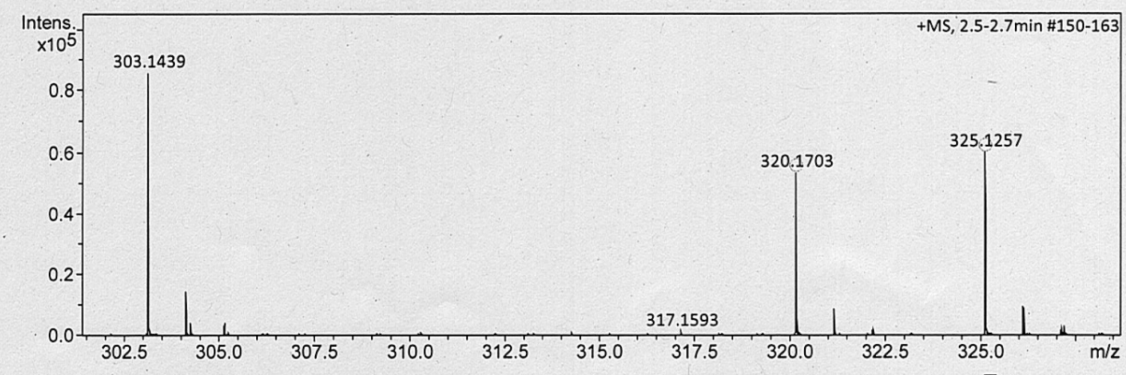

Meas. m/z	#	Ion Formula	m/z	err [ppm]	mSigma	# mSigma	Score	rdb	e⁻ Conf	N-Rule
303.1439	1	C14H23O7	303.1438	-0.2	14.5	1	100.00	3.5	even	ok
320.1703	1	C14H26NO7	320.1704	0.1	2.6	1	100.00	2.5	even	ok
325.1257	1	C14H22NaO7	325.1258	0.1	6.1	1	100.00	3.5	even	ok

S27.NMR Table of Compound 4 (DMSO-d_6, ^{1}H: 600MHz, ^{13}C: 150 MHz)

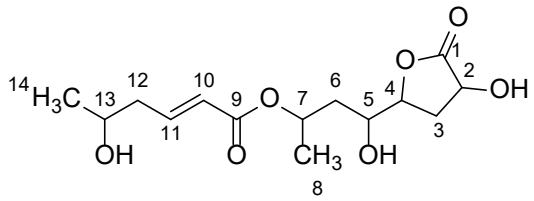

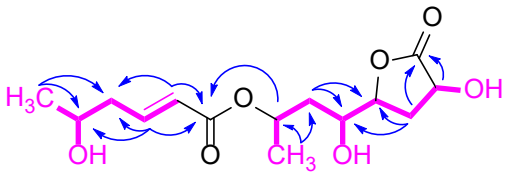

4-hydroxy-4-(4-hydroxy-5-oxotetrahydrofuran-2-yl)butan-2-yl (*E*)-5-hydroxyhex-2-enoate
Chemical Formula: $C_{14}H_{22}O_7$
Molecular Weight: 302,32

COSY —— key HMBC ⌒

position	δ_C	δ_H, m (J in Hz)
1*	177.0, C	
2	67.4, CH	4.45, dd (11.2, 8.1)
3	32.8, CH_2	2.38, ddd (12.0, 8.6, 5.4) 1.87, dt (12.0, 10.9)
4	78.3, CH	4.21, dt (10.3, 5.1)
5	67.8, CH	3.51, q (4.5)
6	38.3, CH_2	1.78, ddd (13.5, 9.3, 5.5) 1.59, ddd (13.5, 8.1, 4.1)
7	67.9, CH	5.04, dp (8.0, 6.3)
8	19.3, CH_3	1.22, d (6.2) 3H
9*	165.0, C	
10	122.7, CH	5.85, dt (15.6, 1.5)
11*	146.6, CH	6.89, dt (15.6, 7.3)
12	41.4, CH_2	2.25, m 2H
13	65.0, CH	3.74, h (6.1)
14	23.4, CH_3	1.05, d (6.2) 3H
2-OH		5.89, m
5-OH		5.19, d (5.7)
13-OH		4.67, br s

*signals were extracted from HSQC and HMBC spectra.

S28.[1]H-NMR Spectrum of Compound 4 (DMSO-d_6, 600 MHz)

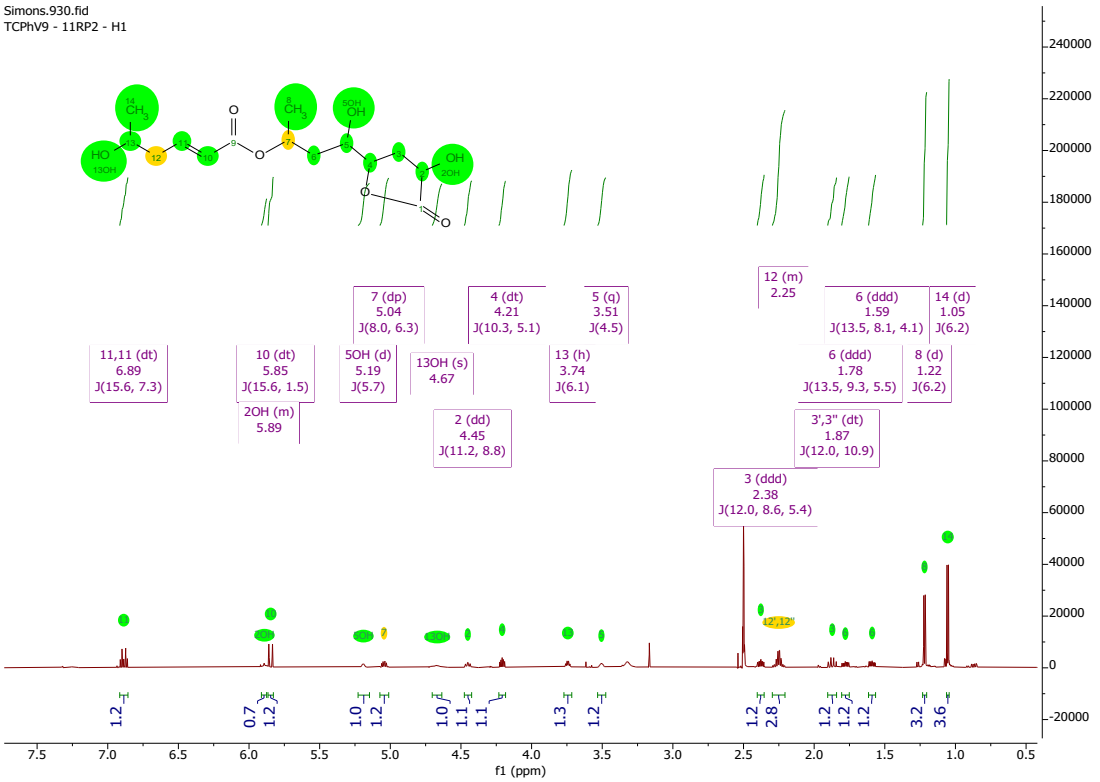

S29.[13]C-NMR Spectrum of Compound 4 (DMSO-d_6, 150 MHz)

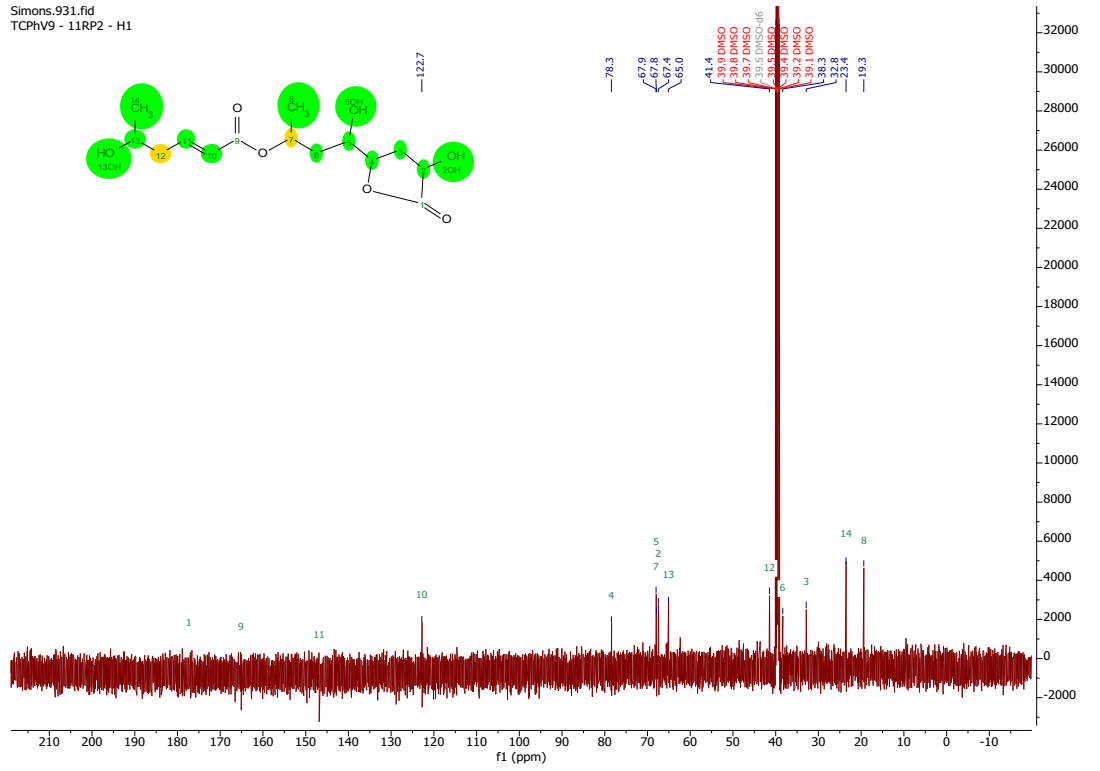

S30.^{1}H-^{13}C-HSQC Spectrum of Compound 4 (DMSO-d_6, ^{1}H: 600MHz, ^{13}C: 150 MHz)

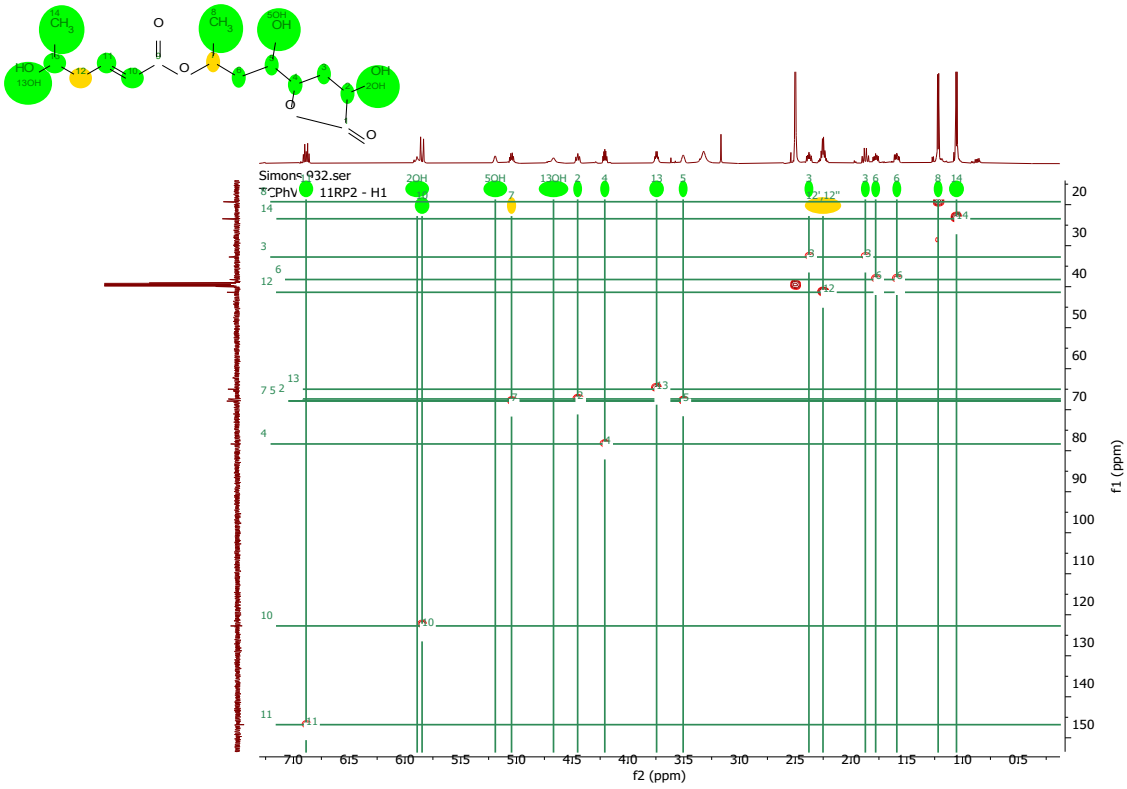

S31.^{1}H-^{13}C-HMBC Spectrum of Compound 4 (DMSO-d_6, ^{1}H: 600MHz, ^{13}C: 150 MHz)

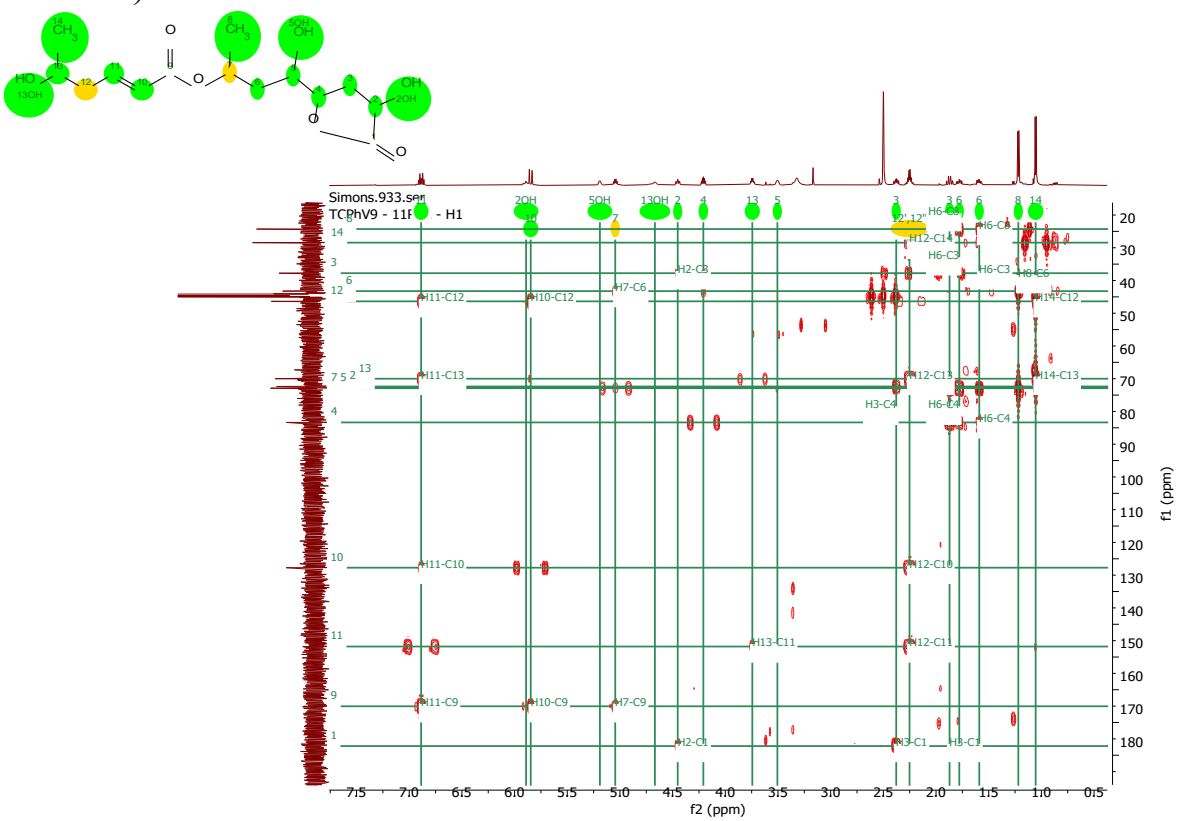

S32.^{1}H-^{1}H-COSY Spectrum of Compound 4 (DMSO-d_6, 600MHz)

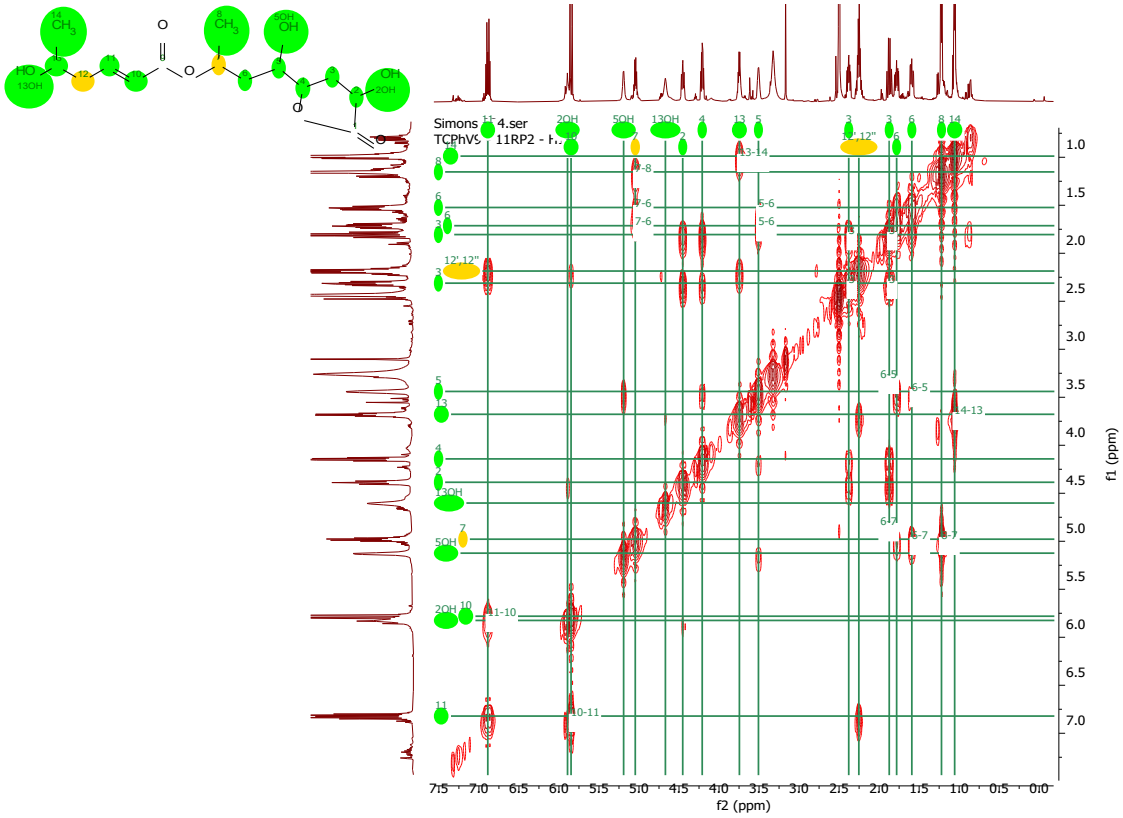

S33.HPLC-DAD UV-Vis Spectrum of Compound 4 (Methanol)

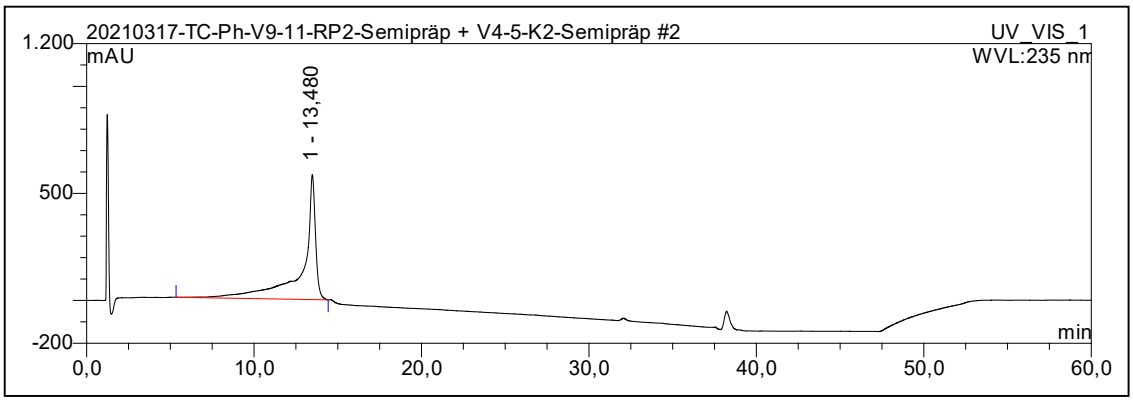

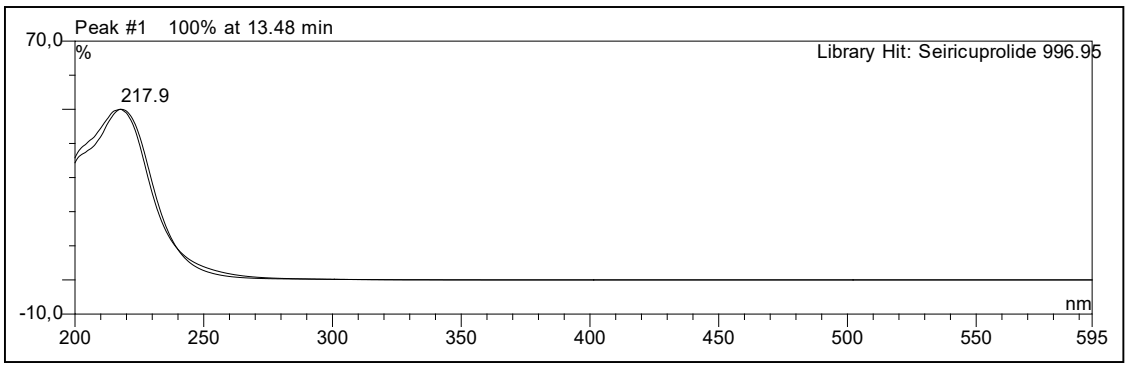

S34.ESI(+)MS Spectrum of Compound 4

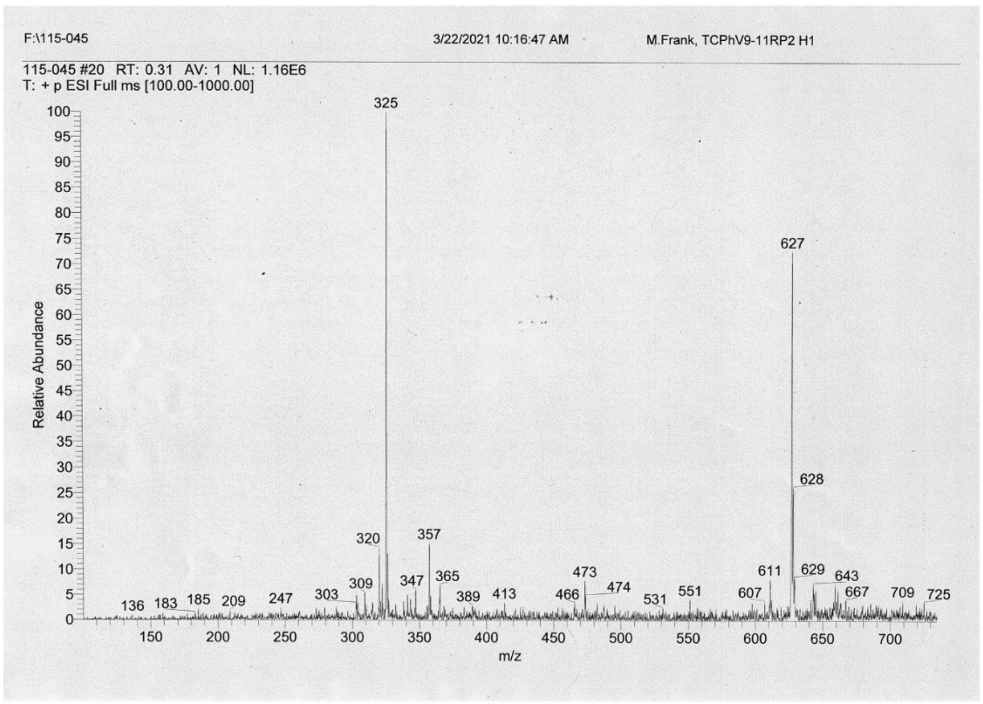

S35.High Resolution ESI(+)MS Spectrum of Compound 4

Mass Spectrum SmartFormula Report

Analysis Info

Analysis Name	D:\Data\Spektren 2021\KAL21HR000030.d	Acquisition Date	3/29/2021 9:58:06 AM
Method	tune_low_new.m	Operator	Peter Tommes
Sample Name	Simons TCPhV9-11RP2H1 (CH3OH)	Instrument	maXis 288882.20213
Comment			

Acquisition Parameter

Source Type	ESI	Ion Polarity	Positive	Set Nebulizer	0.3 Bar
Focus	Not active	Set Capillary	4000 V	Set Dry Heater	180 °C
Scan Begin	50 m/z	Set End Plate Offset	-500 V	Set Dry Gas	4.0 l/min
Scan End	1500 m/z	Set Collision Cell RF	600.0 Vpp	Set Divert Valve	Source

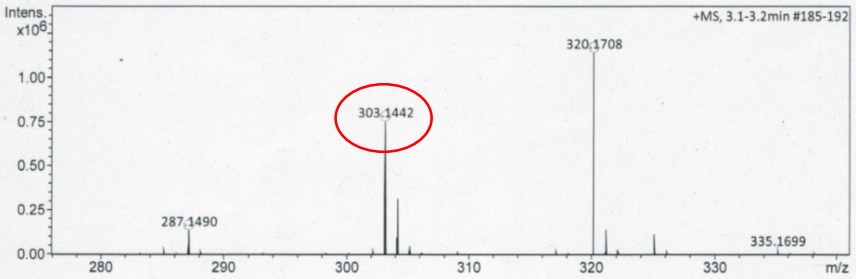

Meas. m/z	#	Ion Formula	m/z	err [ppm]	mSigma	# mSigma	Score	rdb	e⁻ Conf	N-Rule
287.1490	1	C14H23O6	287.1489	-0.3	1.9	1	100.00	3.5	even	ok
	2	C13H20N4NaO2	287.1478	-4.0	4.5	2	56.01	5.5	even	ok
	3	C11H15N10	287.1476	-5.0	6.4	3	45.55	9.5	even	ok
	4	C15H19N4O2	287.1503	4.4	15.2	4	42.62	8.5	even	ok
303.1442	1	C14H23O7	303.1438	-1.2	17.5	1	100.00	3.5	even	ok
	2	C11H15N10O	303.1425	-5.7	17.7	2	45.44	9.5	even	ok
	3	C13H20N4NaO3	303.1428	-4.8	18.1	3	54.54	5.5	even	ok
	4	C15H19N4O3	303.1452	3.2	30.6	4	55.23	8.5	even	ok
320.1708	1	C14H26NO7	320.1704	-1.3	21.7	1	100.00	2.5	even	ok
	2	C11H18N11O	320.1690	-5.5	21.9	2	45.20	8.5	even	ok
	3	C13H23N5NaO3	320.1693	-4.6	22.4	3	54.19	4.5	even	ok
	4	C15H22N5O3	320.1717	2.9	34.9	4	55.87	7.5	even	ok

S36.NMR Table of Compound 5 (DMSO-d_6, ^{1}H: 600MHz, ^{13}C: 150 MHz)

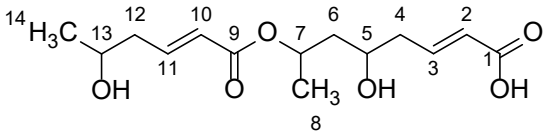

(*E*)-5-hydroxy-7-(((*E*)-5-hydroxyhex-2-enoyl)oxy)oct-2-enoic acid
Chemical Formula: $C_{14}H_{22}O_6$
Molecular Weight: 286,32

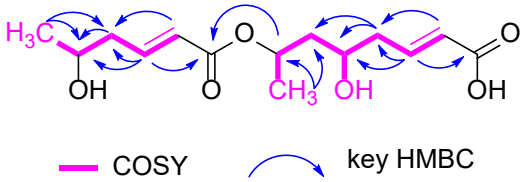

position	δ_C	δ_H, m (*J* in Hz)
1	167.2, C	
2	122.5, C	5.66, dd (15.7, 0.9)
3	149.3, CH	6.66, dd (15.7, 9.1)
4	41.2, CH_2	2.37, ddd (15.7, 8.1, 3.7) 2.26, m 3H
5	63.7, CH	3.37, dt (6.3, 3.6)
6	36.2, CH_2	1.78, ddd (13.8, 9.7, 3.8) 1.54, ddd (13.9, 10.3, 3.5)
7	68.0, CH	4.79, dqd (9.7, 6.1, 3.4)
8	20.1, CH_3	1.17, d (6.2)
9	165.1, C	
10	122.1, CH	5.84, dt (15.6, 1.5)
11	146.8, CH	6.89, dt (15.6, 7.3)
12	41.2, CH_2	2.26, m 3H
13	64.6, CH	3.75, m
14	23.0, CH_3	1.06, d (6.2)
5-OH		4.71, br s

S37.[1]H-NMR Spectrum of Compound 5 (DMSO-d_6, 600 MHz)

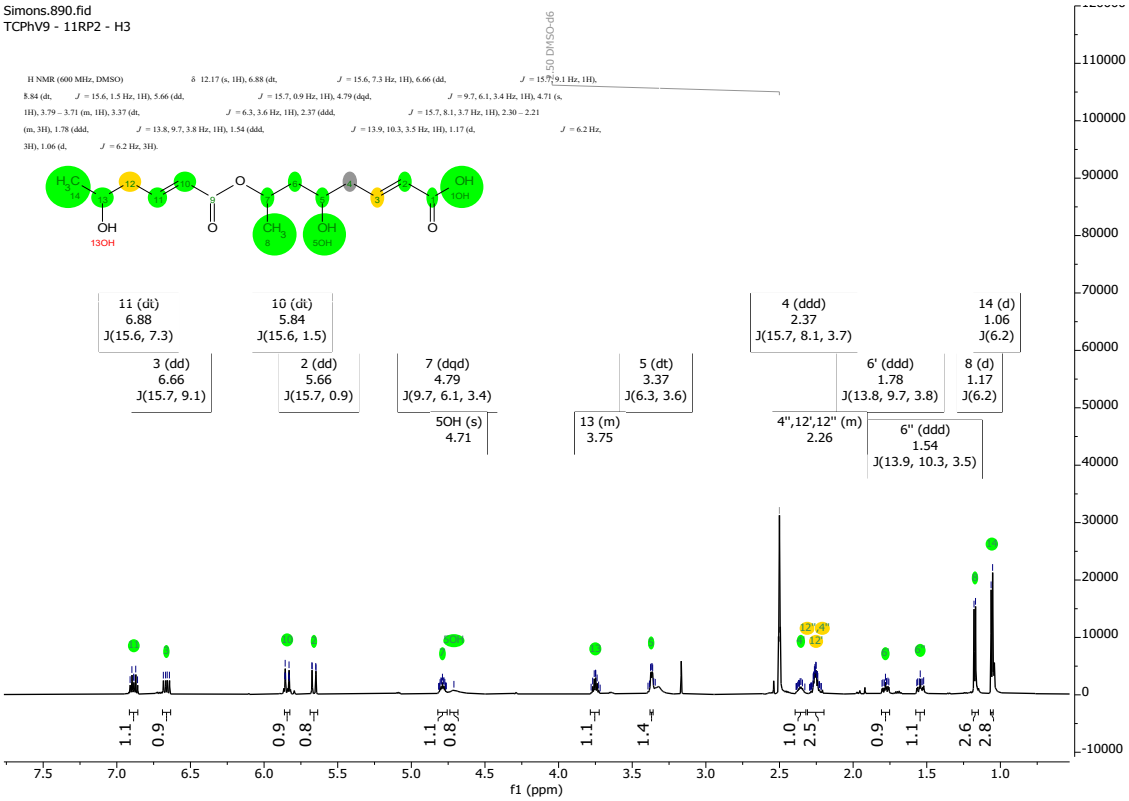

S38.[13]C-NMR Spectrum of Compound 5 (DMSO-d_6, 150 MHz)

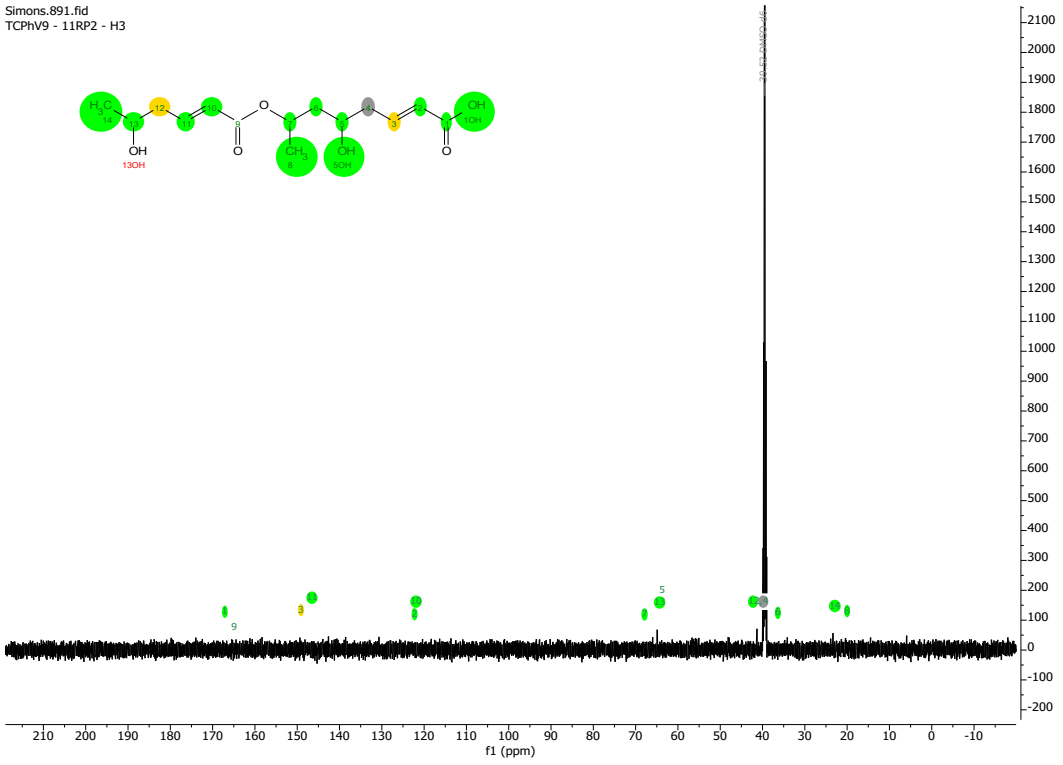

S39.^{1}H-^{13}C-HSQC Spectrum of Compound 5 (DMSO-d_6, ^{1}H: 600MHz, ^{13}C: 150 MHz)

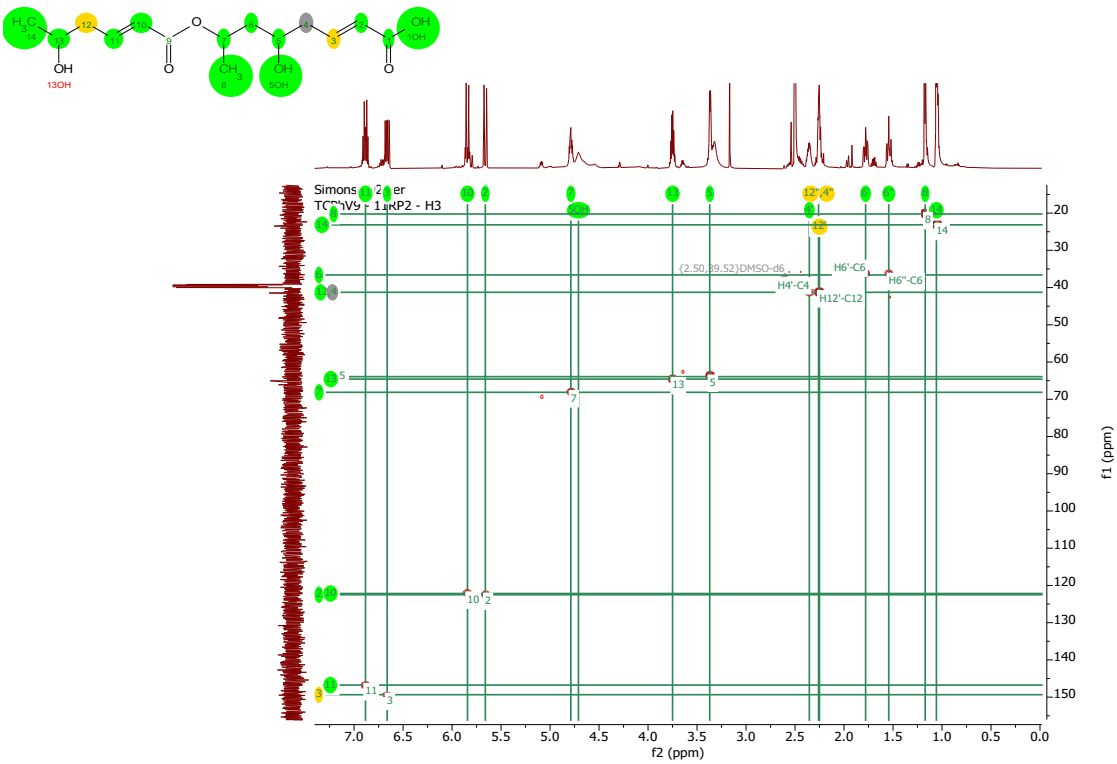

S40.^{1}H-^{13}C-HMBC Spectrum of Compound 5 (DMSO-d_6, ^{1}H: 600MHz, ^{13}C: 150 MHz)

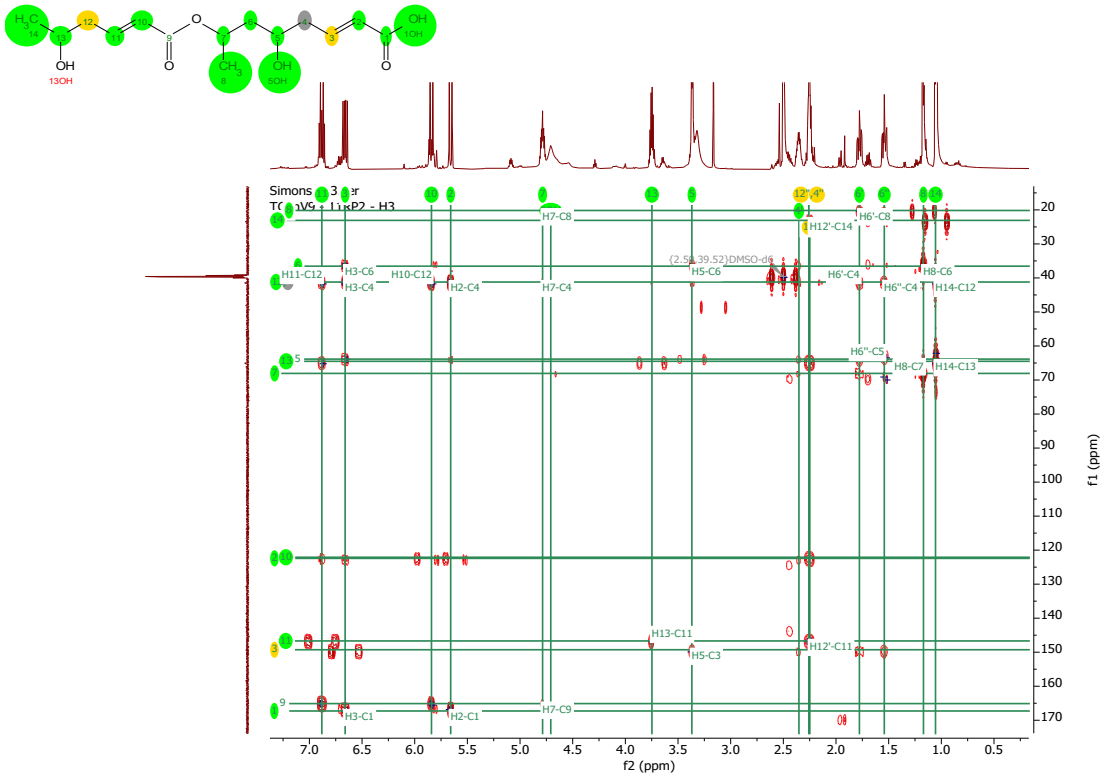

S41.^{1}H-^{1}H-COSY Spectrum of Compound 5 (DMSO-d_6, 600MHz)

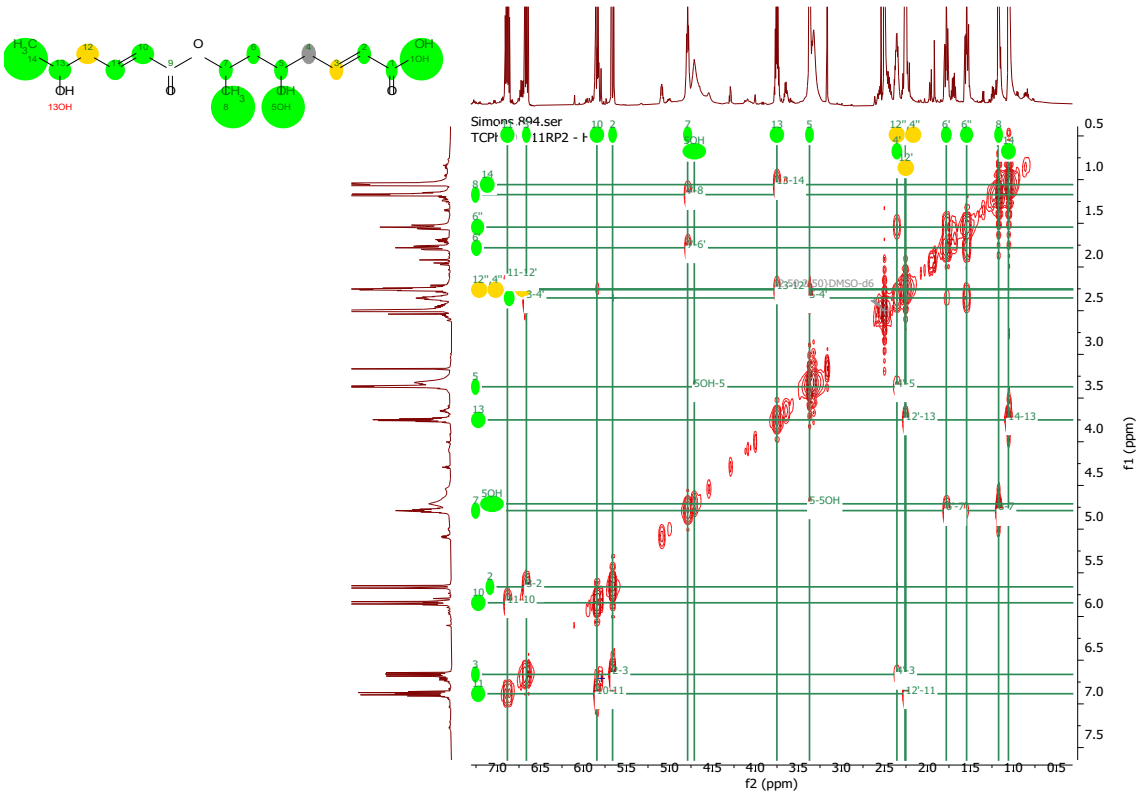

S42.UV-Vis Spectrum of Compound 5 (Methanol)

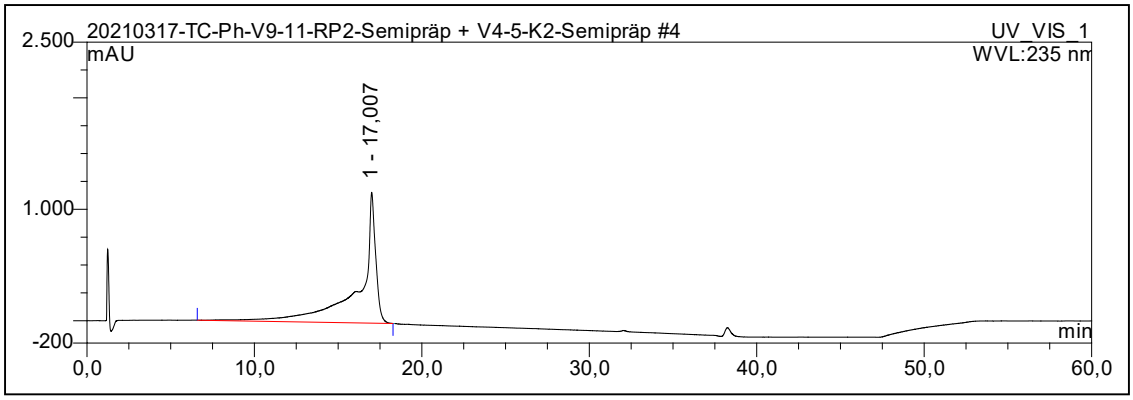

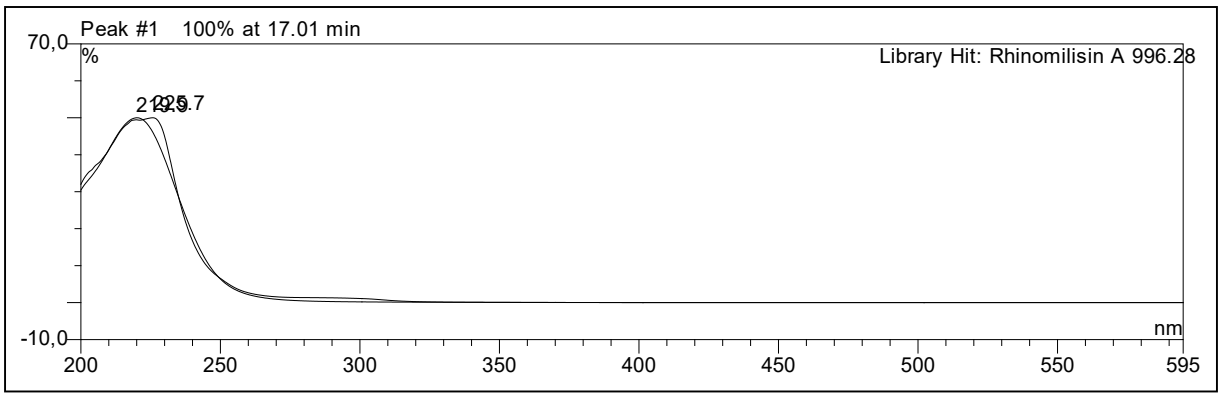

S43.ESI(+)MS Spectrum of Compound 5

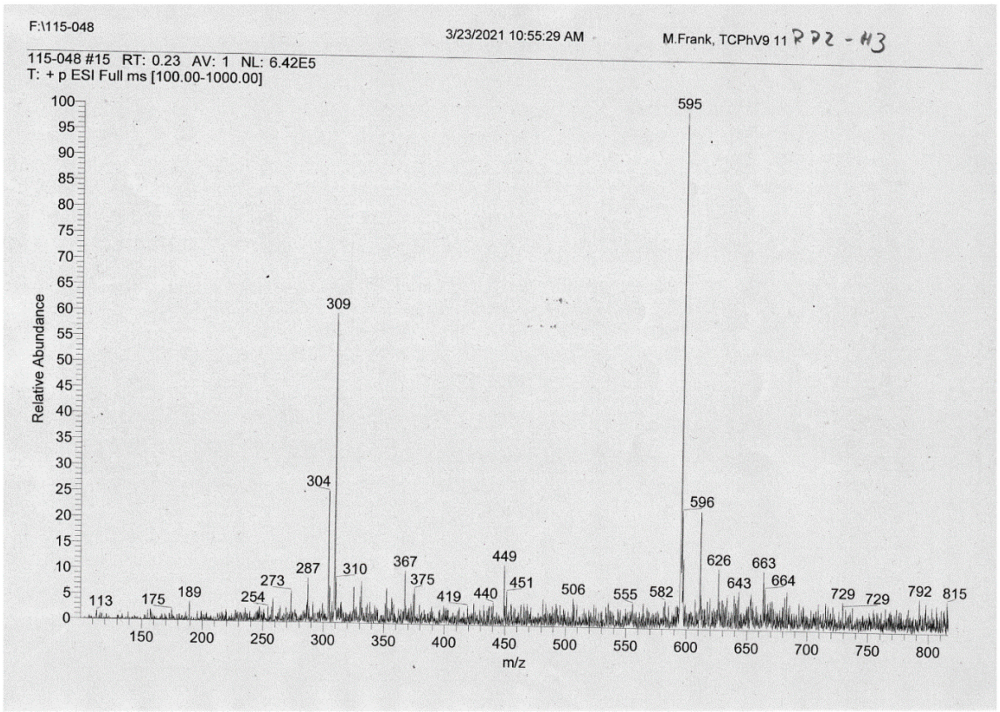

S44.High Resolution ESI(+)MS Spectrum of Compound 5

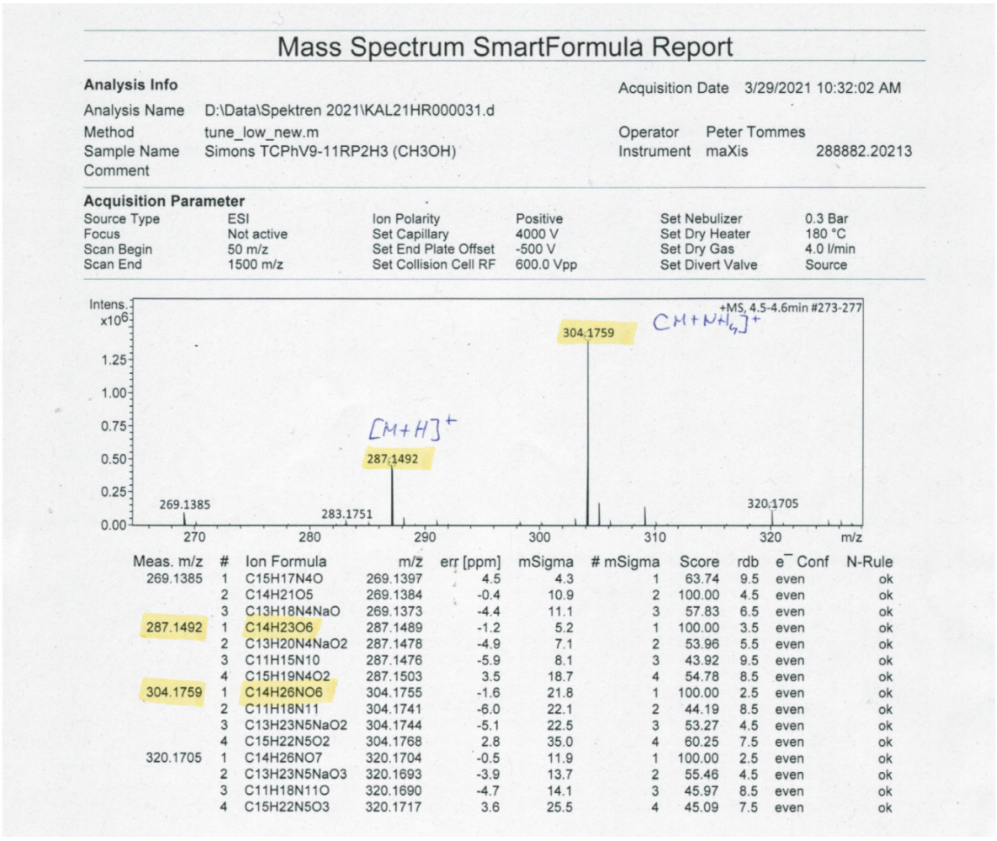

Mass Spectrum SmartFormula Report

Analysis Info

Analysis Name	D:\Data\Spektren 2021\KAL21HR000031.d	Acquisition Date	3/29/2021 10:32:02 AM
Method	tune_low_new.m	Operator	Peter Tommes
Sample Name	Simons TCPhV9-11RP2H3 (CH3OH)	Instrument	maXis 288882.20213
Comment			

Acquisition Parameter

Source Type	ESI	Ion Polarity	Positive	Set Nebulizer	0.3 Bar
Focus	Not active	Set Capillary	4000 V	Set Dry Heater	180 °C
Scan Begin	50 m/z	Set End Plate Offset	-500 V	Set Dry Gas	4.0 l/min
Scan End	1500 m/z	Set Collision Cell RF	600.0 Vpp	Set Divert Valve	Source

Meas. m/z	#	Ion Formula	m/z	err [ppm]	mSigma	# mSigma	Score	rdb	e⁻ Conf	N-Rule
269.1385	1	C15H17N4O	269.1397	4.5	4.3	1	63.74	9.5	even	ok
	2	C14H21O5	269.1384	-0.4	10.9	2	100.00	4.5	even	ok
	3	C13H18N4NaO	269.1373	-4.4	11.1	3	57.83	6.5	even	ok
287.1492	1	C14H23O6	287.1489	-1.2	5.2	1	100.00	3.5	even	ok
	2	C13H20N4NaO2	287.1478	-4.9	7.1	2	53.96	5.5	even	ok
	3	C11H15N10	287.1476	-5.9	8.1	3	43.92	9.5	even	ok
	4	C15H19N4O2	287.1503	3.5	18.7	4	54.78	8.5	even	ok
304.1759	1	C14H26NO6	304.1755	-1.6	21.8	1	100.00	2.5	even	ok
	2	C11H18N11	304.1741	-6.0	22.1	2	44.19	8.5	even	ok
	3	C13H23N5NaO2	304.1744	-5.1	22.5	3	53.27	4.5	even	ok
	4	C15H22N5O2	304.1768	2.8	35.0	4	60.25	7.5	even	ok
320.1705	1	C14H26NO7	320.1704	-0.5	11.9	1	100.00	2.5	even	ok
	2	C13H23N5NaO3	320.1693	-3.9	13.7	2	55.46	4.5	even	ok
	3	C11H18N11O	320.1690	-4.7	14.1	3	45.97	8.5	even	ok
	4	C15H22N5O3	320.1717	3.6	25.5	4	45.09	7.5	even	ok

S45.NMR Table of Compound 6 (600 MHz, CDCl3)

Chaetochromin A (KOYAMA et al. 1987)

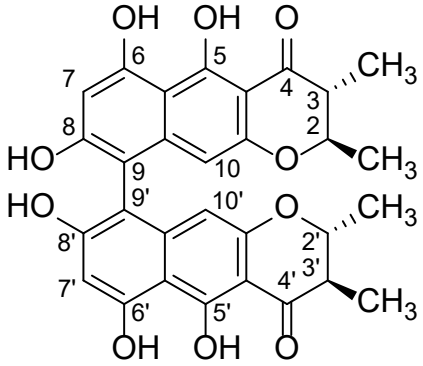

Chemical Formula: $C_{30}H_{26}O_{10}$
Molecular Weight: 546,53

position	δ_H, m (*J* in Hz)
2, 2’	4.16, dq (12.3, 6.1)
3, 3’	2.58, dq (11.1, 6.9)
7, 7’	5.91, s
10, 10’	6.36, s
2-CH_3, 2’-CH_3	1.40, d (6.2)
3-CH_3, 3’-CH_3	1.20, d (6.9)
5-OH, 5’-OH	15.07, s
6-OH, 6’-OH	9.42, s

S46.[1]H-NMR Spectrum of Compound 6 (600 MHz, CDCl3)

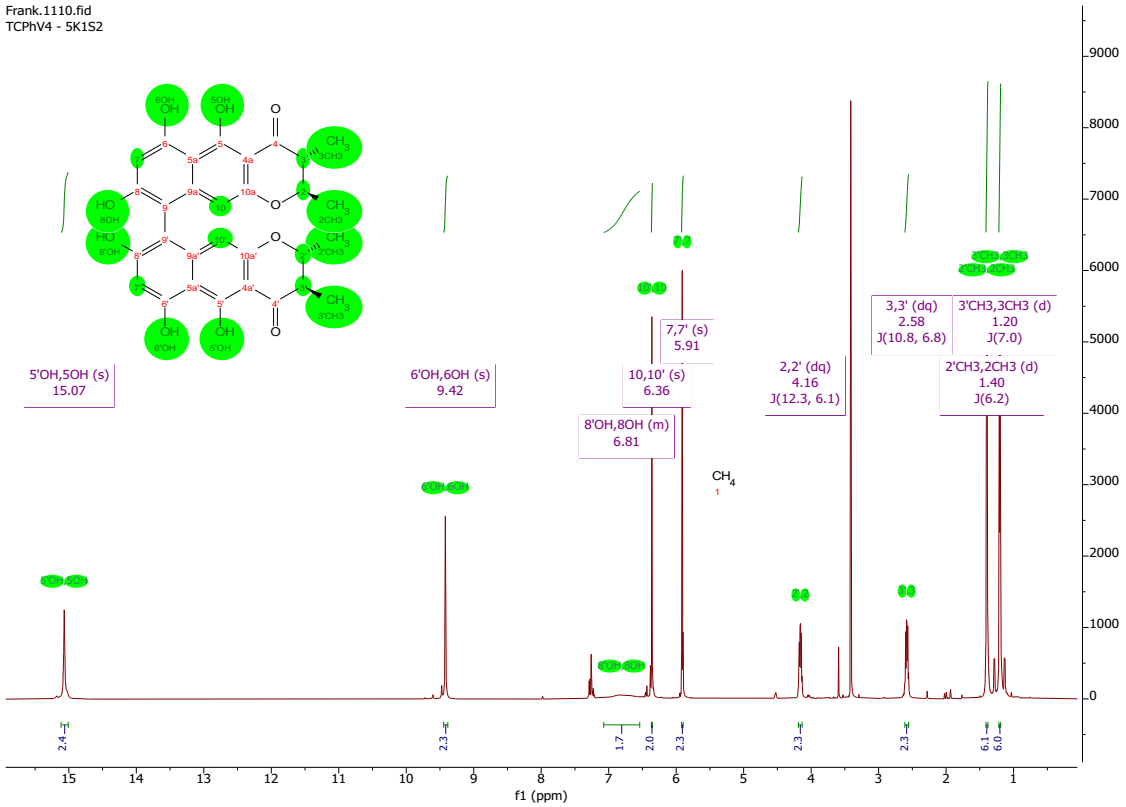

S47.UV-Vis Spectrum of Compound 6 (Methanol)

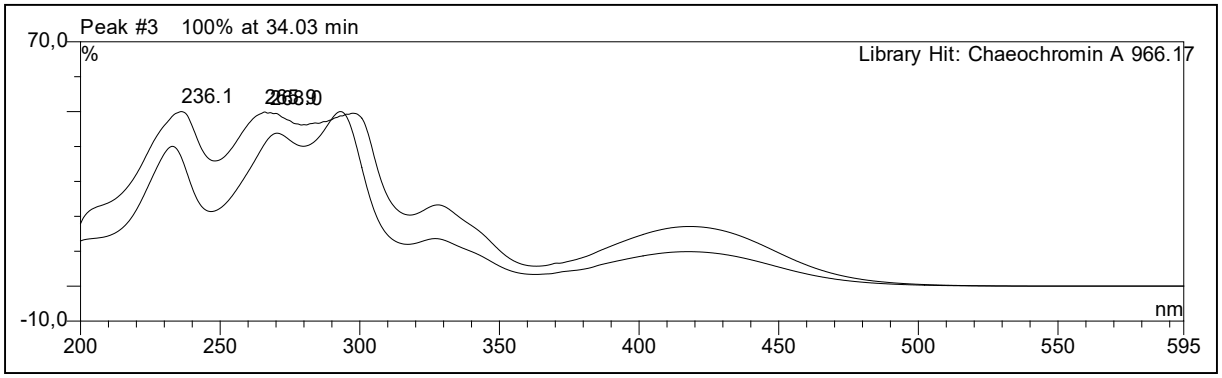

S48.ESI(+)MS Spectrum of Compound 6

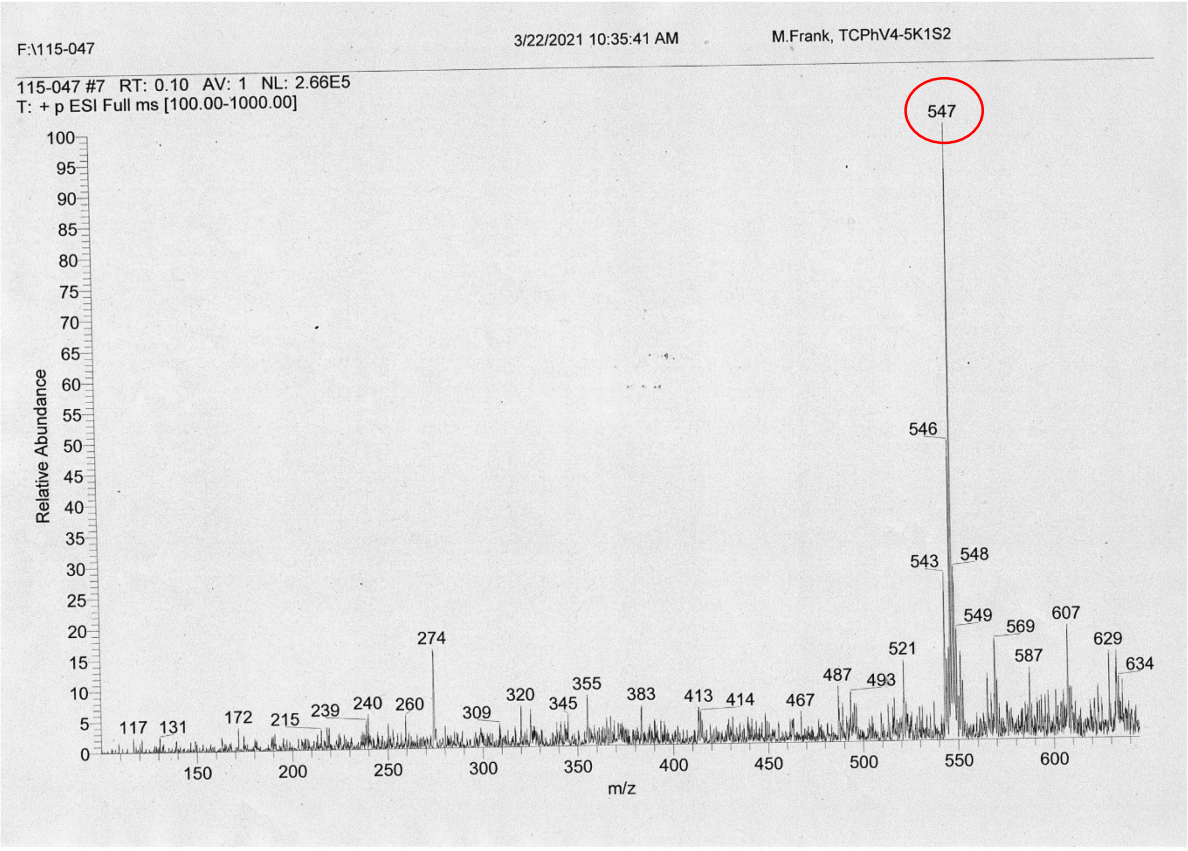

S49.NMR Table of Compound 7 (DMSO-d_6, ^{1}H: 600MHz, ^{13}C: 150 MHz)

Phenazine-1-carboxylic acid (Mehnaz et al. 2013)

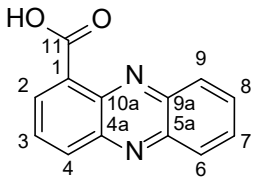

Chemical Formula: $C_{13}H_8N_2O_2$
Molecular Weight: 224,22

position	δ_C*	δ_H, m (J in Hz)
1	129.4, C	
2	133.0, CH	8.49, d (8.1) 2H
3	130.4, CH	8.08, m 3H
4	128.5, CH	8.39, dd (7.7, 1.3)
4a	143.3, C	
5a	141.0, C	
6	129.2, CH	8.35, dd (7.3, 2.0)
7	132.1, CH	8.08, m 3H
8	132.1, CH	8.08, m 3H
9	133.0, CH	8.49, d (8.1) 2H
9a	139.9	
10a	139.9	
11	166.8, C	
11-OH		14.43, br s

*signals were extracted from HSQC and HMBC spectra.

S50.[1]H-NMR Spectrum of Compound 7 (DMSO-d_6, 600 MHz)

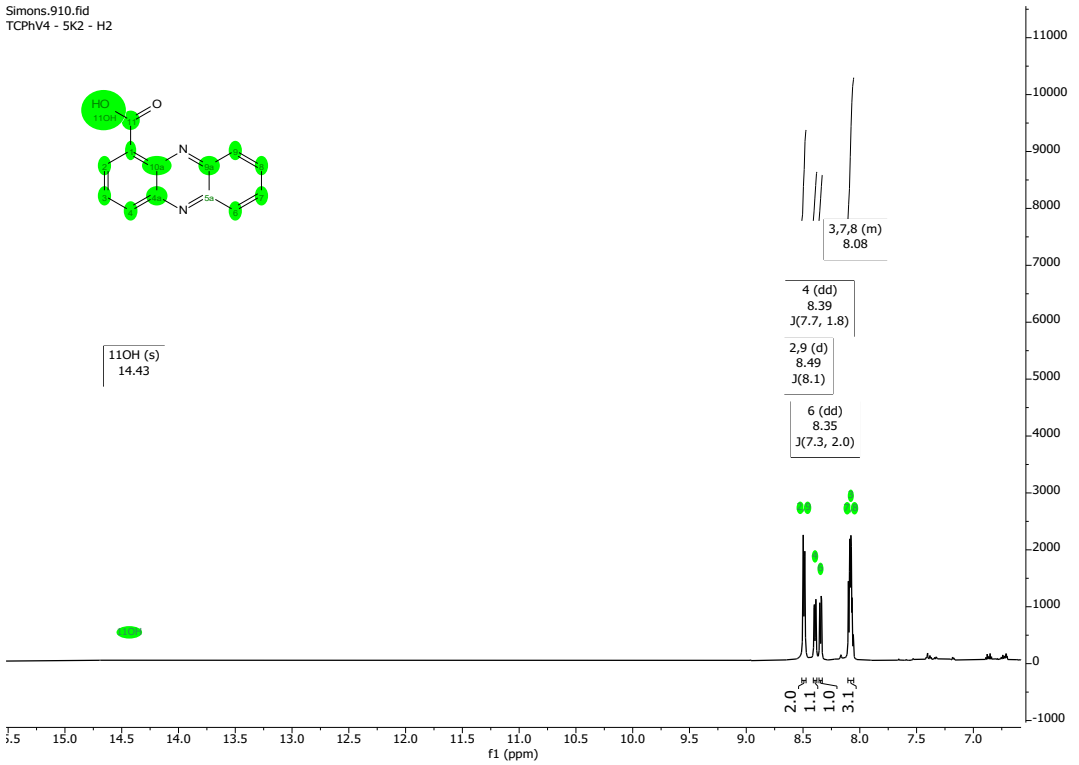

S51.[13]C-NMR Spectrum of Compound 7 (DMSO-d_6, 150 MHz)

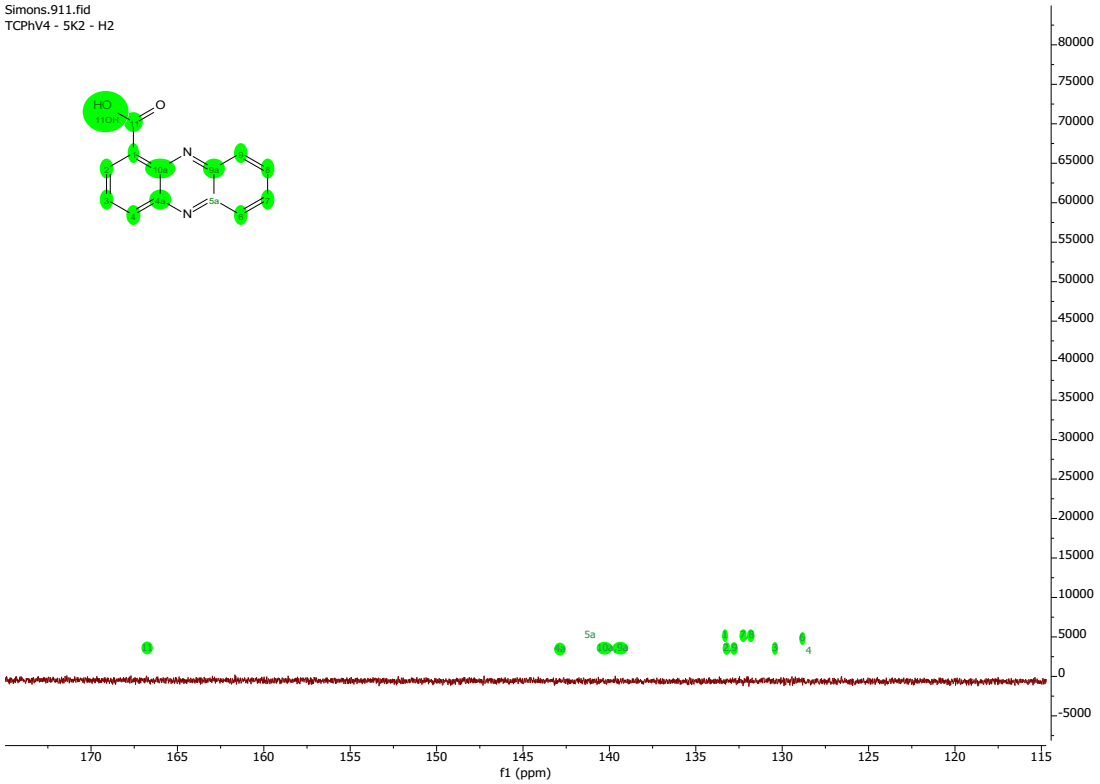

S52.^{1}H-^{13}C-HSQC Spectrum of Compound 7 (DMSO-d_6, ^{1}H: 600MHz, ^{13}C: 150 MHz)

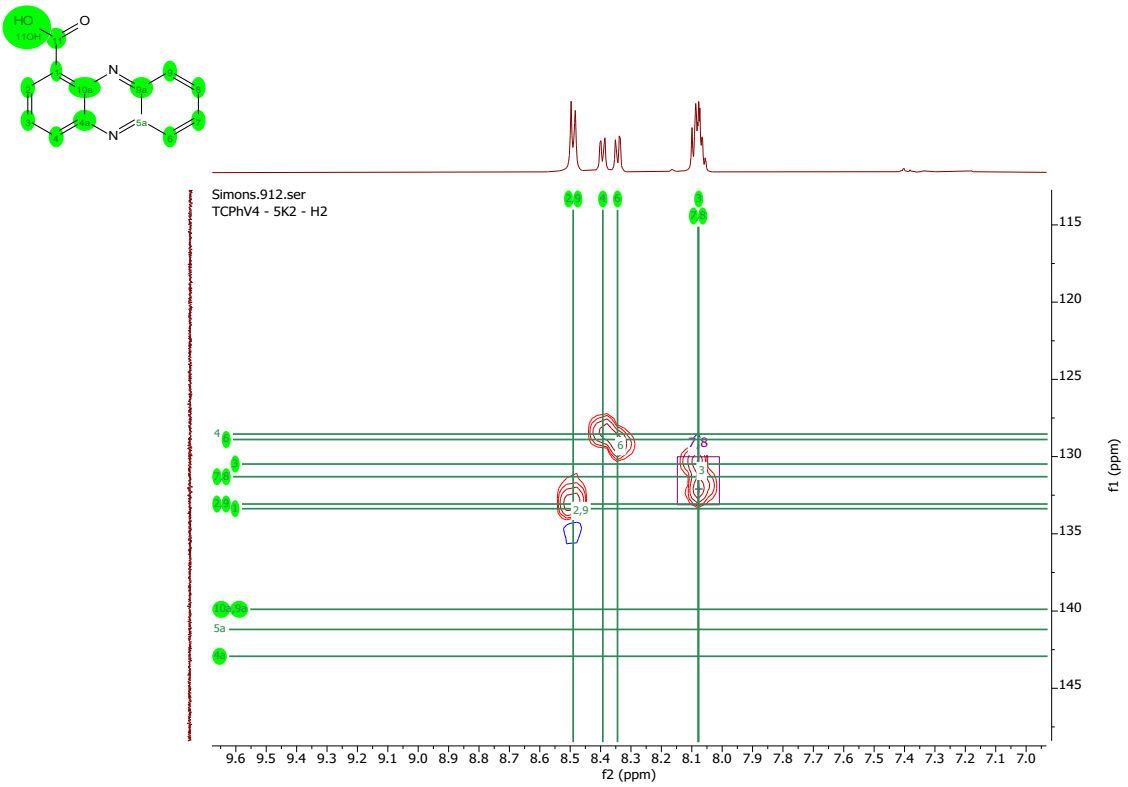

S53.^{1}H-^{13}C-HMBC Spectrum of Compound 7 (DMSO-d_6, ^{1}H: 600MHz, ^{13}C: 150 MHz)

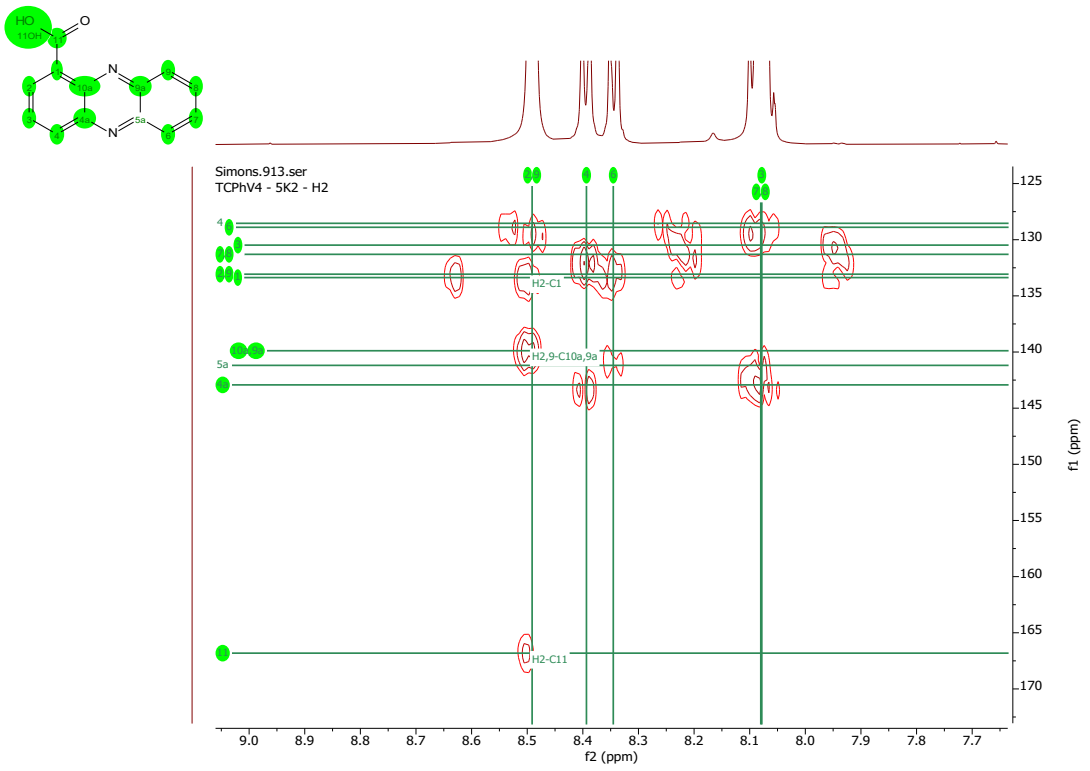

S54.^{1}H-^{1}H-COSY Spectrum of Compound 7 (DMSO-d_6, 600MHz)

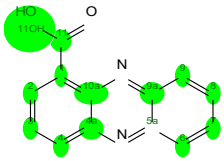

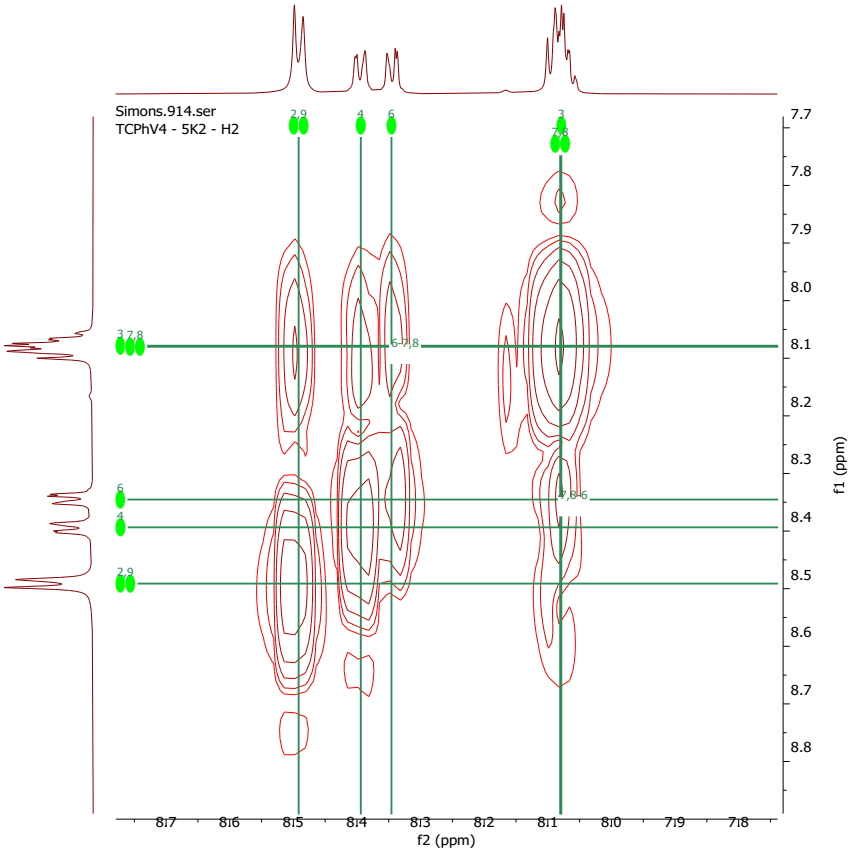

S55.UV-Vis Spectrum of Compound 7 (Methanol)

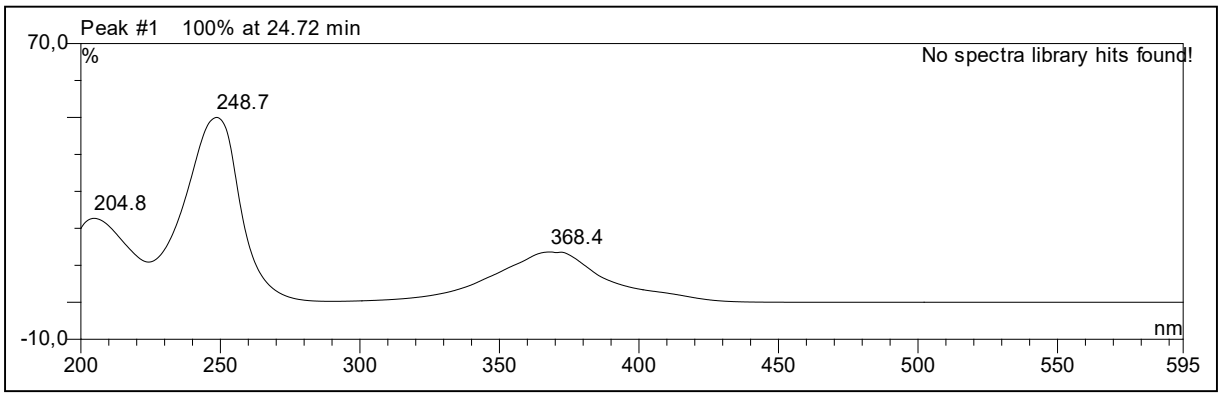

S56.ESI(+)MS Spectrum of Compound 7

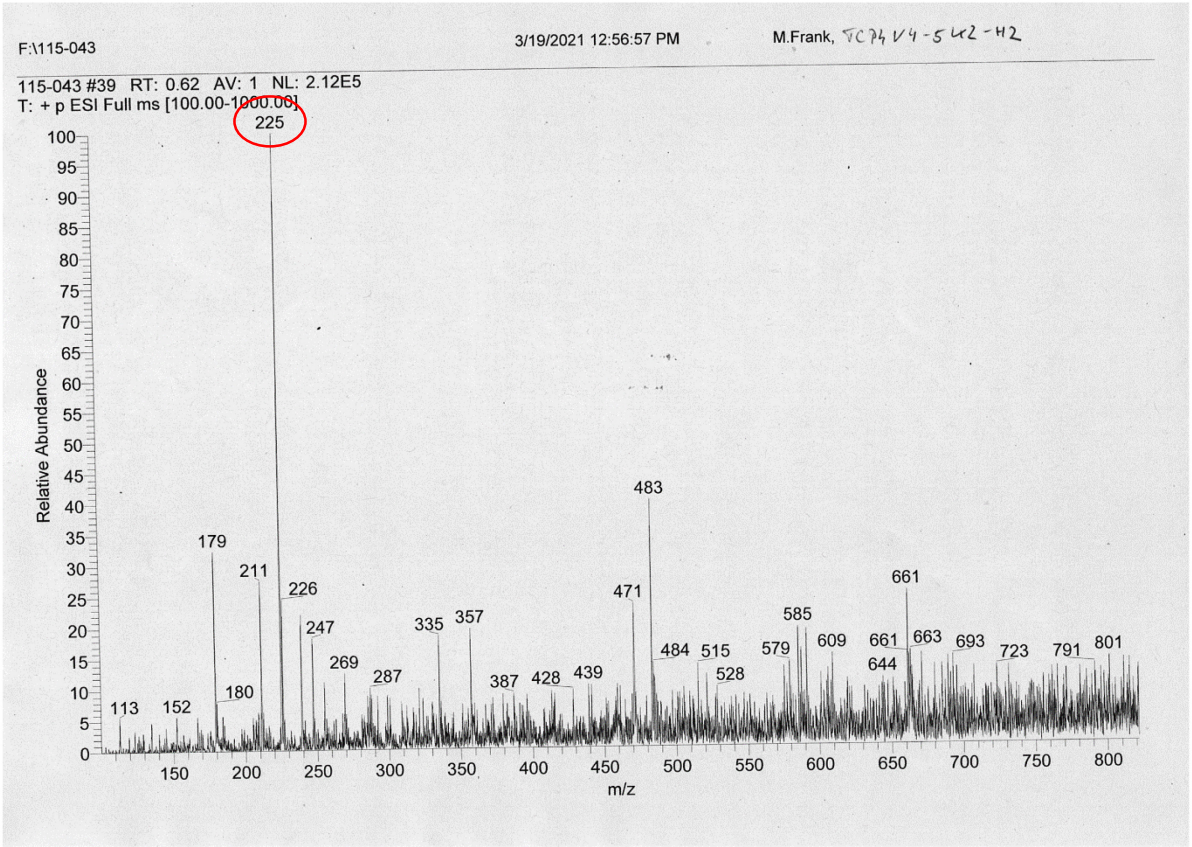

S57.NMR Table of Compound 8 (DMSO-d_6, ^{1}H: 600MHz, ^{13}C: 150 MHz)

Phenazine-1-carboxamide (Kumar et al. 2005)

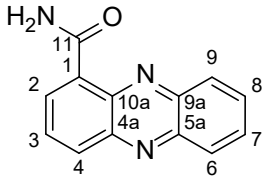

Chemical Formula: $C_{13}H_9N_3O$
Molecular Weight: 223,24

position	δ_C	δ_H, m (J in Hz)
1	131.0, C	
2	134.1, CH	8.68, dd (7.0, 1.5)
3	130.3, CH	8.07, dd (8.7, 7.0)
4	133.1, CH	8.43, dd (8.6, 1.5)
4a	142.8, C	
5a	142.6, C	
6	129.4, CH	8.41, m
7	131.7, CH	8.04, m 2H
8	132.1, CH	8.04, m 2H
9	129.2, CH	8.30, m
9a	141.4, C	
10a	140.2, C	
11	165.8, C	
11-NH_2		9.74, br s 8.10, br s

S58.[1]H-NMR Spectrum of Compound 8 (DMSO-d_6, 600 MHz)

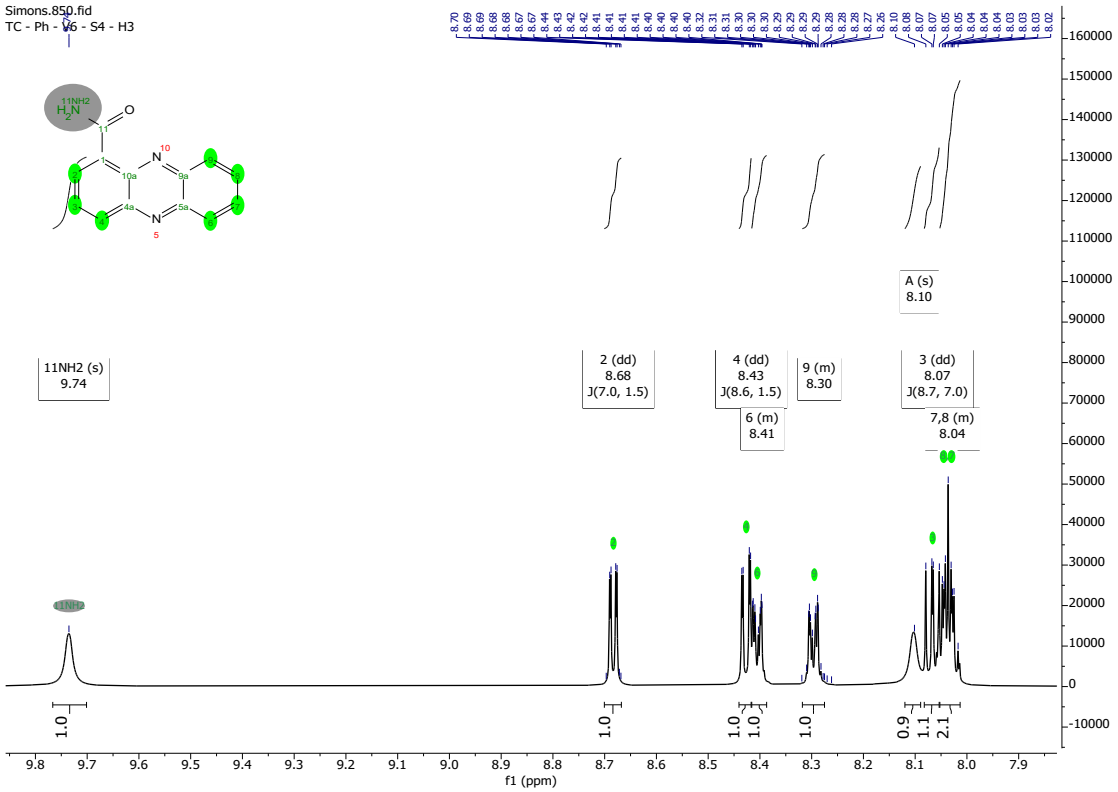

S59.[13]C-NMR Spectrum of Compound 8 (DMSO-d_6, 150 MHz)

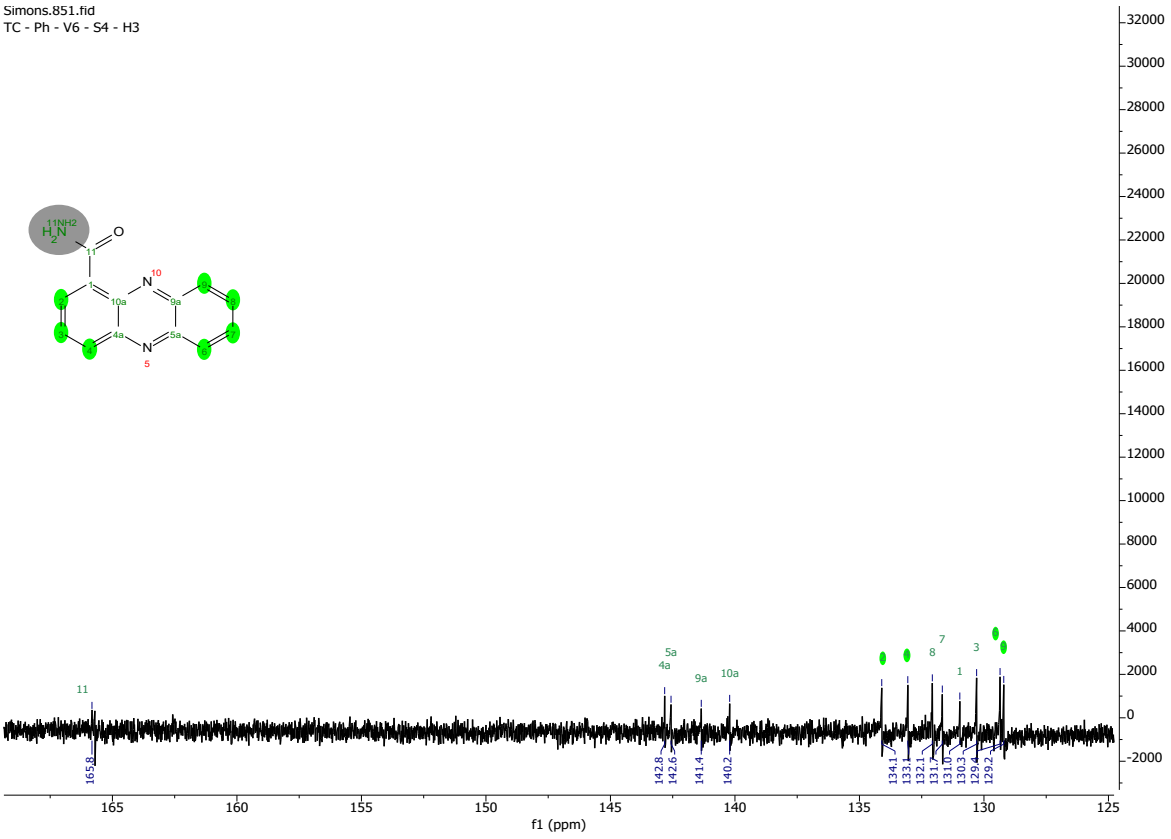

S60.^{1}H-^{13}C-HSQC Spectrum of Compound 8 (DMSO-d_6, ^{1}H: 600MHz, ^{13}C: 150 MHz)

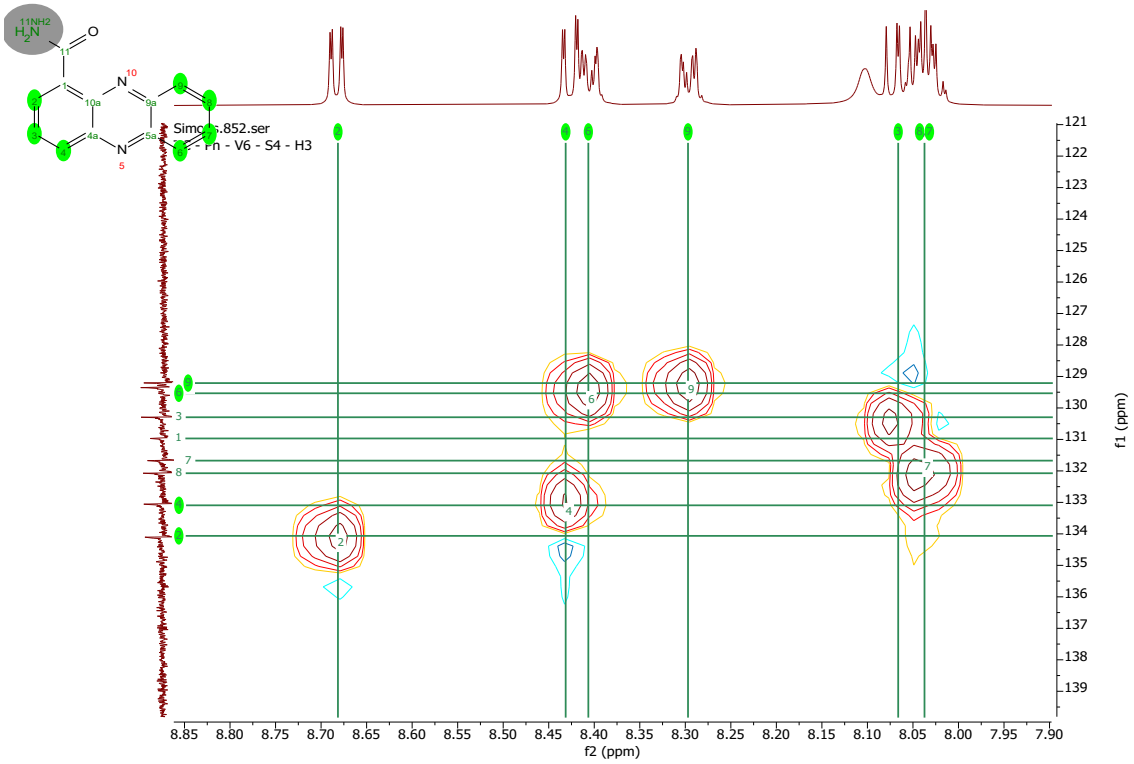

S61.^{1}H-^{13}C-HMBC Spectrum of Compound 8 (DMSO-d_6, ^{1}H: 600MHz, ^{13}C: 150 MHz)

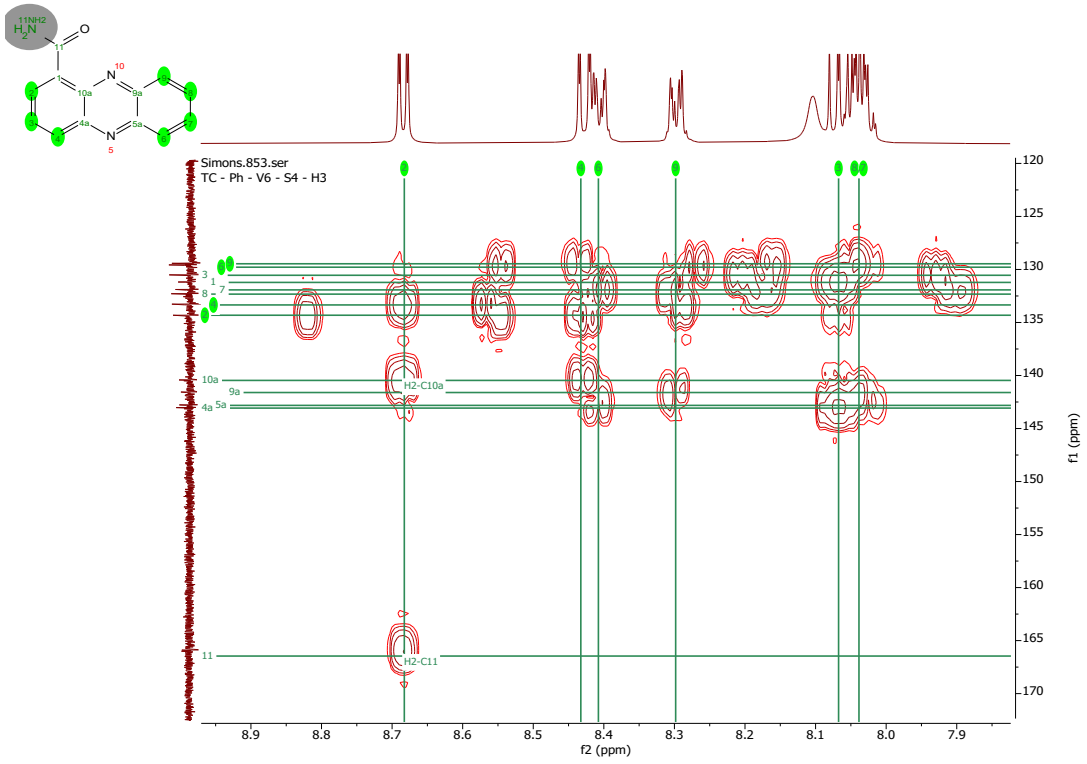

S62.^{1}H-^{1}H-COSY Spectrum of Compound 8 (DMSO-d_6, 600MHz)

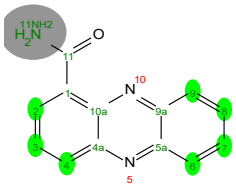

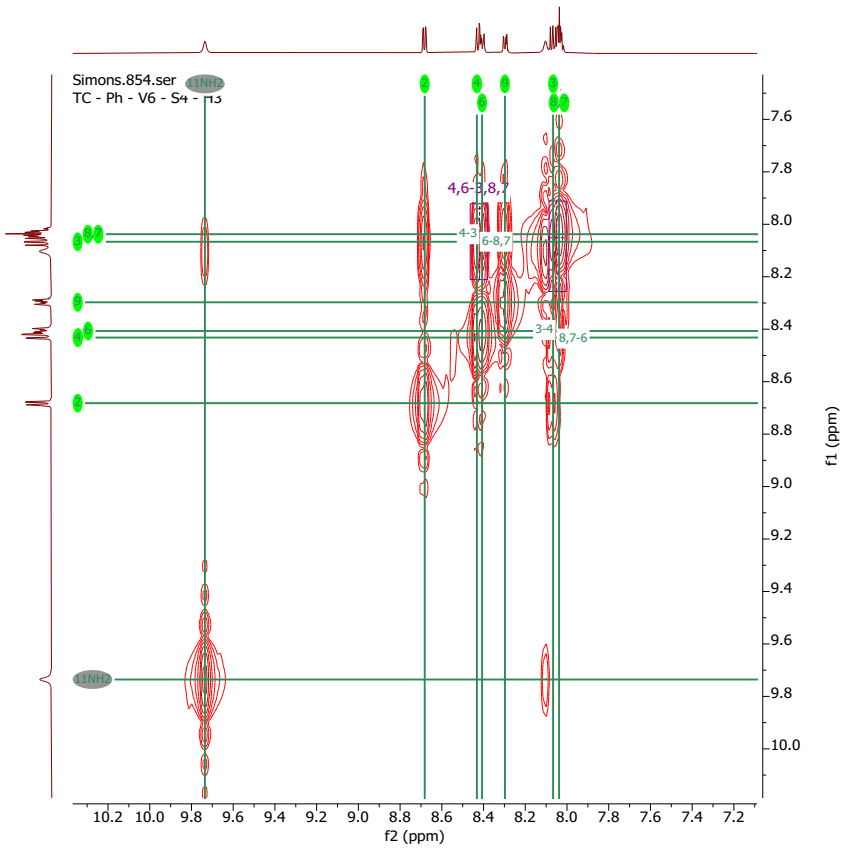

S63.UV-Vis Spectrum of Compound 8 (Methanol)

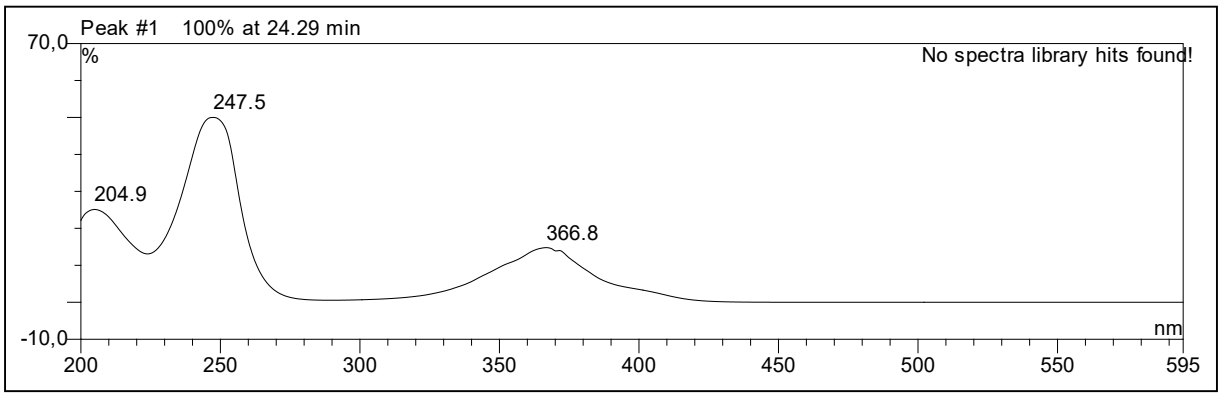

S64.ESI(+)MS Spectrum of Compound 8

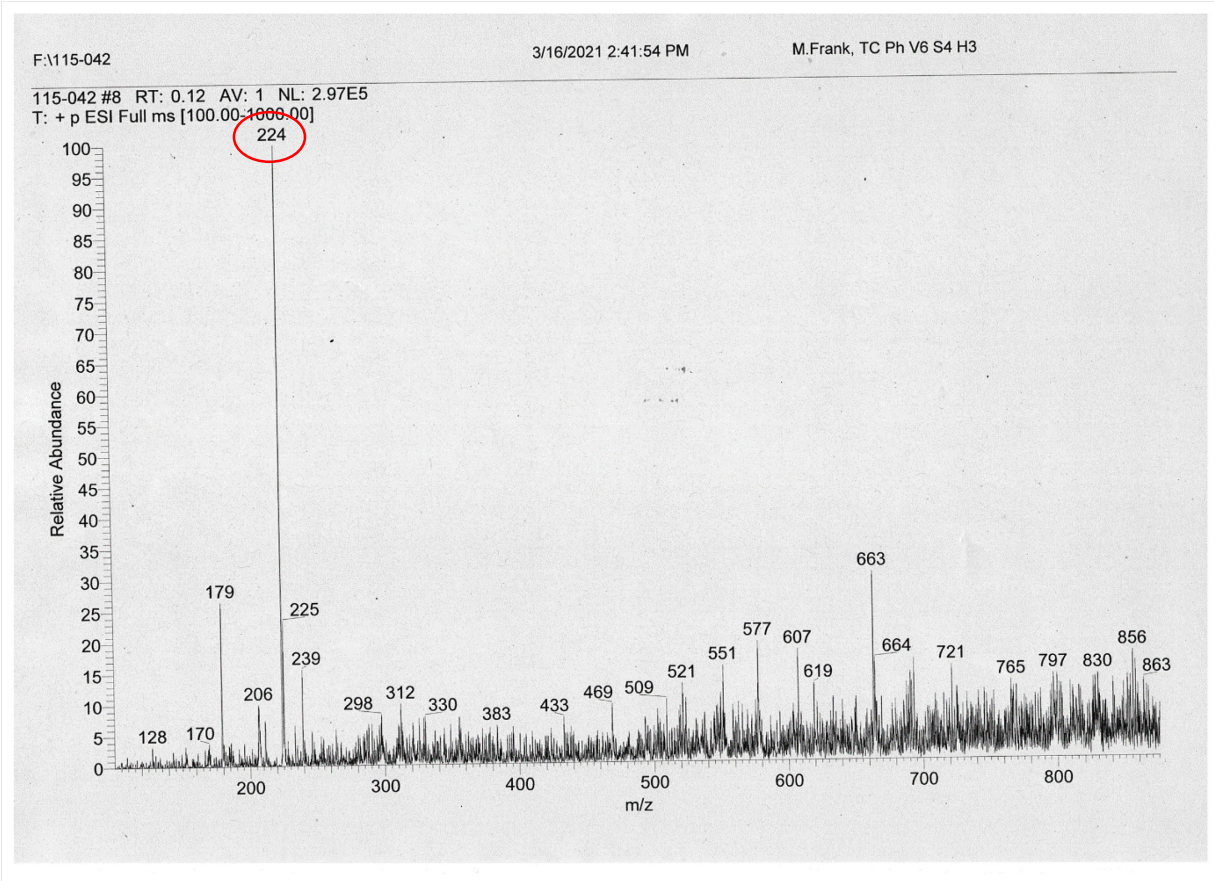

S65.High Resolution ESI(+)MS Spectrum of Compound 8

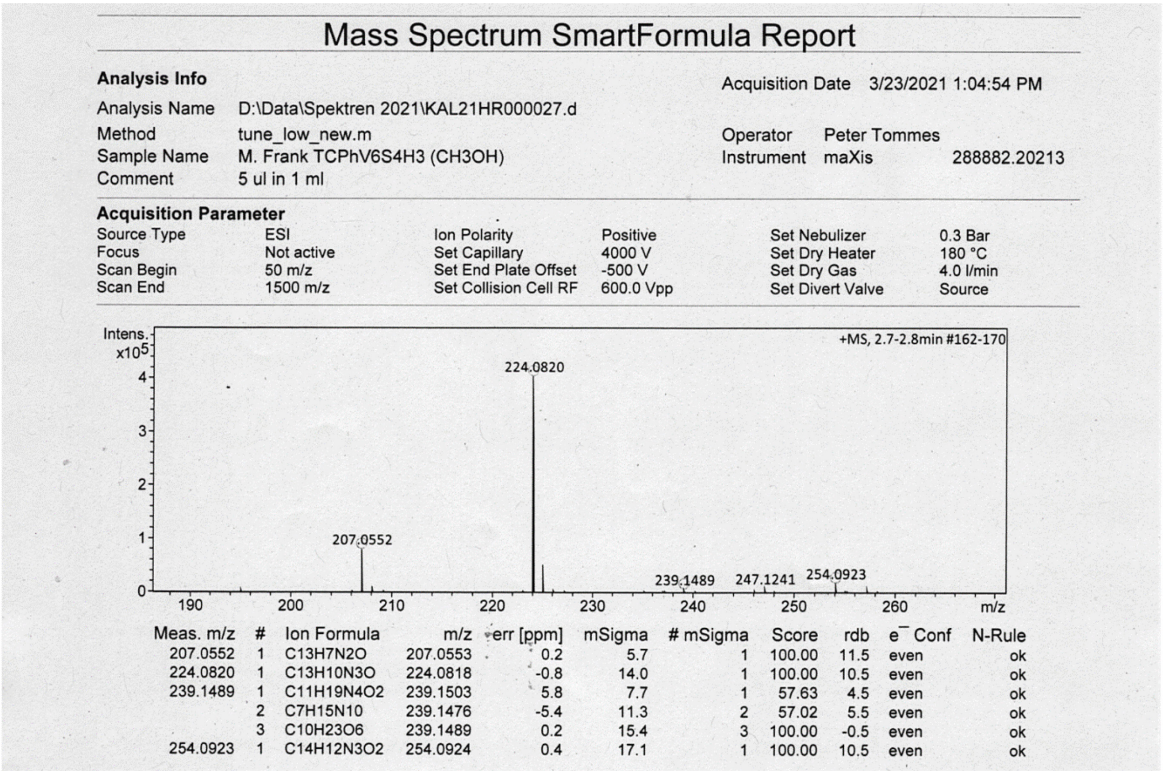

Mass Spectrum SmartFormula Report

Analysis Info

Analysis Name	D:\Data\Spektren 2021\KAL21HR000027.d	Acquisition Date	3/23/2021 1:04:54 PM
Method	tune_low_new.m	Operator	Peter Tommes
Sample Name	M. Frank TCPhV6S4H3 (CH3OH)	Instrument	maXis 288882.20213
Comment	5 ul in 1 ml		

Acquisition Parameter

Source Type	ESI	Ion Polarity	Positive	Set Nebulizer	0.3 Bar
Focus	Not active	Set Capillary	4000 V	Set Dry Heater	180 °C
Scan Begin	50 m/z	Set End Plate Offset	-500 V	Set Dry Gas	4.0 l/min
Scan End	1500 m/z	Set Collision Cell RF	600.0 Vpp	Set Divert Valve	Source

Meas. m/z	#	Ion Formula	m/z	err [ppm]	mSigma	# mSigma	Score	rdb	e⁻ Conf	N-Rule
207.0552	1	C13H7N2O	207.0553	0.2	5.7	1	100.00	11.5	even	ok
224.0820	1	C13H10N3O	224.0818	-0.8	14.0	1	100.00	10.5	even	ok
239.1489	1	C11H19N4O2	239.1503	5.8	7.7	1	57.63	4.5	even	ok
	2	C7H15N10	239.1476	-5.4	11.3	2	57.02	5.5	even	ok
	3	C10H23O6	239.1489	0.2	15.4	3	100.00	-0.5	even	ok
254.0923	1	C14H12N3O2	254.0924	0.4	17.1	1	100.00	10.5	even	ok

S66.NMR Table of Compound 9 (MeOH-d4, ^{1}H: 600MHz, ^{13}C: 150 MHz)

Dechlorodihydromaldoxin (Yu und Snider 2011)

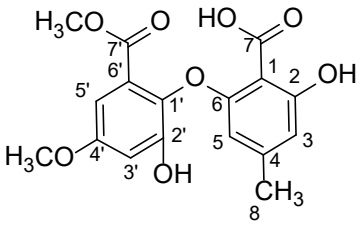

Chemical Formula: $C_{17}H_{16}O_8$
Molecular Weight: 348,31

position	δ_C*	δ_H, m (*J* in Hz)
1	undetected*	
2	160.1, C	
3	106.8, CH	5.85, br s
4	146.2, C	
5	112.1, CH	6.42, br s
6	163.2, C	
7	undetected*	
8	21.5, CH_3	2.13, s
1’	136.7, C	
2’	153.2, C	
3’	107.9, CH	6.75, d (3.1)
4’	158.8, C	
5’	107.0, CH	6.96, d (3.1)
6’	126.3, C	
7’	167.1, C	
4’-OCH_3	55.8, CH_3	3.82, s
7’-OCH_3	52.4, CH_3	3.72, s

*signals were extracted from HSQC and HMBC spectra.
*matches observation from literature data.

S67.[1]H-NMR Spectrum of Compound 9 (MeOH-d4, 600 MHz)

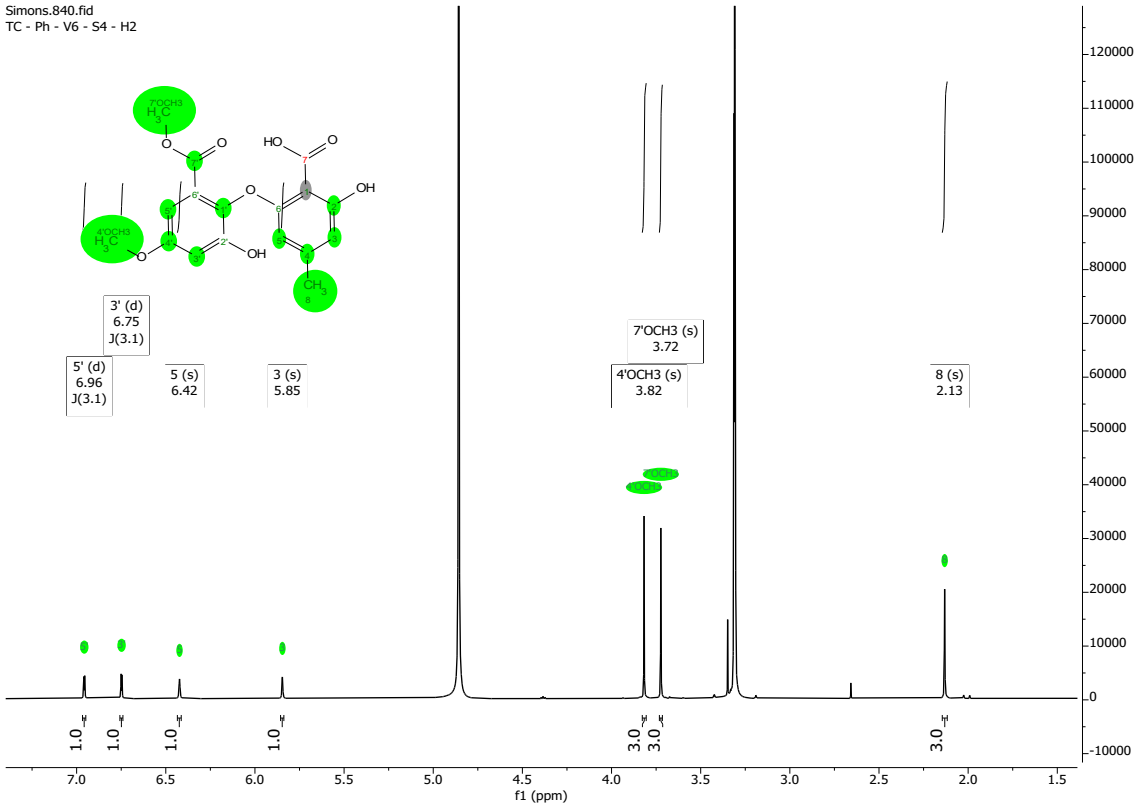

S68.[13]C-NMR Spectrum of Compound 9 (MeOH-d4, 150 MHz)

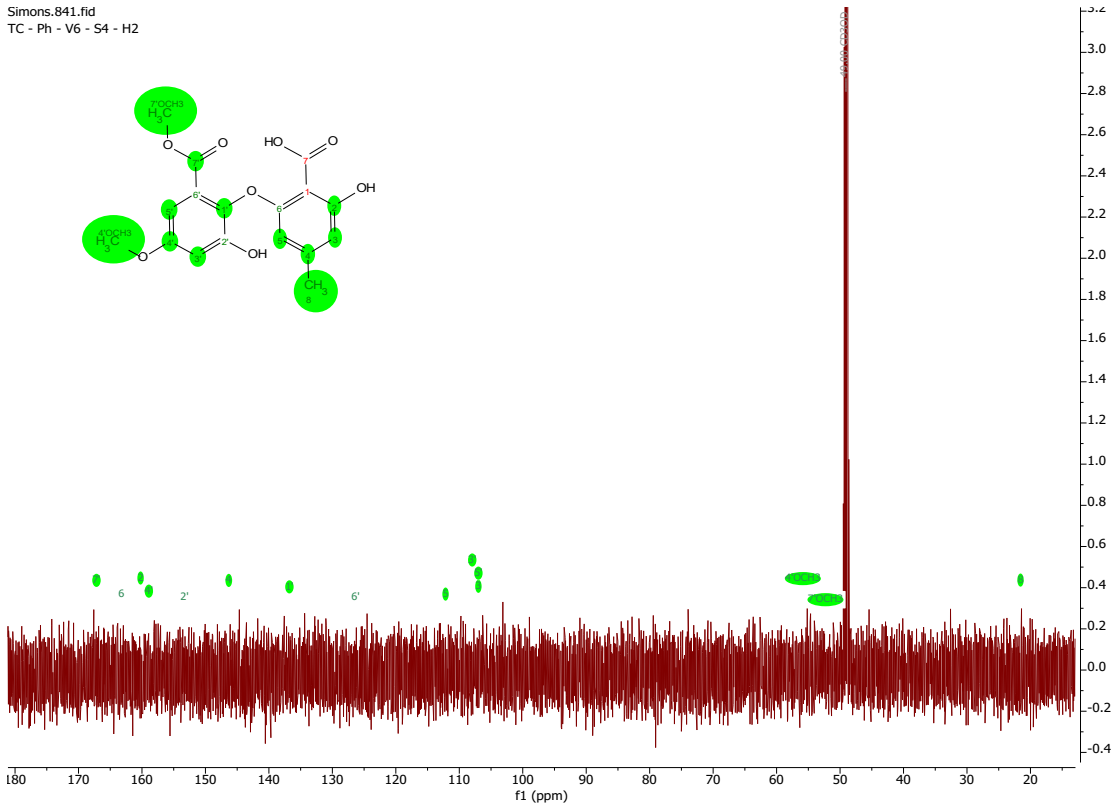

S69.^{1}H-^{13}C-HSQC Spectrum of Compound 9 (MeOH-d4, ^{1}H: 600MHz, ^{13}C: 150 MHz)

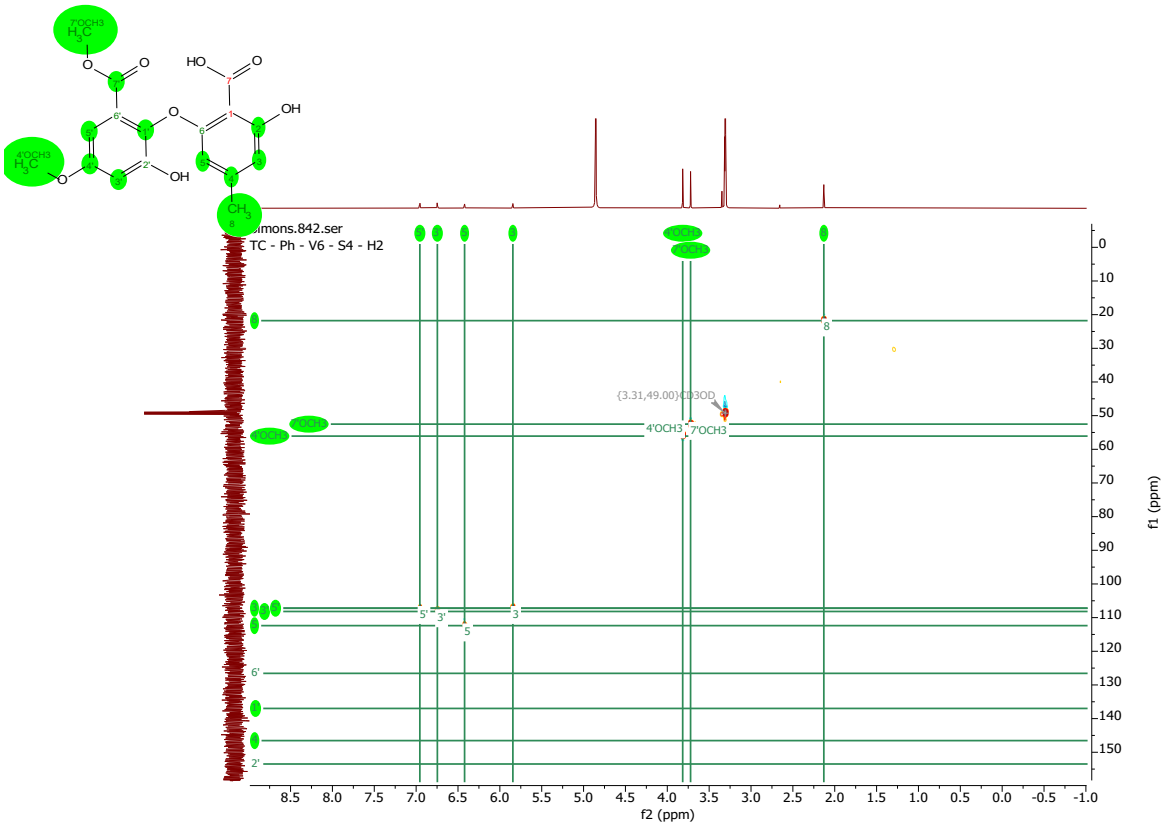

S70.^{1}H-^{13}C-HMBC Spectrum of Compound 9 (MeOH-d4, ^{1}H: 600MHz, ^{13}C: 150 MHz)

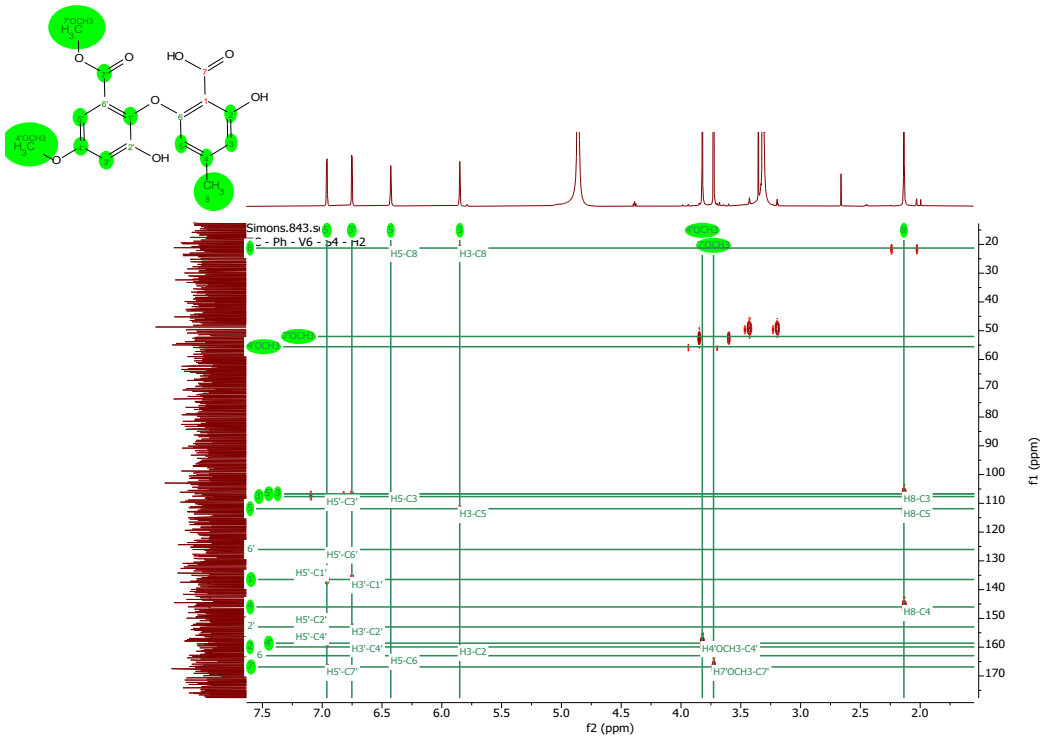

S71.^{1}H-^{1}H-NOESY Spectrum of Compound 9 (MeOH-d4, 600MHz)

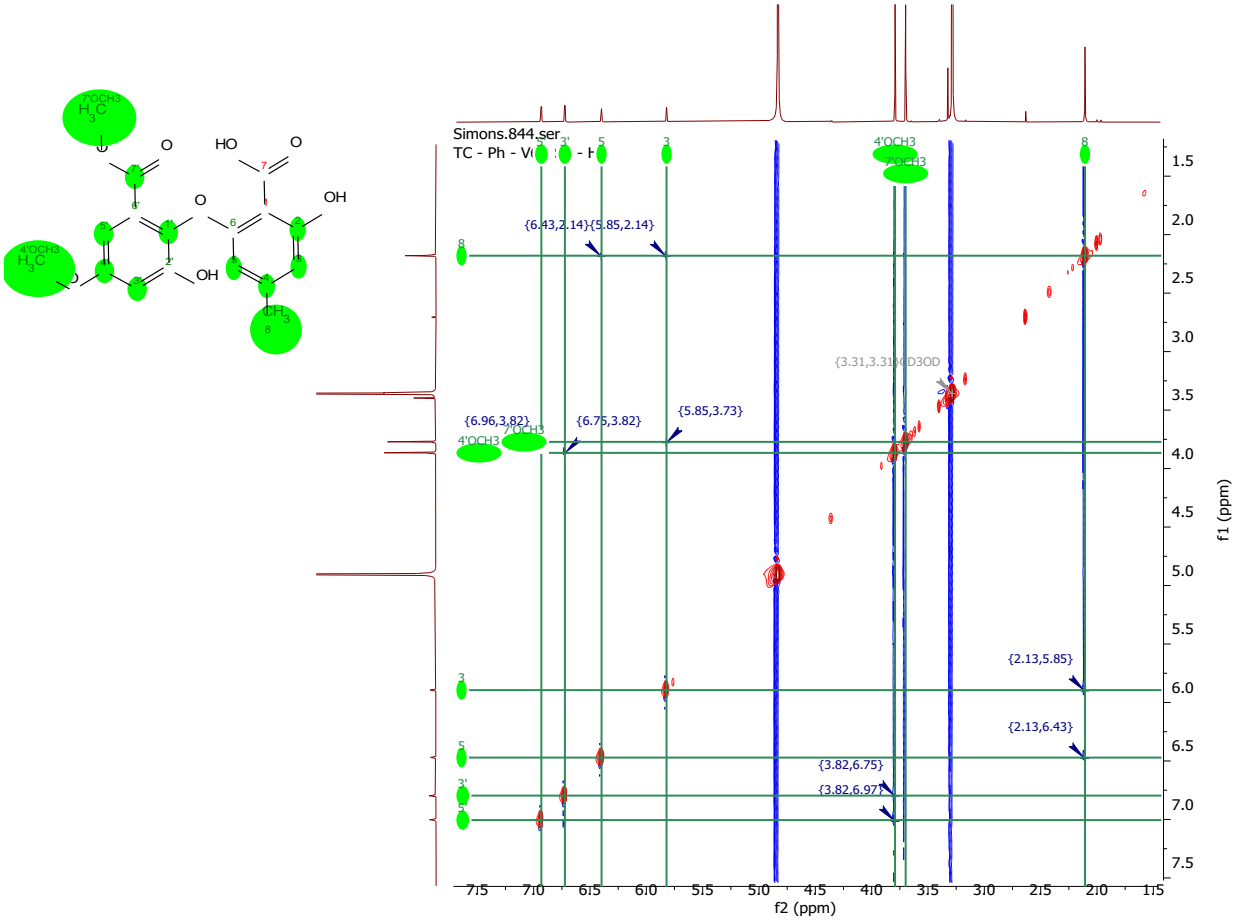

S72.UV-Vis Spectrum of Compound 9 (Methanol)

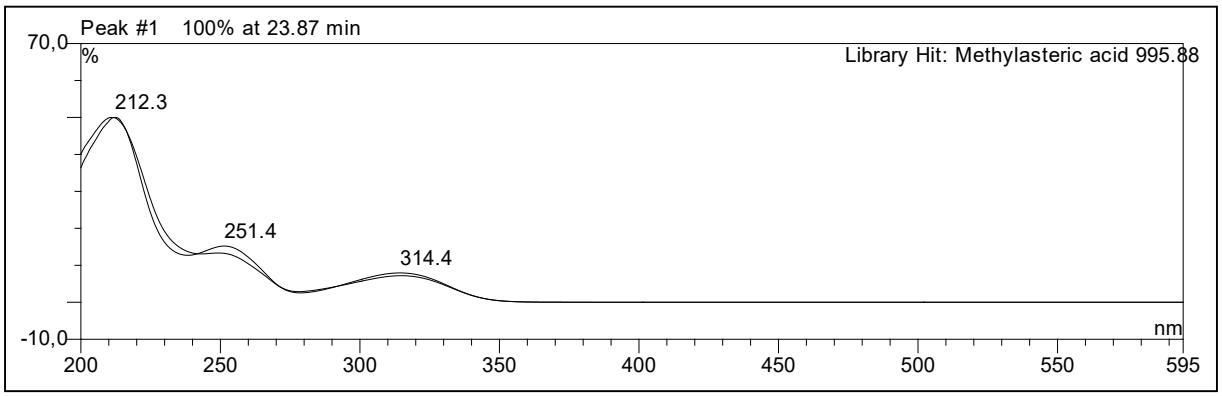

S73.ESI(+)MS Spectrum of Compound 9

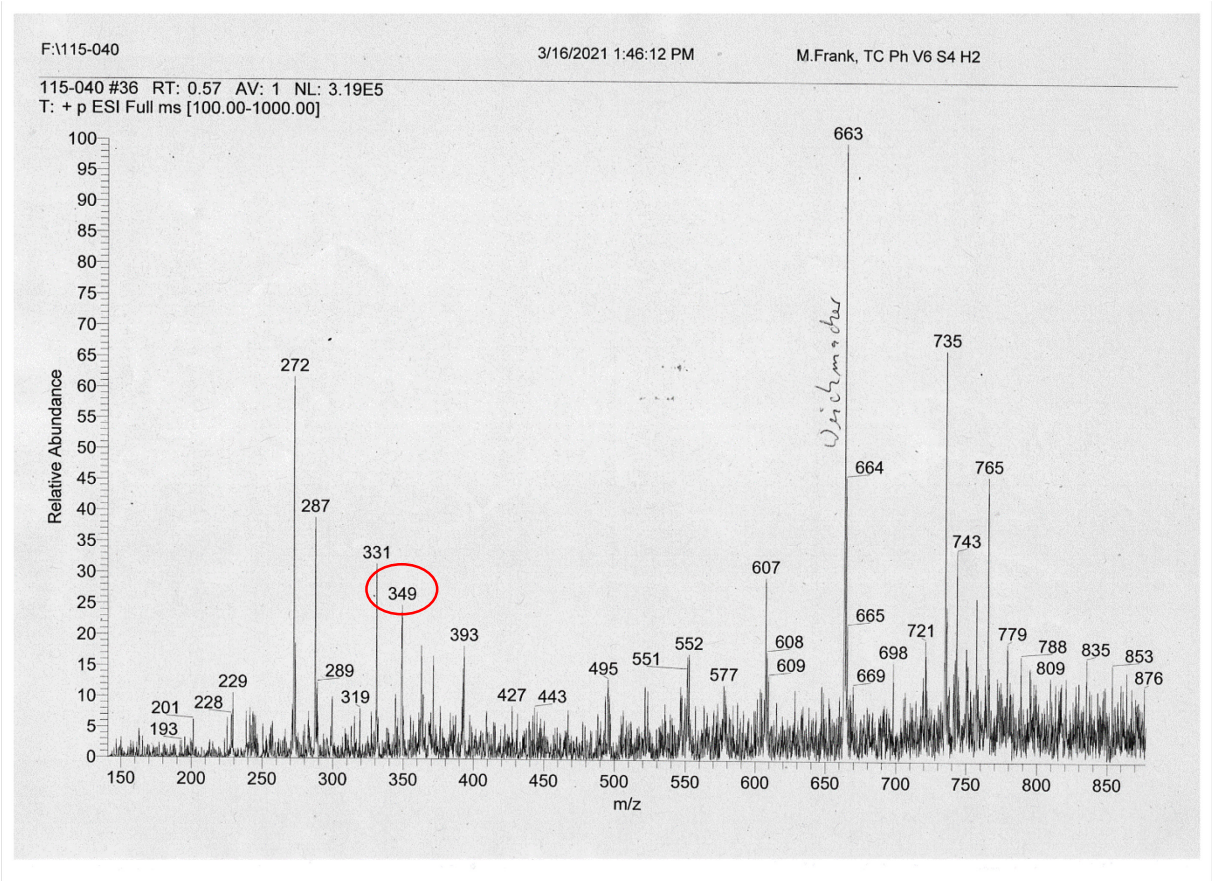

S74.High Resolution ESI(+)MS Spectrum of Compound 9

Mass Spectrum SmartFormula Report

Analysis Info

Analysis Name	D:\Data\Spektren 2021\KAL21HR000029.d	Acquisition Date	3/29/2021 9:13:28 AM
Method	tune_low_new.m	Operator	Peter Tommes
Sample Name	Simons TCPhV6S4H2 (CH3OH)	Instrument	maXis 288882.20213
Comment	10 ul in 1 ml		

Acquisition Parameter

Source Type	ESI	Ion Polarity	Positive	Set Nebulizer	0.3 Bar
Focus	Not active	Set Capillary	4000 V	Set Dry Heater	180 °C
Scan Begin	50 m/z	Set End Plate Offset	-500 V	Set Dry Gas	4.0 l/min
Scan End	1500 m/z	Set Collision Cell RF	600.0 Vpp	Set Divert Valve	Source

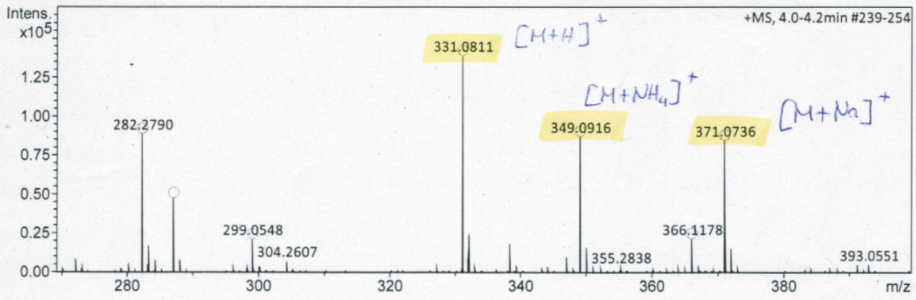

Meas. m/z	#	Ion Formula	m/z	err [ppm]	mSigma	# mSigma	Score	rdb	e⁻ Conf	N-Rule
282.2790	1	C18H36NO	282.2791	0.6	38.4	1	100.00	1.5	even	ok
287.0911	1	C16H15O5	287.0914	0.9	5.5	1	100.00	9.5	even	ok
	2	C15H12N4NaO	287.0903	-2.8	9.0	2	72.57	11.5	even	ok
	3	C17H11N4O	287.0927	5.6	19.1	3	36.33	14.5	even	ok
299.0548	1	C16H11O6	299.0550	0.9	2.1	1	100.00	11.5	even	ok
	2	C15H8N4NaO2	299.0539	-2.7	5.6	2	72.28	13.5	even	ok
	3	C13H3N10	299.0537	-3.6	7.6	3	59.74	17.5	even	ok
	4	C17H7N4O2	299.0564	5.4	15.8	4	36.80	16.5	even	ok
331.0811	1	C17H15O7	331.0812	0.5	6.9	1	100.00	10.5	even	ok
	2	C16H12N4NaO3	331.0802	-2.7	8.5	2	68.64	12.5	even	ok
	3	C14H7N10O	331.0799	-3.5	9.2	3	57.70	16.5	even	ok
	4	C18H11N4O3	331.0826	4.6	20.4	4	37.12	15.5	even	ok
349.0916	1	C17H17O8	349.0918	0.5	3.6	1	100.00	9.5	even	ok
	2	C16H14N4NaO4	349.0907	-2.6	5.9	2	67.46	11.5	even	ok
	3	C14H9N10O2	349.0904	-3.4	7.3	3	55.98	15.5	even	ok
	4	C18H13N4O4	349.0931	4.3	17.1	4	37.59	14.5	even	ok
	5	C17H10N8Na	349.0921	1.3	19.0	5	66.13	16.5	even	ok
366.1178	1	C17H20NO8	366.1183	1.3	1.4	1	100.00	8.5	even	ok
	2	C16H17N5NaO4	366.1173	-1.6	5.0	2	90.55	10.5	even	ok
	3	C14H12N11O2	366.1170	-2.3	7.4	3	74.96	14.5	even	ok
	4	C18H16N5O4	366.1197	5.0	12.5	4	36.70	13.5	even	ok
	5	C15H21NNaO8	366.1159	-5.2	14.0	5	33.59	5.5	even	ok
	6	C17H13N9Na	366.1186	2.1	15.0	6	68.15	15.5	even	ok
371.0736	1	C17H16NaO8	371.0737	0.5	2.5	1	97.83	9.5	even	ok
	2	C15H11N6O6	371.0735	-0.3	3.3	2	100.00	13.5	even	ok
	3	C14H8N10NaO2	371.0724	-3.1	7.8	3	53.85	15.5	even	ok
	4	C12H3N16	371.0721	-3.9	9.9	4	43.45	19.5	even	ok
	5	C14H15N2O10	371.0721	-3.9	11.6	5	42.38	8.5	even	ok
	6	C16H7N10O2	371.0748	3.3	16.2	6	43.93	18.5	even	ok
	7	C18H12N4NaO4	371.0751	4.1	16.2	7	36.68	14.5	even	ok

Bruker Compass DataAnalysis 4.2 printed: 3/29/2021 9:19:32 AM by: Peter Tommes Page 1 of 1

S75.NMR Table of Compound 10 (DMSO-d_6, ^{1}H: 600MHz, ^{13}C: 150 MHz)

Fuscoatramide (Joshi et al. 2002)

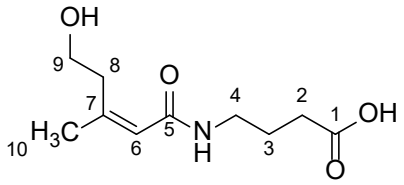

Chemical Formula: $C_{10}H_{17}NO_4$
Molecular Weight: 215,25

position	δ_C*	δ_H, m (J in Hz)
1	174.6, C	
2	31.1, CH_2	2.20, t (7.4)
3	24.3, CH_2	1.61, p (7.2)
4	37.6, CH_2	3.06, q (6.8)
5	166.3, C	
6	120.4, CH	5.68, d (1.6)
7	149.4, C	
8	35.6, CH_2	2.69, t (6.7)
9	59.3, CH_2	3.51, t (6.7)
10	25.0, CH_3	1.80, d (1.4)
4-NH		7.88, m

*signals were extracted from HSQC and HMBC spectra.

S76.[1]H-NMR Spectrum of Compound 10 (DMSO-d_6, 600 MHz)

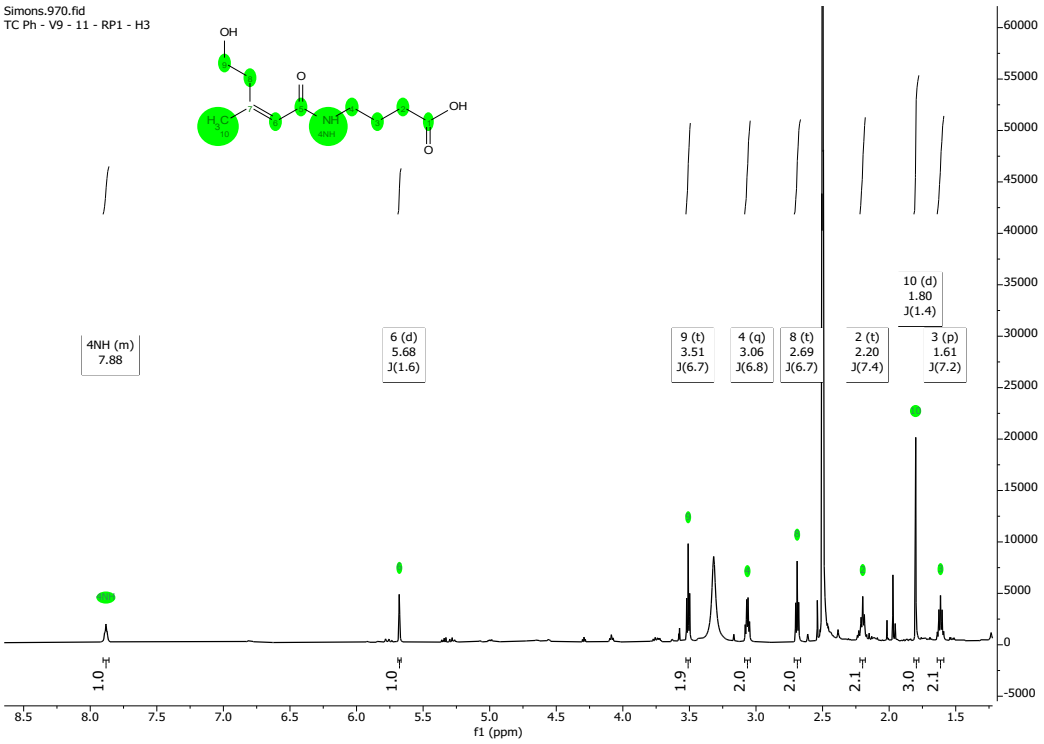

S77.[13]C-NMR Spectrum of Compound 10 (DMSO-d_6, 150 MHz)

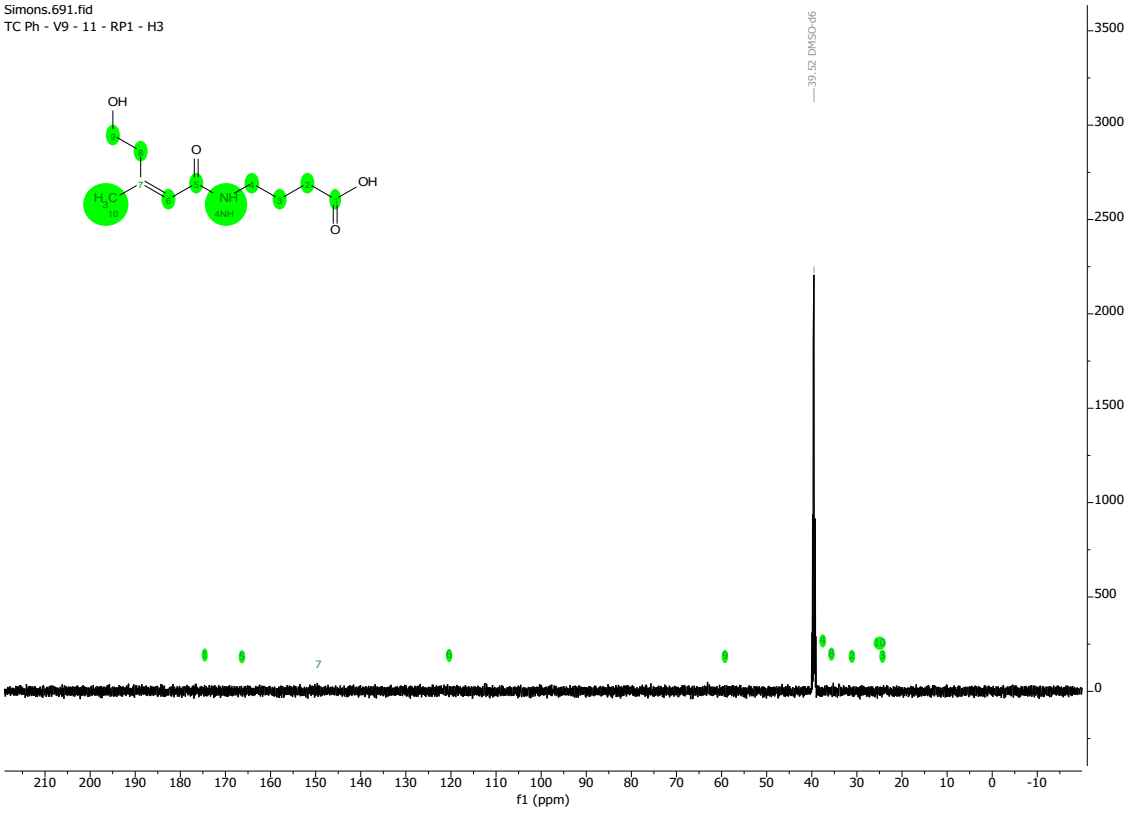

S78.^{1}H-^{13}C-HSQC Spectrum of Compound 10 (DMSO-d_6, ^{1}H: 600MHz, ^{13}C: 150 MHz)

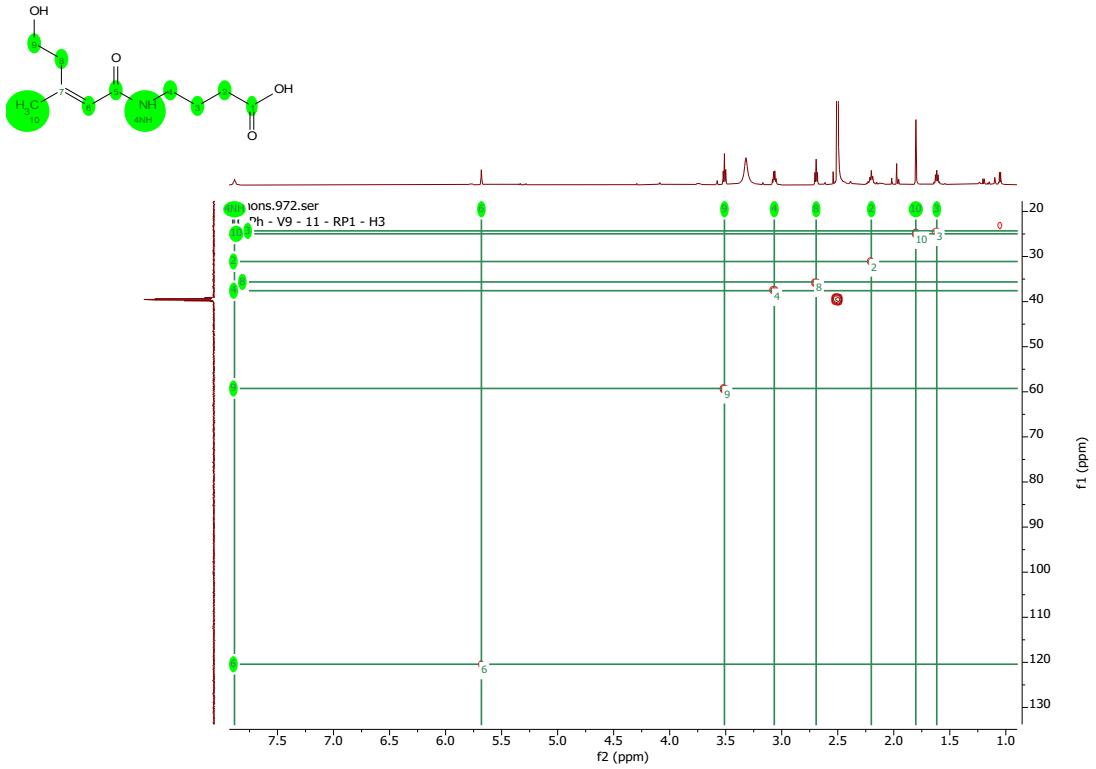

S79.^{1}H-^{13}C-HMBC Spectrum of Compound 10 (DMSO-d_6, ^{1}H: 600MHz, ^{13}C: 150 MHz)

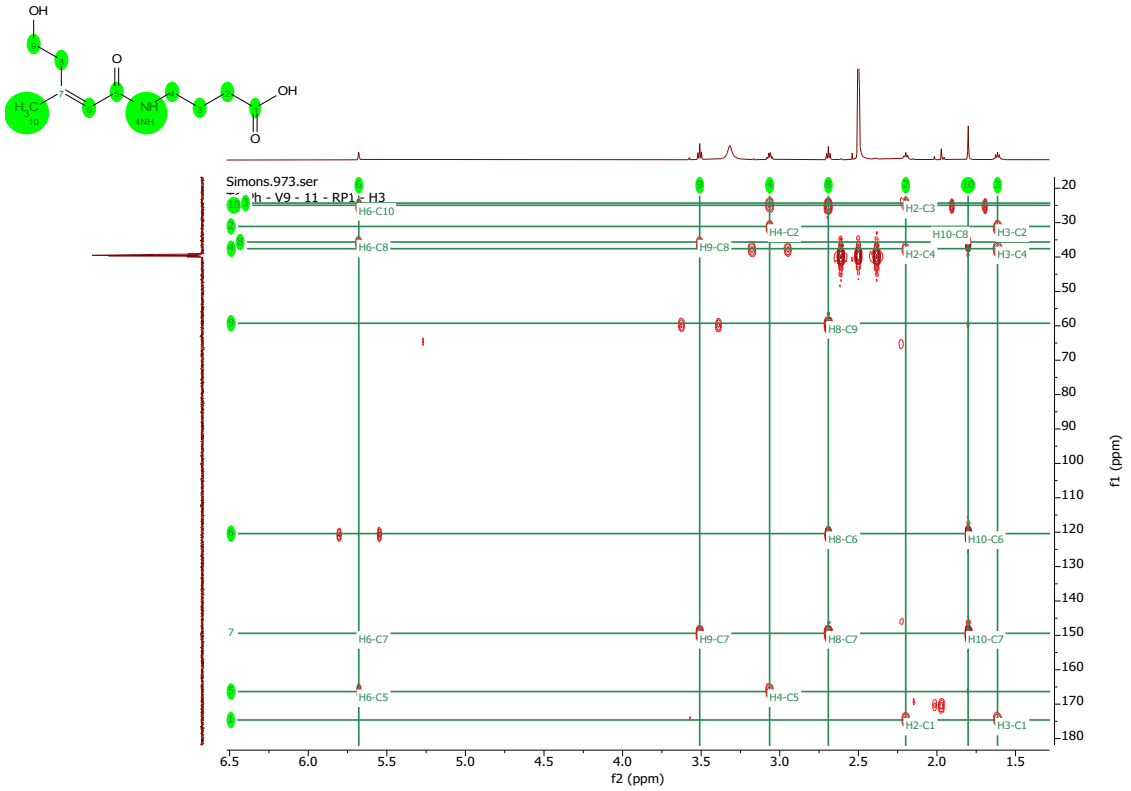

S80.^{1}H-^{1}H-COSY Spectrum of Compound 10 (DMSO-d_6, 600MHz)

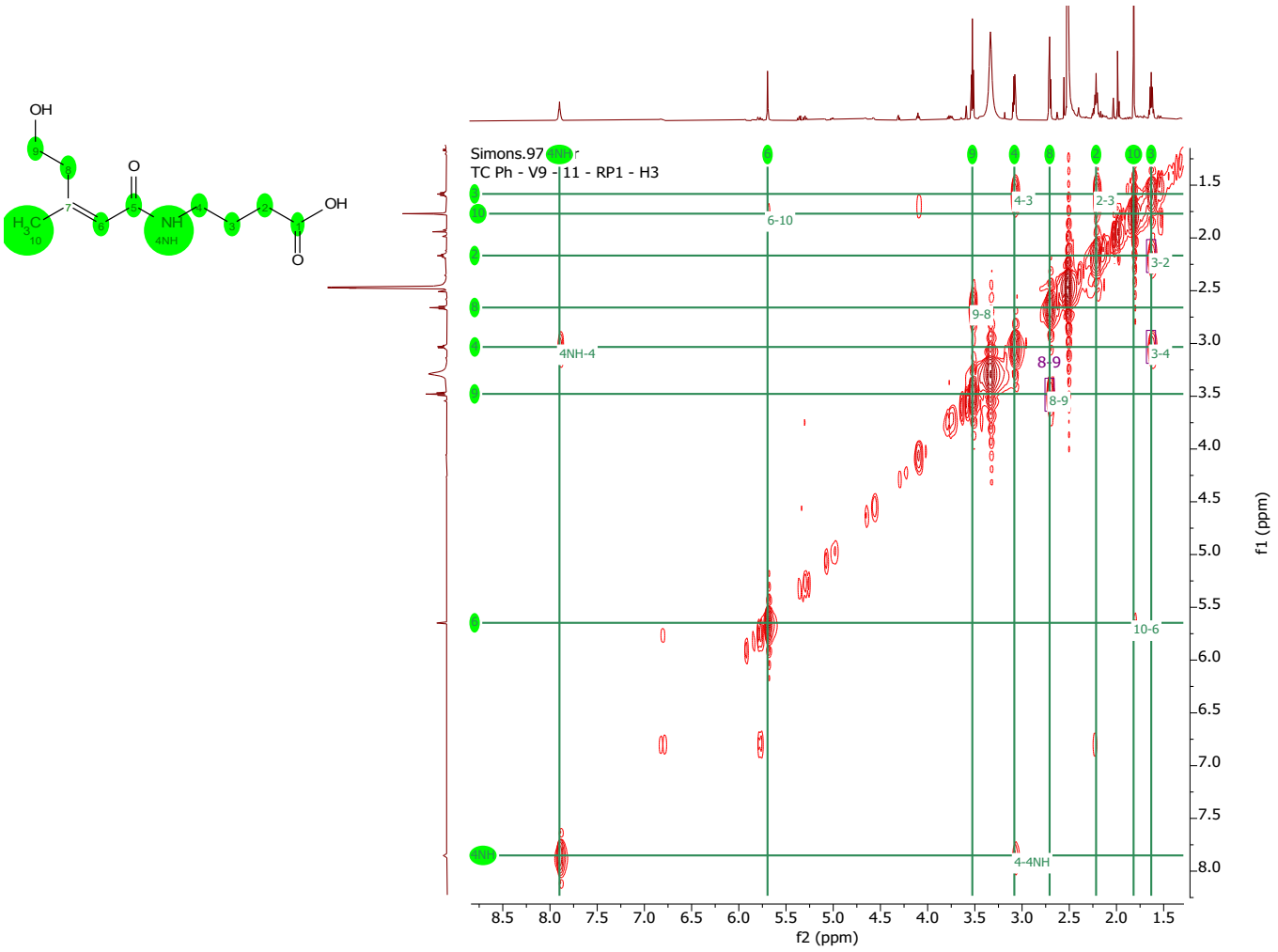

S81.UV-Vis Spectrum of Compound 10 (Methanol)

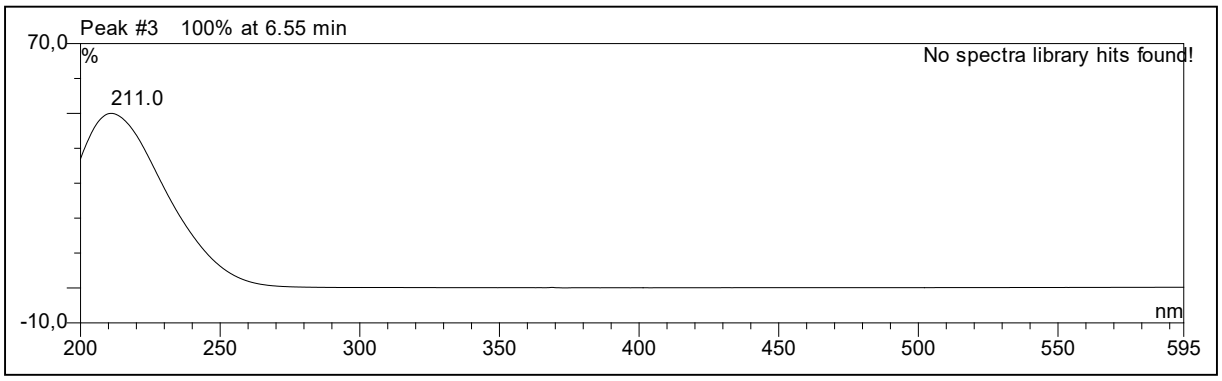

S82.ESI(+)MS Spectrum of Compound 10

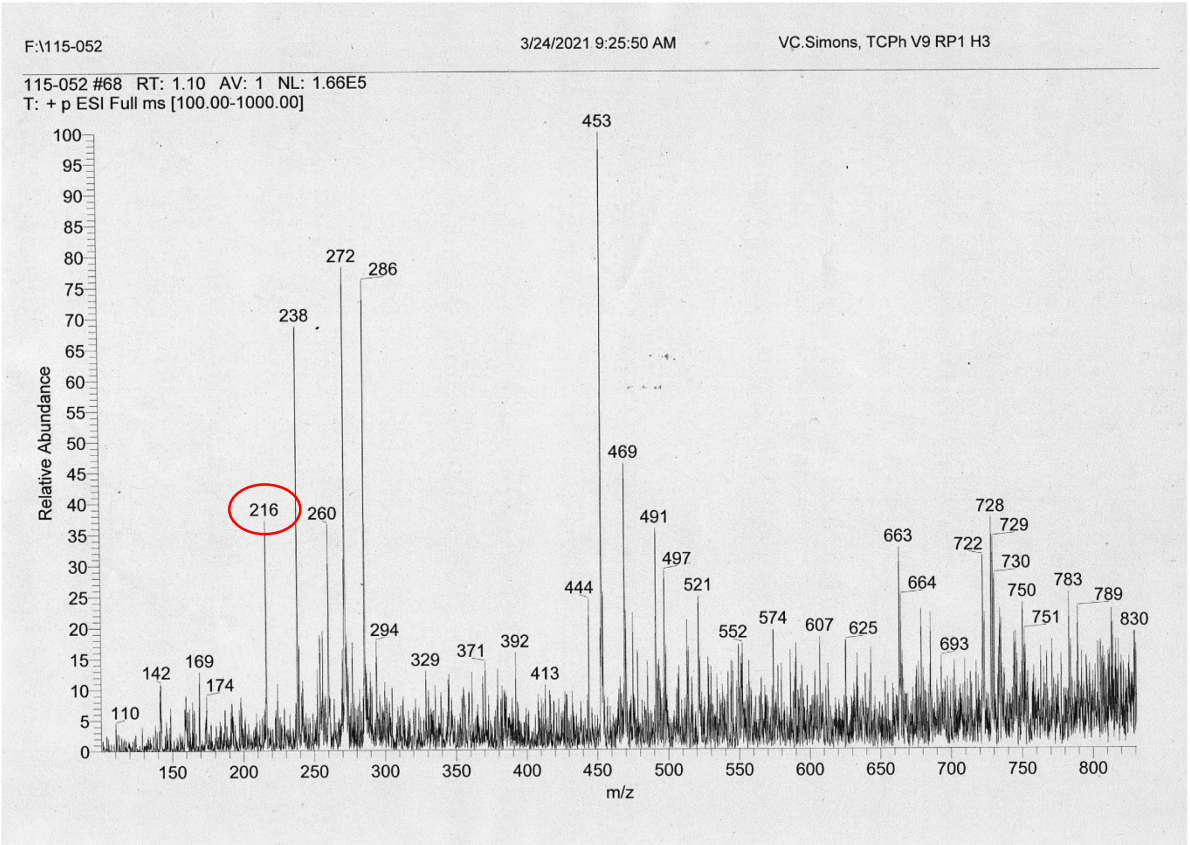

6. Fusarubin derivatives with biofilm-dispersing activities derived from *Fusarium oxysporum*

Manuscript draft (unpublished)

Overall contribution:

- Isolation of the fungus from a soil sample
- Fermentation in co-cultivation with different bacteria
- Extraction and preparation of the crude extract
- Isolation and purification of the fungal metabolites
- Structure elucidation of isolated compounds
- Writing of the first version of the complete manuscript draft

Fusarubin derivatives with biofilm-dispersing activities derived from *Fusarium oxysporum*

Viktor E. Simons[a], Lasse van Geelen[a], Dennis Woschko[b], Sebastian Scharf[c], Philipp Spohr[d], Marian Frank[a], Christoph Janiak[b], Klaus Pfeffer[c], Rainer Kalscheuer[a,*]

[a]Institute of Pharmaceutical Biology and Biotechnology, Heinrich Heine University, Universitätsstrasse 1, 40225 Düsseldorf, Germany

[b]Institute for Nanoporous and Nanoscale Materials, Heinrich Heine University, Universitätsstrasse 1, 40225 Düsseldorf, Germany

[c]Institute of Medical Microbiology and Hospital Hygiene, Heinrich Heine University, Universitätsstrasse 1, 40225 Düsseldorf, Germany

[d]Algorithmic Bioinformatics, Heinrich Heine University, Universitätsstrasse 1, 40225 Düsseldorf, Germany

*Corresponding author. E-mail address:
Rainer Kalscheuer: rainer.kalscheuer@hhu.de;
ORCID ID orcid.org/0000-0002-3378-2067

Abstract: The genus *Fusarium* is known for its versatility in the production of secondary metabolites. Based on the OSMAC (one strain many compounds) concept, in this study, the co-cultivation of the soil-borne fungus *Fusarium oxysporum* with the soil-borne bacterium *Paenibacillus ehimensis* yielded the three new natural products fusachinon (**2**), fusapurpurin A (**3**) and fusapurpurin B (**4**), together with seven previously described compounds (**1 and 5-10**). The structures were elucidated based on comprehensive spectroscopic measurements. The unusually bridged structures of fusapurpurin A and B were confirmed via single crystal X-ray diffraction analysis. Nanopore whole genome sequencing of *F. oxysporum* together with antiSMASH analysis led to the identification of a biosynthetic gene cluster (BGC) likely responsible for the biosynthesis of fusarubin base structures, which are structurally closely related to the novel fusapurpurins. On this basis, a possible biosynthetic route to fusapurpurin A and B is being proposed. Fusapurpurin A and B showed potent biofilm-desintegrating activities against *Staphylococcus aureus* Mu50 with IC90 = 6.25 µM and *Pseudomonas aeruginosa* PAO1 with IC90 = 12.5 µM. Additionally, fusapurpurin B also showed moderate biofilm-disrupting activity against *Mycobacterium tuberculosis* H37Rv and reduced pre-formed biofilm by more than 50% at 100 µM. Of the three new compounds (**2-4**), only fusapurpurin B showed a weak direct antibacterial activity against *S. aureus* Mu50 with a minimal inhibitory concentration (MIC) of 100 µM. Compound **9** had weak activity against *S. aureus* Mu50 with a MIC of 50 µM and strong activity against *Mycobacterium tuberculosis* H37Rv with a MIC of 3.125 µM. Fusapurpurin A and B showed weak to moderate cytotoxic effects against the tested human cell lines THP1 (40.66 vs. 11.57 µM), Huh-7 (47.85 vs. 12.67 µM) and HEK 293 (>100 vs. 26.81 µM).

Keywords: Fusarium oxysporum; OSMAC; fusarubin; fusapurpurin; natural products; co-cultivation; biofilms; biofilm disruption; antibiofilm activity; antibacterial activity; cytotoxicity; whole-genome sequencing; antiSMASH

1. Introduction

Antimicrobial resistance has become a steadily increasing threat to human health during the last decades. The golden era between 1950 and 1970, where a lot of new antibiotics have been introduced to the clinic, was followed by decades of underdevelopment of new antibiotic compounds [1]. Environmental microorganisms are still a very fruitful natural source of novel antibiotics since new chemical skeletons derived from these sources have been continuously being identified during the last decades [2]. Even though there is a long history of isolation of bioactive natural products, various approaches for the activation of silent gene clusters have emerged during recent years leading to a substantial expansion of our portfolio of natural compounds, highlighting the huge hidden treasure chest of what is still to be found [3-5]. Especially fungi belonging to the genus *Fusarium* have been shown to be very versatile when it comes to the activation of silent gene clusters for the production of cryptic metabolites [6-10]. In this regard, the so-called OSMAC concept (One Strain Many Compounds) [Bode *et al.* 2002] is an easy and valuable tool to manipulate *Fusarium* species under laboratory conditions [11, 12]. One of the possible activating parameters of the OSMAC concept is co-cultivation with other microorganisms since it mimics naturally occurring interactions and competition [13, 14]. Interestingly, co-cultivation with different bacteria can also induce different cryptic metabolites [15, 16].

The ability of many pathogenic bacteria to form biofilms is severely complicating antiinfective treatment and a major factor promoting the development of antimicrobial resistance. Bacterial biofilms are one of the main reasons for the establishment of chronic bacterial infections [17]. Biofilms represent a robust physical barrier that effectively protects the imbedded bacteria from being reached by most antibiotics. In addition, the majority of imbedded cells are in a metabolically inactive and non-replicating state that causes phenotypic resistance, meaning that the bacteria are tolerant to antibiotics, which typically target processes of active metabolism and cell division. On the flip side, this also promotes the development of genetic resistance because the amount of antibiotics reaching the bacteria is lower than expected and the treatment is therefore at subinhibitory concentrations promoting the occurrence of mutations [18]. A recent study suggests that biofilms can even put mechanical stress on the infected tissues, leading to additional damage [19]. This shows the huge importance of finding new biofilm-inhibiting and disrupting compounds.

In this study, the soil-borne fungus *Fusarium oxysporum* was co-cultivated with the soil-borne bacterium *Paenibacillus ehimensis* resulting in the production and isolation of one new anthrachinone and two new naphthoquinones together with seven known compounds. The two new naphthoquinones, fusapurpurin A and B, inherit a completely new structural subclass of fusarubin derivatives, where the addition of a phenyl pyruvic acid moiety adds a complex bridged element to the 9-O-methylfusarubin base structure. The absolute configurations of novel compounds **3** and **4** were determined *via* single crystal X-ray diffraction analysis. A whole genome nanopore sequencing of *F. oxysporum* was accomplished and analysed by the antiSMASH fungi version to identify a possible biosynthesic

pathway for fusapurpurins A and B. Fusapurpurins A and B exhibit dispersing activity against pre-formed biofilms of methicillin-resistant *Staphylococcus aureus* Mu50 and *Pseudomonas aeruginosa* PAO1 and to a lesser extent also against *Mycobacterium tuberculosis* H37Rv.

2. Results and Discussion

2.1 Influence of bacterial co-cultivation on the secondary metabolite profile of Fusarium oxysporum

In our ongoing search for new antimicrobial compounds derived from microorganisms, we isolated the filamentous fungus *Fusarium oxysporum* from a soil sample collected in Texel, the Netherlands. Since members of the genus *Fusarium* appear to be particularly amenable to the OSMAC concept for the induction of silent biosynthetic gene clusters [20], *F. oxysporum* was grown in co-culture with cells of five different bacterial species on solid rice medium enriched with LB-medium including one lab strain (*Acinetobacter baylyi* ADP1) and four strains that have been isolated from various soil samples in our laboratory (*Bacillus amyloliquefaciens, Pseudomonas sp., Lysinibacillus sp.* and *Paenibacillus ehimensis*). Interestingly, the fungus responded in very distinct ways to the presence of the different bacteria. While *B. amyloliquefaciens* supressed growth of *F. oxysporum* almost completely, presence of *A. baylyi* ADP1, *Lysinibacillus sp., Pseudomonas sp.* and *P. ehimensis* led to the production of red-coloured pigments after four weeks of culturing. However, only during co-cultivation with *P. ehimensis*, the fungus responded by strong production of darker, purple-coloured pigments (**Fig. 1**).

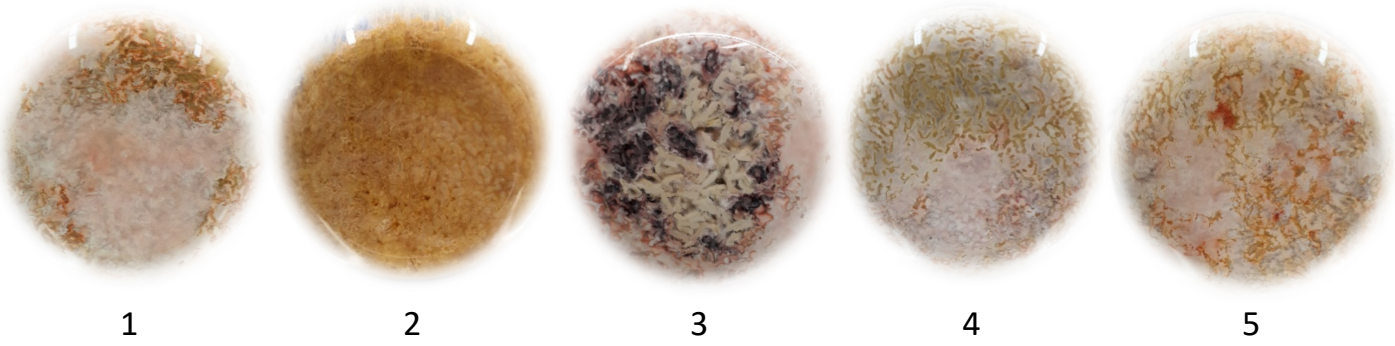

Figure 1. Co-cultivations of different bacteria with *Fusarium oxysporum* on rice medium supplemented with LB-medium. Co-cultivation with *Lysinibacillus sp.* (**1**), *Bacillus amyloliquefaciens* (**2**), *Paenibacillus ehimensis* (**3**), *Pseudomonas sp.* (**4**) and *Acinetobacter baylyi* ADP1 (**5**) after four weeks of growth at room temperature. Captured is the bottom view of the 1-l Erlenmeyer flasks containing the solidified rice cultures.

To compare the co-cultures analytically, crude extracts were obtained from small-scale cultivations and measured via High-Performance Liquid Chromatography (HPLC). HPLC-chromatograms of different crude extracts from co-cultivations with *F. oxysporum* and axenic cultures are shown in **Fig. 2**. Comparison of the HPLC-chromatograms of extracts obtained from co-cultivation with *A. baylyi* ADP1, *Lysinibacillus sp.*and *Pseudomonas sp.* showed only moderate differences to the extract obtained from the axenic *F. oxysporum* culture, while co-cultivation with *B. amyloliquefaciens* strongly repressed overall production of secondary metabolites. In contrast, co-culture with *P. ehimensis* resulted in the elicitation of a very different metabolite profile with strong induction of a peak at retention-time 24.32 minutes that was later identified as 9-O-methylfusarubin (compound **1**, see 2.2), among some additional minor peaks (**Fig. 2**). These new peaks were not detactable in the HPLC-chromatograms of extracts from the axenic *F. oxysporum* and *P. ehimensis* controls (**Fig. 2**).

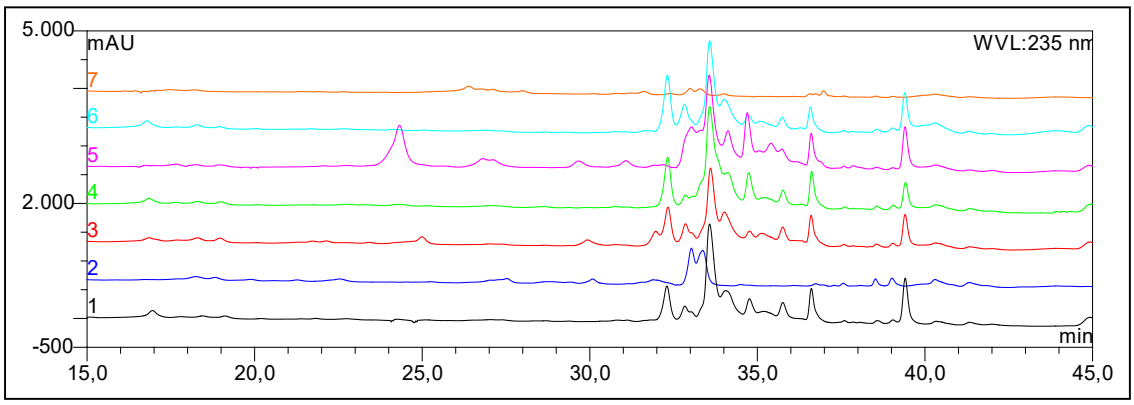

Figure 2. Overlay of HPLC-chromatograms from different axenic and co-culture extracts measured at 235 nm. The chromatograms of crude extracts from *F. oxysporum* axenic (1), *P. ehimensis* axenic (2) and co-cultures of *F. oxysporum with Pseudomonas* sp. (3), *Lysinibacillus sp.* (4), *P. ehimensis* (5), *A. baylyi* ADP1 (6) and *B. amyloliquefaciens* (7) are overlayed.

2.2 Compound isolation and structure elucidation

The crude ethyl acetate extract of the co-cultivation of *F. oxysporum* with *P. ehimensis* was purified via silica and Sephadex column chromatography and semi-preparative HPLC to yield one new anthrachinone (**2)** and the two new naphthoquinone derivatives **3-4** together with seven known compounds including the five naphthoquinones 9-O-methylfusarubin (**1**) [21], 9-O-methylbostrycoidin (**5)** [21], 2,5-dihydroxy-6,8-dimethoxy-3-(2-oxopropyl)-1,4-naphthalenedione (**6)** [22], 9-O-methylanhydrofusarubin (**7)** [22], 9-O-methylanhydrofusarubinlactol (**8)** [23], and the two cyclopeptides beauvericin (**9)** [24] and beauvericin J (**10)** [25]. An overview of the chemical structures of the isolated compounds is provided in **Fig. 3**. The absolute configuration of compounds **3** and **4** was determined via single crystal X-ray diffraction.

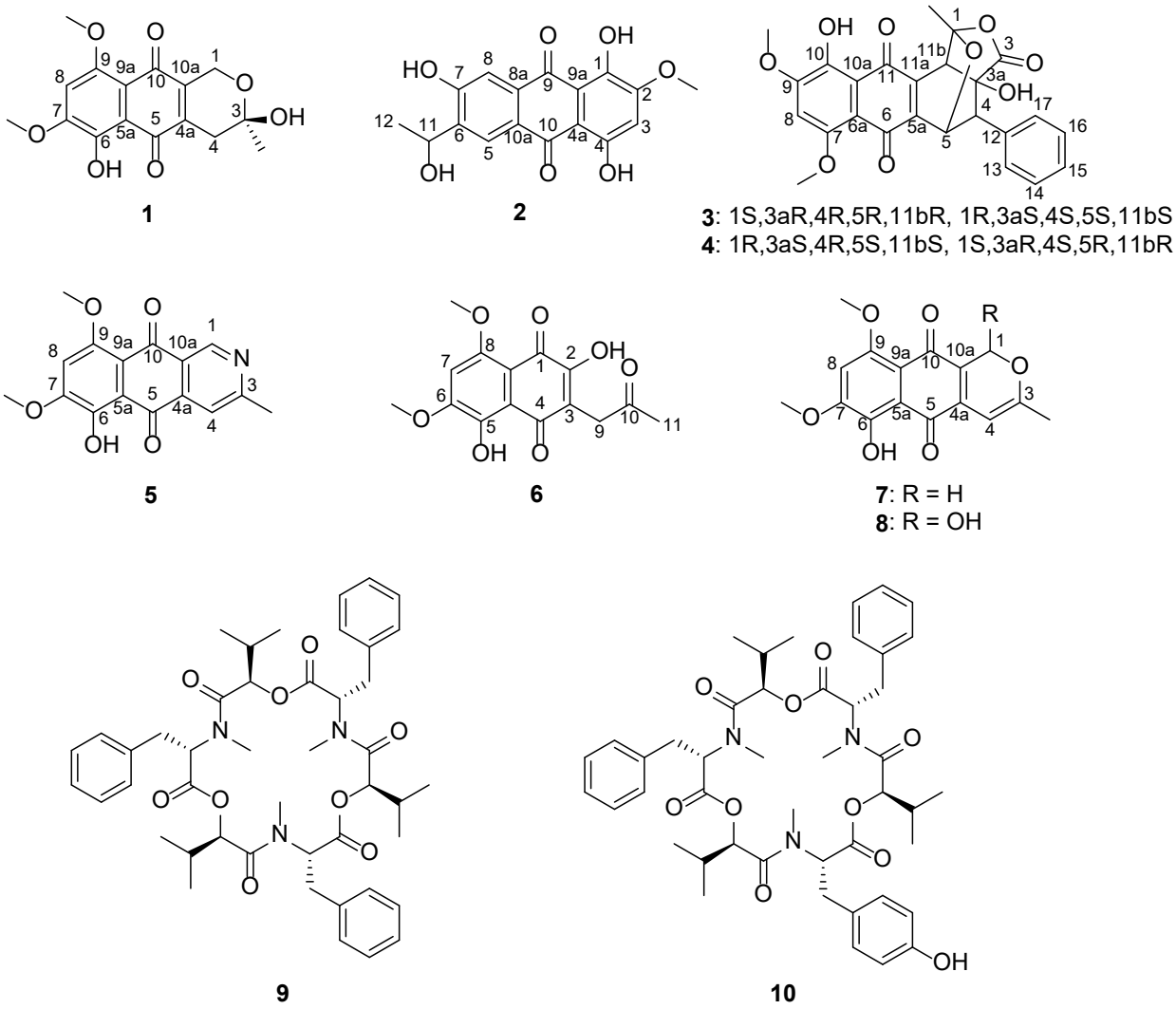

Figure 3. Chemical structures of the isolated compounds from co-culture of *F. oxysporum* with *P. ehimensis*. 9-O-methylfusarubin (**1**), fusachinon (**2**), fusapurpurin A (**3 – racemic mixture**), fusapurpurin B (**4 – racemic mixture**), 9-O-methylbostrycoidin (**5**), 2,5-dihydroxy-6,8-dimethoxy-3-(2-oxopropyl)-1,4-naphthalenedione (**6**), 9-O-methylanhydrofusarubin (**7**), 9-O-methylanhydrofusarubinlactol (**8**), beauvericin (**9**), beauvericin J (**10**).

Structure elucidation of compound **2**:

Compound **2** was isolated as an amorphous orange solid. The molecular formula was assigned as $C_{17}H_{14}O_7$ based on the high-resolution quasi-molecular ion peak at 331.0817 m/z (calcd. for $C_{17}H_{15}O_7$ 311.0812 m/z). The UV spectrum exhibited high similarity to other co-isolated fusarubin derivatives. Detailed analysis of the HMBC and HSQC correlations of aromatic methoxy-unit 2-OCH3 (δ 3.96 ppm), aromatic protons H-3 (δ 6.96 ppm), H-5 (δ 8.35 ppm), H-8 (δ 7.62 ppm) and phenolic protons OH-1 (δ 13.17 ppm), OH-4 (δ 13.70 ppm) and OH-7 (δ 11.21 ppm) revealed an anthraquinone core structure. The position of C9 (δ 187.6 ppm) was confirmed through a strong HMBC correlation from H-8 and a weak *J4* correlation from H-5. The position of C10 (δ 183.8 ppm)

was confirmed the same way mirrored through a strong correlation from H-5 and a weak *J4* correlation from H-8. The COSY correlations between H3-12 (δ 1.33 ppm) and H-11 (δ 5.03 ppm), in addition to HMBC correlations from H-12 to C-11 (δ 62.6 ppm) and C-6 (δ 141.6 ppm), a strong HMBC correlation between H-5 and C11 and an NOE correlation between H-5 and H11 revealed the presence of the hydroxyethyl group at position C-6. The position of OH-1 was confirmed by strong HMBC correlations between OH-1 and C-1 (δ 149.0 ppm), C-2 (δ 156.6 ppm) and C-9a (δ 112.0 ppm). In the same manner, position of OH-4 was revealed by HMBC correlations with C-3 (δ 107.2 ppm), C-4 and C-4a (δ 104.7 ppm). OH-7 was confirmed by correlations with C-6, C-7 (δ 158.9 ppm) and C8 (δ 111.3 ppm).

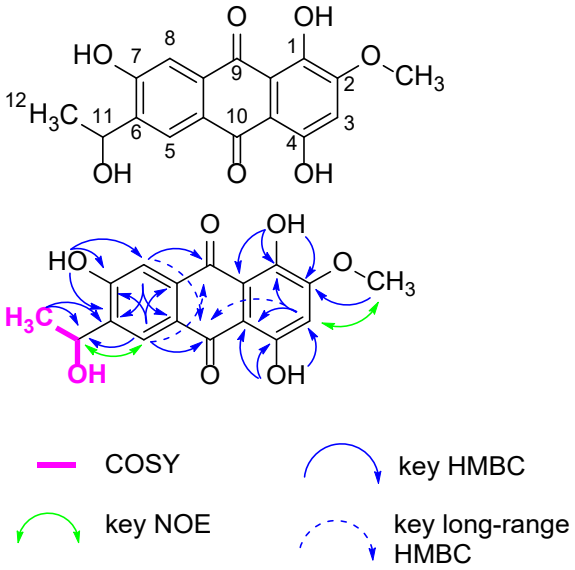

Figure 4. Key NMR correlations for **2** (fusachinon)

Table 1. NMR data for **2** (measured in DMSO-d_6 at 150 MHz for the ^{13}C- and at 600 MHz for the ^{1}H-NMR spectrum)

position	δ_C*	δ_H, m (J in Hz)
1	149.0, C	
2	156.6, C	
3	107.2, CH	6.96, s
4	159.2, C	
4a	104.7, C	
5	124.8, CH	8.35, s
6	141.6, C	
7	158.9, C	
8	111.3, CH	7.62, s
8a	132.9, C	
9	186.7, C	
9a	112.0, C	
10	183.8, C	
10a	125.0, C	
11	62.6, CH	5.03, dq (4.2, 6.4)
12	23.5, CH_3	1.33, d (6.4)
1-OH		13.17, s
2-OCH_3	56.5, CH_3	3.96, s
4-OH		13.70, s
7-OH		11.21, s
11-OH		5.42, d (4.2)

*signals were extracted from HSQC and HMBC spectra.

Structure elucidation of compounds **3** and **4**:

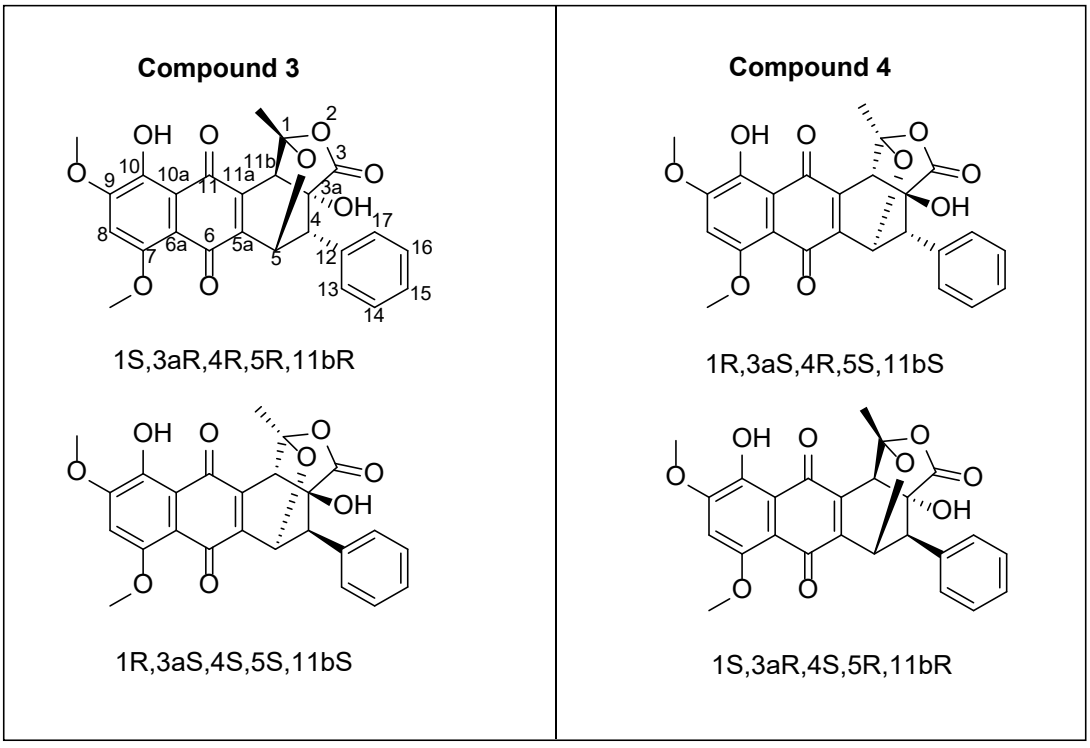

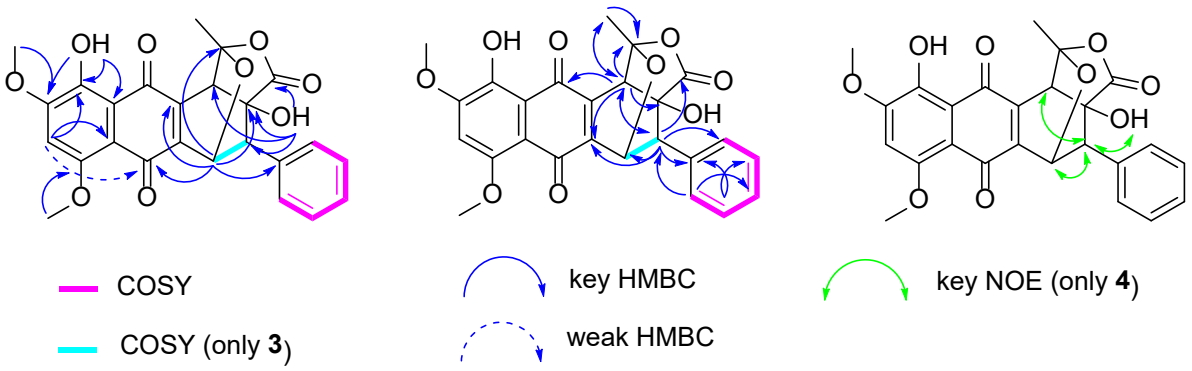

Figure 5. Key NMR correlations for **3** (fusapurpurin A) and **4** (fusapurpurin B)

Compound **3** was isolated as an amorphous purple solid, which crystallized in form of pink square crystals from a mixture of ethyl acetate and *n*-heptane. The molecular formula was assigned as $C_{25}H_{20}O_9$ based on the high-resolution quasi-molecular ion peak at 465.1177 m/*z* (calcd. for $C_{25}H_{21}O_9$ 465.1180 m/*z*). The UV spectrum exhibited high similarity to other co-isolated fusarubin derivatives, suggesting a shared chromophore, but had a stronger bathochromic shift in the highest maximum at around 520 nm. Detailed analysis of the HMBC and HSQC correlations of aromatic methoxy units 9-OCH_3 (δ 4.02 ppm), 7-OCH_3 (δ 3.88 ppm), isolated aromatic proton H-8 (δ 7.10 ppm) and chelated phenolic proton OH-10 (12.99 ppm) revealed a naphthoquinone core structure identical to 8-*O*-methylfusarubin. The position of carbonyl C-6 (δ 175.4 ppm) was confirmed based on a weak J_4-HMBC correlation from H-8, while carbonyl C-11 (δ 186.7 ppm) was inferred from the chelated nature of OH-10 as well as the absence of an HMBC correlation from H-8. The remaining ^{1}H-NMR signals revealed a phenyl-moiety expressing the typical overlapping multiplet pattern of protons H-13 to H-17 (δ 7.03 – 7.12 ppm), a strongly deshielded hydroxyl proton 3a-OH (δ 6.71 ppm), three deshielded methine protons H-5 (δ 5.30 ppm), H-11b (δ 4.34 ppm), H-4 (δ 3.97 ppm) and an aliphatic methyl unit H_3-1-CH3 (δ 1.44 ppm). Detailed analysis of the HMBC and HSQC correlations of signals H-5, H-11b and H_3-1-CH3 revealed the presence of a pyrano-unit connected to the formerly established naphthoquinone core via fusing carbons C-5a (δ 148.9 ppm) and C-11a (δ 138.9 ppm). The orientation of the pyrano-unit relative to the naphthoquinone core was established based on the strong J_3-HMBC correlations of H-11b to C-11 & C-5a and H-5 to C-6 & C-11a.

Compound **4** was isolated as an amorphous purple solid, which crystallized in form of purple crystals from MeOH. The molecular formula was assigned as $C_{25}H_{20}O_9$ based on the high-resolution quasi-molecular ion peak at 465.1174 m/z (calcd. for $C_{25}H_{21}O_9$ 465.1180 m/z). The UV spectrum was identical to that of **3**. The NMR data (**Table 2**) for compounds **3** and **4** also showed that they are largely structurally identical. Surprisingly for compound **4,** we could observe a lower chemical shift for position H-4 (δ 2.91 ppm) compared to that of compound **3** and positions H-4 and H-5 (δ 5.41 ppm) both showing singlet signals instead of doublets. Besides these findings, both compounds share the same information with only very low differences in the chemical shifts. The missing COSY signals

for H-4 and H-5 also supported the missing doublet signals in the ^{1}H-NMR. This could be caused by a dihedral angle that is close to 90° as described by the Karplus equation [26]. Nevertheless, HMBC signals from H-5 to C-12 (δ 136.8 ppm) and H-4 to C-13/17 (δ 127.7 ppm) showed a close range and connection to the phenyl moiety and also proved H-4 and H-5 being directly adjacent to each other. These findings were independently confirmed through X-ray crystallographic measurements that gave the absolute configurations shown in **Fig. 5**. The absolute configuration is also congruent to the relative configuration found through the NOE signals from the same NMR measurement finding 3a-OH (δ 6.65 ppm), H-4, H-5 and H-11b (δ 4.30 ppm) all having the same orientation.

Table 2: NMR data for **3** and **4** (measured in DMSO-d_6 at 150 MHz for the ^{13}C- and at 600 MHz for the ^{1}H-NMR spectrum)

position	*Compound 3*		*Compound 4*	
	δ_C*	δ_H, m (*J* in Hz)	δ_C*	δ_H, m (*J* in Hz)
1	105.5, C		104.7, C	
3	176.7, CO		173.3, CO	
3a	76.4, C		75.1, C	
4	51.6, CH	3.97, d (4.2)	51.5, CH	2.91, s
5	70.9, CH	5.30, d (4.2)	69.1, CH	5.41, s
5a	148.9, C		149.8, C	
6	175.4, CO		175.5, CO	
6a	109.0, C		109.5, C	
7	157.2, CO		156.4, CO	
8	105.1, CH	7.10, s	104.2, CH	7.14, s
9	156.3, CO		155.9, CO	
10	148.9, C		148.1, C	
10a	114.6, C		114.2, C	
11	186.7, CO		187.2, CO	
11a	138.9, C		135.5, C	
11b	46.9, CH	4.34, s	47.2, CH	4.30, s
12	130.7, C		136.8, C	
13/17	131.3, CH	7.03, m, 2H	127.7, CH	7.37, m, 2H
14/16	127.9, CH	7.12, m, 2H	128.6, CH	7.33, m, 2H
15	127.9, CH	7.08, m	128.1, CH	7.29, m
1-CH_3	22.9, CH_3	1.44, s, 3H	22.4, CH_3	1.47, s, 3H
3a-OH		6.71, s		6.65, s
7-OCH_3	57.1, OCH_3	3,88, s, 3H	56.2, OCH_3	3.97, s, 3H
9-OCH_3	57.1, OCH_3	4.02, s, 3H	56.2, OCH_3	4.03, s, 3H
10-OH		12.99, s		12.94, s

*signals were extracted from HSQC and HMBC spectra

The constitutions of compounds **3** and **4** with their absolution configurations were confirmed through single crystal X-ray structures. Before the X-ray structure measurements the compounds were assumed to be chiral. During the crystallographic data collection no restraints were applied with respect to acentric or centrosymmetric space groups. Therefore measurement parameters were chosen for the highest quality absolute configuration data with the Friedel pairs being non-equivalent. During the data integration and data reduction process the Friedel pairs were also not merged to retain the

highest quality absolute configuration data. The resulting reduction statistics suggested centrosymmetric space groups for both compound **3** and **4** for the later solution and refinement of both compounds, indicating racemic mixtures. Thus, the X-ray structures of both compounds **3** and **4** were solved and refined in centrosymmetric space groups. Upon structure solution no acentric space group was suggested.

A centrosymmetric space group contains an inversion centre as a symmetry element. Thus, a chiral molecule in such a space group will be present in both enantiomeric forms in perfectly equal amounts, that is, as a racemate or practically very close to a racemic mixture.

For compound **3** this means that the investigated single crystal contained the enantiomers with configuration 1S,3aR,4R,5R,11bR and 1R,3aS,4S,5S,11bS.

For compound **4** the single crystal had the enantiomers 1R,3aS,4R,5S,11bS and 1S,3aR,4S,5R,11bR, which are the diastereomers and epimers to the content of compound **3**.
In the solid state, the O-H groups are engaged in intra- and inter-molecular hydrogen bonding (**Supplementary Fig. S1**). The intramolecular packing is further controlled by π-π stacking interactions (**Supplementary Fig. S**2). The molecular structures of **3** and **4** cannot pack very efficiently in the solid state so that solvent filled voids are formed in the crystal lattice (**Supplementary Fig. S**3).

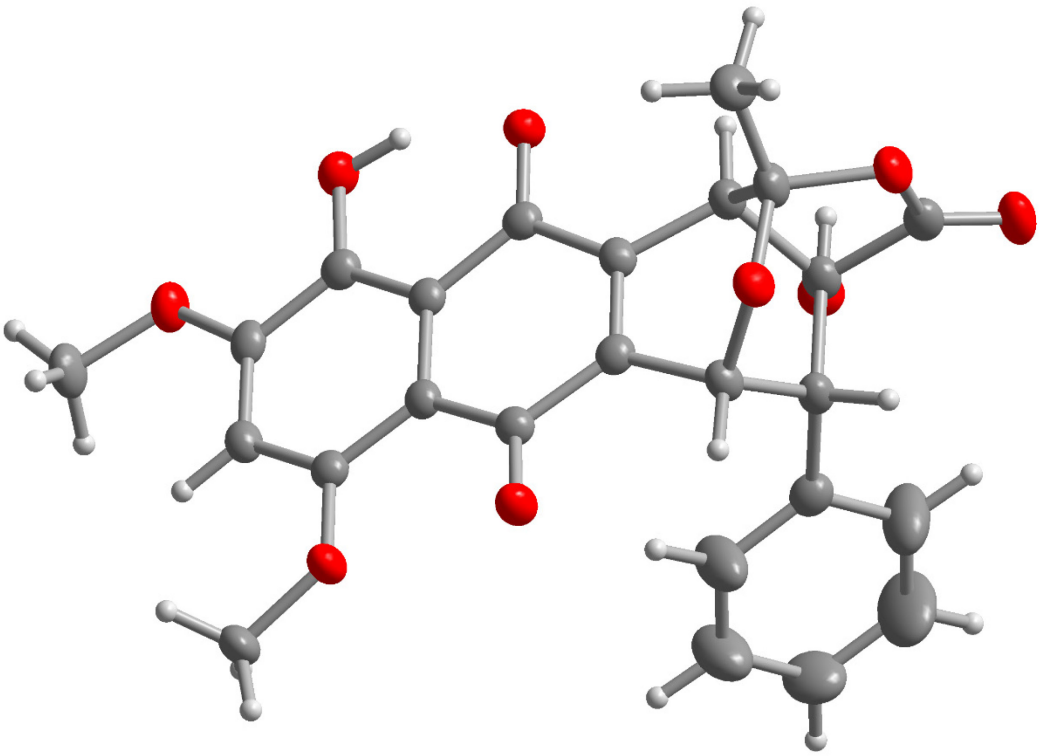

(a)

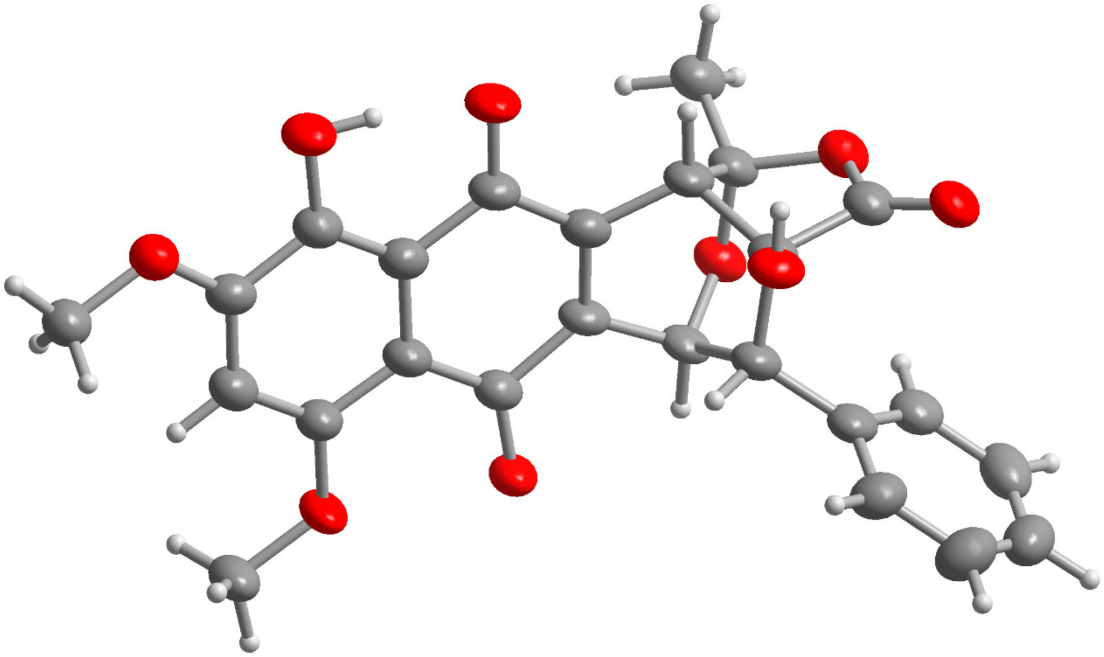

(b)

Figure 6. Molecular structures of compounds **3** (a) and **4** (b) from the single crystal X-ray structure (50% thermal ellipsoids, H atoms with arbitrary radii). Compound **3** crystallizes with a partially occupied ethyl acetate molecule (not shown here; see **Supplementary Fig. S**4), compound **4** with disordered methanol molecules which were removed by solvent masking during the refinement. (See **Supplementary Fig. S**4 and **Supplementary Fig. S**5 for the atom numbering.)

*2.3 Whole genome sequencing, assembly, biosynthetic gene cluster identification and proposed biosynthesis of compounds **3** and **4***

To gather more information about the possible synthesis route of compounds **3** and **4**, whole genome sequencing of *F. oxysporum* employing nanopore sequencing followed by antiSMASH processing and comparison was carried out. Because of the high structural relationship to 9-O-methylfusarubin, the focus was put on biosynthetic gene clusters (BGCs) with high similarity to BGCs known to be involved in the biosynthesis of fusarubin and derivatives. A core genome identity (ANI) of 97.073% with the NCBI reference GCF_000271745.1 using FastANI was established [27], clearly labelling the assembly as *F. oxysporum*. The genome assembly consisted of 537 contigs, with 11 contigs exceeding 1,000,000 base pairs (Total assembly length: 53,627,915, Fragment N50: 3253949, Mean coverage: 215X). An overview of the top 20 assembled contigs and the overall distribution of contigs from the nanopore sequencing sorted by lengths is provided in the supplementary information (**Supplementary Fig. S6)**. Subsequently, the assembly was transferred to the antiSMASH fungal version for comparison to known *Fusarium* BGCs. This led to identification of a cluster [Region 1] in contig 160 of the type 1 polyketide synthase (T1PKS) that had a reported similarity of 87% to the known cluster BGC0001242 from *Fusarium fujikuroi* IMI 58289, which is responsible for the biosynthesis of oxyjavanicin (= fusarubin) [23]. For this gene cluster, besides the core biosynthetic

gene region, nine additional genes with one regulatory gene were reported together with four other putative genes with unknown functions (**Fig. 7**).

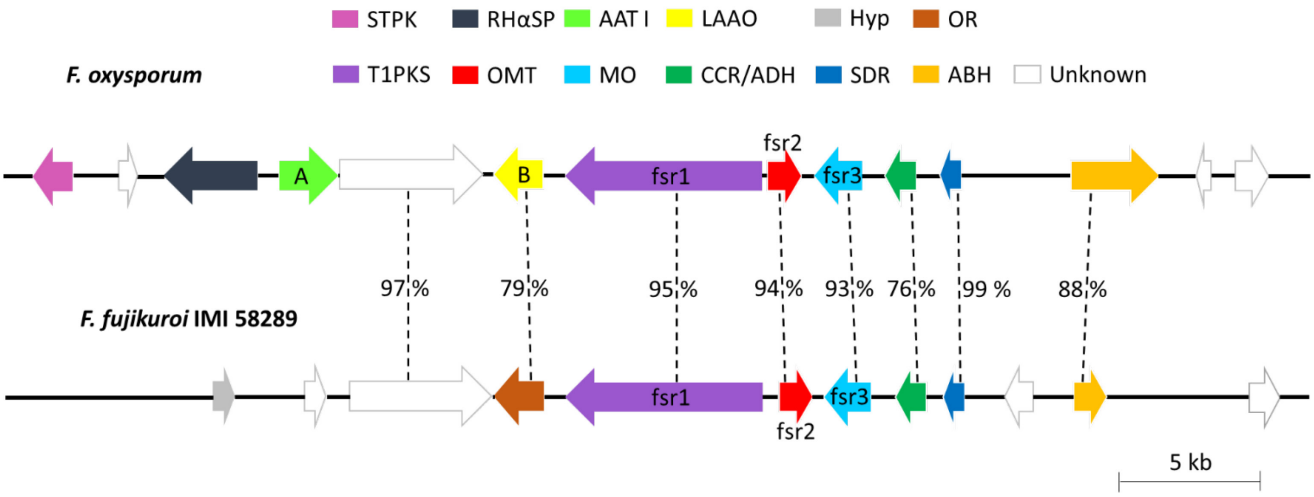

Figure 7. Comparison of the *fsr* cluster in *F. fujikuroi* with the *F. oxysporum* cluster of contig 160 region 1. The sequence identities on the amino acid level are given as percentages. Abbreviations of the enzymes encoded by the genes are as follows: STPK = serine/threonine protein kinase, RHαSP = ring-hydroxylating α-subunit domain-containing protein, AAT = amino acid transporter, LAAO = L-amino acid oxidase, Hyp = hydrophobin, OR = oxidoreductase, T1PKS = type-1 polyketide synthase, OMT = O-methyltransferase, MO = monooxygenase, CCR/ADH = crotonyl-CoA-reductase/alcohol dehydrogenase, SDR = short-chain dehydrogenase/reductase, ABH = alpha/beta hydrolase

Compounds **3** and **4** (fusapurpurin A and B) share the same 9-O-methylfusarubin core structure, which was isolated by us from the crude ethyl acetate extract of the co-cultivation of *F. oxysporum* with *P. ehimensis* as known natural compound **1**. 9-O-methylfusarubin has already been previously described as a pigment produced from different members of the genus *Fusarium* including *Fusarium oxysporum* [21, 22]. In the case of fusapurpurins A and B, the 9-O-methylfusarubin core is extended by a phenyl pyruvic acid moiety. To our best knowledge, this has never been described for a fusarubin derivative before and therefore represents a completely new structural subclass. The reported route to form naphthoquinone structures as basis for different fusarubins is accomplished through polyketide synthases. While the core structure is built by *Fsr1*, the introduction of keto- and O-methyl groups is carried out by *Fsr2* and *Fsr3* as described in the literature [23]. Interestingly, gene *A* codes for an amino acid transporter exhibiting 84.5 % identity to the amino acid/polyamine transporter I from an unrelated *F. oxysporum* strain that is not present in the reference gene cluster (Accession Nr. KAH7221724.1). Furthermore, gene *B* encodes an L-amino acid oxidase with 98 % identity with an enzyme from *F. oxysporum sp. vasinfectum* (Accession Nr. EXM20109.1). Thus, we propose that *A* could introduce L-phenylalanine as a phenylpropanoid to the biosynthesis of **3** and **4**, while *B* converts it into phenylpyruvic acid via oxidative deamination to form the α-keto acid that subsequently is added

to the 9-O-methylfusarubin core structure. The complete proposed biosynthesis of fusapurpurin A and B starting from the 9-O-methylfusarubin core structure is presented in **Fig. 8**.

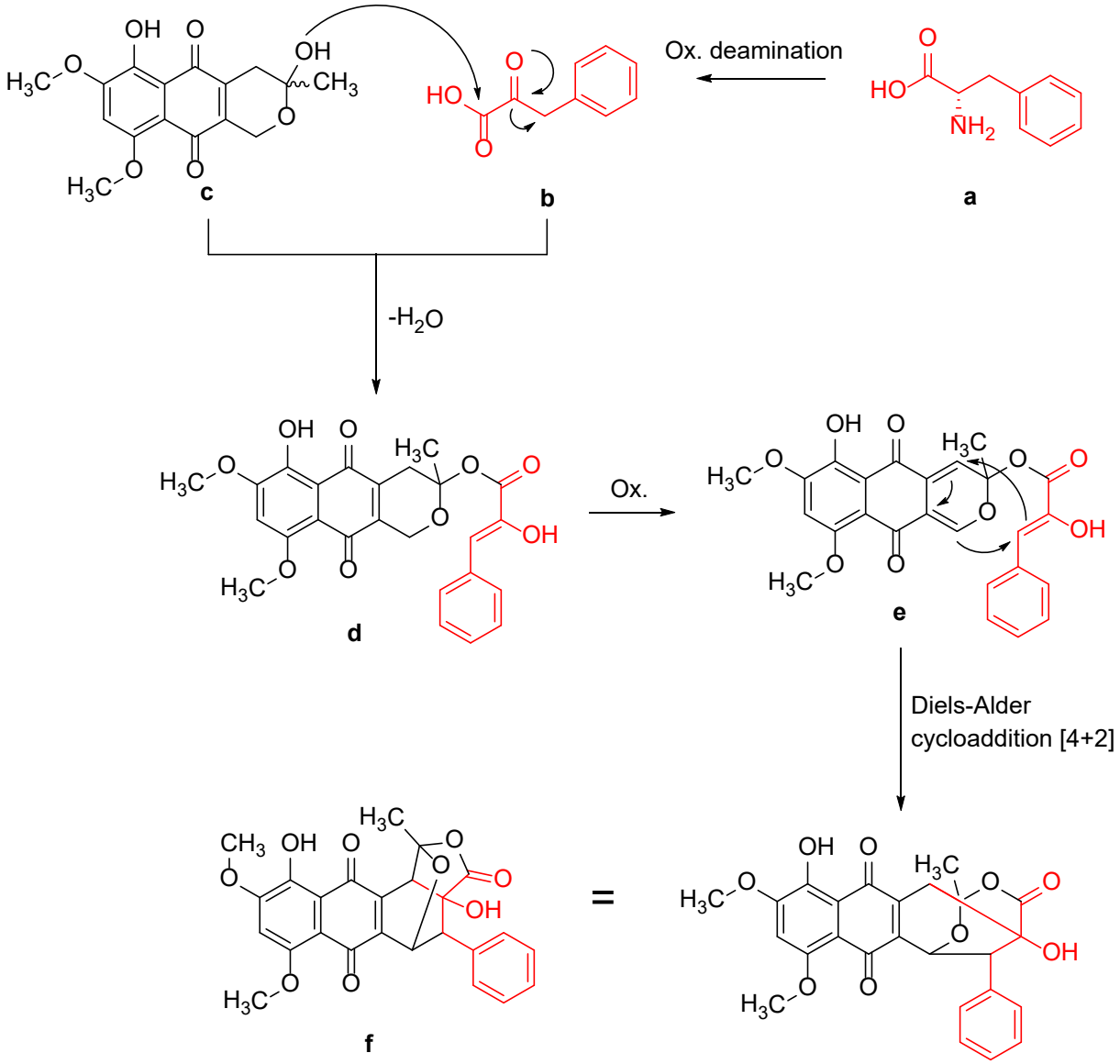

Figure 8. Proposed biosynthetic pathway for formation of compounds **3** and **4**. The amino acid L-phenylalanine (a) is oxidized via oxidative deamination to build phenylpyruvic acid (b). 9-O-Methylfusarubin (c) reacts with phenyl pyruvic acid (b) in a nucleophilic substitution to form intermediate d. After an oxidative step to build intermediate e, structure f (compounds **3** and **4**) is built via a Diels-Alder cycloaddition [4+2] as the final step to build the proposed racemic products.

The Diels-Alder reaction shown in **Fig. 8** could be mediated enzymatically by a Diels-Alderase. While the predicted functions of proteins encoded in the gene cluster shown in **Fig. 7** did not provide such an enzyme, we identified a gene putatively coding for a Diels-Alderase in contig 44 region 8 in our *F. oxysporum* strain. This gene is part of a gene cluster that has 45 % similarity with an equisetin gene cluster from *Fusarium heterosporum* ATCC 74349 (**Fig. 9**).

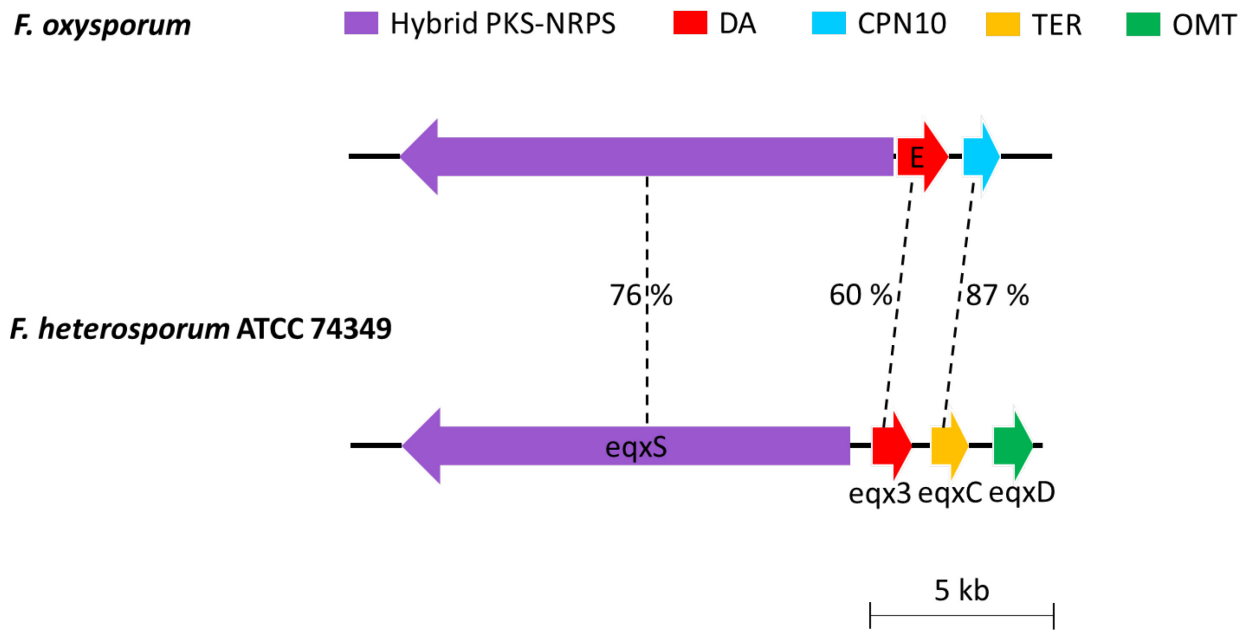

Figure 9. Comparison of a segment of the *eqx* gene cluster in *F. heterosporum* with the *F. oxysporum* cluster of contig 44 region 8. The sequence identities on the amino acid levels are given as percentages. Abbreviations of the enzymes encoded by the genes are as follows: Hybrid PKS-NRPS = hybrid polyketide synthase-nonribosomal peptide synthase, DA = Diels-Alderase, CPN10 = chaperonin 10-like protein, TER = trans-enoyl reductase, OMT = O-methyltransferase

While the known Diels-Alderase gene *eqx3* from *F. heterosporum* has 60 % identity on the amino acid level with *E*, *E* shares 95 % identity on the amino acid level with a putative Diels-Aderase from *F. oxysporum f. sp. matthiolae* (Accession Nr. KAH7489926.1). The essential role of the Diels-Alderase *Fsa2*, which is encoded by *eqx3*, in the biosynthesis of equisetin has already been described [28]. The same reaction is also described for the fungus *Chaetomium globosum* in the biosynthesis of the compound Sch 210972, which is structurally closely related to equisetin [29]. Other examples of fungal Diels-Alderases that are involved in the biosynthesis of secondary metabolites are solanapyrone synthase from *Alternaria solana* in the production of solanapyrone A [30], LovB from *Aspergillus terreus* in the biosynthesis of Lovastatin [31] or the macrophomate synthase MPS from *Macrophoma commeliniae* to yield macrophomic acid [32]. Further work is required to demonstrate whether the proposed biosynthetic pathway shown in **Fig. 8** is plausible and whether P encoded in the *F. oxysporum* cluster of contig 44 region 8 or other Diels-Alderase potentially present in this fungus are indeed involved in the biosynthesis of fusapurpurin A and B.

Another question is how compounds **3** and **4** could be built up as racemic or scalemic mixtures. While natural products most of the time are described as chiral molecules, research about the biosynthesis of racemic natural compounds is rather scarce. On the one hand, the biosynthesis of chiral natural products through enzymatically driven pathways is a reasonable outcome. On the other hand, the biosynthesis of racemic natural products is described in several publications, including alkaloids and polyketides, and often seems to be rather underestimated [33].

In the case of compounds **3** and **4,** the proposed pericyclic reaction described in **Fig. 8** connecting the 9-O-methylfusarubin with the phenylpyruvate moiety could be mediated in a reaction having a radical intermediate, which quickly is being rearranged. This could be a driving factor for the production of different configurations [34]. In general, natural Diels-Alderases are not clearly defined and unified. It is described that often they seem to have a certain stereoselectivity, but also that some enzymes lead to the production of at least two isomers. Also, pericyclic reactions often can happen spontaneously, without enzymatic catalysis, which could support the non-stereoselective production of isomers [35]. The appearance of at least four isomers definitely is intriguing. For future research, it will be of great interest to elucidate the biosynthetic pathway and possible corresponding reactions in detail, which lead to the different isomeric forms of this novel substructure of fusarubin-derivatives.

With respect to the biosynthetic pathway, also the strong promotion of 9-O-methylfusarubin production (compound **1**) during co-culture with *P. ehimensis* is noteworthy (**Fig. 2**) as this molecule likely is the direct precursor for synthesis of the novel fusapurpurins A and B (compounds **3** and **4**). While it is currently not known how presence of *P. ehimensis*, but not of the other tested bacterial species, specifically stimulates 9-O-methylfusarubin formation in *F. oxysporum*, elucidation of the *F. oxysporum* genome sequence now opens an avenue to identify genes potentially involved in fusapurpurin biosynthesis employing comparative transcriptomic and/or proteomic analyses.

2.4 Biofilm-dispersing activities

Initial explorative bioactivity testings with *Mycobacterium tuberculosis* H37Rv revealed a low biofilm-dispersing activity in addition to a direct antibacterial effect of the crude ethyl acetate extract of the co-cultivation of *F. oxysporum* with *P. ehimensis*. Thus, the pure compounds derived from the isolation process were submitted to assays assessing their ability to disperse preformed biofilms against three important human pathogenic bacteria known to notoriously form biofilms during chronic infections: the gram-positive methicillin-resistant *Staphylococcus aureus* (MRSA) strain Mu50, the gram-negative *Pseudomonas aeruginosa* strain PAO1, and *M. tuberculosis* strain H37Rv. Interestingly, the racemic mixtures of compounds **3** and **4** showed potent biofilm-dispersing activities against both MRSA Mu50 and *P. aeruginosa* PAO1 with IC90 of 6.25 µM and 12.5 µM, respectively (**Fig. 10 A+B**), while only **4** caused partial dispersion of *M. tuberculosis* H37Rv biofilms at the highest tested concentration of 100 µM (**Fig. 10 E**). Intriguingly, both fusapurpurins were unable to prevent the formation of biofilms (**Fig. 10 C+D**) . Furthermore, they also did neither impair viability of cells in biofilms (**Supplementary Fig. S7**) nor show any direct antimicrobial effect on actively growing submersed microbial cells (**Table 3**). Quorum sensing has been identified as a cell density-dependent mechanism of cell-cell communication that is involved in all steps of biofilm development and maturation [36]. Consistent with the inability to prevent biofilm-formation, the fusapurpurins also did not interfere with quorum sensing-induced violacein production in a bioassay employing *Chromobacterium violaceum* (**Supplementary Fig. S8**).

Consequently, both fuspurpurins exhibit an unusal, very specific desintegratiung effect at low micromolar concentration only when added to preformed biofilms. This effect appears to be broad spectrum including both gram-positive and gram-negative bacteria and to a lesser extent also mycobacteria.

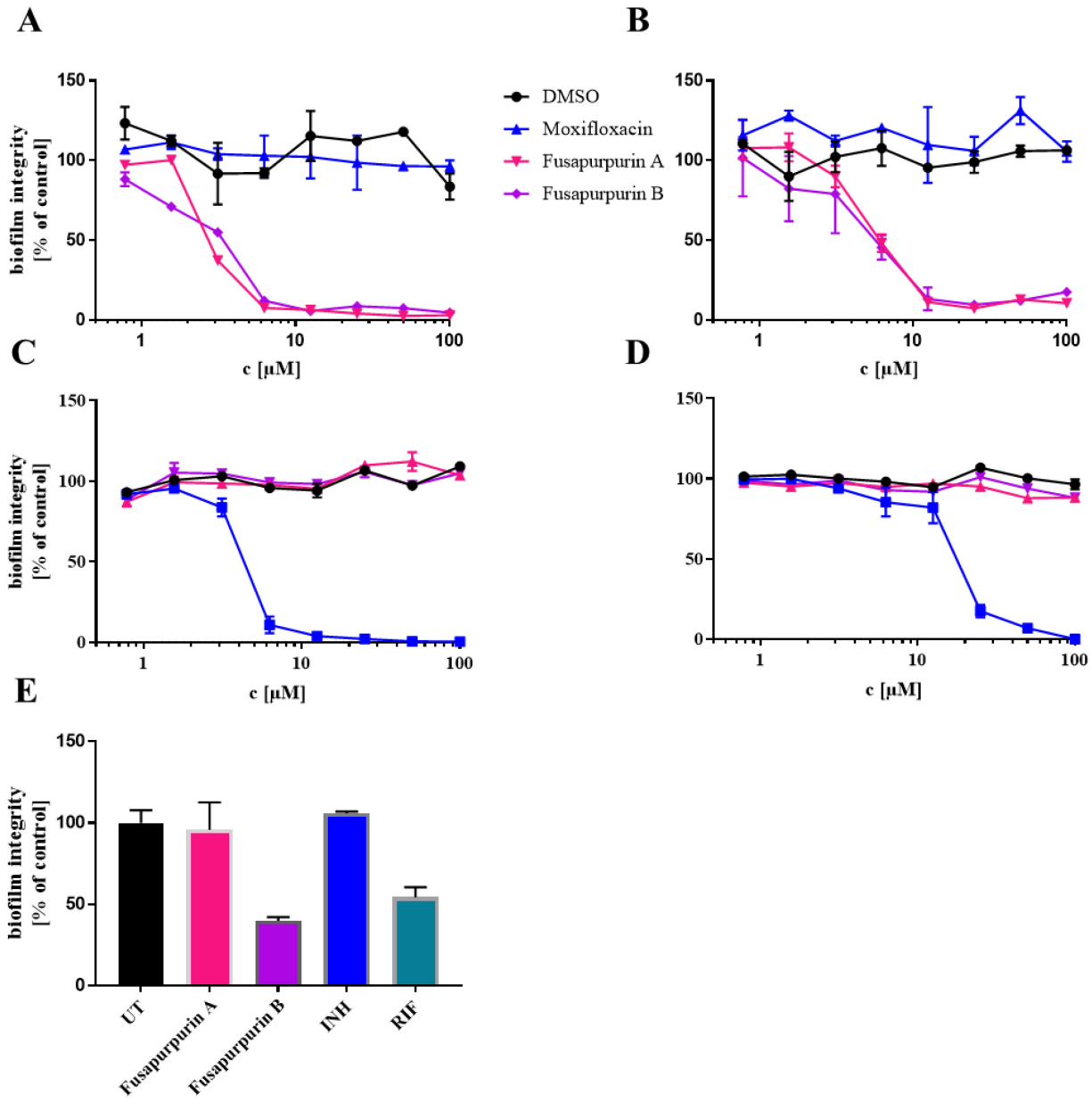

Figure 10. Fusapurpurin A and B (**3** and **4**) mediated dispersion of preformed biofilms in MRSA Mu50 (A) and *P. aeruginosa* PAO1 (B). Moxifloxacin, a bactericidal antibiotic only active gainst replicating bacterial cells, and DMSO were used as negative controls.
Fusapurpurin A and B (**3** and **4**) do not prevent biofilm formation when added to suspended cells of MRSA Mu50 (C) and *P. aeruginosa* PAO1 (D). Moxifloxacin, a bactericidal antibiotic active gainst replicating bacterial cells, was used as positive control, and DMSO was used as negative control. The graphs show the biofilm integrity compared to the control in MRSA Mu50 (C) and *P. aeruginosa* PAO1 (D) when fusapurpurin A and B are added during biofilm formation.

Disruption of biofilm integrity in *Mycobacterium tuberculosis* H37Rv by fusapurpurin B (E). Fusapurpurin A and B were adjusted at 100 µM to the preformed mycobacterial biofilm. Isoniazide (INH, 200 µM) and rifampicin (RIF, 350 µM) were used as controls. UT = Untreated biofilms. All assays (A-E) were carried out in triplicates and graphs show mean ± SEM.

Table 3. MIC_{90} of isolated compounds against MRSA Mu50, *P. aeruginosa* PAO1, *Candida albicans* ATCC 24433 and *M. tuberculosis* H37Rv. All concentrations are shown in µM. Concentrations >100 µM indicate no activity in the experimental setup. The experiment was conducted in triplicates. All compounds except **9** were virtually devoid of antimicrobial activity. Compound **9** (beauvericin) showed weak antibacterial activity against MRSA Mu50 with an MIC_{90} of 50 µM and good activity against Mtb H37Rv at 3.125 µM, which is in agreement with the antibacterial and antimycobacterial activity of this mycotoxin reported in the literature [37].

	MIC_{90} [µM]			
Compound	***S. aureus* Mu50**	***P. aeruginosa* PAO1**	***C. albicans* ATCC 24433**	***M. tuberculosis* H37Rv**
1	>100	>100	>100	>100
2	>100	>100	>100	>100
3	>100	>100	>100	>100
4	100	>100	>100	>100
5	>100	>100	>100	>100
6	>100	>100	>100	>100
7	>100	>100	>100	>100
8	>100	>100	>100	>100
9	50	>100	>100	3.125
10	>100	>100	>100	>100

Bacterial biofilms are virulence factors that are complicating treatment, prolonging infections and increasing mortality of infectious diseases and are therfore a huge health concern [38]. Thus, the discovery of new and potent biofilm-inhibiting compounds is crucial. In addition of compounds that are able to prevent biofilm formation and/or kill bacterial cells imbedded in the biofilms, molecules able to disintegrate the biofilm matrix thereby removing biofilms from biotic and abiotic surfaces are also of great clinical relevance [36]. Therefore, our discovery of the specific biofilm-desintegrating properties of fusapurpurin A and B at low micromolar concentrations are of potential medical interest as these compounds in combination with antibiotics targeting the dispersed bacterial cells might be able to eradicate chronic bacterial infections. In this regard, the unusual broad-spectrum activity of these compounds against a gram-positive, a gram-negative and a mycobacterial organism is a highly beneficial attribute as it might suggest potential broad clinical applicability. For future research, it will be of great interest to distinguish, if the activity of **3** and **4** is connected to either one of the two enantiomers of the mixture or if all isolated isomers show a biofilm disrupting activity. If the shown

activity is only connected to one enantiomer, the biofilm disrupting activity could be stronger than expected, elucidating an even higher potential.

In order to assess the therapeutic potential of the fusapurpurins, the cytotoxic activity of compound enantiomeric mixtures **3** and **4** was evaluated against the human cell lines THP-1 (human monocytic leukaemia cell line), Huh-7 (Human liver carcinoma cell line), and HEK293 (human embryonic kidney cell line). Compound **3** showed weak cytotoxicity against THP-1 and Huh-7 cell lines and no cytotoxic effect on the Hek 293 cell line, while compound **4** showed moderate cytotoxic activities against all three tested cell lines, showing no to moderate cytotoxic effects (**Table 4**). Although this results in some selectivity particularly for fusapurpurin A (compound **3**) (selectivity index = IC50 cytotoxicity / IC90 antibiofilm activity against MRSA ranging from 6 to >16 dependent on human cell type), these properties might not be sufficient for direct clinical application. Nevertheless, elucidation of the mode of action of fusapurpurin A and B and identification of their molecular target might allow the development of more potent and more specific broad-spectrum biofilm-desinteragting drugs in future studies.

Table 4. Mean IC_{50} values of compounds **3** and **4** against human cell lines THP-1, Huh-7 and Hek293. All concentrations are shown in µM. A concentration >100 µM indicates no activity in the experimental setup. All experiments have been conducted in triplicates. The IC_{50} values were calculated using GraphPad Prism 7. 100 % growth control: DMSO. 0 % growth control: cycloheximide.

	Mean IC_{50} [µM]		
Compound	**THP-1**	**Huh-7**	**Hek 293**
3	40.66	47.85	>100
4	11.57	12.67	26.81

3. Experimental section

3.1 General Experimental Procedures

Optical rotations were measured on a Jasco P-2000 polarimeter. UV spectra were obtained by the use of a Dionex P580 system in combination with a diode array detector (UVD340S) and a Eurosphere 10 C18 column (125x4 mm). 1D and 2D NMR spectra were recorded on a Bruker Avance III (^{1}H, 600 MHz; ^{13}C 150 MHz) spectrometer. Mass spectra were measured on a Finnigan LCQ Deca (Thermo Quest) mass spectrometer and for HRESIMS on a UHR-QTOF maXis 4G (Bruker Daltonics) mass spectrometer. Semipreperative HPLC was performed on a Lachrom-Merck Hitachi system (pump L7100, UV-detector L7400, Eurospher 100 C18 column 300x8 mm, Knauer Germany) and a Chromaster-VWR Hitachi system (pump 5110, UV-detector 5410, Eurospher 100 C18 column 300x8 mm, Knauer Germany). VLC and non-vacuum-column chromatography were accomplished using Macherey Nagel silica gel 60M (0.04-0.063 mm). Precoated TLC silica gel 60 F254 plates (Merck) were used for tracking separation using detection under UV light at 254 and 365 nm wavelengths or spraying Anisaldehyde-sulfuric acid reagent. Sephadex LH20 (GE Healthcare Bio. Sciences AB) was used as a stationary phase for column chromatography. The measurement of optical rotations was accomplished by using spectral-grade solvents. The optical density of fungal yeast cultures was measured using a WPA Biowave CO8000 Cell Density Meter.

3.2 Fungal Material

The fungus *Fusarium oxysporum* was obtained from a soil sample collected from Texel, the Netherlands (GPS 53.00 N 4.44 E) by using a co-cultivation method. A spatula of the soil was mixed with 100 µl from an overnight culture of the auxotrophic yeast *Saccharomyces cerevisiae* FY1679-01B with the optical density of 1.0 and 20 ml Lysogeny Broth (LB)-medium in a 100-ml Erlenmeyer flask. The co-cultivation mixture was incubated statically for 14 days at 30 °C, initially aiming at enriching microorganisms that can antagonize yeast growth. 10 µl of the liquid co-culture were spread on an agar plate containing Yeast Nitrogen Base without Amino Acids (BD Difco), enriched with D-glucose and 20 mg/l chloramphenicol, using a spatula and incubated for 3 days at 30 °C. The fungus was growing on top of the agar plate as a white filamentous spot. The isolated strain was identified as *Fusarium oxysporum* by internal transcribed spacer (ITS) sequences with 100 % identity to known *Fusarium oxysporum* (GenBank Accession OP122502). Additionally, the identity was confirmed via whole genome sequencing with a core genome identity (ANI) of 97.073% with the NCBI reference GCF_000271745.1 using FastANI (GenBank Accession PRJNA861985).

3.3 Fermentation and Extraction

The fermentation of the fungus was carried out as a co-cultivation approach, first at a small-scale to compare different co-cultivation attempts followed by large-scale cultivation for isolation purposes. For all samples, solid rice medium enriched with Lysogeny Broth (LB)-medium was used as

the main nutrient. For the small-scale co-cultivation approaches, 100 g of rice and 100 ml of LB-medium were added to seven Erlenmeyer flasks followed by autoclaving. 10 ml of overnight cultures of five different bacteria respectively, namely *Acinetobacter baylyi ADP1*, *Pseudomonas qingdaonensis*, *Bacillus amyloliquefaciens*, *Lysinibacillus macroides* and *Paenibacillus ehimensis* were then each added to one of these Erlenmeyer flasks and incubated for four days at 22 °C under static conditions. Then 1 x 1 cm^2 fungal material was inserted into each of the Erlenmeyer flasks containing bacterial cultures using a flame-sterilized scalpel and into one of the Erlenmeyer flasks not containing bacterial cultures as a control. One Erlenmeyer flask was used as a background control for the LB medium. All flasks were then incubated for four weeks at 22°C under static conditions. For the large-scale co-cultivation approach, ten Erlenmeyer flasks were prepared with rice and LB-medium as mentioned above. 10 ml of an overnight culture of *P. ehimensis* was then added to each flask and incubated for 4 days at 22°C under static conditions followed by the addition of 1 x 1 cm^2 fungal material and incubation for four weeks at 22°C under static conditions. Each flask of the small-scale and large-scale fermentations was extracted with 250 ml Ethylacetate. The rice medium was cut into small pieces and shaken for eight hours followed by evaporation of the EtOAc.

3.4 Isolation

The crude extract (3.89 g) obtained from the large-scale co-cultivation with *P. ehimensis* was separated by the use of Vacuum Liquid Chromatography with silica gel as a stationary phase. A step gradient from 100 % hexane to 100 % EtOAc followed by a step gradient from 100 % CH_2Cl_2 to 100 % CH_3CN and finished with 100 % EtOH, with 500 ml for each eluent, yielded 16 fractions (V1-V16). Fractions V3 (787.9 mg), V4 (901.6 mg) and V5 (328.6 mg) were combined and further separated over a Sephadex LH20 column with Acetone as eluent to give 6 subfractions (V3-5S1-V3-5S6). Subfraction V3-5S5 (35.3 mg) was purified over semi-preparative HPLC using a MeOH-H_2O step gradient from 50-100 % MeOH to give **2** (2.9 mg). Fractions V6 (229.7 mg), V7 (28.0 mg), V8 (2.8 mg), V9 (5.9 mg), V10 (11.0 mg), V11 (13.9 mg), V12 (41.9 mg), V13 (56.8 mg), V14 (72.8 mg) and V15 (38.8 mg) were combined and then separated using a LH20 Sephadex column with 100 % Acetone as an eluent to yield 4 subfractions (V6-15S1-V6-15S4). Subfraction V6-15S1 was finally purified over semi-preparative HPLC using a CH_3CN-H2O step gradient from 30-80 % CH_3CN to give **3** (2.4 mg) and **4** (2.9 mg).

Spectral Data of compounds **2-4**:

Fusachinon (2): orange amorphous solid; $[\alpha]^{25}_D$ *-65 (c 0.8, MeOH)* λ_{max} 230, 277, 480 nm; ^{1}H NMR (DMSO-d_6) and ^{13}C NMR (DMSO-d_6) see **Table 1**; HRESIMS m/z 331.0817 $[M + H]^+$ (calcd. for $C_{17}H_{15}O_7$ 311.0812 m/z).

Fusapurpurin A (3): pink crystals (Ethylacetate); *UV (MeOH)* λ_{max} 200, 226, 284, 520 nm; ^{1}H NMR (DMSO-d_6) and ^{13}C NMR (DMSO-d_6) see **Table 2**; HRESIMS m/z 465.1177 $[M + H]^+$ (calcd. for $C_{25}H_{21}O_9$ 465.1180 m/*z*).

Fusapurpurin B (4): purple crystals (MeOH)*; UV (MeOH)* λ_{max} 201, 226, 283, 520 nm; ^{1}H NMR (DMSO-d_6) and ^{13}C NMR (DMSO-d_6) see **Table 2**; HRESIMS m/z 465.1174 m/z $[M + H]^+$ (calcd. for $C_{25}H_{21}O_9$ 465.1180 m/z).

The detailed NMR- and other spectral data for compounds **1-10** are provided in the supplementary information **S9-S68**.

3.5 X-ray crystallographic data

Suitable crystals were carefully selected under a polarized-light microscope, covered in protective oil and mounted on a cryo-loop. The single crystal diffraction data was collected on a Rigaku XtaLAB Synergy S four circle diffractometer with a Hybrid Pixel Array Detector and a PhotonJet X-ray source for Cu-Kα radiation (λ = 1.54184 Å) with a multilayer mirror monochromator. Data was collected at 100.0 ± 0.1 K using ω-scans. Data reduction and absorption correction were performed with CrysAlisPro 1.171.41.105a [39]. Structure analysis and refinement: The structures were solved by direct methods (SHELXT-2015), Full-matrix least-squares refinements on F^2 were carried out using the SHELXL-2017/1 program package in OLEX 2.1.3 [40-42]. All hydrogen atoms on C were positioned geometrically (with C–H = 0.95 Å for aromatic and aliphatic CH, C–H = 1.00 Å for ternary CH, C–H = 0.99 Å for CH_2 and C–H = 0.98 Å for CH_3) and refined using riding models (AFIX 43, 13, 23 and 137 with $U_{iso(H)}$ = 1.2 U_{eq} (CH, CH_2) and 1.5 U_{eq} (CH_3). The protic hydrogen atom for OH in compound **3** and **4** was found and refined freely. Strongly disorderd solvent molecules of MeOH for compound **4** have been removed with the solvent mask feature as implemented in OLEX 2.1.3. 176 electrons were found in a volume of 1300 Å^3 per unit cell, which may correspond to about 10 methanol molecules (18 electrons each) as the solvent of crystallization per unit cell or about 1.25 methanol per asymmetric unit (Z = 8). Crystal data and details on the structure refinement are given in **Table 5**. Graphics were drawn with the program DIAMOND [43]. Computations on the supramolecular interactions were carried out with PLATON for Windows [44-46]. The crstallographic data for compound **3** and **4** reported in this paper has been deposited in the CCDC under the numbers 2232516 and 2232517. This data can be obtained free of charge from the Cambridge Crystallographic Data Centre *via* www.ccdc.cam.ac.uk/data_request/cif.

Table 5. Crystal data and structure refinement for compounds **3** and **4**.

	Compound 3	**Compound 4**
Formula	$C_{25}H_{20}O_9$, 0.401($C_4H_8O_2$)	$C_{25}H_{20}O_9$, 1.25(CH_3OH)
M_r	499.74	464.41
Cryst. size, mm^3	0.18 × 0.15 × 0.02	0.15 × 0.12 × 0.08
Crystal system	orthorhombic	orthorhombic
Temp. (K)	100	100
Space group	*Pnna*	*Pbcn*
a, Å	14.4569 (2)	17.8013 (5)
b, Å	24.5575 (4)	13.8375 (4)
c, Å	12.8869 (2)	20.7494 (6)
V, $Å^3$	4575.18 (12)	5111.1 (3)
Z	8	8
D_{calcd}, g cm^{-3}	1.451	1.207
μ, mm^{-1}	0.940	0.780
θ range (°)	3.6-67.1	4.1-67.1
F(000)	2090	1936
Trans. (max/min)	0.991/0.991	0.992/0.992
hkl range	±17; ±29 ±15	±21; ±16; ±24
Refl. measured	28841	43551
Refl. unique	4096	4545
R_{int}	0.039	0.061
Param. Refined/Restraints	363/0	316/0
GoF (F^2) [a]	1.162	1.553
R_1/wR_2 [I>2σ (I)] [b]	0.0598/0.1438	0.1095/ 0.3282
R_1/wR_2 (all data) [b]	0.0644/0.1466	0.1182/ 0.3438
Max./min. $\Delta\rho$ (e. $Å^{-3}$) [c]	0.54/–0.42	0.674/–0.556
CCDC number	2232516	2232517

[a] Goodness-of-fit = $[\sum[w(F_o^2 - F_c^2)^2]/(n - p)]^{1/2}$; [b] $R_1=[\sum(||F_o| - |F_c||)/\sum|F_o|]$; $wR_2=[\sum[w(F_o^2 - F_c^2)^2]/\sum[w(F_o^2)^2]]^{1/2}$; [c] Largest difference peak and hole.

3.6 Whole genome nanopore sequencing and genome assembly

For long-read nanopore sequencing, the GDE_9141_v112_revE_01Dec2021 protocol for ligation sequencing of genomic DNA was followed, using the SQK-LSK112 ligation kit and a MinION Flow Cell R10 Version. Reads were assembled using Flye [47]. Assembled contigs are available under the SRA accession [PRJNA861985]. The antiSMASH software [48] was used to detect gene clusters and identify potential genes of interest involved in the production of fusarubin and derivatives.

3.7 Biofilm assays

Biofilm assays were performed as previously described [49]. Briefly, biofilm integrity was evaluated using the crystal violet assay. A bacterial cell suspension was prepared in Mueller-Hinton broth supplemented with 10% glucose and adjusted to an OD equal to 10^8 cells per mL. One hundred microlitres of the bacteria cell solution were added to each well and incubated statically for 24 h at 37 °C to allow the formation of biofilms. The wells were washed twice with PBS to remove planktonic cells and compounds were added in a 1:1 serial dilution to the wells. Crystal violet staining was performed 24 h later as follows. The liquids in the wells were aspirated and each well was washed twice with PBS. After air drying for 30 min, 100 µL of a 0.1% crystal violet solution was added and allowed to stain the biofilms for 15 min. Afterwards, the plates were washed twice with PBS and 100 µL 30% acetic acid was added for 30 min to solubilise the dye. Fifty microlitres were transferred to a fresh 96-well round-bottom plate and absorption was measured at 600 nm in a TECAN plate reader. A sterile and vehicle control were used as controls for calculations.

For mycobacterial biofilms, 24-well polystyrene flat-bottom cell culture plates and Sauton medium without tyloxapol were used. A saturated Mtb H37Rv culture in Sauton medium (OD_{600} = 1.0) was used to start the growth of the biofilms. 450 µL Sauton medium and 50 µL saturated Mtb H37Rv cell suspension was added to each well of the 24-well plate. The plate was covered with a clear sealing foil and was incubated for five weeks at 37 °C, 5% CO_2, and humified atmosphere to allow the formation of the biofilms. Hereafter, test compounds were injected beneath the pellicle to a final concentration of 100 µM. Rifampicin (RIF, 100 µg/mL = 121.5 µM), isoniazid (INH, 50 µg/mL = 365 µM), and DMSO were used as a positive and negative control, respectively. After five days, the medium was carefully removed from each well without disturbing the pellicle and 1000 µL of a 0.1% crystal violet solution was added to stain the extracellular polymeric substances. After staining for 30 minutes, the staining solution was removed and the wells were washed twice with PBS. The pellicles were allowed to air-dry for 15 minutes and 500 µL methanol was added to each well to extract the colour from the pellicles. Using a polystyrene 96-well round bottom plate, 100 µL of each well was transferred into the 96-well plate and absorbance was measured at 600 nm in a TECAN plate reader.

The quorum sensing assay with *Chromobacterium violaceum* was carried out as follows. 100 µL of an overnight culture of *C. violaceum* in Mueller Hinton broth (MHB) were evenly spread over

an agar plate of Mueller Hinton medium. Cotton test discs were put on the surface of the agar medium using forceps. Each disc was soaked with 5 µL of samples or control solutions in DMSO. 125 mg/mL vanillin was used as a positive control. DMSO was used as negative control. Samples were added at concentrations of 10 mg/mL and for fusapurpurin A and B at 100 µM. Test plates were incubated at 30°C over night.

3.8 Cytotoxicity assays

The cytotoxicity assays were performed using THP-1 (human monocytic leukaemia cell line), Huh-7 (Human liver carcinoma cell line) and HEK293 (human embryonic kidney cell line) cell lines as described before [50]. The THP-1 cells were cultured using RPMI 1640 medium containing 2 mM L-glutamine and supplemented with 10 % fetal calf serum (FCS) and 1 % sodium pyruvate. Huh-7 cells were cultured using a 1:1 mixture of RPMI 1640 medium containing 2 mM L-glutamine and 10% FCS medium and DMEM medium containing 10% FCS and 1% sodium pyruvate. The HEK293 cells were cultured with EMEM medium including 2 mM L-glutamine and supplemented with 1% NE amino acids, 1% 1.0 mM sodium pyruvate and 10% FCS. All three cell lines were then incubated at 37 °C in an atmosphere of 5 % CO_2 at humid conditions for 2 weeks while renewing the medium twice weekly. Subsequently, the cells were suspended and adjusted to a density of 2 x 10^5 cells/ml. In a 96-well flat-bottom microtiter plate, the cells were adjusted to a total volume of 100 µl containing 2-fold serial dilutions of the tested compounds **2** and **3** ranging from 100 to 0.78 µM. Cycloheximide (4, 2, 1, 0.5, 0.25, 0.13, 0.06, 0.03 µg/ml) was used as a positive control. After an incubation time of 48 h at 37 °C in an atmosphere of 5 % CO_2 under humid conditions, 10 µl resazurin solution (100 µg/mL) was added to each well and incubated for another 4 h. The fluorescence was then quantified using a Tecan Infinite 200pro microplate reader (excitation 540 nm, emission 590 nm). The residual growth was calculated relative to non-inoculated (0 % growth) and controls treated with DMSO (100 % growth), respectively.

3.9 Media and Strains

Methicillin-resistant *Staphylococcus aureus* (MRSA) Mu50 (ATCC 700699) and *Pseudomonas aeruginosa* PAO1 (ATCC 47085) were grown in Mueller-Hinton-broth (MHB). The yeast *Candida albicans* ATCC 24433 was grown in a standard YPD medium (1% yeast extract, 2% peptone, and 2% glucose). The pathogenic bacterium *Mycobacterium tuberculosis* (Mtb) H37Rv (ATCC 27294) was grown in 7H9 supplemented with ADS (0.85% NaCl, 5% BSA, 2% glucose), 0.5% glycerol, and 0.05% tyloxapol. Nosocomial bacteria and *C. albicans* were grown shaking at 120 rpm and 37 °C, Mtb was grown at 37 °C shaking at 80 rpm.

3.10 Determination of the minimal inhibitory concentration

The minimal inhibitory concentration (MIC_{90}) of compounds was determined via microbroth dilution assays. Briefly, a serial 1:1 dilution of compounds was prepared in a 96-well round-bottom polystyrene plate in 50 µL growth medium ranging from 200 µM to 1.56 µM. Pre-grown bacterial cultures were measured for their OD_{600nm}, and a cell suspension in the growth medium was adjusted to 10^6 CFU/ml. After 50 µL of the cell suspension was added to each well, the compound concentration changed to a range from 100 µM to 0.78 µM. In the case of MRSA Mu50, *P. aeruginosa* PAO1 and *C. albicans* ATCC 24433, the BacTiter Glo assay (Promega) was used to quantify growth after 24 h of incubation as described in the manufacturer's manual. Briefly, equal volumes of BacTiter Glo reagent and bacterial cell suspensions were mixed in a white flat-bottom 96-well plate. After 5 minutes, luminescence was measured with a TECAN plate reader. The positive control for MRSA Mu50 and *P. aeruginosa* PAO1 was moxifloxacin and for *C. albicans* hygromycin was used, while DMSO was used as solvent control for all three organisms. The growth of Mtb H37Rv was quantified via the resazurin assay following a protocol as described earlier [51]. Briefly, 10 µL of a 100 µg/mL resazurin solution was added to each well of the 96-well plate after five days of incubation at 37 °C, 5% CO_2, and in a humidified atmosphere. After incubating the plates for another 18 hours at room temperature, the reaction was stopped by the addition of 100 µL 10% formalin solution to each well. The fluorescence was measured at 535 nm excision and 590 nm emission using a TECAN plate reader. Rifampicin and DMSO were used as positive and vehicle control, respectively. All experiments have been conducted in triplicates.

3.11 Impairment of cell viability in biofilms

The impairment of cell viability in biofilms of *Staphylococcus aureus* (MRSA) Mu50 (ATCC 700699) and *Pseudomonas aeruginosa* PAO1 (ATCC 47085) by fusapurpurin A and B (3 and 4) was tested in a microbroth dilution assay. First, cells were grown to form biofilms as described above. Subsequently, a serial 1:1 dilution of fusapurpurin A and B and moxifloxacin was prepared in a 96-well round-bottom polystyrene plate containing the bacterial biofilms, using 50 µL growth medium ranging from 100 µM to 0.78 µM. The viability of cells in the biofilms was measured using the BacTiter Glo assay (Promega) as described above. DMSO was used as solvent control for both organisms.

Acknowledgements

We thank the CeMSA@HHU (Center for Molecular and Structural Analytics@Heinrich Heine University) for recording the mass-spectrometric and the NMR-spectroscopic data. We thank Heike Goldbach-Gecke for testing the cytotoxic activity against the human cell lines THP-1, Huh-7 and Hek 293. The Rigaku diffractometer was funded by the Deutsche Forschungsgemeinschaft (DFG, German Research Foundation) under grant 440366605.

References:

1. Ventola, C.L., *The antibiotic resistance crisis: part 1: causes and threats.* P T, 2015. **40**(4): p. 277-83.
2. Moloney, M.G., *Natural Products as a Source for Novel Antibiotics.* Trends Pharmacol Sci, 2016. **37**(8): p. 689-701.
3. Rutledge, P.J. and G.L. Challis, *Discovery of microbial natural products by activation of silent biosynthetic gene clusters.* Nat Rev Microbiol, 2015. **13**(8): p. 509-23.
4. Wang, B., et al., *Activation of silent biosynthetic gene clusters using transcription factor decoys.* Nat Chem Biol, 2019. **15**(2): p. 111-114.
5. Okada, B.K. and M.R. Seyedsayamdost, *Antibiotic dialogues: induction of silent biosynthetic gene clusters by exogenous small molecules.* FEMS Microbiol Rev, 2017. **41**(1): p. 19-33.
6. Hoogendoorn, K., et al., *Evolution and Diversity of Biosynthetic Gene Clusters in Fusarium.* Front Microbiol, 2018. **9**: p. 1158.
7. Studt, L., et al., *Knock-down of the methyltransferase Kmt6 relieves H3K27me3 and results in induction of cryptic and otherwise silent secondary metabolite gene clusters in Fusarium fujikuroi.* Environ Microbiol, 2016. **18**(11): p. 4037-4054.
8. Niehaus, E.M., et al., *Apicidin F: characterization and genetic manipulation of a new secondary metabolite gene cluster in the rice pathogen Fusarium fujikuroi.* PLoS One, 2014. **9**(7): p. e103336.
9. von Bargen, K.W., et al., *Isolation and Structure Elucidation of Fujikurins A-D: Products of the PKS19 Gene Cluster in Fusarium fujikuroi.* J Nat Prod, 2015. **78**(8): p. 1809-15.
10. Connolly, L.R., K.M. Smith, and M. Freitag, *The Fusarium graminearum histone H3 K27 methyltransferase KMT6 regulates development and expression of secondary metabolite gene clusters.* PLoS Genet, 2013. **9**(10): p. e1003916.
11. Hemphill, C.F.P., et al., *OSMAC approach leads to new fusarielin metabolites from Fusarium tricinctum.* J Antibiot (Tokyo), 2017. **70**(6): p. 726-732.
12. Rodriguez-Ortiz, R., et al., *Stimulation of bikaverin production by sucrose and by salt starvation in Fusarium fujikuroi.* Appl Microbiol Biotechnol, 2010. **85**(6): p. 1991-2000.
13. Weikl, F., et al., *Sesquiterpene emissions from Alternaria alternata and Fusarium oxysporum: Effects of age, nutrient availability, and co-cultivation.* Sci Rep, 2016. **6**: p. 22152.
14. Moussa, M., et al., *Co-culture of the fungus Fusarium tricinctum with Streptomyces lividans induces production of cryptic naphthoquinone dimers.* RSC Adv, 2019. **9**(3): p. 1491-1500.
15. Ancheeva, E., et al., *Expanding the Metabolic Profile of the FungusChaetomiumsp. through Co-culture with AutoclavedPseudomonas aeruginosa.* European Journal of Organic Chemistry, 2017. **2017**(22): p. 3256-3264.
16. Akone, S.H., et al., *Inducing secondary metabolite production by the endophytic fungus Chaetomium sp. through fungal–bacterial co-culture and epigenetic modification.* Tetrahedron, 2016. **72**(41): p. 6340-6347.
17. Sharma, D., L. Misba, and A.U. Khan, *Antibiotics versus biofilm: an emerging battleground in microbial communities.* Antimicrob Resist Infect Control, 2019. **8**: p. 76.
18. Ciofu, O., et al., *Antibiotic treatment of biofilm infections.* APMIS, 2017. **125**(4): p. 304-319.
19. Cont, A., et al., *Biofilms deform soft surfaces and disrupt epithelia.* Elife, 2020. **9**.
20. Bode, H.B., et al., *Big effects from small changes: possible ways to explore nature's chemical diversity.* ChemBioChem, 2002. **3**: p. 619-627.
21. Steyn, P.S., P.L. Wessels, and W.F.O. Marasas, *Pigments from fusarium moniliforme sheldon.* Tetrahedron, 1979. **35**(12): p. 1551-1555.
22. Tatum, J.H., R.A. Baker, and R.E. Berry, *Naphthoquinones produced by Fusarium oxysporum isolated from citrus.* Phytochemistry, 1985. **24**(3): p. 457-459.
23. Studt, L., et al., *Biosynthesis of fusarubins accounts for pigmentation of Fusarium fujikuroi perithecia.* Appl Environ Microbiol, 2012. **78**(12): p. 4468-80.
24. Hamill, R.L., *THE STRUCTURE OF BEAUVERICIN, A NEW DEPSIPEPTIDE ANTIBIOTIC TOXIC TO ARTEMIA SALINA.* 1969.

25. Isaka, M., et al., *Cyclohexadepsipeptides from Acremonium sp. BCC 28424.* Tetrahedron, 2011. **67**(41): p. 7929-7935.
26. Karplus, M., *Contact Electron-Spin Coupling of Nuclear Magnetic Moments.* The Journal of Chemical Physics, 1959. **30**(1): p. 11-15.
27. Jain, C., et al., *High throughput ANI analysis of 90K prokaryotic genomes reveals clear species boundaries.* Nat Commun, 2018. **9**(1): p. 5114.
28. Li, X., et al., *Chemo-enzymatic synthesis of equisetin.* Chem Commun (Camb), 2017. **53**(34): p. 4695-4697.
29. Watanabe, K., *Discovery and investigation of natural Diels-Alderases.* J Nat Med, 2021. **75**(3): p. 434-447.
30. Kasahara, K., et al., *Solanapyrone synthase, a possible Diels-Alderase and iterative type I polyketide synthase encoded in a biosynthetic gene cluster from Alternaria solani.* Chembiochem, 2010. **11**(9): p. 1245-52.
31. Kim, H.J., et al., *Enzyme-catalysed [4+2] cycloaddition is a key step in the biosynthesis of spinosyn A.* Nature, 2011. **473**(7345): p. 109-12.
32. Oikawa, H., et al., *Biosynthesis of macrophomic acid: Plausible involvement of intermolecular Diels-Alder reaction.* Chemical Communications, 1997(1): p. 97-98.
33. Bitchagno, G.T.M., et al., *Demystifying racemic natural products in the homochiral world.* Nat Rev Chem, 2022. **6**(11): p. 806-822.
34. Kim, H.J., M.W. Ruszczycky, and H.W. Liu, *Current developments and challenges in the search for a naturally selected Diels-Alderase.* Curr Opin Chem Biol, 2012. **16**(1-2): p. 124-31.
35. Klas, K., et al., *Natural Diels-Alderases: Elusive and Irresistable.* J Org Chem, 2015. **80**(23): p. 11672-85.
36. Rumbaugh, K.P. and K. Sauer, *Biofilm dispersion.* Nat Rev Microbiol, 2020. **18**(10): p. 571-586.
37. Wu, Q., et al., *A Review on the Synthesis and Bioactivity Aspects of Beauvericin, a Fusarium Mycotoxin.* Front Pharmacol, 2018. **9**: p. 1338.
38. Schulze, A., et al., *Biofilms by bacterial human pathogens: Clinical relevance - development, composition and regulation - therapeutical strategies.* Microb Cell, 2021. **8**(2): p. 28-56.
39. *CrysAlisPro*. 2021, Rigaku Oxford Diffraction.
40. Sheldrick, G.M., *Crystal structure refinement with SHELXL.* Acta Crystallogr C Struct Chem, 2015. **71**(Pt 1): p. 3-8.
41. Sheldrick, G.M., *A short history of SHELX.* Acta Crystallogr A, 2008. **64**(Pt 1): p. 112-22.
42. Dolomanov, O.V., et al., *OLEX2: a complete structure solution, refinement and analysis program.* Journal of Applied Crystallography, 2009. **42**(2): p. 339-341.
43. Brandenburg, K., *Diamond (Version 4.6), Crystal and Molecular Structure Visualization, Crystal Impact*. copyright 1997-2022, K. Brandenburger & H. Putz Gbr, Bonn, Germany.
44. Spek, A.L., *PLATON - A multipurpose Crystallographic Tool*. 2008, (Utricht University, Utrecht, The Netherlands).
45. Spek, A.L., *Structure validation in chemical crystallography.* Acta Crystallogr D Biol Crystallogr, 2009. **65**(Pt 2): p. 148-55.
46. L.J., F., *Windows implementation, Version 270519*. 2019, (University of Glasgow, Scotland).
47. Kolmogorov, M., et al., *metaFlye: scalable long-read metagenome assembly using repeat graphs.* Nat Methods, 2020. **17**(11): p. 1103-1110.
48. Blin, K., et al., *antiSMASH 6.0: improving cluster detection and comparison capabilities.* Nucleic Acids Res, 2021. **49**(W1): p. W29-W35.
49. van Geelen, L., et al., *Natural brominated phenoxyphenols kill persistent and biofilm-incorporated cells of MRSA and other pathogenic bacteria.* Appl Microbiol Biotechnol, 2020. **104**(13): p. 5985-5998.
50. Meier, D., et al., *The plant-derived chalcone Xanthoangelol targets the membrane of Gram-positive bacteria.* Bioorg Med Chem, 2019. **27**(23): p. 115151.
51. Rehberg, N., et al., *3-O-Methyl-Alkylgallates Inhibit Fatty Acid Desaturation in Mycobacterium tuberculosis.* Antimicrob Agents Chemother, 2019. **63**(9).

Supplementary materials.

Fusarubin derivatives with biofilm dispersing activities derive from *Fusarium oxysporum*

Viktor E. Simons[a], Lasse van Geelen[a], Dennis Woschko[b], Sebastian Scharf[c], Philipp Spohr[d], Marian Frank[a], Christoph Janiak[b], Klaus Pfeffer[c], Rainer Kalscheuer[a,*]

[a]Institute of Pharmaceutical Biology and Biotechnology, Heinrich Heine University, Universitätsstrasse 1, 40225 Düsseldorf, Germany

[b]Institute for Nanoporous and Nanoscale Materials, Heinrich Heine University, Universitätsstrasse 1, 40225 Düsseldorf, Germany

[c]Institute of Medical Microbiology and Hospital Hygiene, Heinrich Heine University, Universitätsstrasse 1, 40225 Düsseldorf, Germany

[d]Algorithmic Bioinformatics, Heinrich Heine University, Universitätsstrasse 1, 40225 Düsseldorf, Germany

Table of contents

S1. Hydrogen bonding interactions of compound 3 and 4

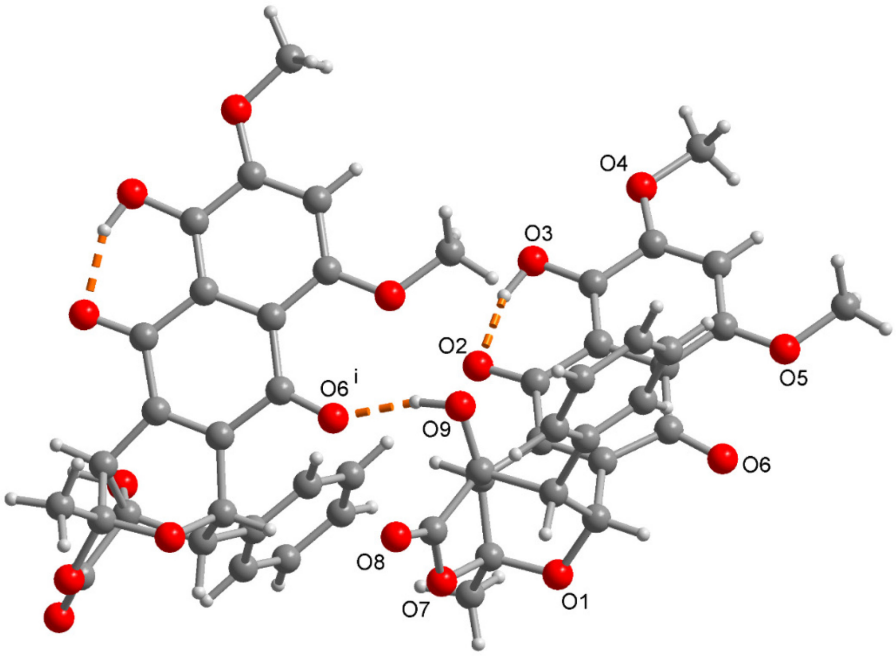

(a)

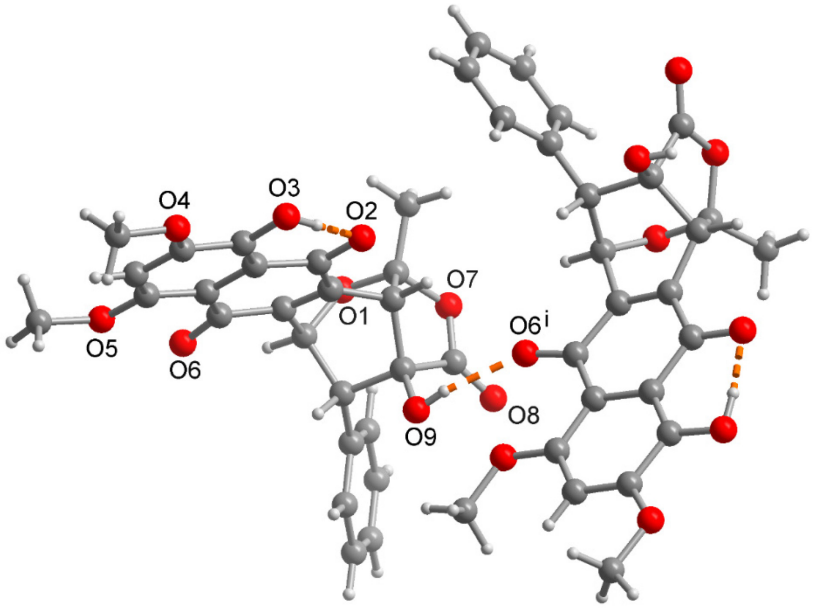

(b)

Hydrogen-bonding interaction in the structures of **3** (a) and **4** (b). The hydrogen-bonding parameters are given in Table S1

Table S1. Hydrogen-bond geometry (Å, º) in the solid-state structures of compound **3** and **4**

D—H···*A*	*D*—H	H···*A*	*D*···*A*	*D*—H···*A*
Compound **3**				
O3—H3···O2	0.90 (4)	1.68 (4)	2.534 (2)	156 (4)
O9—H9···O6^{i}	0.96 (4)	1.75 (4)	2.689 (3)	164 (4)
Compound **4**				
O3—H3···O2	0.87 (6)	1.72 (6)	2.571 (4)	163 (6)
O9—H9···O6^{i}	0.76 (7)	1.96 (7)	2.680 (4)	160 (6)

Symmetry code: Compound **3** (i) *x*-1/2, *y*, -*z*+1. Compound **4** (i) -*x*+3/2, *y*-1/2, *z*

.

S2. π-π stacking interactions in 3 and 4

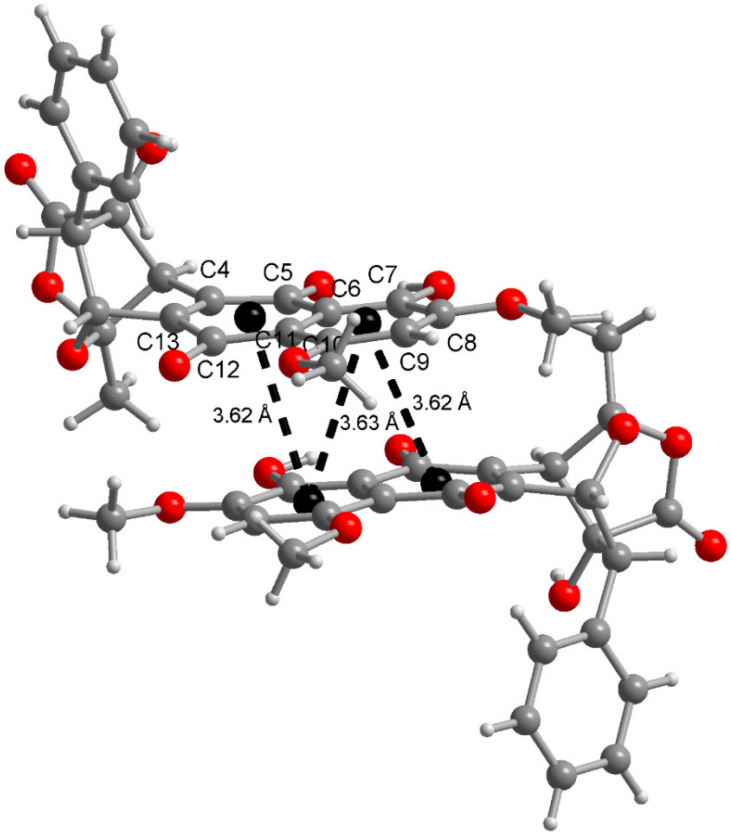

(a)

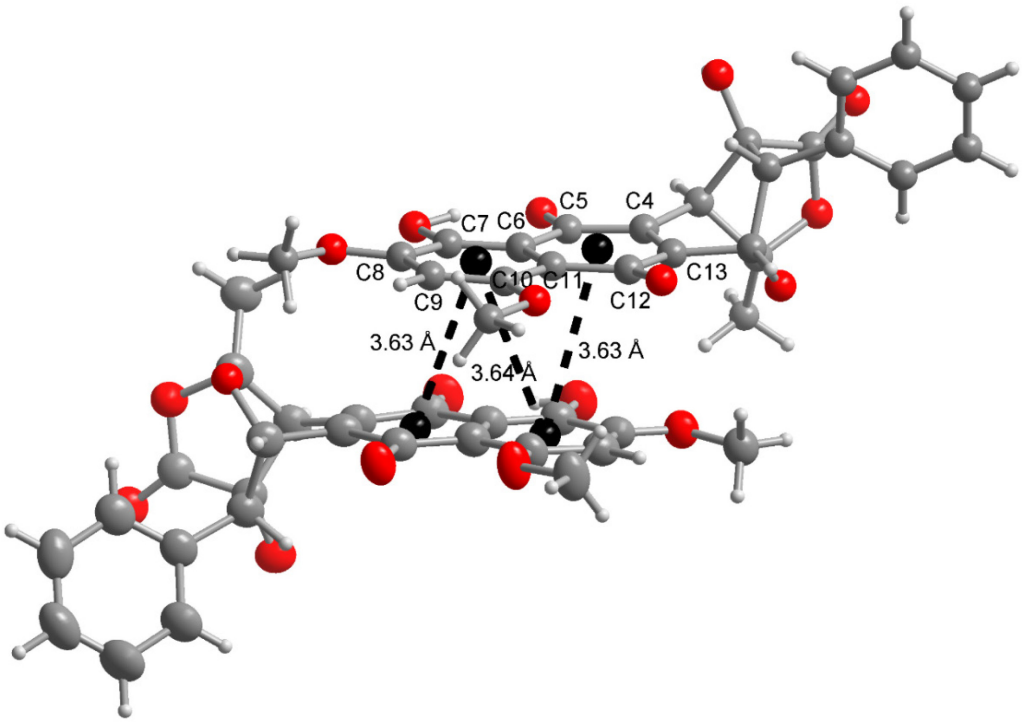

(b)

π-π stacking interactions in compound **3** (a) and **4** (b) with the centroid-centroid distances indicated.

S3. Section of the packing diagram in compound **3** and **4**

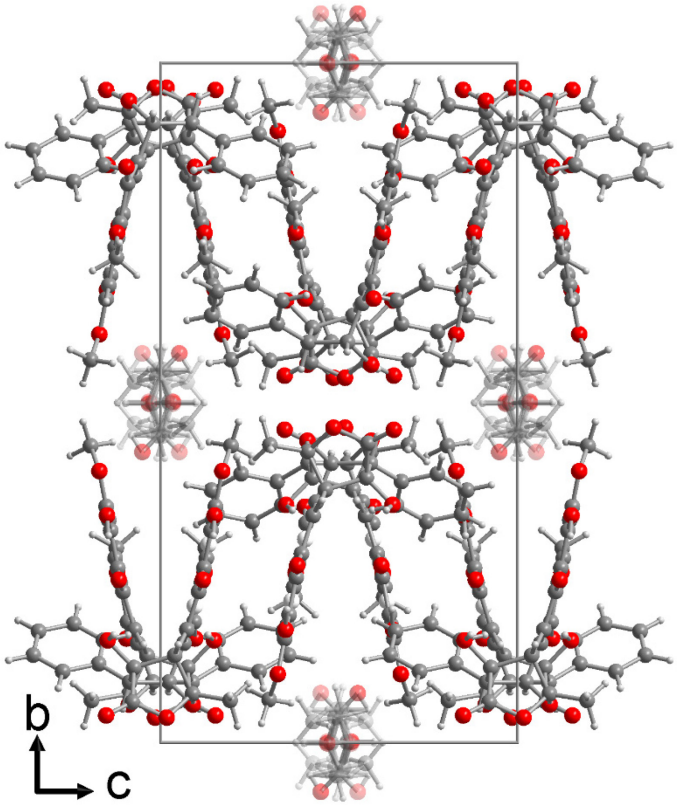

(a)

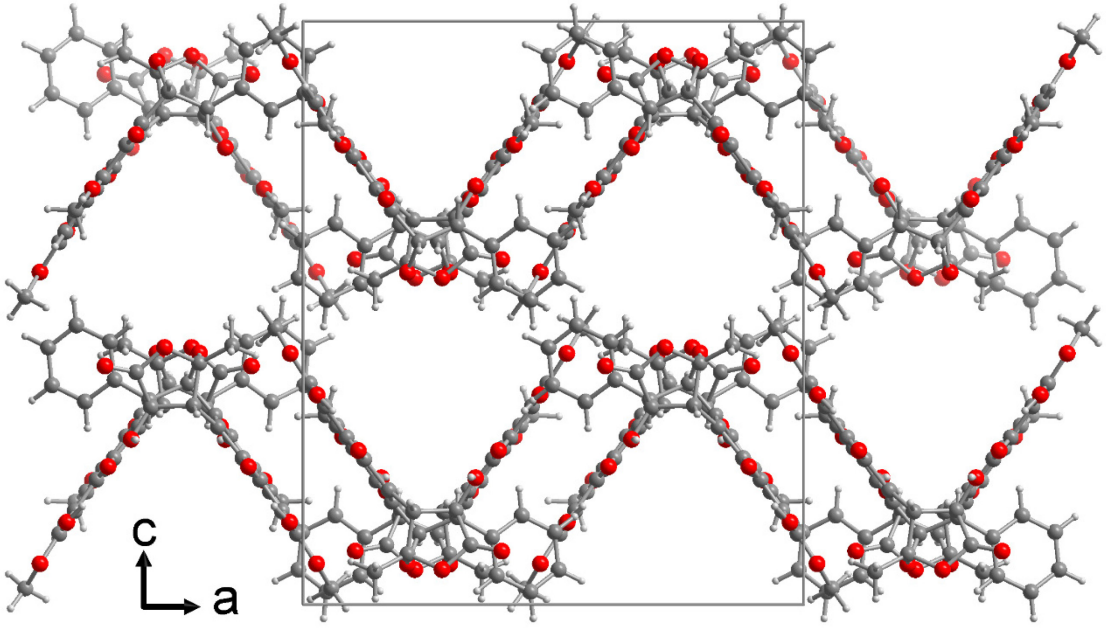

(b)

Section of the packing diagram in compound **3** (a) and **4** (b) showing the solvent-filled voids. For compound **3** the partially-occupied ethyl acetate is indicated semi-transparent. In compound **4** disordered methanol molecules which were removed by solvent masking during the refinement, hence cannot be shown.

S4. Molecular structure of **3** from the single crystal X-ray structure

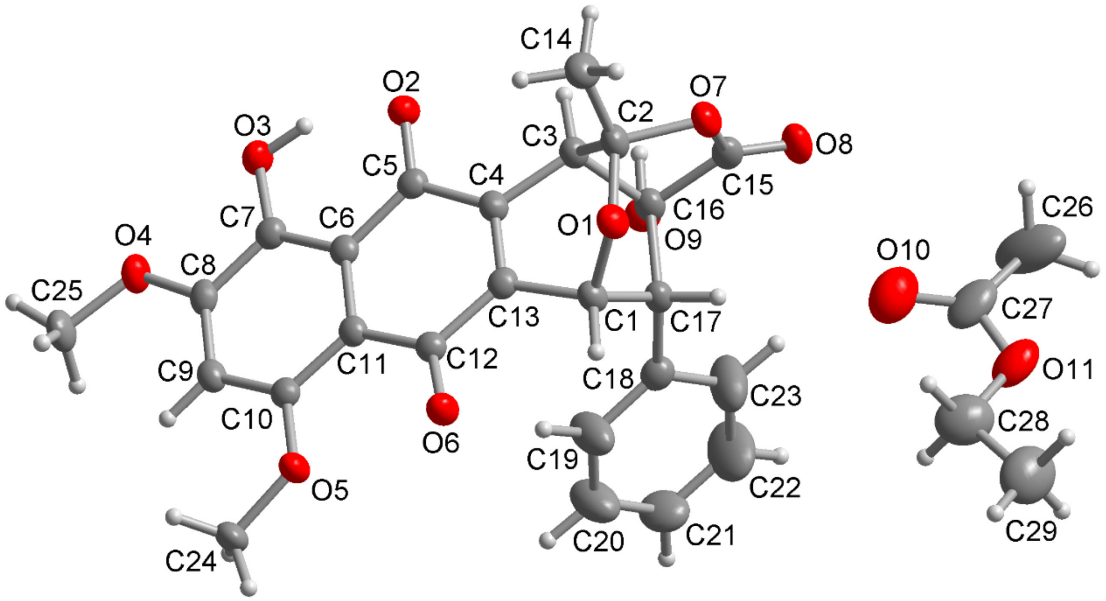

Molecular structure of compounds **3** from the single crystal X-ray structure (50% thermal ellipsoids, H atoms with arbitrary radii) with the ethyl acetate solvent molecule of crystallization. The atoms of the ethyl acetate molecule are only partially occupied (sof = 0.4).

S5. Molecular structures of **3** and **4** with full atom numbering from the single crystal X-ray structure

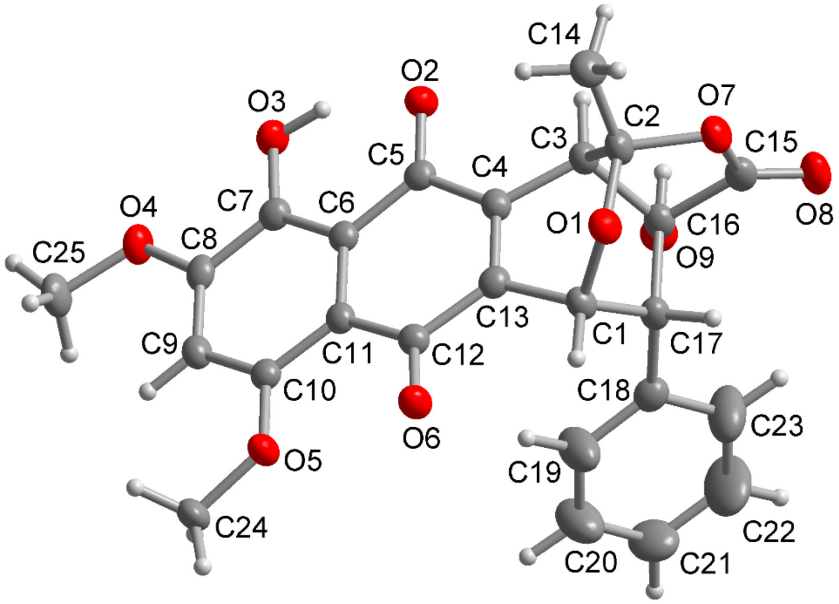

(a)

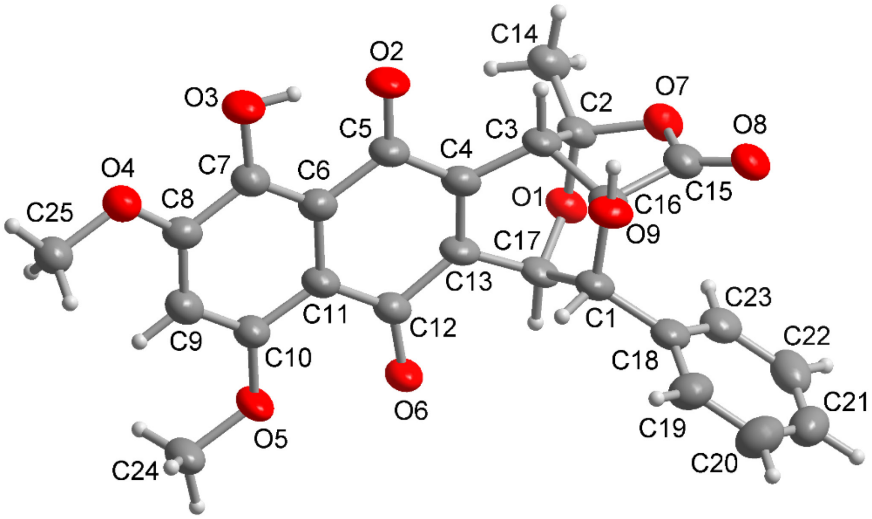

(b)

Molecular structures of compounds **3** (a) and **4** (b) with full atom numbering from the single crystal X-ray structure (50% thermal ellipsoids, H atoms with arbitrary radii).

S6. Top 20 assembled contigs and distribution of contigs

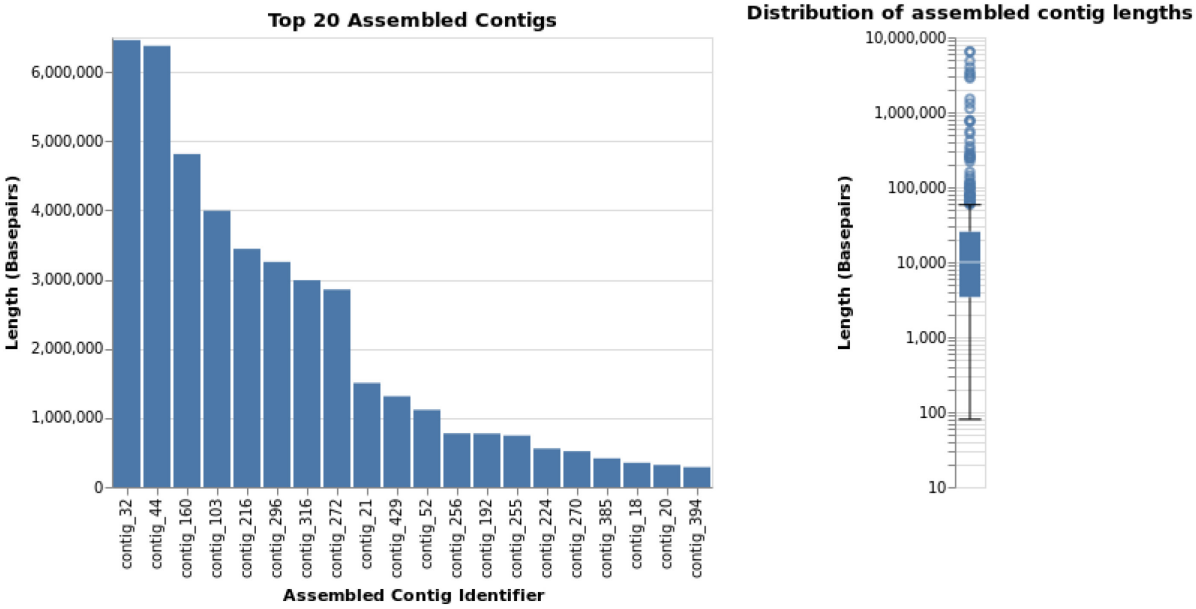

S6 shows the top 20 assembled contigs and the overall distribution of contigs from the nanopore whole genome sequencing, both sorted by lengths

S7. Effect of fusapurpurin A and B (3 and 4) on the cell viability of S. aureus Mu50 and *P. aeruginosa* PAO1 in preformed biofilms

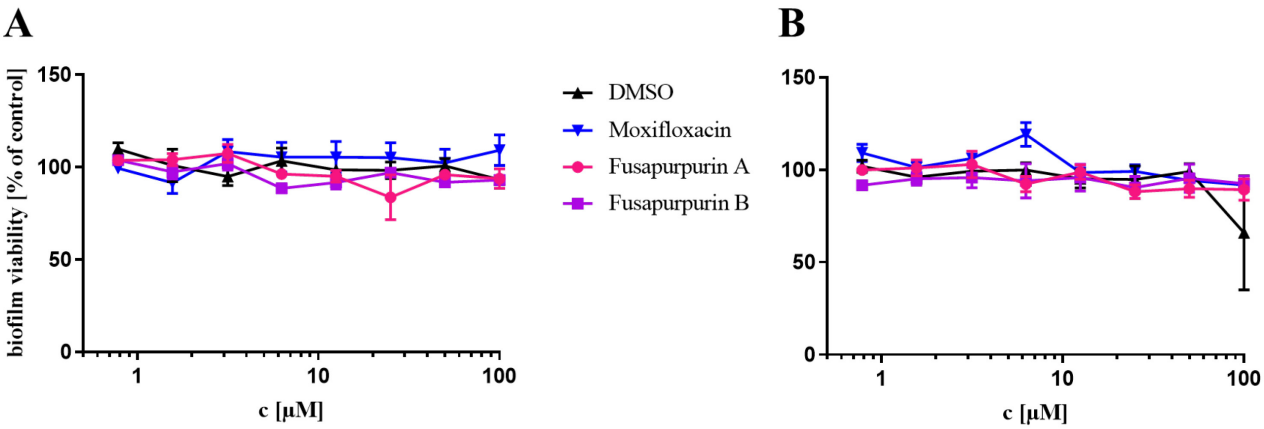

S7 is showing the effect of fusapurpurin A (3), fusapurpurin B (4) and the antibiotic moxifloxacin on the viability of cells in bacterial biofilms formed by MRSA Mu50 (A) and *P. aeruginosa* PAO1 (B). Fusapurpurin A, fusapurpurin B and moxifloxacin do not impair the viability of cells in biofilms. DMSO was used as negative control. Both assays were carried out in triplicates. Graphs show mean ± SEM.

S8. Quorum quenching assay of fusapurpurins in *Chromobacterium violaceum*

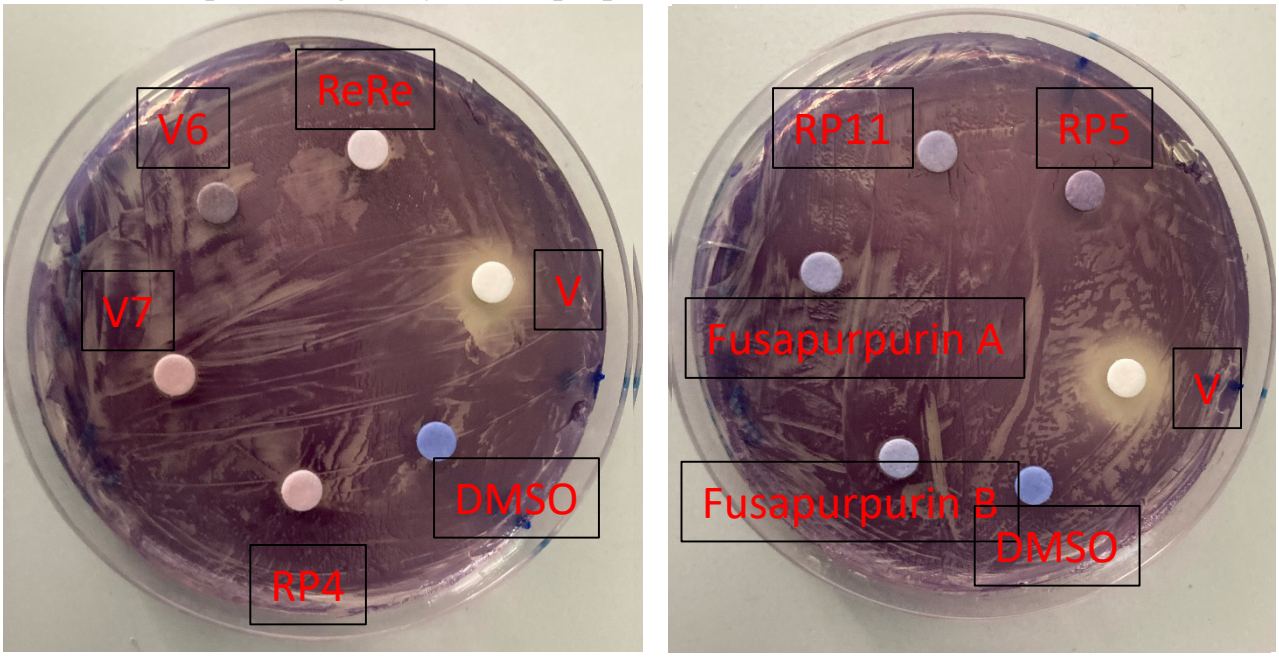

The ability to inhibit quorum sensing (QS) was evaluated using *C. volaceum*. The positive control vanillin (V) inhibits QS, indicated by the colourless circle surrounding the test discs, while negative control DMSO is inactive, indicated by the intensive staining of the test disc and the bacteria around. The different test samples, including fusapurpurin A and B did not inhibit QS.

S9. NMR Table of Compound 1 (9-O-methylfusarubin) (DMSO-d_6, ^{1}H: 600MHz)

9-O-methylfusarubin

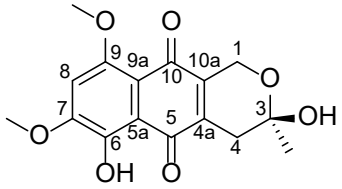

Chemical Formula: $C_{16}H_{16}O_7$
Exact Mass: 320,09
Molecular Weight: 320.30

position	δ_H, m (J in Hz)
1	4.44, m
	4.51, m
4	2.40, m
	2.60, m
8	7.06, s
$3CH_3$	1.44, s, 3H
$7OCH_3$	3.93, s, 3H
$9OCH_3$	3.99, s, 3H
3-OH	6.05, d (1.4)
6-OH	13.00, s

S10. [1]H-NMR Spectrum of Compound 1 (9-O-methylfusarubin) (DMSO-d_6, 600 MHz)

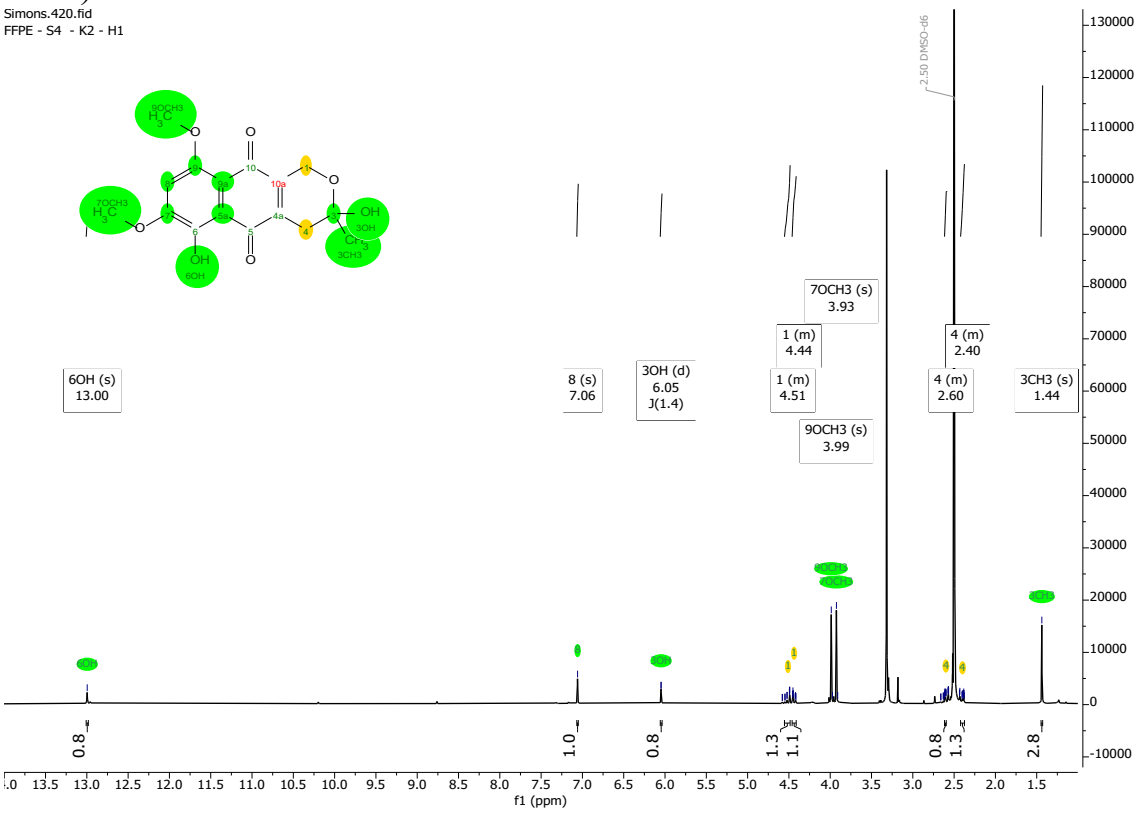

S11. HPLC-DAD UV-Vis Spectrum of Compound 1 (9-O-methylfusarubin) (Methanol)

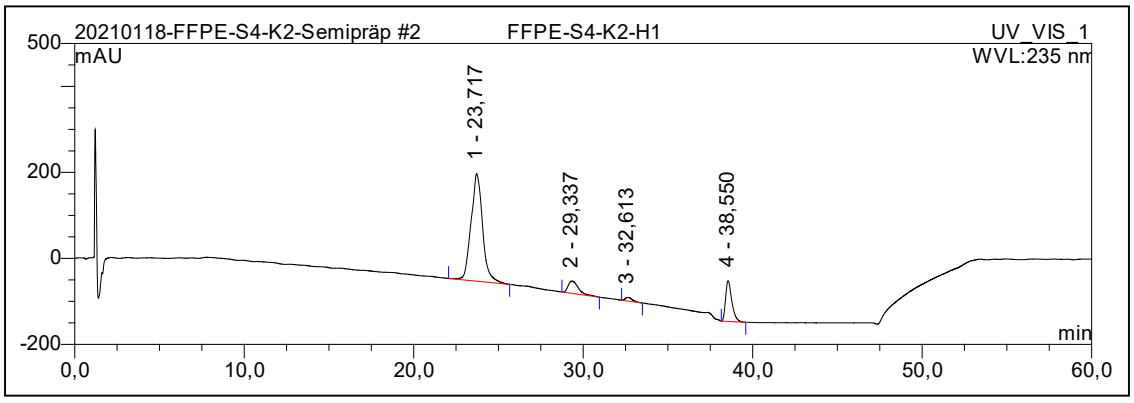

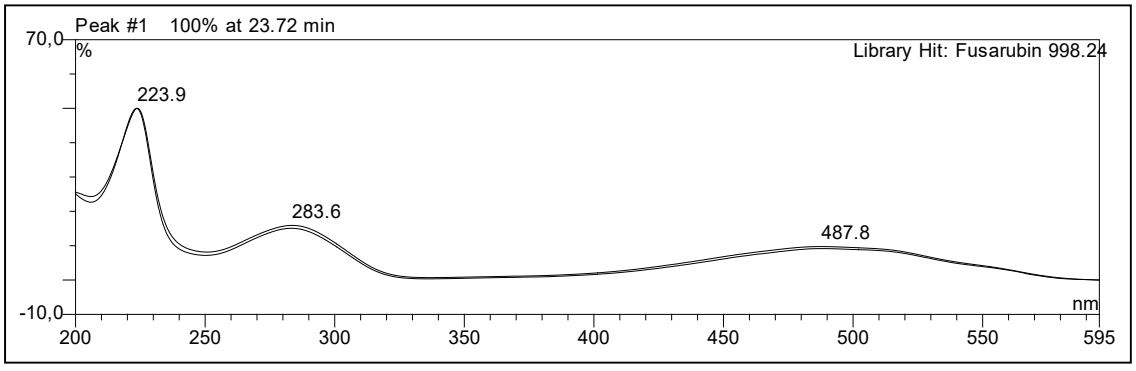

S12. ESI(+)MS Spectrum of 1 (9-O-methylfusarubin)

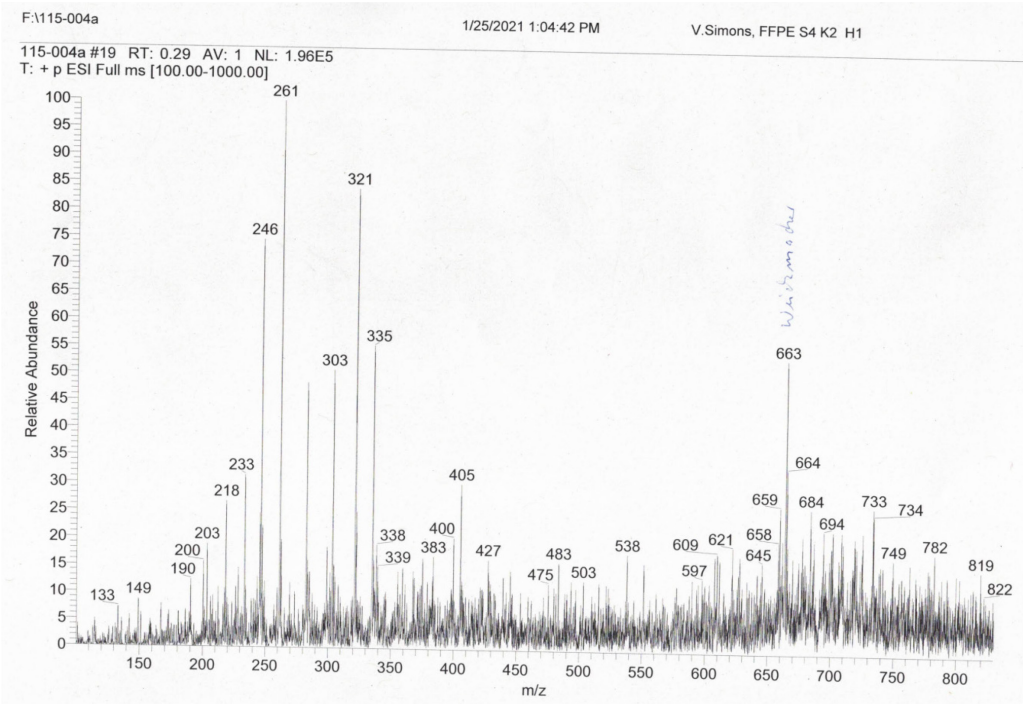

S13. NMR Table of Compound 2 (fusachinon) (DMSO-d_6, ^{1}H: 600MHz, ^{13}C: 150 MHz)

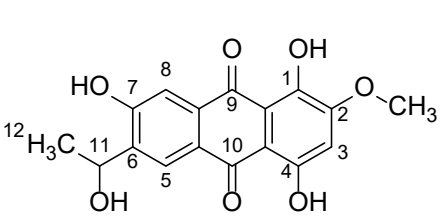

1,4,7-trihydroxy-6-(1-hydroxyethyl)-2-methoxyanthracene-9,10-dione
Chemical Formula: $C_{17}H_{14}O_7$
Molecular Weight: 330,29

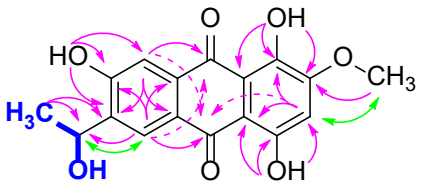

position	δ_C*	δ_H, m (J in Hz)
1	149.0, C	
2	156.6, C	
3	107.2, CH	6.96, s
4	159.2, C	
4a	104.7, C	
5	124.8, CH	8.35, s
6	141.6, Ca	
7	158.9, C	
8	111.3, CH	7.62, s
8a	132.9, C	
9	186.7, C	
9a	112.0, C	
10	183.8, C	
10a	125.0, C	
11	62.6, CH	5.03, dq (4.2, 6.4)
12	23.5, CH_3	1.33, d (6.4)
1-OH		13.17, s
2-OCH_3	56.5, CH_3	3.96, s
4-OH		13.70, s
7-OH		11.21, s
11-OH		5.42, d (4.2)

*signals were extracted from HSQC and HMBC spectra.

S14. ^{1}H-NMR Spectrum of Compound 2 (fusachinon) (DMSO-d_6, 600 MHz)

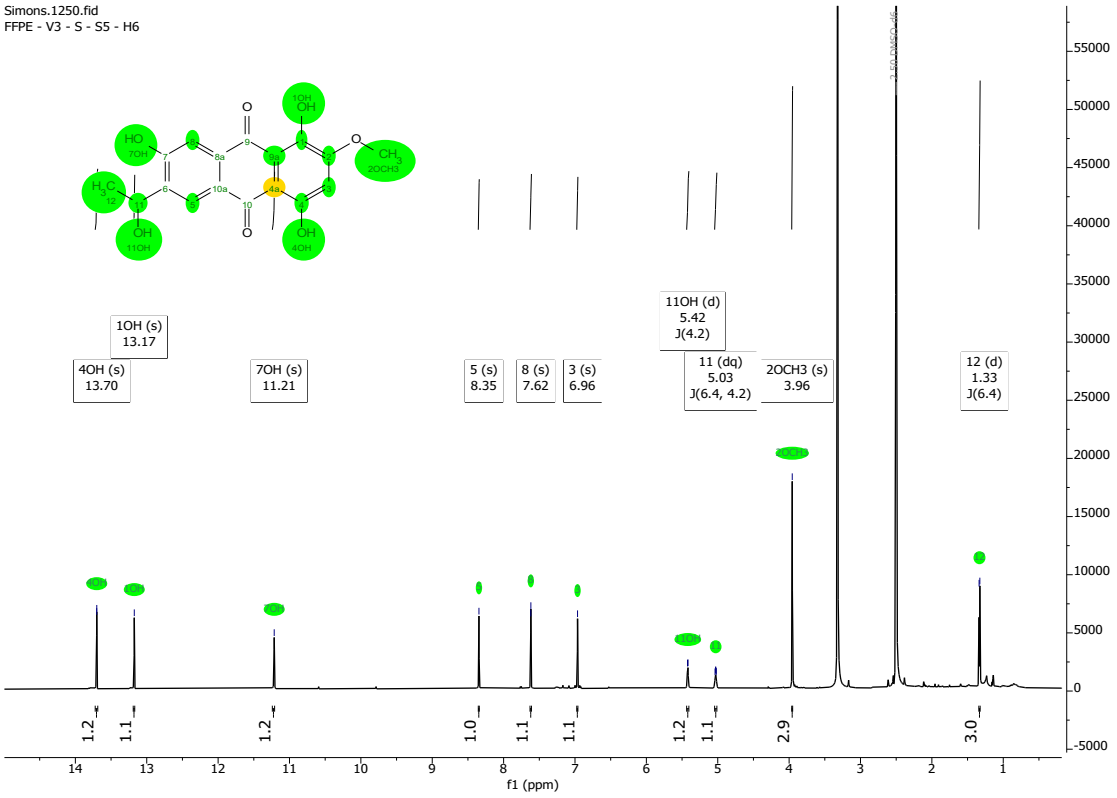

S15. ^{13}C-NMR Spectrum of Compound 2 (fusachinon) (DMSO-d_6, 150 MHz)

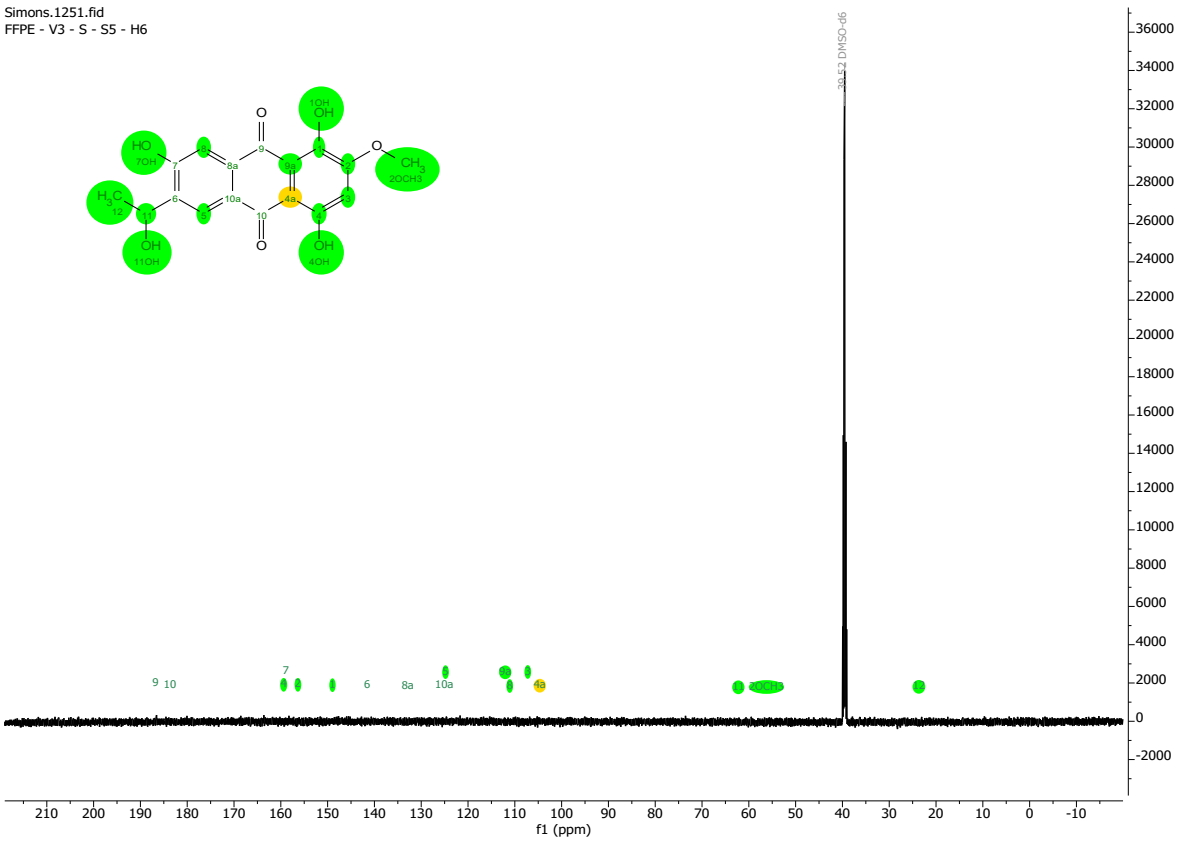

S16. ^{1}H-^{13}C-HSQC Spectrum of Compound 2 (fusachinon) (DMSO-d_6, ^{1}H: 600MHz, ^{13}C: 150 MHz)

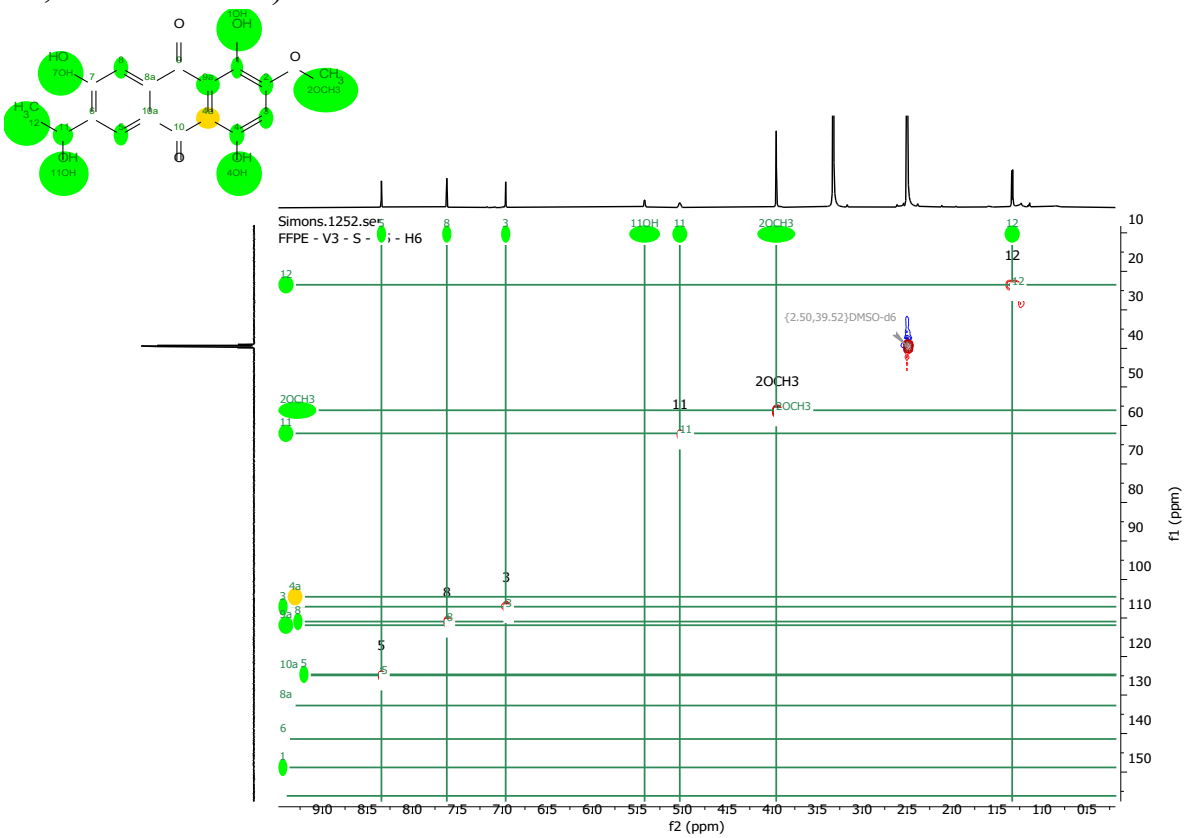

S17. ^{1}H-^{13}C-HMBC Spectrum of Compound 2 (fusachinon) (DMSO-d_6, ^{1}H: 600MHz, ^{13}C: 150 MHz)

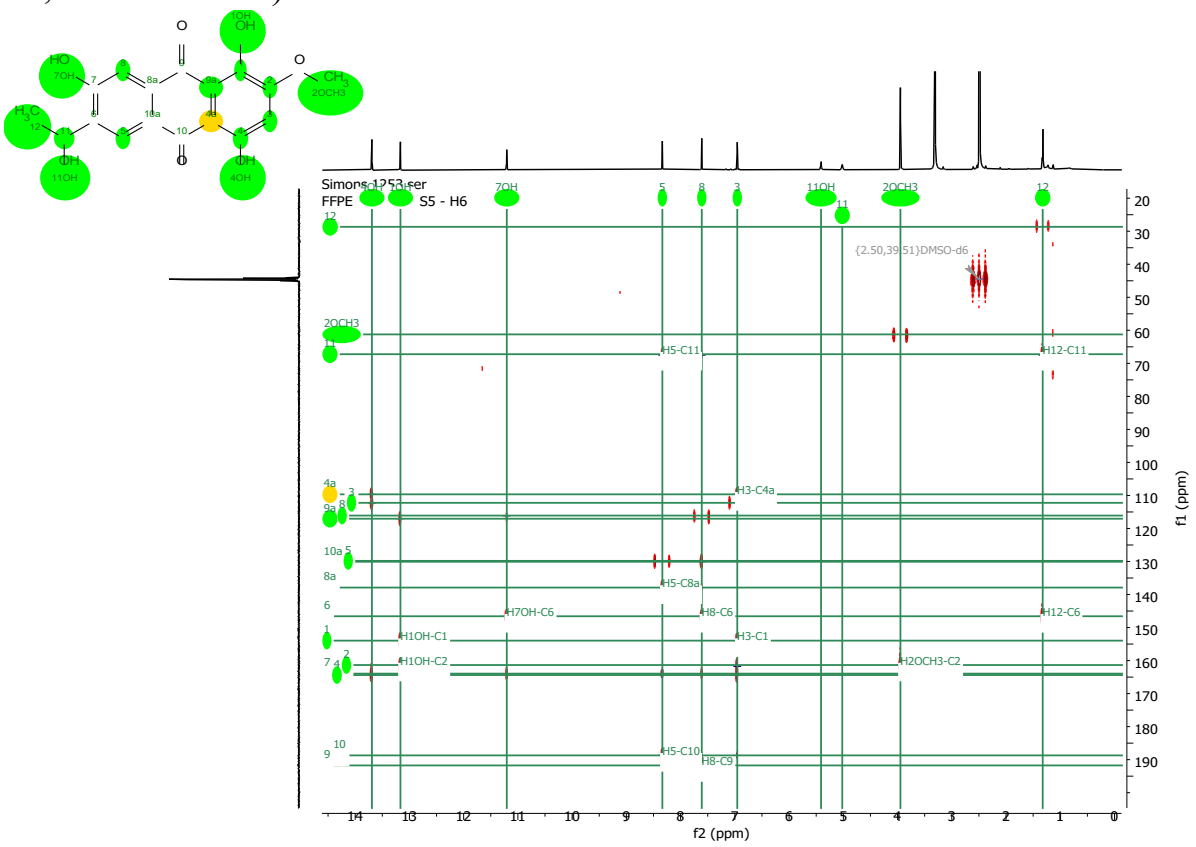

S18. ^{1}H-^{1}H-COSY Spectrum of Compound 2 (fusachinon) (DMSO-d_6, 600MHz)

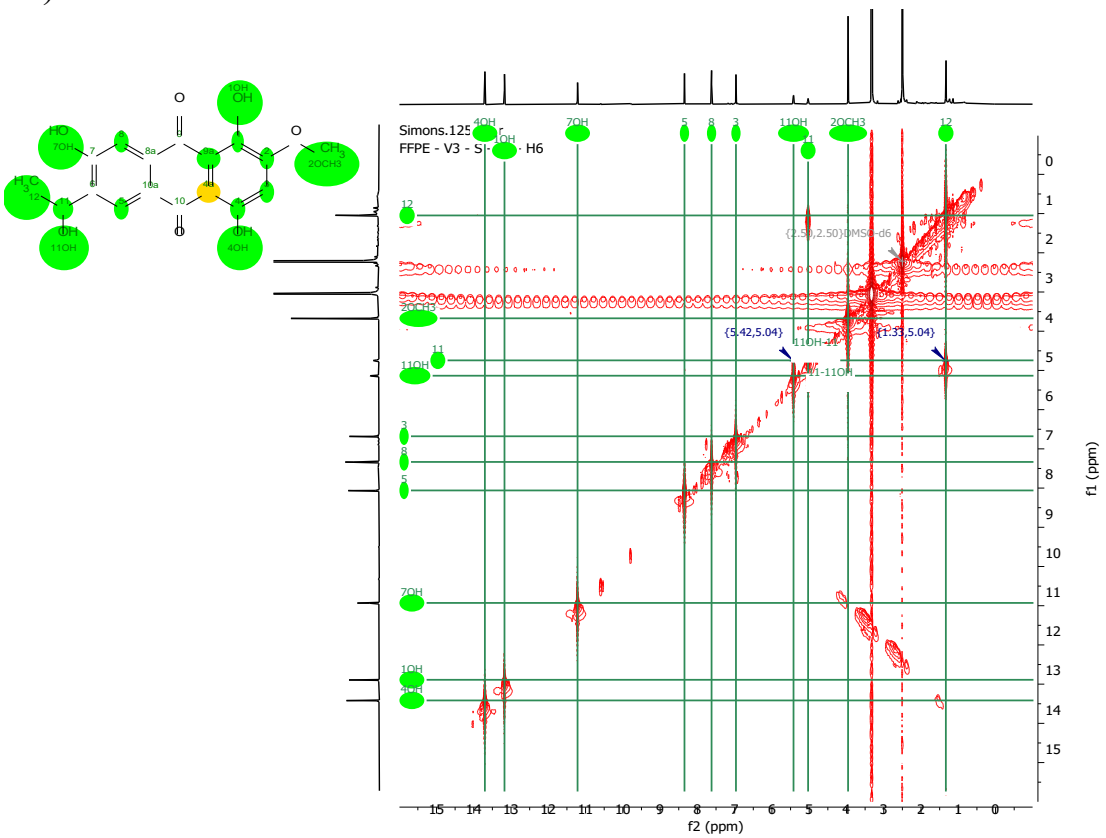

S19. ^{1}H-^{1}H-NOESY Spectrum of Compound 2 (fusachinon) (DMSO-d_6, 600MHz)

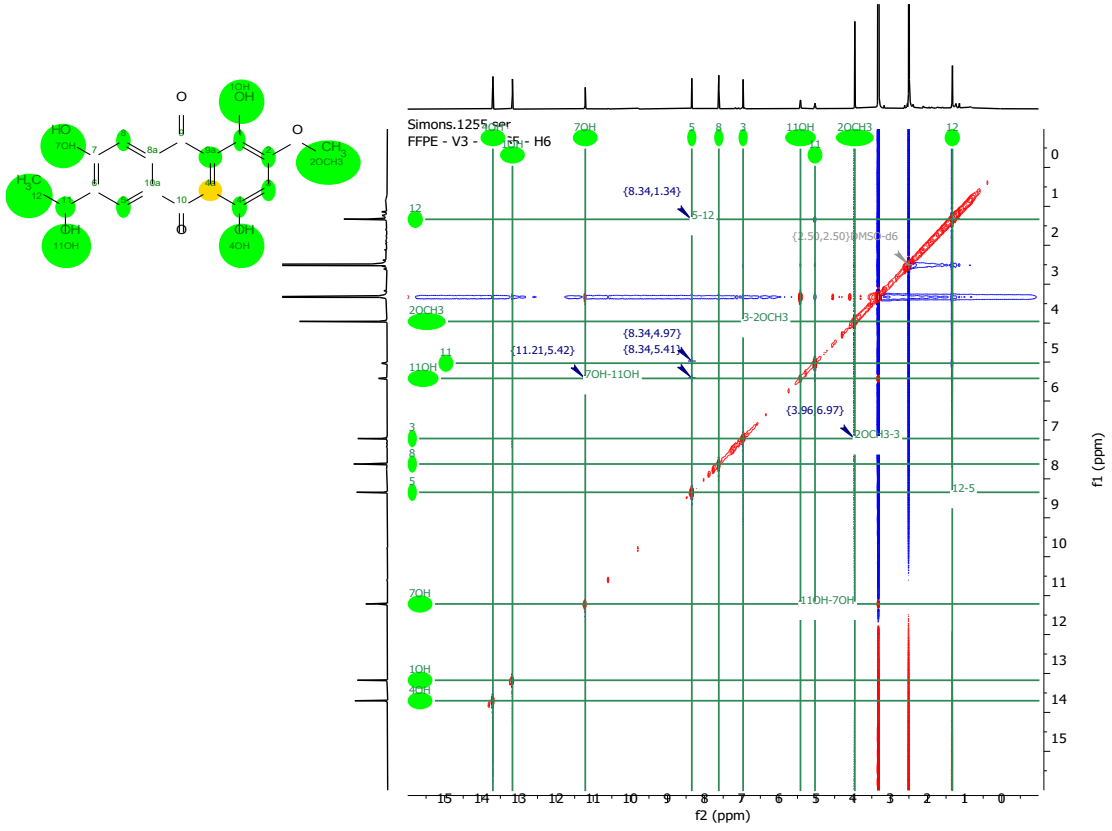

S20. HPLC-DAD UV-Vis Spectrum of Compound 2 (fusachinon) (Methanol)

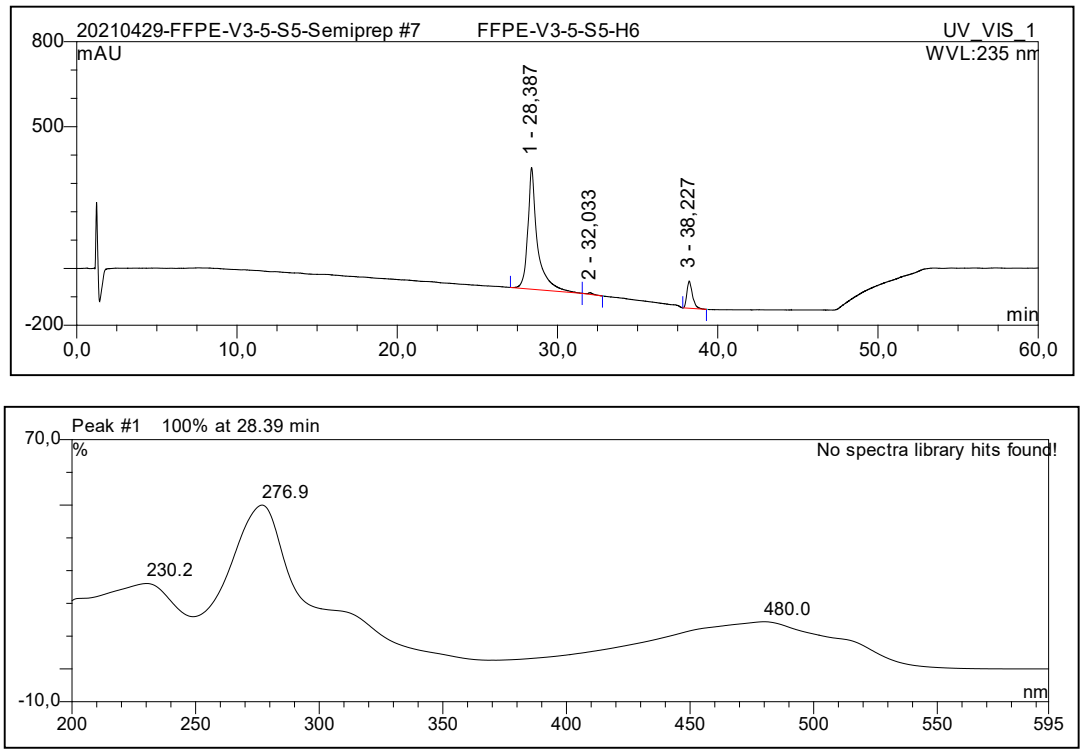

S21. High Resolution ESI(+)MS Spectrum of Compound 2 (fusachinon)

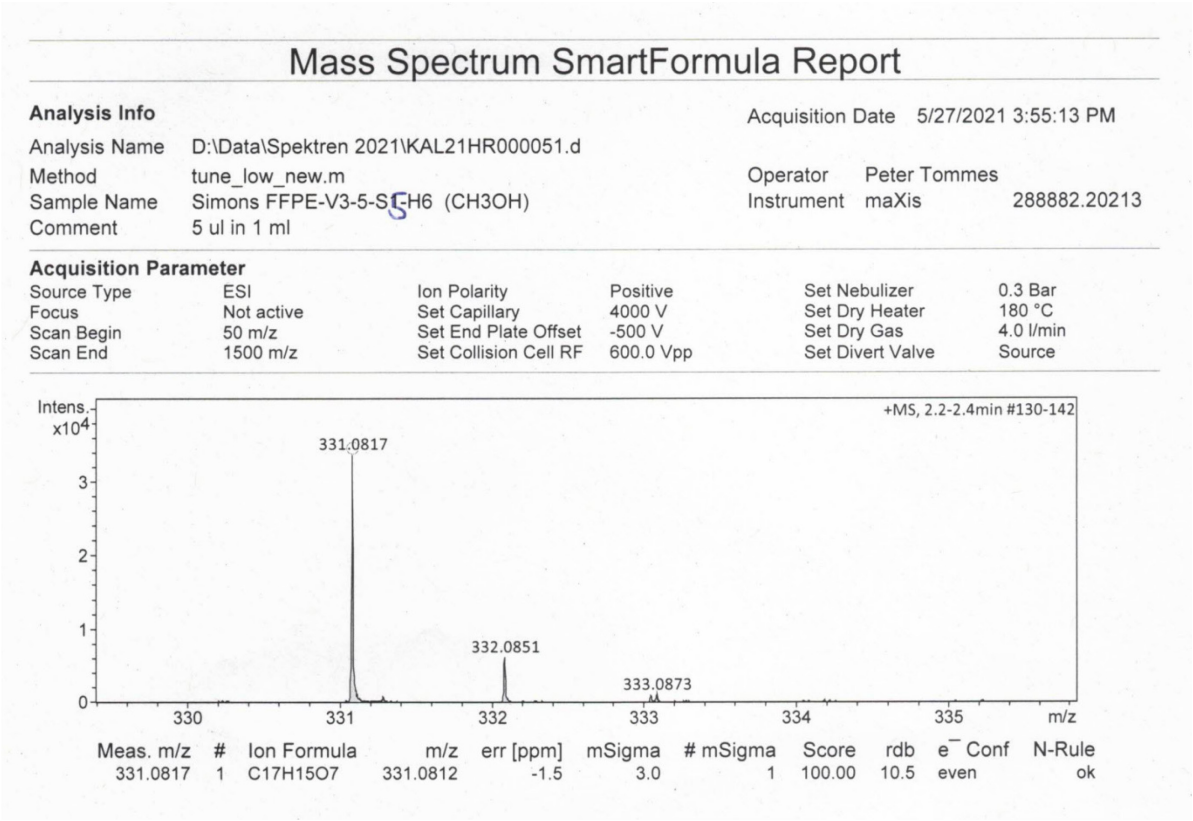

S22. NMR Table of Compound 3 (fusapurpurin A) (DMSO-d_6, ^{1}H: 600MHz, ^{13}C: 150 MHz)

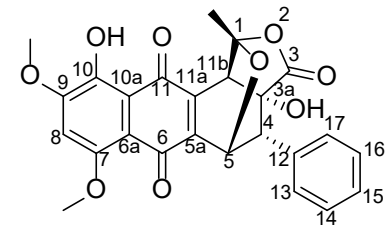

1S,3aR,4R,5R,11bR

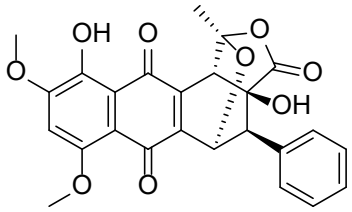

1R,3aS,4S,5S,11bS

Chemical formula: $C_{25}H_{20}O_9$
Molecular weight: 464.43 g/mol

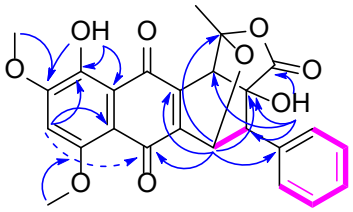

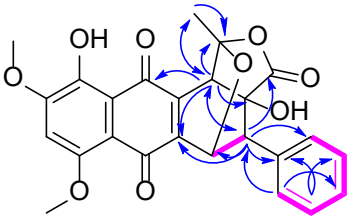

COSY

key HMBC

weak HMBC

position	δ_C*	δ_H, m (J in Hz)
1	105.5, C	
3	176.7, CO	
3a	76.4, C	
4	51.6, CH	3.97, d (4.2)
5	70.9, CH	5.30, d (4.2)
5a	148.9, C	
6	175.4, CO	
6a	109.0, C	
7	157.2, CO	
8	105.1, CH	7.10, s
9	156.3, CO	
10	148.9, C	
10a	114.6, C	
11	186.7, CO	
11a	138.9, C	
11b	46.9, CH	4.34, s
12	130.7, C	
13/17	131.3, CH	7.03, m, 2H
14/16	127.9, CH	7.12, m, 2H
15	127.9, CH	7.08, m
1-CH_3	22.9, CH_3	1.44, s, 3H
3a-OH		6.71, s
7-OCH_3	57.1, OCH_3	3,88, s, 3H
9-OCH_3	57.1, OCH_3	4.02, s, 3H
10-OH		12.99, s

S23. ^{1}H-NMR Spectrum of Compound 3 (fusapurpurin A) (DMSO-d_6, 600 MHz)

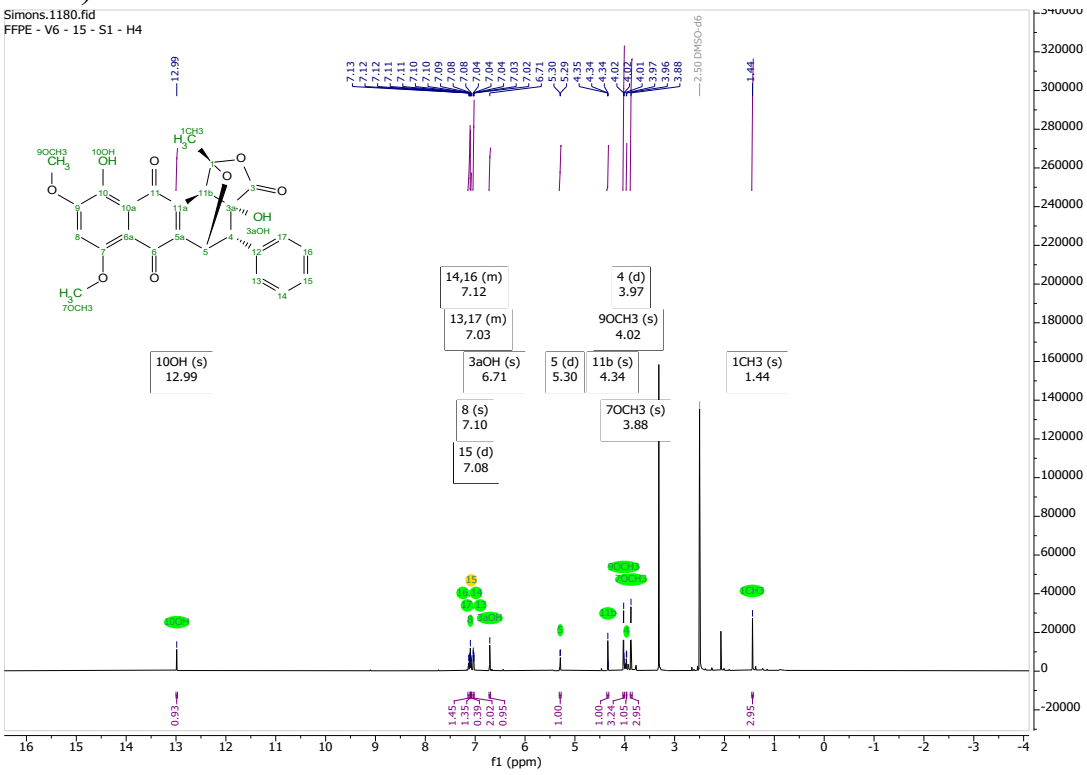

S24. ^{13}C-NMR Spectrum of Compound 3 (fusapurpurin A) (DMSO-d_6, 150 MHz)

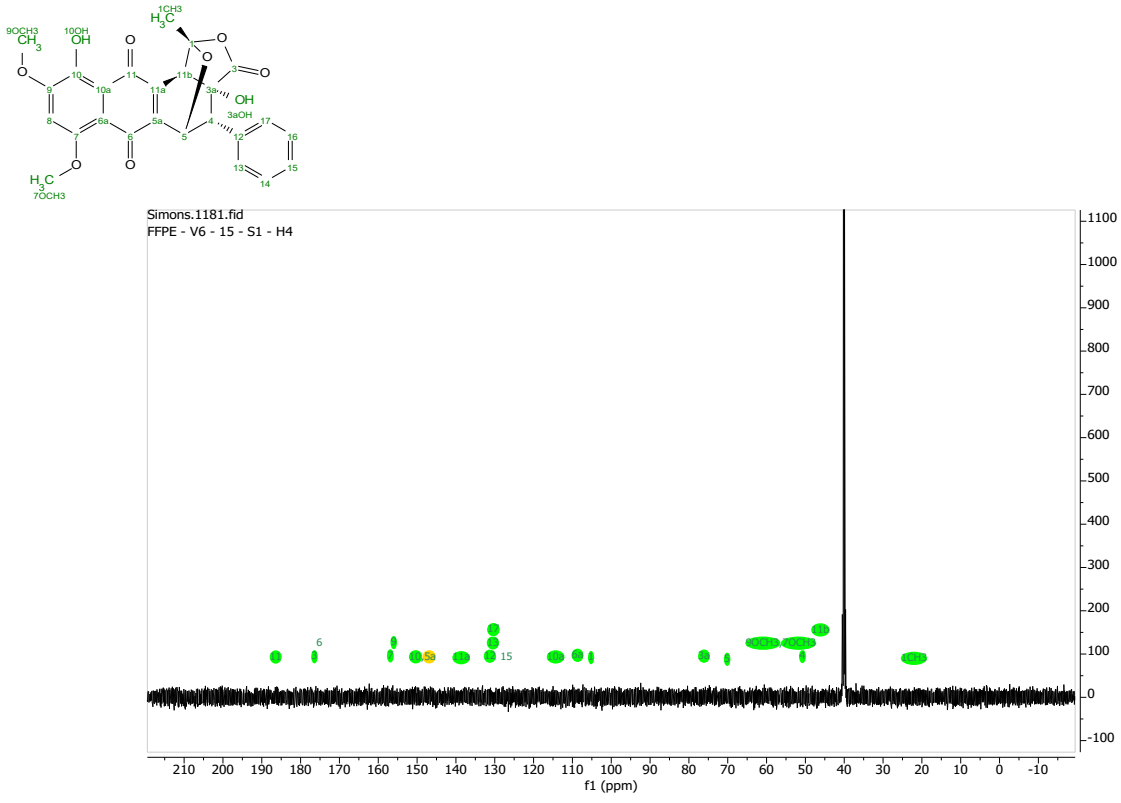

S25. ^{1}H-^{13}C-HSQC Spectrum of Compound 3 (fusapurpurin A) (DMSO-d_6, ^{1}H: 600MHz, ^{13}C: 150 MHz)

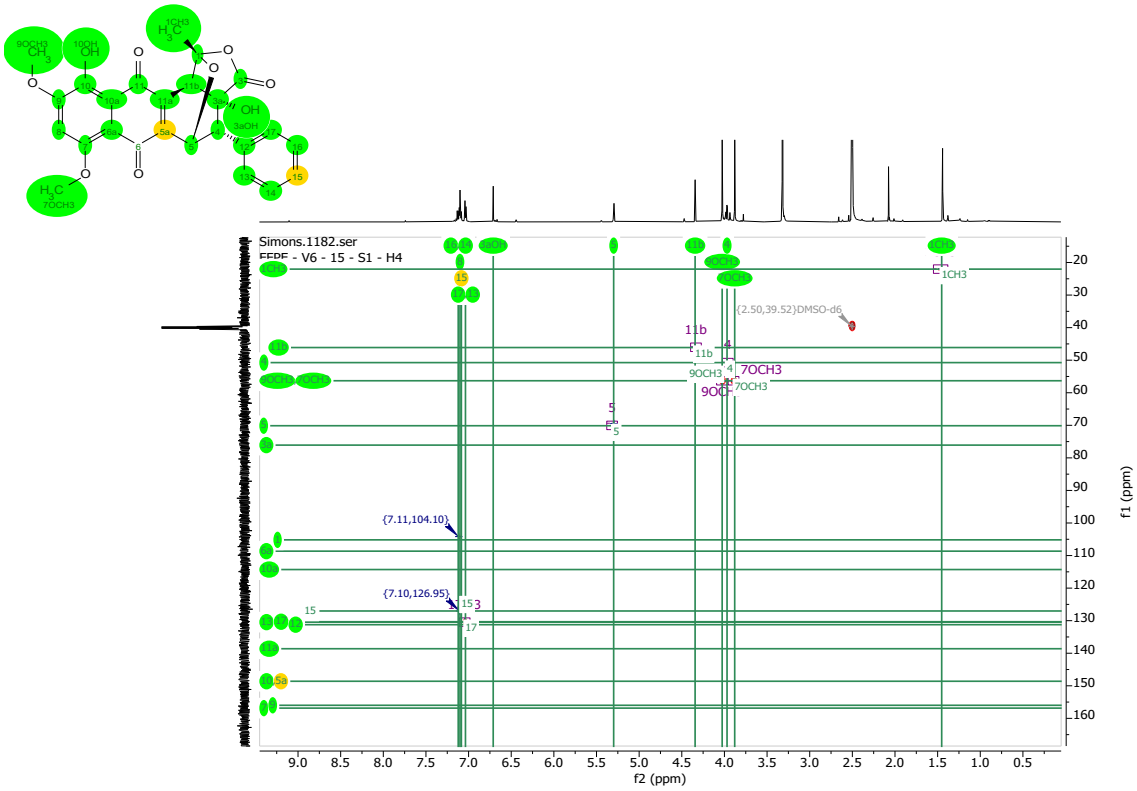

S26. ^{1}H-^{13}C-HMBC Spectrum of Compound 3 (fusapurpurin A) (DMSO-d_6, ^{1}H: 600MHz, ^{13}C: 150 MHz)

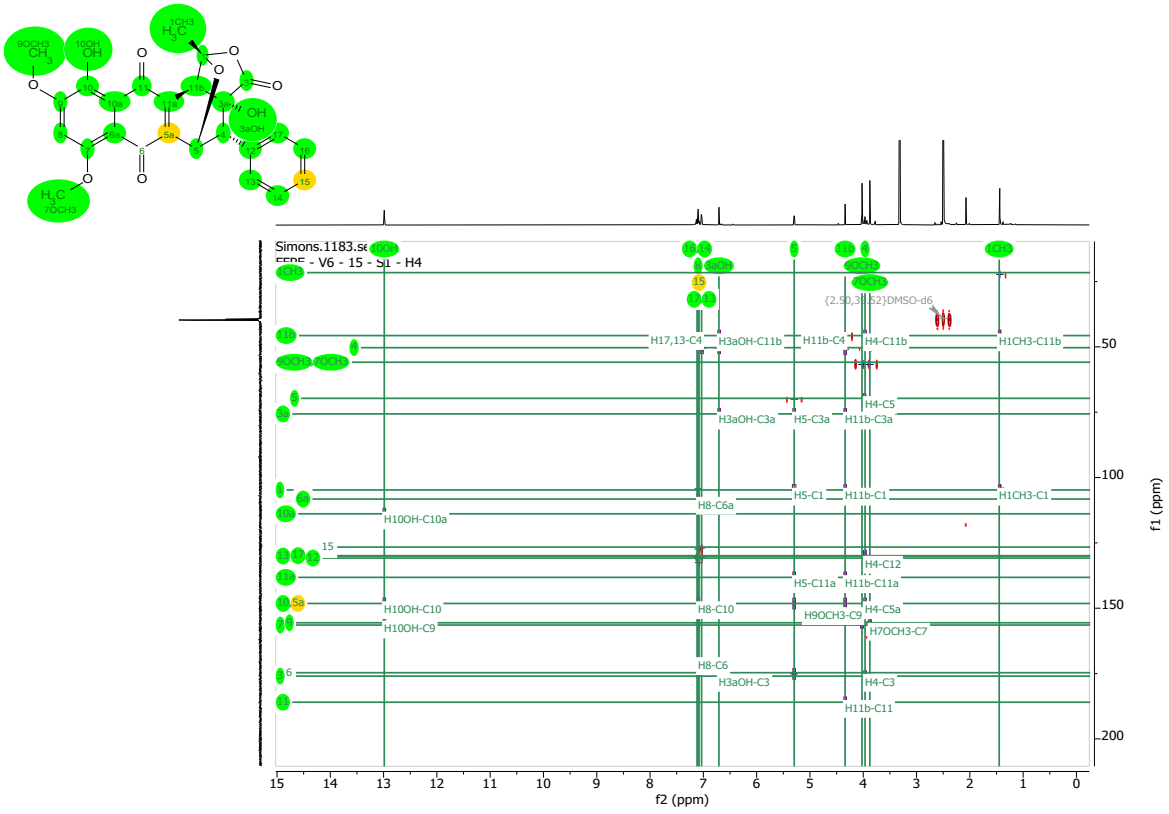

S27. ^{1}H-^{1}H-COSY Spectrum of Compound 3 (fusapurpurin A) (DMSO-d_6, 600MHz)

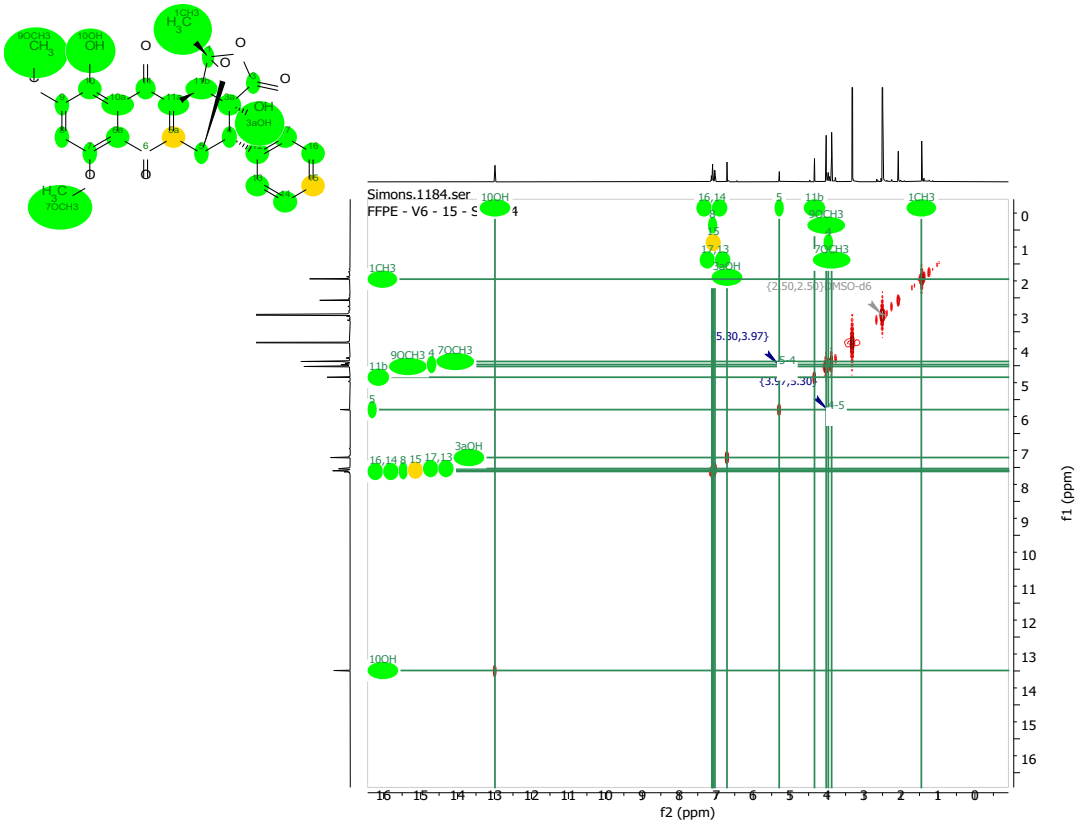

S28. ^{1}H-^{1}H-NOESY Spectrum of Compound 3 (fusapurpurin A) (DMSO-d_6, 600MHz)

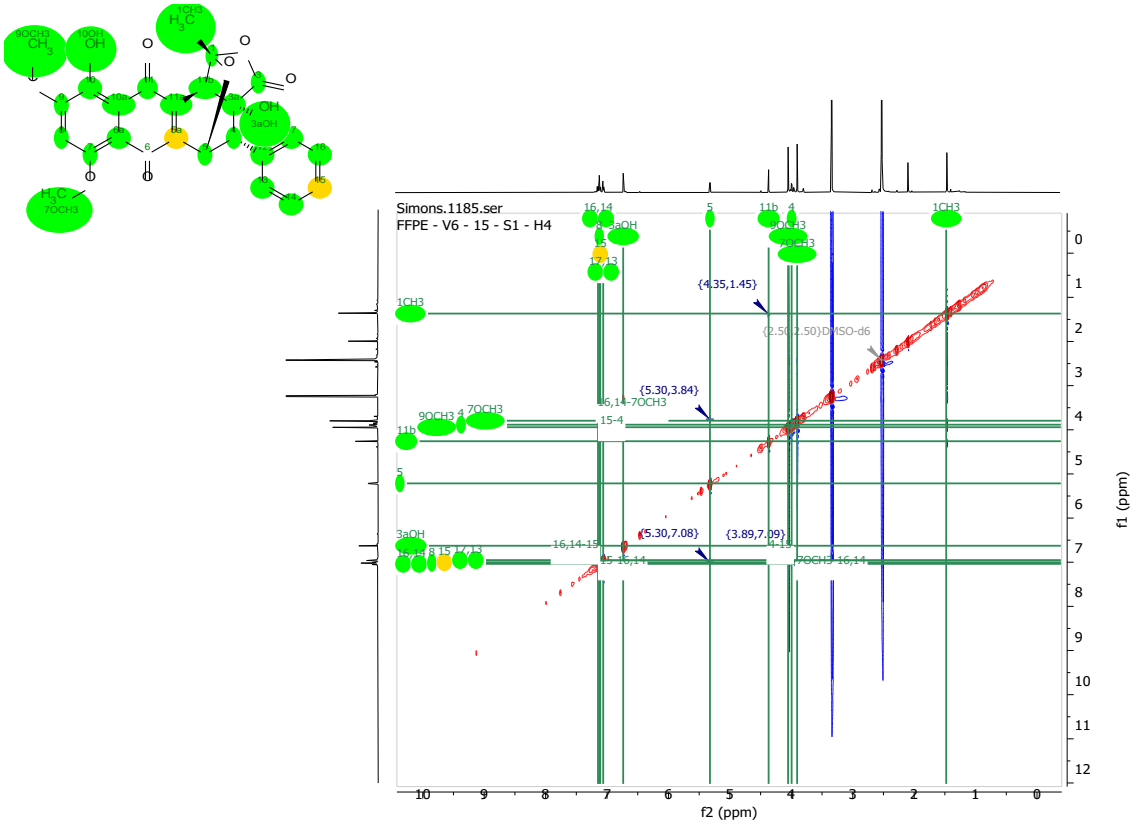

S29. HPLC-DAD UV-Vis Spectrum of Compound 3 (fusapurpurin A) (Methanol)

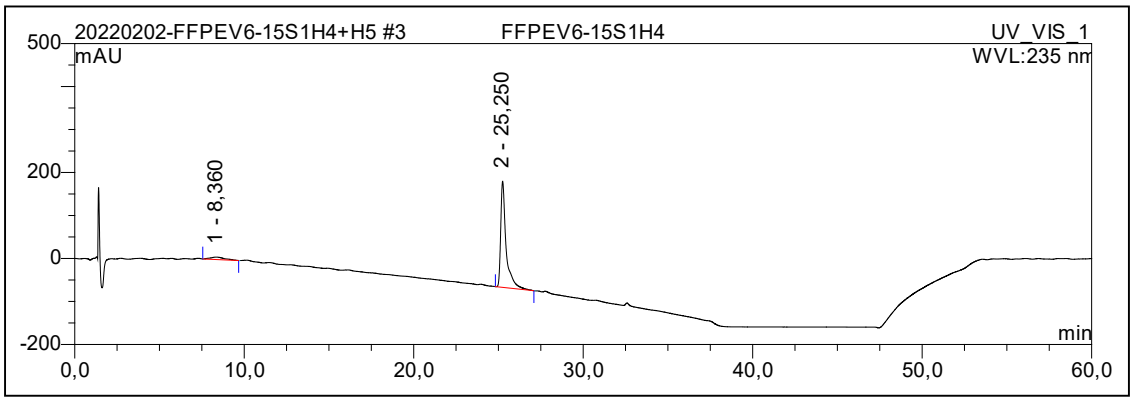

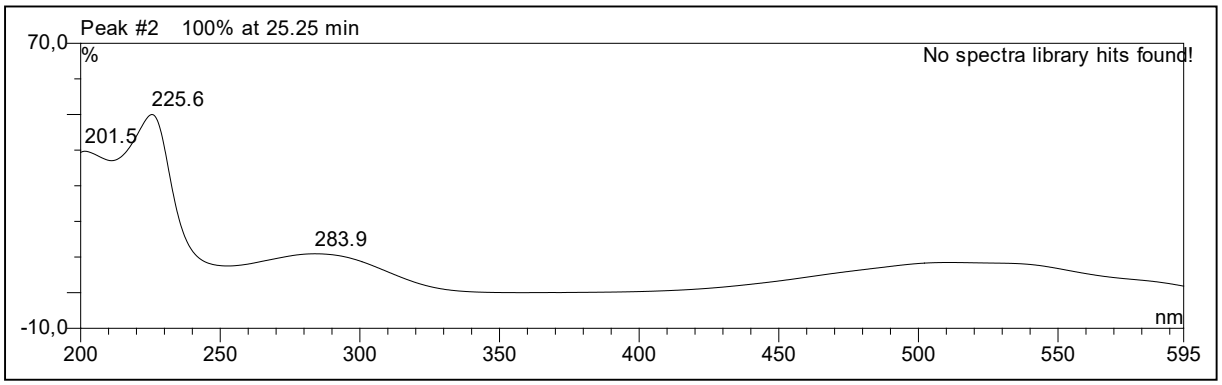

S30. High Resolution ESI(+)MS Spectrum of 3 (fusapurpurin A)

Mass Spectrum SmartFormula Report

Analysis Info

Analysis Name	D:\Data\Spektren 2021\KAL21HR000041.d	Acquisition Date	4/23/2021 10:07:15 AM
Method	tune_low_new.m	Operator	Peter Tommes
Sample Name	Simons FFPE-V6-15-S1-H4 (CH3CN/H2O)	Instrument	maXis 288882.20213
Comment			

Acquisition Parameter

Source Type	ESI	Ion Polarity	Positive	Set Nebulizer	0.3 Bar
Focus	Not active	Set Capillary	4000 V	Set Dry Heater	180 °C
Scan Begin	50 m/z	Set End Plate Offset	-500 V	Set Dry Gas	4.0 l/min
Scan End	1500 m/z	Set Collision Cell RF	600.0 Vpp	Set Divert Valve	Source

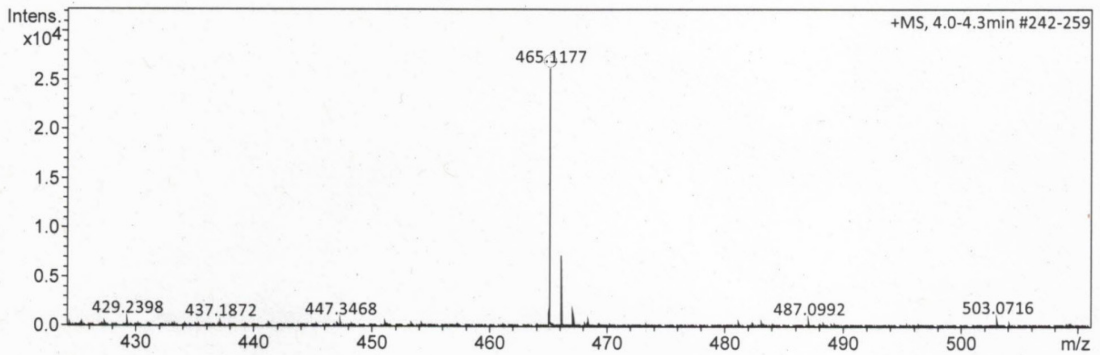

Meas. m/z	#	Ion Formula	m/z	err [ppm]	mSigma	# mSigma	Score	rdb	e⁻ Conf	N-Rule
465.1177	1	C25H21O9	465.1180	0.8	4.8	1	100.00	15.5	even	ok
	2	C22H13N10O3	465.1167	-2.1	11.2	2	48.01	21.5	even	ok
	3	C26H17N4O5	465.1193	3.6	12.0	3	40.62	20.5	even	ok

S31. NMR Table of Compound 4 (fusapurpurin B) (DMSO-d_6, ^{1}H: 600MHz, ^{13}C: 150 MHz)

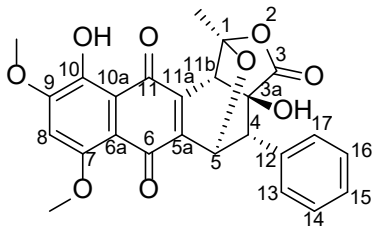

1R,3aS,4R,5S,11bS

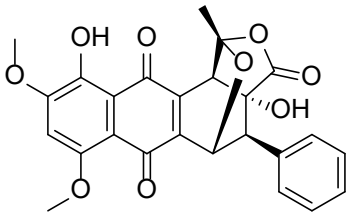

1S,3aR,4S,5R,11bR

Chemical formula: $C_{25}H_{20}O_9$
Molecular weight: 464.43 g/mol

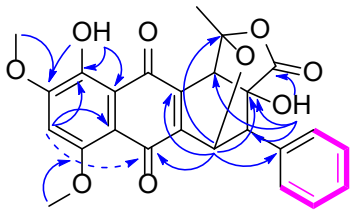

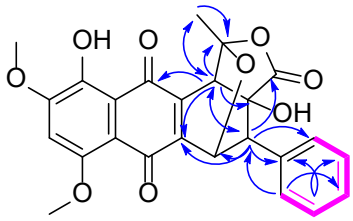

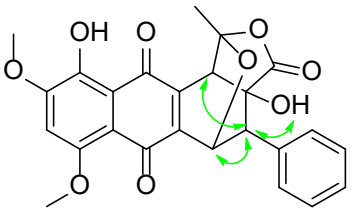

COSY

key HMBC

weak HMBC

key NOE

position	δ_C*	δ_H, m (J in Hz)
1	104.7, C	
3	173.3, CO	
3a	75.1, C	
4	51.5, CH	2.91, s
5	69.1, CH	5.41, s
5a	149.8, C	
6	175.5, CO	
6a	109.5, C	
7	156.4, CO	
8	104.2, CH	7.14, s
9	155.9, CO	
10	148.1, C	
10a	114.2, C	
11	187.2, CO	
11a	135.5, C	
11b	47.2, CH	4.30, s
12	136.8, C	
13/17	127.7, CH	7.37, m, 2H
14/16	128.6, CH	7.33, m, 2H
15	128.1, CH	7.29, m
1-CH_3	22.4, CH_3	1.47, s, 3H
3a-OH		6.65, s
7-OCH_3	56.2, OCH_3	3.97, s, 3H
9-OCH_3	56.2, OCH_3	4.03, s, 3H
10-OH		12.94, s

S32. ^{1}H-NMR Spectrum of Compound 4 (fusapurpurin B) (DMSO-d_6, 600 MHz)

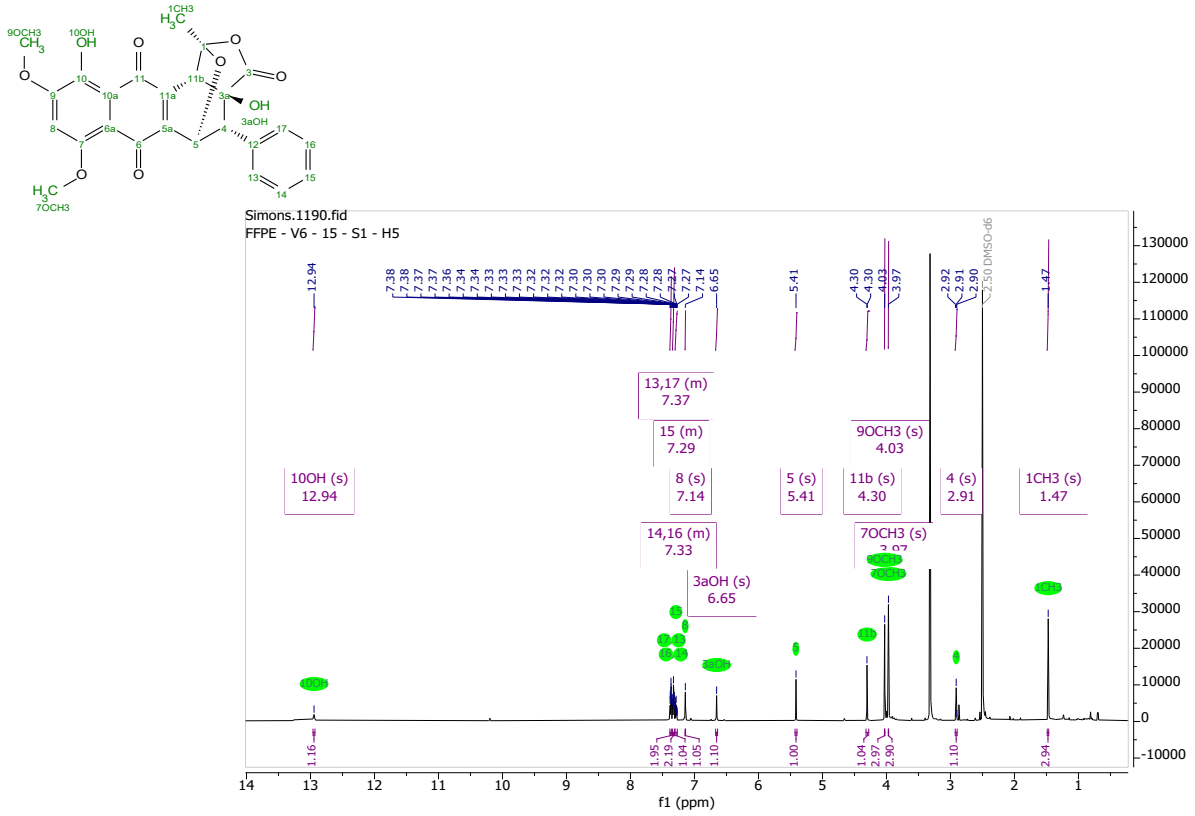

S33. ^{13}C-NMR Spectrum of Compound 4 (fusapurpurin B) (DMSO-d_6, 150 MHz)

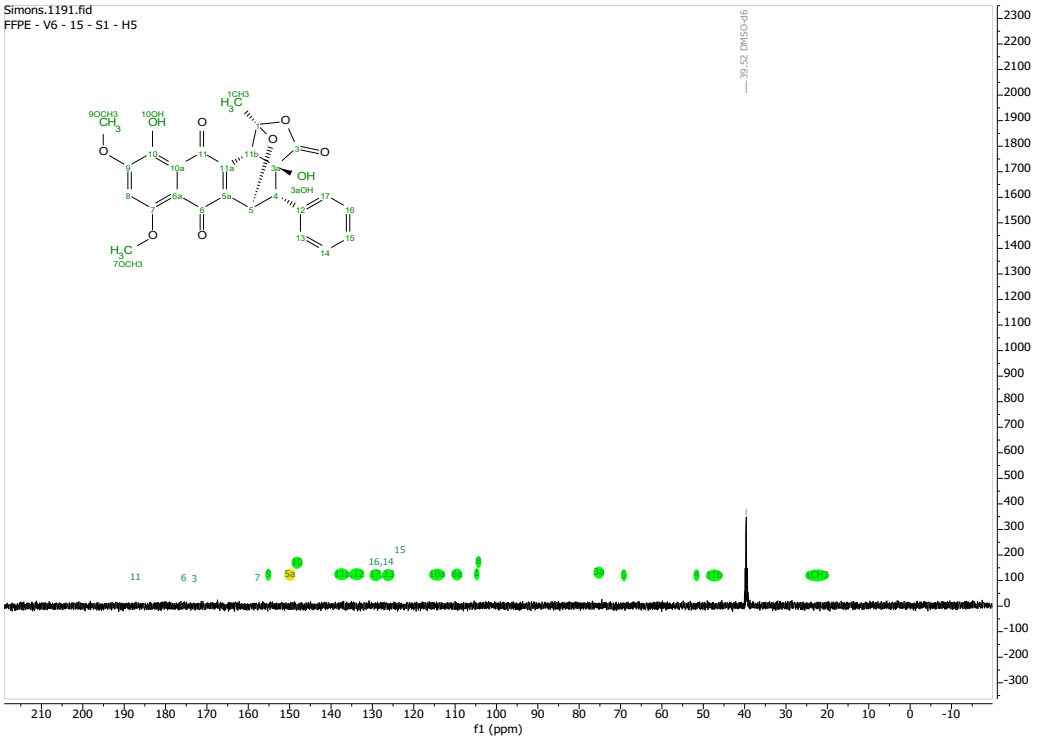

S34. ^{1}H-^{13}C-HSQC Spectrum of Compound 4 (fusapurpurin B) (DMSO-d_6, ^{1}H: 600MHz, ^{13}C: 150 MHz)

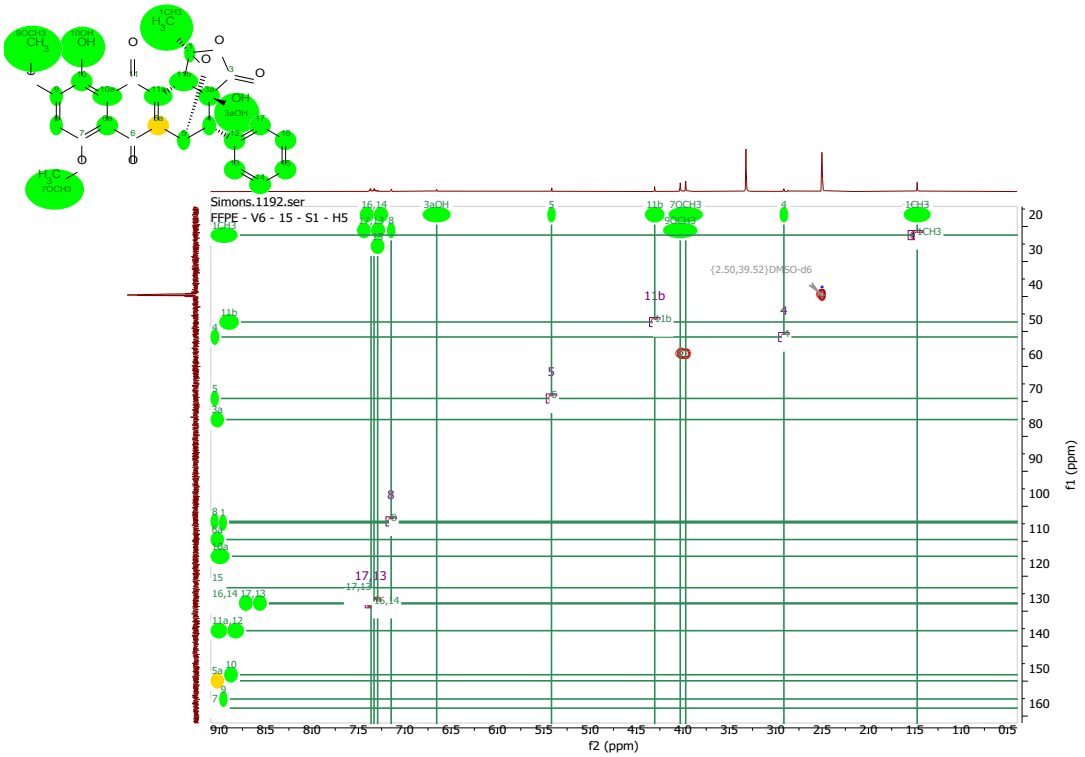

S35. ^{1}H-^{13}C-HMBC Spectrum of Compound 4 (fusapurpurin B) (DMSO-d_6, ^{1}H: 600MHz, ^{13}C: 150 MHz)

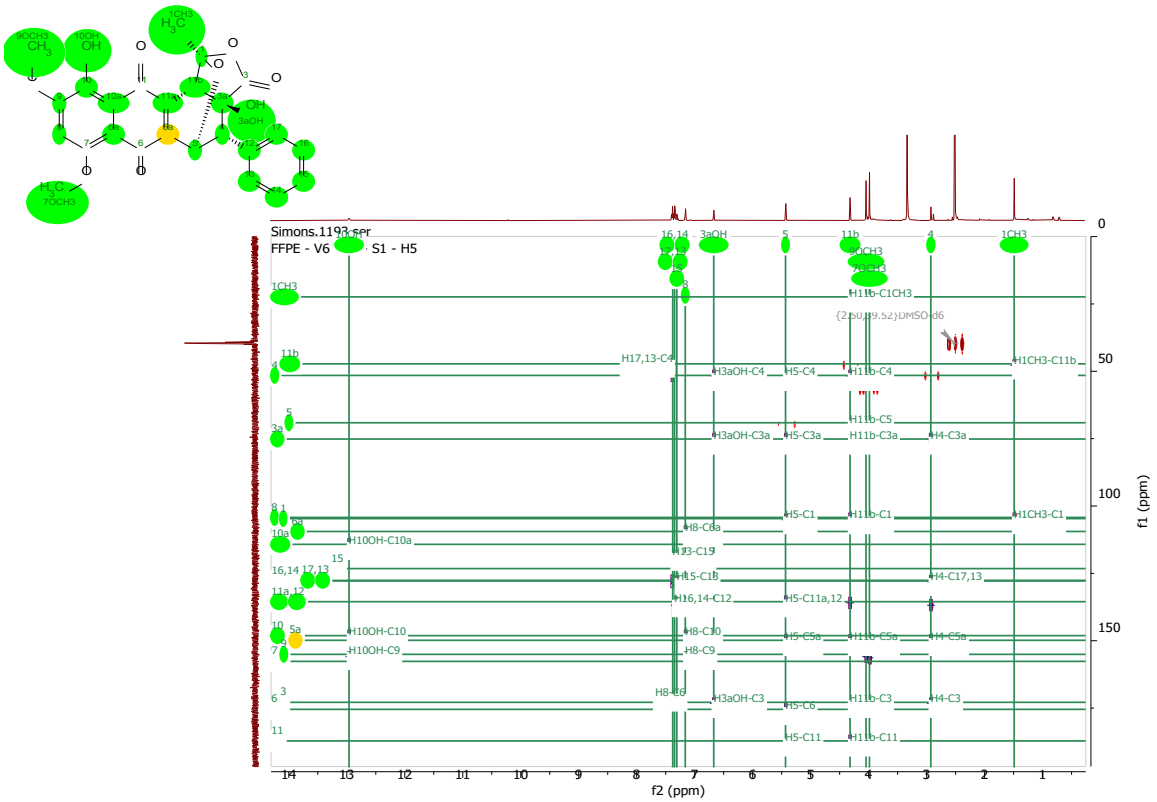

S36. ^{1}H-^{1}H-COSY Spectrum of Compound 4 (fusapurpurin B) (DMSO-d_6, 600MHz)

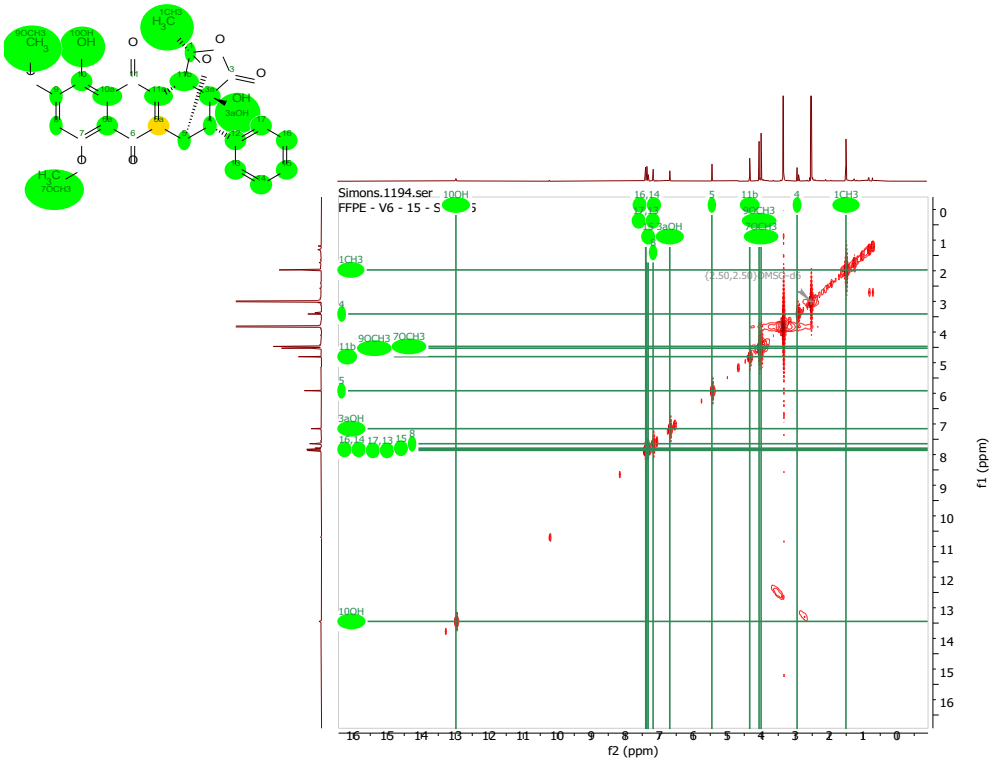

S37. ^{1}H-^{1}H-NOESY Spectrum of Compound 4 (fusapurpurin B) (DMSO-d_6, 600MHz)

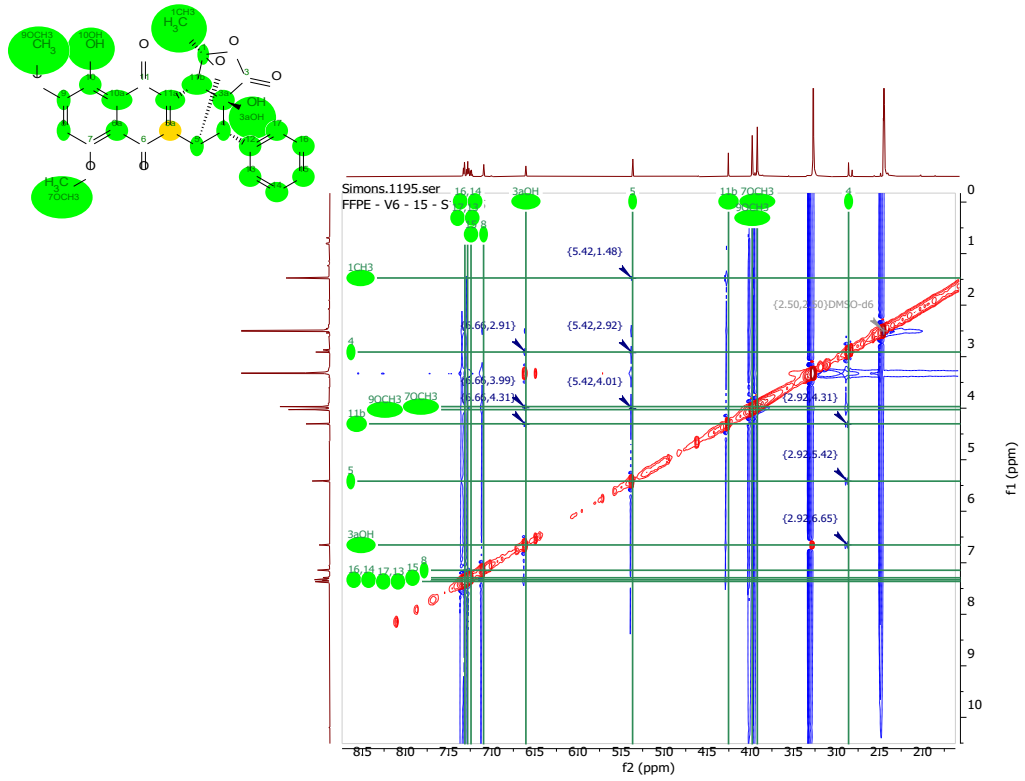

S38. HPLC-DAD UV-Vis Spectrum of Compound 4 (fusapurpurin B) (Methanol)

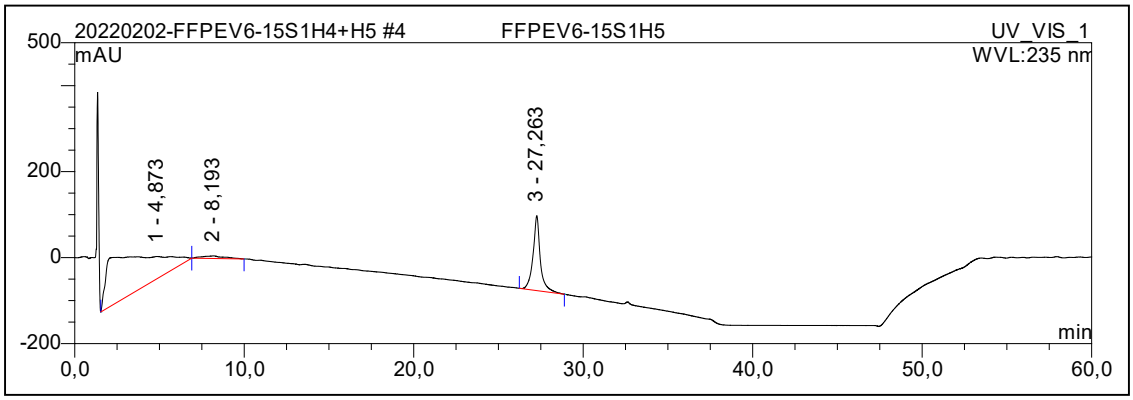

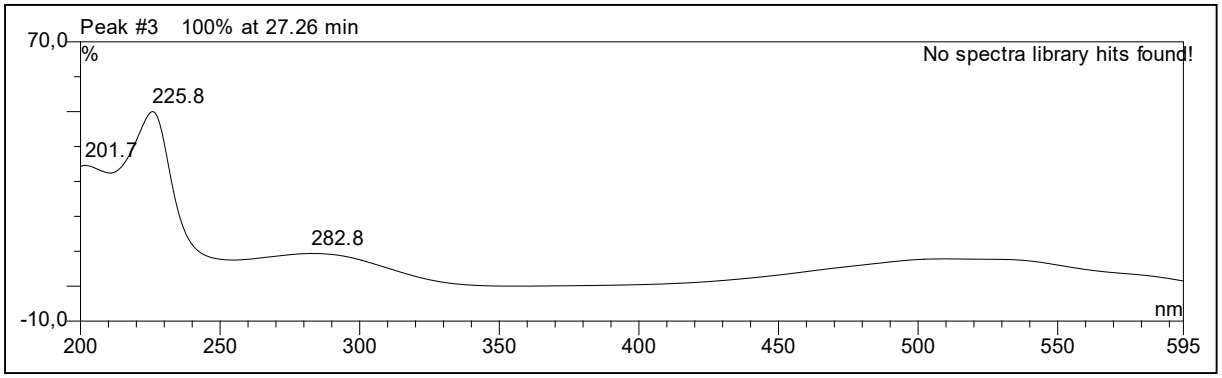

S39. High Resolution ESI(+)MS Spectrum of 4 (fusapurpurin B)

Mass Spectrum SmartFormula Report

Analysis Info

Analysis Name	D:\Data\Spektren 2021\KAL21HR000038.d	Acquisition Date	4/23/2021 8:29:49 AM
Method	tune_low_new.m	Operator	Peter Tommes
Sample Name	Simons FFPE-V6-15-S1-H5 (CH3CN/H2O)	Instrument	maXis 288882.20213
Comment			

Acquisition Parameter

Source Type	ESI	Ion Polarity	Positive	Set Nebulizer	0.3 Bar
Focus	Not active	Set Capillary	4000 V	Set Dry Heater	180 °C
Scan Begin	50 m/z	Set End Plate Offset	-500 V	Set Dry Gas	4.0 l/min
Scan End	1500 m/z	Set Collision Cell RF	600.0 Vpp	Set Divert Valve	Source

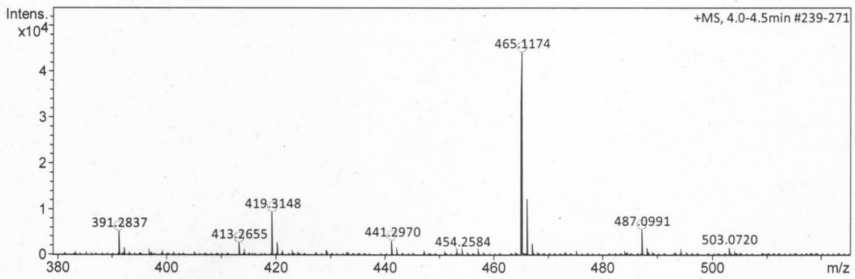

Meas. m/z	#	Ion Formula	m/z	err [ppm]	mSigma	# mSigma	Score	rdb	e⁻ Conf	N-Rule
391.2837	1	C24H39O4	391.2843	1.4	22.0	1	100.00	5.5	even	ok
413.2655	1	C22H33N6O2	413.2660	1.0	23.6	1	100.00	9.5	even	ok
419.3148	1	C26H43O4	419.3156	1.9	12.9	1	100.00	5.5	even	ok
441.2970	1	C26H42NaO4	441.2975	1.2	23.0	1	92.64	5.5	even	ok
	2	C24H37N6O2	441.2973	0.6	25.4	2	100.00	9.5	even	ok
465.1174	1	C25H21O9	465.1180	1.4	1.7	1	100.00	15.5	even	ok
	2	C24H18N4NaO5	465.1169	-0.9	4.7	2	78.38	17.5	even	ok
	3	C22H13N10O3	465.1167	-1.5	7.2	3	65.27	21.5	even	ok
	4	C25H14N8NaO	465.1183	1.9	14.3	4	51.78	22.5	even	ok
487.0991	1	C25H20NaO9	487.1000	1.8	11.4	1	89.88	15.5	even	ok
	2	C23H15N6O7	487.0997	1.2	13.4	2	100.00	19.5	even	ok
	3	C22H12N10NaO3	487.0986	-1.0	16.5	3	75.24	21.5	even	ok
	4	C20H7N16O	487.0983	-1.5	19.0	4	62.03	25.5	even	ok
	5	C22H19N2O11	487.0983	-1.5	20.4	5	80.74	14.5	even	ok

S40. NMR Table of Compound 5 (9-O-methylbostrycoidin) (DMSO-d_6, ^{1}H: 600MHz)

9-*O*-methylbostrycoidin

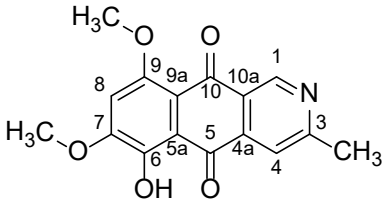

Chemical Formula: $C_{16}H_{13}NO_5$
Molecular Weight: 299,28

position	δ_H, m (J in Hz)
1	9.16, s
4	7.85, s
8	7.18, s
3-CH_3	2.68, s, 3H
6-OH	12.98, s
7-OCH_3	3.97, s, 3H
9-OCH_3	4.01, s, 3H

S41. [1]H-NMR Spectrum of Compound 5 (9-O-methylbostrycoidin)(DMSO-d_6, 600 MHz)

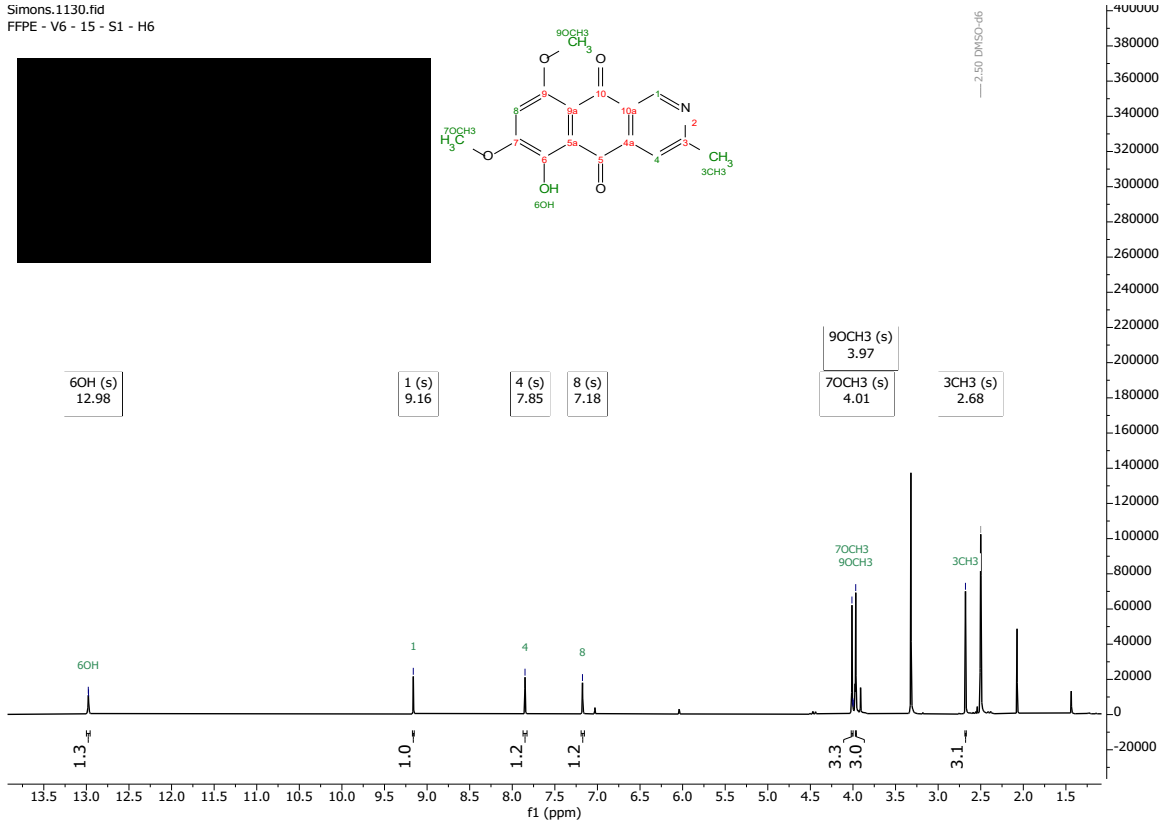

S42. HPLC-DAD UV-Vis Spectrum of Compound 5 (9-O-methylbostrycoidin) (Methanol)

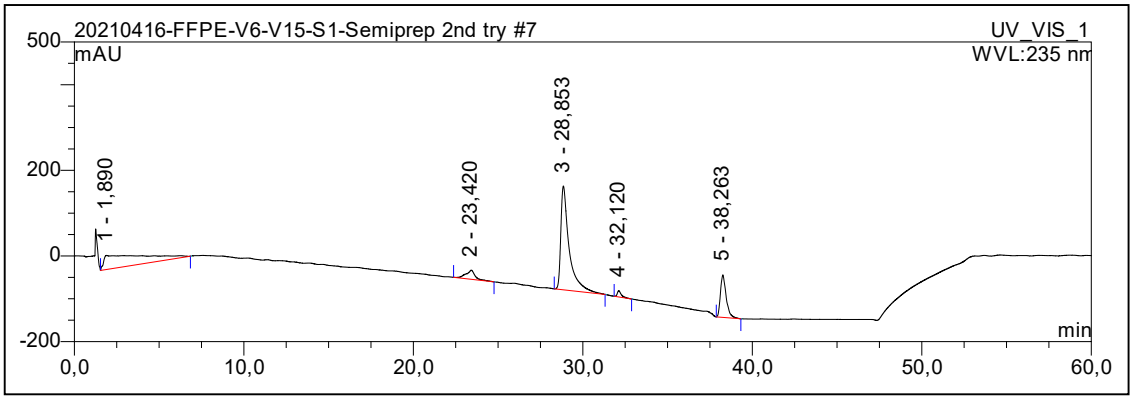

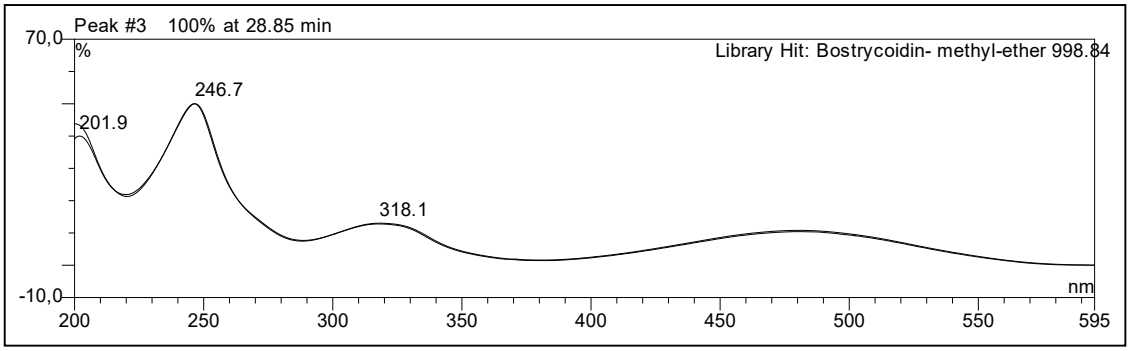

S43. High Resolution ESI(+)MS Spectrum of Compound 5 (9-O-methylbostrycoidin)

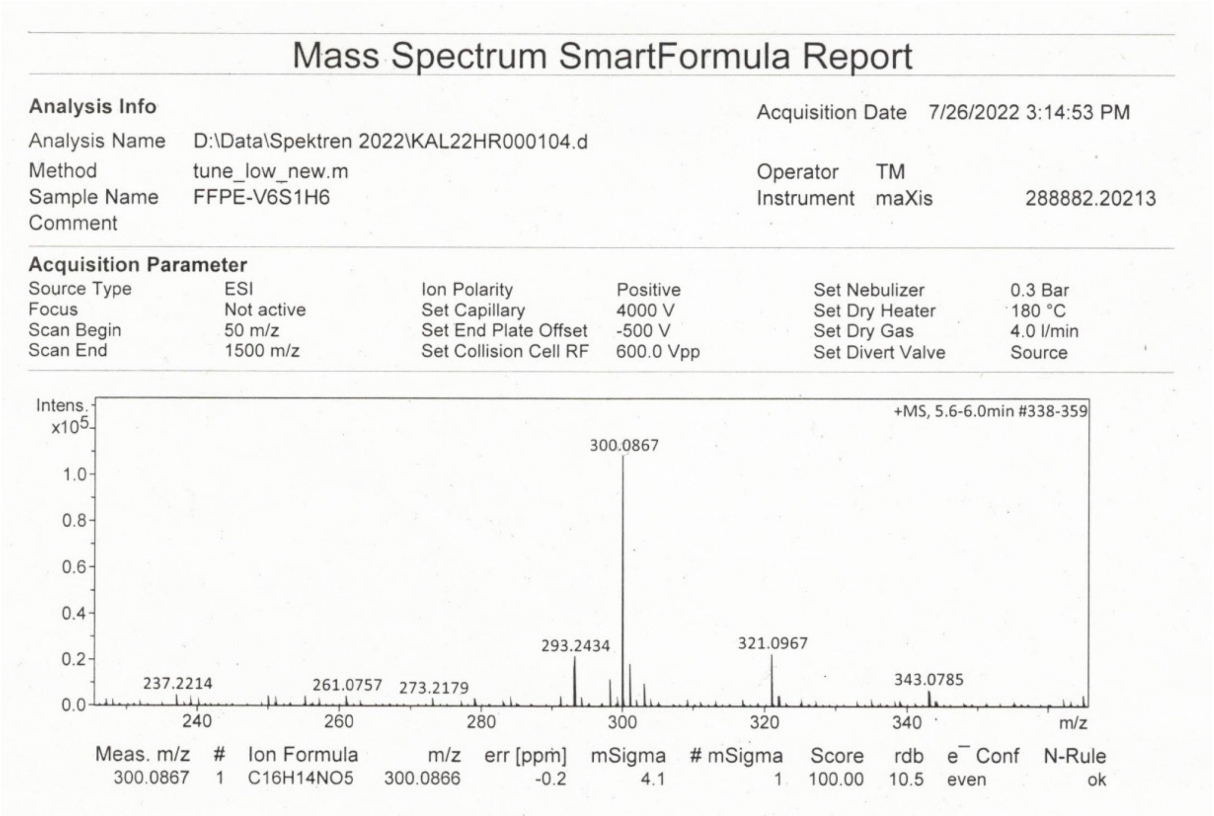

S44. NMR Table of Compound 6 (2,5-Dihydroxy-6,8-dimethoxy-3-(2-oxopropyl)-1,4-naphthalenedione) (DMSO-d6, 600MHz)

2,5-Dihydroxy-6,8-dimethoxy-3-(2-oxopropyl)-1,4-naphthalenedione

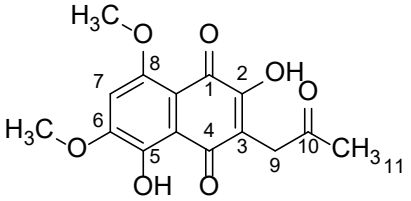

Chemical Formula: $C_{15}H_{14}O_7$
Molecular Weight: 306,27

position	δ_H, m (J in Hz)
7	6.98, s
9	3.53, s 2H
11	2.16, s 3H
2-OH	11.34, br s
5-OH	13.69, s
6-OCH_3	3.99, s 3H
8-OCH_3	3.96, s 3H

S45. 1H-NMR Spectrum of Compound 6 (2,5-Dihydroxy-6,8-dimethoxy-3-(2-oxopropyl)-1,4-naphthalenedione) (DMSO-d6, 600 MHz)

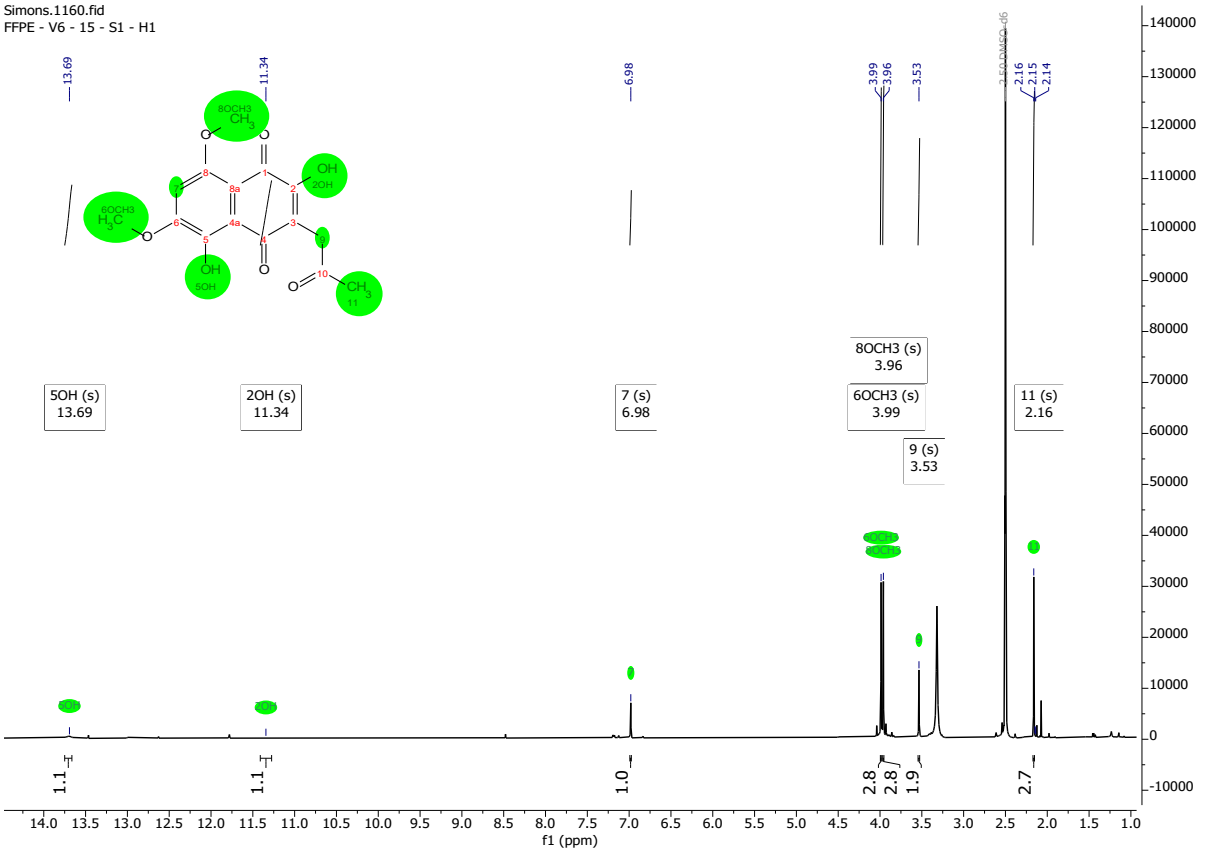

S46. UV-Vis Spectrum of Compound 6 (2,5-Dihydroxy-6,8-dimethoxy-3-(2-oxopropyl)-1,4-naphthalenedione) (Methanol)

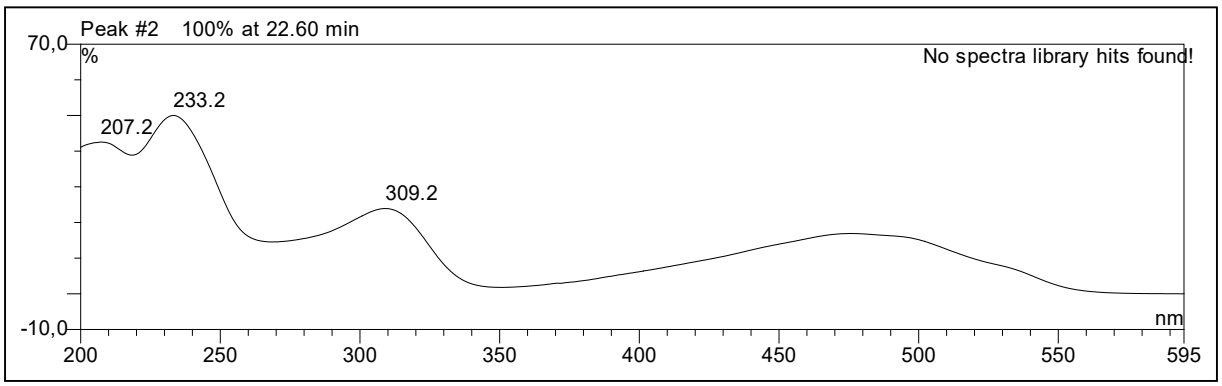

S47. High Resolution ESI(+)MS Spectrum of Compound 6 (2,5-Dihydroxy-6,8-dimethoxy-3-(2-oxopropyl)-1,4-naphthalenedione)

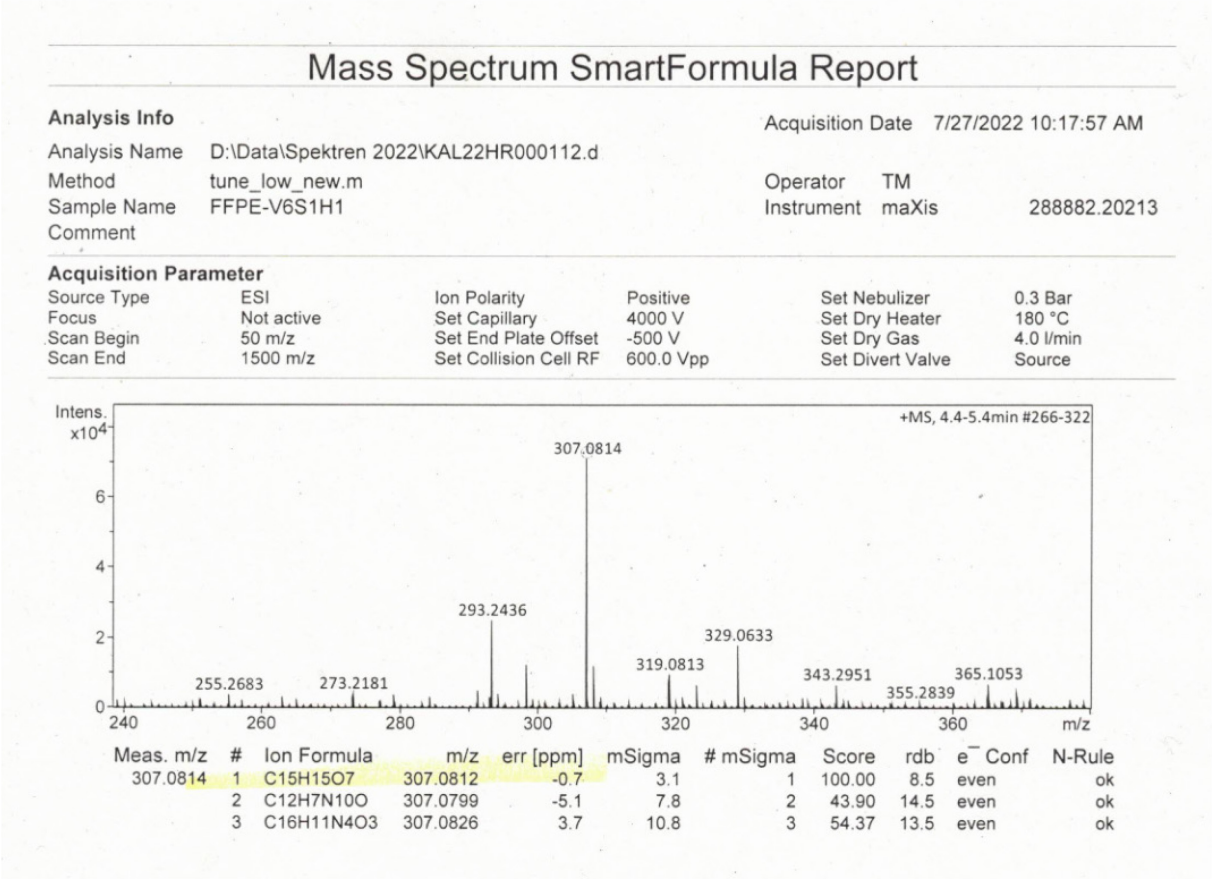

Mass Spectrum SmartFormula Report

Analysis Info

Analysis Name	D:\Data\Spektren 2022\KAL22HR000112.d	Acquisition Date	7/27/2022 10:17:57 AM
Method	tune_low_new.m	Operator	TM
Sample Name	FFPE-V6S1H1	Instrument	maXis 288882.20213
Comment			

Acquisition Parameter

Source Type	ESI	Ion Polarity	Positive	Set Nebulizer	0.3 Bar
Focus	Not active	Set Capillary	4000 V	Set Dry Heater	180 °C
Scan Begin	50 m/z	Set End Plate Offset	-500 V	Set Dry Gas	4.0 l/min
Scan End	1500 m/z	Set Collision Cell RF	600.0 Vpp	Set Divert Valve	Source

Meas. m/z	#	Ion Formula	m/z	err [ppm]	mSigma	# mSigma	Score	rdb	e⁻ Conf	N-Rule
307.0814	1	C15H15O7	307.0812	-0.7	3.1	1	100.00	8.5	even	ok
	2	C12H7N10O	307.0799	-5.1	7.8	2	43.90	14.5	even	ok
	3	C16H11N4O3	307.0826	3.7	10.8	3	54.37	13.5	even	ok

S48. NMR Table of Compound 7 (9-O-methylanhydrofusarubin) (DMSO-d_6, ^{1}H: 600MHz)

9-*O*-methylanhydrofusarubin

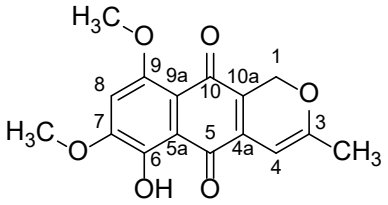

Chemical Formula: $C_{16}H_{14}O_6$
Molecular Weight: 302,28

position	δ_H, m (J in Hz)
1	5.02, s 2H
4	5.83, d (0.9)
8	7.05, s
3-CH_3	1.98, d (0.9)
6-OH	12.91, s
7-OCH_3	3.97, s
9-OCH_3	3.91, s

S49. ^{1}H-NMR Spectrum of Compound 7 (9-O-methylanhydrofusarubin) (DMSO-d_6, 600 MHz)

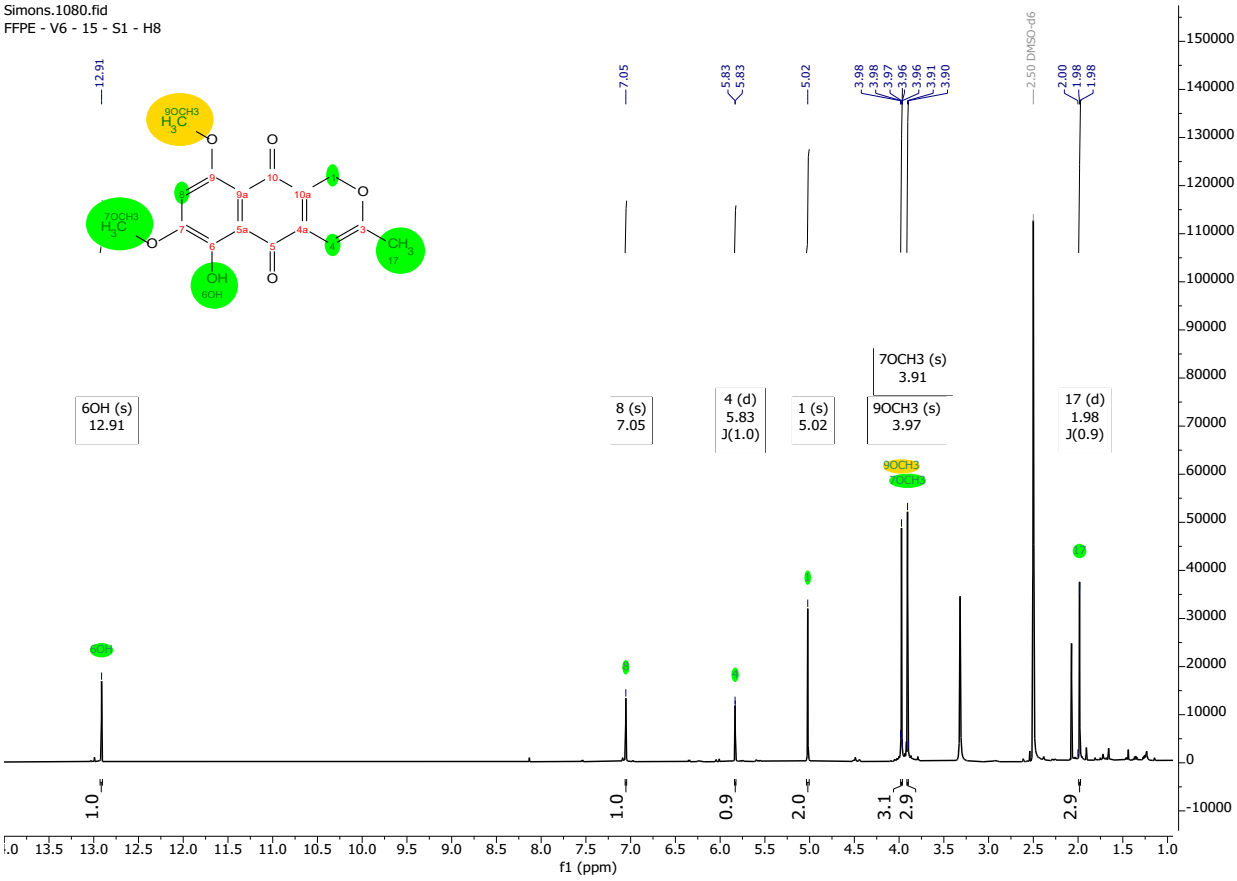

S50. UV-Vis Spectrum of Compound 7 (9-O-methylanhydrofusarubin) (Methanol)

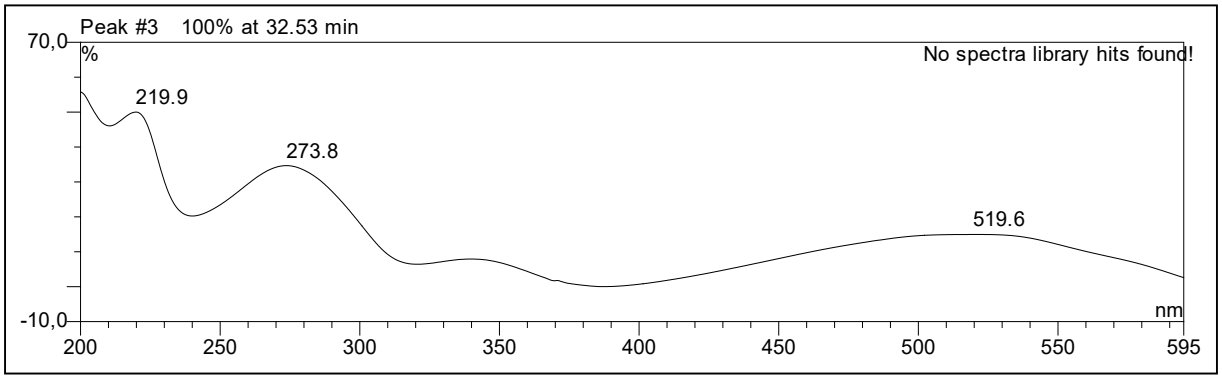

S51. High Resolution ESI(+)MS Spectrum of Compound 7 (9-O-methylanhydrofusarubin)

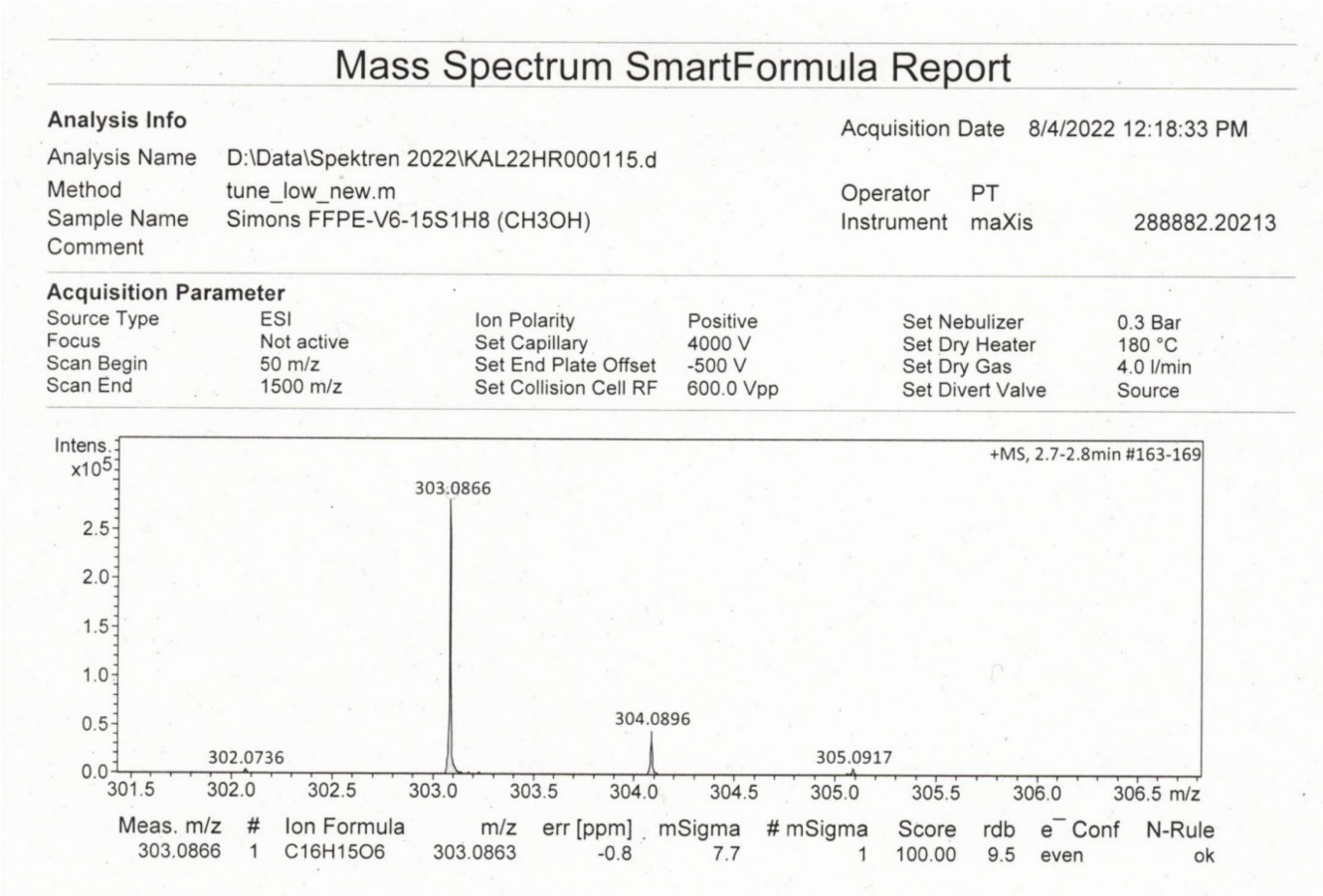

Mass Spectrum SmartFormula Report

Analysis Info

Analysis Name	D:\Data\Spektren 2022\KAL22HR000115.d	Acquisition Date	8/4/2022 12:18:33 PM
Method	tune_low_new.m	Operator	PT
Sample Name	Simons FFPE-V6-15S1H8 (CH3OH)	Instrument	maXis 288882.20213
Comment			

Acquisition Parameter

Source Type	ESI	Ion Polarity	Positive	Set Nebulizer	0.3 Bar
Focus	Not active	Set Capillary	4000 V	Set Dry Heater	180 °C
Scan Begin	50 m/z	Set End Plate Offset	-500 V	Set Dry Gas	4.0 l/min
Scan End	1500 m/z	Set Collision Cell RF	600.0 Vpp	Set Divert Valve	Source

Meas. m/z	#	Ion Formula	m/z	err [ppm]	mSigma	# mSigma	Score	rdb	e⁻ Conf	N-Rule
303.0866	1	C16H15O6	303.0863	-0.8	7.7	1	100.00	9.5	even	ok

S52. NMR Table of Compound 8 (9-O-methylanhydrofusarubinlactol) (DMSO-d_6, ^{1}H: 600MHz, ^{13}C: 150 MHz)

9-*O*-methylanhydrofusarubinlactol

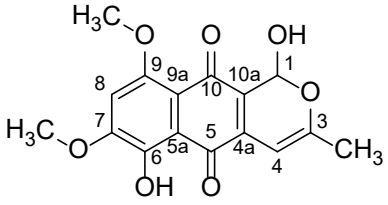

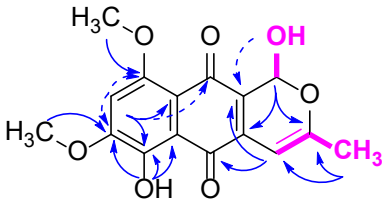

Chemical Formula: $C_{16}H_{14}O_7$
Molecular Weight: 318,28

COSY —— weak HMBC - - ->
key HMBC ⟶

position	δ_C*	δ_H, m (J in Hz)
1	87.5, CH	6.35, d (6.9)
3	159.8, C	
4	91.4, CH	6.01, d (0.9)
4a	133.2, C	
5	188.5, C	
5a	113.8, C	
6	147.8, C	
7	154.6, C	
8	104.6, CH	7.10, s
9	155.1, C	
9a	109.5, C	
10	178.5, C	
10a	125.6, C	
1-OH		7.54, d (6.9)
3-CH_3	20.3, CH_3	2.07, d (0.9)
6-OH		12.92, s
7-OCH_3	56.2, CH_3	3.98, s
9-OCH_3	56.2, CH_3	3.92, s

*signals were extracted from HSQC and HMBC spectra.

S53. [1]H-NMR Spectrum of Compound 8 (9-O-methylanhydrofusarubinlactol) (DMSO-d_6, 600 MHz)

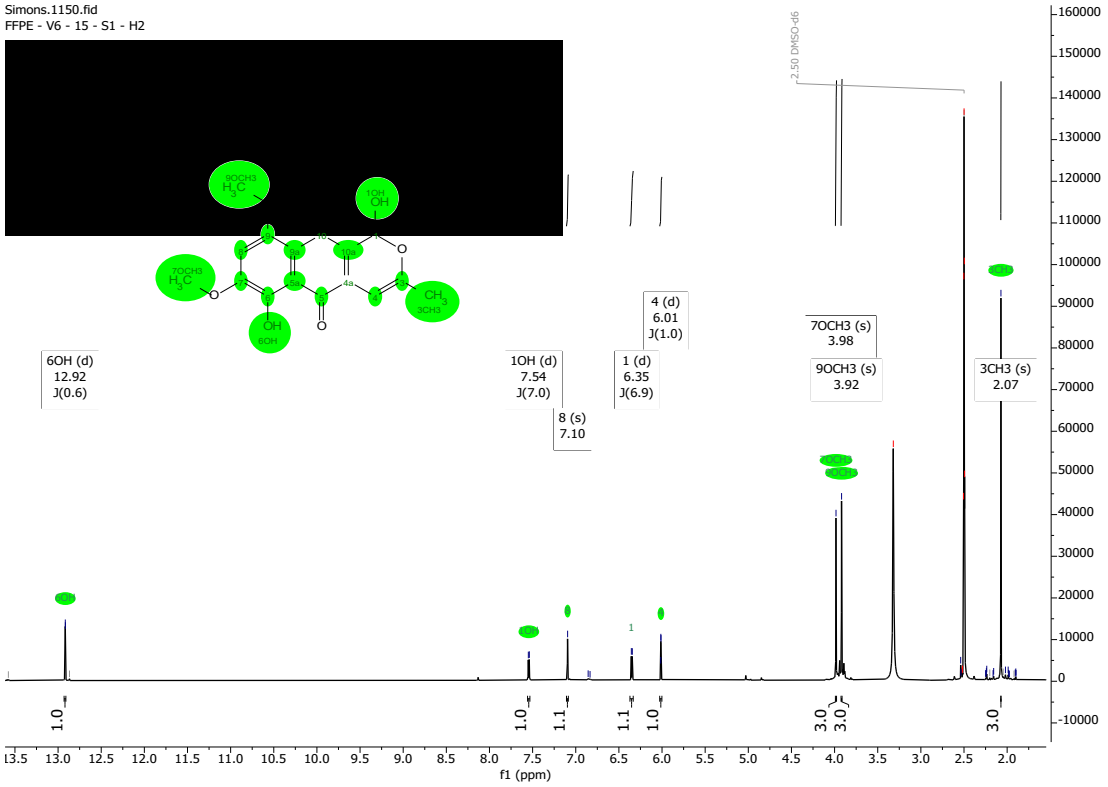

S54. [13]C-NMR Spectrum of Compound 8 (9-O-methylanhydrofusarubinlactol) (DMSO-d_6, 150 MHz)

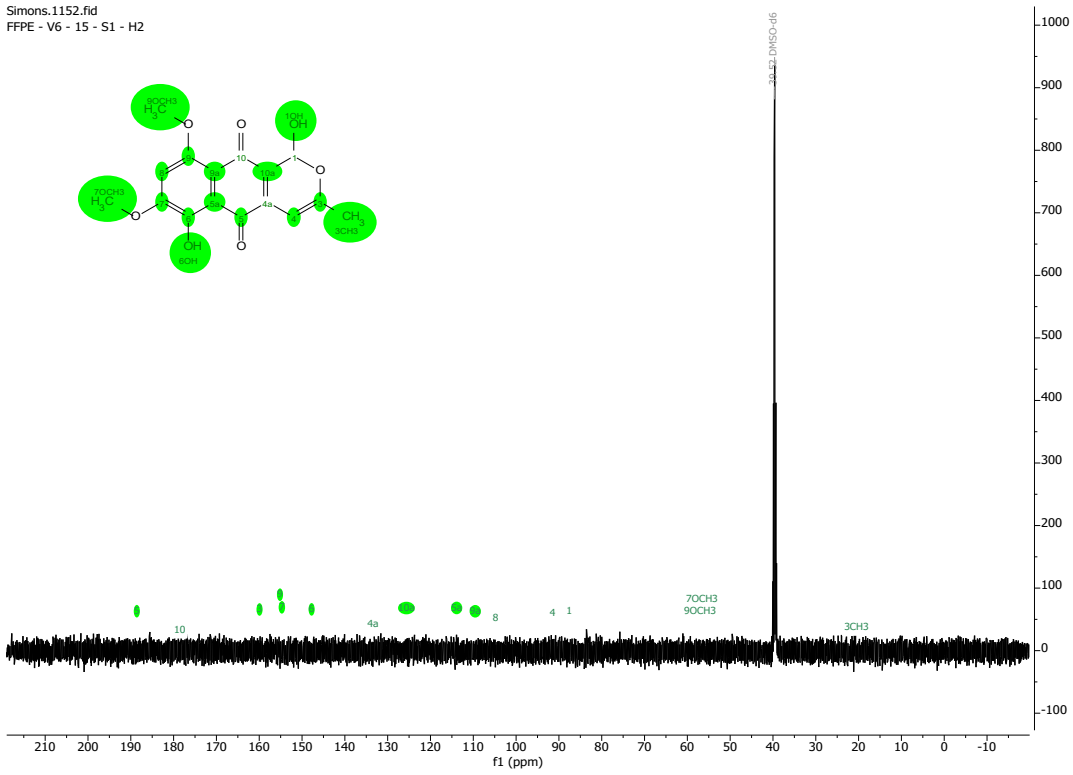

S55. ^{1}H-^{13}C-HSQC Spectrum of Compound 8 (9-O-methylanhydrofusarubinlactol) (DMSO-d_6, ^{1}H: 600MHz, ^{13}C: 150 MHz)

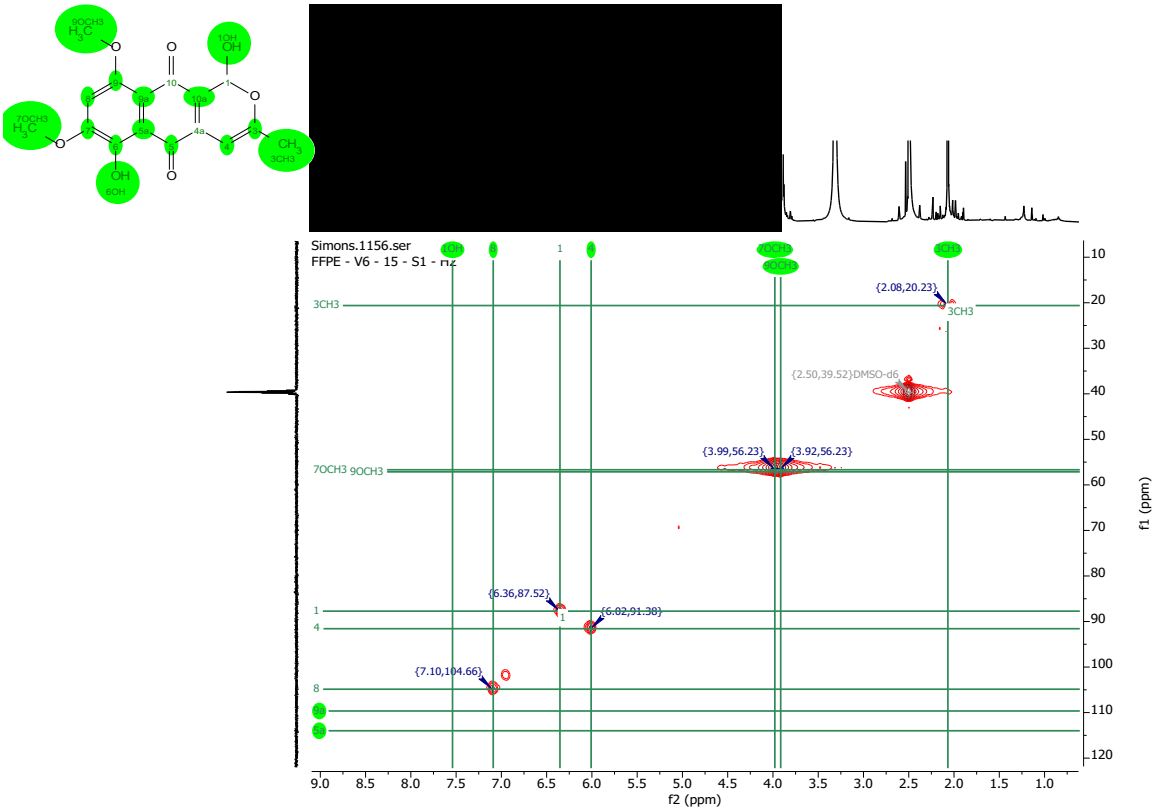

S56. ^{1}H-^{13}C-HMBC Spectrum of Compound 8 (9-O-methylanhydrofusarubinlactol) (DMSO-d_6, ^{1}H: 600MHz, ^{13}C: 150 MHz)

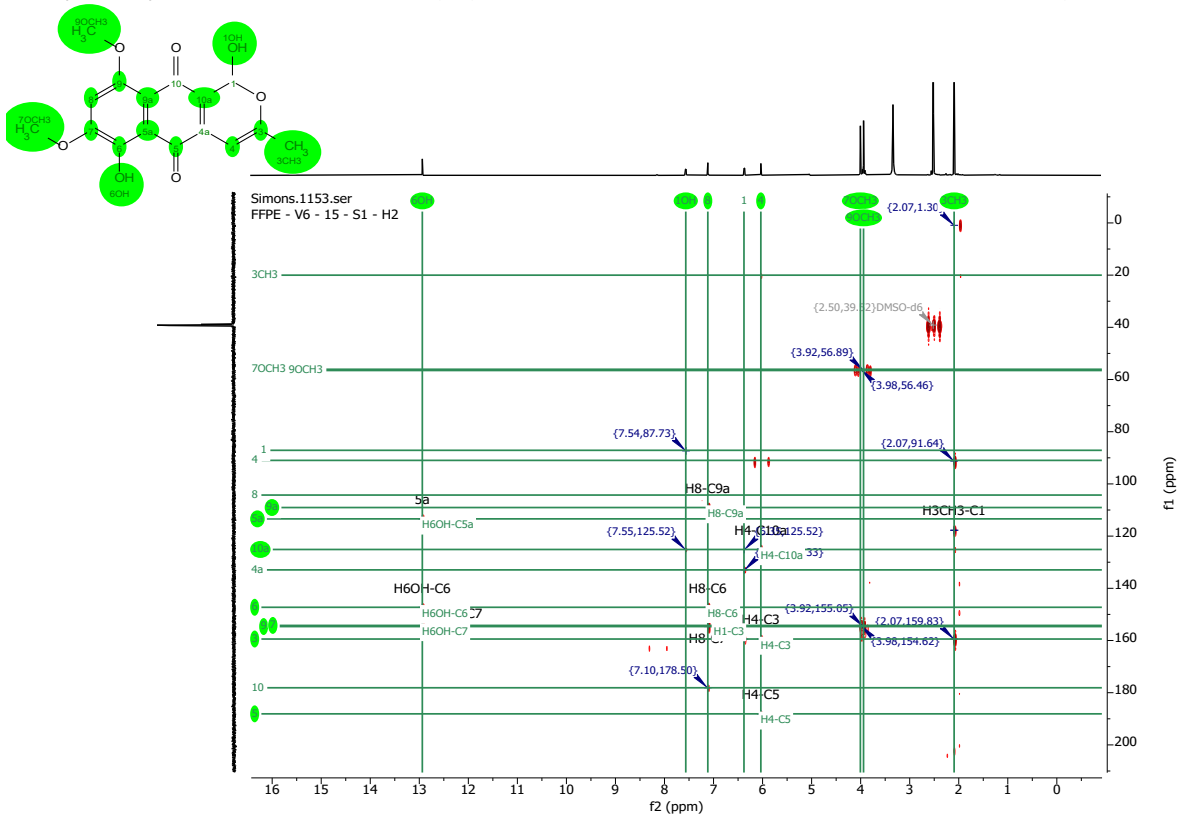

S57. ^{1}H-^{1}H-COSY Spectrum of Compound 8 (9-O-methylanhydrofusarubinlactol) (DMSO-d_6, 600MHz)

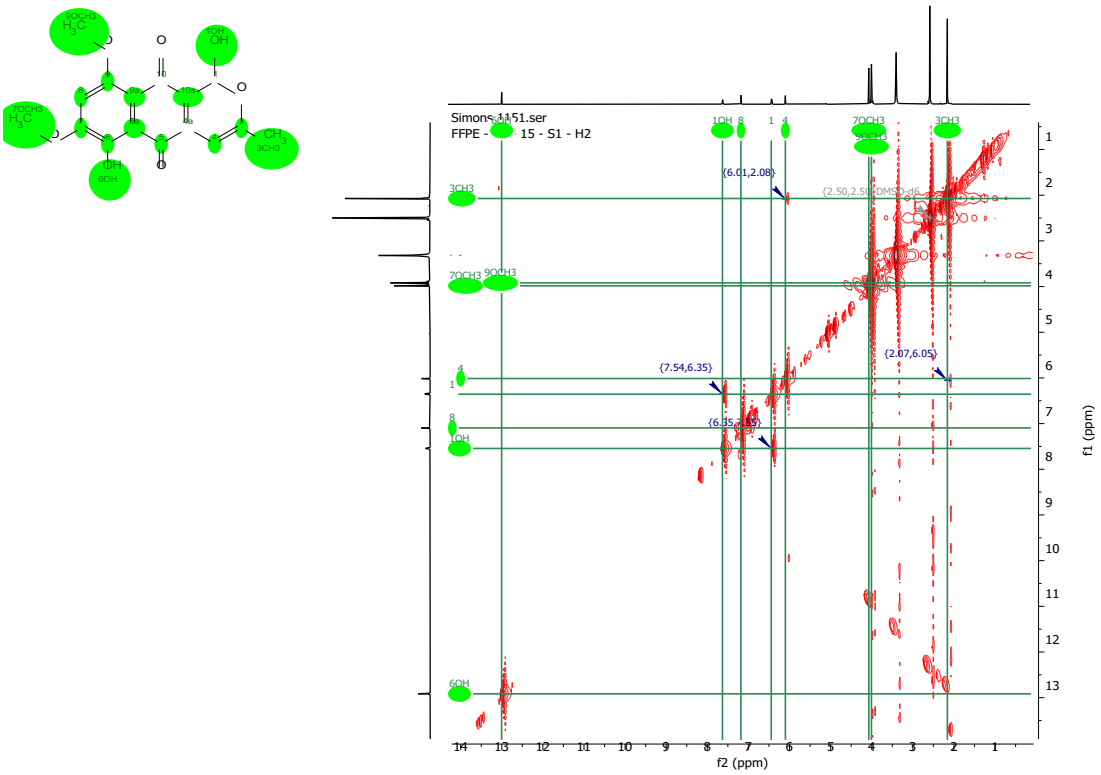

S58. ^{1}H-^{1}H-NOESY Spectrum of Compound 8 (9-O-methylanhydrofusarubinlactol) (DMSO-d_6, 600MHz)

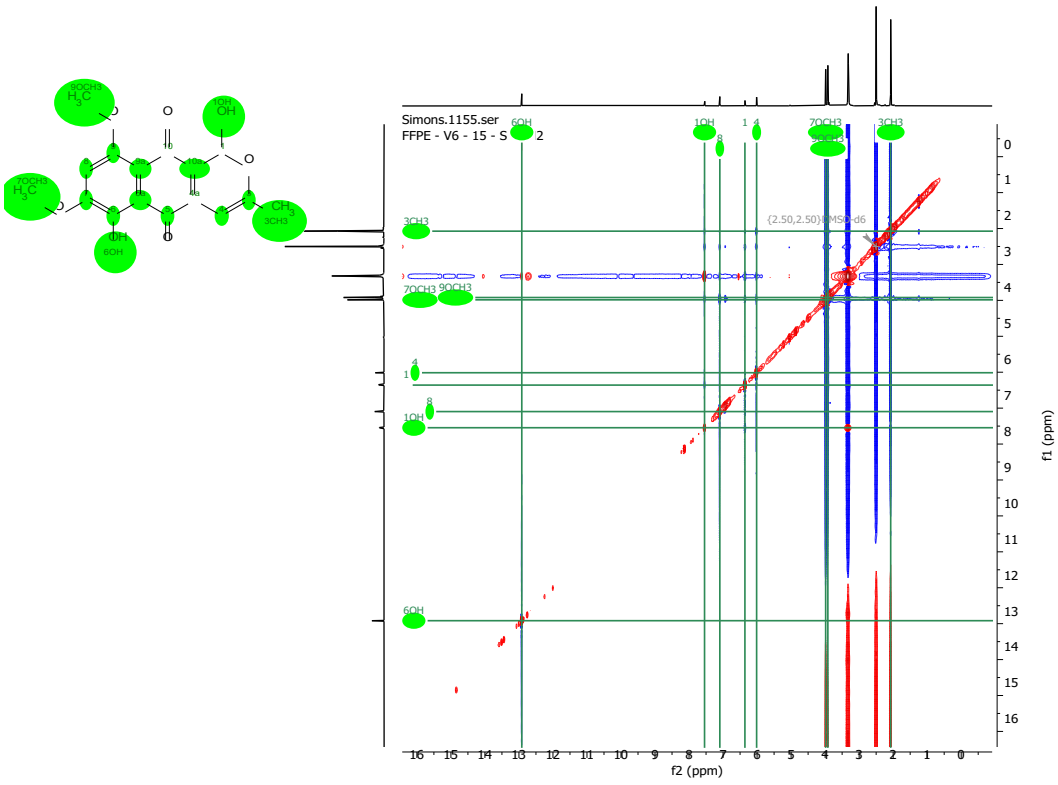

S59. HPLC-DAD UV-Vis Spectrum of Compound 8 (9-O-methylanhydrofusarubinlactol) (Methanol)

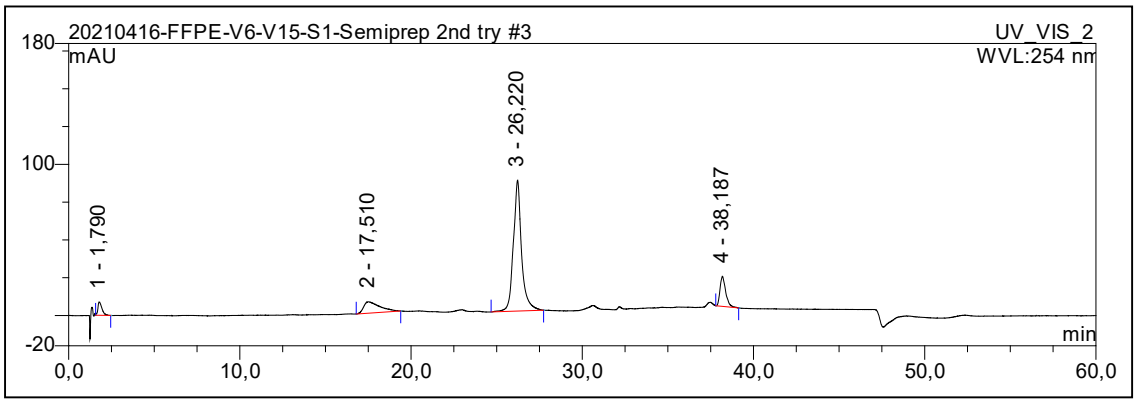

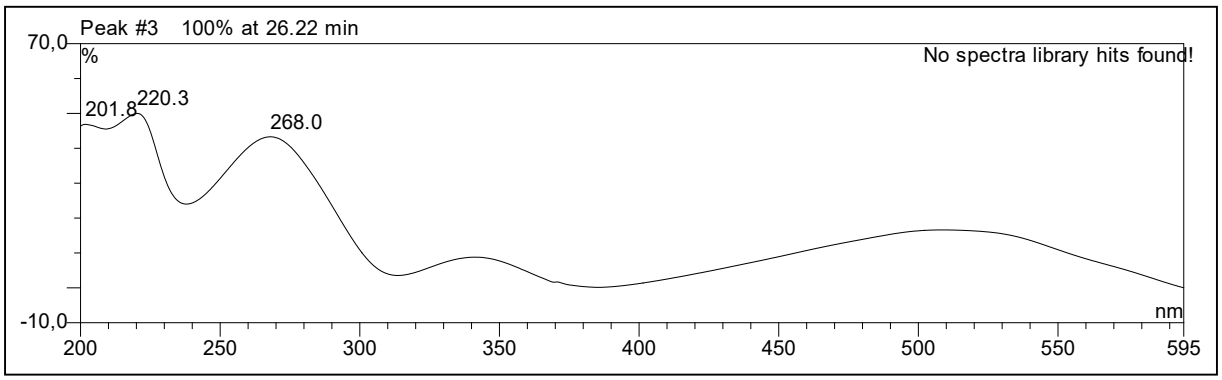

S60. High Resolution ESI(+)MS Spectrum of Compound 8 (9-O-methylanhydrofusarubinlactol)

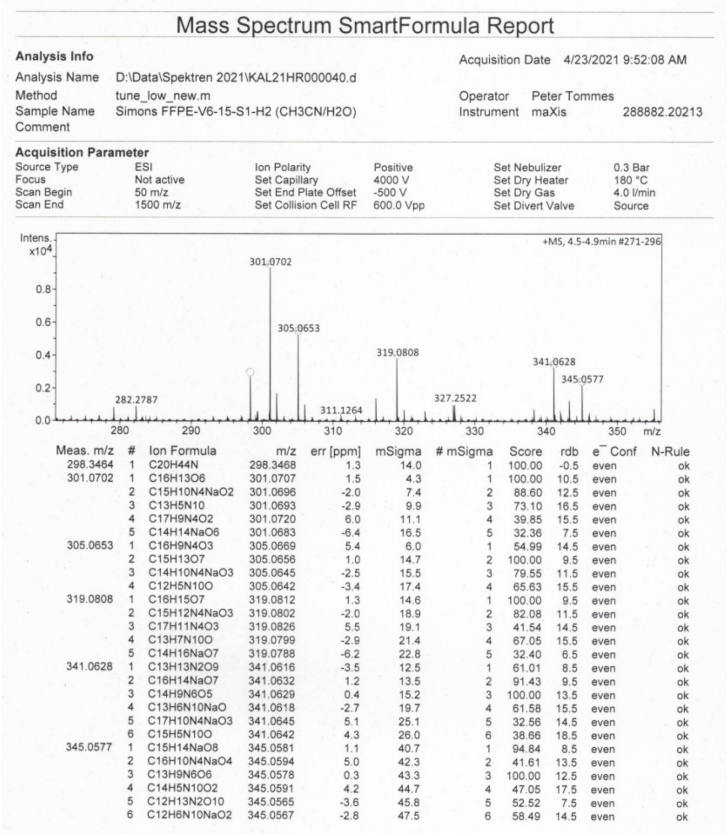

Mass Spectrum SmartFormula Report

Analysis Info

Analysis Name	D:\Data\Spektren 2021\KAL21HR000040.d	Acquisition Date	4/23/2021 9:52:08 AM
Method	tune_low_new.m	Operator	Peter Tommes
Sample Name	Simons FFPE-V6-15-S1-H2 (CH3CN/H2O)	Instrument	maXis 288882.20213
Comment			

Acquisition Parameter

Source Type	ESI	Ion Polarity	Positive	Set Nebulizer	0.3 Bar
Focus	Not active	Set Capillary	4000 V	Set Dry Heater	180 °C
Scan Begin	50 m/z	Set End Plate Offset	-500 V	Set Dry Gas	4.0 l/min
Scan End	1500 m/z	Set Collision Cell RF	600.0 Vpp	Set Divert Valve	Source

Meas. m/z	#	Ion Formula	m/z	err [ppm]	mSigma	# mSigma	Score	rdb	e⁻ Conf	N-Rule
298.3464	1	C20H44N	298.3468	1.3	14.0	1	100.00	-0.5	even	ok
301.0702	1	C16H13O6	301.0707	1.5	4.3	1	100.00	10.5	even	ok
	2	C15H10N4NaO2	301.0696	-2.0	7.4	2	88.60	12.5	even	ok
	3	C13H5N10	301.0693	-2.9	9.9	3	73.10	16.5	even	ok
	4	C17H9N4O2	301.0720	6.0	11.1	4	39.85	15.5	even	ok
	5	C14H14NaO6	301.0683	-6.4	16.5	5	32.36	7.5	even	ok
305.0653	1	C16H9N4O3	305.0669	5.4	6.0	1	54.99	14.5	even	ok
	2	C15H13O7	305.0656	1.0	14.7	2	100.00	9.5	even	ok
	3	C14H10N4NaO3	305.0645	-2.5	15.5	3	79.55	11.5	even	ok
	4	C12H5N10O	305.0642	-3.4	17.4	4	65.63	15.5	even	ok
319.0808	1	C16H15O7	319.0812	1.3	14.6	1	100.00	9.5	even	ok
	2	C15H12N4NaO3	319.0802	-2.0	18.9	2	82.08	11.5	even	ok
	3	C17H11N4O3	319.0826	5.5	19.1	3	41.54	14.5	even	ok
	4	C13H7N10O	319.0799	-2.9	21.4	4	67.05	15.5	even	ok
	5	C14H16NaO7	319.0788	-6.2	22.8	5	32.40	6.5	even	ok
341.0628	1	C13H13N2O9	341.0616	-3.5	12.5	1	61.01	8.5	even	ok
	2	C16H14NaO7	341.0632	1.2	13.5	2	91.43	9.5	even	ok
	3	C14H9N6O5	341.0629	0.4	15.2	3	100.00	13.5	even	ok
	4	C13H6N10NaO	341.0618	-2.7	19.7	4	61.58	15.5	even	ok
	5	C17H10N4NaO3	341.0645	5.1	25.1	5	32.56	14.5	even	ok
	6	C15H5N10O	341.0642	4.3	26.0	6	38.66	18.5	even	ok
345.0577	1	C15H14NaO8	345.0581	1.1	40.7	1	94.84	8.5	even	ok
	2	C16H10N4NaO4	345.0594	5.0	42.3	2	41.61	13.5	even	ok
	3	C13H9N6O6	345.0578	0.3	43.3	3	100.00	12.5	even	ok
	4	C14H5N10O2	345.0591	4.2	44.7	4	47.05	17.5	even	ok
	5	C12H13N2O10	345.0565	-3.6	45.8	5	52.52	7.5	even	ok
	6	C12H6N10NaO2	345.0567	-2.8	47.5	6	58.49	14.5	even	ok

S61. NMR Data of Compound 9 (Beauvericin) ($CDCl_3$, ^1H: 600MHz)

Beauvericin

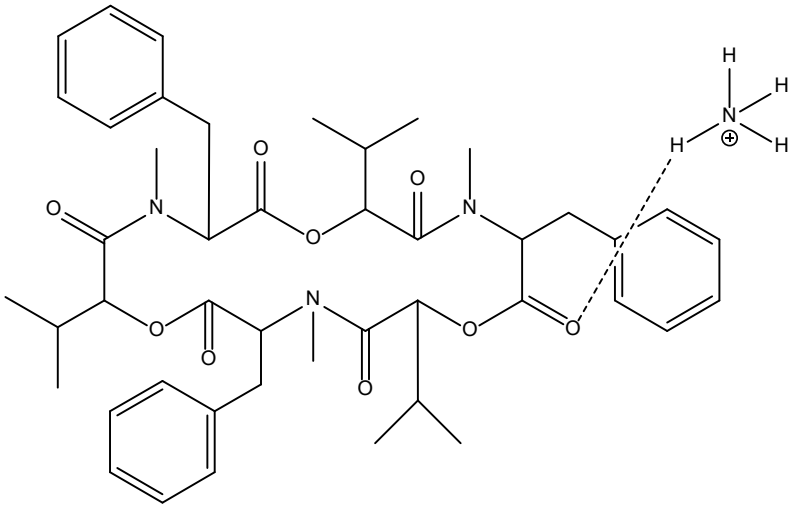

Chemical formula: $C_{45}H_{61}N_4O_9^+$
Molecular weight: 801.44 g/mol

^{1}H-NMR Data: δ 7.29-7.24 (12H, m), 7.21-7.18 (3H, m), 5.48 (3H, dd, J = 12.2, 5.1 Hz), 4.94 (3H, d, J = 8.6 Hz), 3.38 (3H, dd, J = 14.6, 5.0 Hz), 3.02 (9H, s), 2.99 (3H, m), 2.04 (3H, m), 0.82 (9H, d, J = 6.6 Hz), 0.45 (9H, d, J = 6.8 Hz)

S62. ^{1}H-NMR Spectrum of Compound 9 (Beauvericin) ($CDCl_3$, 600 MHz)

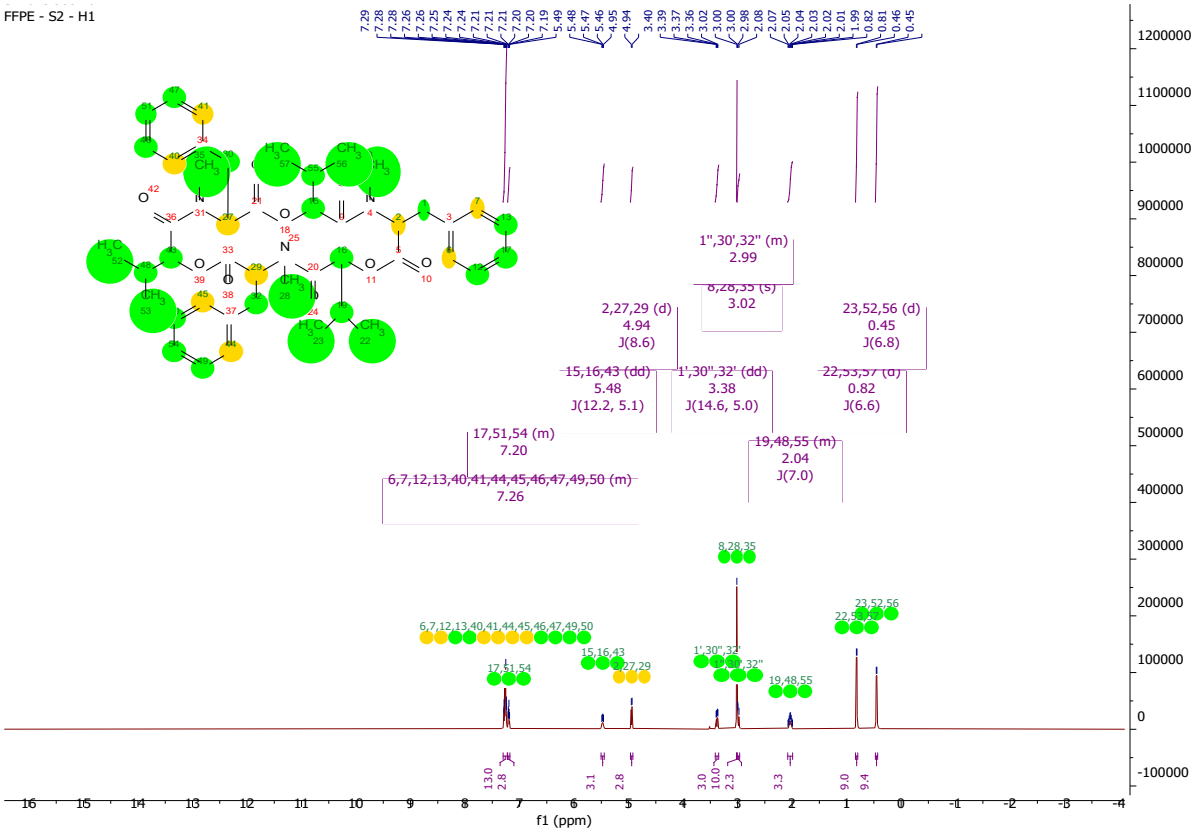

S63. HPLC-DAD UV-Vis Spectrum of Compound 9 (Beauvericin) (Methanol)

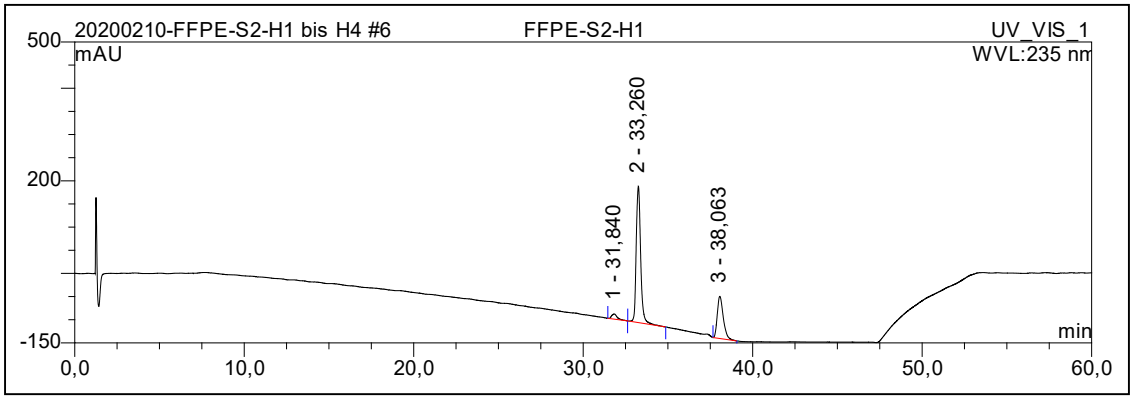

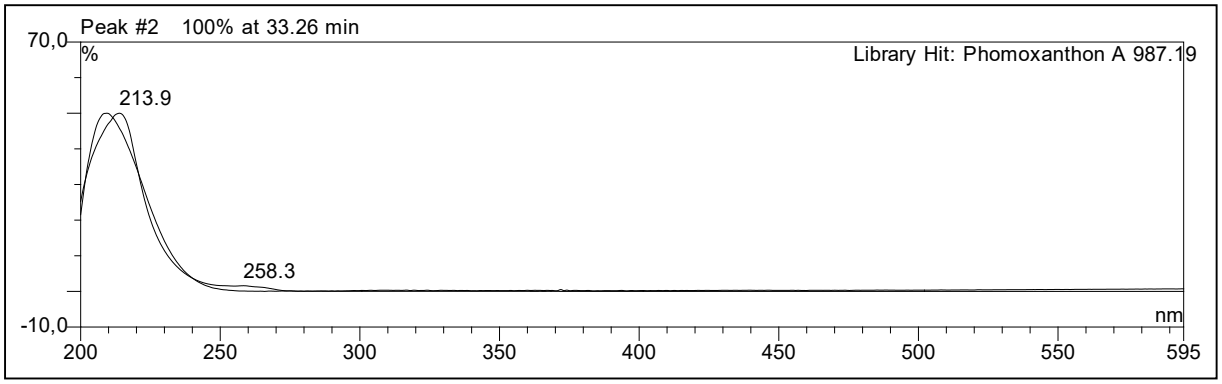

S64. High Resolution ESI(+)MS Spectrum of Compound 9 (Beauvericin)

Mass Spectrum SmartFormula Report

Analysis Info

Analysis Name	D:\Data\Spektren 2021\KAL21HR000011.d	Acquisition Date	2/11/2021 4:20:39 PM
Method	tune_low_new.m	Operator	Peter Tommes
Sample Name	Simons FFPE-S2-H1 (CH3OH)	Instrument	maXis 288882.20213
Comment	10 ul in 1 ml		

Acquisition Parameter

Source Type	ESI	Ion Polarity	Positive	Set Nebulizer	0.3 Bar
Focus	Not active	Set Capillary	4000 V	Set Dry Heater	180 °C
Scan Begin	50 m/z	Set End Plate Offset	-500 V	Set Dry Gas	4.0 l/min
Scan End	1500 m/z	Set Collision Cell RF	600.0 Vpp	Set Divert Valve	Source

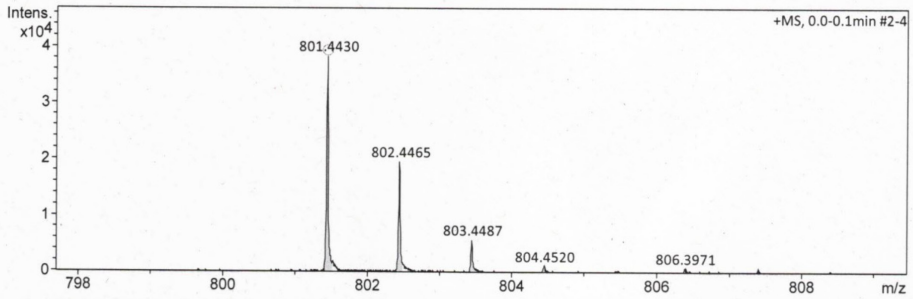

Meas. m/z	#	Ion Formula	m/z	err [ppm]	mSigma	# mSigma	Score	rdb	e⁻ Conf	N-Rule
801.4430	1	C45H61N4O9	801.4433	0.4	1.8	1	100.00	17.5	even	ok
	2	C42H53N14O3	801.4420	-1.2	8.0	2	64.53	23.5	even	ok
	3	C44H65O13	801.4420	-1.2	12.0	3	60.23	12.5	even	ok
	4	C28H45N30	801.4438	1.1	57.6	4	20.06	21.5	even	ok
	5	C30H57N16O10	801.4438	1.1	65.2	5	15.42	10.5	even	ok
	6	C57H57N2O2	801.4415	-1.9	65.2	6	10.41	30.5	even	ok
	7	C27H49N26O4	801.4425	-0.6	67.7	7	16.90	16.5	even	ok
	8	C32H69N2O20	801.4438	1.1	74.4	8	10.90	-0.5	even	ok
	9	C29H61N12O14	801.4425	-0.6	76.0	9	12.41	5.5	even	ok

S65. NMR Data of Compound 10 (Beauvericin J) (DMSO-d6, ^{1}H: 600MHz)

Beauvericin J

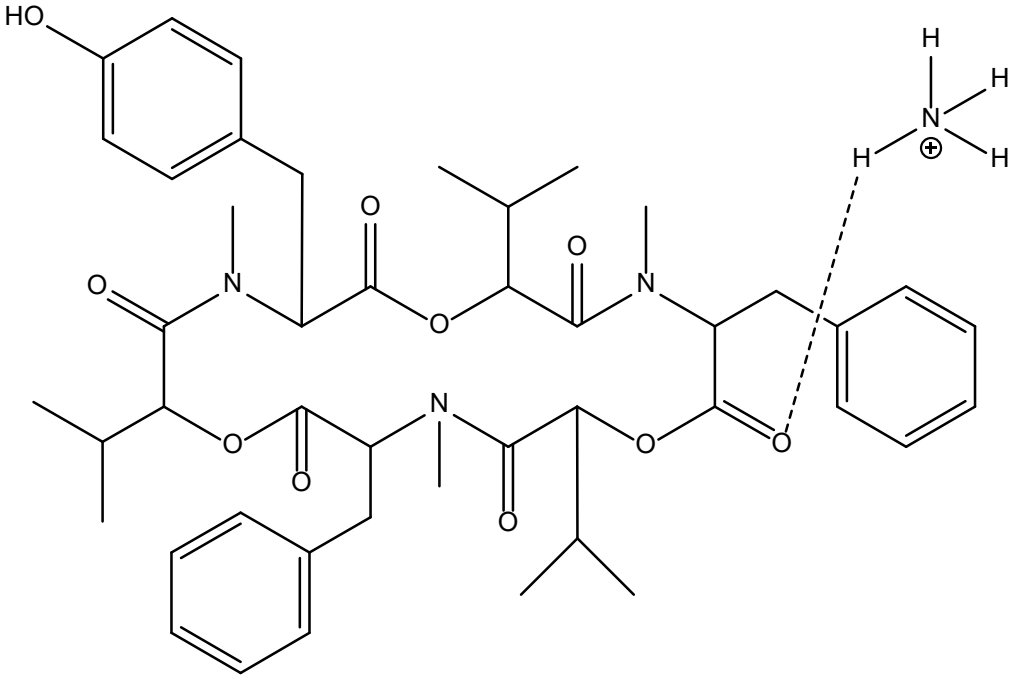

Chemical formula: $C_{45}H_{61}N_4O_{10}^{+}$
Molecular mass: 817.44 g/mol

^{1}H-NMR-data: δ 9.18 (1H, s), 7.27-7.21 (8H, m), 7.18 (2H, tt, J = 7.0, 2.4), 6.99 (2H, m), 6.62 (2H, m), 5.43 (2H, m), 5.32 (1H, dd, J = 11.9, 4.8), 4.83 (3H, m), 3.18 (2H, dt, J = 14.6, 5.3), 3.04 (3H, m), 3.02 (3H, s), 3.01, (3H, s), 3.01 (3H, s), 1.78 (3H, m), 0.78 (3H, d, J = 6.6), 0.74 (6H, dd, J = 6.6, 4.9), 0.33 (3H, d, J = 6.8), 0.23 (6H, dd, J = 10.9, 6.8)

S66. [1]H-NMR Spectrum of Compound 10 (Beauvericin J) (DMSO-d6, 600 MHz)

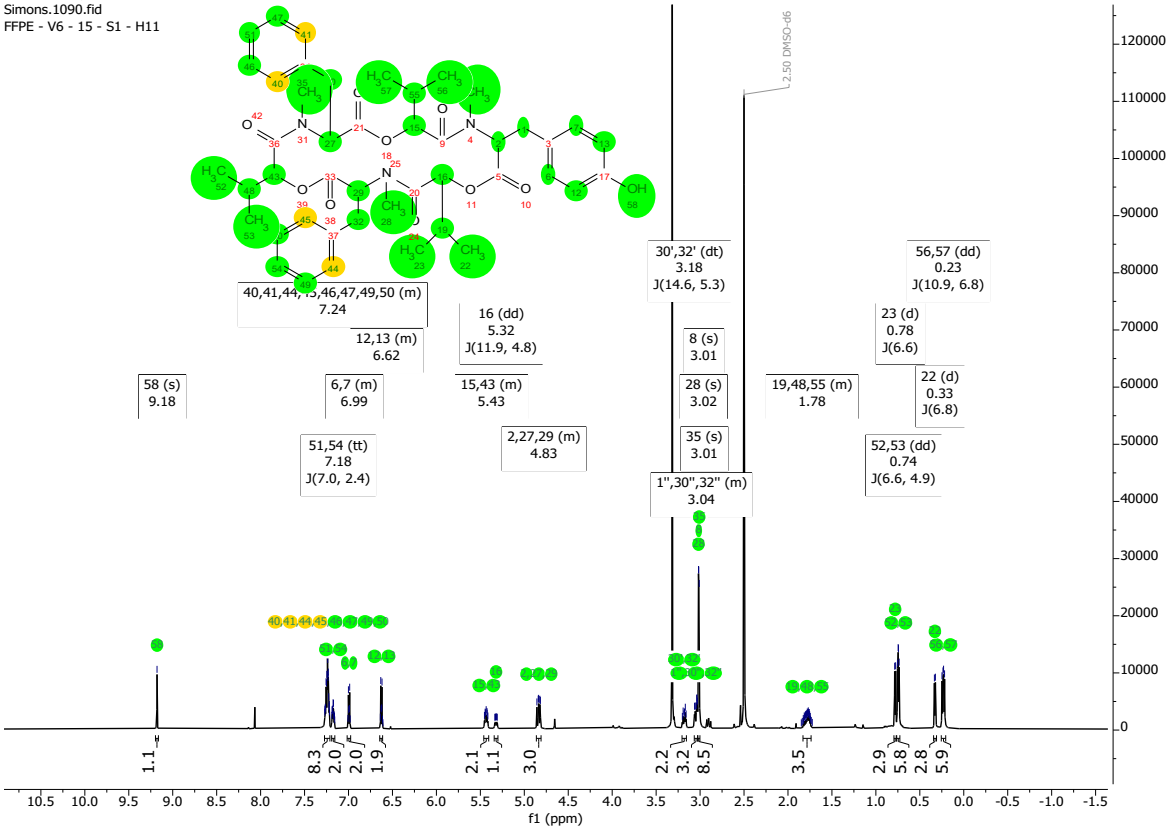

S67. HPLC-DAD UV-Vis Spectrum of Compound 10 (Beauvericin J) (Methanol)

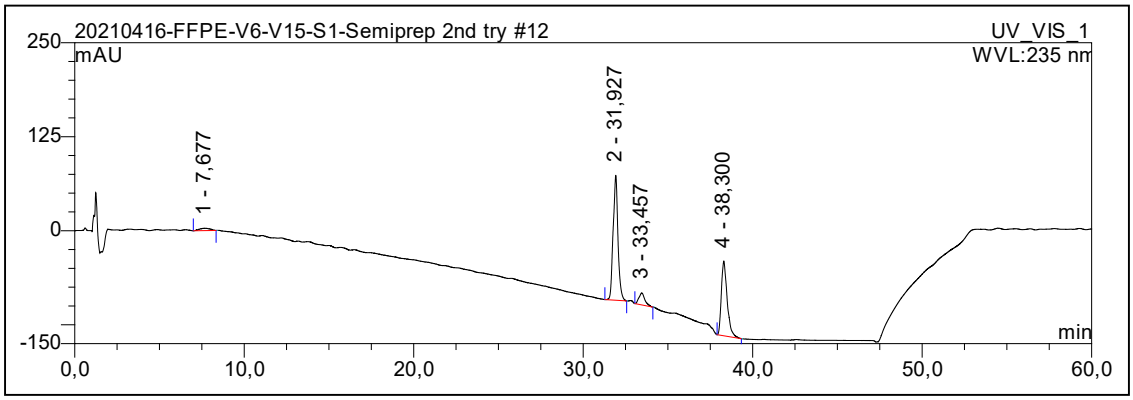

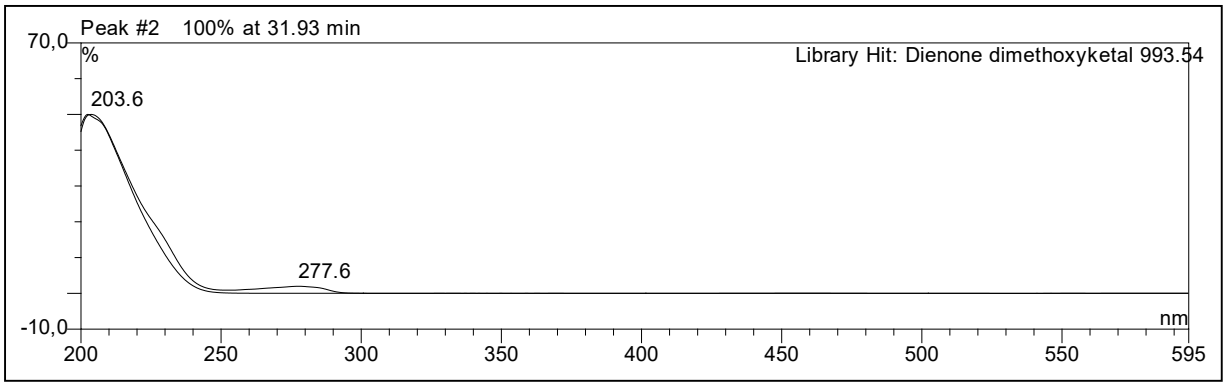

S68. High Resolution ESI(+)MS Spectrum of Compound 10 (Beauvericin J)

Mass Spectrum SmartFormula Report

Analysis Info

Analysis Name	D:\Data\Spektren 2022\KAL22HR000113.d	Acquisition Date	7/27/2022 10:27:21 AM
Method	tune_low_new.m	Operator	TM
Sample Name	FFPE-V6S1H11	Instrument	maXis 288882.20213
Comment			

Acquisition Parameter

Source Type	ESI	Ion Polarity	Positive	Set Nebulizer	0.3 Bar
Focus	Not active	Set Capillary	4000 V	Set Dry Heater	180 °C
Scan Begin	50 m/z	Set End Plate Offset	-500 V	Set Dry Gas	4.0 l/min
Scan End	1500 m/z	Set Collision Cell RF	600.0 Vpp	Set Divert Valve	Source

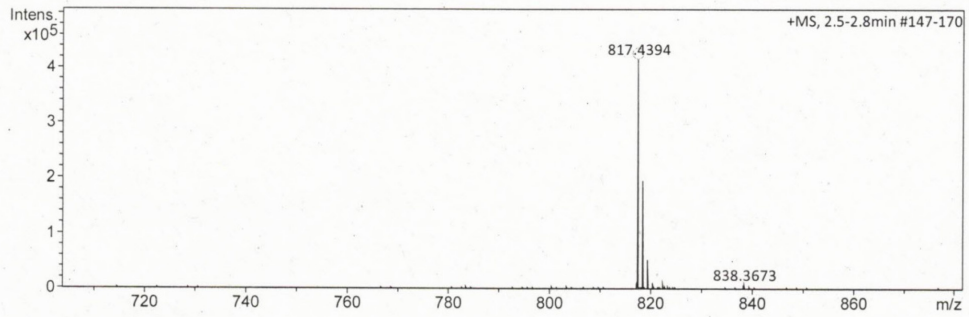

Meas. m/z	#	Ion Formula	m/z	err [ppm]	mSigma	# mSigma	Score	rdb	e⁻ Conf	N-Rule
817.4394	1	C45H61N4O10	817.4382	-1.4	23.2	1	80.86	17.5	even	ok
	2	C43H49N18	817.4382	-1.4	33.6	2	62.75	28.5	even	ok
	3	C46H57N8O6	817.4396	0.2	34.8	3	100.00	22.5	even	ok
	4	C47H53N12O2	817.4409	1.9	46.6	4	34.78	27.5	even	ok
	5	C62H57O	817.4404	1.3	115.4	5	2.85	34.5	even	ok

7. Further contributions

Further minor contributions have been made for the following publications or manuscript drafts:

Peter M Eze, **Viktor Simons**, Tino Seidemann, Lin Wang, Anna-Lene Kiffe-Delf, Marian Frank, Lasse van Geelen, Chika C Abba, Charles O Esimone, Festus BC Okoye, Rainer Kalscheuer, Serratiochelins A and B from *Serratia marcescens* show xenosiderophoric characteristics towards *Acinetobacter baumannii* and *Mycobacterium* tuberculosis.
Status: published in Tropical Journal of Pharmaceutical Research. 20 (12), 2551-2558, (2021).
DOI: 10.4314/tjpr.v20il2.14

Lin Wang, Anna-Lene Kiffe-Delf, **Viktor Simons**, Di He, Philipp Niklas Ostermann, Ying Gao, Lasse van Geelen, Hao-Fu Dai, You-Xing Zhao, Heiner Schaal, Attila Mándi, Sándor Balázs Király, Tibor Kurtán, Zhen Liu, Rainer Kalscheuer, Asperphenalenones isolated from the biocontrol agent *Clonostachys rosea* and their antimicrobial activities.
Status: Submitted to Journal of Agricultural and Food Chemistry

Peter M Eze, Yang Liu, **Viktor E. Simons**, Sherif S. Ebada, Tibor Kurtán, Charles O. Esimone, Festus B.C. Okoye, Peter Proksch, Rainer Kalscheuer, Two new metabolites from coculturing a marine-derived fungus *Penicillium ochrochloron* and *Bacillus subtilis*.
Status: Manuscript draft (unpublished)

8. Discussion and Perspectives

The increasing antimicrobial resistance rates for clinically important pathogens around the world raise the demand for new antibiotics. A lack of innovation of new antimicrobial compounds during the last decades together with a widespread over- and misuse of already established antibiotics have led to the global antimicrobial resistance crisis. While it is now time to improve and strengthen the research for new antimicrobial compounds to help discover new classes of antibiotics, natural products have always been a great source. Over the last four decades, around 60% of clinical antibacterial drugs are based on natural products [188]. Also, nature has always proven to deliver a wide range of different antimicrobial activities comprising all known domains. The studies presented in the chapters 4-7 give examples of the diversity and complexity and the variety of opportunities when it comes to research about natural products derived from microbial sources.

In chapter 4, we introduced a project about the isolation of the endophytic fungus *Pareboeremia selaginellae* from the ornamental plant *Philodendron monstera* and the subsequent isolation of natural products derived from a solid rice fermentation process. We found selective activity against the apicomplexan parasite *Toxoplasma gondii* for six of the eight tested compounds. While the anti-toxoplasma activities ranged from moderate to good, they could not reach the sub-micromolar values of the approved drug and positive control pyrimethamine. Building upon these results, a semisynthetic approach to synthesise more active derivates and decrease the minimal inhibitory concentration to nanomolar levels could be very fruitful. Especially, in the case of the three isolated biphenyl ethers (**1**, **2** and **3** – see **Figure 5**) that showed no cytotoxicity at 100 µM against the tested human cell lines, semisynthesis should be accessible. They exhibit a low molecular weight and no stereocentres, which also makes them perfect for whole synthesis approaches. Interestingly, the two isolated bioxanthracenes (**4** and **5** – see **Figure 5**) differed markedly in their anti-toxoplasma activities and the cytotoxicity assay, preferring compound **4** over **5**. *5S,6S*-Phomalactone (**6** – see **Figure 5**) also is a quite interesting compound, since it is described in the literature to have a wide range of different activities, ranging from antibacterial, antifungal, anti-plasmodium to nematicidal and trypanocidal activities [189-192]. Thus, this compound seems to have a rather unselective mode of action. Nevertheless, in our studies, it had a very low antibacterial activity with an MIC_{90} of 100 µM against *Pseudomonas aeruginosa* ATCC 87110 and >100 µM against methicillin-resistant *Staphylococcus aureus* ATCC 700699.

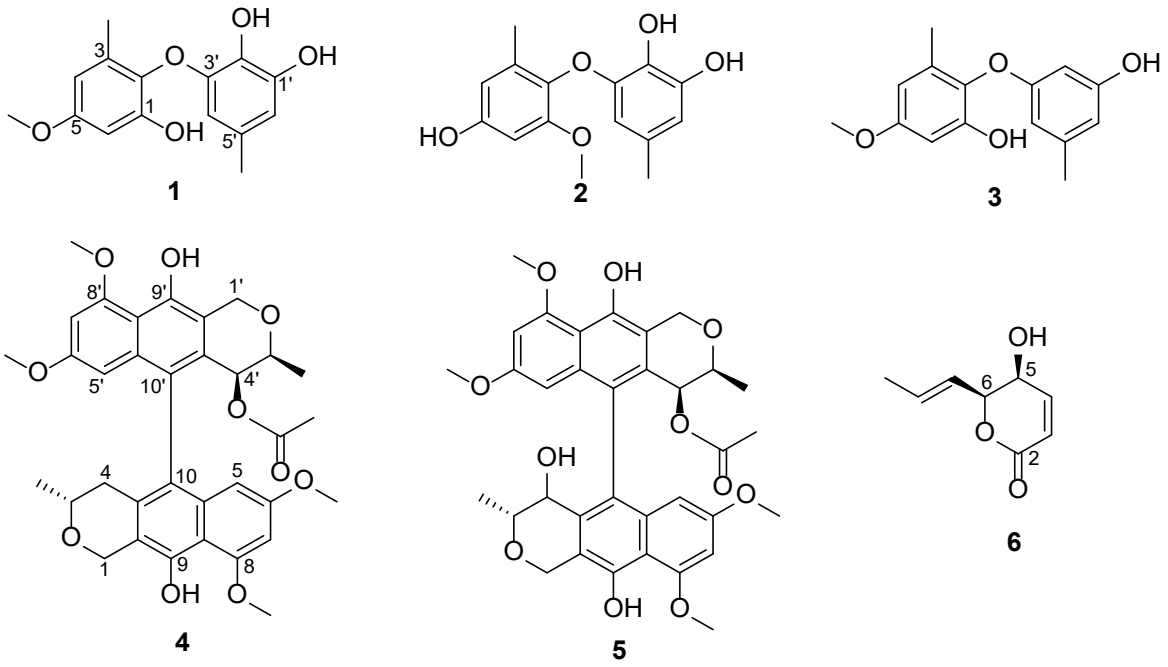

Figure 5. Active compounds against *Toxoplasma gondii* derived from the endophytic fungus *Paraboeremia selaginellae*. Compounds **1-3** are biphenylether-derivatives, **4-5** oxanthracenes and compound **6** is *5S,6S*-phomalactone. All compounds are described in chapter 4 of this thesis.

Since all of the isolated compounds were already known from other microbial sources, this project is a perfect example of the discovery of new activities from already known natural products. Often, the isolation of natural products is linked to the aim of finding specific bioactivities. If a bioassay-guided isolation process is being performed, due to limited time or testing opportunities, it is often restricted to certain types of bioactivity testing systems. Unfortunately, known compounds are often of less interest to natural product researchers, which can lead to the neglect of the inherent undiscovered potential of these molecules. While, of course, it will never be possible for a research group to test for all possible bioactivities, it should still be encouraged to also include known compounds from an isolation process to a variety of bioassays. Approaches that already face this direction focus on the so-called "drug repurposing" or "drug repositioning". While these projects do not focus on non-licensed natural products but include already established drugs or investigational drugs to identify new targets for them to extend their medical indications, they still are exemplary for sustainable research and also extend the possibilities for the scientific outcome [193].

In our second study, presented in chapter 5, we isolated ten compounds from the endophytic fungus *Trichocladium sp.*. Five of the isolated compounds turned out to be undescribed before. This project was interesting from different perspectives. The cultivation was carried out on rice

medium supplemented with the aromatic amino acid L-phenylalanine in an OSMAC-approach. This was already the fourth OSMAC-experiment with this fungus. First, *Trichocladium sp*. was co-cultivated with the bacterium *Bacillus subtilis* on rice medium to yield a new spiro compound. Then the medium was changed from rice to peas medium to increase the protein content. This approach yielded a new sesquiterpene derivative. Further, the fermentation on rice medium with 2.0 % L-tryptophane gave a new bismacrolactone [183]. Now in context of this thesis, the cultivation with 2.5 % L-phenylalanine yielded one new dihydronaphthalenone, one new macrocarpon and three new linear monoester-acids (see **Figure 6**).

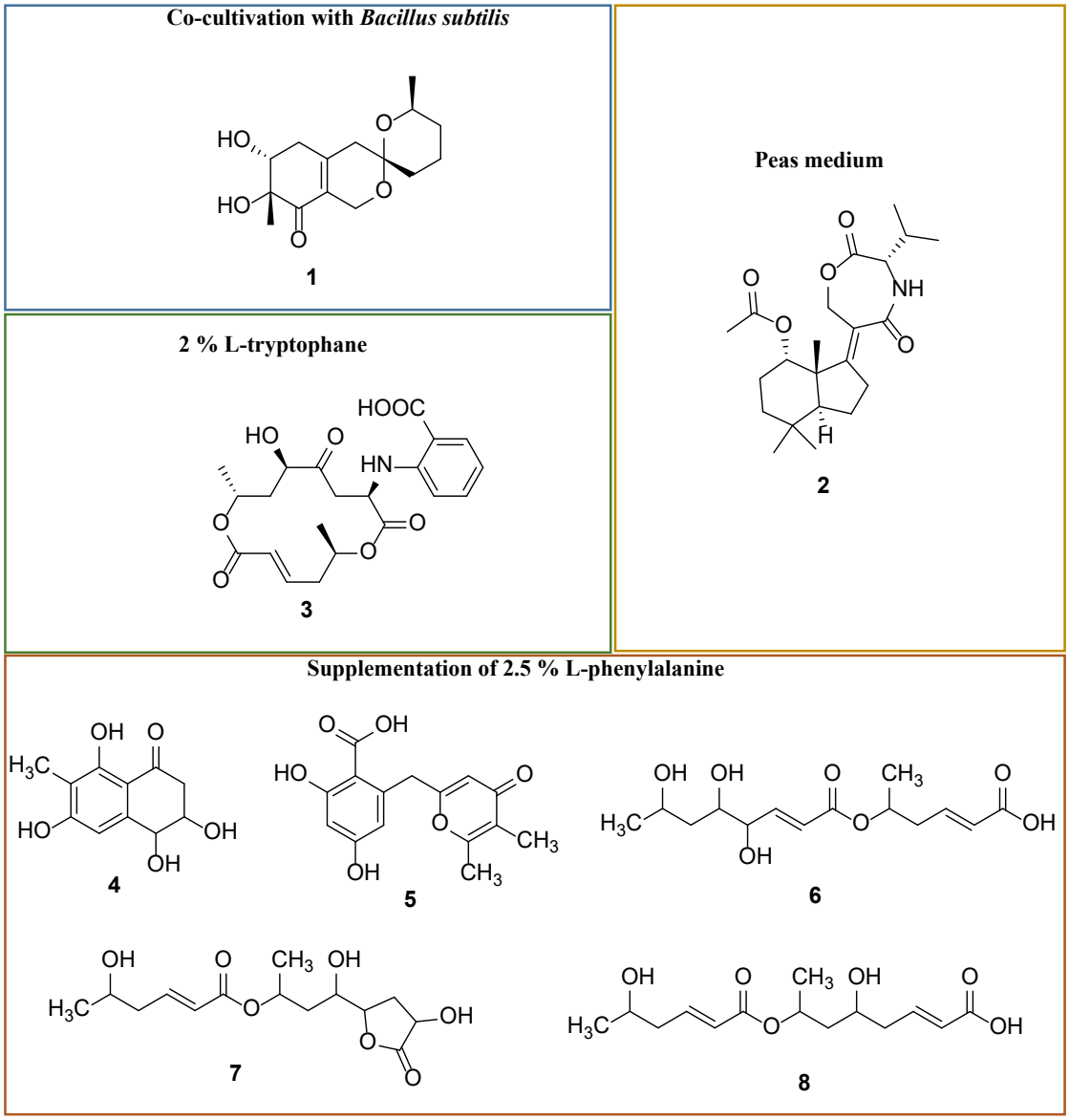

Figure 6. Isolation of new compounds from *Trichocladium sp.* in different OSMAC-approaches. The co-cultivation with *Bacillus subtilis* gave a new spiro compound (**1**). The fermentation on peas medium yielded a new sesquiterpene derivative (**2**). Supplementation of 2 % L-tryptophane to the culture medium led to a new macrobislactone (**3**). The supplementation of 2.5 % L-phenylalanine to the

rice medium yielded five new compounds (**4-8**). Compounds **1-3** were isolated and described by Tran-Cong *et al*. [183]. Compounds **4-8** are described in chapter 5 of this thesis.

This sequence of OSMAC approaches impressively demonstrates the power of this method. While no new bioactivities were found in our last approach, this project shows that OSMAC can influence the production of secondary metabolites on many different levels. Even small changes, like little adaptations of the nutrients, can trigger the production of otherwise cryptic metabolites from BGCs. In this case, we increased the concentration of L-phenylalanine to an unnaturally high level, which could have influenced the biosynthesis of colletodiol and other bislactonic derivatives. This study suggests that L-phenylalanine in high concentrations influences enzymes necessary for the last steps of the biosynthesis of colletodiol and derivatives, where the cyclisation takes place. This influence could happen either directly on enzymes involved in the late biosynthetic steps or indirectly via regulation of genes from BGCs that encode these enzymes. Nevertheless, further studies focussing on the elucidation of our hypothesis are still necessary.

Our experience from this study also provides us with a suggestion for a standard procedure for the application of OSMAC experiments to discover cryptic metabolites efficiently. In the beginning, we start with a large-scale axenic culture to create a secondary metabolite profile for our standard conditions, while creating an HPLC-chromatogram for the crude extract and isolating the main compounds with subsequent structure elucidation. Then, we perform different OSMAC approaches, each in a single fermentation flask to have the opportunity to apply a relatively big number of different OSMAC approaches at the same time without special laboratory equipment. While measuring the HPLC-chromatograms of the crude extracts for each small-scale OSMAC approach, we can directly see the difference in the pattern of metabolite production. The most promising OSMAC approaches can then be conducted in large-scale fermentations to isolate and elucidate the induced metabolites. While the outcome of an OSMAC experiment can hardly be foreseen, this setup still gives the whole methodology a rational design. Afterwards, when secondary metabolites are isolated from the crude extract, a bioassay-guided isolation process can purposefully lead to interesting bioactive metabolites. While modern bioinformatics-based approaches can lead to promising results, they are often still quite sophisticated and time-consuming. The OSMAC- and bioassay-guided isolation is an accessible and relatively fast process with a huge variety of possibilities.

Some results for nutrient-based OSMAC experiments in the past yielded secondary metabolites that can be structurally connected to the nature of the supplemented ingredients. Frank *et al*. for example supplemented solid rice medium with 5% NaBr and thus induced the production of

novel brominated azaphilones from the sponge-associated fungus *Penicillium canescens* [194]. Since chlorinated azaphilones like the chaetoviridins have also been described [195], the high concentrations of NaBr probably lead to a substitution of one halogen atom by the other. Another approach by Yu *et al*. focussed on the supplementation of 3.5% NaI to the solid rice medium of a culture of the endophytic fungus *Pestalotiopsis lespedezae*. This study yielded ten new ambuic acid derivatives, interestingly containing one new iodinated compound that was only produced during NaI substitution [196].

The example of the OSMAC concept can also be transferred to the isolation of microorganisms from environmental samples to improve the inherent potential. With the huge variety of different microorganisms in nature, we have still only been able to isolate a small part of them [118]. Often, we see a rediscovery of already-known species over and over again. In chapter 1.3, we discussed the hidden potential in the isolation of microorganisms from environmental samples that can be tapped through new and alternative approaches. The reason that most of the microorganisms in soil cannot grow under standard laboratory conditions probably is connected to special needs that cannot be fulfilled under artificial circumstances that easily. In very early studies, the role of the soil on the growth of soil-derived microorganisms was already discussed. It was stated that there must be some kind of growth factors inside the soil that specifically induce the growth of certain soil bacteria [197]. Today, we are still not able to understand the nature of the soil completely. We know that it is a specialised ecosystem with complex interactions between the living microbes among each other and the surrounding flora, fauna and soil structure. Interestingly, most microorganisms in soil stay in a dormant, inactive state till the proper circumstances for growth appear. The trigger factors that switch these organisms from the inactive to the active state can be diverse and complex and are still a matter of scientific discussion. Some microorganisms seem to have their micro-niches with special environmental and physicochemical conditions that turn them into an active growth state. Also, the nutrient composition and dynamics in soil are yet to be investigated sufficiently to better understand and influence the growth of uncultivable bacteria under lab conditions [198]. If the secrets about the complex structures and interactions that are inherent in the soil habitat are being deciphered, it will pave the way to more rational cultivation methods to give access to the metabolic profiles of uncultivable microorganisms. This will raise the possibilities for the discovery of new and bioactive natural products.

In chapter 1.3.1, we have discussed another interesting study by Hover *et al*. that circumvents the problem of the cultivation of microorganisms. The bacterial DNA was directly isolated from soil samples and investigated for certain BGCs that encode for a typical calcium-binding motif

to isolate new antimicrobial peptides. The appropriate gene was amplified and transferred into a lab organism for expression. The peptide can then be isolated from the culture of the lab strain [135]. While this study is impressive because of its rational and modern design to tap hidden bioactive molecules from environmental microorganisms, it also bears some limitations. First of all, the authors had to restrict their search to known genetic motifs that are connected to a certain type of activity right from the start. While the structure of certain BGCs can give information about the structural class they are encoding, the complete molecular structure can hardly be predicted precisely by this method when it comes to small molecules. This restricts the method to the isolation of peptidic compounds. Also, this method depends on already known genetic motifs because the structure is isolated based on the genetic information. Standard isolation processes normally work the other way around, since natural products are first isolated, and, if the genetic information is of concern, the elucidation of the BGC is carried out afterwards. Altogether, this sophisticated work enriches and complements the available methods of natural product isolation and is quite valuable, since it can be performed with a variety of different motifs and with DNA from microorganisms of different domains to support the discovery of new compounds from known structural classes. However, it is rather an enhancement than a replacement in the research of antimicrobial compounds derived from microorganisms.

A common problem in the isolation of microorganisms from environmental samples is that often dominant fast-growing species overgrow the slow-growing microbiota during cultivation in standard isolation medium. However, it is known that some bacteria from soil samples are only able to grow in medium with low concentrations of certain nutrients [199]. These oligotrophic bacteria will not be isolated in a standard laboratory medium. Also, some microorganisms are slow-growing and under standard isolation conditions and will not be able to compete against fast-growing opponents. The combination of a medium with low nutrient concentrations together with a prolonged incubation time of up to three months in a study by Davis *et al.* led to the isolation of rare slow-growing soil bacteria, such as members of the phyla Verrucomicrobia and Gemmatimonadetes [200].

The described examples above give an insight into the complex structures and dependencies which are connected to the isolation of microorganisms from environmental samples. Moreover, this also grants us a countless range of varieties starting from how we are taking the sample over to the isolation and the cultivation of the microorganisms. If scientists around the world will continue to creatively improve the isolation and cultivation process of environmental

microorganisms, different combinations and decisions will influence the outcome, enabling us to discover new microbial species and unfold the map to unknown bioactive natural products.

In chapter 6, we isolated biofilm-disrupting fusarubin-derivatives with a new and uncommon substructure. These bioactive molecules, named fusapurpurin A and B, were isolated from a crude extract of a co-cultivation of the soil-derived fungus *Fusarium oxysporum* together with the also soil-derived bacterium *Paenibacillus ehimensis*. This co-cultivation attracted our attention through development of an unusual dark purple colouring on solid rice medium compared to the axenic culture and other bacterial co-cultures. The HPLC-chromatogram showed a strong increase for the 9-*O*-methylfusarubin peak in the crude extract of the *Paenibacillus ehimensis* co-culture compared to the other crude extracts. Interestingly, the molecular structure of the fusapurpurins comprises 9-*O*-methylfusarubin as a core structure that is extended by a phenyl pyruvic acid moiety (see **Figure 7**). The strong induction of the 9-*O*-methylfusarubin in the HPLC-chromatogram thus is comprehensible. Unfortunately, the fusapurpurins cannot be detected in the crude extract even at higher concentrations because they seem to be small side products of the crude extracts. A series of purification steps is necessary to get to a point, where the peaks are being detected. To improve our understanding of the biosynthetic background of the fusapurpurins, we applied nanopore whole genome sequencing. Subsequently, we analysed the whole genome employing the antiSMASH fungi-SMASH algorithm to discover BGCs potentially responsible for fusapurpurin synthesis (antiSMASH version 6.1.1, retrieved at 27.06.2022). Interestingly, we could find a BGC with high similarity to a BGC known to be responsible for the biosynthesis of fusarubin in *Fusarium fujikuroi*. Upstream of the core sequence of this BGC, we discovered genes encoding for an amino acid transporter and a L-amino acid oxidase. These enzymes could be responsible for the transport of the aromatic amino acid L-phenylalanine into the fungal cell and the oxidative deamination to form phenylpyruvic acid and thus support our hypothesis of the fusapurpurin A and B biosynthesis .

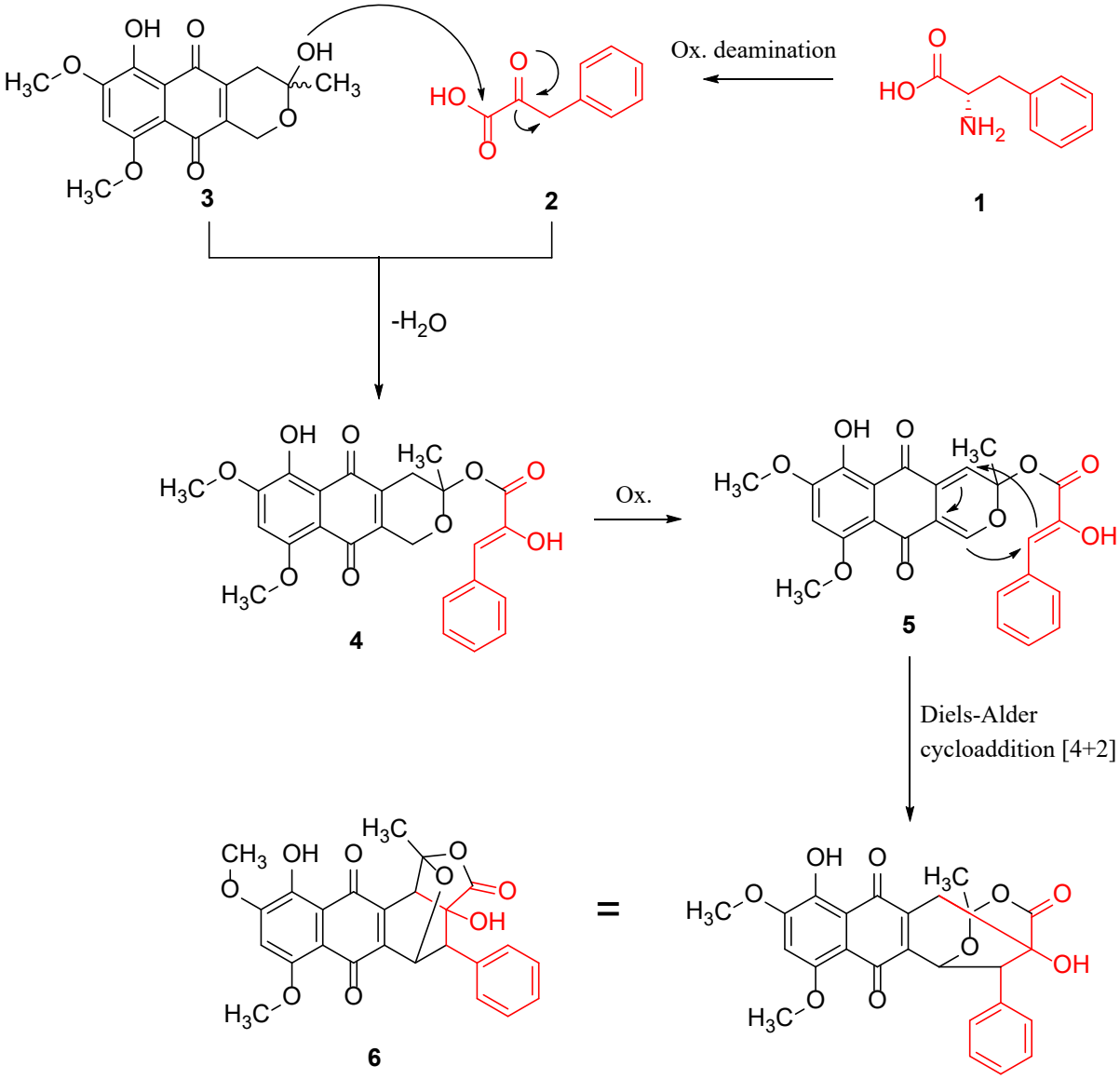

Figure 7: A proposed biosynthetic pathway to form fusapurpurin A and B. The amino acid L-phenylalanine (1) is oxidised via oxidative deamination to build phenylpyruvic acid (2). 9-*O*-Methylfusarubin (3) reacts with phenyl pyruvic acid (2) in a nucleophilic substitution to form intermediate 4. After an oxidative step to building intermediate 5, structure 6 (fusapurpurin A and B) is built over a Diels-Alder cycloaddition [4+2] as the final step.

The biofilm-disrupting activity of the fusapurpurins can be tracked throughout the whole isolation process. In our bioassays, we were able to show this activity for biofilms being produced by *S. aureus* Mu50, *P. aeruginosa* PAO1 and only for fusapurpurin B also on biofilms being produced by *M. tuberculosis* H37Rv. The compounds were not able to inhibit the formation of biofilms but disrupted pre-grown biofilms when administered to them, which was

shown in a serial dilution assay. They had no effect on quorum sensing and no antimicrobial effect alone and did neither improve nor impair the efficacy of moxifloxacin in a checkerboard assay.

This project emphasised that co-culture approaches can be very specific and the use of different types of microorganisms can be significant. Co-cultures are a powerful OSMAC tool because they mimic naturally occurring situations and can activate the biosynthesis of bioactive metabolites. In 2016 for example, Yu *et al.* published an impressive study about a co-cultivation attempt of the marine-derived fungus *Aspergillus flavus* with an actinomycete *Streptomyces sp.* This co-culture led to the induction of six novel cytochalasins that were toxic to *Streptomyces sp.*. Interestingly, the authors could show that direct physical contact between the fungus and the bacterium was necessary to result in these inductions [201].

In our case, the type of influence that *P. ehimensis* has on *F. oxysporum* in comparison to the other bacterial co-cultures remains elusive. *P. ehimensis* can form biofilms on its own [202]. Therefore, the production of compounds that can disrupt the biofilm matrix to compete against this bacterium and open up new spaces for growth is a possible explanation. Also, it might be possible that the fusapurpurins are being synthesized outside of the fungus in cooperation with *P. ehimensis* in a direct or indirect manner. However, this hypothesis is in agreement with the rather unspecific biofilm disrupting activities of fusapurpurin A and B. On the other hand, the exact mode of action of the fusapurpurins remains to be investigated. Fusapurpurin A and B are both inactive during the formation of biofilms and only disrupt pre-formed biofilms. Additionally, they did not inhibit quorum sensing in *Chromobacterium violaceum*. These results indicate that these compounds could have a direct and more generalised effect on the structural integrity of the biofilms. This hypothesis would also be supported by the fact that we could see activities against biofilms of three different pathogens, while it is also interesting that fusapurpurin B, in contrast to fusapurpurin A, was active against *M. tuberculosis* H37Rv biofilms. Also, the mechanism of fusapurpurin biosynthesis has to be confirmed in comprehensive biosynthetic studies. A deeper understanding of how the phenylpyruvate moiety is being added to the 9-*O*-methylfusarubin core structure will give important insights into finding and confirming the responsible BGC. This could pave the way for comprehensive transcriptome analyses. In this regard, it is of concern for future research under which conditions the fusapurpurins are being produced, and which are the best conditions for a maximised yield. It would be interesting to examine the activity of fusapurpurins in *in vivo* assays to see if there is a distinct benefit from it and if it can disrupt biofilms on natural surfaces. Since chemical synthesis of the fusapurpurins appears to be sophisticated because of the

complex structure and five stereocentres, a biotechnological approach can help to improve the yield of these biosynthetic side products. The BGC responsible for the fusapurpurin synthesis could be transformed into a fast-growing lab strain that would produce these compounds in high amounts. Because of the deep purple colour of these metabolites, a guided isolation process is simplified.

The variety and complexity that nature provides to us are noticeable in every detail. Small changes can often have a significant impact, which is underlined in this work and highlights that natural products derived from microorganisms are still of great importance. To tackle the problem of AMR in the future, it is important to approach it from different perspectives and look at it in its entirety. The isolation of antimicrobial compounds is one building block that should be supported by other modern technologies and methods. An example is phage therapy, which have some interesting benefits over common antibiotics. They are host-specific, have low toxicity to humans, can degrade biofilms and are self-amplifying. More scientific research is necessary to unfold their potential since development and application are more sophisticated. The high host-specificity makes it necessary to precisely know the pathogen causing a certain infection if a targeted application should be reached. Also, concerns about phages being vectors of virulence or resistance genes or killing valuable bacteria of the human microbiome are discussed [203, 204]. Also, antibody therapies are of growing interest. Antibodies can target common surface structures of microorganisms, like surface proteins or polysaccharides to mediate an innate immune response through opsonisation. Also, antibodies can target specific bacterial products like toxins. An example is the antibody bezlotoxumab, which can bind and neutralise toxin B produced by the gram-positive bacterium *Clostridium difficile* and reduce recurrence of *C. difficile* infections in patients [205]. While antibody therapies can be quite successful if a specific target is being addressed, downsides have also been described. Correlations of preclinical and clinical study results are not congruent in a variety of cases, and the specific target of the antibody is not always expressed by the targeted bacterium at all times [206].

Anyway, the most crucial and precious possibility to reduce AMR is how we are dealing with already available antibiotics in our dayly life, the medical, industrial and agricultural sector. A widespread and unspecific prescription of antibiotics by doctors is a common issue that paves the way for the development of AMR. A wrong, undifferentiated and unspecific treatment of common infections that often are associated with viruses as pathogens and an insufficient identification of the pathogens before treatment can lead to the unnecessary application of antibiotics. This overprescribing is mainly carried out by general practitioners during treatment

of respiratory tract infections [207, 208]. This problem should be tackled from different sides: increase of laboratory identification of pathogens before treatment, antimicrobial stewardship programs in hospitals, delayed antibiotic prescribing strategies, a structured standard operating procedure for the prescription of antibiotics, and improving and extending the communication with the patients are some examples to lower the overuse and incorrect use of antimicrobial substances. Another problem in the development of AMR is the free access to antibiotics in low- and middle-income countries without medical prescription. While a bad medical prescription management is promoting the development of AMR as described above, the complete lack of it can be even more harmful. Especially in Asian regions, the number of AMR is one of the highest worldwide, where antibiotics often can be directly accessed without prescription by a physician [209-211]. Most of the antibiotics worldwide are used for agriculture and livestock. They are used to promote growth and prevent infections in the animals. However, there is growing evidence that this widespread use has a strong influence on the overall development of AMR. Since, about 70% percent of the antibiotics used in livestock are also relevant in the treatment of human infections, this problem is endangering the effective and successfull application of antibiotics in the future and it is urgently necessary to switch to a more sustainably and responsible use in agriculture and livestock [212-214].

If we continue to invest in basic research and modern technologies and educate ourselves in the careful handling of antibiotics, we will make sure to keep the power of antimicrobial therapies alive and save the lives of millions of people now and in the future.

References

1. Emmerich, R. and O. Löw, *Bakteriolytische Enzyme als Ursache der erworbenen Immunität und die Heilung von Infectionskrankheiten durch dieselben.* Zeitschr. f. Hygiene, 1899. **31**: p. 1-65.
2. Ehrlich, P., *Address in Pathology, ON CHEMIOTHERAPY: Delivered before the Seventeenth International Congress of Medicine.* Br Med J, 1913. **2**(2746): p. 353-9.
3. Fleming, A., *On the Antibacterial Action of Cultures of a Penicillium, with Special Reference to their Use in the Isolation of B. influenza.* Br J Exp Pathol., 1929. **10**: p. 226-236.
4. Waksman, S.A. and H.B. Woodruff, *The soil as a source of microorganisms antagonistic to disease-producing bacteria.* Journal of Bacteriology, 1940. **Volume 40**: p. 581-600.
5. Waksman, S.A. and H.B. Woodruff, *Bacteriostatic and Bactericidal Substanes Produced by a Soil Actinomycete.* 1944.
6. Davies, J., *Where have all the antibiotics gone?* Can J Infect Dis Med Microbiol, 2006. **17**(5): p. 287-289.
7. Ventola, C.L., *The antibiotic resistance crisis: part 1: causes and threats.* P T, 2015. **40**(4): p. 277-83.
8. Berger, F.M., *Preparation of Purified Penicillin.* Br Med J, 1945. **1**(4386): p. 116-7.
9. Behrens, O.K. and M.J. Kingkade, *Biosynthesis of Penicillins.* Journal of Biological Chemistry, 1948. **176**(3): p. 1047-1050.
10. Handsfield, H.H., et al., *Amoxicillin, a new penicillin antibiotic.* Antimicrob Agents Chemother, 1973. **3**(2): p. 262-5.
11. Park, J.T. and J.L. Strominger, *Mode of action of penicillin.* Science, 1957. **125**(3238): p. 99-101.
12. Abraham, E.P., et al., *Cephalosporin N: a new type of penicillin.* Nature, 1953. **171**(4347): p. 343.
13. Newton, G.G. and E.P. Abraham, *Cephalosporin C, a new antibiotic containing sulphur and D-alpha-aminoadipic acid.* Nature, 1955. **175**(4456): p. 548.
14. O'Callaghan, C.H., et al., *Cefuroxime, a new cephalosporin antibiotic: activity in vitro.* Antimicrob Agents Chemother, 1976. **9**(3): p. 511-9.
15. Oxford, A.E., H. Raistrick, and P. Simonart, *Studies in the biochemistry of micro-organisms: Griseofulvin, C(17)H(17)O(6)Cl, a metabolic product of Penicillium griseo-fulvum Dierckx.* Biochem J, 1939. **33**(2): p. 240-8.
16. Brian, P.W., *Studies on the Biological Activity of Griseofulvin.* Annals of Botany, 1949. **13**(1): p. 59-77.
17. Roobol, A., K. Gull, and C.I. Pogson, *Inhibition by griseofulvin of microtubule assembly in vitro.* FEBS Letters, 1976. **67**(3): p. 248-251.
18. Roth, F.J., Jr., B. Sallman, and H. Blank, *In vitro studies of the antifungal antibiotic griseofulvin.* J Invest Dermatol, 1959. **33**: p. 403-18.
19. Gaumann, E., S. Roth, and et al., *Enniatin, a new antibiotic that works against mycobacteria.* Experientia, 1947. **3**(5): p. 202.
20. Plattner, P.A., U. Nager, and A. Boller, *Withers and antibiotics; On the isolation of novel antibiotics from Fusariums.* Helv Chim Acta, 1948. **31**(2): p. 594-602.
21. Hamill, R.L., *THE STRUCTURE OF BEAUVERICIN, A NEW DEPSIPEPTIDE ANTIBIOTIC TOXIC TO ARTEMIA SALINA.* 1969.
22. Maranghi, F., et al., *In vivo toxicity and genotoxicity of beauvericin and enniatins. Combined approach to study in vivo toxicity and genotoxicity of mycotoxins beauvericin (BEA) and enniatin B (ENNB).* EFSA Supporting Publications, 2018. **15**(5).
23. Kavanagh, F., A. Hervey, and W.J. Robbins, *Antibiotic Substances From Basidiomycetes: VIII. Pleurotus Multilus (Fr.) Sacc. and Pleurotus Passeckerianus Pilat.* Proc Natl Acad Sci U S A, 1951. **37**(9): p. 570-4.
24. Högenauer, G., *The Mode of Action of Pleuromutilin as Compared to Chloramphenicol.* 1975.
25. Maffioli, S.I., *A Chemist's Survey of Different Antibiotic Classes.* 2013.
26. Novak, R., *Are pleuromutilin antibiotics finally fit for human use?* Ann N Y Acad Sci, 2011. **1241**: p. 71-81.

27. Mang, R., *Pleuromutilin derivatives for the treatment of diseases mediated by microbes.* World Intellectual Property Organization International Bureau, 2008. **WO 2008/113089 Al**.
28. Sader, H.S., et al., *Antimicrobial activity of the novel pleuromutilin antibiotic BC-3781 against organisms responsible for community-acquired respiratory tract infections (CARTIs).* J Antimicrob Chemother, 2012. **67**(5): p. 1170-5.
29. Godtfredsen, W.O., et al., *Fusidic acid: a new antibiotic.* Nature, 1962. **193**: p. 987.
30. Bodley, J.W., et al., *Formation of the ribosome-G factor-GDP complex in the presence of fusidic acid.* Biochem Biophys Res Commun, 1969. **37**(3): p. 437-43.
31. Musmade, P.B., *Fusidic acid - topical antimicrobial in the management of staphylococcus aureus.* International Journal of Pharmacy and Pharmaceutical Sciences, 2013. **5**(4): p. 381-90.
32. Hutchings, M.I., A.W. Truman, and B. Wilkinson, *Antibiotics: past, present and future.* Curr Opin Microbiol, 2019. **51**: p. 72-80.
33. Lambert, P.A., *Cellular impermeability and uptake of biocides and antibiotics in Gram-positive bacteria and mycobacteria.* Journal of Applied Microbiology, 2002. **92**: p. 46S-54S.
34. Delcour, A.H., *Outer membrane permeability and antibiotic resistance.* Biochim Biophys Acta, 2009. **1794**(5): p. 808-16.
35. Hancock, R.E. and F.S. Brinkman, *Function of pseudomonas porins in uptake and efflux.* Annu Rev Microbiol, 2002. **56**: p. 17-38.
36. Donhofer, A., et al., *Structural basis for TetM-mediated tetracycline resistance.* Proc Natl Acad Sci U S A, 2012. **109**(42): p. 16900-5.
37. Li, W., et al., *Mechanism of tetracycline resistance by ribosomal protection protein Tet(O).* Nat Commun, 2013. **4**: p. 1477.
38. Floss, H.G. and T.W. Yu, *Rifamycin-mode of action, resistance, and biosynthesis.* Chem Rev, 2005. **105**(2): p. 621-32.
39. Tooke, C.L., et al., *beta-Lactamases and beta-Lactamase Inhibitors in the 21st Century.* J Mol Biol, 2019. **431**(18): p. 3472-3500.
40. Biswas, T., et al., *The structural basis for substrate versatility of chloramphenicol acetyltransferase CATI.* Protein Sci, 2012. **21**(4): p. 520-30.
41. Shaw, W.V., *Chloramphenicol acetyltransferase: enzymology and molecular biology.* CRC Crit Rev Biochem, 1983. **14**(1): p. 1-46.
42. Leslie, A.G., P.C. Moody, and W.V. Shaw, *Structure of chloramphenicol acetyltransferase at 1.75-A resolution.* Proc Natl Acad Sci U S A, 1988. **85**(12): p. 4133-7.
43. Poole, K., *Efflux pumps as antimicrobial resistance mechanisms.* Ann Med, 2007. **39**(3): p. 162-76.
44. Davidson, A.L. and J. Chen, *ATP-binding cassette transporters in bacteria.* Annu Rev Biochem, 2004. **73**: p. 241-68.
45. Tremblay, Y.D., et al., *Method to grow Actinobacillus pleuropneumoniae biofilm on a biotic surface.* BMC Vet Res, 2013. **9**: p. 213.
46. Raghupathi, P.K., et al., *Synergistic Interactions within a Multispecies Biofilm Enhance Individual Species Protection against Grazing by a Pelagic Protozoan.* Front Microbiol, 2017. **8**: p. 2649.
47. Karatan, E. and P. Watnick, *Signals, regulatory networks, and materials that build and break bacterial biofilms.* Microbiol Mol Biol Rev, 2009. **73**(2): p. 310-47.
48. Muhammad, M.H., et al., *Beyond Risk: Bacterial Biofilms and Their Regulating Approaches.* Front Microbiol, 2020. **11**: p. 928.
49. *Review on biofilm formation and its control options.* International Journal of Advanced Research in Biological Sciences (IJARBS), 2017. **4**(8): p. 122-133.
50. Hall-Stoodley, L., J.W. Costerton, and P. Stoodley, *Bacterial biofilms: from the natural environment to infectious diseases.* Nat Rev Microbiol, 2004. **2**(2): p. 95-108.
51. Reffuveille, F., et al., *A broad-spectrum antibiofilm peptide enhances antibiotic action against bacterial biofilms.* Antimicrob Agents Chemother, 2014. **58**(9): p. 5363-71.
52. O'Toole, G., H.B. Kaplan, and R. Kolter, *Biofilm formation as microbial development.* Annu Rev Microbiol, 2000. **54**: p. 49-79.

53. Fisher, R.A., B. Gollan, and S. Helaine, *Persistent bacterial infections and persister cells.* Nat Rev Microbiol, 2017. **15**(8): p. 453-464.
54. Jefferson, K.K., *What drives bacteria to produce a biofilm?* FEMS Microbiol Lett, 2004. **236**(2): p. 163-73.
55. Vestby, L.K., et al., *Bacterial Biofilm and its Role in the Pathogenesis of Disease.* Antibiotics (Basel), 2020. **9**(2).
56. Costerton, J.W., P.S. Stewart, and E.P. Greenberg, *Bacterial biofilms: a common cause of persistent infections.* Science, 1999. **284**(5418): p. 1318-22.
57. Esteban, J. and M. Garcia-Coca, *Mycobacterium Biofilms.* Front Microbiol, 2017. **8**: p. 2651.
58. Mulcahy, L.R., V.M. Isabella, and K. Lewis, *Pseudomonas aeruginosa biofilms in disease.* Microb Ecol, 2014. **68**(1): p. 1-12.
59. Archer, N.K., et al., *Staphylococcus aureus biofilms: properties, regulation, and roles in human disease.* Virulence, 2011. **2**(5): p. 445-59.
60. Srinivasan, R., et al., *Bacterial Biofilm Inhibition: A Focused Review on Recent Therapeutic Strategies for Combating the Biofilm Mediated Infections.* Front Microbiol, 2021. **12**: p. 676458.
61. Worthington, R.J., J.J. Richards, and C. Melander, *Small molecule control of bacterial biofilms.* Org Biomol Chem, 2012. **10**(37): p. 7457-74.
62. Jiang, Q., et al., *Quorum Sensing: A Prospective Therapeutic Target for Bacterial Diseases.* Biomed Res Int, 2019. **2019**: p. 2015978.
63. Yuyama, K.T., et al., *Cytochalasans Act as Inhibitors of Biofilm Formation of Staphylococcus Aureus.* Biomolecules, 2018. **8**(4).
64. Saggu, S.K., G. Jha, and P.C. Mishra, *Enzymatic Degradation of Biofilm by Metalloprotease From Microbacterium sp. SKS10.* Front Bioeng Biotechnol, 2019. **7**: p. 192.
65. Weatherly, L.M. and J.A. Gosse, *Triclosan exposure, transformation, and human health effects.* J Toxicol Environ Health B Crit Rev, 2017. **20**(8): p. 447-469.
66. Blackman, L.D., et al., *Approaches for the inhibition and elimination of microbial biofilms using macromolecular agents.* Chem Soc Rev, 2021. **50**(3): p. 1587-1616.
67. Lu, L., et al., *Developing natural products as potential anti-biofilm agents.* Chin Med, 2019. **14**: p. 11.
68. Fischbach, M.A. and C.T. Walsh, *Antibiotics for emerging pathogens.* Science, 2009. **325**(5944): p. 1089-93.
69. *<Neu, 1992.pdf>*.
70. Murray, C.J.L., et al., *Global burden of bacterial antimicrobial resistance in 2019: a systematic analysis.* The Lancet, 2022. **399**(10325): p. 629-655.
71. Yu, T., et al., *Circumventing antimicrobial-resistance and preventing its development in novel, bacterial infection-control strategies.* Expert Opin Drug Deliv, 2020. **17**(8): p. 1151-1164.
72. Ventola, C.L., *The Antibiotic Resistance Crisis Part 1: Causes and Threats.* P.T., 2015. **40**(2015 Apr): p. 277-283.
73. Renwick, M. and E. Mossialos, *What are the economic barriers of antibiotic R&D and how can we overcome them?* Expert Opin Drug Discov, 2018. **13**(10): p. 889-892.
74. O'Neill, J.A., *Antimicrobial resistance: tackling a crisis for the health and wealth of nations.* Wellcome Collection. Attribution 4.0 International (CC BY 4.0), 2014.
75. Theuretzbacher, U., et al., *The global preclinical antibacterial pipeline.* Nat Rev Microbiol, 2020. **18**(5): p. 275-285.
76. Piddock, L.J.V., *The Global Antibiotic Research and Development Partnership (GARDP): a not-for-profit antibiotic development organisation.* The Lancet Infectious Diseases, 2018. **18**(12): p. 1304-1305.
77. Clancy, C.J. and M.H. Nguyen, *Buying Time: The AMR Action Fund and the State of Antibiotic Development in the United States 2020.* Open Forum Infect Dis, 2020. **7**(11): p. ofaa464.
78. WHO, Global Priority List of Antibiotic resistant Bacteria to guide research, discovery, and development of new antibiotics. 2017.
79. WHO, *Antimicrobial resistance surveillance in Europe 2020 data.* 2022.

80. Boucher, H.W., et al., *Bad bugs, no drugs: no ESKAPE! An update from the Infectious Diseases Society of America.* Clin Infect Dis, 2009. **48**(1): p. 1-12.
81. Jadimurthy, R., et al., *Escaping mechanisms of ESKAPE pathogens from antibiotics and their targeting by natural compounds.* Biotechnol Rep (Amst), 2022. **34**: p. e00728.
82. Mulani, M.S., et al., *Emerging Strategies to Combat ESKAPE Pathogens in the Era of Antimicrobial Resistance: A Review.* Front Microbiol, 2019. **10**: p. 539.
83. Lowy, F.D., *Staphylococcus aureus infections.* N Engl J Med, 1998. **339**(8): p. 520-32.
84. Ogston, A., *Ueber Abscesse.* Arch Klin Chir, 1880. **25**: p. 588-600.
85. Otto, M., *Staphylococcus aureus toxins.* Curr Opin Microbiol, 2014. **17**: p. 32-7.
86. van Hal, S.J., et al., *Predictors of mortality in Staphylococcus aureus Bacteremia.* Clin Microbiol Rev, 2012. **25**(2): p. 362-86.
87. Morikawa, K., et al., *Expression of a cryptic secondary sigma factor gene unveils natural competence for DNA transformation in Staphylococcus aureus.* PLoS Pathog, 2012. **8**(11): p. e1003003.
88. Cheung, G.Y.C., J.S. Bae, and M. Otto, *Pathogenicity and virulence of Staphylococcus aureus.* Virulence, 2021. **12**(1): p. 547-569.
89. Rammelkamp, C.H. and T. Maxon, *Resistance of Staphylococcus aureus to the Action of Penicillin.* Experimental Biology and Medicine, 1942. **51**(3): p. 386-389.
90. Rolinson, G.N., et al., *Bacteriological Studies on a New Penicillin—Brl.1241.* The Lancet, 1960. **276**(7150): p. 564-567.
91. Jevons, M.P., *"Celbenin" - resistant Staphylococci.* Bmj, 1961. **1**(5219): p. 124-125.
92. Stapleton, P.D. and P.W. Taylor, *Methicillin resistance in Staphylococcus aureus: mechanisms and modulation.* Sci Prog, 2002. **85**(Pt 1): p. 57-72.
93. Otto, M., *Staphylococcal Biofilms.* Microbiol Spectr, 2018. **6**(4).
94. Yamada, T., et al., *Evaluation of Daptomycin-Induced Cellular Membrane Injury in Skeletal Muscle.* Biol Pharm Bull, 2020. **43**(9): p. 1338-1345.
95. Choo, E.J. and H.F. Chambers, *Treatment of Methicillin-Resistant Staphylococcus aureus Bacteremia.* Infect Chemother, 2016. **48**(4): p. 267-273.
96. Cong, Y., S. Yang, and X. Rao, *Vancomycin resistant Staphylococcus aureus infections: A review of case updating and clinical features.* J Adv Res, 2020. **21**: p. 169-176.
97. Gessard, C., *On the Blue and Green Coloration that Appears on Bandages.* Clinical Infectious Diseases, 1984. **6**(Supplement_3): p. S775-S776.
98. Jordan, E.O., *Bacillus Pyocyaneus and Its Pigments.* J Exp Med, 1899. **4**(5-6): p. 627-47.
99. Wellinghausen, N., et al., *Superiority of molecular techniques for identification of gram-negative, oxidase-positive rods, including morphologically nontypical Pseudomonas aeruginosa, from patients with cystic fibrosis.* J Clin Microbiol, 2005. **43**(8): p. 4070-5.
100. Walker, T.S., et al., *Pseudomonas aeruginosa-plant root interactions. Pathogenicity, biofilm formation, and root exudation.* Plant Physiol, 2004. **134**(1): p. 320-31.
101. Lore, N.I., et al., *Cystic fibrosis-niche adaptation of Pseudomonas aeruginosa reduces virulence in multiple infection hosts.* PLoS One, 2012. **7**(4): p. e35648.
102. de Bentzmann, S. and P. Plesiat, *The Pseudomonas aeruginosa opportunistic pathogen and human infections.* Environ Microbiol, 2011. **13**(7): p. 1655-65.
103. Huszczynski, S.M., J.S. Lam, and C.M. Khursigara, *The Role of Pseudomonas aeruginosa Lipopolysaccharide in Bacterial Pathogenesis and Physiology.* Pathogens, 2019. **9**(1).
104. Arhin, A. and C. Boucher, *The outer membrane protein OprQ and adherence of Pseudomonas aeruginosa to human fibronectin.* Microbiology (Reading), 2010. **156**(Pt 5): p. 1415-1423.
105. Thi, M.T.T., D. Wibowo, and B.H.A. Rehm, *Pseudomonas aeruginosa Biofilms.* Int J Mol Sci, 2020. **21**(22).
106. Hauser, A.R., *The type III secretion system of Pseudomonas aeruginosa: infection by injection.* Nat Rev Microbiol, 2009. **7**(9): p. 654-65.
107. Lau, G.W., et al., *The role of pyocyanin in Pseudomonas aeruginosa infection.* Trends Mol Med, 2004. **10**(12): p. 599-606.
108. Hall, S., et al., *Cellular Effects of Pyocyanin, a Secreted Virulence Factor of Pseudomonas aeruginosa.* Toxins (Basel), 2016. **8**(8).
109. Bedard, E., M. Prevost, and E. Deziel, *Pseudomonas aeruginosa in premise plumbing of large buildings.* Microbiologyopen, 2016. **5**(6): p. 937-956.

110. Fang, Z.L., et al., *OprD mutations and inactivation in imipenem-resistant Pseudomonas aeruginosa isolates from China.* Infect Genet Evol, 2014. **21**: p. 124-8.
111. Guenard, S., et al., *Multiple mutations lead to MexXY-OprM-dependent aminoglycoside resistance in clinical strains of Pseudomonas aeruginosa.* Antimicrob Agents Chemother, 2014. **58**(1): p. 221-8.
112. Ibrahim, D., J.F. Jabbour, and S.S. Kanj, *Current choices of antibiotic treatment for Pseudomonas aeruginosa infections.* Curr Opin Infect Dis, 2020. **33**(6): p. 464-473.
113. Chegini, Z., et al., *Bacteriophage therapy against Pseudomonas aeruginosa biofilms: a review.* Ann Clin Microbiol Antimicrob, 2020. **19**(1): p. 45.
114. Yim, G., H.H. Wang, and J. Davies, *Antibiotics as signalling molecules.* Philos Trans R Soc Lond B Biol Sci, 2007. **362**(1483): p. 1195-200.
115. Romero, D., et al., *Antibiotics as signal molecules.* Chem Rev, 2011. **111**(9): p. 5492-505.
116. Cornforth, D.M. and K.R. Foster, *Antibiotics and the art of bacterial war.* Proc Natl Acad Sci U S A, 2015. **112**(35): p. 10827-8.
117. Shlaes, D.M., *Antibiotics*. 2010.
118. Ferrari, B.C., S.J. Binnerup, and M. Gillings, *Microcolony cultivation on a soil substrate membrane system selects for previously uncultured soil bacteria.* Appl Environ Microbiol, 2005. **71**(12): p. 8714-20.
119. Chaudhary, D.K., A. Khulan, and J. Kim, *Development of a novel cultivation technique for uncultured soil bacteria.* Sci Rep, 2019. **9**(1): p. 6666.
120. Ling, L.L., et al., *A new antibiotic kills pathogens without detectable resistance.* Nature, 2015. **517**(7535): p. 455-9.
121. Rai, N., et al., *Plant associated fungal endophytes as a source of natural bioactive compounds.* Mycology, 2021. **12**(3): p. 139-159.
122. Karthikeyan, A., A. Joseph, and B.G. Nair, *Promising bioactive compounds from the marine environment and their potential effects on various diseases.* J Genet Eng Biotechnol, 2022. **20**(1): p. 14.
123. Beemelmanns, C., et al., *Natural products from microbes associated with insects.* Beilstein J Org Chem, 2016. **12**: p. 314-27.
124. Jiang, Y., et al., *Diversity and Bioactivity of Cultivable Animal Fecal Actinobacteria.* Advances in Microbiology, 2013. **03**(01): p. 1-13.
125. Schatz, A., E. Bugle, and S.A. Waksman, *Streptomycin, a Substance Exhibiting Antibiotic Activity Against Gram-Positive and Gram-Negative Bacteria.** Experimental Biology and Medicine, 1944. **55**(1): p. 66-69.
126. Duggar, B.M., *Aureomycin; a product of the continuing search for new antibiotics.* Ann N Y Acad Sci, 1948. **51**(Art. 2): p. 177-81.
127. Ehrlich, J., et al., *Chloromycetin, a New Antibiotic From a Soil Actinomycete.* Science, 1947. **106**(2757): p. 417.
128. *Chapter 3 Microflora of Soils*, in *Soil Organic Matter and Its Role in Crop Production*. 1973. p. 41-54.
129. Bardgett, R.D. and W.H. van der Putten, *Belowground biodiversity and ecosystem functioning.* Nature, 2014. **515**(7528): p. 505-11.
130. Torsvik, V., L. Ovreas, and T.F. Thingstad, *Prokaryotic diversity--magnitude, dynamics, and controlling factors.* Science, 2002. **296**(5570): p. 1064-6.
131. Taylor, D.L., et al., *A first comprehensive census of fungi in soil reveals both hyperdiversity and fine-scale niche partitioning.* Ecological Monographs, 2014. **84**(1): p. 3-20.
132. Hao, J., et al., 2020.
133. Bulgarelli, D., et al., *Structure and functions of the bacterial microbiota of plants.* Annu Rev Plant Biol, 2013. **64**: p. 807-38.
134. Stevenson, B.S., et al., *New strategies for cultivation and detection of previously uncultured microbes.* Appl Environ Microbiol, 2004. **70**(8): p. 4748-55.
135. Hover, B.M., et al., *Culture-independent discovery of the malacidins as calcium-dependent antibiotics with activity against multidrug-resistant Gram-positive pathogens.* Nat Microbiol, 2018. **3**(4): p. 415-422.
136. *Bacterial Endophyte Colonization and Distribution within Plants.* Microorganisms, 2017. **5**(4).

137. Furnkranz, M., et al., *Microbial diversity inside pumpkins: microhabitat-specific communities display a high antagonistic potential against phytopathogens.* Microb Ecol, 2012. **63**(2): p. 418-28.
138. García-Latorre, C., S. Rodrigo, and O. Santamaria, *Effect of fungal endophytes on plant growth and nutrient uptake in Trifolium subterraneum and Poa pratensis as affected by plant host specificity.* Mycological Progress, 2021. **20**(9): p. 1217-1231.
139. Iniguez, A.L., Y. Dong, and E.W. Triplett, *Nitrogen fixation in wheat provided by Klebsiella pneumoniae 342.* Mol Plant Microbe Interact, 2004. **17**(10): p. 1078-85.
140. Mengistu, A.A., *Endophytes: Colonization, Behaviour, and Their Role in Defense Mechanism.* Int J Microbiol, 2020. **2020**: p. 6927219.
141. Van Bael, S.A., M.A. Seid, and W.T. Wcislo, *Endophytic fungi increase the processing rate of leaves by leaf-cutting ants (Atta)* Ecological Entomology, 2012. **37**(4): p. 318-321.
142. Newman, M.A., et al., *MAMP (microbe-associated molecular pattern) triggered immunity in plants.* Front Plant Sci, 2013. **4**: p. 139.
143. Armijos Jaramillo, V.D., et al., *Horizontal transfer of a subtilisin gene from plants into an ancestor of the plant pathogenic fungal genus Colletotrichum.* PLoS One, 2013. **8**(3): p. e59078.
144. Wang, S. and J. Huang, *Fungal genes in the innovation and evolution of land plants.* Plant Signal Behav, 2021. **16**(4): p. 1879534.
145. Sachin, N., *Do endophytic fungi possess pathway genes for plant secondary metabolites?* Current Science, 2013. **104**(2): p. 178-182.
146. Stierle, A., G. Strobel, and D. Stierle, *Taxol and taxane production by Taxomyces andreanae, an endophytic fungus of Pacific yew.* Science, 1993. **260**(5105): p. 214-6.
147. Kusari, S., et al., *An endophytic fungus from Hypericum perforatum that produces hypericin.* J Nat Prod, 2008. **71**(2): p. 159-62.
148. Shweta, S., et al., *Endophytic fungal strains of Fusarium solani, from Apodytes dimidiata E. Mey. ex Arn (Icacinaceae) produce camptothecin, 10-hydroxycamptothecin and 9-methoxycamptothecin.* Phytochemistry, 2010. **71**(1): p. 117-22.
149. Martinez-Klimova, E., K. Rodriguez-Pena, and S. Sanchez, *Endophytes as sources of antibiotics.* Biochem Pharmacol, 2017. **134**: p. 1-17.
150. Kjer, J., et al., *Methods for isolation of marine-derived endophytic fungi and their bioactive secondary products.* Nat Protoc, 2010. **5**(3): p. 479-90.
151. Vignesh, S., A. Raja, and R. Arthur Jam, *Marine Drugs: Implication and Future Studies.* International Journal of Pharmacology, 2010. **7**(1): p. 22-30.
152. Ameen, F., S. AlNadhari, and A.A. Al-Homaidan, *Marine microorganisms as an untapped source of bioactive compounds.* Saudi J Biol Sci, 2021. **28**(1): p. 224-231.
153. Feling, R.H., et al., *Salinosporamide A: a highly cytotoxic proteasome inhibitor from a novel microbial source, a marine bacterium of the new genus salinospora.* Angew Chem Int Ed Engl, 2003. **42**(3): p. 355-7.
154. Stonik, V.A., T.N. Makarieva, and L.K. Shubina, *Antibiotics from Marine Bacteria.* Biochemistry (Mosc), 2020. **85**(11): p. 1362-1373.
155. Raveh, A., et al., *Discovery of potent broad spectrum antivirals derived from marine actinobacteria.* PLoS One, 2013. **8**(12): p. e82318.
156. Schulze, C.J., et al., *Salinipostins A-K, long-chain bicyclic phosphotriesters as a potent and selective antimalarial chemotype.* J Org Chem, 2015. **80**(3): p. 1312-20.
157. Hoang, K.L., L.T. Morran, and N.M. Gerardo, *Can a Symbiont (Also) Be Food?* Front Microbiol, 2019. **10**: p. 2539.
158. Okabe, K., *Ecological characteristics of insects that affect symbiotic relationships with mites.* Entomological Science, 2013: p. n/a-n/a.
159. Paniagua Voirol, L.R., et al., *Bacterial Symbionts in Lepidoptera: Their Diversity, Transmission, and Impact on the Host.* Front Microbiol, 2018. **9**: p. 556.
160. Boucias, D.G., et al., *Microbiota in insect fungal pathology.* Appl Microbiol Biotechnol, 2018. **102**(14): p. 5873-5888.
161. Ganley, J.G., et al., *Discovery of Antimicrobial Lipodepsipeptides Produced by a Serratia sp. within Mosquito Microbiomes.* Chembiochem, 2018. **19**(15): p. 1590-1594.

162. Chevrette, M.G., et al., *The antimicrobial potential of Streptomyces from insect microbiomes.* Nat Commun, 2019. **10**(1): p. 516.
163. Nery, J., et al., *Influence of dietary protein content and source on fecal quality, electrolyte concentrations, and osmolarity, and digestibility in dogs differing in body size.* J Anim Sci, 2010. **88**(1): p. 159-69.
164. Chen, H.J., et al., *Impact of dietary ingredients on the interpretation of various fecal parameters in rats fed inulin.* J Food Drug Anal, 2019. **27**(4): p. 869-875.
165. Martinez-Romero, E., et al., *We and herbivores eat endophytes.* Microb Biotechnol, 2021. **14**(4): p. 1282-1299.
166. Yu, H., et al., *Azaphilone pigments and macrodiolides from the coprophilous fungus Coniella fragariae.* Fitoterapia, 2019. **137**: p. 104249.
167. Ma, J., et al., *New anti-inflammatory metabolites produced by Streptomyces violaceoruber isolated from Equus burchelli feces.* J Antibiot (Tokyo), 2017. **70**(10): p. 991-994.
168. Medema, M.H., et al., *antiSMASH: rapid identification, annotation and analysis of secondary metabolite biosynthesis gene clusters in bacterial and fungal genome sequences.* Nucleic Acids Res, 2011. **39**(Web Server issue): p. W339-46.
169. Blin, K., et al., *antiSMASH 6.0: improving cluster detection and comparison capabilities.* Nucleic Acids Res, 2021. **49**(W1): p. W29-W35.
170. Mao, D., et al., *Recent advances in activating silent biosynthetic gene clusters in bacteria.* Curr Opin Microbiol, 2018. **45**: p. 156-163.
171. Chiang, Y.M., et al., *Recent advances in awakening silent biosynthetic gene clusters and linking orphan clusters to natural products in microorganisms.* Curr Opin Chem Biol, 2011. **15**(1): p. 137-43.
172. Nah, H.J., et al., *Cloning and Heterologous Expression of a Large-sized Natural Product Biosynthetic Gene Cluster in Streptomyces Species.* Front Microbiol, 2017. **8**: p. 394.
173. Li, L., L.W. Maclntyre, and S.F. Brady, *Refactoring biosynthetic gene clusters for heterologous production of microbial natural products.* Curr Opin Biotechnol, 2021. **69**: p. 145-152.
174. Guzman-Chavez, F., et al., *Deregulation of secondary metabolism in a histone deacetylase mutant of Penicillium chrysogenum.* Microbiologyopen, 2018. **7**(5): p. e00598.
175. Akiyama, D.Y., et al., 2020.
176. Ding, Z., et al., *Deletion of the Histone Deacetylase HdaA in Endophytic Fungus Penicillium chrysogenum Fes1701 Induces the Complex Response of Multiple Bioactive Secondary Metabolite Production and Relevant Gene Cluster Expression.* Molecules, 2020. **25**(16).
177. Bode, H.B., et al., *Big effects from small changes: possible ways to explore nature's chemical diversity.* ChemBioChem, 2002. **3**: p. 619-627.
178. Romano, S., et al., *Extending the "One Strain Many Compounds" (OSMAC) Principle to Marine Microorganisms.* Mar Drugs, 2018. **16**(7).
179. Yamanaka, K., et al., *Direct cloning and refactoring of a silent lipopeptide biosynthetic gene cluster yields the antibiotic taromycin A.* Proc Natl Acad Sci U S A, 2014. **111**(5): p. 1957-62.
180. De, B.C., et al., *Host-dependent heterologous expression of berninamycin gene cluster leads to linear thiopeptide antibiotics.* Org Biomol Chem, 2021. **19**(41): p. 8940-8946.
181. Hemphill, C.F.P., et al., *OSMAC approach leads to new fusarielin metabolites from Fusarium tricinctum.* J Antibiot (Tokyo), 2017. **70**(6): p. 726-732.
182. Ariantari, N.P., et al., *Expanding the chemical diversity of an endophytic fungus Bulgaria inquinans, an ascomycete associated with mistletoe, through an OSMAC approach.* RSC Adv, 2019. **9**(43): p. 25119-25132.
183. Tran-Cong, N.M., et al., *Induction of cryptic metabolites of the endophytic fungus Trichocladium sp. through OSMAC and co-cultivation.* RSC Adv, 2019. **9**(47): p. 27279-27288.
184. Weller, M.G., *A unifying review of bioassay-guided fractionation, effect-directed analysis and related techniques.* Sensors (Basel), 2012. **12**(7): p. 9181-209.
185. Urgen, M., et al., *Bioassay-guided Isolation of Antibacterial and Cytotoxic Compounds from the Mesophilic Actinomycete M-33-5.* Natural Product Communications, 2010. **5**(2).

186. Kerkoub, N., et al., *Bioassay-Guided Isolation of Anti-Candida Biofilm Compounds From Methanol Extracts of the Aerial Parts of Salvia officinalis (Annaba, Algeria).* Front Pharmacol, 2018. **9**: p. 1418.
187. Kaufmann, K., et al., *Activity-guided screening of bioactive natural compounds implementing a new glucocorticoid-receptor-translocation assay and detection of new anti-inflammatory steroids from bacteria.* Biotechnol Lett, 2013. **35**(1): p. 11-20.
188. Newman, D.J. and G.M. Cragg, *Natural Products as Sources of New Drugs over the Nearly Four Decades from 01/1981 to 09/2019.* J Nat Prod, 2020. **83**(3): p. 770-803.
189. Gusmao, A.S., et al., *Computer-Guided Trypanocidal Activity of Natural Lactones Produced by Endophytic Fungus of Euphorbia umbellata.* Chem Biodivers, 2021. **18**(10): p. e2100493.
190. Wu, H.Y., et al., *Regulation of the growth of cotton bollworms by metabolites from an entomopathogenic fungus Paecilomyces cateniobliquus.* J Agric Food Chem, 2012. **60**(22): p. 5604-8.
191. Jiménez-Romero, C., et al., *Activity againstPlasmodium falciparumof Lactones Isolated from the Endophytic FungusXylariasp.* Pharmaceutical Biology, 2009. **46**(10-11): p. 700-703.
192. Kim, J.C., et al., *Activity against plant pathogenic fungi of phomalactone isolated from Nigrospora sphaerica.* Pest Manag Sci, 2001. **57**(6): p. 554-9.
193. Pushpakom, S., et al., *Drug repurposing: progress, challenges and recommendations.* Nat Rev Drug Discov, 2019. **18**(1): p. 41-58.
194. Frank, M., et al., *Brominated Azaphilones from the Sponge-Associated Fungus Penicillium canescens Strain 4.14.6a.* J Nat Prod, 2019. **82**(8): p. 2159-2166.
195. Chen, C., et al., *Recent advances in the chemistry and biology of azaphilones.* RSC Adv, 2020. **10**(17): p. 10197-10220.
196. Yu, X., et al., *Induction of ambuic acid derivatives by the endophytic fungus Pestalotiopsis lespedezae through an OSMAC approach.* Tetrahedron, 2021. **79**.
197. Lochead, A.G., M.O. Burton, and R.H. Thexton, *A bacterial growth-factor synthesized by a soil bacterium.* Nature, 1952. **170**(4320): p. 282.
198. Nannipieri, P., *Soil Is Still an Unknown Biological System.* Applied Sciences, 2020. **10**(11).
199. Whang, K. and T. Hattori, *Oligotrophic bacteria from rendzina forest soil.* Antonie Van Leeuwenhoek, 1988. **54**(1): p. 19-36.
200. Davis, K.E., S.J. Joseph, and P.H. Janssen, *Effects of growth medium, inoculum size, and incubation time on culturability and isolation of soil bacteria.* Appl Environ Microbiol, 2005. **71**(2): p. 826-34.
201. Yu, L., W. Ding, and Z. Ma, *Induced production of cytochalasans in co-culture of marine fungus Aspergillus flavipes and actinomycete Streptomyces sp.* Nat Prod Res, 2016. **30**(15): p. 1718-23.
202. Panichikkal, J., et al., *Biofilm and Biocontrol Modulation of Paenibacillus sp. CCB36 by Supplementation with Zinc Oxide Nanoparticles and Chitosan Nanoparticles.* Appl Biochem Biotechnol, 2022. **194**(4): p. 1606-1620.
203. Lin, D.M., B. Koskella, and H.C. Lin, *Phage therapy: An alternative to antibiotics in the age of multi-drug resistance.* World J Gastrointest Pharmacol Ther, 2017. **8**(3): p. 162-173.
204. Wahida, A., K. Ritter, and H.P. Horz, *The Janus-Face of Bacteriophages across Human Body Habitats.* PLoS Pathog, 2016. **12**(6): p. e1005634.
205. Chahine, E.B., J.C. Cho, and M.V. Worley, *Bezlotoxumab for the Prevention of Clostridium difficile Recurrence.* Consult Pharm, 2018. **33**(2): p. 89-97.
206. Motley, M.P., K. Banerjee, and B.C. Fries, *Monoclonal antibody-based therapies for bacterial infections.* Curr Opin Infect Dis, 2019. **32**(3): p. 210-216.
207. Llor, C. and L. Bjerrum, *Antimicrobial resistance: risk associated with antibiotic overuse and initiatives to reduce the problem.* Therapeutic Advances in Drug Safety, 2014. **5**(6): p. 229-241.
208. Colgan, R., *appropriate antimicrobial prescribing: approaches that limit antibiotic resistance.* American Family Physician, 2001. **64**(6): p. 999-1004.
209. Belachew, S.A., L. Hall, and L.A. Selvey, *Non-prescription dispensing of antibiotic agents among community drug retail outlets in Sub-Saharan African countries: a systematic review and meta-analysis.* Antimicrob Resist Infect Control, 2021. **10**(1): p. 13.

210. Llor, C. and J.M. Cots, *Dispensing of antibiotics without a medical prescription and communication skills of pharmacists.* Aten Primaria, 2013. **45**(9): p. 496-7.
211. Chang, J., et al., *Assessment of non-prescription antibiotic dispensing at community pharmacies in China with simulated clients: a mixed cross-sectional and longitudinal study.* The Lancet Infectious Diseases, 2019. **19**(12): p. 1345-1354.
212. Martin, M.J., S.E. Thottathil, and T.B. Newman, *Antibiotics Overuse in Animal Agriculture: A Call to Action for Health Care Providers.* Am J Public Health, 2015. **105**(12): p. 2409-10.
213. Landers, T.F., et al., *A review of antibiotic use in food animals: perspective, policy, and potential.* Public Health Rep, 2012. **127**(1): p. 4-22.
214. Van Boeckel, T.P., et al., *Global trends in antimicrobial use in food animals.* Proc Natl Acad Sci U S A, 2015. **112**(18): p. 5649-54.

Declaration of academic honesty/Eidesstattliche Erklärung

Ich versichere an Eides Statt, dass die Dissertation, „**Bioactivities and structural diversity of natural products derived from fungi**", von mir selbstständig und ohne unzulässige fremde Hilfe unter Beachtung der „Grundsätze zur Sicherung guter wissenschaftlicher Praxis an der Heinrich-Heine-Universität Düsseldorf" erstellt worden ist. Außer den angegebenen Quellen und Hilfsmitteln wurden keine weiteren verwendet. Diese Dissertation wurde weder in gleicher noch in abgewandelter Form in einem anderen Prüfungsverfahren vorgelegt. Weiterhin erkläre ich, dass ich früher weder akademische Grade erworben, noch dies versucht habe.

Düsseldorf, den 20.01.2023

Viktor Emanuel Simons